

Biophysical Evaluation of DNMT2 and NSUN6 Inhibitors Designed to Selectively Target Epitranscriptomal Writers



Dissertation

zur Erlangung des Grades

“Doktor der Naturwissenschaften (Dr. rer. nat.)”

im Promotionsfach Pharmazeutische und Medizinische Chemie

am Fachbereich Chemie, Pharmazie, Geographie und Geowissenschaften

der Johannes Gutenberg-Universität in Mainz

Apotheker Robert Alexander Zimmermann

geb. in Worms

Mainz, 2023

Submitted to the Faculty of Chemistry, Pharmacy, Geography, and Geoscience.

Dean:

Name of the first reviewer:

Name of the second reviewer:

Doctoral research: From 01. April 2019 to 28. April 2023

Date of the doctoral examination: 23. June 2023

D77 (Dissertation Universität Mainz)

Declaration of Authorship

I, Robert Alexander Zimmermann, declare that this thesis entitled, “Biophysical evaluation of DNMT2 and NSUN6 inhibitors designed to selectively target epitranscriptomal writers”, and the work presented in it are my own. I hereby declare that:

- ❖ I did this work completely while in candidature for a research degree at this university.
- ❖ I have clearly stated which parts of this thesis have already been submitted for another degree or qualification at this university or other institutions.
- ❖ Where I have consulted the published work of others, this is always clearly attributed.
- ❖ Where I have quoted parts from the work of others, the source is given. Except for such quotations, this thesis is entirely my own work.
- ❖ I have acknowledged all main sources of help.
- ❖ Where the thesis is based on work done by myself jointly with others, I have made clear exactly what was done by others and what I have contributed myself.

Place, Date: Mainz, _____

Signature: _____

“VENIET TEMPUS, QUO POSTERI NOSTRI TAM APERTA NOS NESCISSE MIRENTUR”

**“THERE WILL COME A TIME WHEN OUR DESCENDANTS WILL BE AMAZED
THAT WE DID NOT KNOW THINGS THAT ARE SO PLAIN TO THEM.”**

LUCIUS ANNAEUS SENECA, NATURAL QUESTIONS

Acknowledgements/Danksagung

[Redacted text block 1]

[Redacted text block 2]

[Redacted text block 3]

[Redacted text block 4]

[Redacted text block 5]

[Redacted text block 6]

Acknowledgements/Danksagung

[Redacted text block 1]

[Redacted text block 2]

[Redacted text block 3]

[Redacted text block 4]

[Redacted text block 5]

[Redacted text block 6]

[Redacted text block 7]

[Redacted text block 8]

Table of Contents

Declaration of Authorship	V
Acknowledgements/Danksagung.....	VIII
Table of Contents	X
Abbreviations	XII
Abstract	XIV
Kurzzusammenfassung.....	XV
Introduction.....	1
RNA-modifications.....	1
m ⁶ A modifications	2
m ⁷ G modifications.....	3
m ⁵ C modifications	3
RNA-methyltransferases	4
Class I methyltransferases.....	5
Class IV methyltransferases.....	5
Class VII methyltransferase	5
Class VIII methyltransferases.....	5
Class IX methyltransferases.....	5
DNA methyltransferase 2 (DNMT2)	5
NOP2/Sun RNA methyltransferase 6 (NSUN6).....	10
Methyltransferases from a medicinal chemistry perspective.....	13
Biophysical methods in medicinal chemistry	16
Differential Scanning fluorimetry (DSF).....	18
Microscale Thermophoresis (MST).....	18
Isothermal titration calorimetry.....	20
Aim of this thesis	22
List of publications.....	23
Publications and manuscripts as part of the doctoral thesis	23
1. Research articles.....	23
Publications and manuscripts beyond this doctoral thesis.....	24
1. Research articles.....	24
2. Reviews.....	24
3. Unpublished manuscripts.....	24
Development of selective inhibitors for the human methyltransferases DNMT2 and NSUN6	26

Table of Contents

Discovery of Inhibitors of DNA Methyltransferase 2, an Epitranscriptomic Modulator and Potential Target for Cancer Treatment.....	26
Project summary and own contributions.....	26
An Optimized Microscale Thermophoresis Method for High-Throughput Screening of DNA Methyltransferase 2 Ligands.	88
Project summary and own contributions.....	88
Chemical Space Virtual Screening against Hard-to-Drug RNA Methyltransferases DNMT2 and NSUN6.	114
Project summary and own contributions.....	114
Covalent S-adenosylhomocysteine-based DNA methyltransferase 2 inhibitors with a new type of aryl warhead.....	141
Project summary and own contributions.....	141
Outlook.....	201
References.....	203

Abbreviations

A	adenine
Ala	alanine
Arg	arginine
Asn	asparagine
C	cytosine
Cys	cysteine
DNA	deoxyribonucleic acid
DSF	differential scanning fluorimetry
G	guanine
Glu	glutamic acid
Gly	glycine
I	inosine
Ile	isoleucine
IR	infrared
ITC	isothermal titration calorimetry
L	leucine
Lys	lysine
m¹A	<i>N</i> ¹ -methyladenine
m¹G	<i>N</i> ¹ -methylguanine
m¹ψ	<i>N</i> ¹ -methylpseudouracil
m³C	<i>N</i> ³ -methylcytosine
m⁵C	5-methylcytosine
m⁶A	<i>N</i> ⁶ -methyladenine
m⁷G	<i>N</i> ⁷ -methylguanine
mRNA	messenger RNA
MST	microscale thermophoresis
NMR	nuclear magnetic resonance
PDB	protein data bank
Pmt1	probable methyltransferase 1
Pro	proline

Abbreviations

R	arginine
RNA	ribonucleic acid
rRNA	ribosomal RNA
SAH	S-adenosylhomocysteine
SAM	S-adenosylmethionine
SAR	structure-activity relationship
SAXS	small-angle X-ray scattering
Ser	serine
SPR	surface plasmon resonance
Thr	threonine
tRNA	transfer RNA
Tyr	tyrosine
U	uracil
Val	valine
Ψ	pseudouracil

Abstract

Starting from the natural product inhibitor SAH a structure-activity relationship (SAR) study was conducted to discover DNMT2 inhibitors. Microscale thermophoresis was used to determine the binding of these compounds towards DNMT2. The inhibitory potency of these compounds on DNMT2 was determined in a tritium incorporation assay using radioactively labeled SAM as a methyl group donor. Isothermal titration calorimetry was applied to investigate the thermodynamics behind the binding. The most potent inhibitors have been found to be derivatives of SAH, in which the central sulfur was exchanged for nitrogen. Additionally, these derivatives were branched at the nitrogen with various alkyl moieties. The affinity of the compounds towards DNMT2 was comparable to SAH or sinefungin, a pan-methyltransferase inhibitor. Moreover, these compounds showed improved selectivity towards other RNA methyltransferases.

Since the microscale thermophoresis method used in the first study had its limitations, this method was optimized to gain more information from a single experiment. By altering the labeling strategy from His-tag labeling of DNMT2 to a fluorescent tool compound, which binds to the active site of DNMT2, the signal-to-noise ratio of this method was improved tremendously. Furthermore, the transferability of results was improved, facilitating the screening of the in-house compounds. It also delivered semi-quantitative results, which accelerated the development of new compounds.

A virtual screening for DNMT2 and NSUN6 was conducted to develop inhibitors without a SAH scaffold. Based on the results of this screening, several compounds were ordered and tested for their affinity towards DNMT2 or NSUN6 using microscale thermophoresis. Compounds that exhibited a concentration-dependent binding behavior toward their target were cross-tested on the other enzyme for selectivity. Finally, a few compounds with a binding affinity in the mid-micromolar range could be identified. However, none of these compounds showed inhibition in a tritium incorporation assay, probably due to a lack of affinity.

A second SAR study was conducted starting from a benzylic derivative of SAH developed within the first SAR study. The above-mentioned optimized microscale thermophoresis method was applied to screen the inhibitors. The results of the screenings are in very high accordance with the inhibition determined in the tritium incorporation assay, highlighting the potential of this improved microscale thermophoresis method. Further investigations suggested a covalent inhibition of some inhibitors, which could be confirmed by protein mass spectrometry. The most potent inhibitors within this study showed a covalent binding of DNMT2 with one order of magnitude improved affinity compared to SAH. Additionally, the selectivity towards off-target RNA methyltransferase could be improved.

Kurzzusammenfassung

Ausgehend von dem natürlichen Inhibitor SAH wurde eine Strukturwirkungsbeziehungsstudie durchgeführt, um Inhibitoren der DNMT2 zu entdecken. Um zu bestimmen, ob diese Verbindungen an DNMT2 binden wurde *microscale thermophoresis* angewendet. Die Inhibition von DNMT2 durch diese Verbindungen wurde in einem *tritium incorporation assay* bestimmt. Um die Thermodynamik der Bindungen zu untersuchen, wurde *isothermal titration calorimetry* angewendet. Die potentesten Verbindungen waren Derivate von SAH, in denen das zentrale Schwefelatom gegen ein Stickstoffatom ausgetauscht wurde. Zusätzlich wiesen diese Derivate eine Verzweigung am Stickstoffatom mit verschiedenen Alkinresten auf. Die Affinität dieser Verbindungen zu DNMT2 war vergleichbar mit SAH oder Sinefungin, einem Pan-Methyltransferaseinhibitor. Darüber hinaus zeigten diese Verbindungen eine verbesserte Selektivität gegenüber anderen RNA-Methyltransferasen.

Da die *microscale thermophoresis* Methode, welche in der ersten Studie genutzt wurde, gewisse Limitationen aufwies, wurde sie optimiert, um mehr Informationen aus den einzelnen Experimenten zu gewinnen. Durch eine Änderung der Markierungsstrategie von einer Markierung am *His-tag* zu einem fluoreszierenden *tool compound*, der in die Bindetasche von DNMT2 bindet, konnte das Signal-Rausch Verhältnis der Methode erheblich verbessert werden. Darüber hinaus konnte die Übertragbarkeit der Ergebnisse verbessert werden, was ein *screening* der hauseigenen Verbindungen erleichterte. Die Methode lieferte auch semiquantitative Ergebnisse, was die Entwicklung neuer Verbindungen beschleunigte.

Um Inhibitoren ohne ein SAH-Grundgerüst zu entwickeln, wurde ein *virtual screening* für DNMT2 und NSUN6 durchgeführt. Basierend auf diesen Ergebnissen wurden einige Verbindungen kommerziell erworben und mittels *microscale thermophoresis* auf ihre Affinität zu DNMT2 und NSUN6 getestet. Verbindungen, die ein konzentrationsabhängiges Bindeverhalten gegenüber ihrem Zielenzym aufwiesen, wurden an dem jeweils anderen Enzym auf Selektivität kreuzgetestet. Schlussendlich wurden ein paar Verbindungen mit einer Affinität im mittleren mikromolaren Bereich identifiziert. Jedoch konnte für keine dieser Verbindungen eine Inhibition im *tritium incorporation assay* nachgewiesen werden.

Eine zweite Strukturwirkungsbeziehungsstudie wurde ausgehend von einem benzylichen SAH-Derivat, welches in der ersten Studie entwickelt worden war, durchgeführt. Dabei wurde die oben erwähnte optimierte *microscale thermophoresis* Methode angewandt, um die Verbindungen zu untersuchen. Die Ergebnisse dieser Messungen stimmten in hohem Maße mit den Resultaten aus dem später durchgeführten *tritium incorporation assay* überein, was das Potential dieser verbesserten *microscale thermophoresis* Methode hervorhebt. Weitere Untersuchungen legten nahe, dass einige Verbindungen ein kovalentes Bindeverhalten gegenüber DNMT2 aufweisen könnten, was durch

massenspektrometrische Messungen des Proteins bestätigt werden konnte. Die vielversprechendsten Verbindungen innerhalb dieser Studie zeigten ein kovalentes Bindeverhalten gegenüber DNMT2, die Affinität ist im Vergleich zu SAH um eine Größenordnung verbessert worden. Zusätzlich konnte auch die Selektivität gegenüber anderen RNA-Methyltransferasen verbessert werden.

Introduction

RNA-modifications

Thanks to pioneering advances, particularly in detecting RNA modifications,¹⁻³ the field of “epitranscriptomics” attracted widespread interest. Epitranscriptomics describes an emerging field in modern life sciences, which focuses on information that is coded by RNA modifications rather than the four canonical nucleoside bases (Figure 1).^{2,4-6} The sheer variety of different RNA modifications is only surpassed by their potential role in RNA biochemistry. Modifications can alter the structure and stability of RNA. They can affect the interactions of RNA with proteins or regulate gene expression, to mention just a few potential effects of RNA modifications.^{2,7} Since the attempt of a comprehensive description of all RNA modifications and their significance would go far beyond the scope of this thesis, reference should be made to the excellent literature on this topic.⁸⁻¹³ However, a brief overview focusing on some RNA methylations shall be given at this point.

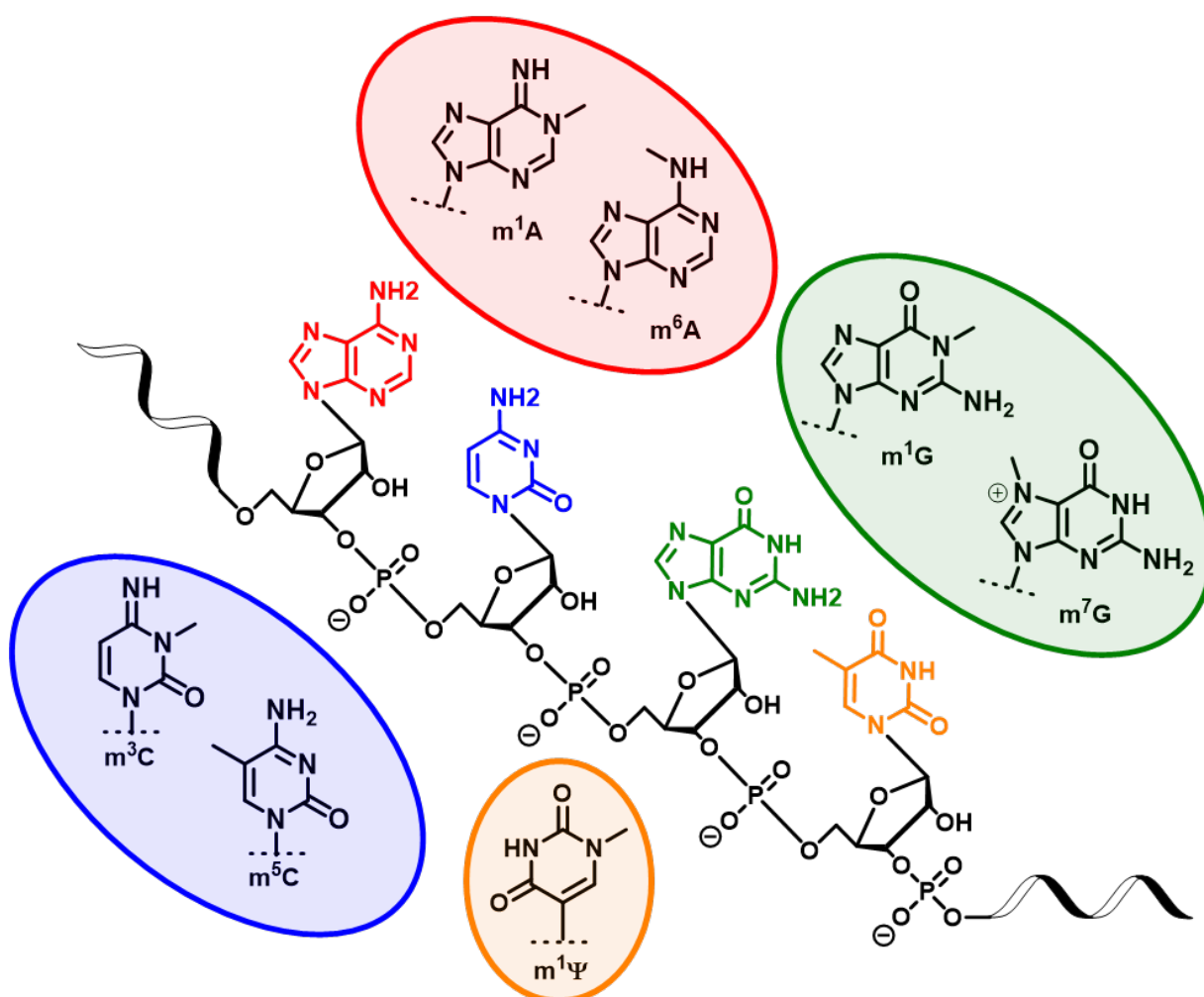


Figure 1: Canonical RNA bases and selection of their modifications. Adenine (red), cytosine (blue), guanine (green), and uracil (orange) are depicted. Highlighted in the respective colors, some methylated modifications of the canonical bases are shown.

Simple methylations may not seem to be the most sophisticated modifications of all the ~ 170 RNA known modifications.^{14–16} Nevertheless, their impact on physiology and pathophysiology should not be underestimated. There are various reports in the literature, highlighting the role of RNA methylations.^{17–21} Figure 1 provides a small overview of selected RNA modifications. Probably some of the most prominent types of RNA methylations are the m⁶A, m⁷G, and m⁵C modifications.

m⁶A modifications

A certain degree of relevance attributed to m⁶A modifications is doubtless due to the fact that this modification is the most common one in mRNA.^{13,22} So-called “writers” are responsible for inserting modifications into RNA. In the case of m⁶A modifications, a three-part multi-protein complex with a molecular weight larger than 1,000 kDa (weights of subcomplexes are 30 kDa, 200 kDa, and 870 kDa, respectively),²³ is responsible for the correct insertion of the modification into the mRNA. The catalytic active part of this multi-protein complex is a methyltransferase called METTL3, which forms a subcomplex with the catalytic inactive METTL14. This subcomplex is depicted in Figure 2.^{7,13}

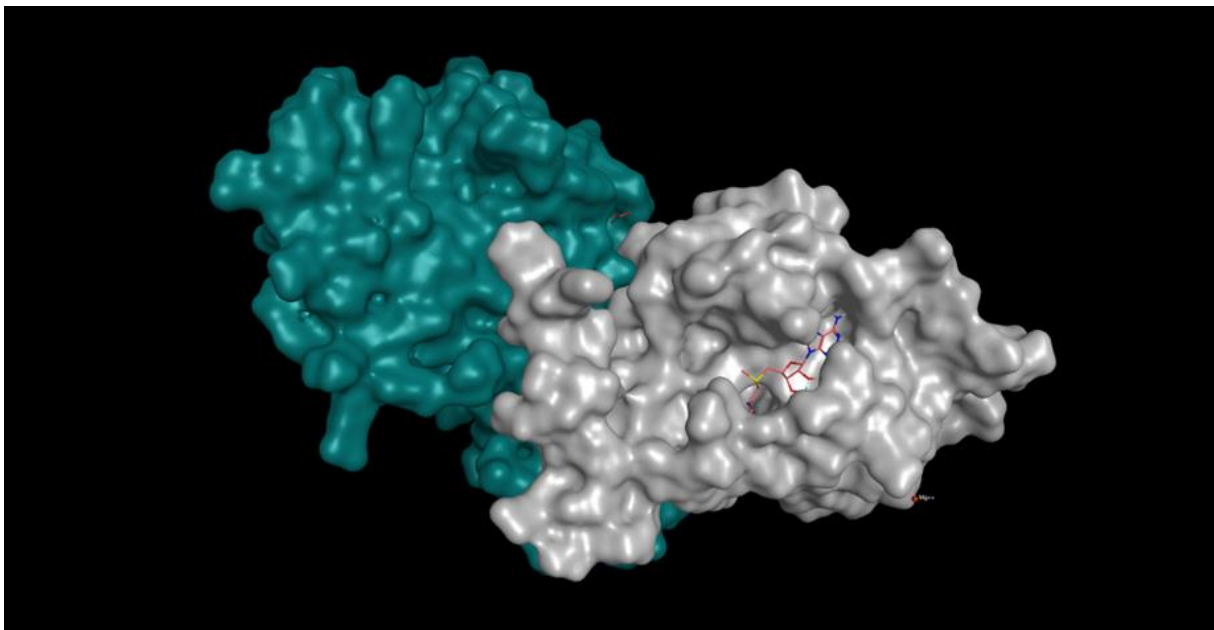


Figure 2: Crystal structure of METTL3 and METTL14 subcomplex (PDB: 5L6E)¹⁵¹. Catalytically active METTL3 (grey), catalytically inactive METTL14 (blue) and methyl group donor SAM (salmon) are depicted. The methyl group donor is bound to the active site of METTL3.

Interestingly, full enzymatic activity can only be achieved if all three subcomplexes work together. Measurements indicated decreasing enzymatic activity of over 90% if only one of the three subcomplexes was removed.²³ The majority of m⁶A modifications in mRNA are linked to conserved DRACH motifs within the mRNA, which are often located in the vicinity of stop codons.^{3,13} While the mere introduction of m⁶A modifications is quite complex, the fate of these modifications is even more sophisticated. It involves “erasers” capable of deleting these modifications, as well as a plethora of “readers” that initiate a multitude of downstream processes in the cell.^{3,13,24} Various studies were conducted to decipher the physiological role of m⁶A modifications and their impact on different

diseases, such as metabolic and neurological disorders or even cancer. The results indicated a significant influence of m⁶A modifications on plenty of diseases, making them potentially worthwhile drug targets in the future.^{3,24}

m⁷G modifications

On average, 0.4% of all guanines show methylation at position N7. These m⁷G modifications are quite conserved in eubacteria and eukaryotes, and even some archaea present this type of modification. Besides in tRNA, this modification was also detected in mRNA, rRNA, miRNA, snRNA, or snoRNA. Moreover, it is involved in constructing the 5' terminal cap structure in eukaryotic mRNA. In tRNA, most of these modifications were found at position 46, where they form a tertiary complex with C13 and G22, which stabilizes the core structure of the tRNA.^{25,26} The "writer" responsible for m⁷G modifications in human tRNA is a complex of METTL1 and WDR4. The catalytical active subunit of the complex is called METTL1. Nevertheless, the catalytic inactive WDR4 is needed to maintain the methylation activity of METTL1. Moreover, METTL1/WDR4 serves as a "writer" for mRNA and miRNA. In rRNA, this function is fulfilled by the WBSR22/Trm112 complex. In contrast to m⁶A modifications, no "readers" or "erasers" have been identified for m⁷G modifications so far.²⁵⁻²⁷ In patients, an R140L missense mutant of WDR4 has been shown to affect the m⁷G levels and has also been linked to the occurrence of primordial dwarfism.²⁸ Furthermore, m⁷G modifications in tRNA seem to promote the progression of lung cancer, hepatocellular carcinoma, and bladder cancer, indicating once more the relevance of RNA modifications for human diseases. The cap structure in eukaryotic mRNA, on the other hand, is crucial for the correct nuclear export, translation, and degradation of mRNA.²⁶

m⁵C modifications

The m⁵C modification has been detected in several types of RNA, such as tRNA, mRNA, mtRNA, or rRNA, and is one of the most eminent RNA modifications. The „writers“ responsible for m⁵C modifications are the members of the NOL1/NOP2/SUN domain (NSUN) family and DNA methyltransferase 2 (DNMT2). The NSUN family consists of seven enzymes from NSUN1 to NSUN7. Some of them, like NSUN1, NSUN2, and NSUN5, are found in an abundance of eukaryotes. The remaining members are limited to higher eukaryotes. In rRNA, the m⁵C modification is inserted by NSUN1 or NSUN5. NSUN2 modifies mRNA, while NSUN3 and NSUN4 are common "writers" for mtRNA. NSUN7 is responsible for m⁵C modifications in enhancer RNA in the nucleus. In tRNAs, NSUN2, NSUN6 as well as DNMT2 function as "writers".²⁹ The physiological role of this modification includes RNA export, as well as translation and tuning of the RNA stability.²⁹⁻³¹ Furthermore, m⁵C modifications are pivotal for cellular and especially neuronal development. Therefore, malfunction of "writers" can lead to severe disorders or diseases. For example, a connection between the occurrence of cardiovascular disease and m⁵C modifications has been suspected, and also the Dubowitz syndrome is reported to be associated with a lack of NSUN2.^{29,32,33} Recent findings even suggest that m⁵C modifications are

involved in cancer metastasis.³⁴ TET2 and ALKBH1 are known to catalyze the oxidation of m⁵C to 5-hydroxymethyl cytosine (5hmC), which alters the properties of the m⁵C modification, making these enzymes “erasers” of m⁵C modifications. The respective “readers” are reported to be ALYREF and YBX1.³⁵

As already stated, the epitranscriptome is involved in countless biological processes, from the early development of cells to the inheritance of information to the next generation. Selective adjustments to the epitranscriptome could therefore offer the possibility of alleviating or even curing diseases and disorders which might otherwise not be druggable. One starting point to make adjustments to the epitranscriptome is the modulation of the “writers” activity. Methyltransferases have been reported to be the active component of many “writer” complexes, so selective inhibition or activation of those enzymes could be very promising.^{8,24,36–40}

RNA-methyltransferases

In 1962 FLEISSNER and BOREK postulated the existence of an enzyme capable of methylating RNA, which they called “RNA-methylase” at that time.⁴¹ Since then, the interest in RNA methyltransferases emerged immensely, culminating in over 16,000 entries for “RNA methyltransferases” in the PubMed library nowadays (February 2023).

Methyltransferases are widely spread in nature and can be found in all three domains of life. Until today over 380 methyltransferases have been classified according to the protein nomenclature and classification list of the International Union of Biochemistry and Molecular Biology (IUBMB).⁴²

Methyltransferases can be categorized according to their substrates to which they transfer the methyl group. Typical substrates for methyltransferases are proteins,^{43–46} DNA,^{47–49} or RNA.^{13,50,51} Most of these enzymes use *S*-adenosyl-L-methionine (SAM) as a cofactor while only a small minority of methyltransferases uses *N*⁵,*N*¹⁰-methylentetrahydrofolate (MTHF) as a donor of the methyl group.^{52,53} One explanation for the considerable predominance of SAM over MTHF as a cofactor in methyltransferases could be the larger gain of free energy released during the conversion from SAM to SAH during the methylation of the substrate compared to MTHF.^{54,55} For a better overview, the SAM-dependent methyltransferases were additionally grouped into classes based on characteristic folding patterns within these methyltransferases. At first, five groups could be identified (class I to class V), but subsequent discoveries led to an extension of up to nine classes (class I to class IX).^{52,56} There is plenty of literature covering the different classes of methyltransferases in detail. Therefore, only the most relevant classes for methylation of RNA are highlighted here.^{52,54,56–60} RNA methyltransferases can be found in classes I, IV, VII, VIII, and IX.

Class I methyltransferases

By far the most frequently occurring one is class I, which members share a common folding pattern called a Rossmann-fold.⁵⁶ It is quite remarkable that the methyltransferases of this class display a high structural similarity, although some of them only share 10% primary sequence similarity.⁵⁷ One of the most conserved motifs in this Rossmann-fold methyltransferases appears to be a glycine-rich loop in the β -turn region, which is crucial for the interaction of the protein with the nucleotide of the SAM substrate.^{56,61} Another conserved motif in these methyltransferases is an acidic residue in the second β -sheet. This acidic residue can form hydrogen bonds to interact with the ribose residue of the substrate.^{56,57} All DNA methyltransferases, most of the RNA methyltransferases, and several protein methyltransferases are class I Rossmann-fold methyltransferases.^{57,62}

Class IV methyltransferases

The SPOUT family or class IV is the second most common, and it is defined by a conserved catalytic domain that forms a trefoil knot structure^{54,63} Beyond this SPOUT knot, the enzymes of this class show a plethora of structural differences, leading to the conclusion that only the core SPOUT knot is relevant for cofactor binding and the catalysis of the methylation.⁵⁴ This class encloses mainly RNA methyltransferases and has been believed for a long time to be limited to RNA methyltransferases until Sfm1, a protein arginine methyltransferase with a typical SPOUT knot, could be crystallized.^{63,64}

Class VII methyltransferase

Some methyltransferases show a cysteine-rich motif, which catalyzes a radical mechanism in order to transfer the methyl group from SAM to the substrate. Especially the Cfr/RlmN family enzymes rely on this sort of mechanism to transfer methyl groups from SAM to different RNAs. These enzymes have been grouped in class VII.⁶⁵⁻⁶⁹

Class VIII methyltransferases

Structural elucidation of TrmO/YaeB indicated that this RNA methyltransferase could not be sorted into one of the existing classes. Therefore, this was the first member of class VIII since it showed a single-sheeted- β -barrel structure, which had not been known from other methyltransferases.⁷⁰

Class IX methyltransferases

The enzymes of the TYW3 family present folding patterns and an (S/T)xSSCxGR motif that is unique for methyltransferases, making it the first representants of class IX, the latest class of SAM-dependent methyltransferases so far.⁷¹

DNA methyltransferase 2 (DNMT2)

For a long time, DNA methyltransferase 2 (DNMT2) was surrounded by mysteries. The literature on DNMT2 invokes the word “enigma” repeatedly.⁷²⁻⁷⁴ Due to structural similarities, it was categorized into the family of DNA methyltransferases together with DNMT1, DNMT3a, and DNMT3b. Their typical

Rossmann-fold identifies them as class I methyltransferases. Furthermore, they were known to catalyze m^5C modifications.⁷⁵ But despite these structural similarities, plenty of questions concerning DNMT2 remained unsolved. For instance, neither a definite substrate nor a specific physiological role could be identified^{72,76–78} Although a particular binding of DNMT2 towards DNA could be detected, the resulting *in vitro* methylation activity did not meet the expectations. So, research for a more suitable substrate continued until in 2006 a report by GOLL *et al.* emerged in general interest. According to their findings, DNMT2 was rather an RNA methyltransferase than a DNA methyltransferase, and its substrate was stated to be a tRNA coding for aspartic acid.^{76,79,80} These results led research on DNMT2 in a different direction, and soon other tRNAs were identified as substrates of DNMT2, confirming its role as an RNA methyltransferase.⁸¹

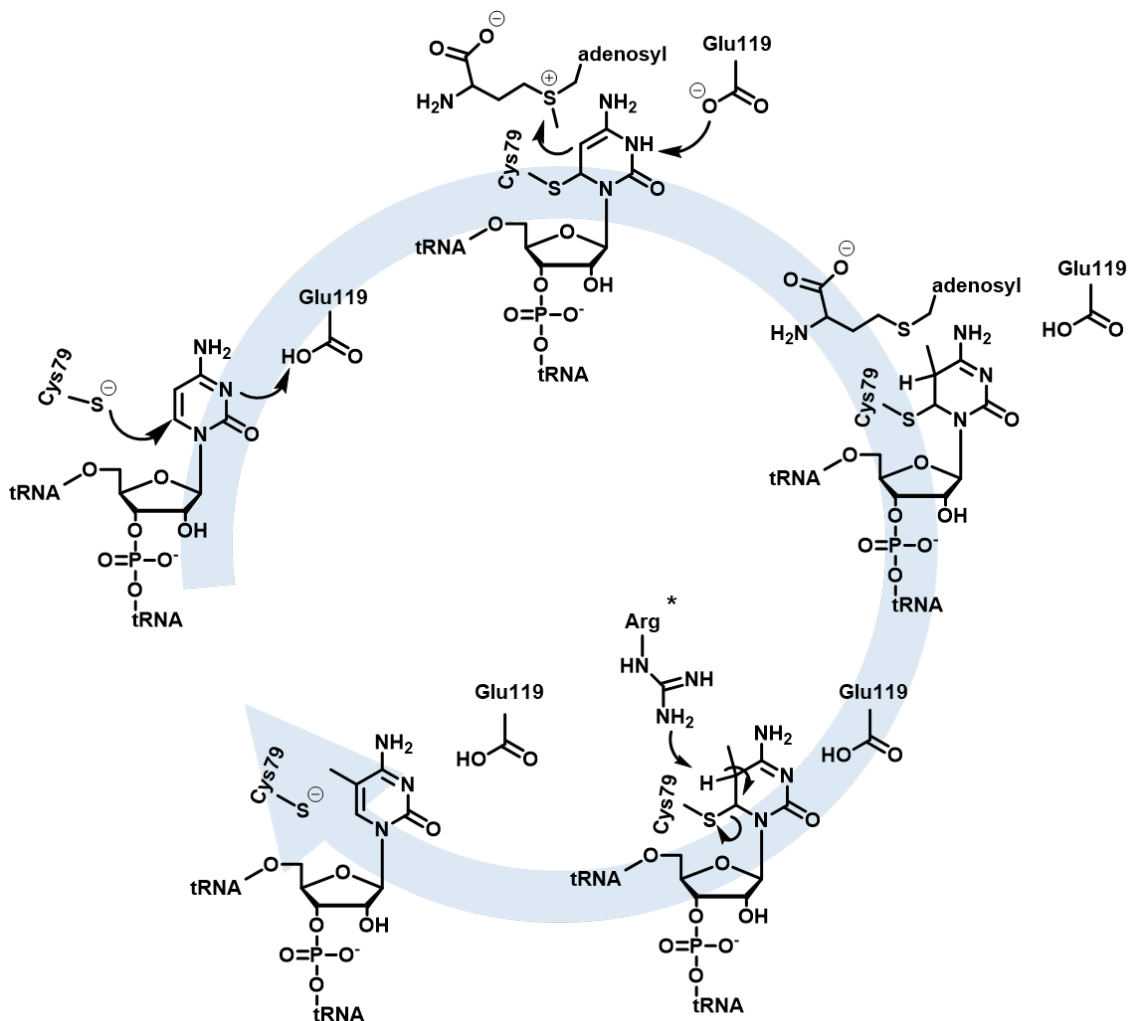


Figure 3: Mechanism of action for DNMT2. A nucleophilic attack of DNMT2 accompanied by the protonation of the substrate by DNMT2 leads to a covalent substrate enzyme complex, which is activated enough to attack the methyl group donor SAM. Afterwards, the substrate is deprotonated by a basic amino acid (*probably an arginine) of DNMT2, which enables resolving the substrate enzyme complex.

Interestingly, the catalytic mechanism used by DNMT2 is not comparable to those of other RNA methyltransferases but rather to those of DNA methyltransferases. Alanine exchange mutants of

DNMT2 revealed that Cys79, Glu119, Arg160, and Arg162 are pivotal for the catalytic mechanism, as the respective alanine mutants did not result in any RNA methylation. These findings were in high accordance with what was known about the catalytic mechanism of DNA methyltransferases.⁸² The main problem with the methylation of cytosine is the electron deficiency of the heterocycle. Even though SAM is an excellent donor, it is insufficient to ensure the transfer of the methyl group to the C5 of cytosine. Therefore, DNA methyltransferases perform a Michael addition to accomplish the reaction. In Figure 3, the catalytic mechanism of DNMT2 is shown. DNMT2 uses the Cys79, which is embedded in a conserved amino acid sequence (motif IV PCQ), for a nucleophilic attack at position 6 of the cytosine. The nucleophilic attack is accompanied by the protonation of the nitrogen at position 3 of the heterocycle, by Glu119. This glutamic acid is also located in a conserved amino acid sequence (motif IV ENV). In consequence of this covalent protein-RNA complex the carbon in position 5 of the cytosine is activated enough to attack the methyl group of SAM. In order to rebuilt aromaticity, the C5 position is deprotonated and Cys79 is eliminated from the heterocycle, which resolved the protein-RNA complex. The above-mentioned arginine residues Arg160 and Arg162 are also part of a conserved amino acid sequence (motif VIII RXR). Besides the fact that they are pivotal for the catalytic mechanism, their exact role remains elusive. It has been discussed that they are involved in the positioning of Glu119 and the cytosine base, or that they are involved in the deprotonation of the C5 carbon.^{82–85}

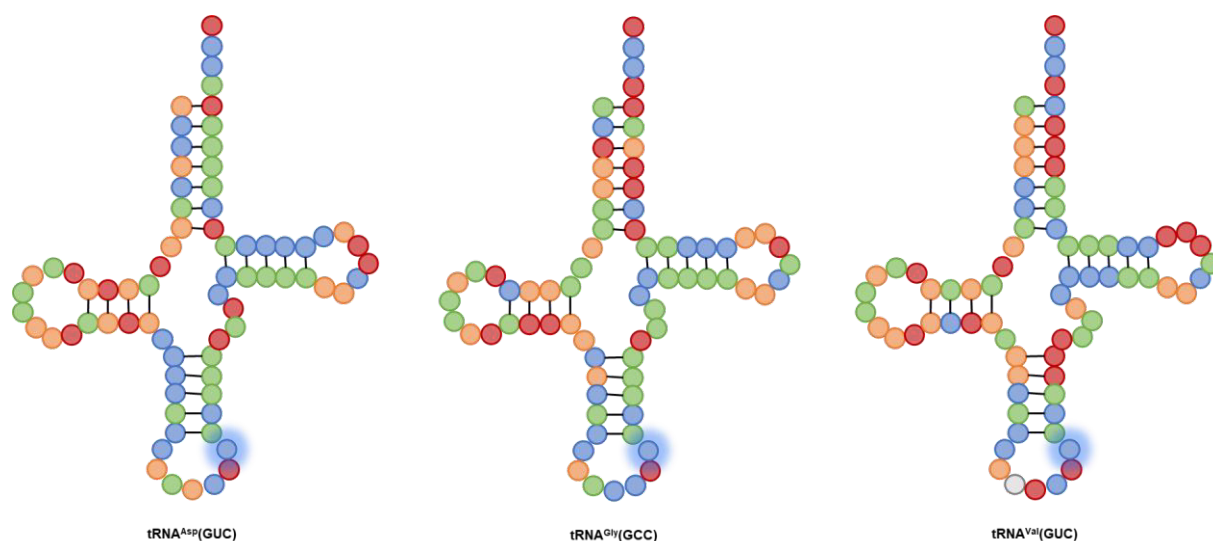


Figure 4: tRNA substrates of DNMT2. (A) tRNA^{Asp}(GUC) (B) tRNA^{Gly}(GCC) (C) tRNA^{Val}(GUC)⁸⁶; color coding of the bases: adenine (red), cytosine (blue), guanine (green), and uracil (orange) inosine (light grey). The cytosine in position 38, which is modified, is highlighted.

A recent study has elucidated the recognition of the RNA substrates by DNMT2 in more detail. In Figure 4, the base sequences of the respective substrates are depicted. It has been demonstrated that DNMT2 demands high requirements for tRNAs to bind. First, the tRNA must be folded properly. Generated mutants that prevented native folding were found to be not methylated by DNMT2. Second, DNMT2 recognizes a seven-nucleoside long pattern C³²U³³(G/I)³⁴N³⁵(C/U)³⁶A³⁷C³⁸ that is crucial for the

methylation of cytidine at position 38. Within this pattern, only position 35, where any nucleoside can be inserted, is not conserved. Positions 34 and 36 are more conserved than position 35. They tolerate only guanosine or inosine and cytidine or uridine, respectively. Any nucleoside exchange at the remaining positions of this pattern will prevent recognition of the substrate. These findings limit the possible substrates of DNMT2 in humans to tRNA^{Asp}(GUC), tRNA^{Gly}(GCC), and probably tRNA^{Val}(AAC). Interestingly, bisulfite sequencing suggested GAC as a triplet, which does not code for valine. So, it was proposed that the adenosine in position 34 might have been modified to inosine and was therefore detected as guanosine by bisulfite sequencing.⁸⁶

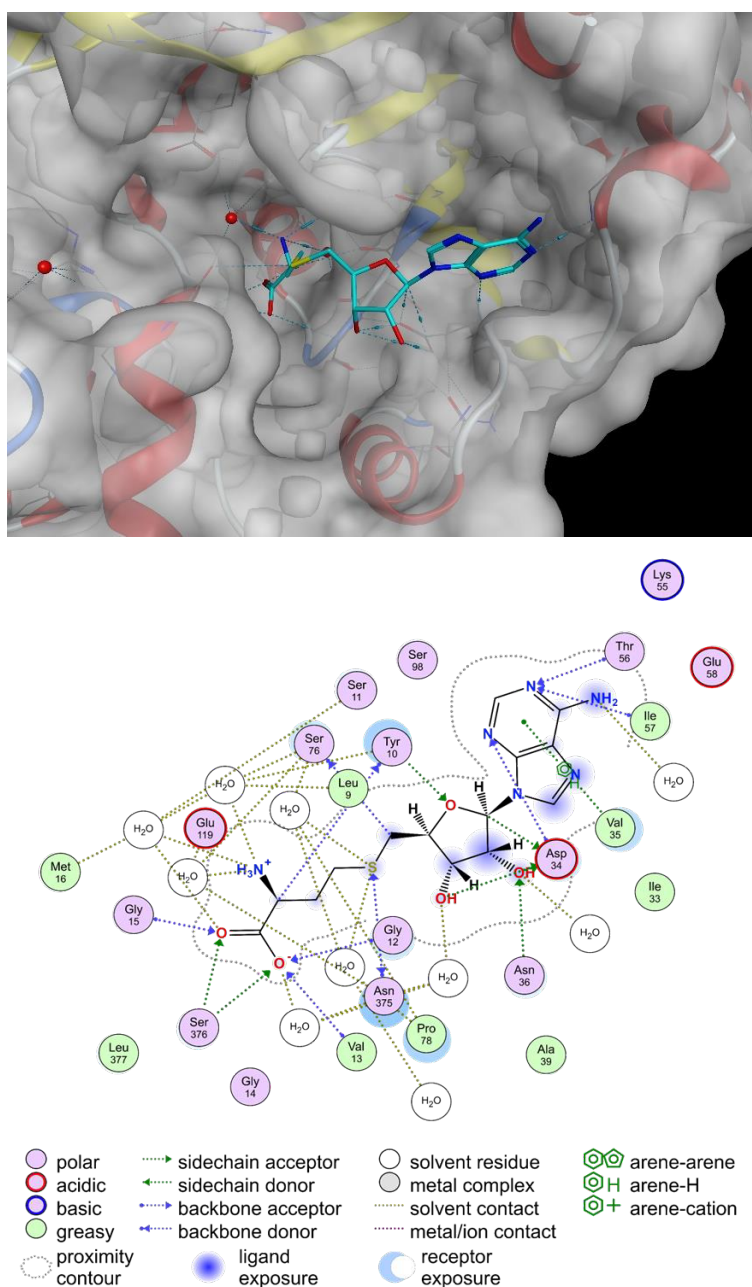


Figure 5: Interaction of SAH with DNMT2. The top figure shows the binding pose of SAH, which is formed during the methylation, in the active site of DNMT2. The bottom figure illustrates this interaction of SAH and DNMT2 in more detail.

A crystal structure of DNMT2 in complex with SAH that was solved by DONG *et al.* in 2001 (PDB: 1G55) had sufficient resolution to estimate potential interactions between DNMT2 and the methyl group donor. Since SAH is created from SAM during the transfer of the methyl group to the tRNA, the interactions found for SAH should be very similar for SAM. Figure 5 gives an overview of the amino acids in DNMT2 that are involved in the binding of SAH.

The N1 of the adenine moiety interacts with the backbones of Thr56 and Ile57, while the N3 forms an interaction with the backbone of Asp34. Furthermore, the sidechain of Val35 forms an interaction with the arene. The ribose moiety forms hydrophilic interaction with the sidechains of Tyr10 and Asn36. In the homocysteine moiety, the carboxyl group interacts with Ser376 and the backbones of Gly12, Val13, and Gly15. The primary amino group that is probably protonated forms an ionic interaction with Glu119. Also, an interaction of the sulfur with the backbone of Asn375 seems plausible.⁷⁶ All these findings revolutionized the knowledge of DNMT2 and paved the way for a better understanding of the physiological role of DNMT2.

The m⁵C modification at position 38 of different tRNAs which is inserted by DNMT2, has been shown to positively affect the stability of these tRNAs. A study could prove that tRNA cleavage into fragments by angiogenin is prevented in the presence of m⁵C modifications catalyzed by DNMT2. This indicates that DNMT2 somehow interferes with the regulation of the protein translation process. Moreover, the m⁵C modification facilitates the recognition of tRNA^{Asp} by aspartyl-tRNA synthetase, which further supports the assumption that DNMT2 could play an important role in regulating protein translation, especially of aspartic acid-rich proteins. Since angiogenin is a stress-induced endonuclease, DNMT2 might also be a part of the cellular stress response. This also matches the finding that cultivation of *S. pombe* in a minimum medium leads to a noteworthy increase in tRNA^{Asp} methylation by Pmt1, a DNMT2 homolog, compared to cultivation in a complete medium. Likewise, overexpression of DNMT2 increased the resistance of *Drosophila* flies against oxidative stress factors and prolonged their life span.^{81,84,87-90} A recent study was able to show that DNMT2 deletion in mice suppresses the transmission of high-fat-diet-induced metabolic disorders to the offspring, indicating that m⁵C modifications have a significant influence on the biological properties of sncRNA by altering their structure. It could mean that DNMT2 is directly connected to the inheritance process and could be a potential target to overcome hereditary obesity.⁴⁰ It has been speculated that DNMT2 might be linked to different types of cancer, as a considerable number of mutants were found to lack activity, which might benefit the tumors and implies an “anti-oncogene” potential of DNMT2. Especially the position Gly155 has been found to be a hotspot for mutations in somatic cancers.⁹¹

Despite all these remarkable discoveries on DNMT2 that have been achieved in the last decades, due to diligent research, our knowledge of DNMT2 is still not complete. It will require more research to complete our understanding of this so-called “enigmatic” enzyme.

NOP2/Sun RNA methyltransferase 6 (NSUN6)

Besides DNMT2, the other “writers” responsible for m⁵C modifications in RNA belong to the NSUN family. Similar to DNMT2, their structure reveals a Rossmann-fold, which identifies them as class I methyltransferases.⁷⁵ Although all seven members of the family recognize various RNAs as substrates, only NSUN2, NSUN6, and to a small extent also, NSUN3 insert m⁵C modifications into tRNA.²⁹ Surprisingly, when compared to DNMT2, the catalytic mechanism of the NSUNs is quite different. Instead of one catalytic cysteine as in DNMT2, the NSUN enzymes use two different cysteines to catalyze the methylation of the C5 position in cytosine.^{92,93}

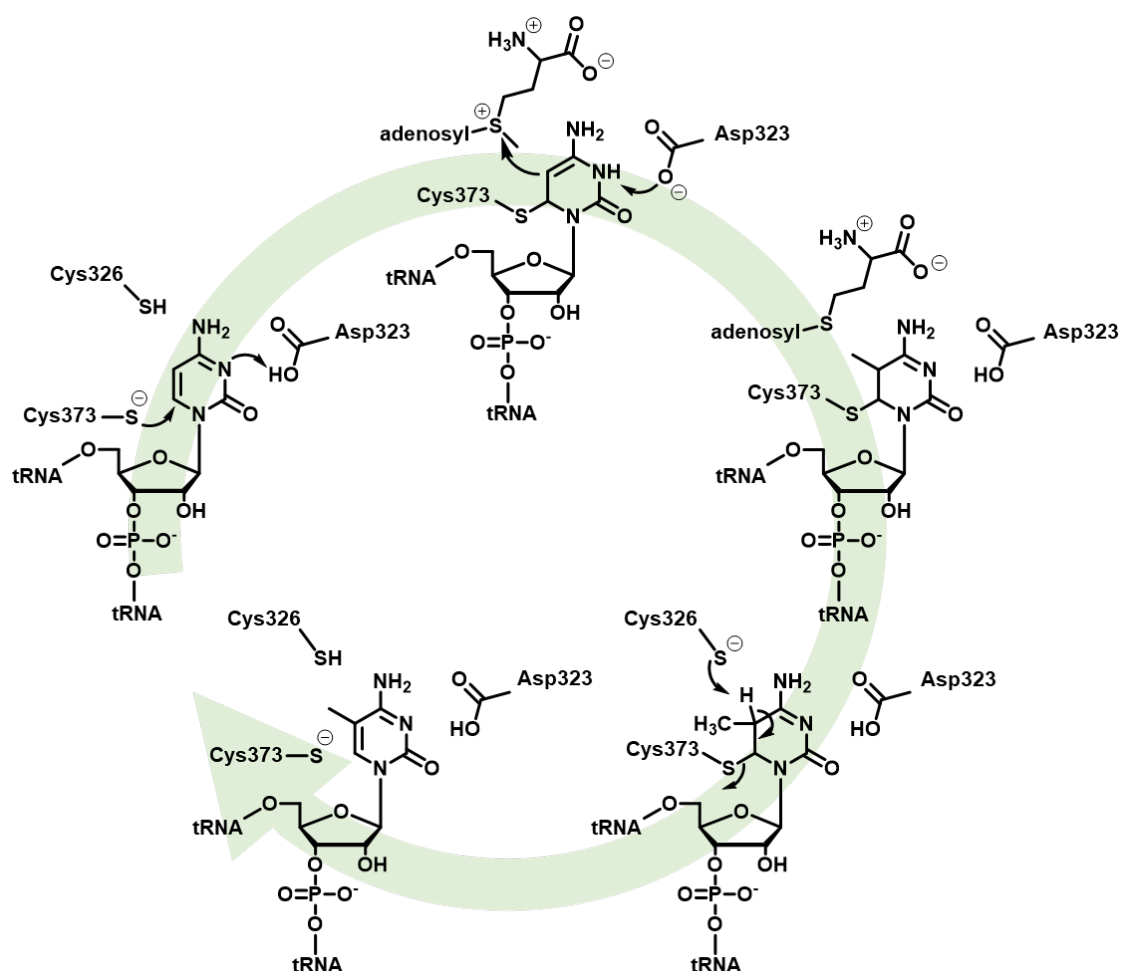


Figure 6: Mechanism of action for NSUN6. A nucleophilic attack of NSUN6 leads to a covalent substrate enzyme complex. This step is accompanied by protonation of the substrate by NSUN6. The covalent complex is able to attack the methyl group donor SAM. In contrast to the mechanism of DNA methyltransferases, the deprotonation of the substrate, which enables resolving the covalent substrate enzyme complex, is catalyzed by a second cysteine instead of a basic amino acid.

Exemplary for the NSUN family, the mechanism for NSUN6 is shown in detail (Figure 6). In a first step, the conserved Cys373 performs a nucleophilic attack on the carbon at position 6 within the cytosine.

This attack is facilitated by the protonation of the nitrogen in position 3 by Asp323. Similar to DNMT2, some conserved motifs, namely motif IV and motif VI, are involved in the mechanisms of the NSUN family. The Cys373 is embedded in a characteristic amino acid sequence called motif VI, while the Asp323 is part of motif IV. The now following inverse protonation of the Asp323 by the nitrogen allows the carbon in position 5 to attack the methyl group donor SAM. In the next step, Cys326, which together with Asp323 is part of motif IV, deprotonates the carbon in position 5, which enables the elimination of the Cys373 under restoration of the aromatic system. It could nicely be shown in several studies that motif IV is responsible for the formation of a covalent protein-RNA complex, while motif VI is crucial for the unraveling of the covalent complex. The respective roles of both cysteines could be shown by mutation studies, in which mutants of Cys326 were unable to release covalently bound RNA, while mutations of the Cys373 led to a complete loss of methyltransferase activity.^{93–96} Also, the spatial arrangement of the respective amino acids, which could be derived from the crystal structures of NSUN6 obtained by Liu *et al.* in 2017, makes this mechanism seem plausible.⁹⁶

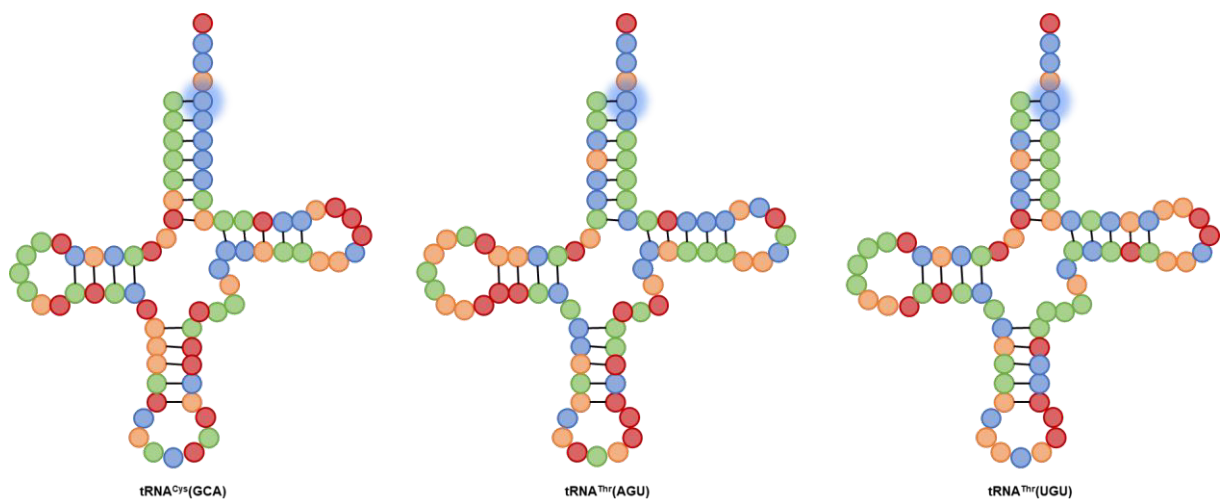


Figure 7: tRNA substrates of NSUN6. (A) tRNA^{Cys}(GCA), (B) tRNA^{Thr}(AGU), tRNA^{Thr}(UGU). Color coding of the bases: adenine (red), cytosine (blue), guanine (green), and uracil (orange); the cytosine in position 72, which is modified, is highlighted.

The search for substrates revealed that the tRNA^{Cys} and tRNA^{Thr} are the primary substrates of NSUN6. Figure 7 displays the base sequences of the respective substrates. All tRNAs are modified at a cytosine in position 72 by the methyltransferase. The recently reported crystal structures of NSUN6 apoprotein (PDB:5WWQ) and NSUN6 in complex with tRNA (PDB:5WWT), SAM/tRNA (PDB:5WWS), and tRNA/Sinefungin (PDB:5WWR) allow us, to further understand the RNA recognition and binding behavior of NSUN6. Interestingly, the before-mentioned cytosine72 is usually paired with the guanine1 of the acceptor region double strand. In complex with NSUN6, this base pairing is resolved, which can be assumed to be energetically quite unfavorable. Furthermore, the base pairing in positions 2 and 71 of the acceptor loop is disrupted by NSUN6. The so-called PUA domain (~ 90 amino acids) of NSUN6 recognizes the D-stem region of tRNA by electrostatic interactions. Moreover, it binds the last three

bases CCA of the tRNA by extensive hydrogen bonding. The catalytic core of the methyltransferase domain (~ 250 amino acids), on the other hand, recognizes the unpaired cytosine72 and the bases in the closest vicinity. Another relevant domain is the RNA-recognition motif (RRM) (~ 60 amino acids), which helps to bind and locate the bases cytosine72 and uracil73 in the active site of NSUN6. The uracil base in position 73 seems to play a critical role as a discriminator of tRNA recognition by the enzyme. Altogether, this sophisticated recognition and binding mechanism of NSUN6 would limit the suitable substrates to tRNA^{Cys} and tRNA^{Thr}₉₅₋₉₇.

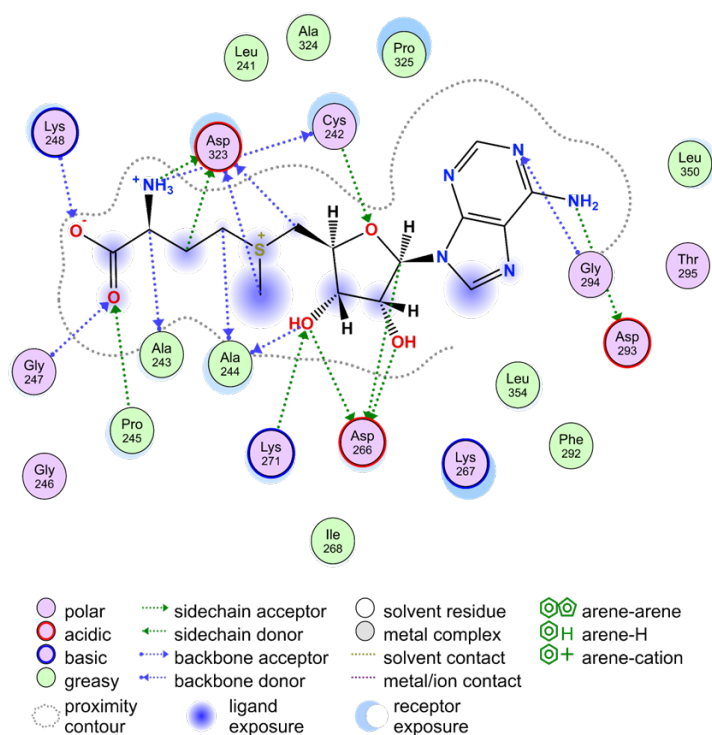
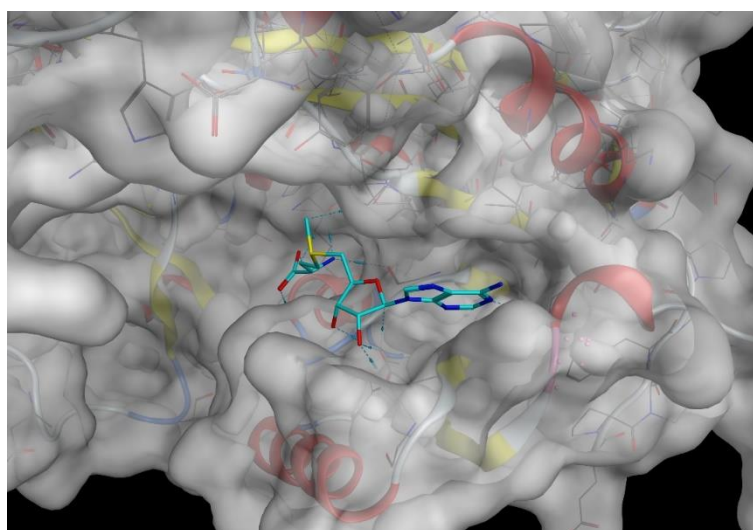


Figure 8: Interaction of SAM with NSUN6. The top figure shows the binding pose of the methyl group donor SAM in the active site of NSUN6. The bottom figure illustrates this interaction of SAM and NSUN6 in more detail.

The crystal structures also helped to elucidate the recognition of the methyl group donor SAM by NSUN6 and the interactions in the active site (Figure 8). Four conserved amino acids, Leu241, Cys242, Pro325, and Leu 354, form a hydrophobic pocket that the adenine moiety of SAM fits into, while the primary amino group interacts with the side chain of Asp293. The alcohol groups of the ribose moiety interact with the side chains of Asp266 and Lys271 and the backbone of Ala244. The oxygen within the furanose ring can interact with the side chain of Cys242. The backbone of Cys242 can interact with the amino group of the methionine moiety, which itself can interact with the side chain of Asp323. Additionally, the carboxyl group of SAM interacts with the backbones of Gly247, Lys248, and the side chain of Pro245. The most conserved amino acids in the active side are Lys248, Asp 323, Cys326, and Cys373, indicating their significance during the catalysis.⁹⁶

There are many reports about the potential physiological and pathophysiological roles of NSUN6 in the literature. In patients with pancreatic cancer, high expression levels of NSUN6 seemed to suppress tumor growth by interfering with the cell proliferation. This matches with the findings that overexpression of NSUN6 could suppress cell growth in liver cancer since, in most liver hepatocellular carcinomas, NSUN6 was found to be downregulated.^{98,99} In complex with the adapter protein LLGL2 and lncRNA MAYA, NSUN6 was detected to methylate the MST1 kinase, which facilitated bone metastasis in breast cancer.¹⁰⁰ Just recently, decreased expression levels of NSUN6 were reported in patients with Alzheimer's disease and in patients with a history of traumatic brain injuries.¹⁰¹ The physiological role was also investigated in knock-out mice. The results suggested that NSUN6 was not necessary for the development or the homeostasis of the animals, leaving the possibility that NSUN6 is only required under special stress conditions.¹⁰² Unfortunately, we do not understand the comprehensive role of NSUN6 at this moment. Therefore, further research is required to increase our knowledge about this mysterious but also promising methyltransferase.

Methyltransferases from a medicinal chemistry perspective

Methyltransferases are quite rare drug targets in clinical use. The first generation of methyltransferase inhibitors consists of anti-metabolites like 5-azacytidine and decitabine (Figure 9). They were approved for myelodysplastic syndrome, chronic myelomonocytic leukemia, and acute myeloid leukemia. Their main targets are DNA methyltransferases. To exert their effect, the antimetabolites must be incorporated into the DNA, where they act like a trap for the methyltransferase. Although they show dose-dependent effects, selectivity issues, and adverse side effects are not to be dismissed. Besides inhibition of DNA methyltransferases, it was reported that 5-azacytidine was capable of inhibiting the RNA methyltransferase DNMT2, whereas decitabine did not display any inhibition of DNMT2. Based on the structure of these drugs, these results are not surprising. While decitabine has a DNA-like deoxyribose moiety, 5-azacytidine contains a ribose moiety, which can typically be found in RNA.

Therefore, 5-azacytidine can easily be inserted in RNA. This certainly underlines the selectivity problems these inhibitors are facing.^{103,104}

GSK received widespread interest for its noncovalent selective DNMT1 inhibitor (GSK3685032). Choosing a noncovalent inhibition might help with selectivity and adverse side effects, but it also comes with the risk of weak inhibitory effects. Luckily, GSK3685032 showed increased potency and tolerability compared to decitabine *in vivo*. In a recent study, PAPPALARDI and coworkers could show that very selective inhibition of DNMT1 over a broad panel of methyltransferases and even over DNMT3a and DNMT3b is possible. They started with high-throughput screening of 1.8 million compounds. Further optimization led to a compound with an IC₅₀ value in the nanomolar range towards DNMT1 but no noteworthy inhibition towards DNMT3a or DNMT3b. This chemically stable compound presented reversible inhibition of DNMT1, which suggests noncovalent binding of the enzyme. However, they did not stop optimizing their research, and by improving potency, solubility, and lipophilicity, they synthesized GSK3685032 (Figure 9). This inhibitor has an IC₅₀ value in the two-digit nanomolar range towards DNMT1, while the inhibition of the DNMT3 enzymes is more than 2500-fold weaker. Also, when tested against 34 methyltransferases and over 350 kinases, no off-target inhibition stronger than 10 µM was detectable. Crystal structures in complex with DNMT1 and DNA (PDB: 6X9J) revealed that GSK3685032 binds to an enzyme domain that is involved in DNA binding, which might explain the selectivity over DNMT3a and DNMT3b. Furthermore, GSK3685032 seems to bind DNMT1, preferably in the presence of hemimethylated DNA. Quite a unique finding that might benefit the selectivity of this compound. Subsequent *in vivo* testing in leukemia models showed promising results. Hypomethylation could be achieved, and anti-tumor effects were measurable. Despite all these promising results, GSK3685032 will have to prove its value in clinical trials yet to come.^{104,105}

The clinical outlook for selective RNA methyltransferase inhibitors is also relatively sparse but nevertheless hopeful. Only one potential drug, namely STC-15 from Storm Therapeutics (structure not available, but the structure of the precursor STM2457 is depicted in Figure 9) has entered phase I of clinical trials for the treatment of solid tumors (ClinicalTrials.gov Identifier: NCT05584111). The target of STC-15 and STM2457 is the earlier-mentioned RNA methyltransferase METTL3. In a recent study by YANKOVA *et al.*, the discovery process of STM2457 has been reported. In brief, a high-throughput screening with 250,000 compounds resulted in only two hits with a non-SAM-like scaffold. Starting from one of these compounds with an affinity in the middle two-digit micromolar range YANKOVA and coworkers ended up with STM2457, which has an affinity towards METTL3 in the low nanomolar range. The obtained crystal structure (PDB: 7O2I) indicated that STM2457 binds to the SAM binding site, even though the scaffold is non-SAM-like. However, STM2457 does not reach into the binding pocket, which

is usually addressed by the methionine moiety of SAM. This finding, taken together with the structural dissimilarity to SAM, is assumed to be the reason for the enormous selectivity of this inhibitor. STM2457 was tested against 45 methyltransferases and over 400 kinases, and yet no significant off-target inhibition could be detected. A distinct decrease of m⁶A modifications, which was observed *in cellulo*, was followed up by *in vivo* testing. The results confirmed the previous findings, as STM2457 showed therapeutic effects against myeloid leukemia in mouse models.¹⁰⁶

In 2020 the American admission authority FDA approved a first-in-class methyltransferase inhibitor targeting the histone-lysine-*N*-methyltransferase EZH2. This inhibitor, named tazemethostat (Tazverik™), formerly known as EPZ643 (figure 9) is indicated for epithelioid sarcoma. Also, in this case, the discovery started with a high-throughput screening, and after several optimizations, KNUTSON *et al.* ended up with EPZ643. This inhibitor competes with the methyl group donor SAM and has an IC₅₀ value in the one-digit nanomolar range. The selectivity over EZH1 is 35-fold and even 4500-fold over 14 other histone methyltransferases.^{107–109}

In summary, the current state in the development of methyltransferase inhibitors might be comparable to the early phase of kinase inhibitors decades ago. It was assumed that kinases were poor drug targets due to two major obstacles: First, the high intracellular concentration of ATP, which would compete with potential inhibitors. Second, a plethora of enzymes all sharing the same substrate, which would make selectivity hard to archive. And yet, after years of diligent research, there are 72 FDA-approved kinase inhibitors available.^{110,111}

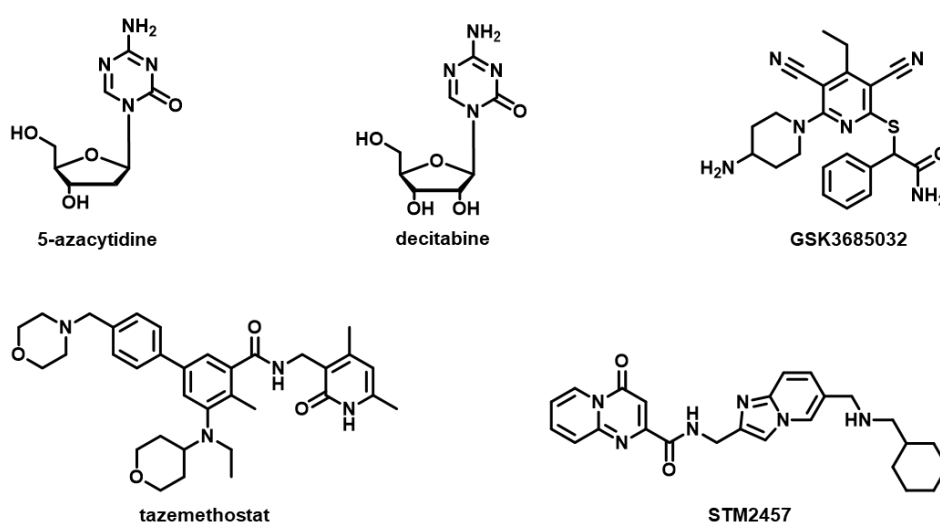


Figure 9: Methyltransferase inhibitors. The figure shows the structures of the antimetabolites 5-azacytidine and decitabine, which are used to inhibit DNA methyltransferases. GSK3685032, a potential DNMT1 inhibitor, tazemethostat an approved EZH2 inhibitor, and STM2457, which was developed to inhibit METTL3.

So far, more than 200 human methyltransferases have been discovered, and as mentioned above, most of these methyltransferases use SAM as a methyl group donor, which means selectivity will be

challenging.¹¹² One solution to overcome this issue could be to address not only the recognition side of SAM but also protein domains that interact with the second substrate, the methyl group acceptor. Therefore, novel inhibitors might need to be deviated from a SAM-like scaffold more and more. GSK and Storm Therapeutics chose this path with GSK3685032 and STM2457, and the results proved them right. Leaving the SAM scaffold behind and reaching out into the binding site of the substrate DNA or RNA was quite successful.

Right after ATP, SAM is the second most common enzyme substrate, so inhibitors will have to face massive competition for the binding site of the substrate.^{55,113} Also, in this case leaving the binding site of SAM and rather targeting the methyl group acceptors' binding site could be promising. Another approach would be the covalent inhibition of methyltransferases. For example, systematic investigations in the 1960s and 1970s revealed that 5-fluorouracil binds the MTHF-dependent methyltransferase thymidylate synthase covalently.^{114–117} Although the history of covalent inhibitors is quite old, the general interest in medicinal chemistry remained limited. But in recent years, the interest emerged tremendously, which is also displayed in literature.^{118–122} β -lactam antibiotics^{123,124} proton pump inhibitors^{125–128} and acetylsalicylic acid¹²⁹ are well-known covalent inhibitors. However, they were not intentionally designed to react covalently.¹²² It is fair to say that their discovery was more or less driven by serendipity.¹²² In recent years, a paradigm shift can be observed as various drugs that utilize covalent mechanisms of action have been developed on purpose. These examples disprove the long-predominant fear that covalent inhibition is accompanied by unmanageable consequences, such as lack of selectivity, adverse side effects, hepatotoxicity, *et cetera*.¹²² Nevertheless, it should be pointed out that reactivity and selectivity of these drugs require excellent fine-tuning, in order to achieve the best therapeutic outcome, without severe side effects caused by promiscuous binding.

To summarize, it can be said that further interplay of rational drug design based on novel and improved crystal structures, high-throughput- and fragment-based screenings, as well as computer-aided screening approaches, might pave the road for potent and selective methyltransferase inhibitors. Although targeting methyltransferases might still be in its infancy, this enzyme class will hopefully become a valid starting point for the selective manipulation of the epigenome and epitranscriptome. This approach could help to alleviate or cure diseases that are not treatable today or improve existing treatments that are limited today.

Biophysical methods in medicinal chemistry

The examples above show that screenings of massive compound libraries via fragment-based or high-throughput screenings can be very promising. Compiling such a library evokes a great deal of effort. However, researchers also need powerful methods capable of discriminating auspicious from poor compounds. Given the fact that these libraries contain up to millions of compounds, the required

methods need to be reliable yet little time- and resource-consuming. Therefore, biophysical methods attract more and more interest. The demands on these methods are quite high given the fact that they have to detect an interaction of a small compound with a total mass in the three-digit Da area towards a biomolecule that can easily exceed the mass of the compound in two orders of magnitude. The following Table 1 is excerpted and adapted from a review by RENAUD *et al.*, which gives an excellent overview of currently used biophysical methods in medicinal chemistry.¹³⁰

Table 1: Overview of biophysical methods frequently applied in medicinal chemistry. The table is adapted from a review by Renaud.¹³⁰ Listed are some of the most frequently used biophysical methods in medicinal chemistry, the affinity range they cover, and the possible throughput of the methods per day.

Method	Affinity range	Throughput per day
NMR	100 nM to 10 mM	100
SPR (immobilized protein)	1 nM to 500 μ M	100
SPR (immobilized compound library)	Up to 500 μ M	10,000
DSF	1 nM to 100 μ M	1,000
ITC	1 nM to 100 μ M	10
MST	1 pM to 1 mM	100
SAXS	up to 30 μ M	100
X-ray crystallography	Up to 1 M	100

Unfortunately, there is no method that is generally the best. All biophysical methods have their advantages but also their limitations. Some methods are more suitable to handle large numbers of compounds, but they deliver only a few details on the binding event. Other methods are limited in the number of compounds that can be screened. However, the results obtained from such a method can hold extensive information on the ligand-protein interaction. In some cases, the resources can limit the method. NMR or x-ray crystallization need very pure protein, which can be quite a problem, but they allow deep insight into the ligand-protein interaction. Likewise, ITC is way too resource-consuming to be used as a primary screening method, but it can deliver quite comprehensive results on ligand-protein interactions. The most suitable biophysical methods for extensive high-throughput screenings are considered to be thermal shift assays. However, the information gained in most cases is not as profound as with other methods. So, the methods have to be chosen very carefully according to the purpose. Furthermore, a thoughtful combination of different methods can increase the outcome of these methods tremendously.^{130–133}

Differential Scanning fluorimetry (DSF)

A very common thermal shift method is differential scanning fluorimetry (DSF), where the unfolding of a protein over a temperature rampage is observed. Usually, hydrophobic amino acids reach into the core of a protein, while hydrophilic amino acids are on the surface of the protein. As a consequence of temperature-induced unfolding, the hydrophobic amino acids reach the surface and become solvent exposed. A fluorometric readout of this process can be enabled by a fluorescent dye, like sypro orange, that binds to hydrophobic patches of the protein, which become solvent exposed upon unfolding. In an aqueous solution, the fluorescence of this dye is quenched, but in the hydrophobic environment of the hydrophobic amino acids, the fluorescence increases. This allows a fast-tracking of the temperature-induced unfolding process (Figure 10).^{133–136} An even more sophisticated method is nanoDSF. This method utilizes the fact that the fluorescence of tryptophan is strongly depending on its environment. During the unfolding process, the surrounding of the tryptophans within the protein is changed and which will alter the detected fluorescence.¹³⁷

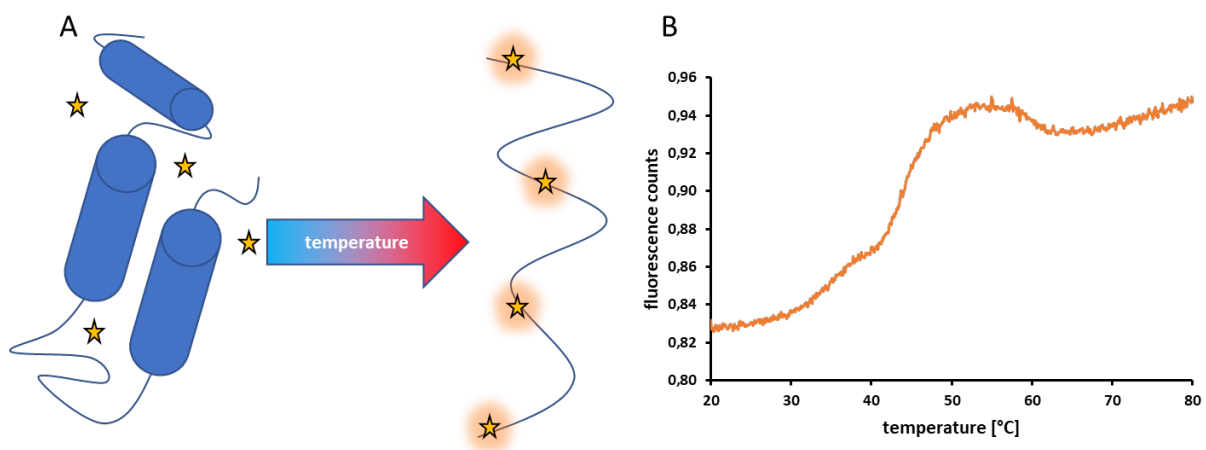


Figure 10: Differential scanning fluorimetry. A) Schematic scheme of the measurement procedure. Properly folded protein is not interacting with the fluorescent dye. Increased temperature leads to the unfolding of the protein, which allows interactions of the proteins' hydrophobic amino acids and the fluorescent dye. The interaction increases the fluorescence of the dye. B) Diagram resulting from a DSF experiment.

Microscale Thermophoresis (MST)

In recent years microscale thermophoresis (MST) attracted emerging interest within the field of medicinal chemistry. This principle was first described in 1856 by C. LUDWIG, and was then used in 2010 by BAASKE *et al.* to develop a method that allowed quantification of thrombin binding to a DNA aptamer. The beauty of this method was that it did not require immobilization of any kind, and it could be performed in a variety of buffers and even blood serum. Since then, the method has become a recognized part of the biophysical toolbox. MST takes advantage of the fact that molecules move along a temperature gradient, a phenomenon called thermophoresis. The detection of this movement is accomplished by a fluorescent dye that is attached to one of the binding partners. After loading this

fluorescently labeled mixture in a glass capillary, an IR laser will heat the mixture in a defined area. As a consequence of the established temperature gradient, the molecules will start to migrate into or out of the heated area. Due to the fluorescent label, only the molecules of interest are detected by an epifluorescent microscope. Movement out of the heated area will result in a decreased fluorescence signal, whereas movement into the heated area will result in an increased fluorescence signal. After switching off the laser, the solution will cool down, and the molecules will diffuse back. Figure 11 illustrates the measurement procedure schematically. However, the signal obtained is an overlay of two different processes. On the one hand, there is thermophoresis, which happens on a scale of seconds. On the other hand, there is temperature-related intensity change (TRIC), which happens within milliseconds. TRIC is, as the name implies, caused by a change in the fluorescence intensity of the dye that is induced by a temperature change. In most cases, the fluorescence intensity drops with increasing temperatures. Both thermophoresis and TRIC are robust under constant conditions, but they can also be altered by external factors. Thermophoresis depends, amongst other factors, mainly on the size, hydration shell, and charge of a molecule, whereas TRIC strongly depends on the environment of the dye. A binding process of two molecules, e.g., protein to protein, protein to an aptamer, and even a small molecule to a protein, can alter both thermophoresis behavior and TRIC. This allows us to use this method as a powerful tool for the detection of various interactions. Another helpful feature is the concentration dependence that can be observed. This allows not only yes/no assays but also the quantification of binding affinities. Further optimizations and adaptations of this method even allow the determination of thermodynamic properties.¹³⁸⁻¹⁴¹ However, MST is not the method of choice for the investigation of thermodynamics. One of the main disadvantages of MST is that the method is susceptible to aggregation. This means the assay conditions have to be optimized for every protein to have a robust and reliable system. Although the extent of the effects observed is concentration dependent, which is a requirement for quantification, a major disadvantage of this method is undoubtedly the lack of transferability of results. Different binding interactions can and will alter thermophoresis and TRIC differently. This is due to the fact that thermophoresis depends on various factors, as mentioned before. However, suitable tool compounds can help to overcome most of these issues.¹⁴² In a noteworthy review by RAINARD *et al.*, the authors highlighted the potential of MST for drug discovery and gave several examples of successful deployment of this method. While MST may not be the best method for high-throughput screenings with thousands of compounds, wherefore DSF is better suited, MST is an excellent orthogonal method for hit validation and all the further optimization steps from hit to lead to drug candidate. Furthermore, they nicely described the synergy of two orthogonal biophysical methods for a screening. Unfortunately, every method has its blind spots, which will result in the loss of potential hits. By combining two or more different methods, it is possible to reduce this loss since one method can compensate for the shortcoming of other

methods.¹⁴¹ Especially due to the commercialization of this technology by NanoTemper, MST experiments can be easily performed. Different labeling kits, various types of capillaries, and robust devices that can be purchased facilitate assay development and ensure reproducible data generation.

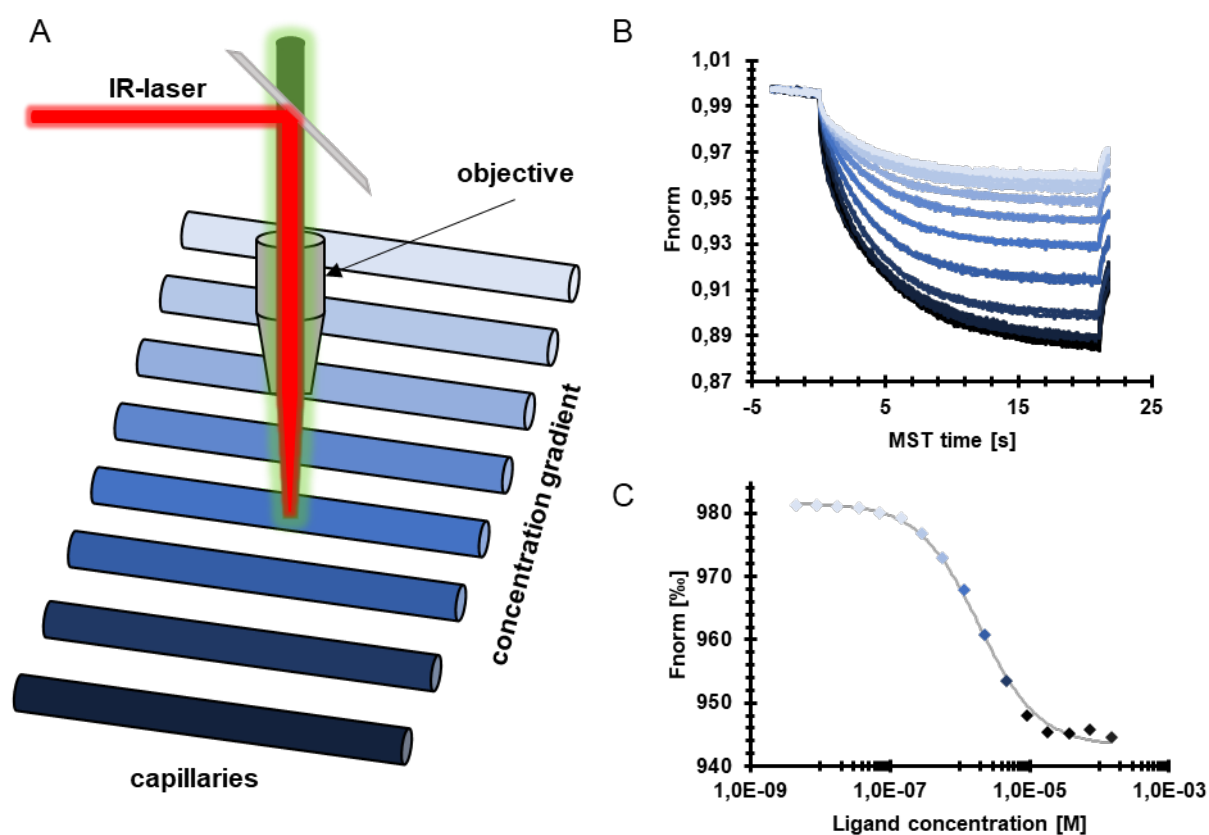


Figure 11: Schematic overview of microscale thermophoresis. A) Scheme of the measuring procedure. The capillaries contain fluorescent-labeled protein and a dilution series of a potential ligand. B) Raw traces of an MST experiment. The experiment starts with a calibration time -5s to 0s. At 0s, the IR laser is switched on and increases the temperature in the capillaries, which leads to the migration of the fluorescent tracer out of the heated area. At 20s, the IR laser is switched off, and the fluorescent tracer migrates back into the cooling area C) Diagram showing the normalized fluorescence obtained from B) plotted against the respective concentration. Figures 11B and 11C are adapted from ZIMMERMANN *et al.*¹⁴²

Isothermal titration calorimetry

Isothermal titration calorimetry (ITC) has been successfully employed in drug development for decades. This calorimetric method basically measures the energy that is released or consumed during a binding process. Therefore, two different cells are needed, one reference cell and one sample cell. Both cells are maintained at the exact same temperature by a system of connected heaters. At equilibrium, both cells require the same energy to be maintained at a constant temperature. For measurements, the reference cell is usually filled with water and the sample cell with an aqueous enzyme solution. Successive titrations of ligand to the enzyme will result in binding, which releases or consumes energy in the sample cell. As a consequence, different energies are required to maintain both cells at the exact same temperature. Exotherm binding will result in less energy that is needed to maintain the temperature in the sample cell compared to the reference cell and *vice versa*. If all ligand

molecules that can bind are bound, no more energy will be released or consumed, and both cells go back to equilibrium. Initially, there is an excess of protein, which will result in the quantitative binding of the ligand. During the experiments, the binding sites of the enzyme are more and more saturated until no further ligand binding occurs. At this point of the experiment, the energy required to maintain the same temperature in both cells is progressively converging. Lastly, the remaining differences are due to the dilution heat or dilution cold of the ligand.^{143–145}

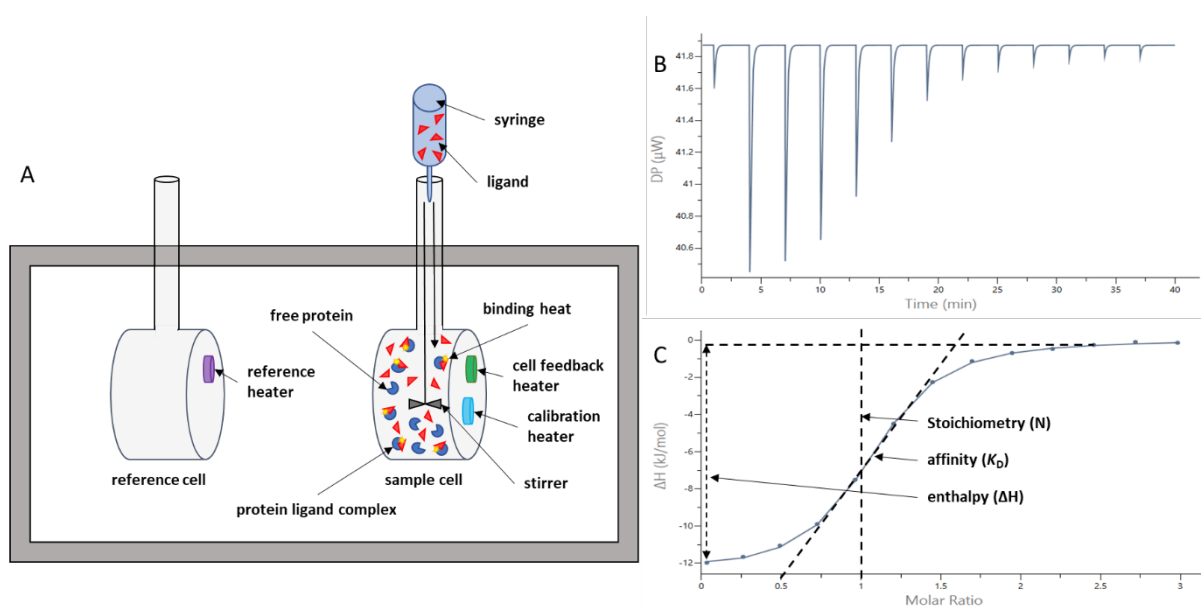


Figure 12: Schematic overview of Isothermal titration calorimetry. A) Scheme of the measuring procedure. B) Thermogram of ITC experiment with 13 titrations. C) Diagram resulting from the peak integration of the thermogram. The diagram highlights how stoichiometry, affinity, and enthalpy can be obtained. Figure 12B and 12C were generated using the MicroCal PEAQ-ITC Analysis software (Malvern Panalytical, Malvern, UK).

Tracking the energy that was required to temperate the sample cell over time will lead to a thermogram, as shown in Fig. 12B. Peak integration results in a diagram that allows the determination of the binding stoichiometry (N), binding affinity (K_D) and enthalpy (ΔH) of the binding (Figure 12C). In Figure 12, a scheme is depicted that describes the measurement itself as well as the results of such a measurement. Furthermore, the free Gibbs energy (ΔG) and the entropy (ΔS) of the binding can be calculated from the measured data using the Gibbs and Gibbs-Helmholtz equations. (R = universal gas constant, T = temperature in Kelvin)

Equation 1: Gibbs equation

$$\Delta G = -RT \ln K_D$$

Equation 2: Gibbs-Helmholtz equation

$$\Delta G = \Delta H - T\Delta S$$

Since the amount of energy that is released by a single binding event is quite small, large numbers of binding events must be enforced to obtain measurable energies. Therefore, high enzyme and ligand

Aim of this thesis

concentrations are needed for this method, which makes this method unsuitable for screenings of large compound libraries. However, ITC enables the determination of binding affinity, stoichiometry, and thermodynamic information with a single measurement. Some ITC experiments allow even more sophisticated evaluation to gain also kinetic information about the binding event. This method is called KinITC. There are reports in the literature that show the kinetic data obtained from KinITC do match the kinetic data from other biophysical methods like SPR.^{143–148}

As stated previously, a combination of different biophysical methods is essential for a successful screening approach. For a screening with a small or medium-sized compound library, isothermal titration calorimetry (ITC) is perfectly suited to be paired with MST. This combination allows fast detection of concentration-dependent binding via MST. Afterward for binding verification and determination of the stoichiometry and thermodynamics of the binding event ITC can be used.

Aim of this thesis

The main aim of this thesis has been the establishment and improvement of biophysical methods that are suitable to screen an in-house library of over a hundred compounds especially designed and synthesized for the inhibition of the human methyltransferases DNMT2 and NSUN6. Furthermore, these biophysical methods should allow the determination of binding affinities. Therefore, particularly microscale thermophoresis and isothermal titration calorimetry have been used.

List of publications

Publications and manuscripts as part of the doctoral thesis

1. Research articles

(1.) Schwickert, M.* , Fischer, T. R.* , Zimmermann, R. A.*, Hoba, S. N., Meidner, J. L., Weber, M., Weber, M., Stark, M. M., Koch, J., Jung, N., Kersten, C., Windbergs, M., Lyko, F., Helm, M., & Schirmeister, T. (2022). **Discovery of Inhibitors of DNA Methyltransferase 2, an Epitranscriptomic Modulator and Potential Target for Cancer Treatment.** *Journal of Medicinal Chemistry*, 65(14), 9750–9788.
<https://doi.org/10.1021/acs.jmedchem.2c00388>

* Authors contributed equally

(2.) Zimmermann, R. A.*, Schwickert, M.* , Meidner, J. L.* , Nidoieva, Z., Helm, M., & Schirmeister, T. (2022). **An Optimized Microscale Thermophoresis Method for High-Throughput Screening of DNA Methyltransferase 2 Ligands.** *ACS Pharmacology & Translational Science*, 5(11), 1079–1085.
<https://doi.org/10.1021/acsptsci.2c00175>

* Authors contributed equally

(3.) Zimmermann, R. A., Fischer, T. R., Schwickert, M., Nidoieva, Z., Schirmeister, T., & Kersten, C. (2023). **Chemical Space Virtual Screening against Hard-to-Drug RNA Methyltransferases DNMT2 and NSUN6.** *International Journal of Molecular Sciences*, 24(7), 6109.
<https://doi.org/10.3390/ijms24076109>

* Authors contributed equally

(4.) Schwickert, M.*; Zimmermann, R.A.*, Habeck, T., Hoba, S.N., Nidoieva, Z., Fischer, T.R., Stark, M.M., Kersten, C., Lermyte, F., Helm, M., & Schirmeister T. (2023). **Covalent S-adenosylhomocysteine-based DNA methyltransferase 2 inhibitors with a new type of aryl warhead** *ACS Medicinal Chemistry Letters*, Article ASAP.
<https://doi.org/10.1021/acsmedchemlett.3c00062>

* Authors contributed equally

Publications and manuscripts beyond this doctoral thesis

1. Research articles

(5.) Welker, A., Kersten, C., Müller, C., Madhugiri, R., Zimmer, C., Müller, P., Zimmermann, R., Hammerschmidt S., Maus H., Ziebuhr J., Sotriffer, C. & Schirmeister, T. (2021). **Structure-activity relationships of benzamides and isoindolines designed as SARS-CoV protease inhibitors effective against SARS-CoV-2.** *ChemMedChem*, 16(2), 340-354.
<https://doi.org/10.1002/cmdc.202000548>

(6.) Amendola G., Ettari R., Previti S., Di Chio C., Messere A., Di Maro S., Hammerschmidt S. J., Zimmer C., Zimmermann R. A., Schirmeister T., Zappalà M., and Cosconati S. (2021). **Lead Discovery of SARS-CoV-2 Main Protease Inhibitors through Covalent Docking-Based Virtual Screening.** *J. Chem. Inf. Model.*, 61(4) 2062-2073.
<https://doi.org/10.1021/acs.jcim.1c00184>

(7.) Jung S., Fuchs N., Johe P., Wagner A., Diehl E., Yuliani T., Zimmer C., Barthels F., Zimmermann R. A., Klein P., Waigel W., Meyr J., Opatz T., Tenzer S., Distler U., Räder H.-J., Kersten C., Engels B., Hellmich U. A., Klein J. & Schirmeister T. (2021) **Fluorovinylsulfones and -Sulfonates as Potent Covalent Reversible Inhibitors of the Trypanosomal Cysteine Protease Rhodesain: Structure–Activity Relationship, Inhibition Mechanism, Metabolism, and In Vivo Studies.** *Journal of Medicinal Chemistry* (64)16, 12322-12358.
<https://doi.org/10.1021/acs.jmedchem.1c01002>

2. Reviews

(8.) Fischer T.R., Meidner L., Schwickert M., Weber M., Zimmermann R. A., Kersten C., Schirmeister T. & Helm M. (2022) **Chemical biology and medicinal chemistry of RNA methyltransferases** 50(8), 4216-4245.
<https://doi.org/10.1093/nar/gkac224>

3. Unpublished manuscripts

(9.) Fuchs N.*, Zimmermann R. A.*, Schwickert M.*, Gunkel A. Zimmer C. Meta M., Schwickert K., Keiser J., Kiefer W., Schirmeister T. **Dual Strategy to Design New Agents Targeting Schistosoma mansoni: Advancing Phenotypic and SmCB1 Inhibitors for Improved Efficacy**

* Authors contributed equally

To be submitted to *ACS Infectious Disease*

- (10.) Maus H.*, Müller P.*, Meta M., Hoba S., Hammerschmidt S. J., Zimmermann R. A., Zimmer C., Fuchs N., Schirmeister T., Barthels F. **Next Generation of Fluorometric Protease Assays: 7-Nitrobenz-2-oxa-1,3-diazol-4-yl-amides (NBD-Amides) as Class-Spanning Protease Substrates**

* Authors contributed equally

Submitted to Angewandte Chemie International Edition on 24th April 2023

Development of selective inhibitors for the human methyltransferases DNMT2 and NSUN6

Discovery of Inhibitors of DNA Methyltransferase 2, an Epitranscriptomic Modulator and Potential Target for Cancer Treatment.

Project summary and own contributions

The human DNA methyltransferase (DNMT2) catalyzes an m⁵C modification at position 38 of different tRNAs, especially tRNA^{Asp}. DNMT2 transfers a methyl group from S-adenosylmethionine (SAM) to the C5 position within the cytidine, whereby SAM is converted into S-adenosylhomocysteine (SAH). SAH binds DNMT2 even stronger than SAM, which can be described as product inhibition.

The main aim of this project was the development of potent yet selective small molecular inhibitors for DNMT2. It was known that besides SAH, the natural product sinefungin (SFG) also inhibits a broad range of methyltransferases due to its structural similarity to SAH. Since the vast majority of methyltransferases use SAM as a methyl group donor, potent DNMT2 inhibition without off-target inhibition was expected to be very challenging. Therefore, a SAR study was conducted to determine which functional groups of the SAH or SFG structure are pivotal to maintaining DNMT2 binding and which moieties can be changed to generate selectivity amongst different methyltransferases. Finally, 36 derivatives of SAH/SFG were synthesized and screened for their affinity towards DNMT2. For this screening, MST was established. To verify the results of the MST screening, a ³H assay was applied, in which the inhibitory effect of the respective compounds was determined. The results of the ³H assay were in high accordance with the results of the MST screening, underlining the good predictive value of this biophysical method. The most potent inhibitors were found to be Y-shaped inhibitors, where the sulfur of the SAH was exchanged with nitrogen allowing further derivatization. Especially Y-shaped inhibitors with rigid linear moieties were found to be equipotent to SAH but showed higher selectivity towards other methyltransferases. The selectivity of the most potent inhibitors was tested against NSUN2, NSUN6, DNMT3a-3sL, and G9a in ³H assays. Moreover, the thermodynamic properties of the most potent inhibitors were investigated using isothermal titration calorimetry (ITC). The results revealed that for all inhibitors, the binding was driven by enthalpy rather than entropy. An *in vivo* assay with the most potent inhibitor showed no significantly reduced amount of m⁵C methylation, which was explained by the poor cell permeability of the compound. Unfortunately, a prodrug of this inhibitor showed only a slight but still significant reduction of m⁵C modifications *in vivo*.

Own contribution: expression and purification of proteins; method development and experimental performing of MST screening and ITC experiments; MTT assay for determination of cell toxicity; partly writing of the manuscript together with [REDACTED] and [REDACTED].

Contributions from other authors: design and synthesis of compounds; method development and experimental performing of ^3H assays; cell permeability assay; in vivo testing of compounds; bisulfide sequencing.

This work has been published in: *Journal of Medicinal Chemistry* (Impact factor: 8.039/CiteScore:11.5)

Reprinted with permission from: *J. Med. Chem.* 2022, 65, 14, 9750–9788. “Discovery of Inhibitors of DNA Methyltransferase 2, an Epitranscriptomic Modulator and Potential Target for Cancer Treatment.” Copyright © 2022 American Chemical Society.

Discovery of Inhibitors of DNA Methyltransferase 2, an Epitranscriptomic Modulator and Potential Target for Cancer Treatment

Published as part of the Journal of Medicinal Chemistry special issue "Epigenetics 2022".

Marvin Schwickert,[‡] Tim R. Fischer,[‡] Robert A. Zimmermann,[‡] Sabrina N. Hoba, J. Laurenz Meidner, Marlies Weber, Moritz Weber, Martin M. Stark, Jonas Koch, Nathalie Jung, Christian Kersten, Maike Windbergs, Frank Lyko, Mark Helm,* and Tanja Schirmeister*Cite This: *J. Med. Chem.* 2022, 65, 9750–9788

Read Online

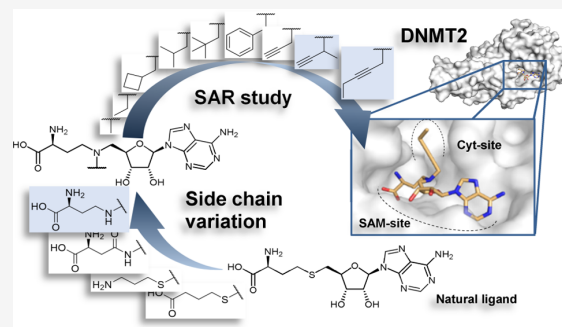
ACCESS |

Metrics & More

Article Recommendations

Supporting Information

ABSTRACT: Selective manipulation of the epitranscriptome could be beneficial for the treatment of cancer and also broaden the understanding of epigenetic inheritance. Inhibitors of the tRNA methyltransferase DNMT2, the enzyme catalyzing the S-adenosyl-methionine-dependent methylation of cytidine 38 to 5-methylcytidine, were designed, synthesized, and analyzed for their enzyme-binding and -inhibiting properties. For rapid screening of potential DNMT2 binders, a microscale thermophoresis assay was established. Besides the natural inhibitors S-adenosyl-L-homocysteine (SAH) and sinefungin (SFG), we identified new synthetic inhibitors based on the structure of N-adenosyl-2,4-diaminobutyric acid (Dab). Structure–activity relationship studies revealed the amino acid side chain and a Y-shaped substitution pattern at the 4-position of Dab as crucial for DNMT2 inhibition. The most potent inhibitors are alkyne-substituted derivatives, exhibiting similar binding and inhibitory potencies as the natural compounds SAH and SFG. CaCo-2 assays revealed that poor membrane permeabilities of the acids and rapid hydrolysis of an ethylester prodrug might be the reasons for the insufficient activity in cellulo.



INTRODUCTION

Epigenetic inheritance is not only mediated by modifications of DNA and histones but also driven by RNA and RNA modifications.^{1–6} Various data suggest that RNA species are involved in the heredity of specific phenotypes such as mental^{7–10} or metabolic disorders.^{4,11–15} As an example, metabolic disorders and their epigenetic transmission were found to be linked to elevated levels of m²G and m⁵C modifications on small noncoding RNAs (sncRNAs) in mouse models,⁴ and it could be shown that deletion of the enzyme responsible for these modifications, namely, the DNA methyltransferase 2 (DNMT2), abolished sperm sncRNA-mediated transmission of high-fat-diet-induced metabolic disorders to descendants.¹¹ The enzyme DNMT2 is also essential for the epigenetic transmission of phenotypes linked to the *Kit* and *Sox9* genes between subsequent generations of mice. These genes encode for a tyrosine kinase and a transcription factor, variants of which lead to white colored tails and feet (*Kit*) or to an enhanced growth (*Sox9*) of *Dnmt2*^{+/+} mice but not *Dnmt2*^{-/-} mice.¹⁶

According to its sequence and structure, human DNMT2 is a member of the DNA methyltransferase (MTase) family.^{17,18}

Also, the catalytic motif is strongly conserved and highly characteristic for DNA methyltransferases. In contrast to DNMT1 and DNMT3, however, DNMT2 is primarily localized in the cytoplasm instead of the nucleus and therefore lacks the properties of a typical DNA methylating enzyme.¹⁹ Although it was discussed that DNMT2 also modifies DNA at CG residues,²⁰ its main function is the methylation of tRNA^{Asp} at position C38 in the anticodon loop.¹⁹ Further substrates are tRNA^{Gly}, tRNA^{Val}, and tRNA^{Glu}, depending on the species.²¹

Besides its role in epigenetics, DNMT2 is involved in other physiological processes, some of which are not quite understood so far. While induced loss of DNMT2 reduced the size of zebrafish morphants and affected retina, liver, and brain development,²² no morphological effects could be observed in

Received: March 11, 2022

Published: July 18, 2022



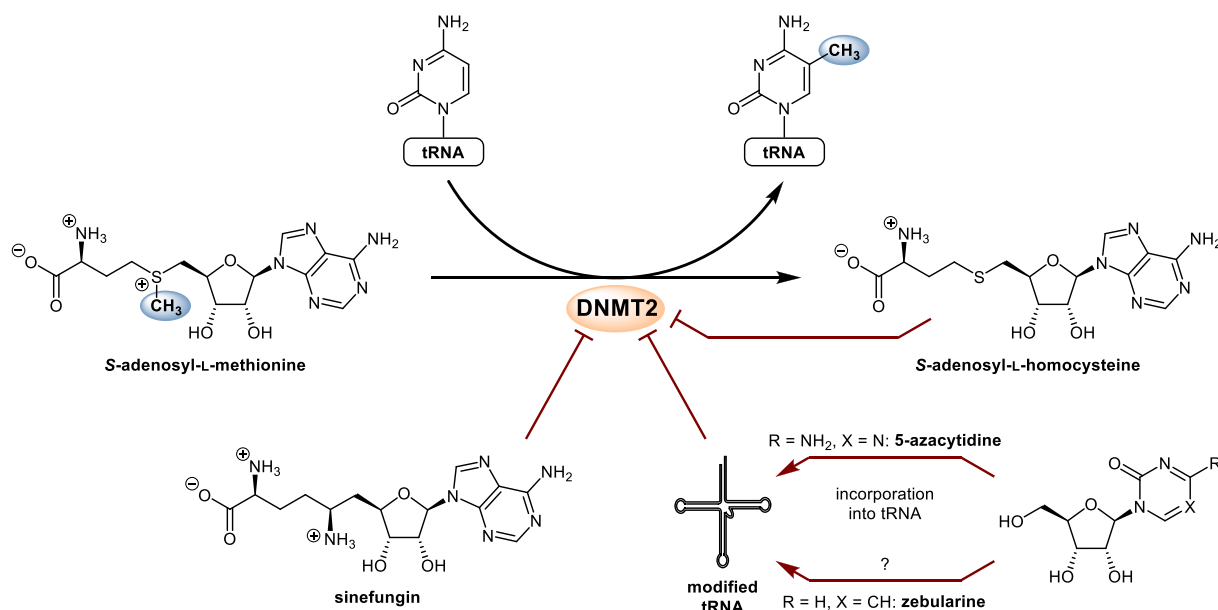


Figure 1. Modification of tRNA by DNMT2 with SAM as a cosubstrate. 5-Azacytidine and sinefungin are inhibitors of DNMT2. Zebularine is a known DNA MTase inhibitor and is supposed to exhibit an analogous mechanism as 5-azacytidine as it has been shown to be incorporated into tRNA.³⁹ Its inhibitory potential against DNMT2 has not been reported yet. However, the *M.HhaI* C5 Mtase, which shows close similarity to DNMT2, is a known target of zebularine.³⁸

flies, mice, and plants.¹⁹ An overexpression of DNMT2 in *Drosophila* flies led to life span prolongation and an increased stress resistance.²³ This is substantiated by the fact that *Drosophila* loss-of-function DNMT2 mutants showed reduced viability under stress conditions.

Methylation of tRNA by DNMT2 prevents ribonuclease-mediated cleavage of tRNA,²⁴ thus regulating RNA stability and correspondingly leading to higher rates of overall protein synthesis.²⁵ Moreover, the methylation of C38-tRNA^{Asp} by DNMT2 is required to ensure accurate polypeptide synthesis by improving codon recognition. Methylation increases the capacity of tRNA to discriminate between Asp and Glu codons improving translational accuracy, which prevents the production of aberrant proteins.²⁶

There are also indications that DNMT2 plays a role in malignancies as it is overexpressed in several cancer tissues, such as cervical²⁷ or bladder tissue.²⁸ According to the COSMIC database, various tumor samples showed upregulation of DNMT2 and numerous somatic mutations in the enzyme were found in tumors originating from different tissues.²⁹

Taken together, DNMT2 represents a potential target in cancer treatment and epigenetic drug discovery.

In 2001, Dong et al. revealed the crystal structure of human DNMT2 (Protein Data Bank (PDB) entry 1G55) in 1.8 Å resolution. Consisting of 391 amino acids corresponding to a size of ca. 40 kDa, the enzyme is a relatively small protein.³⁰ A comparison to DNMT1 and DNMT3 illustrates that in contrast to other eukaryotic MTases DNMT2 lacks the large N-terminal domain.¹⁷ The conserved C-terminal catalytic domain of DNMT2 features a unique cysteine-phenylalanine-threonine (CFT) motif between the catalytic motifs VIII and IX, which is not found in other MTases.^{30,31} In the catalytic motif IV, the protein contains the common proline-cysteine-glutamine (PCQ) motif including the catalytically active cysteine. However, in the crystal structure, this exact part of the catalytic

center is disordered.³⁰ A more defined structure of the loop can be found in the DNMT2 homologue of *Entamoeba histolytica*, which shows an α -helical conformation.³²

DNMT2 requires S-adenosyl-L-methionine (SAM) as cofactor, transferring SAM's methyl group to the 5-position of the tRNA substrate's cytosine, yielding m⁵C38-tRNA^{Asp} and S-adenosyl-L-homocysteine (SAH) (Figure 1).¹⁹

Currently, only a few DNMT2 inhibitors have been reported. The anticancer drugs 5-azacytidine (5-azaC) and 5-aza-2'-deoxycytidine (decitabine) inhibit RNA and DNA MTases (Figure 1) leading to a change of the methylation activity in cancer patients.^{33–35} During transcription and replication, the drugs are randomly incorporated into nascent DNA (decitabine and 5-azaC) and RNA (5-azaC) by respective polymerases. Due to the substitution of cytosine's carbon atom in position 5 with nitrogen in decitabine and 5-azaC, DNA and RNA MTases remain covalently bound to the target nucleic acids, thus inhibiting the catalytic activity of the enzymes.^{36,37} A similar mechanism of inhibition is exhibited by the pyrimidinone derivative zebularine. It forms a covalent complex with DNA MTases, such as C5 Mtase from *Haemophilus hemolyticus* (*M.HhaI*), which shows close similarity to human DNMT2.³⁸ However, inhibition of DNMT2 itself has not been reported yet. Due to the structural similarity to 5-azaC, an analogous mechanism of inhibition by zebularine is supposed as incorporation into tRNA has been found.³⁹

The natural SAM-related nucleoside sinefungin (adenosyl-ornithine, SFG),⁴⁰ originally isolated from *Streptomyces griseolus*, exhibits competitive inhibition of several SAM-dependent MTases.⁴¹ However, the inhibitory potential toward DNMT2 has not been quantified yet. Similarly, the inhibition of DNMT2 by SAH, which has been reported to be a nonselective feedback inhibitor of several SAM-dependent MTases, has not been investigated in detail.⁴²

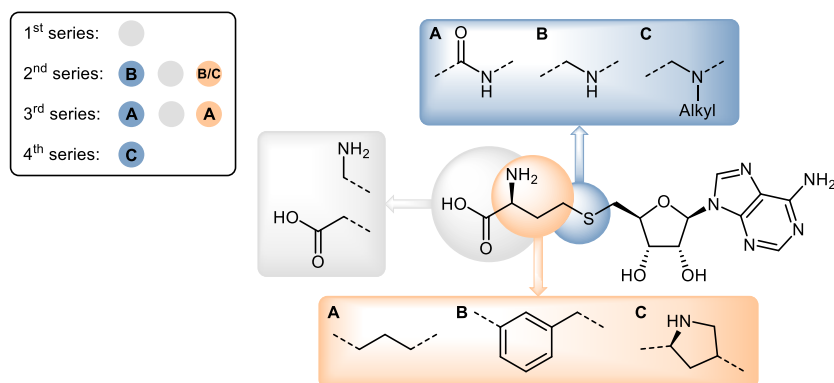
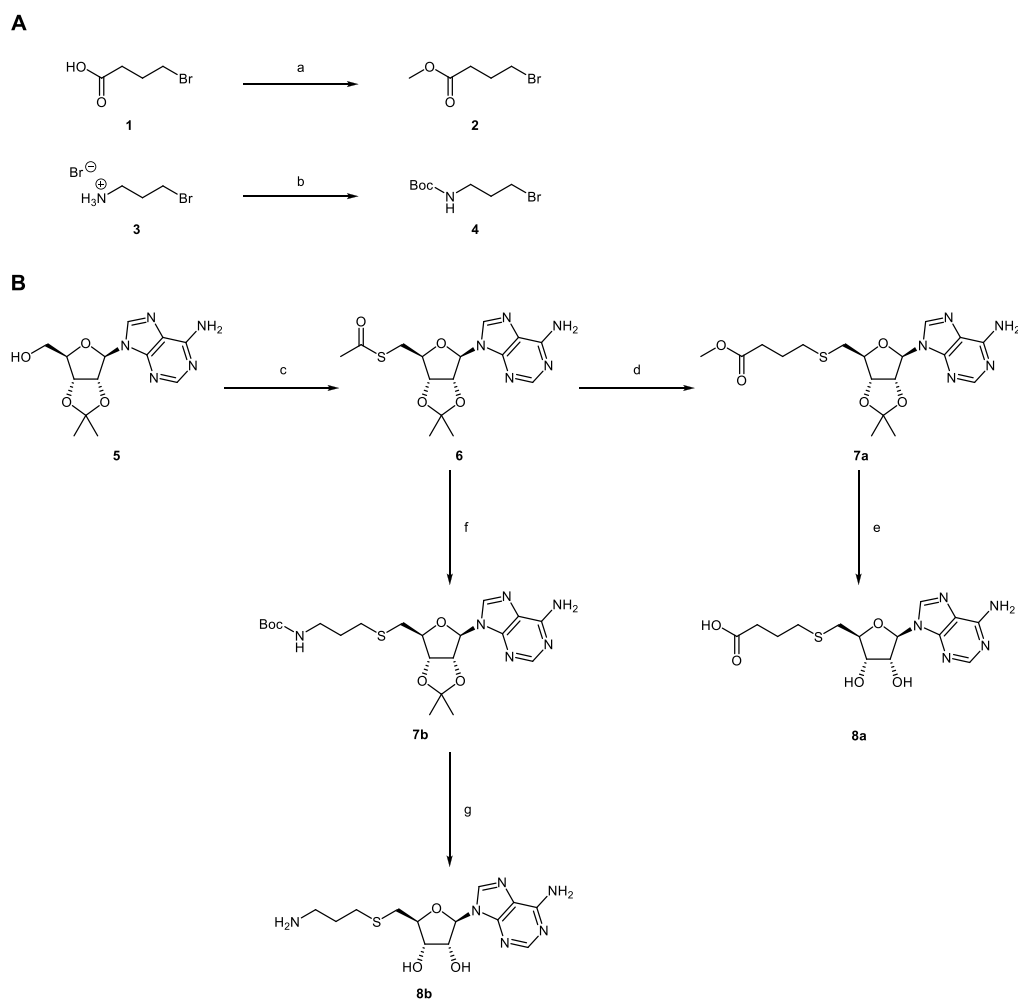
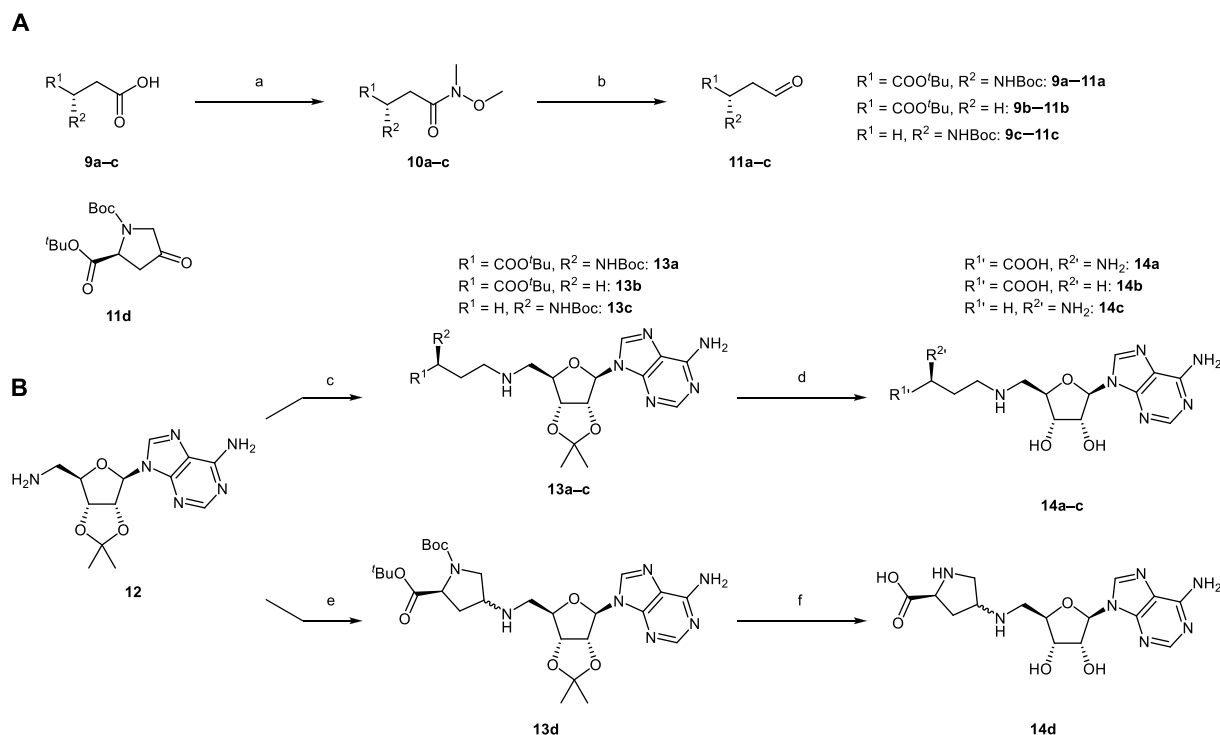


Figure 2. Inhibitor design based on the SAH scaffold.

Scheme 1. Syntheses of Thioethers 8a, 8b: (A) Synthesis of Alkyl Bromides 2 and 4; (B) Synthesis of Acetyl-Protected Thiol Building Block 6 Followed by Nucleophilic Substitution and Deprotection^a



^aReagents and conditions: (a) MeOH, SOCl₂, rt, 16 h, 79%; (b) Boc₂O, THF, NEt₃, rt, 16 h, 70%; (c) PPh₃, DIAD, AcSH, THF, 0 °C, 18 h, 95%; (d) 2, NaOMe, MeOH, rt, 16 h, 75%; (e) (1) LiOH, THF/H₂O, rt, 1 h; (2) DCM/TFA (1:1), H₂O, 5 °C, 1 h, 96%; (f) 4, NaOMe, MeOH, rt, 16 h, 84%; (g) HCOOH, H₂O, 0 °C, 2 d, 96%.

Scheme 2. Syntheses of Aliphatic Amine Derivatives: (A) Synthesis of Aldehyde Building Blocks 11a–c and Structure of the Commercially Available Ketone 11d; (B) Reductive Amination and Deprotection to Yield the Amines 14a–d^a

^aReagents and conditions: (a) *N,O*-dimethylhydroxylamine, CDI, DCM, rt, 18–25 h, 81–89%; (b) DIBAL, THF, -78°C , 2–2.5 h, 34–81%; (c) 11a–c, $\text{NaBH}(\text{OAc})_3$, HOAc, THF, rt, 5–72 h, 57–76%; (d) (1) TFA/DCM 1:1, -20°C ; (2) TFA/ H_2O 1:6, 8°C , 99%; (e) 11d, $\text{NaBH}(\text{OAc})_3$, HOAc, THF, rt, overnight, 68%; (f) (1) TFA/DCM 1:1, -20°C ; (2) TFA/ H_2O 1:6, 8°C , 99%.

As a successful strategy in the search for inhibitors or tools for study of SAM-dependent MTases, the derivatization of the natural binder SAH has been exploited for various targets such as the catechol-*O*-MTase (COMT),^{43–45} protein MTases (PMTs) including histone MTases (HMTs) such as DOT1L,⁴⁶ RNA MTases such as METTL3,⁴⁷ and the SARS-CoV-2 mRNA cap MTase^{48,49} or the previously mentioned DNA MTases DNMT1 and DNMT3B2.^{50,51} The DOT1L inhibitor pinometostat is currently being tested in clinical trials.⁵² For DNMT2, synthetic inhibitors based on SAH were previously described, albeit only with very low affinity.⁵³ However, a systematic approach to identify and improve such inhibitors or tools has not yet been followed so far.

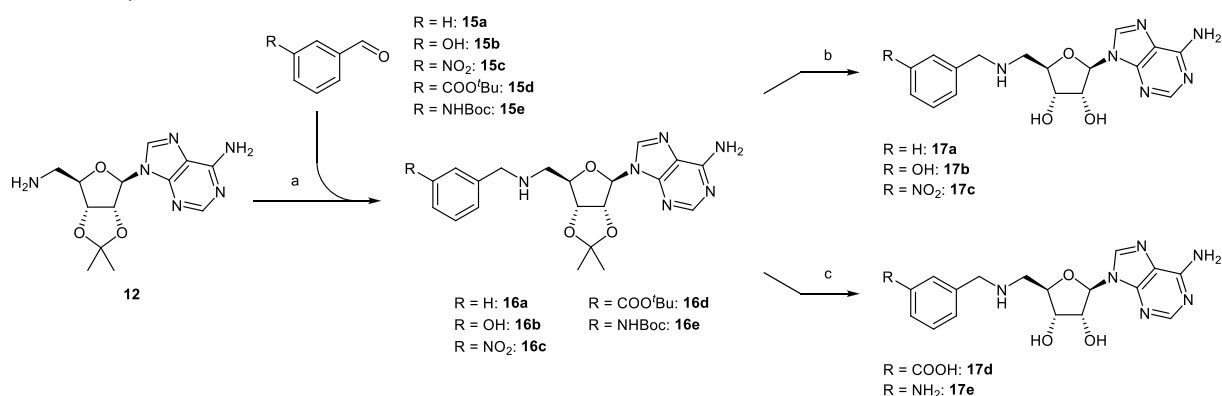
In this work, we present the discovery of potent DNMT2 inhibitors based on SAH's adenosyl scaffold. While this nucleoside substructure was retained, we performed structure–activity relationship studies by investigating different side-chain types (Figure 2). We prepared four compound series:

- (1) First, SAH analogs lacking either the amino or the acid group (8a, 8b) were tested to identify the pharmacophoric significance of these moieties.
- (2) In order to extend the possibilities for substitution, we exchanged the homocysteine's sulfur atom with nitrogen yielding *N*-adenosyl-2,4-diaminobutyric acid (adenosyl-Dab) derivatives (14a–d, 17a–e). This additionally introduces a basic functionality, which—depending on the pH value—can be protonated but does not provide a permanently charged group as found in SAM. Analo-

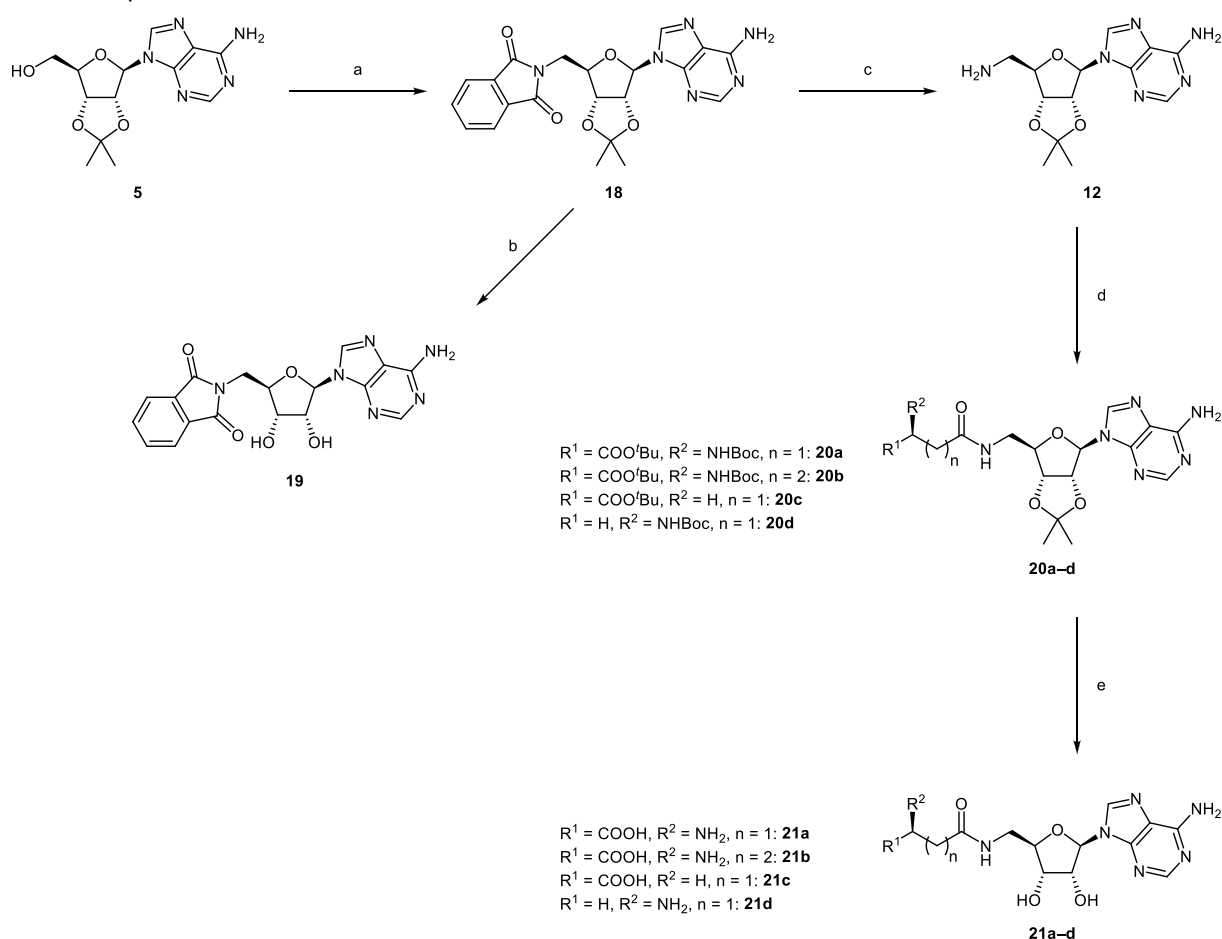
gously to the sulfide derivatives, we generated two compounds, each of which lacks one of the functional groups in the side chain (14b, 14c). To constrain the flexibility of the aliphatic side chain, we implemented a five-membered ring (14d). In addition, we developed derivatives with benzene as a rigidizing element, substituted with and without polar functions (17a–e).

- (3) We also investigated the effect of an amide function as a replacement of the thioether group (21a–d). To enable a comparison of the sulfide and amine derivatives, we also created structures lacking either the amine or the carboxylic acid group of the amino acid side chain (21c, 21d). Since the amide function yields a shorter bond length compared to thioether- or amine-based linkers, we generated a structure with an extended aliphatic side chain (21b).
- (4) In order to target both the SAM- and cytidine-binding site, we designed Y-shaped structures (27a–27t).

The compounds were tested for binding to DNMT2 using microscale thermophoresis (MST). Both DNMT2 binders and nonbinders were evaluated with regard to their inhibitory effect on DNMT2-catalyzed methylation of substrate tRNA^{Asp} in a tritium incorporation assay. This procedure was also followed in order to investigate if DNMT2 binding directly resulted in DNMT2 inhibition and if the MST binding assay can be used as a prescreening method prior to the laborious, time-consuming, and expensive radioactive assay.

Scheme 3. Syntheses of Aromatic Amine Derivatives 17a–e^a

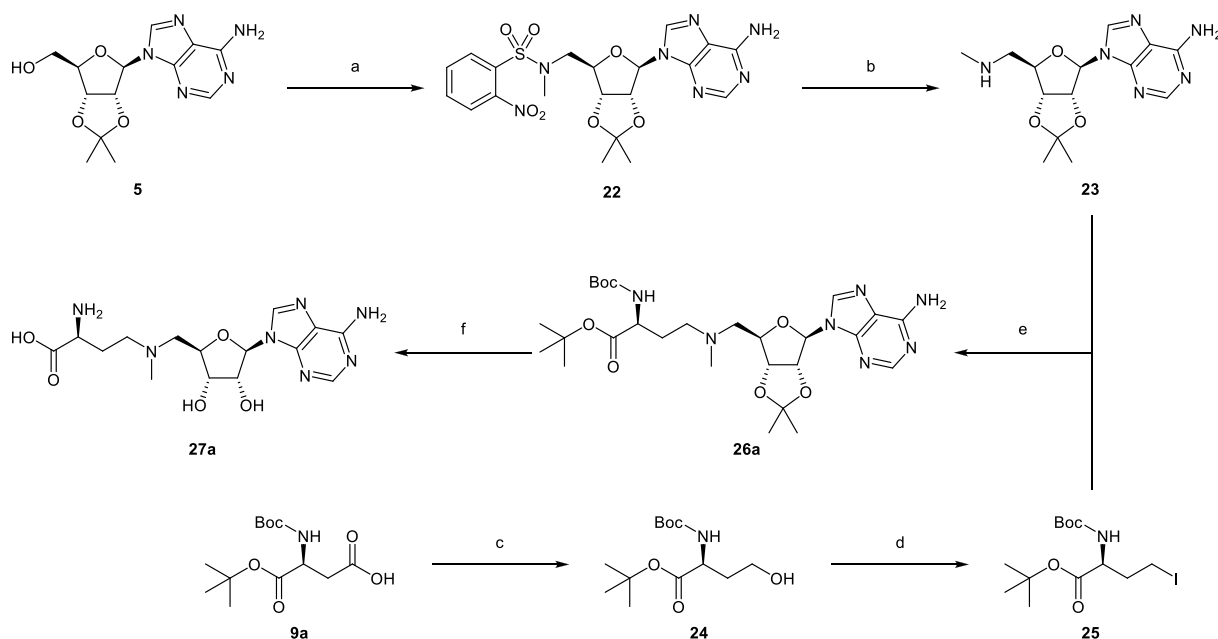
^aReagents and conditions: (a) **15a–e**, NaBH(OAc)₃, HOAc, THF or 1,2-DCE/MeCN, rt, 3.5–24 h, 55–92%; (b) TFA/H₂O 1:6, 5 °C, 91–99%; (c) (1) TFA/DCM 1:1, –20 °C; (2) TFA/H₂O 1:6, 5 °C, 97–99%.

Scheme 4. Syntheses of Amide Derivatives 21a–d and Phthalimide 19^a

^aReagents and conditions: (a) phthalimide, PPh₃, DIAD, THF, rt, 5 h, 71%; (b) TFA/H₂O 1:6, 8 °C, 2 h, 96%; (c) hydrazine, EtOH, Δ, 7 h, 93%; (d) R¹–CHR²–(CH₂)_n–COOH, TBTU, DIPEA, DMF, rt, 2.5–30 h, 76–97%; (e) (1) TFA/DCM 1:1, –20 °C; (2) TFA/H₂O 1:6, 8 °C, 99%.

For the most potent methylation inhibitors, IC₅₀ values were determined in the tritium incorporation assay, and K_D values were determined using isothermal titration calorimetry (ITC).

In our studies, we identified novel SAH-based DNMT2 binders and inhibitors with low micromolar affinity.

Scheme 5. Synthesis of Y-Shaped Methyl Derivative 27a^a

^aReagents and conditions: (a) 2-nitro-*N*-methylbenzenesulfonamide, PPh₃, DIAD, THF, rt, 24 h, 23%; (b) Cs₂CO₃, thiophenol, MeCN, rt, 72 h, 65%; (c) (1) ethyl chloroformate, *N*-methyl morpholine, THF, -10 °C to -5 °C, 15 min; (2) NaBH₄, THF/H₂O, 5 °C to rt, 18 h, 73%; (d) (1) tosyl chloride, DMAP, NEt₃, 1,2-DCE, 0 °C to rt, 4 h; (2) NaI, acetone, rt, 42 h, 66%; (e) DIPEA, MeCN (dry), 18.5 h at rt, 6 h at 55 °C, 28%; (f) TFA/DCM 1:1, H₂O, 5 °C, 99%.

RESULTS AND DISCUSSION

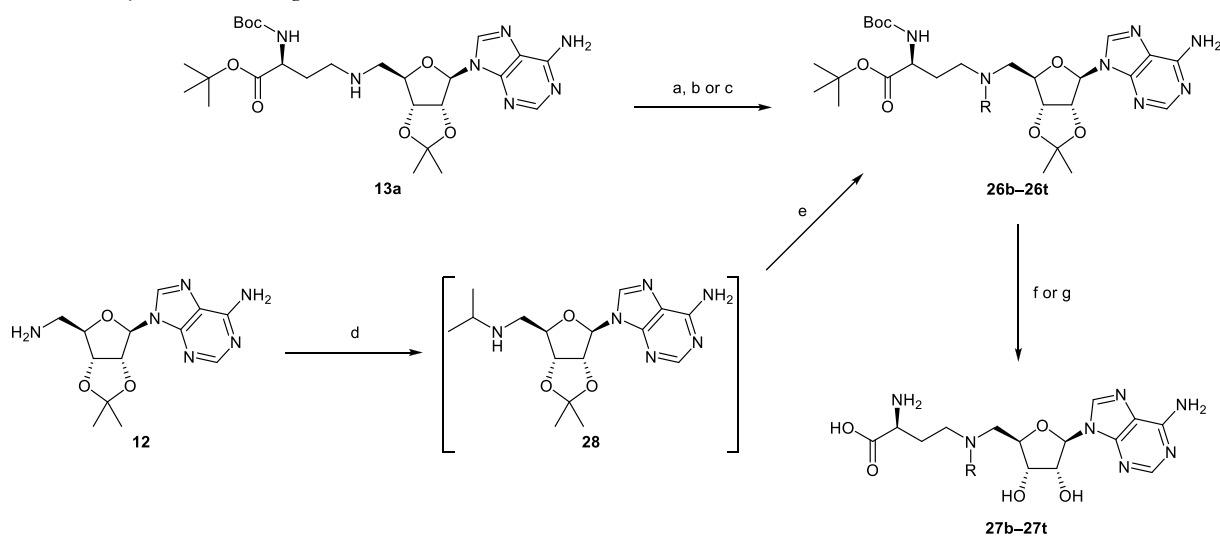
Chemistry. First, SAH analogs lacking either the amino or the acid group (**8a**, **8b**, series 1, Figure 2) were synthesized to identify the pharmacophoric significance of these moieties (Scheme 1). The acetyl-protected thiol building block **6**, used as precursor for both compounds, was synthesized from 2',3'-*O*-isopropylideneadenosine **5** in a Mitsunobu reaction using thioacetic acid and diisopropyl azodicarboxylate (DIAD). The methyl ester **7a** was synthesized by nucleophilic substitution reaction of **6** with methyl-4-bromobutyrate (**2**), which was obtained from 4-bromobutyric acid (**1**) by esterification. The Boc-protected amine **7b** was obtained analogously by reaction of **6** with 3-(Boc-amino)propyl bromide (**4**), which was obtained by reaction of 3-aminopropyl bromide hydrobromide (**3**) with Boc anhydride. The obtained sulfide **7a** was deprotected using lithium hydroxide in THF/water followed by treatment with trifluoroacetic acid (TFA) and water in DCM at 5 °C to yield **8a**. Compound **7b** was deprotected by treatment with formic acid in water at 0 °C yielding **8b**.

In series 2 compounds, the homocysteine's sulfur atom was exchanged with nitrogen yielding *N*-adenosyl-2,4-diaminobutyric acid (adenosyl-Dab) derivatives (**14a–d**, **17a–e**). Also in this series, we generated two compounds that lack either the amino or the carboxylic acid function in the side chain (**14b**, **14c**). In addition, a five-membered ring (**14d**) was introduced in order to constrain the flexibility of the side chain. The necessary precursor aldehydes **11a–c** for reductive amination of 5'-amino-5'-deoxy-2',3'-*O*-isopropylidene adenosine **12** (for the synthesis of **12**, see Scheme 3) were prepared in two-step syntheses starting from the protected carboxylic acids **9a–c** (Scheme 2). These were converted to the respective Weinreb amides **10a–c** with *N,O*-dimethylhydroxylamine and 1,1'-carbonyl-diimida-

zole (CDI) followed by reduction with diisobutylaluminum hydride (DIBAL) at -78 °C. The secondary amines **13a–d** were prepared by reductive amination of the aldehydes **11a–c** and the commercially available ketone **11d**, respectively, with amine **12** using sodium triacetoxyborohydride and acetic acid. Deprotection of **13a–d** to yield **14a–d** was achieved by treatment with 50% (v/v) TFA in dichloromethane at -20 °C followed by 14% (v/v) TFA in water at 8 °C.

The amine building block **12** was also modified with the commercially available aldehydes **15a–e** using sodium triacetoxyborohydride and acetic acid to form the respective benzylic amines **16a–e** (Scheme 3). These were treated with 14% (v/v) TFA in water at 8 °C to yield the target compounds **17a–c**. To accomplish the deprotection of **16d** and **16e** to **17d** and **17e**, respectively, a two-step procedure was required, using 50% (v/v) TFA in dichloromethane at -20 °C first, followed by treatment with 14% (v/v) TFA in water at 8 °C.

For the syntheses of the amides **21a–d** (series 3), 2',3'-*O*-isopropylideneadenosine **5** was modified with phthalimide via Mitsunobu reaction with diisopropyl azodicarboxylate (DIAD) (Scheme 4) to yield compound **18**. In the following Gabriel synthesis, the phthalimide **18** was cleaved with hydrazine to yield 5'-amino-5'-deoxy-2',3'-*O*-isopropylidene adenosine **12**. This intermediate was coupled with different Boc- and *tert*-butyl ester-protected carboxylic acids in the presence of 2-(1*H*-benzotriazole-1-yl)-1,1,3,3-tetramethylammonium tetrafluoroborate (TBTU) to obtain the corresponding amides **20a–d**. Concomitant deprotection of all protecting groups (Boc, *tert*-butyl ester, isopropylidene group) to yield compounds **21a–d** was achieved by performing a two-step procedure, using 50% (v/v) TFA in dichloromethane at -20 °C first, followed by treatment with 14% (v/v) TFA in water at 8 °C. To obtain the

Scheme 6. Synthesis of Y-Shaped Amine Derivatives 27b–t (Series 4)^a

^aReagents and conditions: (a) RCHO, NaBH(OAc)₃, HOAc, 1,2-DCE, 0 °C → rt, overnight, 14–89%; (b) RBr, DIPEA, DMF, rt, overnight, 55–74%; (c) RBr or RCl, DIPEA, CuBr, DMF, rt, 16–48 h, 41–49%; (d) acetone, NaBH₃CN, HOAc, MeOH, 0 °C, 0.5 h; (e) 11a, NaBH(OAc)₃, HOAc, 1,2-DCE, 0 °C → rt, overnight, 66%; (f) TFA/DCM 1:1, H₂O, 5 °C, 99%; (g) (1) TFA/DCM 1:1, 5 °C; (2) TFA/H₂O 1:6, 5 °C, 99%. The structures of compounds 27b–27t are presented in Table 1.

deprotected phthalimide derivative 19, the isopropylidene-protected phthalimide 18 was treated analogously using 14% (v/v) TFA in water.

For the synthesis of the Y-shaped methyl derivative 27a of series 4 (Scheme 5), 2',3'-O-isopropylideneadenosine 5 was functionalized with 2-nitro-*N*-methylbenzenesulfonamide under Mitsunobu conditions. The resulting sulfonamide 22 was hydrolyzed using cesium carbonate and thiophenol. In the following step, the methylated amine 23 was reacted with the alkyl iodide 25 to form the protected Y-shaped methyl derivative 26a, which was deprotected using TFA and water at 5 °C to give 27a. The alkyl iodide 25 was obtained by reducing the protected aspartate 9a with ethyl chloroformate and sodium borohydride followed by treatment first with tosyl chloride, then with sodium iodide.

The other Y-shaped compounds of series 4, 27b–t (Scheme 6, Table 1), were synthesized starting from amine 13a. This intermediate was either reacted with various aldehydes via reductive amination or different alkyl bromides and chlorides via nucleophilic substitution to obtain the tertiary amines 26b–t. To generate the isopropyl derivative 27d, the primary amine 12 was first alkylated with acetone and then with aldehyde 11a, each in a reductive amination reaction. In the final step, all protective groups were removed by treatment with TFA and water at 5 °C yielding compounds 27b–t. Compound 27s was obtained as a 50:50 mixture of two epimers (27s-A/B), but separation by HPLC (hydrophilic C₁₈ column MZ-Aqua Perfect) failed. Therefore, the single epimers 27s-A and 27s-B were obtained by separation of the precursor epimers 26s-A and 26s-B by HPLC (C₁₈) followed by deprotection of these single epimers by treatment with TFA and water at 5 °C.

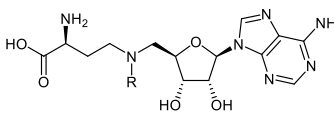
To evaluate the effect of compound 27s-A/B in cells, an ethyl ester prodrug was prepared. Therefore, 27s-A/B was treated with thionyl chloride in ethanol at 60 °C to give the corresponding ethyl ester 28-A/B as a 50:50-mixture of two epimers (Scheme 7). The separation of the epimers was achieved by HPLC yielding 28-A and 28-B. The assignment of


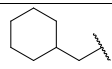
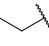
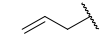
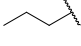
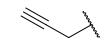
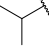
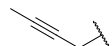
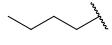
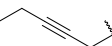
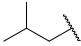
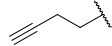
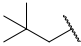
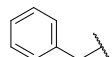
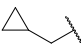
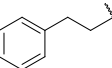
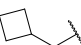
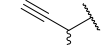

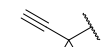
the absolute configuration of the chiral center within the alkyl side chain was not possible, neither for 27s nor for 28. However, since both epimers turned out to be equipotent (see below), we refrained from further efforts to assign the configuration.

Biological Evaluation: DNMT2 Binding and Inhibition.

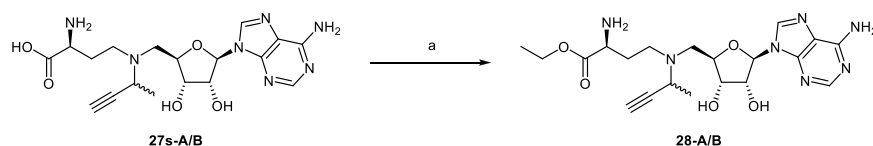
As a preliminary screening, all compounds including SFG and SAH were tested for binding to human DNMT2 at concentrations of 100 μM via MST to discriminate between binders and nonbinders (Figure 3). The readout of the assay was based on the normalized fluorescence signal. If a shift in the normalized fluorescence signal was detected, this was attributed to the formation of a protein–ligand complex. To discriminate binders and nonbinders, the 99% confidence intervals of the respective fluorescence signals were calculated. If the difference between the confidence interval of the measurement and that of the control measurement was more than 1% relative to the normalized fluorescence, the compound was defined as a binder. To evaluate the inhibitory potential of the compounds, tritium incorporation assays using DNMT2, substrate tRNA^{Asp}, and ³H-SAM as cosubstrate were performed with compound concentrations of 100 μM. The results of these assays are presented in Table 2.

To evaluate the quality of an assay, especially of high-throughput screenings (HTS) Zhang et al. developed a tool called Z-factor.⁵⁴ This value can be used to compare assays, or to optimize their quality. A Z-factor of 1 represents an ideal assay, whereas Z-factors > 0.5 classify excellent assays. The same interpretation can be applied to the Z'-factor, which describes the quality of an assay itself. The only difference is that Z' instead compares between negative and positive controls. For the prescreening assay via MST, SFG was chosen as positive control, since it was described as a potent pan-methyltransferase inhibitor in the literature and also showed high inhibition against DNMT2 within this study. Furthermore, 27s-A/B was chosen as another positive control compound because it was the most potent inhibitor within this study. Since both epimers

Table 1. Structures of N-Substituted Adenosyl-Dab Derivatives 27a–t (Series 4)^a


R	Compound 27	R	Compound 27
	a		k
	b		l
	c		m
	d		n
	e		o
	f		p
	g		q
	h		r
	i		s-A/B*
	j		t

^a* indicates that 27s-A/B is a 1:1 mixture of two epimers with different configuration (R or S) at the stereocenter within the alkyl side chain. The single epimers with unknown configuration at this position are 27s-A and 27s-B.

Scheme 7. Synthesis of the Ethyl Esters 28-A and 28-B of Compound 27s-A/B^a

^aReagents and conditions: (a) SOCl₂, EtOH, 0 °C → 60 °C, 9 h, 27%.

showed comparable inhibition of DNMT2, the mixture was used. As negative control DMSO was chosen. A quartet of runs with technical septets were performed, each by three different persons, and revealed Z'-factors of 0.72 (SFG) and 0.76 (27s-A/B) for the prescreening assay via MST. It was stated by Zhang et al. that Z'-factors are always higher than their corresponding Z-factors, but they also stated that a Z-factor > 0 is sufficient for a "yes/no" type assay. Therefore, Z'-factors of 0.72 and 0.76 can be considered sufficient for the desired purposes within this study.

For selected compounds exhibiting both binding to DNMT2 and at least 60% inhibition of the enzymatic methylation activity at a concentration of 100 μM (27m, 27n, 27o, 27s-A/B), K_D and IC₅₀ values for DNMT2 binding and DNMT2 inhibition, respectively, were determined using ITC and the tritium

incorporation assay. The results are summarized in Table 3. Examples of dose–response curves for determination of the IC₅₀ values and examples of ITC thermograms are displayed in Figures 4 and 5.

In general, a very good correlation between DNMT2 binding and DNMT2 inhibition was found (Table 2). Compounds that did not emerge as DNMT2 binders also did not show significant DNMT2 inhibition at 100 μM. Only two compounds (14a and 27b) that were identified as binders in the MST assay were found to be inactive in the tritium incorporation assay. In summary, the MST assay as implemented for this study exhibited good predictive value: 88.9% of all detected binders could be verified as inhibitors in the enzymatic assay. Furthermore, all nonbinders were found to be inactive in the enzyme inhibition assays. Therefore, the MST binding assay is

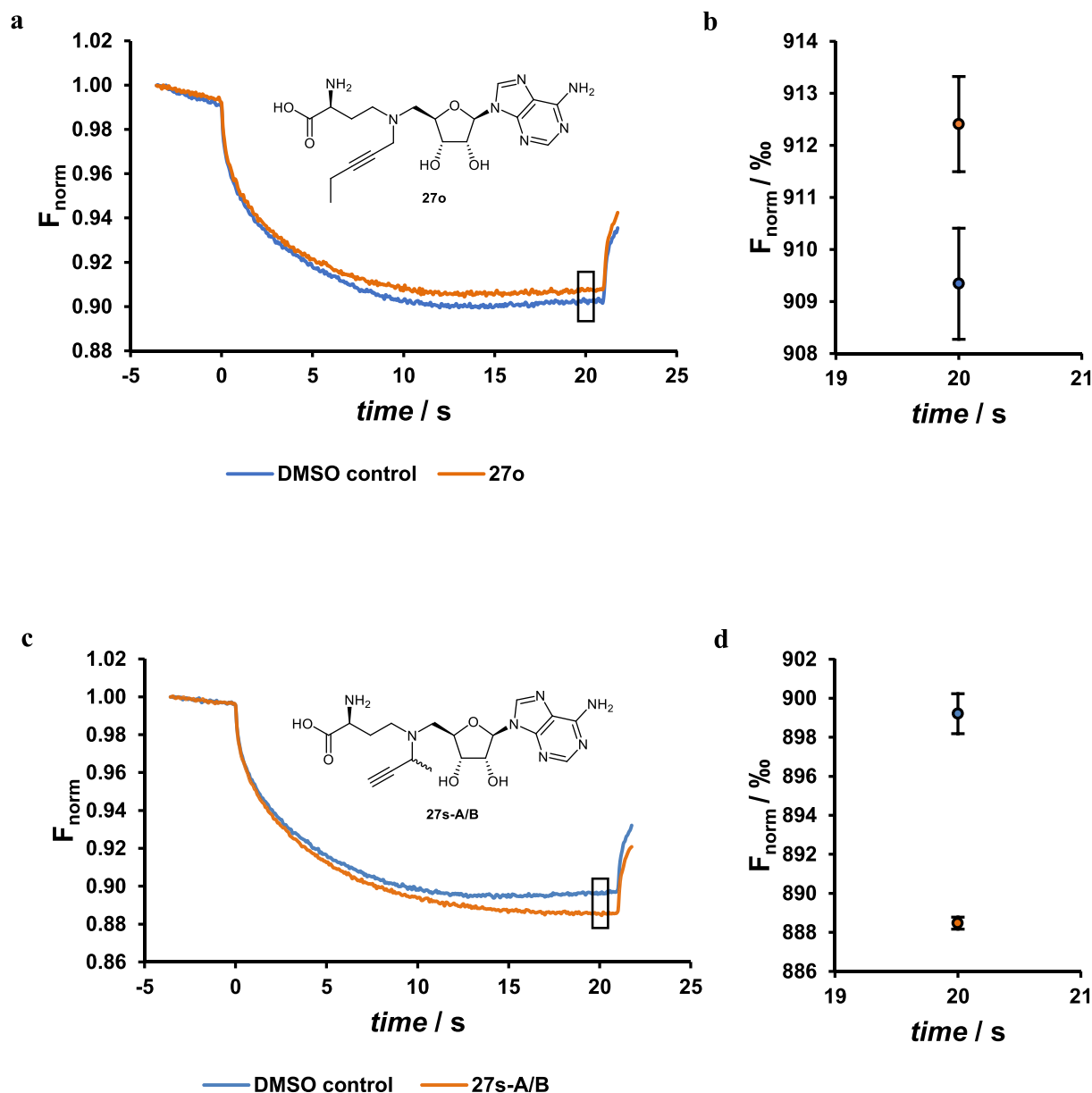


Figure 3. (a, c) MST traces of DNMT2 in absence (control, blue) and presence of 100 μM 27o or 27s-A/B (orange), shown as average of $n = 4$. F_{norm} indicates the fluorescence signal normalized to the initial fluorescence. (b, d) Fluorescence signal at 20 s MST-on time for control and for 27o and 27s-A/B; 99% confident intervals are given.

validated as a suitable method for early discrimination of promising compounds from those with no or low inhibitory activity.

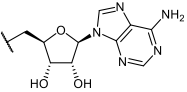
In line with these general findings, both SFG and SAH could be classified as binders in the MST assay and also showed inhibition of the enzymatic activity (ca. 85% at 100 μM). IC_{50} values for SFG and SAH were determined to be $13.2 \pm 0.8 \mu\text{M}$ and $15.8 \pm 1.5 \mu\text{M}$, respectively, while the K_{D} values, determined by ITC, were $7.5 \pm 3.5 \mu\text{M}$ and $13.6 \pm 4.4 \mu\text{M}$.

The truncated SAH analogues 8a and 8b (series 1) exhibited neither DNMT2 binding nor DNMT2 inhibition indicating that both functionalities, that is, the amine and the carboxylic acid,

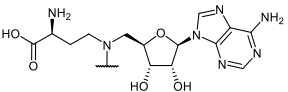
are crucial for an interaction with the enzyme. Within the secondary amine series with aliphatic chains (14a–d, series 2), only the amino acid derivative 14a showed binding to DNMT2, but obviously without affecting the enzymatic activity. Compound 14a was thus investigated at a higher concentration of 1 mM, at which it indeed inhibited the enzyme by 44%, confirming the low affinity toward DNMT2. Also, all the compounds of series 2 with aromatic moieties within the side chain exhibited neither binding to nor inhibition of DNMT2 (17a–e).

Comparably to the amines 14a–c, the amides 21a–d (series 3) contain either an amino acid chain or only the amine or the

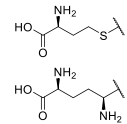
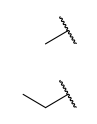
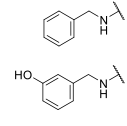
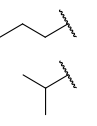
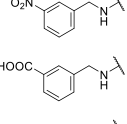
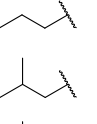
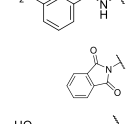
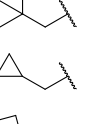
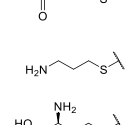
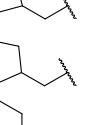
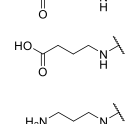
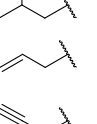
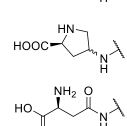
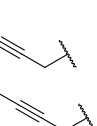
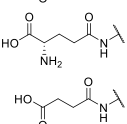
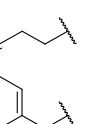
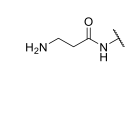
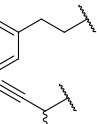
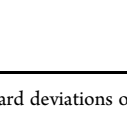
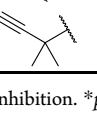






Table 2. Binding of Compounds to DNMT2 as Determined by MST and Inhibition of DNMT2 as Determined in the Tritium Incorporation Assays



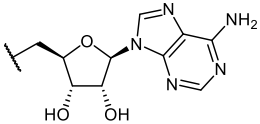
SAH, SFG, 17a–e, 19, 8a–b, 14a–d, 21a–e

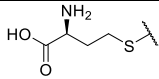
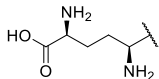
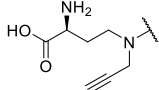
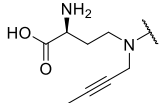
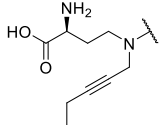
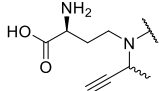


27a–t

Compound		Binding at 100 μ M (MST)	Inhibition at 100 μ M [%] ^a	Compound		Binding at 100 μ M (MST)	Inhibition at 100 μ M [%] ^a
SAH		✓	85.7 \pm 1.7*	27a		✓	30.3 \pm 1.9**
SFG		✓	83.5 \pm 1.1*	27b		✓	n.i.
17a		✗	n.i.	27c		✗	n.i.
17b		✗	n.i.	27d		✓	44.0 \pm 2.7**
17c		✗	n.i.	27e		✗	n.i.
17d		✗	n.i.	27f		✗	n.i.
17e		✗	n.i.	27g		✗	n.i.
19		✗	n.i.	27h		✓	27.5 \pm 0.4*
8a		✗	n.i.	27i		✓	32.0 \pm 2.0*
8b		✗	n.i.	27j		✓	24.5 \pm 8.5*
14a		✓	n.i.	27k		✗	n.i.
14b		✗	n.i.	27l		✓	53.9 \pm 6.4**
14c		✗	n.i.	27m		✓	72.2 \pm 1.2**
14d		✗	n.i.	27n		✓	61.3 \pm 2.1*
21a		✗	n.i.	27o		✓	62.8 \pm 0.1*
21b		✗	n.i.	27p		✓	30.2 \pm 0.8*
21c		✗	n.i.	27q		✓	56.8 \pm 6.8**
21d		✗	n.i.	27r		✓	23.2 \pm 8.2*
				27s-A/B		✓	81.6 \pm 2.1****
				27t		✓	17.3 \pm 1.4***

^aMean values \pm standard deviations of three independent measurements. n.i. = no inhibition. * p < 0.05. ** p < 0.01. *** p < 0.005. **** p < 0.001.

Table 3. K_D Values, as Determined by ITC, and IC_{50} Values of the Most Potent DNMT2 Inhibitors^d


Compound	K_D [μM] ^{a,b}	N	ΔG [$kJ mol^{-1}$]	ΔH [$kJ mol^{-1}$]	$-T\Delta S$ [$kJ mol^{-1}$]	IC_{50} [μM] ^b
SAH 	13.6 ± 4.4^c	1.1 ± 0.1	-27.8 ± 0.8	-55.3 ± 5.8	27.5 ± 6.6	15.8 ± 1.5
SFG 	7.5 ± 3.5	1.3 ± 0.2	-29.3 ± 1.1	-24.5 ± 4.5	-4.8 ± 5.6	13.2 ± 0.8
27m 	11.4 ± 2.4	0.93 ± 0.03	-28.2 ± 0.5	-37.8 ± 3.6	9.6 ± 4.1	77.1 ± 5.3
27n 	10.4 ± 2.2	0.89 ± 0.03	-28.5 ± 0.5	-27.0 ± 1.2	-1.4 ± 3.1	39.7 ± 9.2
27o 	10.5 ± 3.3	1.1 ± 0.1	-28.4 ± 0.8	-27.0 ± 3.6	-1.4 ± 4.4	32.2 ± 4.3
27s-A/B 	8.1 ± 1.4	1.04 ± 0.04	-29.1 ± 0.4	-58.7 ± 4.1	29.6 ± 4.6	12.9 ± 1.9

^aAs determined by ITC. ^bMean values \pm standard deviations of three independent measurements. ^cMean values \pm standard deviations of six independent measurements. ^dN denominates the binding stoichiometry as determined by ITC.

carboxylic acid function with **21b** bearing a glutamate instead of an aspartate residue in the side chain. This should counter the shorter chain length generally found in amides compared to amines or thioethers. All compounds of this series showed neither binding to DNMT2 nor inhibition of the enzymatic activity. The same holds true for phthalimide **19**.

Next, Y-shaped tertiary amines (series 4, Figure 2), which structurally are more related to SFG, were investigated. The "inverse" SFG derivative with a methyl residue at the nitrogen atom (**27a**) displayed binding at $100 \mu M$ and also inhibited the DNMT2 activity by 30%. For the ethyl analogue **27b**, binding could be detected but not DNMT2 inhibition. The *n*-propyl and *n*-butyl derivatives **27c** and **27e** displayed neither binding nor inhibition, suggesting that incorporating linear aliphatic residues at this position is less suitable for the design of DNMT2 inhibitors.

Similar behavior could be observed for the branched derivatives **27d**, **27f**, and **27g**. The smallest derivative, **27d** (*i*-Pr), exhibited binding to the enzyme at $100 \mu M$ in the MST assay and inhibited the enzymatic activity by 44%. The larger

branched derivatives **27f** (*i*-Bu) and **27g** (neopentyl) showed neither binding nor inhibition at $100 \mu M$.

The preference for smaller residues further became evident when investigating cyclic aliphatic residues. For compound **27h**, containing a cyclopropane residue, binding and inhibition (28%) were detected. Analogue **27i** with a four-membered ring was also determined as a binder and a weak inhibitor (32%). Compound **27j**, derivatized with a cyclopentane moiety, displayed binding and weak inhibition (25%). The compound with the largest investigated cyclic aliphatic residue, namely, a cyclohexane ring (**27k**), showed neither inhibition nor binding at $100 \mu M$.

The best inhibitors of the methylation activity of DNMT2 were found within the series of the Y-shaped amines that contain an unsaturated residue. The allylic derivative **27l** was determined as a binder by MST and also inhibited the DNMT2 activity by 54%. Similar behavior was observed for the aromatic compounds **27q** and **27r**, with benzyl or a phenethyl groups, respectively. Both compounds bound to the enzyme at a concentration of $100 \mu M$. Moreover, both compounds reduced the enzymatic activity at $100 \mu M$ by ca.

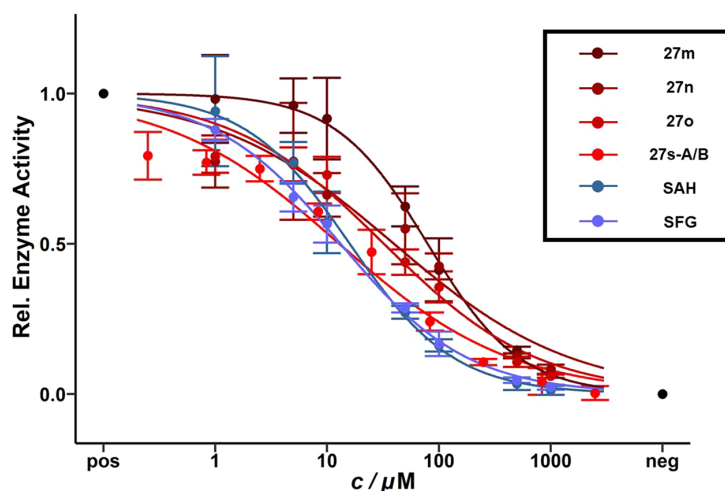


Figure 4. Dose–response curves for determination of the IC_{50} values for DNMT2 inhibition by the investigated compounds as determined by the tritium incorporation assay. Error bars refer to biological triplicates; “pos” describes the relative enzyme activity without compound and “neg” the relative enzyme activity without addition of substrate $tRNA^{Asp}$.

57% and 23%, respectively. The propargylic derivative **27m** also was found to bind to the enzyme at $100 \mu M$ and inhibited it by 72%.

For this compound, we determined the IC_{50} (Figure 4) and K_D values (Figure 5), using the tritium incorporation assay and ITC. While the K_D value of $11.4 \pm 2.4 \mu M$ was very similar to that of the natural products SAH and SFG, the IC_{50} value of $77.1 \pm 5.5 \mu M$ was higher. In order to identify the possible binding site of **27m**, a replacement titration via ITC was performed. For this purpose, DNMT2 was preincubated with **27m** and titrated against SAH. No binding enthalpy was detected suggesting, that **27m** and SAH address the same binding site.

In the next step, **27m** was further derivatized to attain the first structure–activity relationship of this compound class. The propargyl residue was exchanged with a 3-butynyl moiety (**27p**). This compound was found to bind to DNMT2, but only led to weak inhibition of the enzyme (30%) at $100 \mu M$. Also, a methyl or ethyl group was attached to the triple bond. The corresponding compounds **27n** and **27o** were both identified as binders by MST. They also inhibited DNMT2 by ca. 62%. The determined IC_{50} values of $39.7 \pm 9.2 \mu M$ and $32.2 \pm 4.3 \mu M$ (Figure 4) were in the same range as those found for SAH and SFG and slightly better than that of **27m**. With $10.4 \pm 2.2 \mu M$ for **27n** and $10.5 \pm 3.3 \mu M$ for **27o**, the K_D values, as determined by ITC, were also in the same range.

Since both **27d** and **27m** exhibited substantial inhibition at $100 \mu M$, both structures were merged, leading to **27s-A/B** and **27t**. These compounds were identified as binders in the MST assay. While **27t** reduced the enzymatic activity only by 17%, **27s-A/B** inhibited DNMT2 around 82% at $100 \mu M$. The IC_{50} and K_D values (Figure 5) of $12.9 \pm 1.9 \mu M$ and $8.1 \pm 1.4 \mu M$ were comparable to those of SAH and SFG, and the IC_{50} value was found to be nearly 1 order of magnitude lower than that of the unsubstituted propargyl derivative **27m**.

Compound **27s-A/B** is a mixture of two epimers, with either (S) or (R) configuration of the stereocenter within the alkyl side chain. To assess if the single isomers exhibit different biological activities, the separated epimers **27s-A** and **27s-B** were analyzed regarding the inhibition of DNMT2. At 86% and 82%, the inhibition of both epimers was comparable and well in the range

of the 1:1 mixture **27s-A/B** (82% inhibition at $100 \mu M$) indicating no different activities. An exact assignment of the separated epimers to the R or S derivatives was not possible by NMR, but since no preference for one epimer was observed, this was not investigated further.

With the exception of SAH and **27s-A/B**, the K_D values for the tested compounds (SAH, SFG, **27m**, **27n**, **27o**, **27s-A/B**) are generally lower than the IC_{50} values with ratios of $K_D/IC_{50} \approx 2$ (SFG), 7 (**27m**), 4 (**27n**), 3 (**27o**); that is, binding to DNMT2 does not lead to a “productive” inhibition to the same degree. This may be due to the different conditions used in both assays leading to slightly different hydration shells or surface charges, which might result in different binding behaviors. Furthermore, IC_{50} determination is strongly dependent on the experimental conditions, potentially adding to this bias.⁵⁵ The most profound difference between the assays is the lack of the substrate $tRNA^{Asp}$ in ITC measurements. Binding of such a large and strongly charged molecule might induce conformational changes in the enzyme and is probably altering its surface charge significantly. Such differences would explain distinct binding modes of compounds in the presence or absence of RNA.

Our data clearly demonstrated that the amino acid residue is crucial for the interaction with DNMT2. This could be shown by investigating derivatives with aromatic linkers and with analogues lacking either the amino or carboxylic acid function. Exchange of the sulfur atom of SAH with secondary amines or amides abolished the activity of the compounds. With tertiary Y-shaped amines (series 4 compounds) however, DNMT2 activity could be successfully inhibited. In general, smaller residues were superior. The strongest inhibition could be achieved by unsaturated residues, with the propargylic derivatives **27m**, **27n**, **27o**, and **27s-A/B** being the most promising compounds. Remarkably, **27s-A/B**, which resulted from merging the most potent aliphatic compound **27d** with the propargylic derivative **27m**, was the most potent inhibitor of DNMT2, with IC_{50} and K_D values being similar to those of SAH and SFG. The thermodynamic data collected with the ITC measurements indicated that **27s-A/B** is the most enthalpically driven inhibitor ($-58.7 \text{ kJ mol}^{-1}$) within this study, even more enthalpically driven than SAH ($-55.3 \text{ kJ mol}^{-1}$). On the other hand, SFG

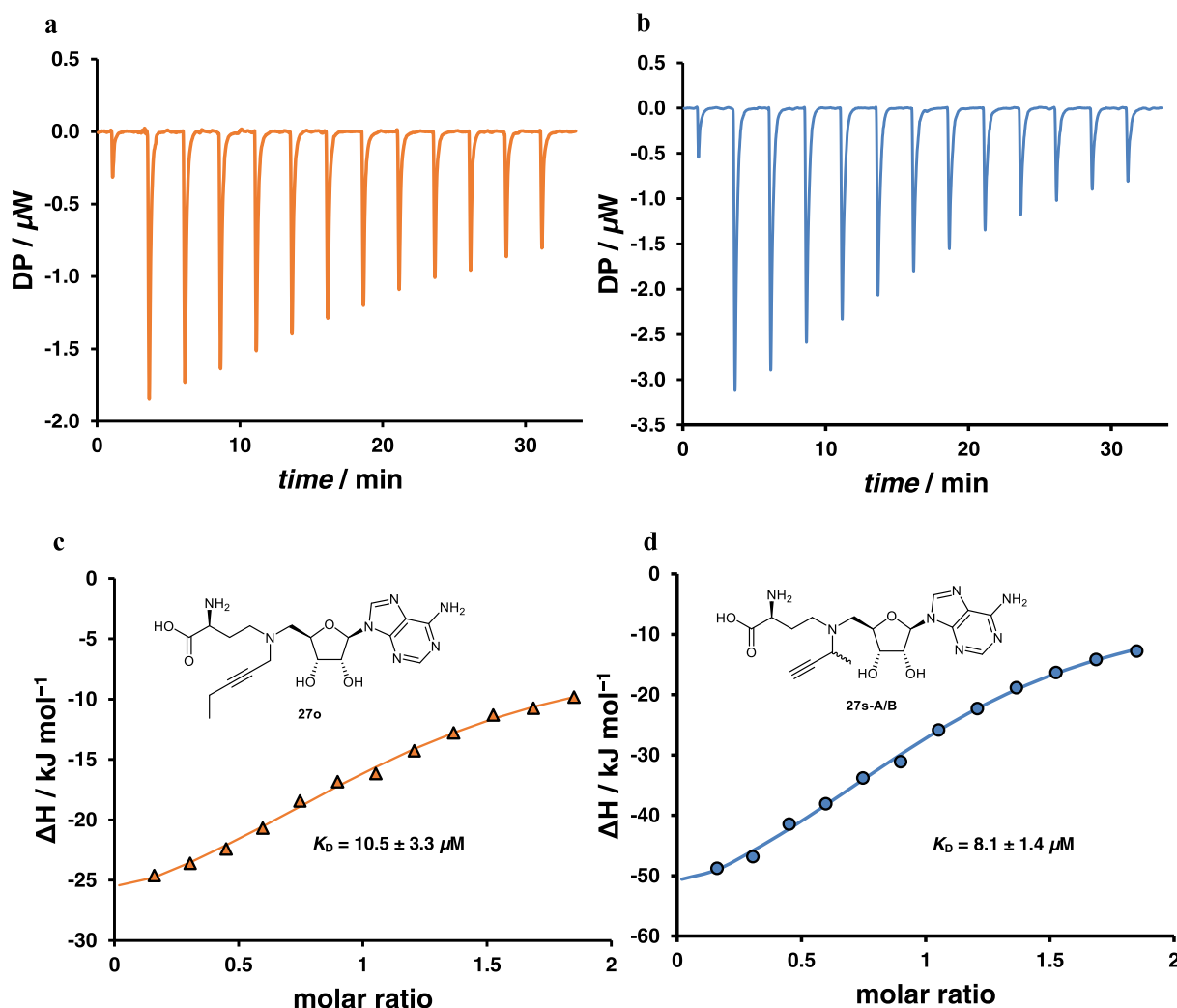


Figure 5. ITC thermograms (a, b) and titration curve fittings (c, d) of 27o (a, c) and 27s-A/B (b, d); K_D values, thermodynamic data, and binding stoichiometry are listed in Table 3.

Table 4. Selectivity Profiles of SAH, SFG, and Several DNMT2 Inhibitors against a Selection of SAM-Dependent MTases^a

compound	DNMT3A-3L ^b	NSUN2 ^b	NSUN6 ^b	G9a ^b	DNMT2 ^b
SAH	96.7 ± 2.8	97.3 ± 0.4	99.6 ± 4.6	94.3 ± 1.2	85.7 ± 1.7
SFG	98.0 ± 3.2	77.1 ± 2.2	70.2 ± 1.8	43.0 ± 9.8	83.5 ± 1.1
27m	97.6 ± 5.6	n.i.	25.9 ± 3.5	22.8 ± 0.3 ^c	72.2 ± 1.2
27n	93.9 ± 2.1	n.i.	12.9 ± 7.6	37.6 ± 5.9	61.3 ± 2.1
27o	95.3 ± 1.6	n.i.	22.7 ± 4.9	32.0 ± 14.5	62.8 ± 0.1
27s-A/B	84.2 ± 0.7	n.i.	n.i.	71.0 ± 5.6	81.6 ± 2.1

^aThe inhibition of the enzymes was investigated at 100 μ M inhibitor concentration in tritium incorporation assays. ^bMean values \pm standard deviations of three independent measurements. ^cMean value \pm standard deviation of two independent measurements. n.i. = no inhibition.

benefits the most from an entropic gain (-4.8 kJ mol^{-1}). Although 27m showed a substantial gain in enthalpy (-37.8 kJ mol^{-1}), this effect is partially compensated by a loss of entropy (9.6 kJ mol^{-1}). The same applies for 27s-A/B with an enthalpic gain of -58.7 kJ mol^{-1} but also a considerable loss of entropy (29.6 kJ mol^{-1}). For the elongated propargylic derivatives 27n and 27o, a remarkable gain in enthalpy (-27.0 kJ mol^{-1}) and a slight gain in entropy (-1.4 kJ mol^{-1}) could be detected.

Selectivity toward Different SAM-Dependent MTases.

Due to the close structural resemblance of the synthesized inhibitors to the ubiquitous MTase cosubstrate SAM, selectivity toward other SAM-dependent MTases is of major concern. The compounds listed in Table 4, including the natural products SAH and SFG, were subjected to tritium incorporation enzyme assays at a concentration of 100 μ M with several different MTases to assess their selectivity profiles. The chosen MTases

included DNMT3A-3L¹⁸ due to its close structural resemblance to DNMT2, the functionally related tRNA m⁵C MTases NSUN2 and NSUN6,^{56–58} as well as the functionally unrelated but SAM-dependent histone MTase G9a.⁵⁹

All investigated compounds showed better inhibition of the DNMT3A-3L construct compared to DNMT2. SAH and SFG both displayed around 100% inhibition at 100 μ M, while **27m**, **27n**, and **27o** reduced the enzyme's activity by 98%, 94%, and 95%, respectively. At 84%, the inhibition by **27s-A/B** was the weakest one in this comparison exhibiting similar inhibition of DNMT2 and DNMT3A-3L.

SAH inhibited both NSUN2 and NSUN6 nearly to 100%, while SFG displayed weaker inhibition of 77% and 70%, respectively. All investigated synthetic compounds did not significantly inhibit NSUN2. NSUN6 activity was only weakly reduced by **27m**, **27n**, and **27o**, while **27s-A/B** inhibited neither NSUN2 nor NSUN6.

The G9a activity was reduced by all investigated inhibitors. SAH and SFG inhibited G9a by 94% and 43%, respectively. While **27m**, **27n**, and **27o** inhibited the histone MTase only weakly (23–38%), **27s-A/B** displayed stronger inhibition (71%).

The profound inhibition of DNMT3A-3L by all synthetic compounds clearly demonstrates that the compounds are not selective in this regard. Due to the high structural similarity between DNMT2 and DNMT3A this is not surprising, especially if one considers the structural similarity of the synthetic inhibitors to the ubiquitous cofactor SAM.

Inhibition of DNMT3A by SAH and SFG was reported with IC₅₀ values in the low- to sub-micromolar range,^{60,61} supporting the obtained results. High inhibition by SAH was also determined for the closely related DNMT3B (IC₅₀ < 500 nM).^{50,51}

In the comparison with the functionally related enzymes NSUN2 and NSUN6, however, the investigated compounds revealed remarkable selectivity. The most active synthetic DNMT2 inhibitor, **27s-A/B**, was not active at 100 μ M against NSUN2 and NSUN6. This might be attributed to the Y-shaped structure, which is also suggested by the slight preference of SAH over SFG by both enzymes.

The inhibition of G9a by SFG was weak compared to other MTases with only around 40% inhibition at 100 μ M. However, reported inhibition of G9a by SFG varies strongly, with IC₅₀ values ranging from the low micromolar range to over 500 μ M, and therefore this observation is not surprising.^{62–64} Furthermore, the reported trend of inhibition by SAH and SFG, with more profound inhibition by SAH (94% at 100 μ M) was reproduced.⁶³

Compounds **27m**, **27n**, and **27o** exhibited only weak inhibition of G9a, which is also lower compared to that of DNMT2. On the other hand, **27s-A/B** reduced G9a activity strongly and comparably to DNMT2.

As expected, the designed DNMT2 inhibitors do not display very pronounced selectivity, most likely due to their close resemblance to the natural cofactor SAM. Especially for DNMT3A-3L, this problem becomes very evident since both proteins share conserved structural motives. Since DNMT1 shares a comparable high structural conservation, a similarly unselective behavior of the compounds can be anticipated.¹⁸ This holds true especially when considering reported inhibition for SFG, SAH, and their most potent synthetic analogues toward DNMT1, which exhibit IC₅₀ values in the low- to sub-micromolar range.^{50,51,65,66} Also, for G9a, no profound

preference of the compounds toward DNMT2 was observed, particularly not for **27s-A/B**, the best synthetic DNMT2 inhibitor so far. Surprisingly, in the comparison with NSUN2 and NSUN6, no or only weak inhibition by the synthetic inhibitors was observed, proving that at least partial selectivity was achieved.

Inhibition of tRNA Methylation In Cellulo. To first determine the hydrolysis of the ethyl ester in aqueous solution at physiological pH value, compound **28-A** (100 μ M) was dissolved in 100 mM TRIS buffer, pH 7.4, and incubated at 37 °C. The amount of hydrolysis product was determined by LC-MS after 3 h, followed by 6 h intervals (Figure 6).

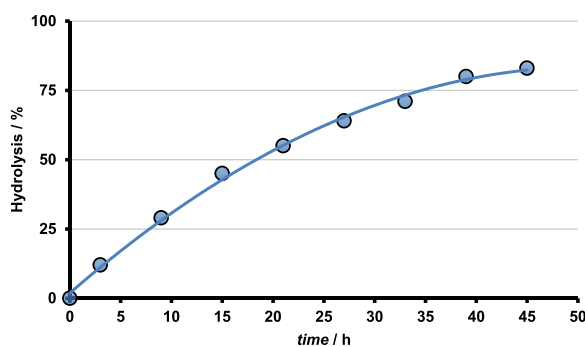


Figure 6. Hydrolysis of prodrug **28-A** (100 μ M) in 100 mM TRIS buffer at pH 7.4 and 37 °C as determined by LC-MS.

Figure 6 shows that the ethyl ester is hydrolyzed to ca. 60% during the first 24 h of incubation.

The most promising compound **27s-A/B**, its ester derivative **28-A/B**, SFG, and a negative control (**27c**) were tested in a cellular context. Since no preference for one compound was identified (*vide supra*), a mixture of the epimers was used both in case of **27s** and **28**.

First, the cell toxicities were investigated in cell viability assays. Therefore, **27s-A/B**, SFG, **28-A/B**, and **27c** were subjected to MTT assays. All compounds showed negligible toxicity against HEK-293 cells up to the highest concentration in the assay, revealing 50% cytotoxic concentration (CC₅₀) values >500 μ M. According to these results, a concentration of 100 μ M was chosen for cell-based experiments. Next, the inhibitors' potencies for modulating DNMT2 activity was elucidated in HEK-293 cells. SFG and derivative **27s-A/B** were chosen as representative molecules. The structurally related compound **27c** containing a propyl side chain was chosen as a negative control since it did not show inhibition of DNMT2 *in vitro*. For estimating inhibition *in vivo*, HEK-293 cells were incubated with 100 μ M compound dissolved in DMSO or with DMSO only as a control for 24 h at 37 °C. Total RNA was extracted from treated cells, and subsequently total tRNA was isolated by gel electrophoresis. To determine m⁵C levels, LC-MS/MS and bisulfite sequencing were conducted. LC-MS/MS analysis was performed using total tRNA. This method allows highly accurate quantification, but information on sequence is lost as the RNA is digested down to nucleosides.⁶⁷ Therefore, bisulfite sequencing was chosen as an orthogonal method being capable of analyzing RNA on nucleotide level while the information about its sequence context is maintained.⁶⁸ With this approach, changes in m⁵C levels at position C38 of tRNA^{Asp}, which are attributed to DNMT2 activity, can be mapped.

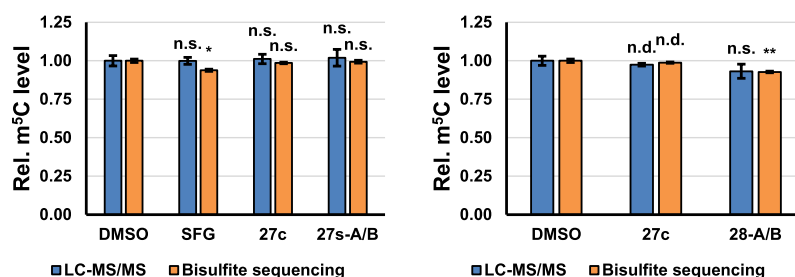


Figure 7. (a) Relative m⁵C levels in HEK-293 cells after treatment with 100 μ M SFG, 27c, or 27s-A/B for 24 h at 37 $^{\circ}$ C. Displayed are relative m⁵C levels normalized to a DMSO control as elucidated by LC-MS/MS (blue) and bisulfite sequencing (orange). Error bars refer to three independent biological replicates. * p < 0.05, n.s. = not significant. (b) Relative m⁵C levels in HEK-293 cells after treatment with 100 μ M 27c or 28-A/B for 24 h at 37 $^{\circ}$ C. Displayed are relative m⁵C levels normalized to a DMSO control as elucidated by LC-MS/MS (blue) and bisulfite sequencing (orange). Error bars refer to four (DMSO, 28-A/B) or two (27c) independent biological replicates, ** p < 0.01, n.s. = not significant, n.d. = significance was not determined due to low number of replicates.

Bisulfite sequencing and LC-MS/MS analysis did not reveal any significant decrease in m⁵C levels relative to the DMSO control for the synthetic compounds 27c and 27s-A/B as shown in Figure 7a. Treatment with SFG on the other hand slightly reduced the m⁵C level down to 94% according to bisulfite sequencing, whereas no significant change could be observed in LC-MS/MS measurements. According to in vitro enzyme assays, 27s-A/B is able to bind and inhibit DNMT2 with comparable affinity as SFG. Changing the in vitro system with its limited components to a more complex cellular environment comes along with an increased number of possible target MTases, as well as the process of cell penetration. Consequently, the overall inhibitor concentration that is accessible for DNMT2 is significantly decreased. Thus, a prodrug approach was followed by converting the acidic moiety of 27s-A/B into the ethyl ester 28-A/B. The enhanced lipophilicity is expected to increase cell permeability, while the ester group can be cleaved by esterases in cellulo to yield the active compound 27s-A/B.⁶⁹

In vitro activity of ester 28-A/B was elucidated using the tritium incorporation assay revealing no significant inhibition at a concentration of 100 μ M. To assess the prodrug's activity in cellulo, HEK-293 cells were treated with the compound as described above.

As depicted in Figure 7b, the usage of ester 28-A/B led to a slight reduction in m⁵C levels in LC-MS/MS and bisulfite sequencing experiments, which was not significant for LC-MS/MS experiments but was significant for the latter ones.

Overall, it can be observed that the investigated compounds are not able to inhibit DNMT2 significantly in a cellular environment. But there is a good perspective in optimizing their physicochemical properties by applying a diverse range of prodrug approaches. Compared to the free acid 27s-A/B, its ester derivative 28-A/B seems to slightly reduce the m⁵C levels indicating an improvement in its cellular concentration. However, this reduction was only perceived when applying bisulfite sequencing. Accordingly, the well-known pan MTase inhibitor SFG also showed a minor decrease in the modification level, only observable when evaluated by bisulfite sequencing.

Among others, possible explanations could be that studied compounds compromise multiple charged functional groups hindering permeation of the molecule through the cell membrane in a quantitative manner. Moreover, differences are present between bisulfite sequencing and LC-MS/MS analysis, which are possibly due to their principle of analyzing RNA: bisulfite sequencing is capable of identifying changes in the m⁵C

level specific to position 38, which is targeted by DNMT2, whereas in LC-MS/MS measurements the determined m⁵C level is restricted to the input RNA and loses its sequence information. Consequently, m⁵C levels in LC-MS/MS data include the total amount of methylated cytidines independent from their position and target enzyme. In combination with the weak inhibitory effect in cellulo, no significant reduction in m⁵C levels could be detected by LC-MS/MS whereas this was possible with bisulfite sequencing.

Cell Permeabilities. To determine the cell permeabilities of acid 27s and its supposed ester prodrug 28, CaCo-2 permeability assays were performed. A CaCo-2 monolayer separating a donor and acceptor compartment was treated with either 27s-A/B or 28-B at 37 $^{\circ}$ C for 24 h, and the solutions from each compartment were analyzed by LC-MS. Analyses of the solutions from the assays with 28-B revealed 20% of ester 28-B and 78% of acid in the donor compartment, whereas the acceptor compartment consisted of 2% acid. In the assays with the acid 27s-A/B, only traces of the compound (0.6%) could be detected in the acceptor compartment. In conclusion, neither 27s-A/B nor 28-B was found to pass the cell barrier in significant amounts. In the case of the ester 28-B, this might be due to its rapid hydrolysis rate observed under the tested conditions. This is in accordance with the results of the assays to detect inhibition of tRNA methylation in cellulo (see above): these assays showed very low, but significant inhibition of tRNA methylation in cells by the ester prodrug but not by the acid.

For stronger cellular effects, future investigations to obtain more potent inhibitors and to optimize the compounds' membrane permeabilities, for example, by strategies yielding prodrugs less susceptible to hydrolysis, are needed.

Structure–Activity Relationship (SAR) Elucidation by Molecular Docking and Solvent Analysis.

To explain the SAR observed in the MST and tritium incorporation assays, molecular docking studies were performed. The chosen docking setup was able to reproduce the crystallographic binding mode of SAH (PDB-ID 1G55,³⁰ redocking RMSD = 0.77 \AA , FlexX-score = -42.0 kJ mol⁻¹) indicating its ability to predict realistic binding modes. Due to the common SAH-related substructure of the molecules reported herein, binding poses showed strong overlap with the reference ligand as well as an overall narrow score distribution complicating discrimination of binders and nonbinders simply by docking score (Table S1). However, some general trends could be observed. For Y-shaped ligands (27a–t, series 4), orientation of the aliphatic side chains toward the

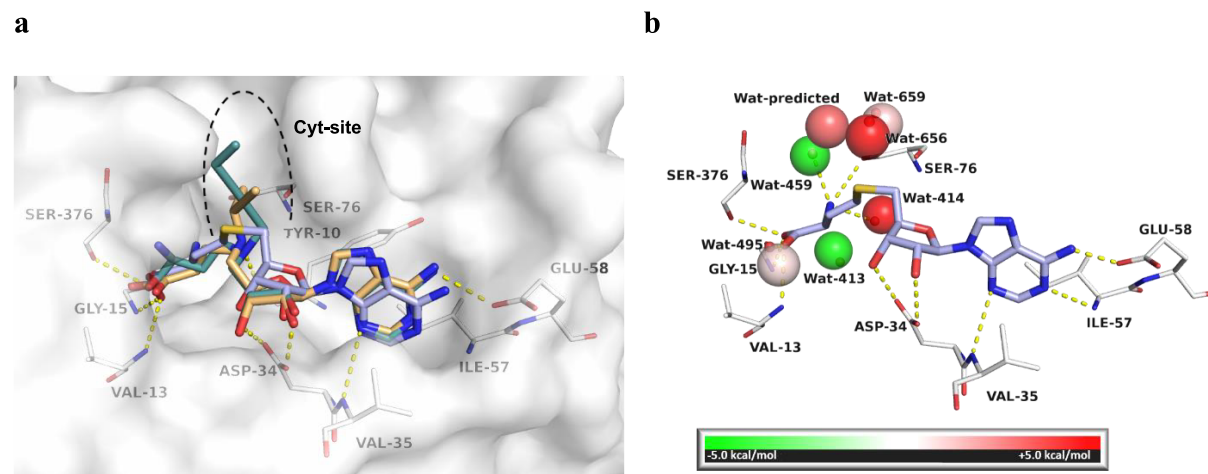


Figure 8. (a) Predicted binding modes of 27s-A/B ((*R*)-epimer, light orange carbon atoms) and 27o (light teal carbon atoms) in complex with hDNMT2 (white carbon atoms and surface) in superposition with crystallographic ligand SAH (light blue carbon atoms). (b) 3D-RISM predicted hydration sites and corresponding water molecules within 4 Å of the SAH homocysteine substructure colored by estimated interaction energy. Identical point of view for panels a and b. For clear view, only residues forming polar interactions (yellow dashes) are depicted as lines and labeled. PDB-ID 1G55. Figures were made with PyMOL.⁷¹

tRNA cytidine binding site was observed (Figure 8a) according to the design hypothesis and described by a favorable score for binders (in order of ascending FlexX-score -44.2 to -39.2 kJ mol^{-1} , Table S1) 27m, 27a, 27r, 27p, 27o, 27q, 27l, 27b, 27h, and 27n and a slightly lower score for bulky, potentially with the pocket clashing, nonbinders 27f, 27k, and 27g (FlexX score -28.5 to -38.5 kJ mol^{-1} , Table S1). This nicely agrees with the experimental results (Table 2, Table 3) but underestimates the affinity of 27s-A/B (-37.0 kJ mol^{-1} for the *R*- and -34.5 kJ mol^{-1} for the *S*-epimer) and the weak binder 27t (-24.9 kJ mol^{-1}). Also, in agreement with the experiments, removal of the acidic moiety resulted in a reduced score (8b FlexX-score -30.4 kJ mol^{-1} , 14c -36.4 kJ mol^{-1} , 21d -35.7 kJ mol^{-1}). Differently from the MST and tritium assay results, removal of the primary amine of the homocysteine moiety was tolerated in the docking studies (8a FlexX-score -42.1 kJ mol^{-1} , 17d -40.2 kJ mol^{-1} , 21c -49.0 kJ mol^{-1}), as was an amide linker (21a -41.4 kJ mol^{-1} , 21b -51.1 kJ mol^{-1}). However, it seems reasonable that basic amines are more likely to mimic the charged sulfur atom of the native substrate SAM and bind with higher affinity compared to uncharged linkers like amides. To further elucidate the discrepancies between docking and experiment, solvent analysis was performed using the three-dimensional reference interaction site model (3D-RISM, Table S2) approach. The detailed analysis of hydration sites within 4 Å of the derivatized homocysteine substructure of SAH demonstrated that crystallographic water molecule positions could be reproduced with high accuracy (Figure 8b). This also includes water molecules being part of the docking setup (Wat-413, Wat-414, Wat-459, and Wat-495) forming three polar interactions with the enzyme or ligand with RMSD between crystallographic positions and 3D-RISM-predicted hydration sites within 0.16–0.93 Å. In close proximity to the primary amine, two hydration sites corresponding to Wat-459 and Wat-413 were further predicted to be highly stable (predicted ΔG of -7.2 and -10.8 kcal mol^{-1} , respectively). This might hold the explanation for the importance of the primary amine group as removal would disrupt the H-bond and water network potentially destabilizing the two hydration sites. Additionally to Wat-659 and Wat-656,

one more hydration site (“Wat-predicted”, Figure 8b) not corresponding to a crystallographic water molecule was identified in the region toward the cytidine binding site. All three hydration sites are rather unfavorable (predicted ΔG of $+0.6$, $+3.3$ and $+5.1$ kcal mol^{-1} , respectively), and removal of the corresponding water molecules by aliphatic groups like in the Y-shaped molecules of series 4 (27a–t), except those with too bulky groups like in 27f, 27g, and 27k, should result in a beneficial desolvation and increased potency. This might also hold an explanation for the more favorable temperature-dependent entropy contribution to binding of 27m, 27n, and 27o ($-T\Delta S$ of $+9.6$, -1.4 and -1.4 kJ mol^{-1} , respectively, Table 3) compared to SAH ($+27.5$ kJ mol^{-1}). While desolvation of a hydrophobic sub-pocket is usually accompanied by a gain (at least a partial one) of entropy,⁷⁰ SAH lacks a substituent to displace these water molecules. This might also account for 27s-A/B whose substituent might not reach deep enough into that sub-pocket (Figure 8a).

Crystal structure analysis indicated that the higher potency of 27m–o against DNMT2 over NSUN6 might be attributed to a close shape-complementarity without larger gaps in the cytidine sub-pocket, which was found to be larger and open in NSUN6 (Figures S239 and S240).⁷² While for NSUN2 no structure is available in the PDB, the most sequentially similar proteins are bacterial methyltransferases from *Pyrococcus horikoshii*, *Enterococcus faecium* or *Methanocaldococcus jannaschii* sharing only 29–32% sequence identity. Hence an AlphaFold2-derived homology model^{73,74} of NSUN2 was analyzed. It revealed both structural and sequential differences between NSUN2 and DNMT2, especially within the binding site, where only 17% identical and 30% similar residues were found. Additionally, an α helix forming one site of the cytidine binding site in DNMT2 (residues V366–L377) is not present in NSUN2 and NSUN6 highlighting a variety of potential selectivity determining features (Figure S241). Differently DNMT2 and DNMT3A share a highly similar fold (Figure S242) and slightly higher sequence similarity of 39%. However, within the binding site, the interaction profile is nearly identical (Figure S243) as is that of the cytidine-site residues. Nevertheless, some of the differences

like L377/W893, N375/R891 or S76/G707 might hold opportunities for selective ligand design.

CONCLUSION

In this study, we introduced new inhibitors of DNMT2 based on the adenosyl scaffold as novel examples for non-natural m⁵C RNA MTase inhibitors, outclassing previously described synthetic specimens but not the natural compounds SAH and SFG.⁵³ Amino and amide analogues of SAH were designed, synthesized, and screened using MST and an enzymatic tritium incorporation assay. A clear correlation between the binding assay (MST) and the inhibition assay (³H incorporation assays) with a high predictivity of the MST was found. Thus, in future studies, the laborious, time-consuming, and expensive tritium-based activity assay can be omitted for initial screenings and can be applied for hit validation. The most promising hits discovered in the present study were further investigated using ITC and detailed enzymatic assays. These revealed the compounds possessing similar binding and inhibition constants as SAH and SFG. As expected, these compounds compete with SAH for the same binding pocket. Our findings clearly indicated the need for a complete amino acid side chain for potent inhibition. Furthermore, a Y-shaped structure with a third substituent at the nitrogen atom was shown to be essential. This structure–activity relationship (SAR) is nicely backed by a computational analysis, which predicted the replacement of unfavorable water molecules by this third residue. As substituents at this position, small aliphatic moieties are favored, with alkyne groups being most potent. In summary, our findings will contribute to the further development of DNMT2 inhibitors and tool compounds, which might help to shed light on the underlying functions of this enzyme in the development of cancer or in epigenetic inheritance.

EXPERIMENTAL SECTION

Syntheses. General Information. All reagents and solvents were commercial grade and used without further purification. Reaction progress was monitored by thin-layer chromatography using Alugram Xtra F254 silica plates from Machery-Nagel. Column chromatography was performed with silica gel (40–63 μm) from Machery-Nagel. NMR spectra were recorded on Bruker Fourier 300 at 300 MHz. Chemical shifts are indicated in parts per million (ppm), with the solvent resonance (CDCl₃, DMSO-*d*₆ or CD₃OD from Deutero GmbH) as internal standard. The identities and purities of final compounds were determined by combined HPLC/ESI-MS analysis using an Agilent 1100 series HPLC system with an Agilent Zorbax SB-Aq (4.6 × 150 mm²; mobile phase MeCN/H₂O = 20:80 + 0.1% HCOOH; flow rate 0.7 mL/min) column. Samples were applied using 5 μL injection with quantitation by AUC at 254 nm. Fourier-transformed ATR-corrected IR spectra were measured on an Avatar 330 single crystal spectrometer from ThermoNicolet. Melting points (uncorrected) were measured with an MPM-H3 using semiopen capillaries. Specific rotations [α]_D²⁰ were determined with a Krüss P3000 polarimeter and are given in deg cm³ g⁻¹ dm⁻¹. The purity of all compounds tested in biological assays was ≥95% as determined by LC-MS.

Methyl 4-Bromobutanoate (2). 4-Bromobutyric acid (2.06 g, 11.98 mmol, 1.0 equiv) was dissolved in methanol (20 mL); then thionyl chloride was added dropwise while stirring the solution. The mixture was kept stirring overnight at rt. The solvent was evaporated under reduced pressure at 40 °C, and the residue was dissolved in ethyl acetate (20 mL). After being washed with saturated NaHCO₃ solution (3 × 10 mL) and with brine (10 mL), the organic phase was dried over anhydrous Na₂SO₄. Evaporation of the solvent under reduced pressure at 40 °C afforded the desired product as an orange oil (1.72 g, 9.50 mmol, 79%). ¹H NMR (300 MHz, CDCl₃): δ/ppm = 3.68 (s, 3H), 3.45 (t, *J* = 6.4 Hz, 2H), 2.50 (t, *J* = 7.1 Hz, 1H), 2.23–2.09 (m, 2H). ¹³C

NMR (75 MHz, CDCl₃): δ/ppm = 173.0, 51.7, 32.7, 32.2, 27.8. FT-IR: ν /cm⁻¹ = 2952, 2028, 1733, 1436, 1367, 1313, 1250, 1206, 1172, 1131, 1060, 1026, 994, 874, 779.

tert-Butyl (3-Bromopropyl)carbamate (3). 3-Bromopropylamine hydrobromide (1.01 g, 4.57 mmol, 1.0 equiv), di-*tert*-butyl dicarbonate (1.20 g, 5.48 mmol, 1.2 equiv), and triethylamine (1.4 mL, 10.05 mmol, 2.2 equiv) were suspended in ethyl acetate (20 mL), and the mixture was stirred overnight at rt. The mixture was then washed with saturated NaHCO₃ solution (3 × 10 mL), 1 M HCl (3 × 10 mL), and brine (10 mL), and the organic phase was dried over anhydrous Na₂SO₄. Evaporation of the solvent under reduced pressure at 40 °C afforded the desired product as a colorless solid (707 mg, 3.22 mmol, 70%). ¹H NMR (300 MHz, CDCl₃): δ/ppm = 3.43 (t, *J* = 6.5 Hz, 2H), 3.26 (t, *J* = 6.6 Hz, 2H), 2.09–1.98 (m, 2H), 1.43 (s, 9H). ¹³C NMR (75 MHz, CDCl₃): δ/ppm = 156.0, 79.5, 39.1, 32.7, 30.8, 28.4. FT-IR: ν /cm⁻¹ = 3375, 2980, 2950, 1682, 1520, 1436, 1387, 1363, 1340, 1295, 1278, 1247, 1221, 1161, 1134, 1086, 1040, 1030, 991, 916, 873. Mp: 39–42 °C.

S-(((3*aS*,4*S*,6*R*,6*aR*)-6-(6-Amino-9*H*-purin-9-yl)-2,2-dimethyltetrahydrofuro[3,4-*d*][1,3]dioxol-4-yl)methyl) Ethane-thioate (6). According to the method of Pignot et al.,⁷⁵ a solution of triphenylphosphine (1.69 g, 6.44 mmol, 2.2 equiv) in dry THF (10 mL) was cooled to 0 °C in an ice bath. Then DIAD (1.26 mL, 6.44 mmol, 2.2 equiv) was added dropwise while stirring, over a period of 10 min. The resulting suspension was stirred for an additional 30 min while keeping it at 0 °C. Compound 5 (902 mg, 2.93 mmol, 1.0 equiv) was added, and the mixture was stirred and cooled for 15 min. Thioacetic acid (0.46 mL, 6.44 mmol, 2.2 equiv) was diluted with dry THF (2 mL) and added dropwise to the suspension, while stirring. The resulting mixture was stirred at 0 °C for an additional hour and subsequently overnight at rt. The solvent was removed under reduced pressure at 40 °C, and the residue was purified by column chromatography (DCM/MeOH = 97:3) to afford the desired product as a pale-yellow solid (1.02 g, 2.79 mmol, 95%). ¹H NMR (300 MHz, CD₃OD): δ/ppm = δ 8.25 (s, 1H), 8.24 (s, 1*H*), 6.18 (d, *J* = 2.3 Hz, 1H), 5.53 (dd, *J* = 6.4, 2.3 Hz, 1H), 4.99 (dd, *J* = 6.4, 3.1 Hz, 1H), 4.26 (td, *J* = 6.9, 3.1 Hz, 1H), 3.29–3.12 (m, 2H), 2.32 (s, 3H), 1.57 (s, 3H), 1.37 (s, 3H). ¹³C NMR (75 MHz, CD₃OD): δ/ppm = 194.2, 155.3, 151.9, 148.1, 139.7, 118.5, 113.4, 89.5, 85.0, 83.2, 82.8, 30.0, 28.3, 25.3, 23.4. FT-IR: ν /cm⁻¹ = 3332, 3183, 2987, 2936, 1690, 1640, 1597, 1578, 1475, 1423, 1373, 1329, 1296, 1237, 1206, 1155, 1134, 1076, 1002, 968. Mp: 54–57 °C. [α]_D²⁰ = –32 (10 mg/mL; MeOH).

Methyl 4-(((3*aS*,4*S*,6*R*,6*aR*)-6-(6-Amino-9*H*-purin-9-yl)-2,2-dimethyltetrahydrofuro[3,4-*d*][1,3]dioxol-4-yl)methyl)thio)butanoate (7a). According to the method of Pignot et al.,⁷⁵ to a solution of compound 6 (150 mg, 0.41 mmol, 1.0 equiv) and 2 (111 mg, 0.62 mmol, 1.5 equiv) in dry methanol (10 mL) was added sodium methoxide (49 mg, 0.90 mmol, 2.2 equiv) while stirring under an argon atmosphere. After stirring overnight at rt, the solvent was removed under reduced pressure at 40 °C, and the residue was purified by column chromatography (DCM/MeOH = 97:3) to afford the desired product as a colorless solid (125 mg, 0.30 mmol, 72%). ¹H NMR (300 MHz, CD₃OD): δ/ppm = 8.29 (s, 1H), 8.24 (s, 1H), 6.19 (d, *J* = 2.4 Hz, 1H), 5.55 (dd, *J* = 6.4, 2.4 Hz, 1H), 5.08 (dd, *J* = 6.4, 3.0 Hz, 1H), 4.35 (td, *J* = 6.9, 3.0 Hz, 1H), 3.65 (s, 3H), 2.81 (d, *J* = 6.9 Hz, 2H), 2.53 (t, *J* = 7.2 Hz, 2H), 2.36 (t, *J* = 7.2 Hz, 2H), 1.78 (p, *J* = 7.3 Hz, 2H), 1.60 (s, 3H), 1.40 (s, 3H). ¹³C NMR (75 MHz, CD₃OD): δ/ppm = 173.1, 155.3, 151.9, 139.8, 113.3, 89.6, 86.2, 83.1, 83.1, 49.9, 32.8, 31.2, 30.3, 25.2, 23.6, 23.4. FT-IR: ν /cm⁻¹ = 3297, 3135, 2990, 2935, 2026, 1732, 1732, 1670, 1600, 1561, 1473, 1365, 1328, 1304, 1267, 1200, 1175, 1092, 1057, 971. Mp: 99–102 °C. [α]_D²⁰ = –14 (10 mg/mL; MeOH).

tert-Butyl (3-(((3*aS*,4*S*,6*R*,6*aR*)-6-(6-Amino-9*H*-purin-9-yl)-2,2-dimethyltetrahydrofuro[3,4-*d*][1,3]dioxol-4-yl)methyl)thio)propyl)carbamate (7b). To a solution of compound 6 (150 mg, 0.41 mmol, 1.0 equiv) and 3 (146 mg, 0.62 mmol, 1.5 equiv) in dry methanol (10 mL) was added sodium methoxide (49 mg, 0.90 mmol, 2.2 equiv) while stirring under an argon atmosphere. After stirring overnight at rt, the solvent was removed under reduced pressure at 40 °C, and the residue was purified by column chromatography (DCM/MeOH = 97:3) to afford the desired product as a colorless solid (165 mg, 0.34 mmol,

84%). ¹H NMR (300 MHz, DMSO-*d*₆): δ/ppm = 8.33 (s, 1H), 8.17 (s, 1H), 7.34 (s, 2H), 6.16 (d, *J* = 2.4 Hz, 1H), 5.50 (dd, *J* = 6.3, 2.4 Hz, 1H), 4.99 (dd, *J* = 6.3, 2.7 Hz, 1H), 4.26–4.21 (m, *J* = 8.0, 6.4, 2.7 Hz, 1H), 2.95–2.89 (m, *J* = 6.4 Hz, 2H), 2.81–2.66 (m, *J* = 13.5, 7.2 Hz, 2H), 2.44 (t, *J* = 7.3 Hz, 2H), 1.53 (s, 3H), 1.36 (s, 9H), 1.33 (s, 3H). ¹³C NMR (75 MHz, DMSO-*d*₆): δ/ppm = 156.1, 155.5, 152.7, 148.7, 140.0, 120.1, 113.2, 89.2, 85.7, 83.34, 83.1, 77.4, 33.4, 29.5, 28.7, 28.2, 26.8, 25.1. FT-IR: ν/cm⁻¹ = 3323, 3181, 2978, 2930, 1695, 1638, 1596, 1508, 1475, 1458, 1420, 1366, 1329, 1248, 1207, 1161, 1075, 982, 868, 798, 782, 723. Mp: 74–77 °C. [α]_D²⁰ = -9 (10 mg/mL; MeOH).

4-(((2*S*,3*R*,4*R*,5*R*)-5-(6-Amino-9*H*-purin-9-yl)-3,4-dihydroxytetrahydrofuran-2-yl)methyl)thio)butanoic Acid (8a). To a solution of compound **7a** (175 mg, 0.41 mmol, 1.0 equiv) in THF (4 mL) and water (3 mL) was added lithium hydroxide monohydrate (52 mg, 1.24 mmol, 3.0 equiv). After stirring at rt for 1 h, the mixture was acidified with 1 M HCl and extracted with CHCl₃/PrOH (3:1). The combined organic extracts were dried over Na₂SO₄, and the solvent was removed under reduced pressure at 40 °C. The residue was taken up in DCM (1.5 mL), and trifluoroacetic acid (1.5 mL), followed by water (200 μL), was added dropwise at 5 °C. After stirring at 5 °C for 1 h, the solvent was removed under reduced pressure and co-distilled with DCM (3 × 40 mL) at 40 °C. Water was added, and the mixture was lyophilized to give the desired product as a colorless resin (146 mg, 0.39 mmol, 96%). ¹H NMR (300 MHz, DMSO-*d*₆): δ/ppm = 8.45 (s, 1H), 8.35 (s, 1H), 6.00 (d, *J* = 4.9 Hz, 1H), 4.69 (t, *J* = 4.9 Hz, 1H), 4.27 (t, *J* = 4.9 Hz, 1H), 4.21–4.12 (m, 1H), 2.97–2.80 (m, 2H), 2.60–2.51 (m, 2H), 2.34–2.26 (m, 2H), 1.85–1.72 (m, 2H). ¹³C NMR (75 MHz, DMSO-*d*₆): δ/ppm = 176.9, 152.4, 150.1, 145.9, 144.0, 120.6, 90.5, 86.0, 75.3, 73.9, 35.1, 33.5, 33.1, 25.9. FT-IR: ν/cm⁻¹ = 3099, 2934, 1693, 1508, 1420, 1324, 1197, 1136, 1096, 1054, 836, 798, 785, 723, 681. [α]_D²⁰ = -2 (10 mg/mL; MeOH). ESI-MS: *m/z* [M + H]⁺ = 370.10 (100%), 371.04 (21.1%), 372.09 (6.4%). Calculated: 370.12 (100%), 371.12 (18.2%), 372.12 (1.4%). Purity: 95% (HPLC, MeCN/H₂O = 20:80 + 0.1% HCOOH); *t*_R = 3.17 min.

(2*R*,3*R*,4*S*,5*S*)-2-(6-Amino-9*H*-purin-9-yl)-5-(((3-aminopropyl)thio)methyl)tetrahydrofuran-3,4-diol (8b). To a suspension of compound **7b** (50 mg, 0.10 mmol) in water (1 mL), formic acid (1 mL) was added at 0 °C. The mixture was stirred for 2 days at rt. The solvent was removed by lyophilization, and the desired product was obtained as a pale-yellow solid (34 mg, 0.99 mmol, 96%). ¹H NMR (300 MHz, DMSO-*d*₆): δ/ppm = 8.17 (s, 1H), 7.34 (s, 2H), 5.89 (d, *J* = 5.6 Hz, 1H), 4.75 (t, *J* = 5.6 Hz, 1H), 4.14 (t, *J* = 4.4 Hz, 1H), 4.00 (d, *J* = 4.4 Hz, 1H), 3.02–2.71 (m, 2H), 2.10 (t, *J* = 7.5 Hz, 1H), 1.72 (q, *J* = 7.5 Hz, 2H). ¹³C NMR (75 MHz, DMSO-*d*₆): δ/ppm = 174.2, 156.4, 152.9, 149.8, 140.3, 119.5, 87.9, 84.4, 72.89, 34.2, 33.0, 31.8, 25.6. FT-IR: ν/cm⁻¹ = 3332, 3183, 2927, 2360, 2341, 1643, 1574, 1477, 1421, 1374, 1333, 1301, 1248, 1209, 1174, 1127, 1088, 1045, 1003, 826, 796, 719. Mp: 66–69 °C. [α]_D²⁰ = -22 (10 mg/mL; MeOH). ESI-MS: *m/z* [M + H]⁺ = 341.13 (100%), 342.11 (15.9%), 343.12 (6.1%). Calculated: 341.14 (100%), 342.14 (17.2%), 343.14 (5.6%). Purity: 97% (HPLC, MeCN/H₂O = 20:80 + 0.1% HCOOH); *t*_R = 4.00 min.

tert-Butyl N²-(tert-Butoxycarbonyl)-N⁴-methoxy-N⁴-methyl-L-asparaginate (10a). According to the method of Zhang et al.,⁷⁶ a solution of Boc-Asp-O^tBu (19.4 g, 67.0 mmol, 1.0 equiv) in DCM (130 mL) was added 1,1-carbonyldiimidazole (12.0 g, 73.7 mmol, 1.1 equiv), and the reaction was stirred at rt for 1 h. Then, *N,O*-dimethylhydroxylamine hydrochloride (7.19 g, 73.7 mmol, 1.1 equiv) was added, and the reaction mixture was stirred at rt for a further 18 h. The mixture was diluted with EtOAc (100 mL), and the residue was filtered off. The filtrate was washed several times with 1 M HCl, saturated NaHCO₃ solution, and brine until no side products were detected by TLC. The combined organic layers were dried over anhydrous Na₂SO₄, filtered, and concentrated under reduced pressure at 40 °C to give **10a** (18.7 g, 56.3 mmol, 84%) as a colorless oil. ¹H NMR (300 MHz, CDCl₃): δ/ppm = 5.65 (d, *J* = 8.9 Hz, 1H), 4.49–4.38 (m, 1H), 3.67 (s, 3H), 3.15 (s, 3H), 3.13–2.80 (m, 2H), 1.44 (s, 9H), 1.42 (s, 9H). ¹³C NMR (75 MHz, CDCl₃): δ/ppm = 171.9, 170.7, 155.9, 81.9, 79.6, 61.3, 50.5, 34.8, 32.1, 28.5, 28.0. FT-IR: ν/cm⁻¹ = 3252, 2984, 2934, 1729, 1703, 1630, 1520, 1250, 1141, 1000, 960, 841. [α]_D²⁰ = +15 (10 mg/mL; CHCl₃).

tert-Butyl 4-(Methoxy(methyl)amino)-4-oxobutanoate (10b). 4-(tert-Butoxy)-4-oxobutanoic acid (500 mg, 2.87 mmol, 1 equiv) and 1,1'-carbonyldiimidazole (512 mg, 3.16 mmol, 1.1 equiv) were dissolved in DCM (10 mL) and stirred at room temperature for 1 h. *N,O*-Dimethylhydroxylamine hydrochloride (308 mg, 3.16 mmol, 1.1 equiv) was added, and the reaction mixture was allowed to stir at room temperature for 19 h. After the solid matter was filtered off, the filtrate was diluted with DCM (10 mL) and washed with 1 M HCl (15 mL), saturated NaHCO₃ solution (15 mL), and brine (15 mL). The organic layer was dried over anhydrous Na₂SO₄ and concentrated under reduced pressure at 40 °C to give the desired product as a colorless oil (552 mg, 2.54 mmol, 89%). ¹H NMR (300 MHz, CDCl₃): δ/ppm = 3.68 (s, 3H), 3.15 (s, 3H), 2.67 (t, *J* = 7.3 Hz, 2H), 2.52 (t, *J* = 7.3 Hz, 2H), 1.42 (s, 9H). ¹³C NMR (75 MHz, CDCl₃): δ/ppm = 173.1, 172.3, 80.5, 61.3, 32.4, 29.9, 28.2, 27.1. FT-IR: ν/cm⁻¹ = 2984, 2934, 1720, 1663, 1360, 1248, 1159, 1105, 987, 888, 847, 751.

tert-Butyl (3-(Methoxy(methyl)amino)-3-oxopropyl)carbamate (10c). Boc-β-Ala-OH (500 mg, 2.64 mmol, 1 equiv) and 1,1'-carbonyldiimidazole (471 mg, 2.91 mmol, 1.1 equiv) were dissolved in DCM (10 mL) and stirred at room temperature for 1 h. *N,O*-Dimethylhydroxylamine hydrochloride (284 mg, 2.91 mmol, 1.1 equiv) was added, and the reaction mixture was allowed to stir at room temperature for 17 h. After the solid matter was filtered off, the filtrate was diluted with DCM (10 mL) and washed with 1 M HCl (15 mL), saturated NaHCO₃ solution (15 mL), and brine (15 mL). The organic layer was dried over anhydrous Na₂SO₄ and concentrated under reduced pressure at 40 °C to give the desired product as a colorless oil (537 mg, 2.31 mmol, 88%). ¹H NMR (300 MHz, CDCl₃): δ/ppm = 6.72 (t, *J* = 5.7 Hz, 1H), 3.65 (s, 3H), 3.14 (q, *J* = 7.0 Hz, 2H), 3.08 (s, 3H), 2.52 (t, *J* = 7.0 Hz, 2H), 1.37 (s, 9H). ¹³C NMR (75 MHz, CDCl₃): δ/ppm = 171.6, 155.5, 77.5, 60.9, 35.9, 31.7, 31.6, 28.2. FT-IR: ν/cm⁻¹ = 3346, 2975, 2937, 1698, 1651, 1505, 1449, 1390, 1365, 1249, 1166, 995, 971, 782.

tert-Butyl (S)-2-((tert-Butoxycarbonyl)amino)-4-oxobutanoate (11a). According to the method of Zhang et al.,⁷⁶ a solution of diisobutylaluminum hydride (DIBAL) in hexane (1 M, 4.06 mmol, 4.06 mL, 1.5 equiv) was added dropwise to a solution of compound **10a** (900 mg, 2.71 mmol, 1 equiv) in anhydrous THF (25 mL) at -78 °C. The reaction mixture was stirred at -78 °C for 2.5 h. KHSO₄ solution (0.35 M, 20 mL) was added, and the mixture was extracted with diethyl ether (3 × 80 mL). The combined organic extracts were washed with 1 M HCl (3 × 50 mL), saturated NaHCO₃ solution (3 × 50 mL), and brine (3 × 50 mL). After drying with anhydrous Na₂SO₄, the solution was concentrated under reduced pressure at 40 °C to obtain the desired product as a colorless oil (600 mg, 2.20 mmol, 81%) that crystallized after storage at -20 °C. ¹H NMR (300 MHz, CDCl₃): δ/ppm = 9.72 (s, 1H), 5.36 (d, *J* = 8.1 Hz, 1H), 4.54–4.39 (m, 1H), 3.07–2.87 (m, 2H), 1.44 (s, 9H), 1.43 (s, 9H). ¹³C NMR (75 MHz, CDCl₃): δ/ppm = 199.5, 170.0, 155.4, 82.7, 80.0, 49.4, 46.4, 28.4, 28.0. FT-IR: ν/cm⁻¹ = 3458, 2977, 2932, 1732, 1711, 1494, 1266, 1333, 1223, 1055, 846. Mp: 67–70 °C. [α]_D²⁰ = +16 (10 mg/mL; CHCl₃).

tert-Butyl 4-Oxobutanoate (11b). A solution of diisobutylaluminum hydride (DIBAL) in hexane (1 M, 3.05 mmol, 3.05 mL, 1.5 equiv) was added dropwise to a solution of compound **10b** (442 mg, 2.03 mmol, 1 equiv) in anhydrous THF (12 mL) at -78 °C. The reaction mixture was stirred at -78 °C for 2 h. KHSO₄ solution (0.35 M, 10 mL) was added, and the mixture was extracted with ethyl acetate (3 × 25 mL). The combined organic extracts were washed with 1 M HCl (3 × 15 mL), saturated NaHCO₃ solution (3 × 15 mL), and brine (3 × 15 mL). After drying with anhydrous Na₂SO₄, the solution was concentrated under reduced pressure at 40 °C to obtain the desired product as a colorless oil (109 mg, 0.69 mmol, 34%). ¹H NMR (300 MHz, CDCl₃): δ/ppm = 10.09 (s, 1H), 3.05–2.98 (m, 2H), 2.87–2.79 (m, 2H), 1.73 (s, 9H). ¹³C NMR (75 MHz, CDCl₃): δ/ppm = 200.5, 171.6, 81.0, 38.8, 30.4, 28.1. FT-IR: ν/cm⁻¹ = 2978, 2932, 1724, 1456, 1392, 1366, 1246, 1151, 1073, 949, 875, 845, 754.

tert-Butyl (3-Oxopropyl)carbamate (11c). A solution of diisobutylaluminum hydride (DIBAL) in hexane (1 M, 2.83 mmol, 2.83 mL, 1.5 equiv) was added dropwise to a solution of compound **10c** (438 mg, 1.89 mmol, 1 equiv) in anhydrous THF (12 mL) at -78 °C. The

reaction mixture was stirred at -78°C for 2 h. KHSO_4 solution (0.35 M, 6 mL) was added, and the mixture was extracted with diethyl ether (3×25 mL). The combined organic extracts were washed with 1 M HCl (3×15 mL), saturated NaHCO_3 solution (3×15 mL), and brine (3×15 mL). After drying with anhydrous Na_2SO_4 , the solution was concentrated under reduced pressure at 40°C to obtain the desired product as a colorless oil (110 mg, 0.64 mmol, 34%). $^1\text{H NMR}$ (300 MHz, CDCl_3): $\delta/\text{ppm} = 10.09$ (s, 1H), 5.32 (d, $J = 7.5$ Hz, 1H), 3.71 (q, $J = 6.0$ Hz, 2H), 2.99 (t, $J = 6.0$ Hz, 2H), 1.71 (s, 9H). $^{13}\text{C NMR}$ (75 MHz, CDCl_3): $\delta/\text{ppm} = 201.5, 155.9, 79.4, 44.4, 34.1, 28.4$. FT-IR: $\nu/\text{cm}^{-1} = 3367, 2978, 2932, 1684, 1510, 1366, 1274, 1249, 1163, 1040, 1003, 751, 666$.

9-(((3aR,4R,6R,6aR)-6-(Aminomethyl)-2,2-dimethyltetrahydrofuro[3,4-d][1,3]dioxol-4-yl)-9H-purin-6-amine (12). According to the method of Liu et al.,²⁷ to a suspension of compound **18** (3.63 g, 8.32 mmol, 1 equiv) in ethanol (100 mL) was added hydrazine monohydrate (6.47 mL, 133.08 mmol, 16 equiv), and the mixture was refluxed for 1 h. After cooling, the precipitate was filtered off, and the solvent was removed under reduced pressure at 40°C . The residues were dissolved in ethanol (60 mL) and stirred for 15 min at room temperature, followed by filtration. The filtrate was concentrated under reduced pressure at 40°C , and the residues were purified by column chromatography (DCM/MeOH + 0.1% NEt_3) to afford the desired product as a white powder (2.32 g, 7.57 mmol, 91%). $^1\text{H NMR}$ (300 MHz, $\text{DMSO}-d_6$): $\delta/\text{ppm} = 8.37$ (s, 1H), 8.15 (s, 1H), 7.34 (s, 2H), 6.08 (d, $J = 3.2$ Hz, 1H), 5.45 (dd, $J = 6.3, 3.2$ Hz, 1H), 4.98 (dd, $J = 6.3, 2.8$ Hz, 1H), 4.09 (td, $J = 5.8, 2.8$ Hz, 1H), 2.70 (dd, $J = 5.8, 2.8$ Hz, 2H), 1.53 (s, 3H), 1.32 (s, 3H). $^{13}\text{C NMR}$ (75 MHz, $\text{DMSO}-d_6$): $\delta/\text{ppm} = 156.2, 152.8, 149.0, 140.0, 119.2, 113.2, 89.1, 87.1, 82.7, 81.6, 43.7, 27.1, 25.2$. FT-IR: $\nu/\text{cm}^{-1} = 3538, 3331, 3176, 1746, 1701, 1660, 1601, 1477, 1381, 1330, 1303, 1270, 1218, 1091, 1016, 902, 872, 798$. Mp: $212-215^{\circ}\text{C}$. $[\alpha]_{\text{D}}^{20} = -32$ (10 mg/mL; MeOH).

tert-Butyl (S)-4-(((3aR,4R,6R,6aR)-6-(6-Amino-9H-purin-9-yl)-2,2-dimethyltetrahydrofuro[3,4-d][1,3]dioxol-4-yl)methyl)amino)-2-((tert-butoxycarbonyl)amino)butanoate (13a). To a 0°C cooled solution of **12** (7.18 g, 28.9 mmol, 1.1 equiv) in THF/MeCN (1:3 = 160 mL) under argon atmosphere were added a suspension of **11a** (7.18 g, 26.3 mmol, 1.0 equiv) in THF/MeCN (1:3 = 12 mL) and HOAc (1.50 mL, 26.3 mmol, 1.0 equiv). After stirring for 30 min, $\text{NaBH}(\text{OAc})_3$ (8.36 g, 39.4 mmol, 1.5 equiv) was added, and the reaction was stirred for 18 h at 5°C . The suspension was diluted with saturated NaHCO_3 solution (250 mL), and the aqueous layer was extracted with DCM (5×50 mL). The combined organic layers were dried over anhydrous Na_2SO_4 , filtered, and concentrated under reduced pressure at 40°C . The residue was purified by column chromatography (DCM/MeOH = 30:1 to 10:1 + 0.5% NEt_3) to give **13a** (9.11 g, 16.2 mmol, 62%) as a colorless solid. $^1\text{H NMR}$ (300 MHz, CDCl_3): $\delta/\text{ppm} = 8.26$ (s, 1H), 7.88 (s, 1H), 6.40 (s, 2H), 6.05 (d, $J = 8.2$ Hz, 1H), 5.93 (d, $J = 3.4$ Hz, 1H), 5.45 (dd, $J = 6.5, 3.4$ Hz, 1H), 5.03 (dd, $J = 6.5, 3.4$ Hz, 1H), 4.37–4.30 (m, 1H), 4.29–4.19 (m, 1H), 2.96–2.66 (m, 3H), 2.65–2.53 (m, 1H), 1.98–1.71 (m, 2H), 1.56 (s, 3H), 1.43–1.29 (m, 21H). $^{13}\text{C NMR}$ (75 MHz, CDCl_3): $\delta/\text{ppm} = 171.9, 156.0, 155.7, 153.1, 149.4, 139.9, 120.4, 114.6, 91.1, 85.0, 83.1, 82.2, 81.7, 79.4, 53.0, 51.4, 46.3, 32.3, 28.4, 28.1, 27.4, 25.5$. FT-IR: $\nu/\text{cm}^{-1} = 2980, 1703, 1640, 1597, 1504, 1476, 1425, 1367, 1330, 1297, 1213, 1152, 1075, 857, 798, 750, 665$. Mp: $96-100^{\circ}\text{C}$. $[\alpha]_{\text{D}}^{20} = -33$ (10 mg/mL; CHCl_3).

tert-Butyl 4-(((3aR,4R,6R,6aR)-6-(6-Amino-9H-purin-9-yl)-2,2-dimethyltetrahydrofuro[3,4-d][1,3]dioxol-4-yl)methyl)amino)-butanoate (13b). To a solution of compound **12** (93 mg, 0.30 mmol, 1 equiv) and compound **11b** (48 mg, 0.30 mmol, 1 equiv) in THF (7 mL) were added acetic acid (17 μL , 0.30 mmol, 1 equiv) and $\text{NaBH}(\text{OAc})_3$ (97 mg, 0.46 mmol, 1.5 equiv). After the mixture was stirred at room temperature overnight, the reaction was quenched by addition of saturated NaHCO_3 solution (15 mL), followed by extraction with DCM (4×15 mL). The combined organic extracts were dried over anhydrous Na_2SO_4 , and the solvent was removed under reduced pressure at 40°C . Purification by column chromatography (DCM/MeOH = 20:1 + 0.1% NEt_3) afforded the desired product as a colorless oil (101 mg, 0.23 mmol, 75%). $^1\text{H NMR}$ (300 MHz, CDCl_3): $\delta/\text{ppm} =$

8.30 (s, 1H), 7.88 (s, 1H), 6.31 (s, 2H), 5.98 (d, $J = 3.2$ Hz, 1H), 5.43 (dd, $J = 6.5, 3.2$ Hz, 1H), 4.99 (dd, $J = 6.5, 3.2$ Hz, 1H), 4.37–4.28 (m, 1H), 2.94–2.78 (m, 2H), 2.67–2.50 (m, 2H), 2.22 (t, $J = 7.4$ Hz, 2H), 1.77–1.65 (m, 2H), 1.57 (s, 3H), 1.38 (s, 9H), 1.35 (s, 3H). $^{13}\text{C NMR}$ (75 MHz, CDCl_3): $\delta/\text{ppm} = 172.9, 156.0, 153.2, 149.5, 139.9, 120.5, 114.6, 90.9, 85.6, 83.5, 82.4, 80.2, 51.3, 49.1, 33.4, 28.2, 27.4, 25.5, 25.4$. FT-IR: $\nu/\text{cm}^{-1} = 2985, 2938, 2852, 1669, 1507, 1426, 1370, 1197, 1178, 1132, 1078, 868, 831, 798, 720$. $[\alpha]_{\text{D}}^{20} = -22$ (10 mg/mL; CHCl_3).

tert-Butyl (3-(((3aR,4R,6R,6aR)-6-(6-Amino-9H-purin-9-yl)-2,2-dimethyltetrahydrofuro[3,4-d][1,3]dioxol-4-yl)methyl)amino)-propyl)carbamate (13c). To a solution of compound **12** (131 mg, 0.43 mmol, 1 equiv) and compound **11c** (74 mg, 0.43 mmol, 1 equiv) in THF (7 mL) was added acetic acid (24 μL , 0.43 mmol, 1 equiv) and $\text{NaBH}(\text{OAc})_3$ (136 mg, 0.64 mmol, 1.5 equiv). After the mixture was stirred at room temperature overnight, the reaction was quenched by addition of saturated NaHCO_3 solution (15 mL), followed by extraction with DCM (4×15 mL). The combined organic extracts were dried over anhydrous Na_2SO_4 , and the solvent was removed under reduced pressure at 40°C . Purification by column chromatography (DCM/MeOH = 30:1 + 0.1% NEt_3) afforded the desired product as a colorless powder (150 mg, 0.32 mmol, 76%). $^1\text{H NMR}$ (300 MHz, CDCl_3): $\delta/\text{ppm} = 8.27$ (s, 1H), 7.94 (s, 1H), 6.16 (s, 2H), 6.00 (d, $J = 3.2$ Hz, 1H), 5.44 (dd, $J = 6.4, 3.2$ Hz, 1H), 5.33 (t, $J = 6.4$ Hz, 1H), 5.06 (dd, $J = 6.4, 3.2$ Hz, 1H), 4.48–4.38 (m, 1H), 3.29–3.11 (m, 2H), 3.02–2.89 (m, 2H), 2.85–2.60 (m, 2H), 1.76–1.63 (m, 2H), 1.59 (s, 3H), 1.41–1.34 (m, 12H). $^{13}\text{C NMR}$ (75 MHz, CDCl_3): $\delta/\text{ppm} = 156.3, 155.8, 153.2, 149.4, 140.1, 120.4, 114.8, 91.1, 85.0, 83.5, 82.4, 79.2, 51.2, 47.7, 39.1, 29.5, 28.5, 27.4, 25.5$. FT-IR: $\nu/\text{cm}^{-1} = 3326, 3182, 2980, 2937, 1642, 1598, 1475, 1366, 1250, 1210, 1159, 1076, 867$. Mp: $46-49^{\circ}\text{C}$. $[\alpha]_{\text{D}}^{20} = -22$ (10 mg/mL; CHCl_3).

Di-tert-butyl (2S)-4-(((3aR,4R,6R,6aR)-6-(6-Amino-9H-purin-9-yl)-2,2-dimethyltetrahydrofuro[3,4-d][1,3]dioxol-4-yl)methyl)amino)pyrrolidine-1,2-dicarboxylate (13d). To a solution of compound **12** (103 mg, 0.34 mmol, 1 equiv) and compound **11d** (96 mg, 0.34 mmol, 1 equiv) in THF (5 mL) was added acetic acid (19 μL , 0.34 mmol, 1 equiv) and $\text{NaBH}(\text{OAc})_3$ (107 mg, 0.50 mmol, 1.5 equiv). After the mixture was stirred at room temperature overnight, the reaction was quenched by addition of saturated NaHCO_3 solution (15 mL), followed by extraction with DCM (4×15 mL). The combined organic extracts were dried over anhydrous Na_2SO_4 , and the solvent was removed under reduced pressure at 40°C . Purification by column chromatography (DCM/MeOH = 30:1 + 0.1% NEt_3) afforded the desired product as a colorless oil (130 mg, 0.23 mmol, 68%). $^1\text{H NMR}$ (300 MHz, CDCl_3): $\delta/\text{ppm} = 8.31$ (s, 1H), 7.90 (s, 1H), 6.02–5.92 (m, 3H), 5.42–5.35 (m, 1H), 5.08–5.01 (m, 1H), 4.41–4.30 (m, 1H), 4.18–4.04 (m, 1H), 3.78–3.67 (m, 1H), 3.34–3.23 (m, 2H), 2.98–2.88 (m, 2H), 2.49–2.29 (m, 1H), 1.91–1.77 (m, 1H), 1.59 (s, 3H), 1.45–1.35 (m, 21H). $^{13}\text{C NMR}$ (75 MHz, CDCl_3): $\delta/\text{ppm} = 172.4, 155.8, 153.9, 149.4, 140.2, 140.1, 120.5, 114.8, 91.0, 85.2, 83.6, 82.2, 81.5, 80.2, 58.7, 56.5, 51.9, 49.636, 36.3, 28.5, 28.1, 27.4, 25.5$. FT-IR: $\nu/\text{cm}^{-1} = 3331, 3181, 2978, 2934, 1694, 1643, 1597, 1476, 1366, 1212, 1152, 1075, 855, 769$. $[\alpha]_{\text{D}}^{20} = -29$ (10 mg/mL; CHCl_3).

(S)-2-Amino-4-(((2R,3S,4R,5R)-5-(6-amino-9H-purin-9-yl)-3,4-dihydroxytetrahydrofuran-2-yl)methyl)amino)butanoic Acid Trifluoroacetate Salt (14a). Cold trifluoroacetic acid (1.5 mL) was added to a solution of compound **13a** (72 mg, 0.13 mmol) in DCM (1.5 mL) at -20°C . The solution was stirred at -20°C until LC-MS analysis indicated complete removal of Boc and ester groups. DCM (40 mL) was added, and the solvent was removed under reduced pressure at 40°C . After co-distillation with DCM (3×40 mL), the residues were dissolved in water (1.5 mL) and cooled down to 5°C . Cold trifluoroacetic acid (250 μL) was added, and the solution was stirred at 5°C overnight. Water (5 mL) was added, and the mixture was lyophilized. The desired product was obtained as the trifluoroacetate salt (colorless solid, 78 mg, 0.13 mmol, 99%). $^1\text{H NMR}$ (300 MHz, CD_3OD): $\delta/\text{ppm} = 8.38$ (s, 1H), 8.26 (s, 1H), 6.02 (d, $J = 5.4$ Hz, 1H), 4.74–4.67 (m, 1H), 4.36–4.27 (m, 2H), 3.95 (dd, $J = 8.6, 4.8$ Hz, 1H), 3.58–3.47 (m, 1H), 3.45–3.36 (m, 1H), 3.34–3.26 (m, 2H), 2.34–2.21 (m, 1H), 2.20–2.07 (m, 1H). $^{13}\text{C NMR}$ (75 MHz, CD_3OD): $\delta/\text{ppm} =$

ppm = 172.7, 153.5, 149.8, 147.6, 144.1, 120.7, 91.1, 81.8, 75.1, 73.2, 53.1, 50.7, 46.5, 28.1. FT-IR: ν/cm^{-1} = 3308, 3166, 3072, 1672, 1508, 1424, 1324, 1198, 1132, 1074, 837, 799, 723, 667. Mp: 58–61 °C. $[\alpha]_{\text{D}}^{20}$ = +2 (10 mg/mL; MeOH). ESI-MS: m/z $[M + H]^+$ = 368.15 (100%), 369.14 (17.0%), 370.15 (2.3%). Calculated: 368.17 (100%), 369.17 (18.2%), 370.17 (2.5%). Purity: > 98% (HPLC, MeCN/H₂O = 20:80 + 0.1% HCOOH); t_{R} = 3.48 min.

4-(((2R,3S,4R,5R)-5-(6-Amino-9H-purin-9-yl)-3,4-dihydroxytetrahydrofuran-2-yl)methyl)amino)butanoic Acid (14b). Cold trifluoroacetic acid (1.5 mL) was added to a solution of compound **13b** (26 mg, 0.06 mmol) in DCM (1.5 mL) at –20 °C. The solution was stirred at –20 °C until LC-MS analysis indicated complete removal of the ester group. DCM (40 mL) was added, and the solvent was removed under reduced pressure at 40 °C. After co-distillation with DCM (3 × 40 mL), the residues were dissolved in water (1.5 mL) and cooled down to 5 °C. Cold trifluoroacetic acid (250 μ L) was added, and the solution was stirred at 5 °C overnight. Water (5 mL) was added, and the mixture was lyophilized to give the desired product as a slightly yellow resin (20 mg, 0.06 mmol, quant.). ¹H NMR (300 MHz, CD₃OD): δ /ppm = 8.43–8.35 (m, 2H), 6.05 (d, J = 5.0 Hz, 1H), 4.78 (t, J = 4.9 Hz, 1H), 4.39–4.26 (m, 2H), 3.61–3.48 (m, 1H), 3.45–3.35 (m, 1H), 3.09 (t, J = 7.8 Hz, 2H), 2.39 (t, J = 6.9 Hz, 2H), 1.98–1.81 (m, 2H). ¹³C NMR (75 MHz, CD₃OD): δ /ppm = 176.1, 153.0, 149.8, 146.9, 144.5, 121.2, 91.9, 81.6, 74.8, 73.3, 50.6, 48.6, 31.5, 22.2. FT-IR: ν/cm^{-1} = 3088, 2846, 1667, 1508, 1423, 1323, 1182, 1129, 1047, 919, 834, 798, 721. $[\alpha]_{\text{D}}^{20}$ = +2 (10 mg/mL; MeOH). ESI-MS: m/z $[M + H]^+$ = 353.13 (100%), 354.11 (17.5%), 355.13 (2.5%). Calculated: 353.16 (100%), 354.16 (15.6%), 355.16 (2.5%). Purity: > 98% (HPLC, MeCN/H₂O = 20:80 + 0.1% HCOOH); t_{R} = 3.85 min.

(2R,3R,4S,5R)-2-(6-Amino-9H-purin-9-yl)-5-(((3-aminopropyl)amino)methyl)tetrahydrofuran-3,4-diol Trifluoroacetate Salt (14c). Cold trifluoroacetic acid (1.5 mL) was added to a solution of compound **13c** (46 mg, 0.10 mmol) in DCM (1.5 mL) at 5 °C. The solution was stirred at 5 °C until LC-MS analysis indicated complete removal of the Boc group. DCM (40 mL) was added, and the solvent was removed under reduced pressure at 40 °C. After co-distillation with DCM (3 × 40 mL), the residues were dissolved in water (1.5 mL) and cooled down to 5 °C. Cold trifluoroacetic acid (250 μ L) was added, and the solution was stirred at 5 °C overnight. Water (5 mL) was added, and the mixture was lyophilized. The desired product was the trifluoroacetate salt (colorless solid, 59 mg, 0.10 mmol, quant.). ¹H NMR (300 MHz, CD₃OD): δ /ppm = 8.37 (s, 1H), 8.35 (s, 1H), 6.05 (d, J = 4.9 Hz, 1H), 4.78 (t, J = 4.9 Hz, 1H), 4.41–4.31 (m, 2H), 3.64–3.53 (m, 1H), 3.48–3.40 (m, 1H), 3.19–3.13 (m, 2H), 3.04–2.96 (m, 2H), 2.11–1.98 (m, 2H). ¹³C NMR (75 MHz, CD₃OD): δ /ppm = 153.7, 149.9, 148.0, 144.1, 121.1, 91.8, 81.4, 74.8, 73.2, 50.7, 46.1, 37.8, 25.2. FT-IR: ν/cm^{-1} = 3065, 2847, 1666, 1427, 1180, 1123, 1065, 1044, 834, 797, 759, 721, 667. Mp: 66–68 °C. $[\alpha]_{\text{D}}^{20}$ = +4 (10 mg/mL; MeOH). ESI-MS: m/z $[M + H]^+$ = 324.17 (100%), 325.14 (16.3%), 326.11 (1.7%). Calculated: m/z : 324.18 (100%), 325.18 (17.0%). Purity: 98% (HPLC, MeCN/H₂O = 20:80 + 0.1% HCOOH); t_{R} = 1.93 min.

(2S)-4-(((2R,3S,4R,5R)-5-(6-Amino-9H-purin-9-yl)-3,4-dihydroxytetrahydrofuran-2-yl)methyl)amino)pyrrolidine-2-carboxylic Acid (14d). Cold trifluoroacetic acid (1.5 mL) was added to a solution of compound **13d** (50 mg, 0.09 mmol) in DCM (1.5 mL) at –20 °C. The solution was stirred at –20 °C until LC-MS analysis indicated complete removal of Boc and ester groups. DCM (40 mL) was added, and the solvent was removed under reduced pressure at 40 °C. After co-distillation with DCM (3 × 40 mL), the residues were dissolved in water (1.5 mL) and cooled down to 5 °C. Cold trifluoroacetic acid (250 μ L) was added, and the solution was stirred at 5 °C overnight. Water (5 mL) was added, and the mixture was lyophilized to give the desired product as a yellow resin (34 mg, 0.09 mmol, quant.). ¹H NMR (300 MHz, DMSO-*d*₆): δ /ppm = 8.51 (s, 1H), 8.29 (s, 1H), 8.09 (s, 2H), 6.00 (d, J = 5.8 Hz, 1H), 4.79–4.72 (m, 1H), 4.47–4.37 (m, 1H), 4.26–4.17 (m, 2H), 4.09–3.97 (m, 1H), 3.61–3.49 (m, 2H), 3.48–3.37 (m, 2H), 2.86–2.71 (m, 1H), 2.18–2.01 (m, 1H). ¹³C NMR (75 MHz, DMSO-*d*₆): δ /ppm = 169.1, 154.3, 150.2, 148.9, 141.4, 119.4, 88.4, 80.1, 72.6, 71.6, 58.0, 54.8, 48.4, 46.4, 30.5. FT-IR: ν/cm^{-1} =

3011, 1669, 1506, 1422, 1180, 1128, 1047, 1024, 997, 827, 798, 763, 720. ESI-MS: m/z $[M + H]^+$ = 380.15 (100%), 381.12 (20.3%), 382.14 (2.6%). Calculated: 380.17 (100%), 381.17 (19.3%), 382.17 (2.7%). Purity: 98% (HPLC, MeCN/H₂O = 20:80 + 0.1% HCOOH); t_{R} = 3.75 min.

9-(((3aR,4R,6R,6aR)-6-((Benzylamino)methyl)-2,2-dimethyltetrahydrofuro[3,4-d][1,3]dioxol-4-yl)-9H-purin-6-amine (16a). To a solution of compound **12** (140 mg, 0.46 mmol, 1 equiv) and benzaldehyde (**15a**; 46 μ g, 0.46 mmol, 1 equiv) in 1,2-DCE/MeCN (2:1, 9 mL) were added acetic acid (26 μ L, 0.46 mmol, 1 equiv) and NaBH(OAc)₃ (145 mg, 0.69 mmol, 1.5 equiv). After the mixture was stirred at room temperature overnight, the reaction was quenched by addition of MeOH (2 mL), and the solvent was removed under reduced pressure at 40 °C. Purification by column chromatography (DCM/MeOH = 30:1 + 0.1% NEt₃) afforded the desired product as a colorless powder (116 mg, 0.40 mmol, 87%). ¹H NMR (300 MHz, CDCl₃): δ /ppm = 8.07 (s, 1H), 7.85 (s, 1H), 7.30–7.17 (m, 5H), 6.25 (s, 2H), 5.96 (d, J = 3.2 Hz, 1H), 5.44 (dd, J = 6.4, 3.2 Hz, 1H), 5.05 (dd, J = 6.4, 3.2 Hz, 1H), 4.42–4.35 (m, 1H), 3.77 (s, 2H), 2.96–2.81 (m, 2H), 1.58 (s, 3H), 1.35 (s, 3H). ¹³C NMR (75 MHz, CDCl₃): δ /ppm = 155.9, 153.1, 149.4, 140.0, 139.8, 128.5, 128.2, 127.1, 120.5, 114.6, 91.2, 85.5, 83.4, 82.4, 53.8, 50.7, 27.4, 25.5. FT-IR: ν/cm^{-1} = 3316, 3159, 2987, 2935, 1643, 1596, 1474, 1373, 1329, 1207, 1073, 863, 732, 698. Mp: 57–60 °C. $[\alpha]_{\text{D}}^{20}$ = –24 (10 mg/mL; CHCl₃).

3-(((3aR,4R,6R,6aR)-6-(6-Amino-9H-purin-9-yl)-2,2-dimethyltetrahydrofuro[3,4-d][1,3]dioxol-4-yl)methyl)amino)phenol (16b). To a solution of compound **12** (157 mg, 0.51 mmol, 1 equiv) and 3-hydroxybenzaldehyde (**15b**; 63 mg, 0.51 mmol, 1 equiv) in THF (2 mL) were added acetic acid (29 μ L, 0.51 mmol, 1 equiv) and NaBH(OAc)₃ (163 mg, 0.77 mmol, 1.5 equiv). After the mixture was stirred at room temperature for 7 h, the reaction was quenched by addition of MeOH (1 mL), and the solvent was removed under reduced pressure at 40 °C. Purification by column chromatography (DCM/MeOH = 10:1 + 0.1% NEt₃) afforded the desired product as a colorless oil (193 mg, 0.47 mmol, 92%). ¹H NMR (300 MHz, CDCl₃): δ /ppm = 8.22 (s, 1H), 8.05 (s, 1H), 7.04 (t, J = 7.8 Hz, 1H), 6.69–6.59 (m, 3H), 6.12 (d, J = 2.8 Hz, 1H), 5.45 (dd, J = 6.3, 2.8 Hz, 1H), 5.00 (dd, J = 6.3, 3.2 Hz, 1H), 4.35 (td, J = 6.0, 3.2 Hz, 1H), 3.62 (s, 2H), 2.83 (d, J = 6.0 Hz, 2H), 1.57 (s, 3H), 1.35 (s, 3H). ¹³C NMR (75 MHz, CDCl₃): δ /ppm = 158.6, 157.3, 153.9, 150.2, 142.0, 141.6, 130.4, 120.7, 120.4, 116.2, 115.5, 115.2, 91.8, 86.9, 84.8, 83.9, 54.2, 51.5, 27.5, 25.6. FT-IR: ν/cm^{-1} = 3543, 3339, 2982, 1645, 1600, 1480, 1457, 1424, 1376, 1331, 1050, 969, 869, 788, 696. Mp: 247 °C (decomposition). $[\alpha]_{\text{D}}^{20}$ = –13 (10 mg/mL; CHCl₃).

9-(((3aR,4R,6R,6aR)-2,2-Dimethyl-6-(((3-nitrobenzyl)amino)methyl)tetrahydrofuro[3,4-d][1,3]dioxol-4-yl)-9H-purin-6-amine (16c). To a solution of compound **12** (402 mg, 1.31 mmol, 1 equiv) and 3-nitrobenzaldehyde (**15c**; 198 mg, 1.31 mmol, 1 equiv) in THF (10 mL) were added acetic acid (75 μ L, 1.31 mmol, 1 equiv) and NaBH(OAc)₃ (417 mg, 1.97 mmol, 1.5 equiv). After the mixture was stirred at room temperature overnight, the reaction was quenched by addition of MeOH (15 mL), and the solvent was removed under reduced pressure at 40 °C. Purification by column chromatography (DCM/MeOH = 40:1 + 0.1% NEt₃) afforded the desired product as a colorless oil (358 mg, 0.81 mmol, 62%). ¹H NMR (300 MHz, CDCl₃): δ /ppm = 8.19–8.13 (m, 1H), 8.11–8.03 (m, 2H), 7.86 (s, 1H), 7.60 (d, J = 7.8 Hz, 1H), 7.43 (t, J = 7.8 Hz, 1H), 6.26 (s, 2H), 5.96 (d, J = 3.2 Hz, 1H), 5.48 (dd, J = 6.4, 3.2 Hz, 1H), 5.08 (dd, J = 6.4, 3.2 Hz, 1H), 4.45–4.34 (m, 1H), 3.90–3.84 (m, 2H), 2.99–2.81 (m, 2H), 1.60 (s, 3H), 1.38 (s, 3H). ¹³C NMR (75 MHz, CDCl₃): δ /ppm = 155.9, 152.9, 149.3, 148.5, 142.5, 140.2, 134.1, 129.3, 122.9, 122.2, 120.4, 114.7, 91.3, 85.6, 83.3, 82.3, 53.0, 50.7, 27.4, 25.5. FT-IR: ν/cm^{-1} = 3323, 3159, 2982, 2935, 1643, 1597, 1525, 1475, 1348, 1207, 1074, 867, 798, 751. $[\alpha]_{\text{D}}^{20}$ = –16 (10 mg/mL; CHCl₃).

tert-Butyl 3-(((3aR,4R,6R,6aR)-6-(6-Amino-9H-purin-9-yl)-2,2-dimethyltetrahydrofuro[3,4-d][1,3]dioxol-4-yl)methyl)amino)benzoate (16d). To a solution of compound **12** (200 mg, 0.65 mmol, 1 equiv) and *tert*-butyl 3-formylbenzoate (**15d**; 135 mg, 0.65 mmol, 1 equiv) in THF (5 mL) was added acetic acid (37 μ L, 0.65 mmol, 1 equiv) and NaBH(OAc)₃ (208 mg, 0.98 mmol, 1.5 equiv). After the mixture was stirred at room temperature overnight, the

reaction was quenched by addition of saturated NaHCO₃ solution (25 mL), followed by extraction with DCM (4 × 20 mL). The combined organic extracts were dried over anhydrous Na₂SO₄, and the solvent was removed under reduced pressure at 40 °C. Purification by column chromatography (DCM/MeOH = 30:1 + 0.1% NEt₃) afforded the desired product as a yellowish oil (177 mg, 0.36 mmol, 55%). ¹H NMR (300 MHz, CDCl₃): δ/ppm = 8.12 (s, 1H), 7.92–7.89 (m, 1H), 7.88–7.83 (m, 2H), 7.49–7.43 (m, 1H), 7.33 (t, J = 7.6 Hz, 1H), 6.06–5.93 (m, 3H), 5.46 (dd, J = 6.4, 3.3 Hz, 1H), 5.07 (dd, J = 6.4, 3.3 Hz, 1H), 4.43–4.36 (m, 1H), 3.83 (s, 2H), 2.99–2.82 (m, 2H), 1.60 (s, 3H), 1.57 (s, 9H), 1.37 (s, 3H). ¹³C NMR (75 MHz, CDCl₃): δ/ppm = 165.9, 155.8, 153.2, 149.5, 140.1, 132.3, 132.2, 129.2, 128.4, 128.3, 120.6, 114.7, 91.2, 85.5, 83.4, 82.4, 81.1, 53.5, 50.7, 28.3, 27.5, 25.6. FT-IR: ν/cm⁻¹ = 3322, 3159, 2980, 2933, 1706, 1643, 1475, 1368, 1294, 1157, 1076, 909, 850, 729. [α]_D²⁰ = -18 (10 mg/mL; CHCl₃).

tert-Butyl 3-((((3*aR*,4*R*,6*R*,6*aR*)-6-(6-Amino-9*H*-purin-9-yl)-2,2-dimethyltetrahydrofuro[3,4-*d*][1,3]dioxol-4-yl)methyl)amino)methyl)phenyl)carbamate (**16e**). To a solution of compound **12** (151 mg, 0.49 mmol, 1 equiv) and *tert*-butyl (3-formylphenyl)carbamate (**15e**) (109 mg, 0.49 mmol, 1 equiv) in 1,2-DCE (5 mL) were added acetic acid (28 μL, 0.49 mmol, 1 equiv) and NaBH(OAc)₃ (157 mg, 0.74 mmol, 1.5 equiv). After the mixture was stirred at room temperature overnight, the reaction was quenched by addition of MeOH (2 mL), and the solvent was removed under reduced pressure at 40 °C. Purification by column chromatography (DCM/MeOH = 30:1 + 0.1% NEt₃) afforded the desired product as a colorless powder (214 mg, 0.42 mmol, 85%). ¹H NMR (300 MHz, CDCl₃): δ/ppm = 8.15 (s, 1H), 7.95 (s, 1H), 7.33 (s, 1H), 7.25–7.15 (m, 2H), 6.95–6.89 (m, 1H), 6.01 (d, J = 3.1 Hz, 1H), 5.94 (s, 2H), 5.44 (dd, J = 6.4, 3.1 Hz, 1H), 5.05 (dd, J = 6.4, 3.1 Hz, 1H), 4.45–4.38 (m, 1H), 3.85–3.71 (m, 2H), 2.95–2.80 (m, 2H), 1.60 (s, 3H), 1.50 (s, 9H), 1.38 (s, 3H). ¹³C NMR (75 MHz, CDCl₃): δ/ppm = 155.8, 153.3, 153.0, 149.5, 140.6, 140.1, 138.8, 129.1, 122.8, 120.5, 118.4, 117.6, 114.6, 91.3, 85.8, 83.7, 82.5, 80.6, 53.8, 50.7, 28.5, 27.4, 25.5. FT-IR: ν/cm⁻¹ = 3319, 3178, 2977, 2977, 2934, 1716, 1643, 1594, 1367, 1239, 1156, 1072, 867, 733. Mp: 68–71 °C. [α]_D²⁰ = -12 (10 mg/mL; CHCl₃).

(2*R*,3*R*,4*S*,5*R*)-2-(6-Amino-9*H*-purin-9-yl)-5-((benzylamino)methyl)tetrahydrofuran-3,4-diol Trifluoroacetate Salt (**17a**). Cold trifluoroacetic acid (250 μL) was added to a suspension of compound **16a** (29 mg, 0.07 mmol) in water (1.5 mL) at 5 °C. The mixture was stirred at 5 °C for 48 h. Water (5 mL) was added, and the mixture was lyophilized to give the desired product as the trifluoroacetate salt (colorless solid, 34 mg, 0.07 mmol, quant.). ¹H NMR (300 MHz, CD₃OD): δ/ppm = 8.36 (s, 1H), 8.16 (s, 1H), 7.42 (s, 5H), 6.06 (d, J = 4.7 Hz, 1H), 4.76 (t, J = 4.7 Hz, 1H), 4.43–4.35 (m, 2H), 4.26 (d, J = 2.8 Hz, 2H), 3.56 (dd, J = 13.0, 9.2 Hz, 1H), 3.43 (dd, J = 13.0, 2.7 Hz, 1H). ¹³C NMR (75 MHz, CD₃OD): δ/ppm = 154.1, 149.8, 148.5, 143.9, 132.1, 131.2, 130.8, 130.3, 121.2, 92.0, 81.5, 74.8, 73.3, 52.4, 49.9. FT-IR: ν/cm⁻¹ = 3326, 3186, 2800, 1644, 1574, 1459, 1423, 1327, 1206, 1067, 825, 797, 699. Mp: 61–63 °C. [α]_D²⁰ = +6 (10 mg/mL; MeOH). ESI-MS: *m/z* [M + H]⁺ = 357.16 (100%), 358.12 (20.8%), 359.14 (2.0%). Calculated: 357.17 (100%), 358.17 (18.7%), 359.17 (2.6%). Purity: 97% (HPLC, MeCN/H₂O = 20:80 + 0.1% HCOOH); *t*_R = 3.44 min.

(2*R*,3*R*,4*S*,5*R*)-2-(6-Amino-9*H*-purin-9-yl)-5-(((3-hydroxybenzyl)amino)methyl)tetrahydrofuran-3,4-diol Trifluoroacetate Salt (**17b**). Cold trifluoroacetic acid (250 μL) was added to a suspension of compound **16b** (37 mg, 0.09 mmol) in water (1.5 mL) at 5 °C. The mixture was stirred at 5 °C overnight. Water (5 mL) was added, and the mixture was lyophilized to give the desired product as the trifluoroacetate salt (yellowish solid, 43 mg, 0.09 mmol, 99%). ¹H NMR (300 MHz, CD₃OD): δ/ppm = 8.35 (s, 1H), 8.18 (s, 1H), 7.16 (t, J = 8.0 Hz, 1H), 6.85–6.74 (m, 3H), 6.02 (d, J = 4.6 Hz, 1H), 4.70 (t, J = 4.6 Hz, 1H), 4.37–4.26 (m, 2H), 4.11 (s, 2H), 3.52–3.31 (m, 2H). ¹³C NMR (75 MHz, CD₃OD): δ/ppm = 159.3, 153.0, 149.7, 146.8, 144.4, 133.3, 131.4, 121.8, 121.2, 117.9, 117.6, 92.1, 81.5, 74.8, 73.3, 52.3, 49.8. FT-IR: ν/cm⁻¹ = 3087, 2840, 1669, 1592, 1427, 1195, 1129, 1040, 834, 797, 721, 697. Mp: 61 °C (decomposition). [α]_D²⁰ = +4 (10 mg/mL; MeOH). ESI-MS: *m/z* [M + H]⁺ = 373.17 (100%), 374.14 (20.1%), 375.17 (2.6%). Calculated: 373.16 (100%), 374.17 (18.8%),

375.17 (2.5%). Purity: 100% (HPLC, MeCN/H₂O = 20:80 + 0.1% HCOOH); *t*_R = 4.06 min.

(2*R*,3*R*,4*S*,5*R*)-2-(6-Amino-9*H*-purin-9-yl)-5-(((3-nitrobenzyl)amino)methyl)tetrahydrofuran-3,4-diol Trifluoroacetate Salt (**17c**). Cold trifluoroacetic acid (500 μL) was added to a suspension of compound **16c** (96 mg, 0.22 mmol) in water (3 mL) at 5 °C. The mixture was stirred at 5 °C overnight. Undissolved residues were filtered off, and water (5 mL) was added to the filtrate. The mixture was lyophilized to give the desired product as a colorless oil (103 mg, 0.20 mmol, 91%). ¹H NMR (300 MHz, CD₃OD): δ/ppm = 8.37 (s, 1H), 8.32–8.29 (m, 1H), 8.27 (s, 1H), 8.23–8.17 (m, 1H), 7.85–7.77 (m, 1H), 7.61 (t, J = 8.0 Hz, 1H), 6.04 (d, J = 4.5 Hz, 1H), 4.70 (t, J = 4.5 Hz, 1H), 4.44–4.29 (m, 4H), 3.61–3.41 (m, 2H). ¹³C NMR (75 MHz, CD₃OD): δ/ppm = 153.9, 149.8 (2x C), 148.2, 143.9, 137.4, 134.3, 131.5, 126.03, 125.4, 121.1, 99.0, 81.3, 74.8, 73.3, 51.4, 50.3. FT-IR: ν/cm⁻¹ = 3326, 3201, 3090, 1672, 1531, 1509, 1482, 1427, 1354, 1199, 1134, 834, 799, 722. [α]_D²⁰ = +14 (10 mg/mL; MeOH). ESI-MS: *m/z* [M + H]⁺ = 402.14 (100%), 403.1 (21.2%), 404.17 (2.7%). Calculated: 402.15 (100%), 403.16 (18.8%), 404.16 (2.7%). Purity: 99% (HPLC, MeCN/H₂O = 20:80 + 0.1% HCOOH); *t*_R = 3.37 min.

3-((((2*R*,3*S*,4*R*,5*R*)-5-(6-Amino-9*H*-purin-9-yl)-3,4-dihydroxytetrahydrofuran-2-yl)methyl)amino)methyl)benzoic Acid Trifluoroacetate Salt (**17d**). Cold trifluoroacetic acid (1.5 mL) was added to a solution of compound **16d** (79 mg, 0.16 mmol) in DCM (1.5 mL) at -20 °C. The solution was stirred at -20 °C until LC-MS analysis indicated complete removal of the ester group. DCM (40 mL) was added, and the solvent was removed under reduced pressure at 40 °C. After co-distillation with DCM (3 × 40 mL), the residues were dissolved in water (1.5 mL) and cooled down to 5 °C. Cold trifluoroacetic acid (250 μL) was added, and the solution was stirred at 5 °C overnight. Water (5 mL) was added, and the mixture was lyophilized. The desired product was obtained as the trifluoroacetate salt (colorless solid, 82 mg, 0.16 mmol, quant.). ¹H NMR (300 MHz, CD₃OD): δ/ppm = 8.34 (s, 1H), 8.21 (s, 1H), 8.04 (d, J = 1.6 Hz, 1H), 7.98 (dt, J = 7.7, 1.6 Hz, 1H), 7.61 (dt, J = 7.7, 1.6 Hz, 1H), 7.46 (t, J = 7.7 Hz, 1H), 6.02 (d, J = 4.5 Hz, 1H), 4.68 (t, J = 4.6 Hz, 1H), 4.37–4.24 (m, 4H), 3.55–3.36 (m, 2H). ¹³C NMR (75 MHz, CD₃OD): δ/ppm = 168.8, 153.0, 149.7, 146.7, 144.4, 135.6, 133.0, 132.7, 132.3, 131.8, 130.5, 121.2, 92.0, 81.4, 74.9, 73.3, 52.0, 50.1. FT-IR: ν/cm⁻¹ = 3076, 3076, 2847, 1667, 1509, 1427, 1280, 1182, 1129, 1042, 826, 797, 749, 721. mp: 65–67 °C. [α]_D²⁰ = +10 (10 mg/mL; MeOH). ESI-MS: *m/z* [M + H]⁺ = 401.14 (100%), 402.12 (22.2%), 403.14 (2.5%). Calculated: 401.16 (100%), 402.16 (19.9%), 403.16 (3.3%). Purity: 100% (HPLC, MeCN/H₂O = 20:80 + 0.1% HCOOH); *t*_R = 3.91 min.

(2*R*,3*R*,4*S*,5*R*)-2-(6-Amino-9*H*-purin-9-yl)-5-(((3-aminobenzyl)amino)methyl)tetrahydrofuran-3,4-diol Trifluoroacetate Salt (**17e**). Cold trifluoroacetic acid (1.5 mL) was added to a solution of compound **16e** (108 mg, 0.21 mmol) in DCM (1.5 mL) at -20 °C. The solution was stirred at -20 °C until LC-MS analysis indicated complete removal of the Boc group. DCM (40 mL) was added, and the solvent was removed under reduced pressure at 40 °C. After co-distillation with DCM (3 × 40 mL), the residues were dissolved in water (1.5 mL) and cooled down to 5 °C. Cold trifluoroacetic acid (250 μL) was added, and the solution was stirred at 5 °C overnight. Water (5 mL) was added, and the mixture was lyophilized. The desired product was obtained as the trifluoroacetate salt (1:1.3; ochrous solid, 111 mg, 0.21 mmol, quant.). ¹H NMR (300 MHz, CD₃OD): δ/ppm = 8.33 (s, 1H), 8.18 (s, 1H), 7.39–7.32 (m, 1H), 7.25–7.20 (m, 2H), 7.19–7.14 (m, 1H), 6.01 (d, J = 4.7 Hz, 1H), 4.72–4.67 (m, 1H), 4.36–4.28 (m, 2H), 4.25–4.14 (m, 2H), 3.56–3.45 (m, 1H), 3.42–3.34 (m, 1H). ¹³C NMR (75 MHz, CD₃OD): δ/ppm = 153.4, 149.7, 147.4, 144.2, 140.0, 133.9, 131.6, 126.8, 122.4, 122.0, 121.1, 92.0, 81.4, 74.8, 73.3, 52.0, 50.1. FT-IR: ν/cm⁻¹ = 2979, 2637, 1666, 1507, 1465, 1427, 1188, 1128, 1041, 836, 797, 721, 695. Mp: 69–72 °C. [α]_D²⁰ = +6 (10 mg/mL; MeOH). ESI-MS: *m/z* [M + H]⁺ = 372.16 (100%), 373.13 (20.9%), 374.15 (2.2%). Calculated: 372.18 (100%), 373.18 (21.3%), 374.19 (1.7%). Purity: 100% (HPLC, MeCN/H₂O = 20:80 + 0.1% HCOOH); *t*_R = 3.88 min.

2-((((3*aR*,4*R*,6*R*,6*aR*)-6-(6-Amino-9*H*-purin-9-yl)-2,2-dimethyltetrahydrofuro[3,4-*d*][1,3]dioxol-4-yl)methyl)isoindoline-1,3-dione (**18**). According to the method of Liu et al.,⁷⁷ to a suspension

of compound **5** (1000 mg, 3.25 mmol, 1 equiv) in THF (40 mL) were added phthalimide (479 mg, 3.25 mmol, 1 equiv) and triphenylphosphine (853 mg, 3.25, 1 equiv). DIAD (639 μ L, 3.25 mmol, 1 equiv) was added dropwise, and the mixture was stirred at room temperature for 5 h. The precipitate was filtered off and washed with cyclohexane to give the desired product as a colorless solid. More product could be obtained by adding cyclohexane to the filtrate and stirring the mixture overnight. The precipitate was filtered off and washed with cyclohexane. Yield: 1.01 g, 2.31 mmol, 71%. $^1\text{H NMR}$ (300 MHz, $\text{DMSO}-d_6$): δ /ppm = 8.28 (s, 1H), 7.86 (s, 1H), 7.81 (s, 4H), 7.31 (s, 2H), 6.18 (d, J = 2.0 Hz, 1H), 5.44 (dd, J = 6.3, 2.0 Hz, 1H), 5.18 (dd, J = 6.3, 3.7 Hz, 1H), 4.43–4.33 (m, 1H), 3.97–3.83 (m, 2H), 1.50 (s, 3H), 1.30 (s, 3H). $^{13}\text{C NMR}$ (75 MHz, $\text{DMSO}-d_6$): δ /ppm = 167.8, 156.1, 152.5, 148.6, 140.3, 134.5, 131.4, 123.1, 119.2, 113.5, 88.7, 83.8, 83.4, 81.8, 27.0, 25.3. FT-IR: ν/cm^{-1} = 3326, 3161, 2979, 1709, 1661, 1597, 1397, 1327, 1208, 1074, 869, 798, 725. Mp: 147–150 $^{\circ}\text{C}$. $[\alpha]_{\text{D}}^{20}$ = +18 (10 mg/mL; DMSO).

2-(((2R,3S,4R,5R)-5-(6-Amino-9H-purin-9-yl)-3,4-dihydroxytetrahydrofuran-2-yl)methyl)isoindoline-1,3-dione (19). Cold trifluoroacetic acid (250 μ L) was added to a suspension of compound **18** (40 mg, 0.09 mmol) in water (1.5 mL) at 5 $^{\circ}\text{C}$. The mixture was stirred at 5 $^{\circ}\text{C}$ overnight. Water (5 mL) was added, and the mixture was lyophilized to give the desired product as a colorless solid (35 mg, 0.09 mmol, 96%). $^1\text{H NMR}$ (300 MHz, $\text{DMSO}-d_6$): δ /ppm = 8.67 (s, 1H), 8.27 (s, 1H), 7.90–7.79 (m, 4H), 5.92 (d, J = 5.3 Hz, 1H), 4.74 (t, J = 5.3 Hz, 1H), 4.24 (t, J = 4.4 Hz, 1H), 4.21–4.13 (m, 1H), 4.02–3.85 (m, 2H). $^{13}\text{C NMR}$ (75 MHz, $\text{DMSO}-d_6$): δ /ppm = 167.9, 158.5, 151.9, 148.6, 147.2, 142.0, 134.6, 131.5, 123.2, 113.0, 87.9, 81.8, 73.1, 71.5. FT-IR: ν/cm^{-1} = 3318, 3120, 2944, 1679, 1395, 1188, 1127, 1029, 1000, 972, 874, 797, 738. mp: 143–147 $^{\circ}\text{C}$. $[\alpha]_{\text{D}}^{20}$ = +32 (10 mg/mL; DMSO). ESI-MS: m/z $[\text{M} + \text{H}]^+$ = 397.12 (100%), 398.06 (19.7%), 399.11 (2.5%). Calculated: 397.13 (100%), 398.13 (19.9%), 399.13 (3.3%). Purity: 97% (HPLC, MeCN/ H_2O = 20:80 + 0.1% HCOOH); t_{R} = 4.20 min.

tert-Butyl N^4 -(((3aR,4R,6R,6aR)-6-(6-Amino-9H-purin-9-yl)-2,2-dimethyltetrahydrofuro[3,4-d][1,3]dioxol-4-yl)methyl)- N^2 -(tert-butoxycarbonyl)-L-asparaginate (20a). To a solution of compound **12** (200 mg, 0.65 mmol, 1 equiv) and DIPEA (111 μ L, 0.65 mmol, 1 equiv) in DMF (2 mL) was added HBTU (248 mg, 0.65 mmol, 1 equiv), and the mixture was stirred at room temperature for 15 min. Boc-Asp-O t Bu (189 mg, 0.65 mmol, 1 equiv) was added, and the mixture was stirred for 1 h. The solution was diluted with saturated NaHCO_3 solution and extracted with ethyl acetate (3 \times 20 mL). The combined organic extracts were dried over anhydrous Na_2SO_4 , and the solvent was removed under reduced pressure at 40 $^{\circ}\text{C}$ to give the desired product as a yellowish solid (352 mg, 0.61 mmol, 93%). $^1\text{H NMR}$ (300 MHz, CDCl_3): δ /ppm = 8.39 (s, 1H), 7.86 (s, 1H), 6.27 (s, 2H), 5.80 (d, J = 4.8 Hz, 1H), 5.73 (d, J = 8.0 Hz, 1H), 5.25 (t, J = 5.7 Hz, 1H), 4.80 (dd, J = 6.3, 2.1 Hz, 1H), 4.50–4.41 (m, 2H), 4.22–4.08 (m, 1H), 3.27–3.17 (m, 1H), 2.96–2.89 (m, 2H), 1.60 (s, 3H), 1.45 (s, 9H), 1.37–1.30 (m, 12H). $^{13}\text{C NMR}$ (75 MHz, CDCl_3): δ /ppm = 170.7, 170.6, 155.9, 155.8, 152.7, 148.9, 140.7, 120.1, 114.9, 92.8, 83.5, 82.3, 82.2, 81.6, 79.8, 51.3, 41.1, 38.4, 28.3, 28.1, 27.6, 25.4. FT-IR: ν/cm^{-1} = 3323, 2980, 2932, 1709, 1643, 1480, 1367, 1296, 1249, 1153, 1096, 1077, 852, 798. Mp: 85 $^{\circ}\text{C}$ (decomposition). $[\alpha]_{\text{D}}^{20}$ = -136 (10 mg/mL; CHCl_3).

tert-Butyl N^5 -(((3aR,4R,6R,6aR)-6-(6-Amino-9H-purin-9-yl)-2,2-dimethyltetrahydrofuro[3,4-d][1,3]dioxol-4-yl)methyl)- N^2 -(tert-butoxycarbonyl)-L-glutamate (20b). To a solution of compound **12** (200 mg, 0.65 mmol, 1 equiv) and DIPEA (111 μ L, 0.65 mmol, 1 equiv) in DMF (2 mL) was added TBTU (210 mg, 0.65 mmol, 1 equiv), and the mixture was stirred at room temperature for 40 min. Boc-Glu-O t Bu (198 mg, 0.65 mmol, 1 equiv) was added, and the mixture was stirred for 2.5 h. The solution was diluted with saturated NaHCO_3 solution and extracted with ethyl acetate (3 \times 20 mL). The combined organic extracts were dried over anhydrous Na_2SO_4 , and the solvent was removed under reduced pressure at 40 $^{\circ}\text{C}$. The residues were dissolved in DCM (2 mL), and *n*-heptane (20 mL) was added. The resulting precipitate was filtered off and washed with *n*-heptane to give the desired product as a colorless solid (322 mg, 0.54 mmol, 84%). ^1H

NMR (300 MHz, CDCl_3): δ /ppm = 8.33 (s, 1H), 8.18 (s, 1H), 8.13 (t, J = 5.8 Hz, 1H), 7.36 (s, 2H), 7.10 (d, J = 7.7 Hz, 1H), 6.11 (d, J = 3.1 Hz, 1H), 5.41 (dd, J = 6.4, 3.1 Hz, 1H), 4.88 (dd, J = 6.4, 3.1 Hz, 1H), 4.22–4.14 (m, 1H), 3.83–3.72 (m, 1H), 3.37–3.32 (m, 2H), 2.25–2.13 (m, 2H), 1.97–1.81 (m, 1H), 1.80–1.64 (m, 1H), 1.53 (s, 3H), 1.40–1.34 (m, 18H), 1.31 (s, 3H). $^{13}\text{C NMR}$ (75 MHz, CDCl_3): δ /ppm = 171.7, 171.6, 156.2, 155.5, 152.7, 148.7, 140.1, 119.3, 113.5, 89.2, 84.1, 82.7, 81.7, 80.2, 78.0, 53.9, 40.8, 31.5, 28.2, 27.6, 27.0, 26.5, 25.2. FT-IR: ν/cm^{-1} = 3323, 3212, 2980, 2932, 1709, 1643, 1480, 1367, 1213, 1153, 1096, 852, 798. Mp: 83–86 $^{\circ}\text{C}$. $[\alpha]_{\text{D}}^{20}$ = -91 (10 mg/mL; CHCl_3).

tert-Butyl 4-(((3aR,4R,6R,6aR)-6-(6-Amino-9H-purin-9-yl)-2,2-dimethyltetrahydrofuro[3,4-d][1,3]dioxol-4-yl)methyl)amino)-4-oxobutanoate (20c). To a solution of compound **12** (204 mg, 0.67 mmol, 1 equiv) and DIPEA (113 μ L, 0.67 mmol, 1 equiv) in DMF (2 mL) was added TBTU (214 mg, 0.67 mmol, 1 equiv), and the mixture was stirred at room temperature for 40 min. 4-(tert-Butoxy)-4-oxobutanoic acid (116 mg, 0.67 mmol, 1 equiv) was added, and the mixture was stirred for 2.5 h. The solution was diluted with saturated NaHCO_3 solution and extracted with ethyl acetate (3 \times 20 mL). The combined organic extracts were dried over anhydrous Na_2SO_4 , and the solvent was removed under reduced pressure at 40 $^{\circ}\text{C}$ to give the desired product as a yellowish solid (300 mg, 0.65 mmol, 97%). $^1\text{H NMR}$ (300 MHz, CDCl_3): δ /ppm = 8.49 (d, J = 8.9 Hz, 1H), 8.35 (s, 1H), 7.85 (s, 1H), 6.17 (s, 2H), 5.80 (d, J = 5.0 Hz, 1H), 5.38–5.32 (m, 1H), 4.84 (dd, J = 6.2, 2.0 Hz, 1H), 4.52–4.44 (m, 1H), 4.26–4.13 (m, 1H), 3.27–3.14 (m, 1H), 2.82–2.61 (m, 2H), 2.59–2.44 (m, 2H), 1.60 (s, 3H), 1.40 (s, 9H), 1.34 (s, 3H). $^{13}\text{C NMR}$ (75 MHz, CDCl_3): δ /ppm = 172.4, 172.3, 156.2, 152.9, 149.0, 140.6, 121.2, 114.6, 92.9, 83.7, 82.3, 81.7, 80.6, 41.1, 30.9, 30.5, 28.2, 27.7, 25.3. FT-IR: ν/cm^{-1} = 3326, 3186, 2980, 2926, 1722, 1642, 1598, 1367, 1332, 1151, 1095, 852, 798. Mp: 62–65 $^{\circ}\text{C}$. $[\alpha]_{\text{D}}^{20}$ = -164 (10 mg/mL; CHCl_3).

tert-Butyl (3-(((3aR,4R,6R,6aR)-6-(6-Amino-9H-purin-9-yl)-2,2-dimethyltetrahydrofuro[3,4-d][1,3]dioxol-4-yl)methyl)amino)-3-oxopropyl)carbamate (20d). To a solution of compound **12** (200 mg, 0.65 mmol, 1 equiv) and DIPEA (111 μ L, 0.65 mmol, 1 equiv) in DMF (2 mL) was added TBTU (210 mg, 0.65 mmol, 1 equiv), and the mixture was stirred at room temperature for 30 min. Boc- β -Ala-OH (124 mg, 0.65 mmol, 1 equiv) was added, and the mixture was stirred overnight. The solution was diluted with saturated NaHCO_3 solution and extracted with ethyl acetate (3 \times 20 mL). The combined organic extracts were dried over anhydrous Na_2SO_4 , and the solvent was removed under reduced pressure at 40 $^{\circ}\text{C}$ to give the desired product as a colorless solid (298 mg, 0.62 mmol, 96%). $^1\text{H NMR}$ (300 MHz, CDCl_3): δ /ppm = 8.36 (s, 1H), 8.22 (d, J = 8.2 Hz, 1H), 7.87 (s, 1H), 6.42 (s, 2H), 5.83 (d, J = 4.5 Hz, 1H), 5.46–5.36 (m, 1H), 5.30–5.23 (m, 1H), 4.80 (dd, J = 6.3, 2.4 Hz, 1H), 4.49–4.42 (m, 1H), 4.17–4.03 (m, 1H), 3.52–3.40 (m, 2H), 3.34–3.23 (m, 1H), 2.67–2.46 (m, 2H), 1.60 (s, 3H), 1.35 (s, 9H), 1.32 (s, 3H). $^{13}\text{C NMR}$ (75 MHz, CDCl_3): δ /ppm = 172.4, 156.2, 156.0, 152.8, 148.9, 140.6, 121.1, 114.9, 92.5, 83.6, 82.5, 81.5, 79.3, 41.1, 36.9, 36.3, 28.5, 27.6, 25.4. FT-IR: ν/cm^{-1} = 3323, 3207, 2980, 2935, 1643, 1600, 1507, 1366, 1247, 1210, 1164, 1077, 854, 750. Mp: 98–101 $^{\circ}\text{C}$. $[\alpha]_{\text{D}}^{20}$ = -132 (10 mg/mL; CHCl_3).

N^4 -(((2R,3S,4R,5R)-5-(6-Amino-9H-purin-9-yl)-3,4-dihydroxytetrahydrofuran-2-yl)methyl)-L-asparagine Trifluoroacetate Salt (21a). Cold trifluoroacetic acid (1.5 mL) was added to a solution of compound **20a** (106 mg, 0.18 mmol) in DCM (1.5 mL) at -20 $^{\circ}\text{C}$. The solution was stirred at -20 $^{\circ}\text{C}$ until LC-MS analysis indicated complete removal of Boc and ester groups. DCM (40 mL) was added, and the solvent was removed under reduced pressure at 40 $^{\circ}\text{C}$. After co-distillation with DCM (3 \times 40 mL), the residues were dissolved in water (1.5 mL) and cooled down to 5 $^{\circ}\text{C}$. Cold trifluoroacetic acid (250 μ L) was added, and the solution was stirred at 5 $^{\circ}\text{C}$ overnight. Water (5 mL) was added, and the mixture was lyophilized. The desired product was obtained as the trifluoroacetate salt (colorless solid, 89 mg, 0.18 mmol, quant.). $^1\text{H NMR}$ (300 MHz, CD_3OD): δ /ppm = 8.35 (s, 1H), 8.29 (s, 1H), 5.91 (d, J = 5.3 Hz, 1H), 4.64 (t, J = 5.3 Hz, 1H), 4.22–4.12 (m, 2H), 4.08–4.00 (m, 1H), 3.61–3.40 (m, 2H), 2.94–2.76 (m, 2H). $^{13}\text{C NMR}$ (75 MHz, CD_3OD): δ /ppm = 171.4, 171.3, 153.2, 149.9, 147.1, 144.1, 120.8, 90.8, 85.0, 75.1, 72.8, 51.0, 42.3, 35.4. FT-IR:

$\nu/\text{cm}^{-1} = 3087, 2981, 1664, 1507, 1423, 1323, 1186, 1129, 1069, 899, 836, 798, 721$. Mp: 72 °C (decomposition). $[\alpha]_{\text{D}}^{20} = -20$ (10 mg/mL; MeOH). ESI-MS: m/z $[M + H]^+ = 382.13$ (100%), 383.12 (17.2%), 384.13 (2.1%). Calculated: 382.15 (100%), 383.15 (15.6%), 384.15 (2.7%). Purity: 95% (HPLC, MeCN/H₂O = 20:80 + 0.1% HCOOH); $t_{\text{R}} = 3.68$ min.

***N*²-(((2*R*,3*S*,4*R*,5*R*)-5-(6-Amino-9*H*-purin-9-yl)-3,4-dihydroxytetrahydrofuran-2-yl)methyl)-L-glutamine Trifluoroacetate Salt (21b)**. Cold trifluoroacetic acid (1.5 mL) was added to a solution of compound **20b** (101 mg, 0.17 mmol) in DCM (1.5 mL) at -20 °C. The solution was stirred at -20 °C until LC-MS analysis indicated complete removal of Boc and ester groups. DCM (40 mL) was added, and the solvent was removed under reduced pressure at 40 °C. After co-distillation with DCM (3 × 40 mL), the residues were dissolved in water (1.5 mL) and cooled down to 5 °C. Cold trifluoroacetic acid (250 μL) was added, and the solution was stirred at 5 °C overnight. Water (5 mL) was added, and the mixture was lyophilized. The desired product was obtained as the trifluoroacetate salt (yellowish solid, 87 mg, 0.17 mmol quant.). ¹H NMR (300 MHz, CD₃OD): $\delta/\text{ppm} = 8.36$ (s, 1H), 8.30 (s, 1H), 5.91 (d, $J = 5.4$ Hz, 1H), 4.66–4.61 (m, 1H), 4.16–4.10 (m, 1H), 4.08–4.00 (m, 1H), 3.95–3.88 (m, 1H), 3.59–3.39 (m, 2H), 2.46–2.38 (m, 2H), 2.19–1.99 (m, 2H). ¹³C NMR (75 MHz, CD₃OD): $\delta/\text{ppm} = 174.5, 171.6, 152.8, 150.0, 146.5, 144.2, 120.9, 90.9, 85.1, 75.2, 72.9, 53.6, 42.5, 32.4, 27.2$. FT-IR: $\nu/\text{cm}^{-1} = 3082, 2945, 1667, 1556, 1507, 1424, 1323, 1184, 1129, 898, 836, 797, 721$. Mp: 77–80 °C. $[\alpha]_{\text{D}}^{20} = -17$ (10 mg/mL; MeOH). ESI-MS: m/z $[M + H]^+ = 396.15$ (100%), 397.14 (18%), 398.15 (2.6%). Calculated: 396.16 (100%), 397.17 (16.7%), 398.17 (2.5%). Purity: 96% (HPLC, MeCN/H₂O = 20:80 + 0.1% HCOOH); $t_{\text{R}} = 2.22$ min.

4-(((2*R*,3*S*,4*R*,5*R*)-5-(6-Amino-9*H*-purin-9-yl)-3,4-dihydroxytetrahydrofuran-2-yl)methyl)amino)-4-oxobutanoic Acid (21c). Cold trifluoroacetic acid (1.5 mL) was added to a solution of compound **20b** (50 mg, 0.11 mmol) in DCM (1.5 mL) at -20 °C. The solution was stirred at -20 °C until LC-MS analysis indicated complete removal of the ester group. DCM (40 mL) was added, and the solvent was removed under reduced pressure at 40 °C. After co-distillation with DCM (3 × 40 mL), the residues were dissolved in water (1.5 mL) and cooled down to 5 °C. Cold trifluoroacetic acid (250 μL) was added, and the solution was stirred at 5 °C overnight. Water (5 mL) was added, and the mixture was lyophilized to give the desired product as a colorless solid (40 mg, 0.11 mmol, quant.). ¹H NMR (300 MHz, CD₃OD): $\delta/\text{ppm} = 8.40$ –8.28 (m, 2H), 5.94 (d, $J = 5.9$ Hz, 1H), 4.77–4.71 (m, 1H), 4.21–4.10 (m, 2H), 3.77–3.66 (m, 1H), 3.41 (dd, $J = 14.3, 4.1$ Hz, 1H), 2.63–2.55 (m, 2H), 2.55–2.47 (m, 2H). ¹³C NMR (75 MHz, CD₃OD): $\delta/\text{ppm} = 175.0, 174.9, 154.6, 150.1, 149.5, 143.5, 120.9, 90.8, 85.6, 74.9, 72.7, 42.1, 31.6, 30.0$. FT-IR: $\nu/\text{cm}^{-1} = 3305, 3102, 2935, 1646, 1553, 1420, 1195, 1129, 1059, 834, 798, 721$. Mp: 64–67 °C. $[\alpha]_{\text{D}}^{20} = -64$ (5 mg/mL; MeOH). ESI-MS: m/z $[M + H]^+ = 367.12$ (100%), 368.09 (16.8%), 369.10 (2.3%). Calculated: 367.14 (100%), 368.14 (15.6%), 369.14 (2.7%). Purity: 100% (HPLC, MeCN/H₂O = 20:80 + 0.1% HCOOH); $t_{\text{R}} = 4.19$ min.

3-Amino-N-(((2*R*,3*S*,4*R*,5*R*)-5-(6-amino-9*H*-purin-9-yl)-3,4-dihydroxytetrahydrofuran-2-yl)methyl)propanamide Trifluoroacetate Salt (21d). Cold trifluoroacetic acid (1.5 mL) was added to a solution of compound **20d** (83 mg, 0.17 mmol) in DCM (1.5 mL) at -20 °C. The solution was stirred at -20 °C until LC-MS analysis indicated complete removal of Boc and ester groups. DCM (40 mL) was added, and the solvent was removed under reduced pressure at 40 °C. After co-distillation with DCM (3 × 40 mL), the residues were dissolved in water (1.5 mL) and cooled down to 5 °C. Cold trifluoroacetic acid (250 μL) was added, and the solution was stirred at 5 °C overnight. Water (5 mL) was added, and the mixture was lyophilized. The desired product was obtained as the trifluoroacetate salt (yellow resin, 78 mg, 0.17 mmol quant.). ¹H NMR (300 MHz, CD₃OD): $\delta/\text{ppm} = 8.44$ (s, 1H), 8.38 (s, 1H), 5.99 (d, $J = 5.2$ Hz, 1H), 4.75–4.68 (m, 1H), 4.25–4.18 (m, 1H), 4.16–4.08 (m, 1H), 3.65–3.51 (m, 2H), 3.20–3.14 (m, 2H), 2.66–2.58 (m, 2H). ¹³C NMR (75 MHz, CD₃OD): $\delta/\text{ppm} = 171.1, 152.2, 148.7, 146.4, 142.4, 119.5, 89.5, 83.6, 73.7, 71.5, 41.0, 35.7, 31.4$. FT-IR: $\nu/\text{cm}^{-1} = 3271, 3088, 1666, 1557, 1507, 1423, 1325, 1183, 1126, 1074, 835, 798, 721$. $[\alpha]_{\text{D}}^{20} = -23$ (10 mg/mL; MeOH). ESI-MS: m/z $[M +$

$H]^+ = 338.13$ (100%), 339.12 (15.5%), 340.11 (2.0%). Calculated: 338.16 (100%), 339.16 (14.4%), 340.16 (2.1%). Purity: 95% (HPLC, MeCN/H₂O = 20:80 + 0.1% HCOOH); $t_{\text{R}} = 4.02$ min.

***N*-(((3*aR*,4*R*,6*R*,6*aR*)-6-(6-Amino-9*H*-purin-9-yl)-2,2-dimethyltetrahydrofuro[3,4-*d*][1,3]dioxol-4-yl)methyl)-*N*-methyl-2-nitrobenzenesulfonamide (22)**. To a solution of 2',3'-*O*-isopropylidenedenosine (**5**) (0.5 g, 1.6 mmol, 1.0 equiv) in THF (12 mL) at 0 °C were added 2-nitro-*N*-methylbenzenesulfonamide (387 mg, 1.8 mmol, 1.1 equiv), PPh₃ (726 mg, 2.8 mmol, 1.7 equiv), and DIAD (0.54 mL, 560 mg, 2.8 mmol, 1.7 equiv), and the mixture was stirred at rt for 24 h. The reaction was concentrated, and the residue was recrystallized in hot MeOH (25 mL) and further purified by column chromatography (DCM/MeOH = 25:1) to give **22** (192 mg, 0.38 mmol, 23%) as a yellow solid. ¹H NMR (300 MHz, CDCl₃): $\delta/\text{ppm} = 8.30$ (d, $J = 9.0$ Hz, 2H), 8.17 (s, 1H), 7.92 (dd, $J = 8.3, 1.4$ Hz, 1H), 7.85–7.78 (m, 2H), 7.76–7.66 (m, 1H), 7.36 (s, 2H), 6.21 (d, $J = 2.3$ Hz, 1H), 5.45 (dd, $J = 6.4, 2.3$ Hz, 1H), 5.08 (dd, $J = 6.4, 3.4$ Hz, 1H), 4.40–4.27 (m, 1H), 3.63 (dd, $J = 14.5, 5.3$ Hz, 1H), 3.51–3.40 (m, 1H), 2.77 (s, 3H), 1.53 (s, 3H), 1.32 (s, 3H). ¹³C NMR (75.5 MHz, CDCl₃): $\delta/\text{ppm} = 156.1, 152.7, 148.7, 147.8, 140.3, 134.5, 132.3, 130.4, 129.8, 124.3, 119.2, 113.6, 89.0, 84.4, 83.2, 81.8, 51.4, 35.7, 27.0, 25.2$. FT-IR: $\nu/\text{cm}^{-1} = 3114, 1543, 1372, 1347, 1217, 1205, 1170, 1103, 1072, 1057, 972, 877, 854, 777, 767, 693$. Mp: 230–233 °C. $[\alpha]_{\text{D}}^{20} = -10$ (10 mg/mL; MeOH). $R_{\text{f}} = 0.25$ (DCM/MeOH = 20:1).

9-(((3*aR*,4*R*,6*R*,6*aR*)-2,2-Dimethyl-6-((methylamino)methyl)-tetrahydrofuro[3,4-*d*][1,3]dioxol-4-yl)-9*H*-purin-6-amine (23). To a solution of **22** (172 mg, 0.34 mmol, 1.0 equiv) in MeCN (3 mL) were added Cs₂CO₃ (332 mg, 1.02 mmol, 3.0 equiv) and thiophenol (0.14 mL, 1.36 mmol, 4.0 equiv), and the suspension was stirred at rt for 72 h. By the addition of 1 M NaOH (20 mL), the reaction was quenched, and the aqueous layer was extracted with DCM (3 × 20 mL). The combined organic layers were dried over anhydrous Na₂SO₄, filtered, and concentrated under reduced pressure at 40 °C. The residue was purified by column chromatography (DCM/MeOH = 90:10 to 70:30) to give **23** (71 mg, 0.22 mmol, 65%) as a yellow oil. ¹H NMR (300 MHz, CDCl₃): $\delta/\text{ppm} = 8.26$ (s, 1H), 7.87 (s, 1H), 6.56 (s, 2H), 5.97 (d, $J = 3.3$ Hz, 1H), 5.42 (dd, $J = 6.6, 3.2$ Hz, 1H), 5.01–4.94 (m, 1H), 4.37–4.30 (m, 1H), 2.83 (d, $J = 4.9$ Hz, 2H), 2.37 (s, 3H), 1.55 (s, 3H), 1.32 (s, 3H). ¹³C NMR (75.5 MHz, CDCl₃): $\delta/\text{ppm} = 156.0, 153.1, 149.3, 139.8, 120.3, 114.6, 90.9, 85.2, 83.5, 82.4, 53.5, 36.4, 27.3, 25.4$. FT-IR: $\nu/\text{cm}^{-1} = 3163, 2986, 1643, 1596, 1474, 1374, 1328, 1296, 1265, 1208, 1155, 1074, 866, 798, 732, 702$. $[\alpha]_{\text{D}}^{20} = -17$ (10 mg/mL; MeOH). $R_{\text{f}} = 0.11$ (DCM/MeOH = 10:1).

***tert*-Butyl (tert-Butoxycarbonyl)-L-homoserinate (24)**. To a solution of Boc-Asp-*O*^tBu (2.5 g, 8.7 mmol, 1.0 equiv) in dry THF (100 mL) under argon atmosphere at -10 °C was added *N*-methyl morpholine (0.95 mL, 875 mg, 8.7 mmol, 1.0 equiv). After 1 min, ethyl chloroformate (0.82 mL, 938 mg, 8.7 mmol, 1.0 equiv) was added, and the mixture was stirred for 15 min at -5 °C. Then, the precipitates were filtered off, and the filtrate was dropwise added to a 5 °C chilled solution of NaBH₄ (0.67 mL, 736 mg, 19.5 mmol, 2.3 equiv) in water. The reaction was slowly warmed up to rt and was stirred at rt for 18 h. The mixture was cooled to 5 °C and acidified to pH 2 with 3 M HCl. Then, the aqueous phase was extracted with EtOAc (2 × 25 mL), and the combined organic layers were washed with brine (3 × 25 mL), dried over anhydrous Na₂SO₄, filtered, and concentrated under reduced pressure at 40 °C. The residue was purified by column chromatography (cyclohexane/EtOAc = 1:1) to give **24** (1.73 g, 6.3 mmol, 73%) as a colorless oil. ¹H NMR (300 MHz, CDCl₃): $\delta/\text{ppm} = 5.48$ –5.23 (m, 1H), 4.45–4.22 (m, 1H), 3.76–3.55 (m, 2H), 3.33 (s, 1H), 2.20–2.04 (m, 1H), 1.44 (d, $J = 6.4$ Hz, 18H). ¹³C NMR (75.5 MHz, CDCl₃): $\delta/\text{ppm} = 172.1, 156.8, 82.4, 80.5, 58.4, 51.0, 36.7, 31.3, 28.4, 28.4, 28.1, 28.0$. FT-IR: $\nu/\text{cm}^{-1} = 3377, 2979, 1715, 1505, 1456, 1392, 1367, 1251, 1154, 1054, 846$. $[\alpha]_{\text{D}}^{20} = -39$ (10 mg/mL; MeOH). $R_{\text{f}} = 0.40$ (cyclohexane/EtOAc = 2:1).

***tert*-Butyl 2-((tert-Butoxycarbonyl)amino)-4-iodobutanoate (25)**. To a solution of **24** (0.5 g, 1.8 mmol, 1.0 equiv) in 1,2-dce at 0 °C were added DMAP (22 mg, 0.18 mmol, 0.1 equiv), tosyl chloride (693 mg, 3.6 mmol, 2.0 equiv), and NEt₃ (1.26 mL, 9.1 mmol, 5.0 equiv). After the mixture was stirred at rt for 4 h, the solvent was removed under

reduced pressure at 40 °C. The obtained residue was dissolved in EtOAc (20 mL) and washed with 1 M HCl (3 × 20 mL), saturated NaHCO₃ solution (3 × 20 mL), and brine (3 × 20 mL). The organic layer was dried over MgSO₄, filtered, and concentrated under reduced pressure at 40 °C to give a yellow oil. To a solution of the oil in acetone (5 mL) was added NaI (4.1 g, 27.3 mmol, 3.0 equiv), and the solution was stirred at rt for 42 h under light exclusion. The reaction was quenched by the addition of 10 mL of ice water and then extracted with EtOAc (3 × 15 mL). The organic layer was washed with brine (3 × 15 mL), dried over Na₂SO₄, filtered, and concentrated under reduced pressure at 40 °C. The obtained oil was purified via column chromatography to give **25** (462 mg, 1.2 mmol, 66%) as a brown oil. ¹H NMR (300 MHz, CDCl₃): δ/ppm = 5.15–5.00 (m, 1H), 4.18 (d, *J* = 5.1 Hz, 1H), 3.25–3.07 (m, 2H), 2.44–2.28 (m, 1H), 2.18–2.07 (m, 1H), 1.46 (d, *J* = 8.0 Hz, 18H). ¹³C NMR (75.5 MHz, CDCl₃): δ/ppm = 170.7, 155.4, 82.7, 80.2, 55.1, 37.8, 28.5, 28.1, –0.4. FT-IR: ν/cm⁻¹ = 2978, 2934, 1714, 1504, 1455, 1392, 1367, 1251, 1153, 1046, 1022, 846. [α]_D²⁰ = –13 (10 mg/mL; MeOH). *R*_f = 0.61 (cyclohexane/EtOAc = 2:1).

tert-Butyl (S)-4-(((3*aR*,4*R*,6*R*,6*aR*)-6-(6-Amino-9*H*-purin-9-yl)-2,2-dimethyltetrahydrofuro-[3,4-*d*][1,3]dioxol-4-yl)methyl)-(methyl)amino)-2-((tert-butoxycarbonyl)amino)butanoate (26a). To a solution of **23** (62 mg, 0.19 mmol, 1.0 equiv) in dry MeCN (1 mL) was added dropwise a solution of **25** (90 mg, 0.23 mmol, 1.2 equiv) in dry MeCN (1 mL). After stirring for 30 min, DIPEA (40 μL, 0.23 mmol, 1.2 equiv) was added, and the mixture was stirred at rt for further 18 h. After the reaction was heated to 55 °C for 6 h, the reaction was quenched by the addition of brine (10 mL), and the aqueous layer was extracted with EtOAc (3 × 15 mL). The combined organic layers were dried over anhydrous Na₂SO₄, filtered, and concentrated under reduced pressure at 40 °C. The residue was purified by column chromatography (DCM/MeOH = 30:1) to give **26a** (30 mg, 0.05 mmol, 28%) as a colorless oil. ¹H NMR (300 MHz, CDCl₃): δ/ppm = 8.33 (s, 1H), 7.94 (s, 1H), 6.05 (d, *J* = 2.2 Hz, 1H), 5.95 (s, 2H), 5.59 (d, *J* = 8.3 Hz, 1H), 5.48–5.40 (m, 1H), 5.02–4.86 (m, 1H), 4.47–4.33 (m, 1H), 4.23–4.10 (m, 1H), 2.85–2.35 (m, 4H), 2.27 (s, 3H), 2.06–1.70 (m, 3H), 1.60 (s, 3H), 1.46–1.32 (m, 21H). ¹³C NMR (75.5 MHz, CDCl₃): δ/ppm = 171.6, 155.8, 155.6, 153.2, 149.4, 140.2, 120.5, 114.7, 90.9, 84.9, 84.0, 83.3, 81.9, 79.7, 59.4, 54.3, 52.9, 42.7, 29.3, 28.5, 28.1, 27.3, 25.5. FT-IR: ν/cm⁻¹ = 2978, 1704, 1642, 1597, 1475, 1366, 1330, 1296, 1249, 1211, 1152, 1076, 909, 870, 729. [α]_D²⁰ = –12 (10 mg/mL; MeOH). *R*_f = 0.41 (DCM/MeOH = 10:1).

tert-Butyl (S)-4-(((3*aR*,4*R*,6*R*,6*aR*)-6-(6-Amino-9*H*-purin-9-yl)-2,2-dimethyltetrahydrofuro-[3,4-*d*][1,3]dioxol-4-yl)methyl)(ethyl)amino)-2-((tert-butoxycarbonyl)amino)butanoate (26b). To a solution of **13a** (204 mg, 0.36 mmol, 1.0 equiv) in 1,2-dce (4 mL) at 0 °C under argon atmosphere were added acetaldehyde (48 mg, 1.09 mmol, 61 μL, 3.0 equiv) and HOAc (31 μL, 0.54 mmol, 1.5 equiv). The mixture was stirred at 0 °C for 30 min, and then NaBH(OAc)₃ (130 mg, 0.62 mmol, 1.7 equiv) was added. The reaction was slowly warmed up to rt and was then stirred overnight. The reaction was quenched by the addition of saturated NaHCO₃ solution (20 mL), and the aqueous layer was extracted with EtOAc (3 × 10 mL). The combined organic layers were dried over Na₂SO₄, filtered, and concentrated under reduced pressure at 40 °C. The residue was purified by column chromatography (DCM/MeOH = 30:1) to give **26b** as a colorless oil (71 mg, 0.12 mmol, 34%). ¹H NMR (300 MHz, CDCl₃): δ/ppm = 8.30 (s, 1H), 7.92 (s, 1H), 6.23 (s, 2H), 6.03 (d, *J* = 2.1 Hz, 1H), 5.73 (d, *J* = 8.1 Hz, 1H), 5.52–5.41 (m, 1H), 4.95 (dd, *J* = 6.5, 3.4 Hz, 1H), 4.36–4.27 (m, 1H), 4.21–4.08 (m, 1H), 2.79–2.69 (m, 1H), 2.63–2.37 (m, 5H), 1.97–1.81 (m, 1H), 1.78–1.62 (m, 1H), 1.58 (s, 3H), 1.44–1.34 (m, 21H), 1.32–1.26 (m, 2H), 0.92 (t, *J* = 6.7 Hz, 3H). ¹³C NMR (75.5 MHz, CDCl₃): δ/ppm = 171.9, 155.9, 155.6, 153.1, 149.3, 140.2, 120.4, 114.4, 91.0, 85.6, 83.9, 83.4, 81.7, 79.4, 55.6, 53.1, 50.1, 48.0, 29.8, 29.2, 28.4, 28.1, 27.2, 25.2, 11.3. FT-IR: ν/cm⁻¹ = 2977, 1704, 1643, 1597, 1366, 1297, 1248, 1210, 1152, 1061, 909, 871, 799, 729. [α]_D²⁰ = –9 (10 mg/mL; MeOH). *R*_f = 0.51 (DCM/MeOH = 10:1).

tert-Butyl (S)-4-(((3*aR*,4*R*,6*R*,6*aR*)-6-(6-Amino-9*H*-purin-9-yl)-2,2-dimethyltetrahydrofuro-[3,4-*d*][1,3]dioxol-4-yl)methyl)(propyl)amino)-2-((tert-butoxycarbonyl)amino)butanoate (26c). To a sol-

ution of **13a** (200 mg, 0.35 mmol, 1.0 equiv) in 1,2-dce (4 mL) at 0 °C under argon atmosphere were added propionaldehyde (51 μL, 0.71 mmol, 2.0 equiv) and HOAc (30 μL, 0.53 mmol, 1.5 equiv). The mixture was stirred at 0 °C for 30 min, and then NaBH(OAc)₃ (128 mg, 0.60 mmol, 1.7 equiv) was added. The reaction was slowly warmed up to rt and was then stirred overnight. The reaction was quenched by the addition of saturated NaHCO₃ solution (20 mL), and the aqueous layer was extracted with EtOAc (3 × 10 mL). The combined organic layers were dried over Na₂SO₄, filtered, and concentrated under reduced pressure at 40 °C. The residue was purified by column chromatography (DCM/MeOH = 30:1) to give **26c** as a colorless oil (129 mg, 0.21 mmol, 60%). ¹H NMR (300 MHz, CDCl₃): δ/ppm = 8.27 (s, 1H), 7.89 (s, 1H), 6.47 (s, 2H), 6.01 (d, *J* = 2.1 Hz, 1H), 5.84 (d, *J* = 8.1 Hz, 1H), 5.52–5.43 (m, 1H), 4.94 (dd, *J* = 6.4, 3.3 Hz, 1H), 4.32–4.25 (m, 1H), 4.17–4.07 (m, 1H), 2.79–2.65 (m, 1H), 2.60–2.20 (m, 5H), 1.94–1.80 (m, 1H), 1.71–1.60 (m, 1H), 1.55 (s, 3H), 1.45–1.30 (m, 21H), 0.76 (t, *J* = 6.8 Hz, 3H). ¹³C NMR (75.5 MHz, CDCl₃): δ/ppm = 172.0, 156.0, 155.6, 153.0, 149.2, 140.1, 120.3, 114.2, 91.0, 85.6, 83.8, 83.5, 81.5, 79.3, 56.6, 56.1, 53.1, 50.8, 29.1, 28.4, 28.0, 27.2, 25.5, 19.8, 11.8. FT-IR: ν/cm⁻¹ = 2978, 1704, 1642, 1597, 1475, 1367, 1297, 1248, 1210, 1153, 1076, 907, 871, 799, 728. [α]_D²⁰ = –22 (10 mg/mL; MeOH). *R*_f = 0.57 (DCM/MeOH = 10:1).

tert-Butyl (S)-4-(((3*aR*,4*R*,6*R*,6*aR*)-6-(6-Amino-9*H*-purin-9-yl)-2,2-dimethyltetrahydrofuro-[3,4-*d*][1,3]dioxol-4-yl)methyl)-(isopropyl)amino)-2-((tert-butoxycarbonyl)amino)butanoate (26d). To a 0 °C cooled solution of **12** (150 mg, 0.49 mmol, 1.0 equiv) were added acetone (72 μL, 0.98 mmol, 2.0 equiv) and HOAc (56 μL, 0.98 mmol, 2.0 equiv). After stirring for 30 min at rt, NaBH₃CN (154 mg, 2.45 mmol, 5.0 equiv) was added, and the reaction was stirred at rt for 18 h. The solvent was removed under reduced pressure at 40 °C, and the residue was dissolved in water (15 mL). The aqueous layer was then extracted with EtOAc (3 × 20 mL). The combined organic layers were dried over anhydrous Na₂SO₄, filtered, and concentrated under reduced pressure at 40 °C. The residue was utilized without further purification. The residue (64 mg, 0.21 mmol, 1.0 equiv) was dissolved in 1,2-dce (4 mL) and was cooled to 0 °C. Compound **11a** (114 mg, 0.42 mmol, 2.0 equiv) and HOAc (18 μL, 0.31 mmol, 1.5 equiv) were added, and the mixture was stirred at 0 °C for 30 min. After the addition of NaBH(OAc)₃ (71 mg, 0.33 mmol, 1.6 equiv), the reaction was stirred at rt for 18 h. By the addition of saturated NaHCO₃ solution (20 mL), the reaction was quenched. The aqueous layer was extracted with EtOAc (3 × 20 mL), and the combined organic layers were dried over anhydrous Na₂SO₄, filtered, and concentrated under reduced pressure at 40 °C. The residue was purified by column chromatography (DCM/MeOH = 30:1) to give **26d** (84 mg, 0.14 mmol, 66%) as a colorless oil. ¹H NMR (300 MHz, CDCl₃): δ/ppm = 8.28 (s, 1H), 7.90 (s, 1H), 6.38 (s, 2H), 6.02 (d, *J* = 2.1 Hz, 1H), 5.84 (d, *J* = 8.1 Hz, 1H), 5.53–5.44 (m, 1H), 4.98 (dd, *J* = 6.5, 3.2 Hz, 1H), 4.33–4.21 (m, 1H), 4.18–4.03 (m, 1H), 3.00–2.83 (m, 1H), 2.77–2.63 (m, 1H), 2.58–2.33 (m, 3H), 1.99–1.85 (m, 1H), 1.78–1.63 (m, 1H), 1.57 (s, 3H), 1.46–1.32 (m, 21H), 0.98 (d, *J* = 6.5 Hz, 3H), 0.77 (d, *J* = 6.5 Hz, 3H). ¹³C NMR (75.5 MHz, CDCl₃): δ/ppm = 172.0, 156.0, 155.6, 153.0, 149.2, 140.3, 120.3, 114.3, 91.1, 86.4, 83.8, 83.4, 81.5, 79.3, 53.1, 52.1, 50.9, 47.1, 30.4, 29.7, 28.4, 28.0, 27.2, 25.5, 19.4, 16.2. FT-IR: ν/cm⁻¹ = 2976, 1704, 1643, 1597, 1366, 1298, 1248, 1210, 1153, 1075, 908, 870, 799, 728. [α]_D²⁰ = –20 (10 mg/mL; MeOH). *R*_f = 0.45 (DCM/MeOH = 10:1).

tert-Butyl (S)-4-(((3*aR*,4*R*,6*R*,6*aR*)-6-(6-amino-9*H*-purin-9-yl)-2,2-dimethyltetrahydrofuro-[3,4-*d*][1,3]dioxol-4-yl)methyl)(butyl)amino)-2-((tert-butoxycarbonyl)amino)butanoate (26e). To a solution of **13a** (200 mg, 0.35 mmol, 1.0 equiv) in 1,2-dce (4 mL) at 0 °C under argon atmosphere were added butanal (51 mg, 0.71 mmol, 64 μL, 2.0 equiv) and HOAc (30 μL, 0.71 mmol, 1.5 equiv). The mixture was stirred at 0 °C for 30 min, and then NaBH(OAc)₃ (128 mg, 0.60 mmol, 1.7 equiv) was added. The reaction was slowly warmed up to rt and was then stirred overnight. The reaction was quenched by the addition of saturated NaHCO₃ solution (20 mL), and the aqueous layer was extracted with EtOAc (3 × 10 mL). The combined organic layers were dried over Na₂SO₄, filtered, and concentrated under reduced pressure at 40 °C. The residue was purified by column chromatography (DCM/MeOH = 30:1) to give **26e** as a colorless oil (155 mg, 0.25 mmol, 71%).

¹H NMR (300 MHz, CDCl₃): δ/ppm = 8.29 (s, 1H), 7.90 (s, 1H), 6.32 (s, 2H), 6.02 (s, 1H), 5.79 (d, *J* = 8.0 Hz, 1H), 5.57–5.41 (m, 1H), 4.95 (dd, *J* = 6.5, 3.3 Hz, 1H), 4.37–4.24 (m, 1H), 4.19–4.08 (m, 1H), 2.79–2.65 (m, 1H), 2.61–2.21 (m, 5H), 1.98–1.79 (m, 1H), 1.77–1.62 (m, 1H), 1.57 (s, 3H), 1.43–1.34 (m, 21H), 1.32–1.08 (m, 5H), 0.81 (t, *J* = 7.1 Hz, 3H). ¹³C NMR (75.5 MHz, CDCl₃): δ/ppm = 171.9, 155.9, 155.6, 153.1, 149.2, 140.2, 120.4, 114.3, 91.0, 85.6, 83.9, 83.5, 81.6, 79.3, 56.1, 54.3, 53.1, 50.8, 29.1, 28.7, 28.4, 28.0, 27.2, 25.5, 20.5, 14.0. FT-IR: ν/cm⁻¹ = 2978, 1704, 1642, 1597, 1475, 1367, 1330, 1297, 1248, 1210, 1153, 1076, 908, 871, 799, 728. [α]_D²⁰ = -23 (10 mg/mL; MeOH). *R*_f = 0.48 (DCM/MeOH = 20:1).

tert-Butyl (5)-4-(((3*aR*,4*R*,6*R*,6*aR*)-6-(6-*amino-9H-purin-9-yl*)-2,2-dimethyltetrahydrofuro-[3,4-*d*][1,3]dioxol-4-yl)methyl)-(isobutylamino)-2-((*tert*-butoxycarbonyl)amino)butanoate (**26f**). To a solution of **13a** (250 mg, 0.44 mmol, 1.0 equiv) in 1,2-dce (4 mL) at 0 °C under argon atmosphere were added isobutanol (49 μL, 0.53 mmol, 1.2 equiv) and HOAc (38 μL, 0.67 mmol, 1.5 equiv). The mixture was stirred at 0 °C for 30 min, and then NaBH(OAc)₃ (160 mg, 0.75 mmol, 1.7 equiv) was added. The reaction was slowly warmed up to rt and was then stirred overnight. The reaction was quenched by the addition of saturated NaHCO₃ solution (20 mL), and the aqueous layer was extracted with EtOAc (3 × 10 mL). The combined organic layers were dried over Na₂SO₄, filtered, and concentrated under reduced pressure at 40 °C. The residue was purified by column chromatography (DCM/MeOH = 30:1) to give **26f** as a colorless oil (162 mg, 0.26 mmol, 59%). ¹H NMR (300 MHz, CDCl₃): δ/ppm = 8.24 (s, 1H), 7.86 (s, 1H), 6.59 (s, 2H), 6.00 (d, *J* = 2.1 Hz, 1H), 5.91 (d, *J* = 8.0 Hz, 1H), 5.53–5.41 (m, 1H), 4.94 (dd, *J* = 6.5, 3.1 Hz, 1H), 4.31–4.22 (m, 1H), 4.17–3.96 (m, 1H), 2.70 (dd, *J* = 13.5, 7.2 Hz, 1H), 2.58–2.25 (m, 3H), 2.12–1.99 (m, 2H), 1.96–1.78 (m, 1H), 1.54 (s, 5H), 1.42–1.26 (m, 21H), 0.82 (d, *J* = 6.6 Hz, 3H), 0.72 (d, *J* = 6.6 Hz, 3H). ¹³C NMR (75.5 MHz, CDCl₃): δ/ppm = 172.1, 156.0, 155.6, 153.0, 149.1, 140.1, 120.2, 114.1, 91.1, 85.6, 83.7, 83.6, 81.4, 79.2, 63.7, 56.6, 53.1, 51.4, 28.8, 28.3, 28.0, 27.1, 26.3, 25.4, 20.9, 20.8. FT-IR: ν/cm⁻¹ = 2978, 1705, 1640, 1597, 1475, 1367, 1248, 1210, 1153, 1091, 907, 872, 727. [α]_D²⁰ = -34 (10 mg/mL; MeOH). *R*_f = 0.52 (DCM/MeOH = 10:1).

tert-Butyl (5)-4-(((3*aR*,4*R*,6*R*,6*aR*)-6-(6-*amino-9H-purin-9-yl*)-2,2-dimethyltetrahydrofuro-[3,4-*d*][1,3]dioxol-4-yl)methyl)-(neopentylamino)-2-((*tert*-butoxycarbonyl)amino)butanoate (**26g**). To a solution of **13a** (250 mg, 0.44 mmol, 1.0 equiv) in 1,2-dce (4 mL) at 0 °C under argon atmosphere were added pivalaldehyde (97 μL, 0.89 mmol, 2.0 equiv) and HOAc (38 μL, 0.67 mmol, 1.5 equiv). The mixture was stirred at 0 °C for 30 min, and then NaBH(OAc)₃ (160 mg, 0.75 mmol, 1.7 equiv) was added. The reaction was slowly warmed up to rt and was then stirred overnight. The reaction was quenched by the addition of saturated NaHCO₃ solution (20 mL), and the aqueous layer was extracted with EtOAc (3 × 10 mL). The combined organic layers were dried over Na₂SO₄, filtered, and concentrated under reduced pressure at 40 °C. The residue was purified by column chromatography (DCM/MeOH = 30:1) to give **26g** as a colorless oil (97 mg, 0.15 mmol, 35%). ¹H NMR (300 MHz, CDCl₃): δ/ppm = 8.29 (s, 1H), 7.88 (s, 1H), 6.27 (s, 2H), 6.02 (d, *J* = 2.2 Hz, 1H), 5.57 (d, *J* = 7.1 Hz, 1H), 5.47 (d, *J* = 6.3 Hz, 1H), 5.04–4.95 (m, 1H), 4.39–4.26 (m, 1H), 4.16–4.02 (m, 1H), 2.85–2.72 (m, 1H), 2.70–2.53 (m, 2H), 2.51–2.40 (m, 1H), 2.20–2.11 (m, 2H), 1.95–1.80 (m, 1H), 1.57 (s, 4H), 1.48–1.31 (m, 21H), 0.80 (s, 9H). ¹³C NMR (75.5 MHz, CDCl₃): δ/ppm = 171.9, 155.9, 155.5, 153.1, 149.3, 140.1, 120.4, 114.3, 91.0, 85.9, 83.9, 83.5, 81.7, 79.4, 68.4, 58.4, 53.2, 53.1, 29.5, 28.4, 28.3, 28.0, 27.3, 25.5. FT-IR: ν/cm⁻¹ = 2977, 1705, 1643, 1598, 1478, 1366, 1248, 1209, 1152, 1075, 909, 871, 730. [α]_D²⁰ = -16 (10 mg/mL; MeOH). *R*_f = 0.55 (DCM/MeOH = 10:1).

tert-Butyl (5)-4-(((3*aR*,4*R*,6*R*,6*aR*)-6-(6-*amino-9H-purin-9-yl*)-2,2-dimethyltetrahydrofuro-[3,4-*d*][1,3]dioxol-4-yl)methyl)-(cyclopropylmethylamino)-2-((*tert*-butoxycarbonyl)amino)butanoate (**26h**). To a solution of **13a** (200 mg, 0.35 mmol, 1.0 equiv) in 1,2-dce (4 mL) at 0 °C under argon atmosphere were added cyclopropanecarbaldehyde (75 μL, 0.71 mmol, 2.0 equiv) and HOAc (30 μL, 0.53 mmol, 1.5 equiv). The mixture was stirred at 0 °C for 30 min, and then NaBH(OAc)₃ (128 mg, 0.60 mmol, 1.7 equiv) was added. The reaction was slowly warmed up to rt and was then stirred

overnight. The reaction was quenched by the addition of saturated NaHCO₃ solution (20 mL), and the aqueous layer was extracted with EtOAc (3 × 10 mL). The combined organic layers were dried over Na₂SO₄, filtered, and concentrated under reduced pressure at 40 °C. The residue was purified by column chromatography (DCM/MeOH = 30:1) to give **26h** (123 mg, 0.20 mmol, 57%) as a colorless oil. ¹H NMR (300 MHz, CDCl₃): δ/ppm = 8.25 (s, 1H), 7.89 (s, 1H), 6.53 (s, 2H), 6.01 (d, *J* = 2.1 Hz, 1H), 5.94 (d, *J* = 8.0 Hz, 1H), 5.53–5.40 (m, 1H), 4.95 (dd, *J* = 6.4, 3.3 Hz, 1H), 4.37–4.24 (m, 1H), 4.13 (dd, *J* = 7.6, 3.0 Hz, 1H), 2.81 (dd, *J* = 13.5, 6.7 Hz, 1H), 2.68–2.41 (m, 3H), 2.27 (d, *J* = 6.5 Hz, 2H), 1.96–1.78 (m, 1H), 1.78–1.59 (m, 1H), 1.54 (s, 3H), 1.39–1.28 (m, 21H), 0.83–0.66 (m, 1H), 0.37 (dd, *J* = 8.0, 3.6 Hz, 2H), 0.06–0.10 (m, 2H). ¹³C NMR (75.5 MHz, CDCl₃): δ/ppm = 171.9, 156.0, 155.6, 153.0, 149.1, 140.0, 120.2, 114.2, 90.9, 85.4, 83.8, 83.4, 81.5, 79.2, 59.3, 56.0, 53.1, 50.6, 29.0, 28.4, 28.2, 28.0, 27.1, 25.5, 8.3, 4.2, 3.7. FT-IR: ν/cm⁻¹ = 2980, 1704, 1640, 1367, 1248, 1211, 1153, 1091, 1077, 907, 871, 727. [α]_D²⁰ = -17 (10 mg/mL; MeOH). *R*_f = 0.50 (DCM/MeOH = 10:1).

tert-Butyl (5)-4-(((3*aR*,4*R*,6*R*,6*aR*)-6-(6-*amino-9H-purin-9-yl*)-2,2-dimethyltetrahydrofuro-[3,4-*d*][1,3]dioxol-4-yl)methyl)-(cyclobutylmethylamino)-2-((*tert*-butoxycarbonyl)amino)butanoate (**26i**). To a solution of **13a** (200 mg, 0.35 mmol, 1.0 equiv) in 1,2-dce (4 mL) at 0 °C under argon atmosphere were added cyclobutanecarbaldehyde (64 μL, 0.71 mmol, 2.0 equiv) and HOAc (30 μL, 0.53 mmol, 1.5 equiv). The mixture was stirred at 0 °C for 30 min, and then NaBH(OAc)₃ (128 mg, 0.60 mmol, 1.7 equiv) was added. The reaction was slowly warmed up to rt and was then stirred overnight. The reaction was quenched by the addition of saturated NaHCO₃ solution (20 mL), and the aqueous layer was extracted with EtOAc (3 × 10 mL). The combined organic layers were dried over Na₂SO₄, filtered, and concentrated under reduced pressure at 40 °C. The residue was purified by column chromatography (DCM/MeOH = 30:1) to give **26i** (97 mg, 0.15 mmol, 43%) as a colorless oil. ¹H NMR (300 MHz, CDCl₃): δ/ppm = 8.29 (s, 1H), 7.89 (s, 1H), 6.38 (s, 2H), 6.02 (d, *J* = 2.1 Hz, 1H), 5.90 (d, *J* = 8.0 Hz, 1H), 5.56–5.43 (m, 1H), 4.93 (dd, *J* = 6.4, 3.2 Hz, 1H), 4.29 (td, *J* = 6.9, 3.2 Hz, 1H), 4.17–4.06 (m, 1H), 2.70 (dd, *J* = 13.5, 7.0 Hz, 1H), 2.59–2.26 (m, 6H), 2.07–1.60 (m, 7H), 1.57 (s, 3H), 1.53–1.46 (m, 1H), 1.45–1.29 (m, 21H). ¹³C NMR (75.5 MHz, CDCl₃): δ/ppm = 172.0, 156.0, 155.6, 153.1, 149.2, 140.2, 120.3, 114.2, 91.1, 85.6, 83.8, 83.5, 81.5, 79.2, 61.0, 56.2, 53.2, 51.1, 33.4, 28.6, 28.4, 28.0, 27.4, 27.2, 27.1, 25.5, 18.7. FT-IR: ν/cm⁻¹ = 2975, 1705, 1644, 1598, 1366, 1297, 1248, 1209, 1152, 1075, 1029, 871, 799. [α]_D²⁰ = -28 (10 mg/mL; MeOH). *R*_f = 0.50 (DCM/MeOH = 10:1).

tert-Butyl (5)-4-(((3*aR*,4*R*,6*R*,6*aR*)-6-(6-*amino-9H-purin-9-yl*)-2,2-dimethyltetrahydrofuro-[3,4-*d*][1,3]dioxol-4-yl)methyl)-(cyclopentylmethylamino)-2-((*tert*-butoxycarbonyl)amino)butanoate (**26j**). To a solution of **13a** (200 mg, 0.35 mmol, 1.0 equiv) in 1,2-dce (4 mL) at 0 °C under argon atmosphere were added cyclopentanecarbaldehyde (76 μL, 0.71 mmol, 2.0 equiv) and HOAc (30 μL, 0.53 mmol, 1.5 equiv). The mixture was stirred at 0 °C for 30 min and then NaBH(OAc)₃ (128 mg, 0.60 mmol, 1.7 equiv) was added. The reaction was slowly warmed up to rt and was then stirred overnight. The reaction was quenched by the addition of saturated NaHCO₃ solution (20 mL), and the aqueous layer was extracted with EtOAc (3 × 10 mL). The combined organic layers were dried over Na₂SO₄, filtered, and concentrated under reduced pressure at 40 °C. The residue was purified by column chromatography (DCM/MeOH = 30:1) to give **26j** as a colorless oil (67 mg, 0.10 mmol, 29%). ¹H NMR (300 MHz, CDCl₃): δ/ppm = 8.25 (s, 1H), 7.85 (s, 1H), 6.13 (s, 2H), 5.99 (d, *J* = 2.1 Hz, 1H), 5.88 (d, *J* = 8.0 Hz, 1H), 5.53–5.39 (m, 1H), 4.94 (dd, *J* = 6.4, 3.2 Hz, 1H), 4.36–4.22 (m, 1H), 4.14–4.03 (m, 1H), 2.81–2.63 (m, 1H), 2.62–2.12 (m, 5H), 1.94–1.62 (m, 5H), 1.57 (s, 3H), 1.49–1.40 (m, 4H), 1.39–1.32 (m, 21H), 1.16–0.91 (m, 2H). ¹³C NMR (75.5 MHz, CDCl₃): δ/ppm = 172.0, 155.9, 155.7, 153.1, 149.2, 140.3, 120.4, 114.3, 91.2, 85.7, 83.9, 83.7, 81.5, 79.3, 60.8, 56.3, 53.4, 51.4, 37.7, 31.3, 31.2, 28.7, 28.5, 28.1, 27.2, 25.5, 25.3, 25.2. FT-IR: ν/cm⁻¹ = 2950, 1705, 1643, 1598, 1366, 1297, 1248, 1209, 1153, 1075, 909, 871, 799, 730, 682. [α]_D²⁰ = -30 (10 mg/mL; MeOH). *R*_f = 0.53 (DCM/MeOH = 10:1).

tert-Butyl (S)-4-(((3aR,4R,6R,6aR)-6-(6-Amino-9H-purin-9-yl)-2,2-dimethyltetrahydrofuro-[3,4-d][1,3]dioxol-4-yl)methyl)-(cyclohexylmethyl)amino)-2-((tert-butoxycarbonyl)-amino)-butanoate (26k). To a solution of 13a (200 mg, 0.35 mmol, 1.0 equiv) in 1,2-dce (4 mL) at 0 °C under argon atmosphere were added cyclohexanecarbaldehyde (51 μ L, 0.43 mmol, 1.2 equiv) and HOAc (30 μ L, 0.53 mmol, 1.5 equiv). The mixture was stirred at 0 °C for 30 min, and then NaBH(OAc)₃ (128 mg, 0.60 mmol, 1.7 equiv) was added. The reaction was slowly warmed up to rt and was then stirred overnight. The reaction was quenched by the addition of saturated NaHCO₃ solution (20 mL), and the aqueous layer was extracted with EtOAc (3 \times 10 mL). The combined organic layers were dried over Na₂SO₄, filtered, and concentrated under reduced pressure at 40 °C. The residue was purified by column chromatography (DCM/MeOH = 30:1) to give 26k (207 mg, 0.31 mmol, 89%) as a colorless oil. ¹H NMR (300 MHz, CDCl₃): δ /ppm = 8.26 (s, 1H), 7.87 (s, 1H), 6.55 (s, 2H), 6.00 (d, *J* = 1.4 Hz, 1H), 5.91 (d, *J* = 8.0 Hz, 1H), 5.46 (d, *J* = 6.4 Hz, 1H), 4.94 (d, *J* = 3.3 Hz, 1H), 4.34–4.22 (m, 1H), 4.16–4.04 (m, 1H), 2.76–2.64 (m, 1H), 2.60–2.40 (m, 2H), 2.40–2.24 (m, 1H), 2.20–1.98 (m, 2H), 1.93–1.70 (m, 2H), 1.69–1.48 (m, 7H), 1.42–1.30 (m, 21H), 1.30–1.12 (m, 3H), 1.10–0.99 (m, 2H), 0.80–0.62 (m, 2H). ¹³C NMR (75.5 MHz, CDCl₃): δ /ppm = 172.0, 156.0, 155.6, 153.0, 149.1, 140.1, 120.3, 114.1, 91.1, 85.6, 83.8, 83.6, 81.4, 79.2, 62.3, 56.7, 53.2, 51.6, 35.7, 31.7, 31.6, 28.9, 28.4, 28.0, 27.1, 26.7, 26.1, 26.0, 25.4. FT-IR: ν /cm⁻¹ = 2926, 1705, 1640, 1597, 1476, 1367, 1330, 1211, 1153, 1076, 907, 871, 799, 727. [α]_D²⁰ = -22 (10 mg/mL; MeOH). *R*_f = 0.59 (DCM/MeOH = 10:1).

tert-Butyl (S)-4-(Allyl(((3aR,4R,6R,6aR)-6-(6-amino-9H-purin-9-yl)-2,2-dimethyltetrahydro-furo[3,4-d][1,3]dioxol-4-yl)methyl)-amino)-2-((tert-butoxycarbonyl)-amino)butanoate (26l). To a solution of 13a (200 mg, 0.35 mmol, 1.0 equiv) in DMF (4 mL) were added allyl bromide (30 μ L, 0.39 mmol, 1.1 equiv) and DIPEA (66 μ L, 0.39 mmol, 1.1 equiv), and the mixture was stirred at rt overnight. The reaction was quenched by the addition of brine (20 mL), and the aqueous layer was extracted with EtOAc (3 \times 10 mL). The combined organic layers were dried over anhydrous Na₂SO₄, filtered, and concentrated under reduced pressure at 40 °C. The residue was purified by column chromatography (DCM/MeOH = 30:1) to give 26l as a colorless oil (117 mg, 0.19 mmol, 55%). ¹H NMR (300 MHz, CDCl₃): δ /ppm = 8.29 (s, 1H), 7.90 (s, 1H), 6.44–6.18 (m, 2H), 6.03 (d, *J* = 2.2 Hz, 1H), 5.81–5.60 (m, 2H), 5.48–5.42 (m, 1H), 5.09–4.98 (m, 2H), 4.97–4.90 (m, 1H), 4.38–4.27 (m, 1H), 4.19–4.09 (m, 1H), 3.18–3.08 (m, 1H), 3.05–2.95 (m, 1H), 2.80–2.67 (m, 1H), 2.64–2.38 (m, 3H), 1.98–1.82 (m, 1H), 1.79–1.62 (m, 1H), 1.58 (s, 3H), 1.46–1.32 (m, 21H). ¹³C NMR (75.5 MHz, CDCl₃): δ /ppm = 171.8, 155.9, 155.6, 153.1, 149.3, 140.1, 134.8, 120.4, 118.2, 114.4, 90.8, 85.5, 83.9, 83.4, 81.7, 79.4, 57.6, 55.7, 52.9, 50.4, 29.3, 28.4, 28.1, 27.2, 25.5. FT-IR: ν /cm⁻¹ = 2979, 1705, 1642, 1597, 1476, 1366, 1330, 1297, 1248, 1210, 1152, 1075, 911, 871, 799, 730. [α]_D²⁰ = -15 (10 mg/mL; MeOH). *R*_f = 0.56 (DCM/MeOH = 10:1).

tert-Butyl (S)-4-(((3aR,4R,6R,6aR)-6-(6-Amino-9H-purin-9-yl)-2,2-dimethyltetrahydrofuro-[3,4-d][1,3]dioxol-4-yl)methyl)(prop-2-yn-1-yl)amino)-2-((tert-butoxycarbonyl)amino)butanoate (26m). To a solution of 13a (200 mg, 0.35 mmol, 1.0 equiv) in DMF (4 mL) were added propargyl bromide (58 mg, 0.49 mmol, 37 μ L, 1.1 equiv) and DIPEA (66 μ L, 0.39 mmol, 1.1 equiv), and the mixture was stirred at rt overnight. The reaction was quenched by the addition of brine (20 mL), and the aqueous layer was extracted with EtOAc (3 \times 10 mL). The combined organic layers were dried over anhydrous Na₂SO₄, filtered, and concentrated under reduced pressure at 40 °C. The residue was purified by column chromatography (DCM/MeOH = 30:1) to give 26m as a colorless oil (155 mg, 0.26 mmol, 74%). ¹H NMR (300 MHz, CDCl₃): δ /ppm = 8.27 (s, 1H), 7.92 (s, 1H), 6.48 (s, 2H), 6.03 (d, *J* = 2.2 Hz, 1H), 5.68 (d, *J* = 8.2 Hz, 1H), 5.48–5.40 (m, 1H), 4.99–4.85 (m, 1H), 4.36–4.25 (m, 1H), 4.22–4.13 (m, 1H), 3.36 (t, *J* = 2.4 Hz, 2H), 2.81–2.60 (m, 2H), 2.52 (t, *J* = 6.8 Hz, 2H), 2.07 (s, 1H), 1.95–1.80 (m, 1H), 1.80–1.64 (m, 1H), 1.55 (s, 3H), 1.42–1.30 (m, 21H). ¹³C NMR (75.5 MHz, CDCl₃): δ /ppm = 171.8, 155.9, 155.5, 153.0, 149.2, 140.0, 120.3, 114.4, 90.8, 85.5, 83.9, 83.1, 81.7, 79.5, 77.9, 73.5, 55.3, 52.7, 50.2, 42.6, 29.8, 28.4, 28.0, 27.1, 25.4. FT-IR: ν /cm⁻¹ =

2980, 1704, 1640, 1597, 1367, 1329, 1297, 1248, 1211, 1153, 1075, 908, 871, 728. [α]_D²⁰ = -13 (10 mg/mL; MeOH). *R*_f = 0.68 (DCM/MeOH = 10:1).

tert-Butyl (S)-4-(((3aR,4R,6R,6aR)-6-(6-Amino-9H-purin-9-yl)-2,2-dimethyltetrahydrofuro-[3,4-d][1,3]dioxol-4-yl)methyl)(but-2-yn-1-yl)amino)-2-((tert-butoxycarbonyl)amino)butanoate (26n). To a solution of 13a (200 mg, 0.35 mmol, 1.0 equiv) in DMF (4 mL) were added 1-bromo-2-butyne (43 μ L, 0.49 mmol, 1.4 equiv) and DIPEA (66 μ L, 0.49), and the mixture was stirred at rt overnight. The reaction was quenched by the addition of brine (20 mL), and the aqueous layer was extracted with EtOAc (3 \times 10 mL). The combined organic layers were dried over anhydrous Na₂SO₄, filtered, and concentrated under reduced pressure at 40 °C. The residue was purified by column chromatography (DCM/MeOH = 30:1) to give 26n as a colorless solid (128 mg, 0.21 mmol, 60%). ¹H NMR (300 MHz, CDCl₃): δ /ppm = 8.31 (s, 1H), 7.96 (s, 1H), 6.32 (s, 2H), 6.05 (d, *J* = 2.2 Hz, 1H), 5.63 (d, *J* = 8.2 Hz, 1H), 5.45 (d, *J* = 6.4 Hz, 1H), 4.99–4.86 (m, 1H), 4.43–4.30 (m, 1H), 4.23–4.12 (m, 1H), 3.38–3.30 (m, 2H), 2.90–2.62 (m, 2H), 2.60–2.49 (m, 2H), 2.03–1.75 (m, 2H), 1.58 (s, 3H), 1.45–1.35 (m, 21H), 1.22 (s, 3H). ¹³C NMR (75.5 MHz, CDCl₃): δ /ppm = 171.8, 155.8, 155.6, 152.9, 149.3, 140.1, 120.3, 114.5, 90.9, 85.4, 84.0, 83.2, 81.7, 79.5, 77.4, 72.8, 55.5, 52.8, 50.3, 42.9, 29.7, 28.0, 27.2, 25.5, 3.4. FT-IR: ν /cm⁻¹ = 2929, 1705, 1642, 1597, 1367, 1329, 1296, 1248, 1210, 1153, 1077, 908, 871, 799, 729. Mp: 83–86 °C. [α]_D²⁰ = -10 (10 mg/mL; MeOH). *R*_f = 0.49 (DCM/MeOH = 10:1).

tert-Butyl (S)-4-(((3aR,4R,6R,6aR)-6-(6-Amino-9H-purin-9-yl)-2,2-dimethyltetrahydrofuro-[3,4-d][1,3]dioxol-4-yl)methyl)(pent-2-yn-1-yl)amino)-2-((tert-butoxycarbonyl)amino)butanoate (26o). To a solution of 13a (200 mg, 0.35 mmol, 1.0 equiv) in DMF (4 mL) were added 1-bromo-2-pentyne (50 μ L, 0.49 mmol, 1.4 equiv) and DIPEA (66 μ L, 0.39 mmol, 1.1 equiv), and the mixture was stirred at rt overnight. The reaction was quenched by the addition of brine (20 mL), and the aqueous layer was extracted with EtOAc (3 \times 10 mL). The combined organic layers were dried over anhydrous Na₂SO₄, filtered, and concentrated under reduced pressure at 40 °C. The residue was purified by column chromatography (DCM/MeOH = 30:1) to give 26o (115 mg, 0.18 mmol, 51%) as a colorless solid. ¹H NMR (300 MHz, CDCl₃): δ /ppm = 8.33 (s, 1H), 7.97 (s, 1H), 6.10 (s, 2H), 6.06 (d, *J* = 2.2 Hz, 1H), 5.58 (d, *J* = 8.2 Hz, 1H), 5.49–5.40 (m, 1H), 5.01–4.82 (m, 1H), 4.41–4.31 (m, 1H), 4.25–4.13 (m, 1H), 3.44–3.31 (m, 2H), 2.88–2.63 (m, 2H), 2.59–2.51 (m, 2H), 2.11 (qt, *J* = 7.5, 2.1 Hz, 2H), 2.01–1.71 (m, 2H), 1.59 (s, 3H), 1.47–1.29 (m, 21H), 1.06 (t, *J* = 7.5 Hz, 3H). ¹³C NMR (75.5 MHz, CDCl₃): δ /ppm = 171.8, 155.7, 155.6, 153.1, 149.4, 140.1, 120.4, 114.5, 90.9, 87.5, 85.4, 84.0, 83.2, 81.8, 79.6, 72.9, 55.5, 52.9, 50.3, 42.9, 29.7, 28.5, 28.1, 27.3, 25.5, 14.3, 12.4. FT-IR: ν /cm⁻¹ = 2926, 1705, 1642, 1366, 1247, 1210, 1153, 1080, 1028, 908, 871, 848, 730. Mp: 51–54 °C. [α]_D²⁰ = -11 (10 mg/mL; MeOH). *R*_f = 0.46 (DCM/MeOH = 10:1).

tert-Butyl (S)-4-(((3aR,4R,6R,6aR)-6-(6-Amino-9H-purin-9-yl)-2,2-dimethyltetrahydrofuro-[3,4-d][1,3]dioxol-4-yl)methyl)(but-3-yn-1-yl)amino)-2-((tert-butoxycarbonyl)amino)butanoate (26p). To a solution of 13a (200 mg, 0.35 mmol, 1.0 equiv) in DMF (4 mL) were added 4-bromo-1-butyne (46 μ L, 0.49 mmol, 1.4 equiv) and DIPEA (66 μ L, 0.39 mmol, 1.1 equiv), and the mixture was stirred at rt overnight. After the reaction was heated to 95 °C for 3 days, the reaction was quenched by the addition of brine (20 mL). The aqueous layer was extracted with EtOAc (3 \times 10 mL). The combined organic layers were dried over anhydrous Na₂SO₄, filtered, and concentrated under reduced pressure at 40 °C. The residue was purified by column chromatography (DCM/MeOH = 30:1) to give 26p (30 mg, 0.05 mmol, 14%) as a colorless solid. ¹H NMR (300 MHz, CDCl₃): δ /ppm = 8.35 (s, 1H), 7.93 (s, 1H), 6.05 (d, *J* = 2.2 Hz, 1H), 5.84 (s, 2H), 5.57–5.45 (m, 2H), 5.04–4.98 (m, 1H), 4.40–4.32 (m, 1H), 4.22–4.13 (m, 1H), 2.89–2.47 (m, 6H), 2.29 (td, *J* = 7.3, 2.7 Hz, 2H), 1.94 (s, 1H), 1.85–1.67 (m, 2H), 1.61 (s, 3H), 1.48–1.37 (m, 21H). ¹³C NMR (75.5 MHz, CDCl₃): δ /ppm = 171.8, 155.6, 153.1, 149.3, 140.5, 124.9, 120.5, 114.6, 91.1, 85.5, 83.9, 83.4, 82.5, 81.9, 79.7, 69.6, 55.8, 53.1, 52.8, 50.7, 29.8, 28.5, 28.1, 27.3, 25.5, 16.7. FT-IR: ν /cm⁻¹ = 2976, 2928, 1709, 1643, 1598, 1476, 1366, 1330, 1297, 1248, 1210, 1153, 1079, 871. Mp: 64–67

$^{\circ}\text{C}$. $[\alpha]_{\text{D}}^{20} = -21$ (10 mg/mL; MeOH). $R_f = 0.55$ (DCM/MeOH = 10:1).

tert-Butyl (S)-4-(((3aR,4R,6R,6aR)-6-(6-Amino-9H-purin-9-yl)-2,2-dimethyltetrahydrofuro[3,4-d][1,3]dioxol-4-yl)methyl)(benzyl-amino)-2-((tert-butoxycarbonyl)amino)butanoate (26q). To a solution of **13a** (200 mg, 0.35 mmol, 1.0 equiv) in 1,2-dce (4 mL) at 0°C under argon atmosphere were added benzaldehyde (72 μL , 0.71 mmol, 2.0 equiv) and HOAc (30 μL , 0.53 mmol, 1.5 equiv). The mixture was stirred at 0°C for 30 min, and then $\text{NaBH}(\text{OAc})_3$ (128 mg, 0.60 mmol, 1.7 equiv) was added. The reaction was slowly warmed up to rt and was then stirred overnight. The reaction was quenched by the addition of saturated NaHCO_3 solution (20 mL), and the aqueous layer was extracted with EtOAc (3×10 mL). The combined organic layers were dried over Na_2SO_4 , filtered, and concentrated under reduced pressure at 40°C . The residue was purified by column chromatography (DCM/MeOH = 30:1) to give **26q** as a colorless oil (142 mg, 0.23 mmol, 63%). ^1H NMR (300 MHz, CDCl_3): $\delta/\text{ppm} = 8.19$ (s, 1H), 7.82 (s, 1H), 7.24–7.15 (m, 5H), 6.24 (s, 2H), 6.01 (d, $J = 2.1$ Hz, 1H), 5.67 (d, $J = 8.1$ Hz, 1H), 5.33 (d, $J = 5.9$ Hz, 1H), 4.84 (dd, $J = 6.4$, 3.4 Hz, 1H), 4.41–4.29 (m, 1H), 4.22–4.09 (m, 1H), 3.69 (d, $J = 13.5$ Hz, 1H), 3.44 (d, $J = 13.5$ Hz, 1H), 2.82–2.70 (m, 1H), 2.66–2.42 (m, 3H), 2.03–1.89 (m, 1H), 1.84–1.69 (m, 1H), 1.57 (s, 3H), 1.45–1.31 (m, 21H). ^{13}C NMR (75.5 MHz, CDCl_3): $\delta/\text{ppm} = 171.8$, 155.8, 155.5, 153.1, 149.2, 139.9, 138.3, 129.1, 128.3, 127.3, 120.3, 114.4, 90.8, 85.3, 83.9, 83.5, 81.7, 79.4, 59.0, 55.7, 53.0, 50.8, 29.3, 28.5, 28.0, 27.2, 25.5. FT-IR: $\nu/\text{cm}^{-1} = 2979$, 1704, 1642, 1597, 1367, 1247, 1209, 1152, 1074, 908, 870, 728, 699. $[\alpha]_{\text{D}}^{20} = -14$ (10 mg/mL; MeOH). $R_f = 0.66$ (DCM/MeOH = 10:1).

tert-Butyl (S)-4-(((3aR,4R,6R,6aR)-6-(6-Amino-9H-purin-9-yl)-2,2-dimethyltetrahydrofuro[3,4-d][1,3]dioxol-4-yl)methyl)(phenethyl-amino)-2-((tert-butoxycarbonyl)amino)butanoate (26r). To a solution of **13a** (250 mg, 0.44 mmol, 1.0 equiv) in 1,2-dce (4 mL) at 0°C under argon atmosphere were added phenylacetaldehyde (103 μL , 0.89 mmol, 2.0 equiv) and HOAc (38 μL , 0.67 mmol, 1.5 equiv). The mixture was stirred at 0°C for 30 min, and then $\text{NaBH}(\text{OAc})_3$ (160 mg, 0.75 mmol, 1.7 equiv) was added. The reaction was slowly warmed up to rt and was then stirred overnight. The reaction was quenched by the addition of saturated NaHCO_3 solution (20 mL), and the aqueous layer was extracted with EtOAc (3×10 mL). The combined organic layers were dried over Na_2SO_4 , filtered, and concentrated under reduced pressure at 40°C . The residue was purified by column chromatography (DCM/MeOH = 30:1) to give **26r** as a colorless oil (140 mg, 0.21 mmol, 48%). ^1H NMR (300 MHz, CDCl_3): $\delta/\text{ppm} = 8.30$ (s, 1H), 7.87 (s, 1H), 7.24–7.01 (m, 5H), 6.52 (s, 2H), 6.03 (d, $J = 2.1$ Hz, 1H), 5.74 (d, $J = 8.1$ Hz, 1H), 5.52–5.42 (m, 1H), 4.95 (dd, $J = 6.5$, 3.4 Hz, 1H), 4.39–4.28 (m, 1H), 4.16–4.06 (m, 1H), 2.94–2.78 (m, 1H), 2.77–2.47 (m, 7H), 2.04–1.86 (m, 1H), 1.83–1.66 (m, 1H), 1.58 (s, 3H), 1.46–1.32 (m, 21H). ^{13}C NMR (75.5 MHz, CDCl_3): $\delta/\text{ppm} = 171.8$, 155.9, 155.5, 152.9, 149.1, 140.1, 139.9, 128.6, 128.4, 126.0, 120.2, 114.3, 90.9, 85.5, 83.7, 83.3, 81.6, 79.4, 56.2, 55.8, 52.8, 50.6, 33.0, 29.2, 28.0, 27.9, 27.1, 25.4. FT-IR: $\nu/\text{cm}^{-1} = 2978$, 1704, 1642, 1598, 1367, 1248, 1209, 1152, 1075, 909, 870, 729, 700. $[\alpha]_{\text{D}}^{20} = -14$ (10 mg/mL; MeOH). $R_f = 0.50$ (DCM/MeOH = 10:1).

tert-Butyl (S)-4-(((3aR,4R,6R,6aR)-6-(6-Amino-9H-purin-9-yl)-2,2-dimethyltetrahydrofuro[3,4-d][1,3]dioxol-4-yl)methyl)((R)/(S)-but-3-yn-2-yl)amino)-2-((tert-butoxycarbonyl)amino)butanoate (26s). To a solution of **13a** (200 mg, 0.35 mmol, 1.1 equiv) in DMF (4 mL) were added 3-bromo-1-butyne (32 μL , 0.35 mmol, 1.0 equiv), DIPEA (66 μL , 0.39 mmol, 1.1 equiv), and CuBr (7 mg, 0.035 mmol, 10 mol %), and the mixture was stirred at rt overnight. The reaction was quenched by the addition of brine (20 mL), and the aqueous layer was extracted with EtOAc (3×10 mL). The combined organic layers were dried over anhydrous Na_2SO_4 , filtered, and concentrated under reduced pressure at 40°C . The residue was purified by column chromatography (DCM/MeOH = 30:1) to give **26s** (107 mg, 0.17 mmol, 49%) as a colorless solid. The diastereomers were separated by semipreparative HPLC (reversed phase C_{18} , MeCN/ $\text{H}_2\text{O} = 25:75 + 0.1\%$ TFA, $t_{\text{R}}(\text{26s-B}) = 24$ min, $t_{\text{R}}(\text{26s-A}) = 26$ min) and directly used in the next step without further characterization. ^1H NMR (300 MHz, CDCl_3): δ/ppm

$= 8.29$ (s, 2H), 7.68 (s, 2H), 6.15 (dd, $J = 4.8$, 2.2 Hz, 1H), 5.44 (s, 1H), 5.25 (td, $J = 6.4$, 2.1 Hz, 1H), 4.97 (q, $J = 4.9$ Hz, 1H), 4.67–4.50 (m, 1H), 4.24 (d, $J = 21.4$ Hz, 1H), 4.12–4.00 (m, 1H), 3.55–2.79 (m, 4H), 2.63–2.41 (m, 1H), 2.25–2.04 (m, 1H), 1.99–1.79 (m, 1H), 1.60 (s, 3H), 1.48 (dd, $J = 20.0$, 6.7 Hz, 3H), 1.44–1.31 (m, 21H). ^{13}C NMR (75.5 MHz, CDCl_3): $\delta/\text{ppm} = 170.6$, 155.7, 152.2, 148.1, 145.0, 142.7, 120.1, 115.9, 90.7, 84.3, 83.9, 82.6, 82.4, 82.3, 80.2, 78.2, 53.6, 52.4, 50.8, 48.9, 28.3, 28.2, 27.9, 27.1, 25.4, 18.0. FT-IR: $\nu/\text{cm}^{-1} = 2982$, 1695, 1505, 1456, 1427, 1369, 1181, 1140, 1082, 911, 832, 799, 722. Mp: $80\text{--}83^{\circ}\text{C}$. $[\alpha]_{\text{D}}^{20} = +3$ (10 mg/mL; CDCl_3). $R_f = 0.69$ (DCM/MeOH = 9:1).

tert-Butyl (S)-4-(((3aR,4R,6R,6aR)-6-(6-Amino-9H-purin-9-yl)-2,2-dimethyltetrahydrofuro[3,4-d][1,3]dioxol-4-yl)methyl)(2-methylbut-3-yn-2-yl)amino)-2-((tert-butoxycarbonyl)amino)butanoate (26t). To a solution of **13a** (150 mg, 0.27 mmol, 1.0 equiv) in DMF (4 mL) were added 3-chloro-3-methyl-1-butyne (33 μL , 0.29 mmol, 1.1 equiv), DIPEA (50 μL , 0.29 mmol, 1.1 equiv), and CuBr (38 mg, 0.27 mmol, 1.0 equiv), and the mixture was stirred at rt for 48 h. The reaction was quenched by the addition of brine (20 mL), and the aqueous layer was extracted with EtOAc (3×10 mL). The combined organic layers were dried over anhydrous Na_2SO_4 , filtered, and concentrated under reduced pressure at 40°C . The residue was purified by column chromatography (DCM/MeOH = 30:1) to give **26t** (69 mg, 0.11 mmol, 41%) as a colorless oil. ^1H NMR (300 MHz, CDCl_3): $\delta/\text{ppm} = 8.30$ (s, 1H), 7.91 (s, 1H), 6.27 (s, 2H), 6.08–5.98 (m, 1H), 5.52–5.41 (m, 1H), 5.36 (d, $J = 8.0$ Hz, 1H), 5.00 (dd, $J = 6.6$, 3.4 Hz, 1H), 4.31 (td, $J = 6.6$, 3.4 Hz, 1H), 4.14–3.97 (m, 1H), 2.97 (dd, $J = 14.1$, 6.7 Hz, 1H), 2.70 (ddd, $J = 16.7$, 11.0, 6.7 Hz, 3H), 2.13 (s, 1H), 2.06–1.87 (m, 1H), 1.82–1.69 (m, 1H), 1.57 (s, 3H), 1.38 (d, $J = 11.3$ Hz, 24H), 1.25 (s, 3H). ^{13}C NMR (75.5 MHz, CDCl_3): $\delta/\text{ppm} = 171.9$, 155.8, 155.5, 152.9, 149.3, 140.4, 120.5, 114.4, 91.0, 87.2, 86.9, 84.0, 83.2, 81.8, 79.6, 70.8, 55.0, 53.7, 52.9, 48.3, 32.4, 29.1, 28.8, 28.4, 28.0, 27.3, 25.6. FT-IR: $\nu/\text{cm}^{-1} = 3307$, 2980, 2935, 1705, 1644, 1598, 1477, 1367, 1249, 1211, 1155, 1094, 871, 755. $[\alpha]_{\text{D}}^{20} = +6$ (10 mg/mL; CHCl_3). $R_f = 0.50$ (DCM/MeOH = 9:1).

(S)-2-Amino-4-(((2R,3S,4R,5R)-5-(6-amino-9H-purin-9-yl)-3,4-dihydroxytetrahydrofuran-2-yl)methyl)(methyl)amino)butanoic Acid Trifluoroacetate Salt (27a). To a solution of **26a** (21 mg, 0.04 mmol) in DCM (1.5 mL) at 5°C were added TFA (1.5 mL) and H_2O (200 μL). The solution was kept at 5°C for 3 d. After the reaction was diluted and co-distilled with DCM (3×20 mL), the residue was once more dissolved in DCM (1.5 mL) and TFA (1.5 mL). The solution was kept again at 5°C until full conversion was detected by LC-MS. Then, the reaction was diluted and co-distilled with DCM (5×20 mL). The residue was dissolved in H_2O (7 mL) and was dried by lyophilization to give **27a** (20 mg, 0.04 mmol, 99%, 1.0 equiv TFA) as a colorless trifluoroacetate salt. ^1H NMR (300 MHz, CD_3OD): $\delta/\text{ppm} = 8.50$ (s, 1H), 8.26 (s, 1H), 6.11 (d, $J = 5.4$ Hz, 1H), 4.74 (t, $J = 5.4$ Hz, 1H), 4.53 (d, $J = 10.9$ Hz, 1H), 4.31 (t, $J = 4.4$ Hz, 1H), 4.04 (dd, $J = 9.2$, 3.6 Hz, 1H), 3.77 (t, $J = 12.1$ Hz, 1H), 3.62–3.50 (m, 2H), 3.49–3.38 (m, 1H), 2.93 (s, 3H), 2.48–2.30 (m, 1H), 2.24–2.08 (m, 1H). ^{13}C NMR (75.5 MHz, CD_3OD): $\delta/\text{ppm} = 171.3$, 153.3, 149.8, 149.8, 144.0, 142.4, 90.5, 80.3, 74.9, 73.4, 59.4, 56.1, 53.3, 39.7, 26.1. FT-IR: $\nu/\text{cm}^{-1} = 3093$, 1668, 1507, 1425, 1325, 1196, 1129, 835, 799, 722. Mp: $86\text{--}89^{\circ}\text{C}$. $[\alpha]_{\text{D}}^{20} = +14$ (6 mg/mL; MeOH). ESI-MS: m/z $[\text{M} + \text{H}]^+ = 382.2$ (100%), 383.1 (18.7%), 384.1 (2.5%). Calculated: 382.2 (100%), 383.2 (16.2%), 384.2 (1.2%). Purity: 99% (HPLC, MeCN/ $\text{H}_2\text{O} = 20:80 + 0.1\%$ HCOOH); $t_{\text{R}} = 1.89$ min.

(S)-2-Amino-4-(((2R,3S,4R,5R)-5-(6-Amino-9H-purin-9-yl)-3,4-dihydroxytetrahydrofuran-2-yl)methyl)(ethyl)amino)butanoic Acid Trifluoroacetate Salt (27b). To a solution of **26b** (66 mg, 0.11 mmol) in DCM (1.5 mL) at 5°C were added TFA (1.5 mL) and H_2O (200 μL). The solution was kept at 5°C for 3 d. After the reaction was diluted and co-distilled with DCM (3×20 mL), the residue was once more dissolved in DCM (1.5 mL) and TFA (1.5 mL). The solution was kept again at 5°C until full conversion was detected by LC-MS. Then, the reaction was diluted and co-distilled with DCM (5×20 mL). The residue was dissolved in H_2O (7 mL) and was dried by lyophilization to give **27b** (69 mg, 0.11 mmol, 99%, 2.0 equiv TFA) as a colorless trifluoroacetate salt. ^1H NMR (300 MHz, CD_3OD): $\delta/\text{ppm} = 8.35$ (s,

1H), 8.25 (s, 1H), 6.01 (d, $J = 4.2$ Hz, 1H), 4.61 (t, $J = 4.7$ Hz, 1H), 4.43–4.24 (m, 2H), 3.94 (dd, $J = 8.2, 4.5$ Hz, 1H), 3.70–3.46 (m, 2H), 3.46–3.10 (m, 4H), 2.39–2.19 (m, 1H), 2.19–2.03 (m, 1H), 1.20 (t, $J = 7.2$ Hz, 3H). ^{13}C NMR (75.5 MHz, CD_3OD): $\delta/\text{ppm} = 170.7, 151.5, 148.3, 145.2, 142.9, 119.4, 90.2, 78.8, 73.4, 72.0, 54.5, 51.2, 50.2, 24.6, 7.2$. FT-IR: $\nu/\text{cm}^{-1} = 2471, 2074, 1663, 1506, 1424, 1183, 1128, 973, 833, 799, 721$. Mp: 80–83 °C. $[\alpha]_{\text{D}}^{20} = +18$ (10 mg/mL; MeOH). ESI-MS: m/z $[\text{M} + \text{H}]^+ = 396.2$ (100%), 397.2 (20.1%), 398.2 (2.5%). Calculated: 396.2 (100%), 397.2 (17.3%), 398.2 (1.4%). Purity: 99% (HPLC, MeCN/ $\text{H}_2\text{O} = 20:80 + 0.1\%$ HCOOH); $t_{\text{R}} = 2.82$ min.

(*S*)-2-Amino-4-(((2*R*,3*S*,4*R*,5*R*)-5-(6-amino-9*H*-purin-9-yl)-3,4-dihydroxytetrahydrofuran-2-yl)methyl)(propyl)amino)butanoic Acid Trifluoroacetate Salt (**27c**). To a solution of **26c** (121 mg, 0.20 mmol) in DCM (1.5 mL) at 5 °C were added TFA (1.5 mL) and H_2O (200 μL). The solution was kept at 5 °C for 3 d. After the reaction was diluted and co-distilled with DCM (3 \times 20 mL), the residue was once more dissolved in DCM (1.5 mL) and TFA (1.5 mL). The solution was kept again at 5 °C until full conversion was detected by LC-MS. Then, the reaction was diluted and co-distilled with DCM (5 \times 20 mL). The residue was dissolved in H_2O (7 mL) and was dried by lyophilization to give **27c** (106 mg, 0.20 mmol, 99%, 1.0 equiv TFA) as a colorless trifluoroacetate salt. ^1H NMR (300 MHz, CD_3OD): $\delta/\text{ppm} = 8.19$ (s, 1H), 8.13 (s, 1H), 5.85 (d, $J = 4.0$ Hz, 1H), 4.45 (t, $J = 4.5$ Hz, 1H), 4.26–4.12 (m, 2H), 3.78 (dd, $J = 7.8, 5.0$ Hz, 1H), 3.54–3.11 (m, 4H), 3.05–2.84 (m, 2H), 2.25–2.07 (m, 1H), 2.05–1.91 (m, 1H), 1.47 (dt, $J = 9.3, 7.0$ Hz, 2H), 0.68 (t, $J = 7.3$ Hz, 3H). ^{13}C NMR (75.5 MHz, CD_3OD): $\delta/\text{ppm} = 171.6, 152.5, 149.6, 146.0, 144.4, 120.9, 91.9, 80.0, 74.7, 73.4, 56.4, 56.2, 52.1, 51.8, 25.9, 17.9, 11.0$. FT-IR: $\nu/\text{cm}^{-1} = 2979, 2473, 2074, 1662, 1506, 1425, 1183, 1130, 973, 834, 798, 721$. Mp: 64–67 °C. $[\alpha]_{\text{D}}^{20} = +21$ (10 mg/mL; MeOH). ESI-MS: m/z $[\text{M} + \text{H}]^+ = 410.2$ (100%), 411.2 (24.5%), 412.2 (3.6%). Calculated: 410.2 (100%), 411.2 (18.4%), 412.2 (1.6%). Purity 100% (HPLC, MeCN/ $\text{H}_2\text{O} = 20:80 + 0.1\%$ HCOOH); $t_{\text{R}} = 2.61$ min.

(*S*)-2-Amino-4-(((2*R*,3*S*,4*R*,5*R*)-5-(6-amino-9*H*-purin-9-yl)-3,4-dihydroxytetrahydrofuran-2-yl)methyl)(isopropyl)amino)butanoic Acid Trifluoroacetate Salt (**27d**). To a solution of **26d** (65 mg, 0.11 mmol) in DCM (1.5 mL) at 5 °C were added TFA (1.5 mL) and H_2O (200 μL). The solution was kept at 5 °C for 3 d. After the reaction was diluted and co-distilled with DCM (3 \times 20 mL), the residue was once more dissolved in DCM (1.5 mL) and TFA (1.5 mL). The solution was kept again at 5 °C until full conversion was detected by LC-MS. Then, the reaction was diluted and co-distilled with DCM (5 \times 20 mL). The residue was dissolved in H_2O (7 mL) and was dried by lyophilization to give **27d** (77 mg, 0.11 mmol, 99%, 2.5 equiv TFA) as a colorless trifluoroacetate salt. ^1H NMR (300 MHz, CD_3OD): $\delta/\text{ppm} = 8.34$ (s, 1H), 8.29 (s, 1H), 6.01 (d, $J = 3.6$ Hz, 1H), 4.58 (s, 1H), 4.37–4.29 (m, 2H), 3.88 (dd, $J = 8.4, 4.4$ Hz, 1H), 3.78–3.63 (m, 1H), 3.58–3.49 (m, 2H), 3.46–3.23 (m, 2H), 3.19 (d, $J = 3.0$ Hz, 1H), 2.41–2.22 (m, 1H), 2.13 (d, $J = 12.2$ Hz, 1H), 1.28 (d, $J = 6.5$ Hz, 3H), 1.19 (d, $J = 5.7$ Hz, 3H). ^{13}C NMR (75.5 MHz, CD_3OD): $\delta/\text{ppm} = 172.0, 152.8, 149.7, 146.6, 144.2, 121.0, 92.0, 81.0, 74.7, 73.5, 57.9, 53.8, 52.7, 49.9, 27.0, 17.0, 16.0$. FT-IR: $\nu/\text{cm}^{-1} = 2992, 2488, 1663, 1506, 1425, 1182, 1128, 975, 833, 799, 721$. Mp: 88–91 °C. $[\alpha]_{\text{D}}^{20} = +19$ (10 mg/mL; MeOH). ESI-MS: m/z $[\text{M} + \text{H}]^+ = 410.2$ (100%), 411.2 (18.4%), 412.2 (1.6%). Calculated: 410.2 (100%), 411.2 (20.2%), 412.2 (3.0%). Purity: 98% (HPLC, MeCN/ $\text{H}_2\text{O} = 20:80 + 0.1\%$ HCOOH); $t_{\text{R}} = 3.81$ min.

(*S*)-2-Amino-4-(((2*R*,3*S*,4*R*,5*R*)-5-(6-amino-9*H*-purin-9-yl)-3,4-dihydroxytetrahydrofuran-2-yl)methyl)(butyl)amino)butanoic Acid Trifluoroacetate Salt (**27e**). To a solution of **26e** (150 mg, 0.24 mmol) in DCM (1.5 mL) at 5 °C were added TFA (1.5 mL) and H_2O (200 μL). The solution was kept at 5 °C for 3 d. After the reaction was diluted and co-distilled with DCM (3 \times 20 mL), the residue was once more dissolved in DCM (1.5 mL) and TFA (1.5 mL). The solution was kept again at 5 °C until full conversion was detected by LC-MS. Then, the reaction was diluted and co-distilled with DCM (5 \times 20 mL). The residue was dissolved in H_2O (7 mL) and was dried by lyophilization to give **27e** (123 mg, 0.24 mmol, 99%, 1.0 equiv TFA) as a colorless trifluoroacetate salt. ^1H NMR (300 MHz, CD_3OD): $\delta/\text{ppm} = 8.19$ (s, 1H), 8.13 (s, 1H), 5.85 (d, $J = 3.9$ Hz, 1H), 4.45 (t, $J = 4.4$ Hz, 1H), 4.24–4.13 (m, 2H), 3.78 (dd, $J = 7.7, 5.0$ Hz, 1H), 3.57–3.11 (m, 4H),

2.97 (d, $J = 5.0$ Hz, 2H), 2.21–2.07 (m, 1H), 2.01 (dd, $J = 9.6, 5.0$ Hz, 1H), 1.40 (dd, $J = 11.9, 6.0$ Hz, 2H), 1.07 (dd, $J = 7.5, 2.3$ Hz, 2H), 0.63 (t, $J = 6.7, 6.0$ Hz, 3H). ^{13}C NMR (75.5 MHz, CD_3OD): $\delta/\text{ppm} = 171.5, 152.5, 149.7, 146.0, 144.5, 120.9, 91.9, 80.0, 74.7, 73.4, 56.4, 54.6, 52.1, 51.7, 26.3, 25.9, 20.7, 13.8$. FT-IR: $\nu/\text{cm}^{-1} = 2969, 1663, 1506, 1424, 1182, 1129, 976, 834, 799, 721$. Mp: 74–77 °C. $[\alpha]_{\text{D}}^{20} = +17$ (10 mg/mL; MeOH). ESI-MS: m/z $[\text{M} + \text{H}]^+ = 424.2$ (100%), 425.2 (19.8%), 426.2 (3.3%). Calculated: 424.2 (100%), 425.2 (19.5%), 426.2 (1.8%). Purity: 99% (HPLC, MeCN/ $\text{H}_2\text{O} = 20:80 + 0.1\%$ HCOOH); $t_{\text{R}} = 2.63$ min.

(*S*)-2-Amino-4-(((2*R*,3*S*,4*R*,5*R*)-5-(6-amino-9*H*-purin-9-yl)-3,4-dihydroxytetrahydrofuran-2-yl)methyl)(isobutyl)amino)butanoic Acid Trifluoroacetate Salt (**27f**). To a solution of **26f** (160 mg, 0.26 mmol) in DCM (1.5 mL) at 5 °C were added TFA (1.5 mL) and H_2O (200 μL). The solution was kept at 5 °C for 3 d. After the reaction was diluted and co-distilled with DCM (3 \times 20 mL), the residue was once more dissolved in DCM (1.5 mL) and TFA (1.5 mL). The solution was kept again at 5 °C until full conversion was detected by LC-MS. Then, the reaction was diluted and co-distilled with DCM (5 \times 20 mL). The residue was dissolved in H_2O (7 mL) and was dried by lyophilization to give **27f** (200 mg, 0.26 mmol, 99%, 3.0 equiv TFA) as a colorless trifluoroacetate salt. ^1H NMR (300 MHz, CD_3OD): $\delta/\text{ppm} = 8.14$ (d, $J = 12.3$ Hz, 2H), 5.84 (d, $J = 3.2$ Hz, 1H), 4.36 (t, $J = 3.9$ Hz, 1H), 4.23–4.13 (m, 2H), 3.75 (dd, $J = 7.8, 4.8$ Hz, 1H), 3.53–3.26 (m, 3H), 3.24–3.11 (m, 1H), 2.94–2.71 (m, 2H), 2.24–1.92 (m, 2H), 1.90–1.72 (m, 1H), 0.70 (dd, $J = 14.9, 6.5$ Hz, 6H). ^{13}C NMR (75.5 MHz, CD_3OD): $\delta/\text{ppm} = 171.6, 152.6, 149.6, 146.0, 144.4, 120.9, 92.2, 79.6, 74.7, 73.4, 63.0, 56.7, 53.0, 52.3, 25.7, 25.5, 20.5, 20.4$. FT-IR: $\nu/\text{cm}^{-1} = 2476, 2241, 2072, 1666, 1426, 1186, 1136, 973, 834, 799, 722$. Mp: 67–70 °C. $[\alpha]_{\text{D}}^{20} = +14$ (10 mg/mL; MeOH). ESI-MS: m/z $[\text{M} + \text{H}]^+ = 424.2$ (100%), 425.2 (21.5%), 426.2 (2.9%). Calculated: 424.2 (100%), 425.2 (19.5%), 426.2 (1.8%). Purity: 98% (HPLC, MeCN/ $\text{H}_2\text{O} = 20:80 + 0.1\%$ HCOOH); $t_{\text{R}} = 3.88$ min.

(*S*)-2-Amino-4-(((2*R*,3*S*,4*R*,5*R*)-5-(6-amino-9*H*-purin-9-yl)-3,4-dihydroxytetrahydrofuran-2-yl)methyl)(neopentyl)amino)butanoic Acid Trifluoroacetate Salt (**27g**). To a solution of **26g** (67 mg, 0.11 mmol) in DCM (1.5 mL) at 5 °C were added TFA (1.5 mL) and H_2O (200 μL). The solution was kept at 5 °C for 3 d. After the reaction was diluted and co-distilled with DCM (3 \times 20 mL), the residue was once more dissolved in DCM (1.5 mL) and TFA (1.5 mL). The solution was kept again at 5 °C until full conversion was detected by LC-MS. Then, the reaction was diluted and co-distilled with DCM (5 \times 20 mL). The residue was dissolved in H_2O (7 mL) and was dried by lyophilization to give **27g** (73 mg, 0.11 mmol, 99%, 2.0 equiv TFA) as a colorless trifluoroacetate salt. ^1H NMR (300 MHz, CD_3OD): $\delta/\text{ppm} = 8.35$ (d, $J = 9.2$ Hz, 2H), 6.04 (d, $J = 2.9$ Hz, 1H), 4.51 (dd, $J = 4.8, 2.9$ Hz, 1H), 4.45–4.35 (m, 2H), 3.90 (dd, $J = 8.8, 4.2$ Hz, 1H), 3.77–3.34 (m, 4H), 3.17–3.01 (m, 2H), 2.41–2.23 (m, 1H), 2.23–2.08 (m, 1H), 1.02 (s, 9H). ^{13}C NMR (75.5 MHz, CD_3OD): $\delta/\text{ppm} = 172.0, 152.8, 149.6, 146.5, 144.1, 121.0, 92.4, 79.9, 74.6, 73.6, 68.4, 59.4, 56.4, 53.0, 32.6, 27.9, 26.2$. FT-IR: $\nu/\text{cm}^{-1} = 2969, 1667, 1507, 1485, 1423, 1185, 1132, 976, 833, 799, 721$. Mp: 86–89 °C. $[\alpha]_{\text{D}}^{20} = -13$ (10 mg/mL; MeOH). ESI-MS: m/z $[\text{M} + \text{H}]^+ = 438.2$ (100%), 439.2 (24.6%), 440.3 (3.9%). Calculated: 438.3 (100%), 439.3 (20.5%), 440.3 (2.0%). Purity: 100% (HPLC, MeCN/ $\text{H}_2\text{O} = 20:80 + 0.1\%$ HCOOH); $t_{\text{R}} = 3.82$ min.

(*S*)-2-Amino-4-(((2*R*,3*S*,4*R*,5*R*)-5-(6-amino-9*H*-purin-9-yl)-3,4-dihydroxytetrahydrofuran-2-yl)methyl)(cyclopropylmethyl)amino)butanoic Acid Trifluoroacetate Salt (**27h**). To a solution of **26h** (114 mg, 0.18 mmol) in DCM (1.5 mL) at 5 °C were added TFA (1.5 mL) and H_2O (200 μL). The solution was kept at 5 °C for 3 d. After the reaction was diluted and co-distilled with DCM (3 \times 20 mL), the residue was once more dissolved in DCM (1.5 mL) and TFA (1.5 mL). The solution was kept again at 5 °C until full conversion was detected by LC-MS. Then, the reaction was diluted and co-distilled with DCM (5 \times 20 mL). The residue was dissolved in H_2O (7 mL) and was dried by lyophilization to give **27h** (124 mg, 0.18 mmol, 99%, 2.4 equiv TFA) as a colorless trifluoroacetate salt. ^1H NMR (300 MHz, CD_3OD): $\delta/\text{ppm} = 8.48$ (s, 1H), 8.39 (s, 1H), 6.14 (d, $J = 3.9$ Hz, 1H), 4.71 (t, $J = 4.5$ Hz, 1H), 4.56–4.42 (m, 2H), 4.06 (dd, $J = 8.3, 4.5$ Hz, 1H), 3.86–3.74 (m, 2H), 3.71–3.51 (m, 2H), 3.26–3.18 (m, 2H), 2.54–2.37 (m,

1H), 2.35–2.19 (m, 1H), 1.19–1.05 (m, 1H), 0.82–0.67 (m, 2H), 0.45 (q, $J = 3.9, 2.7$ Hz, 2H). ^{13}C NMR (75.5 MHz, CD_3OD): $\delta/\text{ppm} = 172.0, 152.8, 149.7, 146.5, 144.2, 120.8, 91.8, 80.0, 74.8, 73.4, 59.5, 56.3, 52.6, 52.2, 26.1, 6.2, 5.1$. FT-IR: $\nu/\text{cm}^{-1} = 2973, 1667, 1507, 1467, 1424, 1322, 1185, 1129, 1064, 949, 898, 833, 799, 721$. mp: 70–73 °C. $[\alpha]_{\text{D}}^{20} = +17$ (10 mg/mL; MeOH). ESI-MS: m/z $[\text{M} + \text{H}]^+ = 422.2$ (100%), 423.2 (17.8%), 424.2 (2.1%). Calculated: 422.2 (100%), 423.2 (19.5%), 424.2 (1.8%). Purity: 100% (HPLC, MeCN/ $\text{H}_2\text{O} = 20:80 + 0.1\%$ HCOOH); $t_{\text{R}} = 2.13$ min.

(S)-2-Amino-4-(((2R,3S,4R,5R)-5-(6-amino-9H-purin-9-yl)-3,4-dihydroxytetrahydrofuran-2-yl)methyl)(cyclobutylmethyl)amino)-butanoic Acid Trifluoroacetate Salt (27i). To a solution of 26i (114 mg, 0.18 mmol) in DCM (1.5 mL) at 5 °C was added TFA (1.5 mL). The solution was kept at 5 °C until complete deprotection of the amine and carboxylic acid was detected by LC-MS. The reaction was diluted and co-distilled with DCM (3 × 20 mL), and the residue was dissolved in water (1.8 mL) and TFA (0.3 mL) at 5 °C. The solution was kept again at 5 °C until full conversion was detected by LC-MS. Then, the reaction was dried by lyophilization to give 27i (91 mg, 0.13 mmol, 99%, 2.3 equiv TFA) as a colorless trifluoroacetate salt. ^1H NMR (300 MHz, CD_3OD): $\delta/\text{ppm} = 8.49$ (s, 1H), 8.38 (s, 1H), 6.14 (d, $J = 3.9$ Hz, 1H), 4.72 (t, $J = 4.5$ Hz, 1H), 4.55–4.37 (m, 2H), 4.02 (dd, $J = 8.8, 4.1$ Hz, 1H), 3.79–3.24 (m, 6H), 2.89–2.70 (m, 1H), 2.50–2.31 (m, 1H), 2.29–2.05 (m, 3H), 2.01–1.76 (m, 4H). ^{13}C NMR (75.5 MHz, CD_3OD): $\delta/\text{ppm} = 172.5, 153.1, 149.7, 147.0, 144.1, 117.9, 114.1, 91.6, 80.1, 74.7, 73.5, 59.6, 56.6, 53.0, 31.5, 28.2, 28.0, 26.1, 19.4$. FT-IR: $\nu/\text{cm}^{-1} = 2977, 2461, 2073, 1664, 1506, 1423, 1182, 1128, 975, 833, 799, 721$. mp: 63–66 °C. $[\alpha]_{\text{D}}^{20} = +19$ (10 mg/mL; MeOH). ESI-MS: m/z $[\text{M} + \text{H}]^+ = 436.2$ (100%), 437.2 (23.4%), 438.2 (3.3%). Calculated: 436.2 (100%), 437.2 (20.5%), 438.2 (1.0%). Purity: 100% (HPLC, MeCN/ $\text{H}_2\text{O} = 20:80 + 0.1\%$ HCOOH); $t_{\text{R}} = 3.89$ min.

(S)-2-Amino-4-(((2R,3S,4R,5R)-5-(6-amino-9H-purin-9-yl)-3,4-dihydroxytetrahydrofuran-2-yl)methyl)(cyclopentylmethyl)amino)-butanoic Acid Trifluoroacetate Salt (27j). To a solution of 26j (55 mg, 0.09 mmol) in DCM (1.5 mL) at 5 °C were added TFA (1.5 mL) and H_2O (200 μL). The solution was kept at 5 °C for 3 d. After the reaction was diluted and co-distilled with DCM (3 × 20 mL), the residue was once more dissolved in DCM (1.5 mL) and TFA (1.5 mL). The solution was kept again at 5 °C until full conversion was detected by LC-MS. Then, the reaction was diluted and co-distilled with DCM (5 × 20 mL). The residue was dissolved in H_2O (7 mL), and was dried by lyophilization to give 27j (51 mg, 0.09 mmol, 99%, 1.0 equiv TFA) as a colorless trifluoroacetate salt. ^1H NMR (300 MHz, CD_3OD): $\delta/\text{ppm} = 8.36$ (d, $J = 21.6$ Hz, 2H), 6.11 (d, $J = 3.5$ Hz, 1H), 4.74 (s, 1H), 4.50 (d, $J = 7.2$ Hz, 2H), 4.05–3.84 (m, 1H), 3.80–3.40 (m, 4H), 3.30–3.11 (m, 2H), 2.56–2.04 (m, 3H), 2.02–1.72 (m, 2H), 1.72–1.43 (m, 4H), 1.38–1.11 (m, 2H). ^{13}C NMR (75.5 MHz, CD_3OD): $\delta/\text{ppm} = 173.0, 154.8, 149.9, 149.7, 143.3, 120.9, 91.9, 80.3, 74.4, 73.7, 60.7, 56.5, 54.4, 54.3, 36.5, 32.1, 32.0, 26.3, 25.9, 25.8$. FT-IR: $\nu/\text{cm}^{-1} = 2961, 1669, 1421, 1199, 1131, 978, 833, 799, 721$. mp: 121–124 °C. $[\alpha]_{\text{D}}^{20} = +15$ (10 mg/mL; MeOH). ESI-MS: m/z $[\text{M} + \text{H}]^+ = 450.2$ (100%), 451.2 (25.2%), 452.2 (3.9%). Calculated: 450.3 (100%), 451.3 (21.6%), 452.3 (2.2%). Purity: 95% (HPLC, MeCN/ $\text{H}_2\text{O} = 20:80 + 0.1\%$ HCOOH); $t_{\text{R}} = 3.99$ min.

(S)-2-Amino-4-(((2R,3S,4R,5R)-5-(6-amino-9H-purin-9-yl)-3,4-dihydroxytetrahydrofuran-2-yl)methyl)(cyclohexylmethyl)amino)-butanoic Acid Trifluoroacetate Salt (27k). To a solution of 26k (150 mg, 0.23 mmol) in DCM (1.5 mL) at 5 °C were added TFA (1.5 mL) and H_2O (200 μL). The solution was kept at 5 °C for 3 d. After the reaction was diluted and co-distilled with DCM (3 × 20 mL), the residue was once more dissolved in DCM (1.5 mL) and TFA (1.5 mL). The solution was kept again at 5 °C until full conversion was detected by LC-MS. Then, the reaction was diluted and co-distilled with DCM (5 × 20 mL). The residue was dissolved in H_2O (7 mL) and was dried by lyophilization to give 27k (122 mg, 0.23 mmol, 99%, 0.6 equiv TFA) as a colorless trifluoroacetate salt. ^1H NMR (300 MHz, CD_3OD): $\delta/\text{ppm} = 8.28$ (s, 1H), 8.23 (s, 1H), 5.96 (d, $J = 3.3$ Hz, 1H), 4.50 (t, $J = 3.9$ Hz, 1H), 4.36–4.24 (m, 2H), 3.84 (dd, $J = 8.6, 4.3$ Hz, 1H), 3.65–3.22 (m, 4H), 3.02–2.82 (m, 2H), 2.32–2.14 (m, 1H), 2.14–1.99 (m, 1H), 1.69–1.37 (m, 6H), 1.16–0.66 (m, 6H). ^{13}C NMR (75.5 MHz,

CD_3OD): $\delta/\text{ppm} = 172.2, 153.0, 149.7, 146.8, 144.2, 120.9, 92.1, 79.9, 74.7, 73.5, 62.0, 56.8, 53.8, 52.8, 34.5, 31.7, 31.6, 26.8, 26.4, 25.9$. FT-IR: $\nu/\text{cm}^{-1} = 2932, 2857, 1666, 1506, 1423, 1182, 1130, 976, 833, 799, 721$. mp: 126–129 °C. $[\alpha]_{\text{D}}^{20} = +16$ (10 mg/mL; MeOH). ESI-MS: m/z $[\text{M} + \text{H}]^+ = 464.2$ (100%), 464.6 (10.2%), 465.5 (4.6%). Calculated: 464.3 (100%), 465.3 (22.7%), 466.3 (2.5%). Purity: 96% (HPLC, MeCN/ $\text{H}_2\text{O} = 20:80 + 0.1\%$ HCOOH); $t_{\text{R}} = 2.77$ min.

(S)-4-(Allyl(((2R,3S,4R,5R)-5-(6-Amino-9H-purin-9-yl)-3,4-dihydroxytetrahydrofuran-2-yl)methyl)amino)-2-aminobutanoic Acid Trifluoroacetate Salt (27l). To a solution of 26l (100 mg, 0.17 mmol) in DCM (1.5 mL) at 5 °C were added TFA (1.5 mL) and H_2O (200 μL). The solution was kept at 5 °C for 3 d. After the reaction was diluted and co-distilled with DCM (3 × 20 mL), the residue was once more dissolved in DCM (1.5 mL) and TFA (1.5 mL). The solution was kept again at 5 °C until full conversion was detected by LC-MS. Then, the reaction was diluted and co-distilled with DCM (5 × 20 mL). The residue was dissolved in H_2O (7 mL) and was dried by lyophilization to give 27l (119 mg, 0.17 mmol, 99%, 2.6 equiv TFA) as a colorless trifluoroacetate salt. ^1H NMR (300 MHz, CD_3OD): $\delta/\text{ppm} = 8.19$ (s, 1H), 8.13 (s, 1H), 5.85 (d, $J = 4.0$ Hz, 1H), 5.76–5.59 (m, 1H), 5.40–5.26 (m, 2H), 4.45 (t, $J = 4.7$ Hz, 1H), 4.30–4.10 (m, 2H), 3.78 (dd, $J = 7.9, 5.0$ Hz, 1H), 3.73–3.57 (m, 2H), 3.54–3.10 (m, 4H), 2.25–2.08 (m, 1H), 2.07–1.92 (m, 1H). ^{13}C NMR (75.5 MHz, CD_3OD): $\delta/\text{ppm} = 171.7, 152.5, 149.7, 146.0, 144.5, 127.6, 126.8, 120.8, 91.7, 80.0, 74.7, 73.4, 56.7, 56.3, 52.2, 51.5, 25.9$. FT-IR: $\nu/\text{cm}^{-1} = 2981, 1672, 1509, 1427, 1196, 1136, 836, 799, 723$. mp: 78–81 °C. $[\alpha]_{\text{D}}^{20} = +14$ (10 mg/mL; MeOH). ESI-MS: m/z $[\text{M} + \text{H}]^+ = 408.2$ (100%), 409.2 (20.8%), 410.2 (3.4%). Calculated: 408.2 (100%), 409.2 (18.4%), 410.2 (1.6%). Purity: 100% (HPLC, MeCN/ $\text{H}_2\text{O} = 20:80 + 0.1\%$ HCOOH); $t_{\text{R}} = 2.71$ min.

(S)-2-Amino-4-(((2R,3S,4R,5R)-5-(6-amino-9H-purin-9-yl)-3,4-dihydroxytetrahydrofuran-2-yl)methyl)(prop-2-yn-1-yl)amino)-butanoic Acid Trifluoroacetate Salt (27m). To a solution of 26m (134 mg, 0.22 mmol) in DCM (1.5 mL) at 5 °C were added TFA (1.5 mL) and H_2O (200 μL). The solution was kept at 5 °C for 3 d. After the reaction was diluted and co-distilled with DCM (3 × 20 mL), the residue was once more dissolved in DCM (1.5 mL) and TFA (1.5 mL). The solution was kept again at 5 °C until full conversion was detected by LC-MS. Then, the reaction was diluted and co-distilled with DCM (5 × 20 mL). The residue was dissolved in H_2O (7 mL) and was dried by lyophilization to give 27m (157 mg, 0.22 mmol, 99%, 2.7 equiv TFA) as a colorless trifluoroacetate salt. ^1H NMR (300 MHz, CD_3OD): $\delta/\text{ppm} = 8.23$ (s, 1H), 8.06 (s, 1H), 5.83 (d, $J = 4.9$ Hz, 1H), 4.45 (t, $J = 4.9$ Hz, 1H), 4.20 (d, $J = 7.0$ Hz, 1H), 4.09 (t, $J = 4.9$ Hz, 1H), 3.88 (t, $J = 2.8$ Hz, 2H), 3.85–3.76 (m, 1H), 3.51–3.28 (m, 2H), 3.24 (t, $J = 7.1$ Hz, 2H), 2.96 (s, 1H), 2.22–2.04 (m, 1H), 1.99–1.84 (m, 1H). ^{13}C NMR (75.5 MHz, CD_3OD): $\delta/\text{ppm} = 172.2, 152.3, 149.7, 145.8, 144.5, 120.6, 91.1, 81.1, 80.7, 74.9, 73.4, 72.9, 56.8, 52.8, 52.5, 42.9, 26.3$. FT-IR: $\nu/\text{cm}^{-1} = 3097, 1671, 1509, 1428, 1323, 1195, 1137, 837, 799, 723$. mp: 76–79 °C. $[\alpha]_{\text{D}}^{20} = +12$ (10 mg/mL; MeOH). ESI-MS: m/z $[\text{M} + \text{H}]^+ = 406.2$ (100%), 407.2 (21.0%), 408.1 (2.5%). Calculated: 406.2 (100%), 407.2 (18.4%), 408.2 (1.6%). Purity: 97% (HPLC, MeCN/ $\text{H}_2\text{O} = 20:80 + 0.1\%$ HCOOH); $t_{\text{R}} = 2.70$ min.

(S)-2-Amino-4-(((2R,3S,4R,5R)-5-(6-amino-9H-purin-9-yl)-3,4-dihydroxytetrahydrofuran-2-yl)methyl)(but-2-yn-1-yl)amino)-butanoic Acid Trifluoroacetate Salt (27n). To a solution of 26n (119 mg, 0.19 mmol) in DCM (1.5 mL) at 5 °C were added TFA (1.5 mL) and H_2O (200 μL). The solution was kept at 5 °C for 3 d. After the reaction was diluted and co-distilled with DCM (3 × 20 mL), the residue was once more dissolved in DCM (1.5 mL) and TFA (1.5 mL). The solution was kept again at 5 °C until full conversion was detected by LC-MS. Then, the reaction was diluted and co-distilled with DCM (5 × 20 mL). The residue was dissolved in H_2O (7 mL) and was dried by lyophilization to give 27n (131 mg, 0.19 mmol, 99%, 2.4 equiv TFA) as a colorless trifluoroacetate salt. ^1H NMR (300 MHz, CD_3OD): $\delta/\text{ppm} = 8.61$ (s, 1H), 8.31 (s, 1H), 6.17 (d, $J = 5.4$ Hz, 1H), 4.77 (t, $J = 5.3$ Hz, 1H), 4.62–4.50 (m, 1H), 4.38 (t, $J = 4.4$ Hz, 1H), 4.28–4.09 (m, 3H), 3.85–3.50 (m, 4H), 2.55–2.36 (m, 1H), 2.33–2.13 (m, 1H), 1.92 (s, 3H). ^{13}C NMR (75.5 MHz, CD_3OD): $\delta/\text{ppm} = 173.0, 152.4, 149.7, 146.1, 144.3, 120.2, 90.4, 89.3, 80.6, 75.1, 73.3, 67.4, 56.6, 53.2,$

52.8, 42.7, 26.1, 3.2. FT-IR: ν/cm^{-1} = 2925, 1666, 1507, 1423, 1184, 1131, 976, 897, 835, 799, 722. Mp: 121–124 °C. $[\alpha]_{\text{D}}^{20}$ = +13 (10 mg/mL; MeOH). ESI-MS: m/z $[M + H]^+$ = 420.2 (100%), 421.2 (20.6%), 422.2 (3.5%). Calculated: 420.2 (100%), 421.2 (19.5%), 422.2 (1.8%). Purity: 99% (HPLC, MeCN/H₂O = 20:80 + 0.1% HCOOH); t_{R} = 1.95 min.

(S)-2-Amino-4-(((2R,3S,4R,5R)-5-(6-amino-9H-purin-9-yl)-3,4-dihydroxytetrahydrofuran-2-yl)methyl)(pent-2-yn-1-yl)amino)butanoic Acid Trifluoroacetate Salt (**27o**). To a solution of **26o** (98 mg, 0.16 mmol) in DCM (1.5 mL) at 5 °C were added TFA (1.5 mL) and H₂O (200 μ L). The solution was kept at 5 °C for 3 d. After the reaction was diluted and co-distilled with DCM (3 \times 20 mL), the residue was once more dissolved in DCM (1.5 mL) and TFA (1.5 mL). The solution was kept again at 5 °C until full conversion was detected by LC-MS. Then, the reaction was diluted and co-distilled with DCM (5 \times 20 mL). The residue was dissolved in H₂O (7 mL) and was dried by lyophilization to give **27o** (93 mg, 0.16 mmol, 99%, 1.3 equiv TFA) as a colorless trifluoroacetate salt. ¹H NMR (300 MHz, CD₃OD): δ /ppm = 8.61 (s, 1H), 8.29 (s, 1H), 6.17 (d, J = 5.5 Hz, 1H), 4.75 (t, J = 5.3 Hz, 1H), 4.59–4.49 (m, 1H), 4.38 (t, J = 4.4 Hz, 1H), 4.30–4.10 (m, 3H), 3.83–3.47 (m, 4H), 2.46 (dt, J = 15.6, 7.9 Hz, 1H), 2.36–2.26 (m, 2H), 2.25–2.14 (m, 1H), 1.17 (t, J = 7.5 Hz, 3H). ¹³C NMR (75.5 MHz, CD₃OD): δ /ppm = 173.3, 152.7, 149.7, 146.5, 144.2, 120.1, 94.6, 90.3, 80.7, 75.1, 73.3, 67.9, 56.6, 53.5, 53.1, 42.4, 26.2, 13.7, 13.0. FT-IR: ν/cm^{-1} = 2981, 1669, 1507, 1422, 1321, 1198, 1130, 1061, 900, 833, 799, 721. Mp: 110–113 °C. $[\alpha]_{\text{D}}^{20}$ = +14 (10 mg/mL; MeOH). ESI-MS: m/z $[M + H]^+$ = 434.2 (100%), 435.4 (9.4%), 436.2 (2.7%). Calculated: 434.2 (100%), 435.2 (20.5%), 436.2 (1.0%). Purity: 100% (HPLC, MeCN/H₂O = 20:80 + 0.1% HCOOH); t_{R} = 2.78 min.

(S)-2-Amino-4-(((2R,3S,4R,5R)-5-(6-amino-9H-purin-9-yl)-3,4-dihydroxytetrahydrofuran-2-yl)methyl)(but-3-yn-1-yl)amino)butanoic Acid Trifluoroacetate Salt (**27p**). To a solution of **26p** (25 mg, 0.04 mmol) in DCM (1.5 mL) at 5 °C was added TFA (1.5 mL). The solution was kept at 5 °C until complete deprotection of the amine and carboxylic acid was detected by LC-MS. The reaction was diluted and co-distilled with DCM (3 \times 20 mL), and the residue was dissolved in water (1.8 mL) and TFA (0.3 mL) at 5 °C. The solution was kept again at 5 °C until full conversion was detected by LC-MS. Then, the reaction was dried by lyophilization to give **27p** (28 mg, 0.04 mmol, 99%, 2.5 equiv TFA) as a colorless trifluoroacetate salt. ¹H NMR (300 MHz, CD₃OD): δ /ppm = 8.63–8.24 (m, 2H), 6.11 (s, 1H), 4.74 (s, 1H), 4.55–4.35 (m, 2H), 4.01 (dd, J = 13.9, 7.3 Hz, 1H), 3.74–3.33 (m, 6H), 2.75–2.64 (m, 2H), 2.47 (d, J = 2.3 Hz, 1H), 2.43–2.26 (m, 1H), 2.19–1.99 (m, 1H). ¹³C NMR (75.5 MHz, CD₃OD): δ /ppm = 172.6, 154.1, 148.7, 148.7, 143.2, 125.5, 91.6, 80.9, 80.2, 74.6, 73.5, 73.1, 56.7, 53.8, 53.6, 52.8, 26.5, 15.3. FT-IR: ν/cm^{-1} = 2926, 1673, 1506, 1423, 1200, 1132, 834, 800, 722. Mp: 163–166 °C. $[\alpha]_{\text{D}}^{20}$ = +28 (10 mg/mL; MeOH). ESI-MS: m/z $[M + H]^+$ = 420.2 (100%), 421.2 (21.8%), 422.2 (2.9%). Calculated: 420.2 (100%), 421.2 (19.5%), 422.2 (1.8%). Purity: 100% (HPLC, MeCN/H₂O = 20:80 + 0.1% HCOOH); t_{R} = 3.94 min.

(S)-2-Amino-4-(((2R,3S,4R,5R)-5-(6-amino-9H-purin-9-yl)-3,4-dihydroxytetrahydrofuran-2-yl)methyl)(benzyl)amino)butanoic Acid Trifluoroacetate Salt (**27q**). To a solution of **26q** (115 mg, 0.18 mmol) in DCM (1.5 mL) at 5 °C were added TFA (1.5 mL) and H₂O (200 μ L). The solution was kept at 5 °C for 3 d. After the reaction was diluted and co-distilled with DCM (3 \times 20 mL), the residue was once more dissolved in DCM (1.5 mL) and TFA (1.5 mL). The solution was kept again at 5 °C until full conversion was detected by LC-MS. Then, the reaction was diluted and co-distilled with DCM (5 \times 20 mL). The residue was dissolved in H₂O (7 mL) and was dried by lyophilization to give **27q** (104 mg, 0.18 mmol, 99%, 1.0 equiv TFA) as a colorless trifluoroacetate salt. ¹H NMR (300 MHz, CD₃OD): δ /ppm = 8.19 (s, 1H), 8.04 (s, 1H), 7.27–7.19 (m, 2H), 7.17–7.08 (m, 3H), 5.90 (d, J = 3.3 Hz, 1H), 4.39 (dd, J = 5.2, 3.3 Hz, 1H), 4.36–4.11 (m, 4H), 3.76–3.67 (m, 1H), 3.52–3.20 (m, 4H), 2.29–2.10 (m, 1H), 2.10–1.96 (m, 1H). ¹³C NMR (75.5 MHz, CD₃OD): δ /ppm = 172.5, 152.8, 149.6, 146.5, 144.2, 132.3, 131.1, 130.6, 130.3, 120.8, 92.0, 80.1, 74.8, 73.5, 58.9, 56.1, 53.1, 52.9, 26.2. FT-IR: ν/cm^{-1} = 3088, 2475, 1664, 1504, 1423, 1182, 1127, 975, 833, 799, 721, 702. Mp: 122–125 °C. $[\alpha]_{\text{D}}^{20}$ =

+19 (10 mg/mL; MeOH). ESI-MS: m/z $[M + H]^+$ = 458.2 (100%), 459.2 (24.4%), 460.2 (3.9%). Calculated: 458.2 (100%), 459.2 (22.7%), 460.2 (2.5%). Purity: 100% (HPLC, MeCN/H₂O = 20:80 + 0.1% HCOOH); t_{R} = 2.90 min.

(S)-2-Amino-4-(((2R,3S,4R,5R)-5-(6-amino-9H-purin-9-yl)-3,4-dihydroxytetrahydrofuran-2-yl)methyl)(phenethyl)amino)butanoic Acid Trifluoroacetate Salt (**27r**). To a solution of **26r** (113 mg, 0.17 mmol) in DCM (1.5 mL) at 5 °C were added TFA (1.5 mL) and H₂O (200 μ L). The solution was kept at 5 °C for 3 d. After the reaction was diluted and co-distilled with DCM (3 \times 20 mL), the residue was once more dissolved in DCM (1.5 mL) and TFA (1.5 mL). The solution was kept again at 5 °C until full conversion was detected by LC-MS. Then, the reaction was diluted and co-distilled with DCM (5 \times 20 mL). The residue was dissolved in H₂O (7 mL) and was dried by lyophilization to give **27r** (103 mg, 0.17 mmol, 99%, 1.5 equiv TFA) as a colorless trifluoroacetate salt. ¹H NMR (300 MHz, CD₃OD): δ /ppm = 8.31 (s, 1H), 8.19 (s, 1H), 7.17–6.93 (m, 5H), 5.98 (d, J = 4.2 Hz, 1H), 4.61 (t, J = 4.7 Hz, 1H), 4.45–4.36 (m, 1H), 4.34–4.28 (m, 1H), 3.91 (dd, J = 8.2, 4.7 Hz, 1H), 3.72–3.28 (m, 6H), 2.94–2.82 (m, 2H), 2.43–2.23 (m, 1H), 2.21–2.07 (m, 1H). ¹³C NMR (75.5 MHz, CD₃OD): δ /ppm = 171.8, 152.9, 149.7, 146.7, 144.3, 137.2, 129.9, 129.7, 128.2, 121.0, 91.9, 80.3, 74.5, 73.5, 56.3, 55.7, 52.5, 52.3, 30.6, 26.0. FT-IR: ν/cm^{-1} = 3066, 1666, 1505, 1425, 1187, 1131, 976, 835, 799, 722, 702. Mp: 79–82 °C. $[\alpha]_{\text{D}}^{20}$ = +18 (10 mg/mL; MeOH). ESI-MS: m/z $[M + H]^+$ = 472.2 (100%), 473.3 (26.7%), 474.2 (3.8%). Calculated: 472.2 (100%), 473.2 (23.8%), 474.2 (2.7%). Purity: 99% (HPLC, MeCN/H₂O = 20:80 + 0.1% HCOOH); t_{R} = 3.87 min.

(2S)-2-Amino-4-(((2R,3S,4R,5R)-5-(6-amino-9H-purin-9-yl)-3,4-dihydroxytetrahydrofuran-2-yl)methyl)(but-3-yn-2-yl)amino)butanoic Acid Trifluoroacetate Salt (**27s-A/B**). To a solution of **26s** (31 mg, 0.05 mmol) in DCM (1.5 mL) at 5 °C was added TFA (1.5 mL). The solution was kept at 5 °C until complete deprotection of the amine and carboxylic acid was detected by LC-MS. The reaction was diluted and co-distilled with DCM (3 \times 20 mL), and the residue was dissolved in water (1.8 mL) and TFA (0.3 mL) at 5 °C. The solution was kept again at 5 °C until full conversion was detected by LC-MS. Then, the reaction was dried by lyophilization to give **27s** (39 mg, 0.05 mmol, 99%, 3.0 equiv TFA) as a colorless trifluoroacetate salt. ¹H NMR (300 MHz, CD₃OD): δ /ppm = 8.43–8.28 (m, 2H), 6.02 (t, J = 3.8 Hz, 1H), 4.68–4.56 (m, 1H), 4.38–4.12 (m, 3H), 4.00–3.83 (m, 1H), 3.53–3.25 (m, 4H), 3.04 (dd, J = 3.6, 2.2 Hz, 1H), 2.32–2.14 (m, 1H), 2.13–1.98 (m, 1H), 1.42 (dd, J = 29.3, 6.9 Hz, 3H). ¹³C NMR (75.5 MHz, CD₃OD): δ /ppm = 172.1, 171.7, 152.9, 149.8, 146.7, 144.1, 121.0, 91.8, 91.5, 82.6, 81.6, 79.6, 79.1, 78.4, 78.1, 74.8, 73.5, 73.3, 55.0, 54.6, 53.7, 52.3, 51.4, 51.2, 50.7, 27.4, 27.3, 18.2, 18.2. FT-IR: ν/cm^{-1} = 3091, 1670, 1508, 1427, 1323, 1196, 1134, 835, 799, 722. Mp: 60–63 °C. $[\alpha]_{\text{D}}^{20}$ = +12 (10 mg/mL; MeOH). ESI-MS: m/z $[M + H]^+$ = 420.2 (100%), 421.1 (21.7%), 422.2 (3.2%). Calculated: 420.2 (100%), 421.2 (19.5%), 422.2 (1.8%). Purity: 100% (HPLC, MeCN/H₂O = 20:80 + 0.1% HCOOH); t_{R} = 3.95 min.

(2S)-2-Amino-4-(((2R,3S,4R,5R)-5-(6-amino-9H-purin-9-yl)-3,4-dihydroxytetrahydrofuran-2-yl)methyl)(but-3-yn-2-yl)amino)butanoic Acid Trifluoroacetate Salt (**27s-A**). To a solution of **26s-A** (36 mg, 0.06 mmol) in DCM (1.5 mL) at 5 °C was added TFA (1.5 mL). The solution was kept at 5 °C until complete deprotection of the amine and carboxylic acid was detected by LC-MS. The reaction was diluted and co-distilled with DCM (3 \times 20 mL), and the residue was dissolved in water (3 mL) and TFA (0.5 mL) at 5 °C. The solution was kept again at 5 °C until full conversion was detected by LC-MS. Then, the reaction was dried by lyophilization to give **27s-A** (39 mg, 0.06 mmol, 99%, 2.1 equiv TFA) as a colorless trifluoroacetate salt (resin). ¹H NMR (300 MHz, DMSO-*d*₆): δ /ppm = 8.53 (s, 1H), 8.36 (s, 1H), 5.94 (d, J = 4.9 Hz, 1H), 4.63 (t, J = 4.9 Hz, 1H), 4.20–4.06 (m, 2H), 3.99–3.85 (m, 2H), 3.33 (d, J = 2.0 Hz, 1H), 3.16–3.04 (m, 1H), 2.9–2.81 (m, 2H), 2.80–2.63 (m, 1H), 2.04–1.92 (m, 2H), 1.32 (d, J = 6.9 Hz, 3H). ¹³C NMR (75.5 MHz, DMSO-*d*₆): δ /ppm = 170.8, 153.4, 148.9, 148.8, 141.4, 119.2, 88.3, 82.5, 81.5, 76.3, 72.8, 71.9, 53.6, 50.8, 49.2, 47.9, 27.7, 19.1. FT-IR: ν/cm^{-1} = 2952, 2256, 2126, 1670, 1505, 1419, 1324, 1197, 1127, 1024, 997, 826, 798, 719. $[\alpha]_{\text{D}}^{20}$ = –3 (10 mg/mL; MeOH). ESI-MS: m/z $[M + H]^+$ = 420.2 (100%), 421.1 (21.3%),

422.2 (3.5%). Calculated: 420.2 (100%), 421.2 (19.5%), 422.2 (1.8%). Purity: 96% (HPLC, MeCN/H₂O = 20:80 + 0.1% HCOOH); t_R = 3.31 min.

(2*S*)-2-Amino-4-(((2*R*,3*S*,4*R*,5*R*)-5-(6-amino-9*H*-purin-9-yl)-3,4-dihydroxytetrahydrofuran-2-yl)methyl)(but-3-yn-2-yl)amino)butanoic Acid Trifluoroacetate Salt (27*s*-B). To a solution of 26*s*-B (74 mg, 0.12 mmol) in DCM (1.5 mL) at 5 °C was added TFA (1.5 mL). The solution was kept at 5 °C until complete deprotection of the amine and carboxylic acid was detected by LC-MS. The reaction was diluted and co-distilled with DCM (3 × 20 mL), and the residue was dissolved in water (3 mL) and TFA (0.5 mL) at 5 °C. The solution was kept again at 5 °C until full conversion was detected by LC-MS. Then, the reaction was dried by lyophilization to give 27*s*-B (58 mg, 0.12 mmol, 99%, 0.8 equiv TFA) as a colorless trifluoroacetate salt (resin). ¹H NMR (300 MHz, DMSO-*d*₆): δ /ppm = 8.57 (s, 1H), 8.43 (s, 1H), 5.97 (d, *J* = 4.7 Hz, 1H), 4.62 (t, *J* = 4.7 Hz, 1H), 4.25–4.13 (m, 2H), 4.07–3.90 (m, 2H), 3.51–3.42 (m, 1H), 3.23–3.09 (m, 1H), 3.07–2.81 (m, 3H), 2.15–2.02 (m, 1H), 2.02–1.87 (m, 1H), 1.27 (d, *J* = 6.7 Hz, 3H). ¹³C NMR (75.5 MHz, DMSO-*d*₆): δ /ppm = 171.0, 153.1, 149.1, 148.3, 142.2, 119.5, 88.8, 81.3 (2x C), 77.5, 73.6, 72.1, 53.7, 51.5, 49.4, 48.8, 27.3, 18.7. FT-IR: ν /cm⁻¹ = 2941, 2255, 2127, 1674, 1505, 1418, 1322, 1197, 1128, 1024, 1001, 824, 798, 719. $[\alpha]_D^{20}$ = +20 (10 mg/mL; MeOH). ESI-MS: m/z [M + H]⁺ = 420.2 (100%), 421.1 (21.9%), 422.2 (3.2%). Calculated: 420.2 (100%), 421.2 (19.5%), 422.2 (1.8%). Purity: 98% (HPLC, MeCN/H₂O = 20:80 + 0.1% HCOOH); t_R = 3.39 min.

(*S*)-2-Amino-4-(((2*R*,3*S*,4*R*,5*R*)-5-(6-amino-9*H*-purin-9-yl)-3,4-dihydroxytetrahydrofuran-2-yl)methyl)(2-methylbut-3-yn-2-yl)amino)butanoic Acid Trifluoroacetate Salt (27*t*). To a solution of 26*t* (25 mg, 0.04 mmol) in DCM (1.5 mL) at 5 °C was added TFA (1.5 mL). The solution was kept at 5 °C until complete deprotection of the amine and carboxylic acid was detected by LC-MS. The reaction was diluted and co-distilled with DCM (3 × 20 mL), and the residue was dissolved in water (1.8 mL) and TFA (0.3 mL) at 5 °C. The solution was kept again at 5 °C until full conversion was detected by LC-MS. Then, the reaction was dried by lyophilization to give 27*t* (73 mg, 0.11 mmol, 99%, 2.0 equiv TFA) as a colorless trifluoroacetate salt. ¹H NMR (300 MHz, CD₃OD): δ /ppm = 8.24 (s, 2H), 5.95 (d, *J* = 3.5 Hz, 1H), 4.51 (t, *J* = 3.5 Hz, 1H), 4.38–4.24 (m, 2H), 3.85 (t, *J* = 6.4 Hz, 1H), 3.69–3.35 (m, 4H), 3.17 (s, 1H), 2.37–2.20 (m, 1H), 2.16–1.97 (m, 1H), 1.55 (d, *J* = 4.7 Hz, 6H). ¹³C NMR (75.5 MHz, CD₃OD): δ /ppm = 170.8, 151.8, 145.8, 145.7, 116.5, 112.8, 90.5, 81.5, 80.6, 77.0, 73.4, 72.1, 61.1, 54.3, 49.9, 27.4, 25.1, 24.9. FT-IR: ν /cm⁻¹ = 3095, 1663, 1506, 1427, 1186, 1133, 834, 799, 722. Mp: 74–77 °C. $[\alpha]_D^{20}$ = +21 (10 mg/mL; MeOH). ESI-MS: m/z [M + H]⁺ = 434.2 (100%), 435.2 (22.6%), 436.2 (2.9%). Calculated: 434.2 (100%), 435.2 (20.5%), 436.2 (2.0%). Purity: 96% (HPLC, MeCN/H₂O = 20:80 + 0.1% HCOOH); t_R = 2.18 min.

Ethyl (2*S*)-2-Amino-4-(((2*R*,3*S*,4*R*,5*R*)-5-(6-amino-9*H*-purin-9-yl)-3,4-dihydroxytetrahydrofuran-2-yl)methyl)(but-3-yn-2-yl)amino)butanoate (28-A/B). To a solution of 27-A/B (99 mg, 0.13 mmol) in absolute ethanol (6 mL) was added thionyl chloride (77 μ L, 1.07 mmol, 8.0 equiv) at 0 °C. The solution was stirred at 0 °C for 5 min and then heated for 9 h at 50 °C. After the solvent was evaporated under reduced pressure at 40 °C, the residue was purified by column chromatography (DCM/MeOH = 10:1 + 1% NEt₃) to give 28-A/B (15 mg, 0.04 mmol, 27%) as a colorless powder. The diastereomers 28-A and 28-B were separated using a hydrophilic column (MZ Aqua Perfect), MeCN/H₂O = 9:91 + 0.1% TFA. After lyophilization 28-A (10 mg, 0.01 mmol, 2.7 equiv TFA) and 28-B (6 mg, 0.01 mmol, 2.0 equiv TFA) were obtained as colorless trifluoroacetate salts (resins). 28-A: ¹H NMR (300 MHz, DMSO-*d*₆): δ /ppm = 8.52 (s, 1H), 8.35 (s, 1H), 5.93 (d, *J* = 5.0 Hz, 1H), 4.61 (t, *J* = 5.0 Hz, 1H), 4.25–4.12 (m, 3H), 4.11–4.01 (m, 2H), 3.91–3.80 (m, 1H), 3.35–3.27 (m, 1H), 3.12–2.99 (m, 1H), 2.94–2.72 (m, 2H), 2.68–2.56 (m, 1H), 2.04–1.90 (m, 2H), 1.31 (d, *J* = 6.9 Hz, 3H), 1.20 (t, *J* = 7.1 Hz, 3H). $[\alpha]_D^{20}$ = -1 (10 mg/mL; MeOH). ESI-MS: m/z [M + H]⁺ = 448.2 (100%), 449.2 (24.1%), 450.2 (3.2%). Calculated: 448.2 (100%), 449.2 (24.2%), 450.2 (3.4%). Purity: 99% (HPLC, MeCN/H₂O = 20:80 + 0.1% HCOOH); t_R = 3.78 min. 28-B: ¹H NMR (300 MHz, DMSO-*d*₆): δ /ppm = 8.46 (s, 1H), 8.30 (s, 1H),

5.92 (d, *J* = 4.9 Hz, 1H), 4.61 (t, *J* = 4.9 Hz, 1H), 4.23–4.03 (m, 5H), 3.87–3.76 (m, 1H), 3.38–3.28 (m, 1H), 3.04–2.90 (m, 1H), 2.89–2.75 (m, 2H), 2.74–2.65 (m, 1H), 2.03–1.84 (m, 2H), 1.25–1.17 (m, 6H). $[\alpha]_D^{20}$ = +33 (3 mg/mL; MeOH). ESI-MS: m/z [M + H]⁺ = 448.2 (100%), 449.2 (26.0%), 450.1 (3.6%). Calculated: 448.2 (100%), 449.2 (24.2%), 450.2 (3.4%). Purity: 99% (HPLC, MeCN/H₂O = 20:80 + 0.1% HCOOH); t_R = 3.68 min.

Molecular Docking. Molecular docking was conducted using the FlexX algorithm within the LeadIT-2.3.2 software under default parameters.^{78,79} The protein structure of the human DNMT2–SAH complex (PDB-ID 1G55)³⁰ was obtained from the Protein Data Bank (PDB).⁸⁰ The binding site was defined to include all amino acids within a 6.5 Å radius around the crystallographic ligand SAH and water molecules 413, 414, 459, and 495 in a predefined orientation forming at least three interactions with SAH and the binding site. The receptor was protonated using the Protoss module⁸¹ within LeadIT. For molecular docking, all ligands were energy-minimized using the Merck molecular force field (MMFF94x)⁸² within MOE 2020.09.⁸³ The docking setup was validated by redocking of SAH (Table S1 Supporting Information).

Solvent analysis was performed using the 3D-RISM approach⁸⁴ within MOE.⁸⁵ The DNMT2–SAH complex structure PDB-ID 1G55 was prepared using the QuickPrep module to add missing atoms and for assignment of protonation states without further energy minimization to preserve crystallographic water positions (structure resolution 1.80 Å). Receptor and ligand atoms 10 Å around SAH were considered in solvent analysis using a grid spacing of 0.25 Å.

Expression and Purification of Human Full-Length DNMT2.

The plasmid coding for the full-length protein of human DNMT2 as described by Dong et al.³⁰ was kindly provided by Albert Jeltsch (University of Stuttgart, Germany). The protein was expressed in *E. coli* Rosetta 2 (DE3) pLysS cells (Merck KGaA, Darmstadt, Germany), using a pET-28a vector to obtain an N-terminal polyhistidine tagged protein. The sequence was then verified by Eurofins Genomics Europe (Ebersberg, Germany). Cells were grown in TB medium at 37 °C until they reached an optical density at 600 nm of 0.8. Overexpression was induced by adding IPTG up to a final concentration of 500 μ M and was maintained overnight at 20 °C. Cells were harvested by centrifugation at 4000g for 30 min at 4 °C; afterward the cell pellets were resuspended in lysis buffer (50 mM sodium phosphate, pH 8.0, 150 mM NaCl, 25 mM imidazole, 0.1% polysorbate-20). After incubation on ice for 40 min with lysozyme (Carl Roth, Karlsruhe, Germany), cells were disrupted by sonication on ice in 15 s intervals. Cell debris was removed by centrifugation at 17 500g for 60 min at 4 °C. The clear supernatant was filtered using Chromafil Xtra RC 25 mm 0.45 μ m syringe filters (Macherey-Nagel, Düren, Germany). For purification, an ÄKTA start system (Cytiva, Marlborough, Chicago, USA) was used. Therefore, the supernatant was loaded on a HisTrap HP 5 mL column (Cytiva, Marlborough, Chicago, USA), a wash-out with several column volumes lysis buffer was conducted, and finally DNMT2 was eluted using a gradient up to 100% elution buffer (50 mM sodium phosphate, pH 8.0, 150 mM NaCl, 800 mM imidazole, 0.1% polysorbate-20). To remove DNA and RNA fragments, eluted DNMT2 was diluted 1:10 with IEX buffer A (10 mM sodium phosphate, pH 8.0, 0.1% polysorbate-20) and loaded on a HiTrap Q HP 5 mL column (Cytiva, Marlborough, USA). Several column volumes of IEX buffer A were used for wash-out of unspecific bound anions, followed by a gradient up to 100% IEX buffer B (10 mM sodium phosphate, 1 M NaCl, 0.1% polysorbate-20) to elute DNMT2. DNA and RNA fragments eluted at higher concentrations of NaCl compared to DNMT2. For further purification, size exclusion chromatography using a Superdex 16/600 75 μ g column (Cytiva, Marlborough, USA) equilibrated in SEC buffer (50 mM sodium phosphate, pH 8.0, 300 mM NaCl, 1 mM EDTA, 2 mM DTT, 0.1% polysorbate-20) was performed. DNMT2 was then concentrated using Amicon Ultra 4 10K centrifugal filters (Merck KGaA, Darmstadt, Germany) and diluted 1:4 with storage buffer (50 mM sodium phosphate, pH 8.0, 300 mM NaCl, 1 mM EDTA, 2 mM DTT, 0.1% polysorbate-20, 60% glycerol). Protein was stored in liquid state at -20 °C for further use.

Expression and Purification of Murine DNMT3A-3L Single Chain Fusion Protein. The plasmid coding for the murine

DNMT3A-3L single chain fusion protein (pET-Dnmt3A3L-sc27) was kindly gifted from Albert Jeltsch (Addgene plasmid no. 71827; <http://n2t.net/addgene:71827>; RRID:Addgene_71827).⁸⁵ The sequence was verified by Eurofins genomics (Ebersberg, Germany). For protein expression, *E. coli* Rosetta 2 (DE3) pLysS cells (Merck KGaA, Darmstadt, Germany) were transformed and grown in TB medium to an optical density of 0.5. Overexpression was induced by addition of IPTG to a final concentration of 500 μ M, and cells were maintained overnight at 16 °C. Cells were harvested by centrifugation at 4500g at 4 °C for 30 min; afterward cells were washed in lysis buffer (30 mM sodium phosphate, pH 7.3, 500 mM NaCl, 10 mM imidazole, 0.2 mM DTT, 0.1% polysorbate-20, 10% glycerol) and centrifuged again at 10 000g at 4 °C for 10 min. Clear supernatant was removed, and cells were flash frozen in liquid nitrogen to be stored at -80 °C until further use.

Frozen cells were resuspended in lysis buffer and incubated with lysozyme on ice for 30 min. Afterward, cells were lysed by sonication in 45 s intervals on ice, and cell debris was removed by centrifugation at 17 000g at 4 °C for 90 min. Clear supernatant was filtered using Chromafil Xtra RC 25 mm 0.45 μ m syringe filters (Macherey-Nagel, Düren, Germany) and loaded on a HisTrap HP 5 mL column (Cytiva, Marlborough, Chicago, USA). A wash-out step with several column volumes of lysis buffer was conducted, and finally the DNMT3A-3L single chain fusion protein was eluted using a gradient up to 100% elution buffer (30 mM sodium phosphate, pH 7.3, 500 mM NaCl, 500 mM imidazole, 0.2 mM DTT, 0.1% polysorbate-20, 10% glycerol). A further purification step was conducted using a Superdex 16/600 75 μ g column (Cytiva, Marlborough, USA) equilibrated in SEC buffer (20 mM HEPES, pH 7.3, 200 mM sodium chloride, 1 mM DTT, 0.1% polysorbate-20, 10% glycerol). Eluted protein was then concentrated using Amicon Ultra 4 10K centrifugal filters (Merck KGaA, Darmstadt, Germany) and adjusted to a final concentration of 40% glycerol. Protein was stored at -20 °C until further use.

Expression and Purification of Human NSUN2. The gene coding for the full-length human NSUN2 (Uniprot ID Q08J23) was synthesized and inserted into a pET28a(+) vector between *EcoRI* and *XhoI* sites by Genscript (Piscataway, New Jersey, USA) as previously described.⁸⁶ The sequence was verified by Eurofins Genomics Europe (Ebersberg, Germany). The plasmid used for this study will be available at Addgene (Addgene ID: 188059). For protein expression, *E. coli* Rosetta 2 (DE3) pLysS cells (Merck KGaA, Darmstadt, Germany) were transformed and grown as described for the murine DNMT3A-3L single chain fusion protein. Purification was conducted quite similarly to that described for DNMT3A-3L with some adjustments to the buffers used. Cells were lysed and washed with lysis buffer (50 mM sodium phosphate, pH 8.0, 300 mM NaCl, 10 mM imidazole, 0.1% polysorbate-20) and then eluted with elution buffer (50 mM sodium phosphate, pH 8.0, 300 mM NaCl, 10 mM imidazole, 0.1% polysorbate-20). For size-exclusion chromatography, a Superdex 16/600 75 μ g column (Cytiva, Marlborough, USA) equilibrated in SEC buffer (50 mM sodium phosphate, pH 8.0, 300 mM NaCl, 1 mM EDTA, 2 mM DTT, 0.1% polysorbate-20) was used. The eluted protein was then concentrated using Amicon Ultra 4 10K centrifugal filters (Merck KGaA, Darmstadt, Germany) and adjusted to a final concentration of 40% glycerol. The protein was stored at -20 °C until further use.

Expression and Purification of Human NSUN6. The gene coding for the full-length human NSUN6 (Uniprot ID Q8TEA1) was synthesized and inserted into a pET22b(+) plasmid between *NdeI* and *XhoI* sites by Genscript (Piscataway, New Jersey, USA), as described earlier in literature.⁸⁷ The sequence was verified by Eurofins Genomics Europe (Ebersberg, Germany). The plasmid used for this study will be available at Addgene (Addgene ID: 188060). For protein expression, *E. coli* Rosetta 2 (DE3) pLysS cells (Merck KGaA, Darmstadt, Germany) were transformed and grown as described for the murine DNMT3A-3L single chain fusion protein. Purification was conducted quite similarly to that described for DNMT3A-3L with some adjustments to the buffers used. Cells were lysed and washed with lysis buffer (50 mM sodium phosphate, pH 7.5, 150 mM NaCl, 10 mM imidazole, 0.1% polysorbate-20) and then eluted with elution buffer (50 mM sodium phosphate, pH 7.5, 150 mM NaCl, 500 mM imidazole, 0.1% polysorbate-

20). For size-exclusion chromatography, a Superdex 16/600 75 μ g column (Cytiva, Marlborough, USA) equilibrated in SEC buffer (25 mM HEPES, pH 7.5, 300 mM NaCl, 1 mM DTT, 0.1% polysorbate-20, 10% glycerol) was used. The protein was concentrated using Amicon Ultra 4 10K centrifugal filters (Merck KGaA, Darmstadt, Germany) and diluted 1:4 with storage buffer (25 mM HEPES, pH 7.5, 300 mM NaCl, 1 mM DTT, 0.1% polysorbate-20, 60% glycerol). Protein was stored at -20 °C until further use.

Expression and Purification of the Methyltransferase Domain of Human EHMT2 (G9a). The plasmid coding for the methyltransferase domain of human EHMT2 (G9a) was a kind gift from Cheryl Arrowsmith (Addgene plasmid no. 25503; <http://n2t.net/addgene:25503>; RRID:Addgene_25503). The sequence was verified by Eurofins Genomics Europe (Ebersberg, Germany). For protein expression, *E. coli* Rosetta 2 (DE3) pLysS cells (Merck KGaA, Darmstadt, Germany) were transformed and grown as described for the murine DNMT3A-3L single chain fusion protein. The purification was conducted quite similarly to that described for DNMT3A-3L with some adjustments to the buffers used. Cells were lysed in lysis buffer (100 mM sodium phosphate, pH 7.4, 250 mM NaCl, 0.1% 2-mercaptoethanol, 0.1% polysorbate-20, 5% glycerol), washed with wash buffer (100 mM sodium phosphate, pH 7.4, 250 mM NaCl, 50 mM imidazole, 0.1% polysorbate-20, 5% glycerol), and then eluted with elution buffer (100 mM sodium phosphate, pH 7.4, 250 mM NaCl, 250 mM imidazole, 0.1% polysorbate-20, 5% glycerol). For size-exclusion chromatography, a Superdex 16/600 75 μ g column (Cytiva, Marlborough, USA) equilibrated in SEC buffer (20 mM Tris-HCl, pH 8.0, 150 mM NaCl, 0.1% polysorbate-20) was used. The protein was flash frozen in liquid nitrogen and stored at -80 °C until further use.

Expression and Purification of T7 Polymerase. For the protein expression, competent BL21 (DE3) pLysS cells (Merck KGaA, Darmstadt, Germany) were transformed with plasmid obtained by Addgene (pQE 80L Kan T7WT was a gift from Andrew Ellington (Addgene plasmid no. 102790; <http://n2t.net/addgene:102790>; RRID:Addgene_102790). Cells were grown in LB medium at 37 °C until an optical density of 0.8 at 600 nm was reached. After induction of the expression by 500 μ M IPTG, the expression was maintained overnight at 37 °C. Disruption of cells was performed as described above using lysis buffer_{T7} (25 mM sodium phosphate, pH 7.4, 500 mM NaCl, 25 mM imidazole). For purification, the clear supernatant was loaded onto a HisTrap HP 5 mL column, and protein was eluted performing a gradient up to 100% elution buffer_{T7} (25 mM sodium phosphate, pH 7.4, 500 mM NaCl, 500 mM imidazole). For storage, the eluted protein was rebuffered into 2 \times storage buffer_{T7} (100 mM Tris-HCl, pH 7.8, 200 mM NaCl, 0.2 mM EDTA, 2 mM DTT, 0.2% Triton X-100) using Amicon Ultra 4 10K centrifugal filters (Merck KGaA, Darmstadt, Germany) and was diluted 1:1 very gently with glycerol. Protein was stored until further use at -20 °C.

Polymerase Chain Reaction (PCR). For the preparation of IVT templates for tRNA^{Asp}, PCR reactions were carried out in final volumes of 200 μ L. Taq DNA Polymerase (0.05 U μ L⁻¹; NEB; units defined by the supplier) was added to the reaction buffer (10 mM Tris-HCl, pH 8.3, 50 mM KCl, 1.5 mM MgCl₂) containing 3 mM MgCl₂, 400 mM dNTP-Mix, 2 μ M of each primer (forward, 5'-CGC GCG AAG CTT AAT ACG ACT CAC TAT A-3'; reverse, 5'-TGG CGG GCC GTC G-3') and 10 nM template (5'-TGG CGG GCC GTC GGG GAA TCG AAC CCC GGT CTC CCG CGT GAC AGG CGG GGA TAC TCA CCA CTA TAC TAA CGA CCC TAT AGT GAG TCG TAT T-3'). After an initial denaturation step (2 min at 90 °C), 35 PCR cycles were performed with annealing (30 s at 59 °C), elongation (45 s at 72 °C), and denaturation (30 s at 90 °C) and a final elongation step of 5 min.

The template of tRNA^{Thr} was prepared accordingly with primers 5'-CGC GCG AAG CTT AAT ACG ACT CAC TAT A-3' (forward) and 5'-TGG AGG CCC CGC TGG GAG TCG AA-3' (reverse) and the following template: 5'-TAG TCG TAA GCT GAT ATG GCT GAT TAG TCG GAA GCA TCG AAC GCT GAT GAG AGG CCC CGC TGG GAG TCG AAC CCA GGA TCT CCT GTT TAC TAG ACA GGC GCT TTA ACC AAC TAA GCT ACG GAG CCT ATA GTG AGT CGT ATT A-3'.

In Vitro Transcription (IVT) and Purification of tRNA^{Asp} and tRNA^{Thr}. A portion (400 μL) of the PCR reaction product without further purification was added to reaction mix to reach a final volume of 1 mL in transcription buffer (40 mM Tris-HCl, pH 8.8, 1 mM spermidine, 5 mM DTT, 0.01% Triton X-100) containing 30 mM MgCl_2 , 5 mM DTT, 5 mM of each NTP, 2.5 $\mu\text{g mL}^{-1}$ BSA, and 50 $\mu\text{g mL}^{-1}$ of T7 polymerase. Reactions were carried out at 37 °C for 4 h.

The DNA template was digested by addition of 1 U RNase-free DNase I (Thermo Scientific; units defined by the supplier) and 100 μL DNase I buffer (100 mM Tris-HCl, pH 7.5, 25 mM MgCl_2 , 1 mM CaCl_2 , Thermo Scientific) to the transcription reaction and incubation for 1 h at 37 °C.

In vitro transcribed RNA was purified by 10% denaturing polyacrylamide gel electrophoresis (PAGE) for 90 min at 15 W. RNA was visualized by UV shadowing and the corresponding gel area was excised from the gel. After overnight elution in 0.5 M NH_4OAc and Nanosep filtering (0.45 μm , VWR), the RNA was precipitated with EtOH.

Purified RNA was dissolved in Milli-Q water. The quality was checked on 10% denaturing PAGE gels after staining with GelRed (Biotrend Chemikalien GmbH, Köln, Germany) and visualizing RNA on a Typhoon 9400 at an excitation wavelength of 525 nm. The concentration was determined on a Nanodrop 2000 Spectrometer (Thermo Scientific, Waltham, USA) by measuring the absorption at 260 and 280 nm.

Microscale Thermophoresis (MST). A screening of all compounds for binding was performed on a Monolith NT.115 Pico instrument (NanoTemper Technologies, Muenchen, Germany). His6-tagged DNMT2 was labeled using the Monolith His-Tag Labeling Kit RED-Tris-NTA second generation, according to the manufacturer's instructions. The labeling strategy was chosen due to the existence of a His6 tag within the recombinant protein, which should allow specific labeling without interfering with the binding site of the protein. Labeled protein was diluted to 10 nM into MST buffer (50 mM HEPES, pH 7.5, 150 mM NaCl, 10 mM MgCl_2 , 1 mM DTT, 0.05% polysorbate-20, 0.1% PEG-8000), and the compound was added in a final concentration of 100 μM . HEPES was recommended by the manufacturer as a reasonable buffer; moreover, addition of 0.05% polysorbate-20 and 0.1% PEG-8000 stabilized the protein and prevented aggregation during the measurements. Measurements were performed in quadruplets in MST buffer at 25 °C and at medium MST power in Monolith NT.115 Capillaries (NanoTemper Technologies, Muenchen, Germany). Medium MST power was sufficient to induce a shift in thermophoresis; therefore the usage of high MST power was waived to avoid stress for the protein. Furthermore, special care was taken to always use fresh protein and buffers to reduce adsorption and aggregation and also to maintain reducing conditions for the protein, which was crucial for the interactions. The protein was incubated with compound for 5 min at room temperature prior to measurements. The raw data were analyzed using the MO.Affinity Analysis software (NanoTemper Technologies, Muenchen, Germany). For binder/nonbinder discrimination, a 99% confidence interval of normalized fluorescence was calculated. If there was at least a 1% fluorescence shift, based on normalized fluorescence between the confidence intervals of testing compound and control, the compound was defined as a binder.

Isothermal Titration Calorimetry (ITC). Calorimetric experiments for determination of binding affinity of detected inhibitors were conducted with a MicroCal PEAQ-ITC Automated (Malvern Panalytical, Malvern, UK). DNMT2 was concentrated and buffer was exchanged into ITC buffer (50 mM sodium phosphate, pH 7.5, 300 mM NaCl, 0.5 mM EDTA, 2 mM β -mercaptoethanol, 0.05% polysorbate-20) using Amicon Ultra 4 10K centrifugal filters (Merck KGaA, Darmstadt, Germany) to a final concentration of 30 μM . Stocks of compounds were provided as 25 mM stocks in DMSO and were diluted to 300 μM with ITC buffer. Measurements were performed in 13 injections at 25 °C in triplicate. Data were analyzed and fitted using MicroCal PEAQ-ITC Analysis Software 1.21. (Malvern Panalytical, Malvern, UK). Values were not buffer-corrected, considering the low ionization heat of phosphate buffers.⁸⁸

For analysis of the binding site, DNMT2 was spiked with 300 μM 27m instead of DMSO and the titration was performed with 300 μM SAH, which served as a known binder. Parameters and analysis were as described in the preceding.

DNMT2 Activity Assay. The enzymatic assay was carried out in 100 mM Tris-HCl, pH 8, 100 mM NH_4OAc , 0.1 mM EDTA, 10 mM MgCl_2 , and 10 mM DTT. SAM was added as a mixture of ^3H -SAM (Hartmann Analytics) and cold SAM (NEB) to final concentrations of 0.025 $\mu\text{Ci } \mu\text{L}^{-1}$ and 0.9 μM . tRNA^{Asp} was heated to 75 °C for 5 min and cooled down to room temperature before it was added to the reaction mixture to a final concentration of 5 μM . The amount of DMSO was adjusted to 5%. The reactions were started by adding 250 nM DNMT2 to a final volume of 20 μL and carried out at 37 °C.

At 0 and 20 min, aliquots of 8 μL were taken from the reaction mixture and spotted on Whatman glass microfiber filters (GF/C, 25 mm). The RNA was precipitated on the filters in 5% ice cold TCA for at least 15 min. The filters were washed twice with 5% TCA at room temperature for 20 and 10 min and once in EtOH for 10 min. After drying, the filters were transferred into scintillation vials and 3 mL of Gold MV liquid scintillation cocktail (PerkinElmer, Waltham, USA) was added. Scintillation was measured on a scintillation counter (TriCarb Liquid Scintillation Analyzer 4810TR) with a measurement time of 1 min.

For compound screening, compounds were added to final concentrations of 100 μM . Percentage of inhibition at this concentration was obtained by referencing scintillation increase to a positive control without compound. Errors refer to the standard deviation of three independent measurements.

For IC₅₀ value determination, compounds were analyzed at a minimum of seven different concentrations in experimental triplicates. IC₅₀ values were calculated by exponential fitting of the relative enzymatic activities against the inhibitor concentrations using the LL.2 function of the drc package, version 3.0-1,⁸⁹ in RStudio.⁹⁰ IC₅₀ errors are given as standard errors.

DNMT3A-3L Activity Assay. The enzymatic assay was carried out in 50 mM KPi, pH 7.8, 1.0 mM EDTA, 20 mM NaCl, 0.2 mg mL^{-1} BSA, and 1.0 mM DTT. ^3H -SAM (Hartmann Analytics) was added to a final concentration of 0.63 μM and 0.05 $\mu\text{Ci } \mu\text{L}^{-1}$.

Substrate DNA was prepared by annealing 7.5 μM of oligos 5'-GTC GTC GTC GTC GTC GTC GTC GTC GTC GTC GTC GTC-3' and 5'-GAC GAC GAC GAC GAC GAC GAC GAC GAC GAC GAC GAC-3' (Biomers) in 100 mM HEPES, pH 7.5, and 15 mM KOAc by heating to 95 °C and slowly cooling down to room temperature.

Duplex DNA was added to the reaction mixture to a final concentration of 750 nM. The amount of DMSO was adjusted to 5%. The reactions were started by adding 1 μM DNMT3A-3L to a final volume of 20 μL and carried out at 37 °C.

At 0 and 150 min, aliquots of 8 μL were taken from the reaction mixture and spotted on Whatman glass microfiber filters (GF/C, 25 mm). The DNA was precipitated on the filters in 5% ice cold TCA for at least 15 min. The filters were washed twice with 5% TCA at room temperature for 10 and 20 min and once in EtOH for 10 min, respectively. After drying, the filters were transferred into scintillation vials, and 3 mL of Gold MV liquid scintillation cocktail (PerkinElmer, Waltham, USA) was added. Scintillation was measured on a scintillation counter (TriCarb Liquid Scintillation Analyzer 4810TR) with a measurement time of 1 min.

Compounds were added to final concentrations of 100 μM . Percentage of inhibition at this concentration was obtained by referencing scintillation increase to a positive control without compound. Errors refer to the standard deviation of three independent measurements.

NSUN2 Activity Assay. The enzymatic assay was carried out in 50 mM Tris-HCl, pH 7.5, 5.0 mM EDTA, 5.0 mM MgCl_2 , 10% glycerol, and 1.5 mM DTT. SAM was added as a mixture of ^3H -SAM (Hartmann Analytics) and cold SAM (NEB) to final concentrations of 0.025 $\mu\text{Ci } \mu\text{L}^{-1}$ and 0.9 μM . Total tRNA of *E. coli* (Roche Diagnostics GmbH) was heated to 75 °C for 5 min and cooled down to room temperature before it was added to the reaction mixture to a final concentration of 123 ng μL^{-1} . The amount of DMSO was adjusted to 5%. The reactions

were started by adding 250 nM NSUN2 to a final volume of 20 μL and carried out at 37 $^{\circ}\text{C}$.

At 0 and 20 min, aliquots of 8 μL were taken from the reaction mixture and spotted on Whatman glass microfiber filters (GF/C, 25 mm). The RNA was precipitated on the filters in 5% ice cold TCA for at least 15 min. The filters were washed twice with 5% TCA at room temperature for 10 and 20 min and once in EtOH for 10 min, respectively. After drying, the filters were transferred into scintillation vials and 3 mL of Gold MV liquid scintillation cocktail (PerkinElmer, Waltham, USA) was added. Scintillation was measured on a scintillation counter (TriCarb Liquid Scintillation Analyzer 4810TR) with a measurement time of 1 min.

Compounds were added to final concentrations of 100 μM . Percentage of inhibition at this concentration was obtained by referencing scintillation increase to a positive control without compound. Errors refer to the standard deviation of three independent measurements.

NSUN6 Activity Assay. The enzymatic assay was carried out in 50 mM Tris-HCl, pH 7.0, 50 mM NaCl, 5.0 mM MgCl_2 , and 1.0 mM DTT. SAM was added as a mixture of ^3H -SAM (Hartmann Analytics) and cold SAM (NEB) to final concentrations of 1.2 μM and 0.038 $\mu\text{Ci mL}^{-1}$. tRNA^{Thr} was heated to 75 $^{\circ}\text{C}$ for 5 min and cooled down to room temperature before it was added to the reaction mixture to a final concentration of 1 μM . The amount of DMSO was adjusted to 5%. The reactions were started by adding 30 nM NSUN6 to a final volume of 20 μL and carried out at 37 $^{\circ}\text{C}$.

At 0 and 20 min, aliquots of 8 μL were taken from the reaction mixture and spotted on Whatman glass microfiber filters (GF/C, 25 mm). The RNA was precipitated on the filters in 5% ice cold TCA for at least 15 min. The filters were washed twice with 5% TCA at room temperature for 20 and 10 min and once in EtOH for 10 min. After drying, the filters were transferred into scintillation vials, and 3 mL of Gold MV liquid scintillation cocktail (PerkinElmer, Waltham, USA) was added. Scintillation was measured on a scintillation counter (TriCarb Liquid Scintillation Analyzer 4810TR) with a measurement time of 1 min.

Compounds were added to final concentrations of 100 μM . Percentage of inhibition at this concentration was obtained by referencing scintillation increase to a positive control without compound. Errors refer to the standard deviation of three independent measurements.

G9a Activity Assay. The enzymatic assay was carried out in 20 mM KPi, pH 8.0, 2.0 mM MgCl_2 , 0.01% Tween-20. SAM was added as a mixture of ^3H -SAM (Hartmann Analytics) and cold SAM (NEB) to final concentrations of 0.025 $\mu\text{Ci mL}^{-1}$ and 0.9 μM . Histone H3 (AAs 1–25, Eurogentec) was added to the reaction mixture to a final concentration of 1.6 μM . The amount of DMSO was adjusted to 5%. The reactions were started by adding 30 nM G9a to a final volume of 20 μL and carried out at 37 $^{\circ}\text{C}$.

At 0 and 20 min, aliquots of 8 μL were taken from the reaction mixture and spotted on Whatman glass microfiber filters (GF/C, 25 mm). The peptide was precipitated on the filters in 0.2 M ice cold NH_4OAc for at least 15 min. The filters were washed twice with 0.2 M NH_4OAc at room temperature for 10 and 20 min and once in acetone for 10 min. After drying, the filters were transferred into scintillation vials, and 3 mL of Gold MV liquid scintillation cocktail (PerkinElmer, Waltham, USA) was added. Scintillation was measured on a scintillation counter (TriCarb Liquid Scintillation Analyzer 4810TR) with a measurement time of 1 min.

Compounds were added to final concentrations of 100 μM . Percentage of inhibition at this concentration was obtained by referencing scintillation increase to a positive control without compound. Errors refer to the standard deviation of three independent measurements.

Cell Culture. HEK-293 cells were cultured in DMEM high glucose medium (Thermo Scientific) supplied with 10% (v/v) fetal bovine serum (FBS, Thermo Scientific) and 1% (v/v) Penicillin-Streptomycin (10000 U mL^{-1} , Thermo Scientific) in 175 cm^2 cell culture flasks at 37 $^{\circ}\text{C}$ and 5% CO_2 . At a confluency of 80–90%, passaging was performed by washing once with 5 mL of Dulbecco's phosphate-buffered saline

(DPBS, Thermo Scientific) followed by adding 1 mL of trypsin-EDTA (Thermo Scientific) before splitting in a ratio of 1:20. Cells were passaged every 2–3 days.

Cell Viability Assays. Cell viability assays were performed as described in the literature⁹¹ with minor adaptations. Briefly, HEK-293 cells were cultured in a humidified incubator at 37 $^{\circ}\text{C}$ with 5% CO_2 atmosphere as described in the previous section. Cell viability assay were performed in Dulbecco's modified Eagle medium (DMEM, no glucose, no glutamine, no phenol red, Thermo Scientific) supplemented with 10% (v/v) fetal bovine serum, 1% pyruvate (Thermo Scientific), and 1% Penicillin-Streptomycin (10000 U mL^{-1}). Cells (10000 per well) were seeded into 96-well microplates in a volume of 200 μL of supplemented DMEM. Compounds, provided as 50 mM stocks in DMSO, were added in a range of 500 μM to 800 nM (1% to 0.0016% DMSO, respectively) in duplicates to the wells. Negative controls were performed with DMSO treatment in the same concentrations as the compound solutions. After incubation for 24 h at 37 $^{\circ}\text{C}$ and 5% CO_2 , 40 μL of a 3 mg mL^{-1} solution of 3-(4,5-dimethyl-2-thiazolyl)-2,5-diphenyl-2H-tetrazolium bromide (MTT, Sigma-Aldrich) was added to each well. After a further incubation at 37 $^{\circ}\text{C}$ and 5% CO_2 for 20 min, the medium was removed and 225 μL of an 8:1 mixture of DMSO/(0.1 M glycine pH 10.5 (Merck KGaA), 0.1 M NaCl) was added to each well. Plates were shaken for 20 min, and the absorbance was determined at 595 and 670 nm using an Infinite M200 Pro plate reader (Tecan, Männedorf, Switzerland). Background absorbance at 670 nm was subtracted from absorbance at 595 nm. The cell viability was calculated as the ratio of corrected absorbance in compound treated cells to DMSO treated cells with corresponding DMSO concentrations.

In Vivo Methylation Assay. 750 000 cells per well were seeded in 6-well plates, and 2.5 mL of DMEM supplemented with 10% FBS and 1% Penicillin-Streptomycin was added. After 24 h, the medium was removed, and the experiment was initiated by the addition of 2.5 mL of supplemented DMEM including a final concentration of 100 μM compound (5 μL of a 50 mM stock in DMSO) or 5 μL of DMSO. Incubation was carried out for 24 h at 37 $^{\circ}\text{C}$ and 5% CO_2 . To terminate the experiment, the medium was removed, and cells were washed with DPBS and directly harvested using 0.5 mL of Tri Reagent (Sigma-Aldrich).

CaCo-2 Cell Permeability Assay. Cell permeabilities of 27s-A/B and 28-B were assessed in transport studies across monolayers of a human enterocyte cell line. CaCo-2 cells (clone C2Bbe1, passage 49, LGC Standards, Wesel, Germany) were seeded at a density of 5×10^4 cells/ cm^2 in 24-well Transwell inserts with a pore diameter of 3.0 μm (Corning Life Science, Corning, USA) in DMEM cell culture medium (Gibco, Thermo Fisher Scientific, Waltham, USA) supplemented with 10% fetal calf serum (Sigma-Aldrich, St. Louis, USA) and 1% nonessential amino acids (Gibco, Thermo Fisher Scientific, Waltham, USA). Cells were cultured for 14 days at 37 $^{\circ}\text{C}$ and 5% CO_2 , and medium was exchanged every 2–3 days. Before and after the transport study, barrier integrity was evaluated via the transepithelial electrical resistance using chop stick electrodes (Millicell ERS-2, Merck Millipore, Burlington, USA). Compounds 27s-A/B and 28-B were dissolved in DMSO and applied to the apical side of CaCo-2 cell layers at a final concentration of 200 μM in cell culture medium (final concentration of 1% DMSO v/v) in four separate experiments. Compound-free DMSO solutions were used as controls. After 24 h, cell culture media from the apical and basolateral compartments were collected and lyophilized. The residues were each taken up in 200 μL of MeOH, centrifuged, and analyzed by LC-MS using an Agilent Zorbax SB-Aq column ($4.6 \times 150 \text{ mm}^2$) with the mobile phases $\text{MeCN}/\text{H}_2\text{O} = 10:90 + 0.1\% \text{ HCOOH}$ or $\text{MeCN}/\text{H}_2\text{O} = 5:95 + 0.1\% \text{ HCOOH}$. The flow rate was 0.7 mL/min. Samples were applied using 5 μL injection, and the quantitation of the compounds in the apical and basolateral compartment was conducted using the AUCs of the respective peaks at 254 nm. The retention times using the two different mobile phases were as follows: t_{R} (27s-A/B) = 3.21 min ($\text{MeCN}/\text{H}_2\text{O} = 10:90 + 0.1\% \text{ HCOOH}$); t_{R} (28-B) = 9.25 min ($\text{MeCN}/\text{H}_2\text{O} = 10:90 + 0.1\% \text{ HCOOH}$); 4.96 min (27s-A, $\text{MeCN}/\text{H}_2\text{O} = 5:95 + 0.1\% \text{ HCOOH}$), 5.68 min (27s-B, $\text{MeCN}/\text{H}_2\text{O} = 5:95 + 0.1\% \text{ HCOOH}$). Analyses of

the solutions from the assays with **28-B** revealed 20% of ester **28-B** and 78% of acid in the donor compartment, whereas the acceptor compartment contained 2% acid. In the assays with the acid **27s-A/B**, only traces of the compound (ca. 0.6%) could be detected in the acceptor compartment. All values are mean values from the four independent experiments.

Extraction of Total RNA. Total RNA was extracted in Tri Reagent according to the manufacturer's protocol with chloroform (Honeywell Riedel-de Haën). Chloroform (200 μ L per milliliter of Tri Reagent) was added, and the samples were vortexed and incubated at 25 $^{\circ}$ C for 2 min followed by centrifugation for 15 min at 12 000g at 4 $^{\circ}$ C. Total RNA contained in the upper phase was transferred into a new tube, and the procedure was repeated. Afterward, RNA was precipitated by addition of 500 μ L of isopropanol (Honeywell Riedel-de Haën), incubation for 10 min, and centrifugation at 13 000g at 4 $^{\circ}$ C for 30–45 min. The supernatant was discarded, and pellets were washed with 300 μ L of 75% ethanol (Carl Roth) and centrifuged again. Following this procedure, the pellet was dried and RNA was dissolved in 10 μ L of RNase-free water. Concentrations were determined on a Nanodrop 2000 Spectrometer (Thermo Scientific, Waltham, USA) by measuring the absorption at 260 and 280 nm.

Isolation of Total tRNA. Total tRNA was isolated from total RNA by 10% denaturing polyacrylamide gel elution as described in previous sections with minor adaptations: the gel bands containing small RNA species (75 to 120 nucleotides) were excised after running the gel for 90 min at 15 W, staining, and visualization as described previously. RNA was eluted from the gel by adding 300 μ L of NH_4OAc (0.5 M), shaking overnight at 850 rpm and 20 $^{\circ}$ C, and filtering through a Nanosep device (0.45 μ m, VWR). Finally, RNA was EtOH precipitated, and the concentration was determined on a Nanodrop 2000 Spectrometer (Thermo Scientific, Waltham, USA) by measuring the absorption at 260 and 280 nm.

LC-MS/MS-Based Quantification of $m^5\text{C}$. Before measuring $m^5\text{C}$ levels via LC-MS/MS, samples were digested down to nucleosides. Therefore, RNA was incubated for 2 h at 37 $^{\circ}$ C in 5 mM Tris-HCl (pH 8), 1 mM MgCl_2 , 0.3 U of nuclease P1 from *Penicillium citrinum* (Merck KGaA), 0.1 U of phosphodiesterase I (venom exonuclease, Worthington Biochemical Corporation), 1 U of alkaline phosphatase from bovine intestinal mucosa (Merck KGaA), and 10 U of Benzonase Nuclease (Merck KGaA).

For relative quantification of $m^5\text{C}$, deuterated $m^5\text{C}$ ($\text{D}_3\text{-}m^5\text{C}$) was added to digested samples as an internal standard. Samples were measured using an Agilent 1260 HPLC Infinity system equipped with a diode array detector (DAD) and a Synergy Fusion RP column (4 μ m particle size, 80 \AA pore size, 250 mm length, 2 mm inner diameter, Phenomenex). The HPLC was coupled to a triple quadrupole mass spectrometer (Agilent 6470) equipped with an electrospray ion source (ESI, Agilent Jet Stream). Column temperature was set to 35 $^{\circ}$ C and elution was performed at a flow rate of 0.350 mL min^{-1} using a gradient over 30 min with the following mobile phases: A (5 mM NH_4OAc adjusted to pH 5.3 using acetic acid) and B (100% acetonitrile, CHROMASOLV, Honeywell Riedel-de Haën). The gradient included a linear increase from 0–8% B (0–10 min) followed by 8–40% B (10–20 min), 40–0% B (20–23 min), and a final constant composition of 0% B (23–30 min). HPLC separation was followed by a photometrical measurement of the main nucleosides using a DAD at 254 nm prior to entering the triple quadrupole mass spectrometer, which was run at a gas temperature of 300 $^{\circ}$ C, gas flow of 7 L min^{-1} , nebulizer pressure of 60 psi, sheath gas temperature of 400 $^{\circ}$ C, sheath gas flow of 12 L min^{-1} , capillary voltage of 3000 V, and nozzle voltage of 0 V. Measurement was performed in the positive ion mode using the Agilent MassHunter software, and modified nucleosides were monitored in the dynamic multiple reaction monitoring (dynamic MRM) mode. The following nucleoside-to-base mass transitions were used for detection of $m^5\text{C}$ and $\text{D}_3\text{-}m^5\text{C}$: 258 \rightarrow 126 ($m^5\text{C}$), 261 \rightarrow 129 ($\text{D}_3\text{-}m^5\text{C}$) with a retention time ($m^5\text{C}$ and $\text{D}_3\text{-}m^5\text{C}$) of 7.6 min. Analysis was performed using the Agilent MassHunter Qualitative Analysis Software V10.0. For relative quantification, the ratio of unlabeled $^{12}\text{C}\text{-}m^5\text{C}$ and $\text{D}_3\text{-}m^5\text{C}$ was calculated and normalized to the UV peak area of adenosine. The final

$m^5\text{C}$ levels were related to the negative control with DMSO, which was set to 1.

tRNA-Bisulfite-MiSeq. For tRNA-bisulfite-MiSeq, primers were designed to in silico converted (C > U), unmethylated regions of tRNA^{Asp} according to Bormann et al.⁹² Within the amplified region, target cytosine residue 38 was contained. For compatibility with Illumina index and sequencing adapters, 5' and 3' Illumina overhang adapters were appended to the tRNA^{Asp}-specific primer sequences (*vide infra*). For sequencing library preparation, 1 μ g of total RNA isolated from compound-treated HEK-293 cells was bisulfite-converted using the EZ RNA Methylation Kit (Zymo Research). Target amplicons were generated by RT-PCR. cDNA first-strand synthesis was performed using the SuperScript III First-Strand Synthesis kit (Invitrogen). Briefly, 200 ng of bisulfite-converted total RNA was reverse-transcribed using the tRNA^{Asp}-specific reverse primer listed below and subsequently amplified via PCR. PCR reactions were separated on agarose gels and purified using the QIAquick Gel Extraction Kit (Qiagen). Dual indices and sequencing adapters were attached to the amplicons by an indexing PCR using the Illumina Nextera XT Index Kit v2 Set B (Illumina) and the 2 \times KAPA HiFi Hot Start Ready Mix (KAPA Biosystems). Amplicons were purified using AMPure XP beads (Beckman Coulter Genomics) according to the 16S Metagenomic Sequencing Library Preparation Protocol (Illumina). The final library was quantified via the Qubit dsDNA BR Assay Kit (Life Technologies), pooled at equimolar ratios, and submitted for MiSeq at the Genomic and Proteomic Core Facility (German Cancer Research Center). Sequencing data processing and methylation heatmap generation were performed using the BisAMP pipeline.⁹² The forward primer used for library preparation was 5'-tcg tcg gca gcg tca gat gtt tat aag aga cag TGT TAG TAT AGT GGT GAG TAT-3' and the reverse primer 5'-gtc tcg tgg gct cgg aga tgt gta gaa gaa gca gCT CCC CAT CAA AAA ATT A-3'. Capital letters correspond to target-specific sequences that were designed to in silico converted (C > U), unmethylated regions of tRNA^{Asp}. Small letters represent Illumina overhang adapter sequences that are compatible with Illumina index and sequencing adapters.

Statistics. *P*-values were determined with the Rstatix package⁹³ in RStudio⁹⁰ using unpaired two-tailed Welch *t* tests and adjusted to reduce the number of false positive hits appearing due to performing multiple comparisons. Adjustment of *p*-values was conducted using the Benjamini–Hochberg method, a method based on the false discovery rate (FDR), reducing false positive hits while minimizing adjustment-based false negative results.^{94,95}

■ ASSOCIATED CONTENT

SI Supporting Information

The Supporting Information is available free of charge at <https://pubs.acs.org/doi/10.1021/acs.jmedchem.2c00388>.

3D-RISM results for hydration sites, synthesis protocols and analytical data for all compounds, MST traces, ITC curves, NMR spectra, mass spectra, and LC-MS chromatograms of all tested compounds (PDF)

Molecular docking results and predicted binding modes (ZIP)

Molecular formula strings (CSV)

■ AUTHOR INFORMATION

Corresponding Authors

Mark Helm – Institute of Pharmaceutical and Biomedical Sciences, Johannes Gutenberg University Mainz, D-55128 Mainz, Germany; orcid.org/0000-0002-0154-0928; Phone: ++49 (0) 6131 39 25731; Email: mhelm@uni-mainz.de

Tanja Schirmeister – Institute of Pharmaceutical and Biomedical Sciences, Johannes Gutenberg University Mainz, D-55128 Mainz, Germany; Phone: ++49 (0) 6131 39 25742; Email: schirmei@uni-mainz.de

Authors

Marvin Schwickert – Institute of Pharmaceutical and Biomedical Sciences, Johannes Gutenberg University Mainz, D-55128 Mainz, Germany; orcid.org/0000-0002-1385-1416

Tim R. Fischer – Institute of Pharmaceutical and Biomedical Sciences, Johannes Gutenberg University Mainz, D-55128 Mainz, Germany

Robert A. Zimmermann – Institute of Pharmaceutical and Biomedical Sciences, Johannes Gutenberg University Mainz, D-55128 Mainz, Germany

Sabrina N. Hoba – Institute of Pharmaceutical and Biomedical Sciences, Johannes Gutenberg University Mainz, D-55128 Mainz, Germany

J. Laurenz Meidner – Institute of Pharmaceutical and Biomedical Sciences, Johannes Gutenberg University Mainz, D-55128 Mainz, Germany

Marlies Weber – Institute of Pharmaceutical and Biomedical Sciences, Johannes Gutenberg University Mainz, D-55128 Mainz, Germany

Moritz Weber – Institute of Pharmaceutical and Biomedical Sciences, Johannes Gutenberg University Mainz, D-55128 Mainz, Germany

Martin M. Stark – Institute of Pharmaceutical and Biomedical Sciences, Johannes Gutenberg University Mainz, D-55128 Mainz, Germany

Jonas Koch – Division of Epigenetics, DKFZ-ZMBH Alliance, German Cancer Research Center, D-69120 Heidelberg, Germany; orcid.org/0000-0002-2080-6293

Nathalie Jung – Institute of Pharmaceutical Technology, Goethe University Frankfurt, D-60438 Frankfurt am Main, Germany

Christian Kersten – Institute of Pharmaceutical and Biomedical Sciences, Johannes Gutenberg University Mainz, D-55128 Mainz, Germany; orcid.org/0000-0001-9976-7639

Maike Windbergs – Institute of Pharmaceutical Technology, Goethe University Frankfurt, D-60438 Frankfurt am Main, Germany

Frank Lyko – Division of Epigenetics, DKFZ-ZMBH Alliance, German Cancer Research Center, D-69120 Heidelberg, Germany

Complete contact information is available at:
<https://pubs.acs.org/10.1021/acs.jmedchem.2c00388>

Author Contributions

[‡]M.S., T.R.F., and R.A.Z. contributed equally. The manuscript was written through contributions of all authors. All authors have given approval to the final version of the manuscript.

Funding

Financial support by the DFG (Deutsche Forschungsgemeinschaft) in the framework of the Transregio Collaborative Research Center TRR 319 (RMaP, RNA Modification and Processing), projects A01 (T.S., F.L.), C01, and C03 (M.H.), is gratefully acknowledged.

Notes

The authors declare no competing financial interest.

ACKNOWLEDGMENTS

We thank the Genomic and Proteomic Core Facility at the DKFZ for their support of this project. Furthermore, we thank Nina Jacobs (University of Mainz) for her support in optimization of the MST assay, Chloé Walter (University of

Mainz) for her support with the biophysical measurements, and Thea Bruchhardt (University of Mainz) for her support in the establishment of protein expression.

ABBREVIATIONS USED

5-azaC, 5-azacytidine; C, cytidine; CC₅₀, half maximal cytotoxic concentration; CDI, 1,1'-carbonyldiimidazole; COMT, catechol-O-MTase; Dab, 2,4-diaminobutyric acid; 1,2-DCE, 1,2-dichloroethane; DCM, dichloromethane; DIAD, diisopropyl azodicarboxylate; DIBAL, diisobutylaluminum hydride; DIPEA, *N,N*-diisopropylethylamine; DMAP, 4-dimethylaminopyridine; DMEM, Dulbecco's modified Eagle medium; DMF, *N,N*-dimethylformamide; DMSO, dimethyl sulfoxide; DNMT, DNA methyltransferase; DOT1L, histone-lysine *N*-methyltransferase, H3 lysine-79 specific; DTT, dithiothreitol; EDTA, ethylenediaminetetraacetic acid; HBTU, hexafluorophosphate benzotriazole tetramethyl uronium; HMT, histone methyltransferase; IEX, ion exchange chromatography; ITC, isothermal titration calorimetry; m³C, 5-methylcytidine; m²G, 2-methylguanosine; METTL, N⁶-adenosine MTase; MMFF94x, Merck molecular force field; MTase, methyltransferase; MST, microscale thermophoresis; NTMT, N-terminal methyltransferase; PCR, polymerase chain reaction; PDB, Protein Data Bank; PMT, protein methyltransferase; 3D-RISM, three-dimensional reference interaction site model; RMSD, root-mean-square deviation of atomic positions; SAH, S-adenosyl-L-homocysteine; SAM, S-adenosyl-L-methionine; SAR, structure-activity relationship; SARS-CoV-2, severe acute respiratory syndrome coronavirus type 2; SFG, sinefungin; snRNA, small noncoding RNA; TBTU, (1*H*-benzotriazole-1-yl)-1,1,3,3-tetramethylammonium tetrafluoroborate; TCA, trichloroacetic acid; THF, tetrahydrofuran; Tris, tris(hydroxymethyl)aminomethane

REFERENCES

- Ganesan, A.; Arimondo, P. B.; Rots, M. G.; Jeronimo, C.; Berdasco, M. The Timeline of Epigenetic Drug Discovery: From Reality to Dreams. *Clin. Epigenetics* **2019**, *11* (1), 174.
- Jonkhout, N.; Tran, J.; Smith, M. A.; Schonrock, N.; Mattick, J. S.; Novoa, E. M. The RNA Modification Landscape in Human Disease. *RNA* **2017**, *23* (12), 1754–1769.
- Chen, Q.; Yan, W.; Duan, E. Epigenetic Inheritance of Acquired Traits through Sperm RNAs and Sperm RNA Modifications. *Nat. Rev. Genet.* **2016**, *17* (12), 733–743.
- Chen, Q.; Yan, M.; Cao, Z.; Li, X.; Zhang, Y.; Shi, J.; Feng, G.; Peng, H.; Zhang, X.; Zhang, Y.; Qian, J.; Duan, E.; Zhai, Q.; Zhou, Q. Sperm TsRNAs Contribute to Intergenerational Inheritance of an Acquired Metabolic Disorder. *Science* **2016**, *351* (6271), 397–400.
- Rassoulzadegan, M.; Grandjean, V.; Gounon, P.; Vincent, S.; Gillot, I.; Cuzin, F. RNA-Mediated Non-Mendelian Inheritance of an Epigenetic Change in the Mouse. *Nature* **2006**, *441* (7092), 469–474.
- Liebers, R.; Rassoulzadegan, M.; Lyko, F. Epigenetic Regulation by Heritable RNA. *PLoS Genet.* **2014**, *10* (4), No. e1004296.
- Wang, Y.; Chen, Z.-P.; Hu, H.; Lei, J.; Zhou, Z.; Yao, B.; Chen, L.; Liang, G.; Zhan, S.; Zhu, X.; Jin, F.; Ma, R.; Zhang, J.; Liang, H.; Xing, M.; Chen, X.-R.; Zhang, C.-Y.; Zhu, J.-N.; Chen, X. Sperm MicroRNAs Confer Depression Susceptibility to Offspring. *Sci. Adv.* **2021**, *7* (7), eabd7605.
- Gapp, K.; Jawaid, A.; Sarkies, P.; Bohacek, J.; Pelczar, P.; Prados, J.; Farinelli, L.; Miska, E.; Mansuy, I. M. Implication of Sperm RNAs in Transgenerational Inheritance of the Effects of Early Trauma in Mice. *Nat. Neurosci.* **2014**, *17* (5), 667–669.
- Rodgers, A. B.; Morgan, C. P.; Leu, N. A.; Bale, T. L. Transgenerational Epigenetic Programming via Sperm MicroRNA Recapitulates Effects of Paternal Stress. *Proc. Natl. Acad. Sci. U. S. A.* **2015**, *112* (44), 13699–13704.

- (10) Gapp, K.; van Steenwyk, G.; Germain, P. L.; Matsushima, W.; Rudolph, K. L. M.; Manuella, F.; Roszkowski, M.; Vernaz, G.; Ghosh, T.; Pelczar, P.; Mansuy, I. M.; Miska, E. A. Alterations in Sperm Long RNA Contribute to the Epigenetic Inheritance of the Effects of Postnatal Trauma. *Mol. Psychiatry* **2020**, *25* (9), 2162–2174.
- (11) Zhang, Y.; Zhang, X.; Shi, J.; Tuorto, F.; Li, X.; Liu, Y.; Liebers, R.; Zhang, L.; Qu, Y.; Qian, J.; Pahima, M.; Liu, Y.; Yan, M.; Cao, Z.; Lei, X.; Cao, Y.; Peng, H.; Liu, S.; Wang, Y.; Zheng, H.; Woolsey, R.; Quilici, D.; Zhai, Q.; Li, L.; Zhou, T.; Yan, W.; Lyko, F.; Zhang, Y.; Zhou, Q.; Duan, E.; Chen, Q. Dnmt2 Mediates Intergenerational Transmission of Paternally Acquired Metabolic Disorders through Sperm Small Non-Coding RNAs. *Nat. Cell Biol.* **2018**, *20* (5), 535–540.
- (12) Sharma, U.; Conine, C. N.; Shea, J. M.; Boskovic, A.; Derr, A. G.; Bing, X. Y.; Belleannee, C.; Kucukural, A.; Serra, R. W.; Sun, F.; Song, L.; Carone, B. R.; Ricci, E. P.; Li, X. Z.; Fauquier, L.; Moore, M. J.; Sullivan, R.; Mello, C. C.; Garber, M.; Rando, O. J. Biogenesis and Function of TRNA Fragments during Sperm Maturation and Fertilization in Mammals. *Science* **2016**, *351* (6271), 391–396.
- (13) Sarker, G.; Sun, W.; Rosenkranz, D.; Pelczar, P.; Opitz, L.; Efthymiou, V.; Wolfrum, C.; Peleg-Raibstein, D. Maternal Over-nutrition Programs Hedonic and Metabolic Phenotypes across Generations through Sperm TsRNAs. *Proc. Natl. Acad. Sci. U. S. A.* **2019**, *116* (21), 10547–10556.
- (14) Swanson, G. M.; Estill, M.; Diamond, M. P.; Legro, R. S.; Coutifaris, C.; Barnhart, K. T.; Huang, H.; Hansen, K. R.; Trussell, J. C.; Coward, R. M.; Zhang, H.; Goodrich, R.; Krawetz, S. A. Human Chromatin Remodeler Cofactor, RNA Interactor, Eraser and Writer Sperm RNAs Responding to Obesity. *Epigenetics* **2020**, *15* (1–2), 32–46.
- (15) Zhang, Y.; Shi, J.; Rassoulzadegan, M.; Tuorto, F.; Chen, Q. Sperm RNA Code Programmes the Metabolic Health of Offspring. *Nat. Rev. Endocrinol.* **2019**, *15* (8), 489–498.
- (16) Kiani, J.; Grandjean, V.; Liebers, R.; Tuorto, F.; Ghanbarian, H.; Lyko, F.; Cuzin, F.; Rassoulzadegan, M. RNA-Mediated Epigenetic Heredity Requires the Cytosine Methyltransferase Dnmt2. *PLoS Genet.* **2013**, *9* (5), No. e1003498.
- (17) Yoder, J. A.; Bestor, T. H. A Candidate Mammalian DNA Methyltransferase Related to Pmt1p of Fission Yeast. *Hum. Mol. Genet.* **1998**, *7* (2), 279–284.
- (18) Lyko, F. The DNA Methyltransferase Family: A Versatile Toolkit for Epigenetic Regulation. *Nat. Rev. Genet.* **2018**, *19* (2), 81–92.
- (19) Goll, M. G.; Kirpekar, F.; Maggert, K. A.; Yoder, J. A.; Hsieh, C. L.; Zhang, X.; Golic, K. G.; Jacobsen, S. E.; Bestor, T. H. Methylation of TRNAAsp by the DNA Methyltransferase Homolog Dnmt2. *Science* (80-). **2006**, *311* (5759), 395–398.
- (20) Hermann, A.; Schmitt, S.; Jeltsch, A. The Human Dnmt2 Has Residual DNA-(Cytosine-C5) Methyltransferase Activity. *J. Biol. Chem.* **2003**, *278* (34), 31717–31721.
- (21) Jeltsch, A.; Ehrenhofer-Murray, A.; Jurkowski, T. P.; Lyko, F.; Reuter, G.; Ankri, S.; Nellen, W.; Schaefer, M.; Helm, M. Mechanism and Biological Role of Dnmt2 in Nucleic Acid Methylation. *RNA Biol.* **2017**, *14* (9), 1108–1123.
- (22) Rai, K.; Chidester, S.; Zavala, C. V.; Manos, E. J.; James, S. R.; Karpf, A. R.; Jones, D. A.; Cairns, B. R. Dnmt2 Functions in the Cytoplasm to Promote Liver, Brain, and Retina Development in Zebrafish. *Genes Dev.* **2007**, *21*, 261–266.
- (23) Lin, M. J.; Tang, L. Y.; Reddy, M. N.; Shen, C. K. J. DNA Methyltransferase Gene DDnmt2 and Longevity of *Drosophila*. *J. Biol. Chem.* **2005**, *280* (2), 861–864.
- (24) Schaefer, M.; Pollex, T.; Hanna, K.; Tuorto, F.; Meusburger, M.; Helm, M.; Lyko, F. RNA Methylation by Dnmt2 Protects Transfer RNAs against Stress-Induced Cleavage. *Genes Dev.* **2010**, *24* (15), 1590–1595.
- (25) Tuorto, F.; Liebers, R.; Musch, T.; Schaefer, M.; Hofmann, S.; Kellner, S.; Frye, M.; Helm, M.; Stoecklin, G.; Lyko, F. RNA Cytosine Methylation by Dnmt2 and NSun2 Promotes TRNA Stability and Protein Synthesis. *Nat. Struct. Mol. Biol.* **2012**, *19*, 900.
- (26) Tuorto, F.; Herbst, F.; Alerasool, N.; Bender, S.; Popp, O.; Federico, G.; Reitter, S.; Liebers, R.; Stoecklin, G.; Gröne, H.; Dittmar, G.; Glimm, H.; Lyko, F. The TRNA Methyltransferase Dnmt2 Is Required for Accurate Polypeptide Synthesis during Haematopoiesis. *EMBO J.* **2015**, *34* (18), 2350–2362.
- (27) Li, L.; Wang, S. DNA Methyltransferase (DNMTs) Expression in Cervical Cancer Tissues and Its Relationship with HPV Infection and Tumor Malignancy. *J. Hainan Med. Univ.* **2017**, *23*, 136–139.
- (28) Towns, W. L.; Begley, T. J. Transfer RNA Methyltransferases and Their Corresponding Modifications in Budding Yeast and Humans: Activities, Predications, and Potential Roles in Human Health. *DNA and Cell Biology.* **2012**, *31*, 434–454.
- (29) Forbes, S. A.; Beare, D.; Gunasekaran, P.; Leung, K.; Bindal, N.; Boutselakis, H.; Ding, M.; Bamford, S.; Cole, C.; Ward, S.; Kok, C. Y.; Jia, M.; De, T.; Teague, J. W.; Stratton, M. R.; McDermott, U.; Campbell, P. J. COSMIC: Exploring the World's Knowledge of Somatic Mutations in Human Cancer. *Nucleic Acids Res.* **2015**, *43* (D1), D805–D811.
- (30) Dong, A. Structure of Human DNMT2, an Enigmatic DNA Methyltransferase Homolog That Displays Denaturant-Resistant Binding to DNA. *Nucleic Acids Res.* **2001**, *29* (2), 439–448.
- (31) Jurkowski, T. P.; Jeltsch, A. On the Evolutionary Origin of Eukaryotic DNA Methyltransferases and Dnmt2. *PLoS One* **2011**, *6* (11), e28104.
- (32) Schulz, E. C.; Roth, H. M.; Ankri, S.; Ficner, R. Structure Analysis of *Entamoeba histolytica* DNMT2 (EhMeth). *PLoS One* **2012**, *7* (6), e38728.
- (33) Tran, H. T. T.; Kim, H. N.; Lee, I.-K.; Kim, Y.-K.; Ahn, J.-S.; Yang, D.-H.; Lee, J.-J.; Kim, H.-J. DNA Methylation Changes Following 5-Azacytidine Treatment in Patients with Myelodysplastic Syndrome. *J. Korean Med. Sci.* **2011**, *26* (2), 207–213.
- (34) Mund, C.; Hackanson, B.; Stresemann, C.; Lübbert, M.; Lyko, F. Characterization of DNA Demethylation Effects Induced by 5-Aza-2'-Deoxycytidine in Patients with Myelodysplastic Syndrome. *Cancer Res.* **2005**, *65* (16), 7086–7090.
- (35) Yang, A. S.; Doshi, K. D.; Choi, S.-W.; Mason, J. B.; Mannari, R. K.; Gharybian, V.; Luna, R.; Rashid, A.; Shen, L.; Estecio, M. R. H.; Kantarjian, H. M.; Garcia-Manero, G.; Issa, J.-P. J. DNA Methylation Changes after 5-Aza-2'-Deoxycytidine Therapy in Patients with Leukemia. *Cancer Res.* **2006**, *66* (10), 5495–5503.
- (36) Santi, D. V.; Norment, A.; Garrett, C. E. Covalent Bond Formation between a DNA-Cytosine Methyltransferase and DNA Containing 5-Azacytosine. *Proc. Natl. Acad. Sci. U. S. A.* **1984**, *81* (22), 6993–6997.
- (37) Khoddami, V.; Cairns, B. R. Identification of Direct Targets and Modified Bases of RNA Cytosine Methyltransferases. *Nat. Biotechnol.* **2013**, *31* (5), 458–464.
- (38) Zhou, L.; Cheng, X.; Connolly, B. A.; Dickman, M. J.; Hurd, P. J.; Hornby, D. P. Zebularine: A Novel DNA Methylation Inhibitor That Forms a Covalent Complex with DNA Methyltransferases. *J. Mol. Biol.* **2002**, *321* (4), 591–599.
- (39) Cho, H. D.; Oyelere, A. K.; Strobel, S. A.; Weiner, A. M. Use of Nucleotide Analogs by Class I and Class II CCA-Adding Enzymes (TRNA Nucleotidyltransferase): Deciphering the Basis for Nucleotide Selection. *RNA* **2003**, *9* (8), 970–981.
- (40) Hamill, R. L.; Hoehn, M. M. A9145, a New Adenine-Containing Antifungal Antibiotic: I. Discovery and Isolation. *J. Antibiot. (Tokyo).* **1973**, *26* (8), 463–465.
- (41) Borchardt, R. T.; Eiden, L. E.; Wu, B. S.; Rutledge, C. O. Sinefungin, a Potent Inhibitor of S-Adenosylmethionine: Protein O-Methyltransferase. *Biochem. Biophys. Res. Commun.* **1979**, *89* (3), 919–924.
- (42) Richon, V. M.; Johnston, D.; Sneeringer, C. J.; Jin, L.; Majer, C. R.; Elliston, K.; Jerva, L. F.; Scott, M. P.; Copeland, R. A. Chemogenetic Analysis of Human Protein Methyltransferases. *Chem. Biol. Drug Des.* **2011**, *78* (2), 199–210.
- (43) Lerner, C.; Masjost, B.; Ruf, A.; Gramlich, V.; Jakob-Roetne, R.; Zürcher, G.; Borroni, E.; Diederich, F. Bisubstrate Inhibitors for the Enzyme Catechol-O-Methyltransferase (COMT): Influence of Inhibitor Preorganisation and Linker Length between the Two Substrate Moieties on Binding Affinity. *Org. Biomol. Chem.* **2003**, *1* (1), 42–49.

- (44) Paulini, R.; Lerner, C.; Jakob-Roetne, R.; Zürcher, G.; Borroni, E.; Diederich, F. Bisubstrate Inhibitors of the Enzyme Catechol O-Methyltransferase (COMT): Efficient Inhibition despite the Lack of a Nitro Group. *Chembiochem* **2004**, *5* (9), 1270–1274.
- (45) Ellermann, M.; Paulini, R.; Jakob-Roetne, R.; Lerner, C.; Borroni, E.; Roth, D.; Ehler, A.; Schweizer, W. B.; Schlatter, D.; Rudolph, M. G.; Diederich, F. Molecular Recognition at the Active Site of Catechol-O-Methyltransferase (COMT): Adenine Replacements in Bisubstrate Inhibitors. *Chemistry* **2011**, *17* (23), 6369–6381.
- (46) Anglin, J. L.; Deng, L.; Yao, Y.; Cai, G.; Liu, Z.; Jiang, H.; Cheng, G.; Chen, P.; Dong, S.; Song, Y. Synthesis and Structure-Activity Relationship Investigation of Adenosine-Containing Inhibitors of Histone Methyltransferase DOT1L. *J. Med. Chem.* **2012**, *55* (18), 8066–8074.
- (47) Bedi, R. K.; Huang, D.; Eberle, S. A.; Wiedmer, L.; Ślędz, P.; Cafilisch, A. Small-Molecule Inhibitors of METTL3, the Major Human Epitranscriptomic Writer. *ChemMedChem* **2020**, *15* (9), 744–748.
- (48) Ferron, F.; Decroly, E.; Selisko, B.; Canard, B. The Viral RNA Capping Machinery as a Target for Antiviral Drugs. *Antiviral Res.* **2012**, *96* (1), 21–31.
- (49) Ahmed-Belkacem, R.; Sutto-Ortiz, P.; Guiraud, M.; Canard, B.; Vasseur, J.-J.; Decroly, E.; Debart, F. Synthesis of Adenine Dinucleosides SAM Analogs as Specific Inhibitors of SARS-CoV Nsp14 RNA Cap Guanine-N7-Methyltransferase. *Eur. J. Med. Chem.* **2020**, *201*, 112557.
- (50) Saavedra, O. M.; Isakovic, L.; Llewellyn, D. B.; Zhan, L.; Bernstein, N.; Claridge, S.; Raepel, F.; Vaisburg, A.; Elowe, N.; Petschner, A. J.; Rahil, J.; Beaulieu, N.; MacLeod, A. R.; Delorme, D.; Besterman, J. M.; Wahhab, A. SAR around (1)-S-Adenosyl-L-Homocysteine, an Inhibitor of Human DNA Methyltransferase (DNMT) Enzymes. *Bioorg. Med. Chem. Lett.* **2009**, *19* (10), 2747–2751.
- (51) Isakovic, L.; Saavedra, O. M.; Llewellyn, D. B.; Claridge, S.; Zhan, L.; Bernstein, N.; Vaisburg, A.; Elowe, N.; Petschner, A. J.; Rahil, J.; Beaulieu, N.; Gauthier, F.; MacLeod, A. R.; Delorme, D.; Besterman, J. M.; Wahhab, A. Constrained (1)-S-Adenosyl-L-Homocysteine (SAH) Analogues as DNA Methyltransferase Inhibitors. *Bioorg. Med. Chem. Lett.* **2009**, *19* (10), 2742–2746.
- (52) Stein, E. M.; Garcia-Manero, G.; Rizzieri, D. A.; Tibes, R.; Berdeja, J. G.; Savona, M. R.; Jongen-Lavrenic, M.; Altman, J. K.; Thomson, B.; Blakemore, S. J.; Daigle, S. R.; Waters, N. J.; Suttle, A. B.; Clawson, A.; Pollock, R.; Krivtsov, A.; Armstrong, S. A.; DiMartino, J.; Hedrick, E.; Löwenberg, B.; Tallman, M. S. The DOT1L Inhibitor Pinometostat Reduces H3K79 Methylation and Has Modest Clinical Activity in Adult Acute Leukemia. *Blood* **2018**, *131* (24), 2661–2669.
- (53) Halby, L.; Marechal, N.; Pechalieu, D.; Cura, V.; Franchini, D.-M.; Faux, C.; Alby, F.; Troffer-Charlier, N.; Kudithipudi, S.; Jeltsch, A.; Aouadi, W.; Decroly, E.; Guillemot, J.-C.; Page, P.; Ferroud, C.; Bonnefond, L.; Guianvarc'h, D.; Cavarelli, J.; Arimondo, P. B. Hijacking DNA Methyltransferase Transition State Analogues to Produce Chemical Scaffolds for PRMT Inhibitors. *Philos. Trans. R. Soc. London. Ser. B, Biol. Sci.* **2018**, *373* (1748), 20170072.
- (54) Zhang, J. H.; Chung, T. D.; Oldenburg, K. R. A Simple Statistical Parameter for Use in Evaluation and Validation of High Throughput Screening Assays. *J. Biomol. Screen.* **1999**, *4* (2), 67–73.
- (55) Kalliokoski, T.; Kramer, C.; Vulpetti, A.; Gedeck, P. Comparability of Mixed IC₅₀ Data - a Statistical Analysis. *PLoS One* **2013**, *8* (4), No. e61007.
- (56) Chellamuthu, A.; Gray, S. G. The RNA Methyltransferase NSUN2 and Its Potential Roles in Cancer. *Cells* **2020**, *9* (8), 1758.
- (57) Trixl, L.; Lusser, A. The Dynamic RNA Methylation 5-Methylcytosine and Its Emerging Role as an Epitranscriptomic Mark. *Wiley Interdiscip. Rev. RNA* **2019**, *10* (1), No. e1510.
- (58) Xue, C.; Zhao, Y.; Li, L. Advances in RNA Cytosine-5 Methylation: Detection, Regulatory Mechanisms, Biological Functions and Links to Cancer. *Biomark. Res.* **2020**, *8*, 43.
- (59) Shankar, S. R.; Bahirvani, A. G.; Rao, V. K.; Bharathy, N.; Ow, J. R.; Taneja, R. G9a, a Multipotent Regulator of Gene Expression. *Epigenetics* **2013**, *8* (1), 16–22.
- (60) Yokochi, T.; Robertson, K. D. Dimethyl Sulfoxide Stimulates the Catalytic Activity of de Novo DNA Methyltransferase 3a (Dnmt3a) in Vitro. *Bioorg. Chem.* **2004**, *32* (4), 234–243.
- (61) Gros, C.; Chauvigné, L.; Poulet, A.; Menon, Y.; Ausseil, F.; Dufau, I.; Arimondo, P. B. Development of a Universal Radioactive DNA Methyltransferase Inhibition Test for High-Throughput Screening and Mechanistic Studies. *Nucleic Acids Res.* **2013**, *41* (19), No. e185.
- (62) Liu, Q.; Cai, X.; Yang, D.; Chen, Y.; Wang, Y.; Shao, L.; Wang, M. W. Cycloalkane Analogues of Sinefungin as EHMT1/2 Inhibitors. *Bioorg. Med. Chem.* **2017**, *25* (17), 4579–4594.
- (63) Rotili, D.; Tarantino, D.; Marrocco, B.; Gros, C.; Masson, V.; Poughon, V.; Ausseil, F.; Chang, Y.; Labella, D.; Cosconati, S.; Di Maro, S.; Novellino, E.; Schnekenburger, M.; Grandjennet, C.; Bouvy, C.; Diederich, M.; Cheng, X.; Arimondo, P. B.; Mai, A. Properly Substituted Analogues of BIX-01294 Lose Inhibition of G9a Histone Methyltransferase and Gain Selective Anti-DNA Methyltransferase 3A Activity. *PLoS One* **2014**, *9* (5), No. e96941.
- (64) Devkota, K.; Lohse, B.; Liu, Q.; Wang, M.-W.; Stärk, D.; Berthelsen, J.; Clausen, R. P. Analogues of the Natural Product Sinefungin as Inhibitors of EHMT1 and EHMT2. *ACS Med. Chem. Lett.* **2014**, *5* (4), 293–297.
- (65) Zheng, W.; Ibáñez, G.; Wu, H.; Blum, G.; Zeng, H.; Dong, A.; Li, F.; Hajian, T.; Allali-Hassani, A.; Amaya, M. F.; Siarheyeva, A.; Yu, W.; Brown, P. J.; Schapira, M.; Vedadi, M.; Min, J.; Luo, M. Sinefungin Derivatives as Inhibitors and Structure Probes of Protein Lysine Methyltransferase SETD2. *J. Am. Chem. Soc.* **2012**, *134* (43), 18004–18014.
- (66) Kilgore, J. A.; Du, X.; Melito, L.; Wei, S.; Wang, C.; Chin, H. G.; Posner, B.; Pradhan, S.; Ready, J. M.; Williams, N. S. Identification of DNMT1 Selective Antagonists Using a Novel Scintillation Proximity Assay. *J. Biol. Chem.* **2013**, *288* (27), 19673–19684.
- (67) Thüring, K.; Schmid, K.; Keller, P.; Helm, M. Analysis of RNA Modifications by Liquid Chromatography-Tandem Mass Spectrometry. *Methods* **2016**, *107*, 48–56.
- (68) Schaefer, M.; Pollex, T.; Hanna, K.; Lyko, F. RNA Cytosine Methylation Analysis by Bisulfite Sequencing. *Nucleic Acids Res.* **2008**, *37* (2), No. e12.
- (69) Rautio, J.; Meanwell, N. A.; Di, L.; Hageman, M. J. The Expanding Role of Prodrugs in Contemporary Drug Design and Development. *Nat. Rev. Drug Discovery* **2018**, *17* (8), 559–587.
- (70) Biela, A.; Nasief, N. N.; Betz, M.; Heine, A.; Hangauer, D.; Klebe, G. Dissecting the Hydrophobic Effect on the Molecular Level: The Role of Water, Enthalpy, and Entropy in Ligand Binding to Thermolysin. *Angew. Chem., Int. Ed. Engl.* **2013**, *52* (6), 1822–1828.
- (71) *The PyMOL Molecular Graphics System*; Schrödinger, LLC.
- (72) Liu, R.-J.; Long, T.; Li, J.; Li, H.; Wang, E.-D. Structural Basis for Substrate Binding and Catalytic Mechanism of a Human RNA:MSC Methyltransferase NSun6. *Nucleic Acids Res.* **2017**, *45* (11), 6684–6697.
- (73) Jumper, J.; Evans, R.; Pritzel, A.; Green, T.; Figurnov, M.; Ronneberger, O.; Tunyasuvunakool, K.; Bates, R.; Židek, A.; Potapenko, A.; Bridgland, A.; Meyer, C.; Kohli, S. A. A.; Ballard, A. J.; Cowie, A.; Romera-Paredes, B.; Nikolov, S.; Jain, R.; Adler, J.; Back, T.; Petersen, S.; Reiman, D.; Clancy, E.; Zielinski, M.; Steinegger, M.; Pacholska, M.; Berghammer, T.; Bodensteiner, S.; Silver, D.; Vinyals, O.; Senior, A. W.; Kavukcuoglu, K.; Kohli, P.; Hassabis, D. Highly Accurate Protein Structure Prediction with AlphaFold. *Nature* **2021**, *596* (7873), 583–589.
- (74) Varadi, M.; Anyango, S.; Deshpande, M.; Nair, S.; Natassia, C.; Yordanova, G.; Yuan, D.; Stroe, O.; Wood, G.; Laydon, A.; Židek, A.; Green, T.; Tunyasuvunakool, K.; Petersen, S.; Jumper, J.; Clancy, E.; Green, R.; Vora, A.; Lutfi, M.; Figurnov, M.; Cowie, A.; Hobbs, N.; Kohli, P.; Kleywegt, G.; Birney, E.; Hassabis, D.; Velankar, S. AlphaFold Protein Structure Database: Massively Expanding the Structural Coverage of Protein-Sequence Space with High-Accuracy Models. *Nucleic Acids Res.* **2022**, *50* (D1), D439–D444.
- (75) Pignot, M.; Pljevaljčić, G.; Weinhold, E. Efficient Synthesis of S-Adenosyl-L-Homocysteine Natural Product Analogues and Their Use to Elucidate the Structural Determinant for Cofactor Binding of the

DNA Methyltransferase M-HhaI. *Eur. J. Org. Chem.* **2000**, *2000* (3), 549–555.

(76) Zhang, G.; Richardson, S. L.; Mao, Y.; Huang, R. Design, Synthesis, and Kinetic Analysis of Potent Protein N-Terminal Methyltransferase 1 Inhibitors. *Org. Biomol. Chem.* **2015**, *13* (14), 4149–4154.

(77) Liu, Q.; Cai, X.; Yang, D.; Chen, Y.; Wang, Y.; Shao, L.; Wang, M.-W. Cycloalkane Analogues of Sinefungin as EHMT1/2 Inhibitors. *Bioorg. Med. Chem.* **2017**, *25* (17), 4579–4594.

(78) Kramer, B.; Rarey, M.; Lengauer, T. Evaluation of the FlexX Incremental Construction Algorithm for Protein-Ligand Docking. *Proteins Struct. Funct. Genet.* **1999**, *37* (2), 228–241.

(79) *LeadIT*; BioSolveIT GmbH: Sankt Augustin, Germany, 2017.

(80) Berman, H. M.; Westbrook, J.; Feng, Z.; Gilliland, G.; Bhat, T. N.; Weissig, H.; Shindyalov, I. N.; Bourne, P. E. The Protein Data Bank. *Nucleic Acids Res.* **2000**, *28* (1), 235–242.

(81) Bietz, S.; Urbaczek, S.; Schulz, B.; Rarey, M. Protoss: A Holistic Approach to Predict Tautomers and Protonation States in Protein-Ligand Complexes. *J. Cheminform.* **2014**, *6* (1), 12.

(82) Halgren, T. A. Merck Molecular Force Field V. Extension of MMFF94 Using Experimental Data, Additional Computational Data, and Empirical Rules. *J. Comput. Chem.* **1996**, *17* (5–6), 616–641.

(83) *Molecular Operating Environment (MOE)*; Chemical Computing Group, 2019.

(84) Beglov, D.; Roux, B. An Integral Equation To Describe the Solvation of Polar Molecules in Liquid Water. *J. Phys. Chem. B* **1997**, *101* (39), 7821–7826.

(85) Siddique, A. N.; Nunna, S.; Rajavelu, A.; Zhang, Y.; Jurkowska, R. Z.; Reinhardt, R.; Rots, M. G.; Ragozin, S.; Jurkowski, T. P.; Jeltsch, A. Targeted Methylation and Gene Silencing of VEGF-A in Human Cells by Using a Designed Dnmt3a-Dnmt3L Single-Chain Fusion Protein with Increased DNA Methylation Activity. *J. Mol. Biol.* **2013**, *425* (3), 479–491.

(86) Zhang, X.; Liu, Z.; Yi, J.; Tang, H.; Xing, J.; Yu, M.; Tong, T.; Shang, Y.; Gorospe, M.; Wang, W. The TRNA Methyltransferase NSun2 Stabilizes P16INK⁴ mRNA by Methylating the 3'-Untranslated Region of P16. *Nat. Commun.* **2012**, *3*, 712.

(87) Long, T.; Li, J.; Li, H.; Zhou, M.; Zhou, X.-L.; Liu, R.-J.; Wang, E.-D. Sequence-Specific and Shape-Selective RNA Recognition by the Human RNA 5-Methylcytosine Methyltransferase NSun6. *J. Biol. Chem.* **2016**, *291* (46), 24293–24303.

(88) Goldberg, R. N.; Kishore, N.; Lennen, R. M. Thermodynamic Quantities for the Ionization Reactions of Buffers. *J. Phys. Chem. Ref. Data* **2002**, *31* (2), 231–370.

(89) Ritz, C.; Baty, F.; Streibig, J. C.; Gerhard, D. Dose-Response Analysis Using R. *PLoS One* **2015**, *10* (12), No. e0146021.

(90) *RStudio*; RStudio Team: Boston, MA, 2020.

(91) Barthels, F.; Marincola, G.; Marciniak, T.; Konhäuser, M.; Hammerschmidt, S.; Bierlmeier, J.; Distler, U.; Wich, P. R.; Tenzer, S.; Schwarzer, D.; Ziebuhr, W.; Schirmeister, T. Asymmetric Disulfanylbenzamides as Irreversible and Selective Inhibitors of Staphylococcus Aureus Sortase A. *ChemMedChem* **2020**, *15* (10), 839–850.

(92) Bormann, F.; Tuorto, F.; Cirzi, C.; Lyko, F.; Legrand, C. BisAMP: A Web-Based Pipeline for Targeted RNA Cytosine-5 Methylation Analysis. *Methods* **2019**, *156*, 121–127.

(93) Kassambara, A. *Rstatix: Pipe-Friendly Framework for Basic Statistical Tests*; 2021.

(94) Benjamini, Y.; Hochberg, Y. Controlling the False Discovery Rate: A Practical and Powerful Approach to Multiple Testing. *J. R. Stat. Soc. Ser. B* **1995**, *57* (1), 289–300.

(95) Jafari, M.; Ansari-Pour, N. Why, When and How to Adjust Your P Values? *Cell J.* **2019**, *20* (4), 604–607.

Recommended by ACS

Discovery of Novel Src Homology-2 Domain-Containing Phosphatase 2 and Histone Deacetylase Dual Inhibitors with Potent Antitumor Efficacy and Enhanced Antitumor Imm...

Meng Liu, Xuben Hou, *et al.*

SEPTEMBER 12, 2022
JOURNAL OF MEDICINAL CHEMISTRY

READ 

Structure-Based Design, Optimization, and Evaluation of Potent Stabilized Peptide Inhibitors Disrupting MTDH and SND1 Interaction

Hailing Chen, Zigang Li, *et al.*

AUGUST 31, 2022
JOURNAL OF MEDICINAL CHEMISTRY

READ 

Discovery of a Novel Potent STAT3 Inhibitor HP590 with Dual p-Tyr⁷⁰⁵/Ser⁷²⁷ Inhibitory Activity for Gastric Cancer Treatment

Peng He, Yihua Chen, *et al.*

SEPTEMBER 14, 2022
JOURNAL OF MEDICINAL CHEMISTRY

READ 

Structure-Based Discovery of a Series of NSD2-PWWP1 Inhibitors

Na Li, Tongchao Liu, *et al.*

JUNE 15, 2022
JOURNAL OF MEDICINAL CHEMISTRY

READ 

Get More Suggestions >

Supporting Information

Discovery of inhibitors of DNA methyltransferase 2, an epitranscriptomic modulator and potential target for cancer treatment

Marvin Schwickert,^{‡,#} Tim R. Fischer,^{‡,#} Robert A. Zimmermann,^{‡,#} Sabrina N. Hoba,[#] J. Laurenz Meidner,[#] Marlies Weber,[#] Moritz Weber,[#] Martin M. Stark,[#] Jonas Koch,⁺ Nathalie Jung,[†] Christian Kersten,[#] Maike Windbergs,[†] Frank Lyko,⁺ Mark Helm^{#} and Tanja Schirmeister^{#*}*

[#]Institute of Pharmaceutical and Biomedical Sciences, Johannes Gutenberg University Mainz, Staudinger Weg 5, D-55128 Mainz, Germany

⁺Division of Epigenetics, DKFZ-ZMBH Alliance, German Cancer Research Center, Im Neuenheimer Feld 280, D-69120 Heidelberg, Germany.

[†]Institute of Pharmaceutical Technology and Buchmann Institute for Molecular Life Sciences Goethe University Frankfurt, Max-von-Laue-Str. 9, D-60438 Frankfurt am Main

[‡]These authors contributed equally.

*Corresponding authors:

Prof. Dr. Tanja Schirmeister, Phone: +49 6131 39-25742, E-Mail: schirmei@uni-mainz.de.

Prof. Dr. Mark Helm, Phone: +49 6131 39 25731, E-Mail: mhelm@uni-mainz.de

Content:

Figure S1–S218 (NMR Spectra and Chromatograms).....	S3–S130
Figure S219–S234 (MST Curves).....	S131–S138
Figure S235–S238 (ITC Curves).....	S140–S140
Table S1–S2 (Docking).....	S142–S143
Figure S239–S243 (Docking Poses).....	S144–S146
Figure 244–S248 (Caco-2 Cell Permeability Assay Chromatograms).....	S147–S149

MST Curves

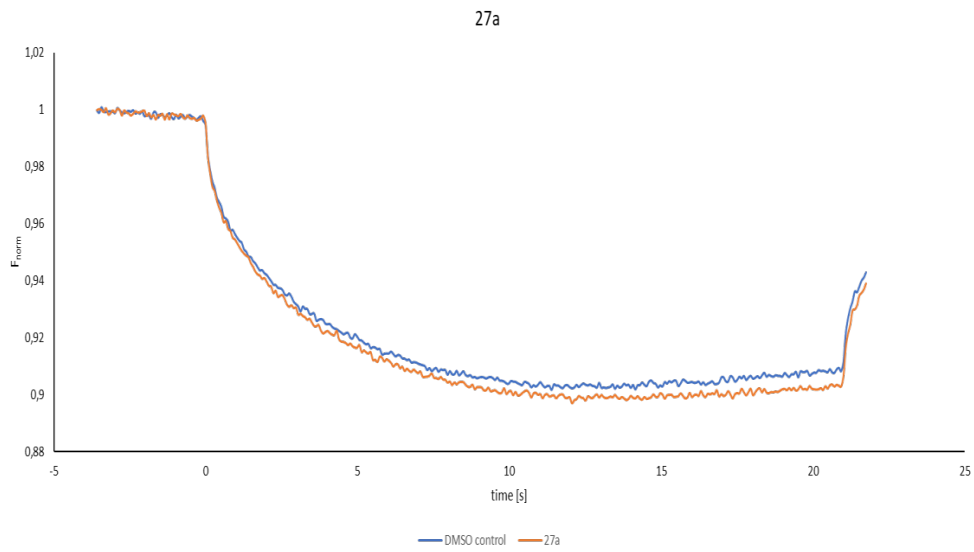


Figure S219. MST curve of **27a**.

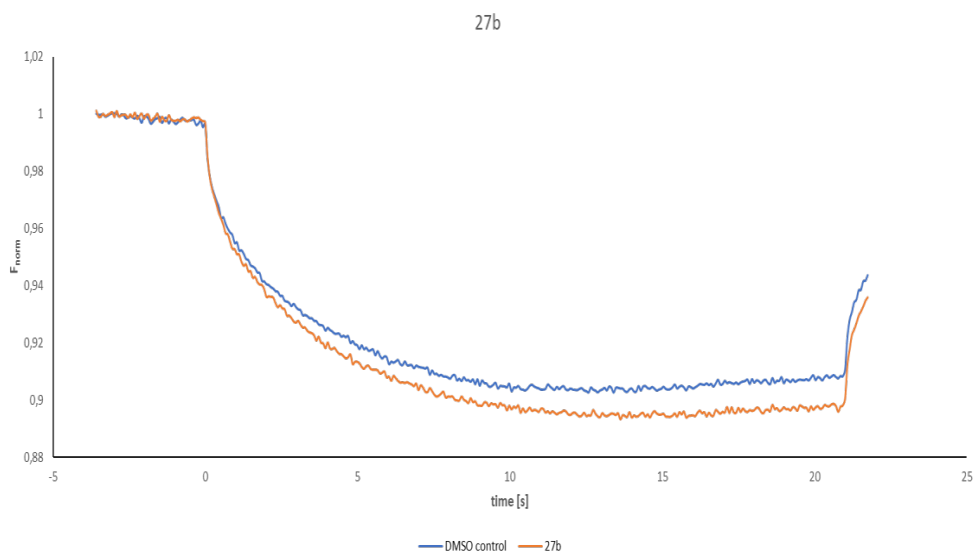


Figure S220. MST curve of **27b**.

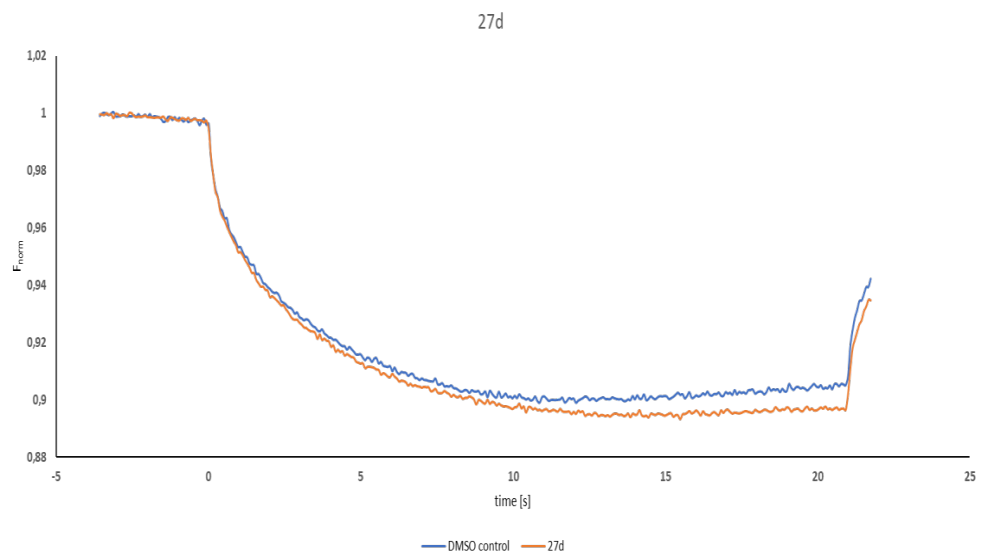


Figure S221. MST curve of **27d**.

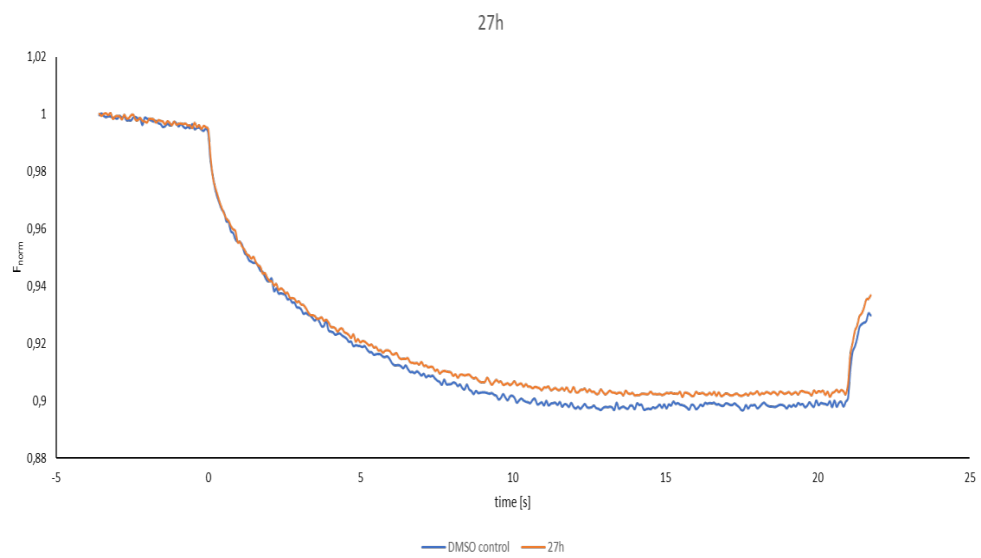


Figure S222. MST curve of **27h**.

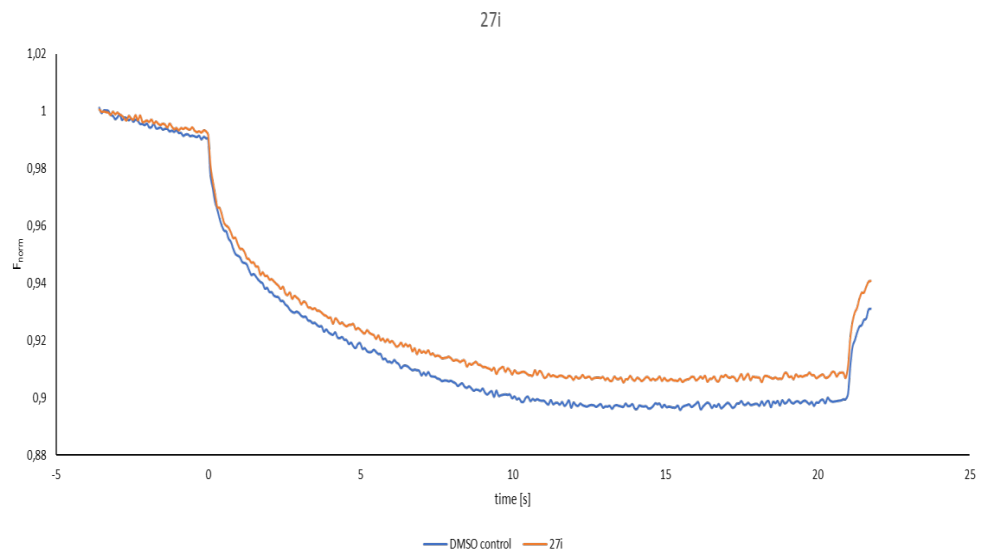


Figure S223. MST curve of 27i.

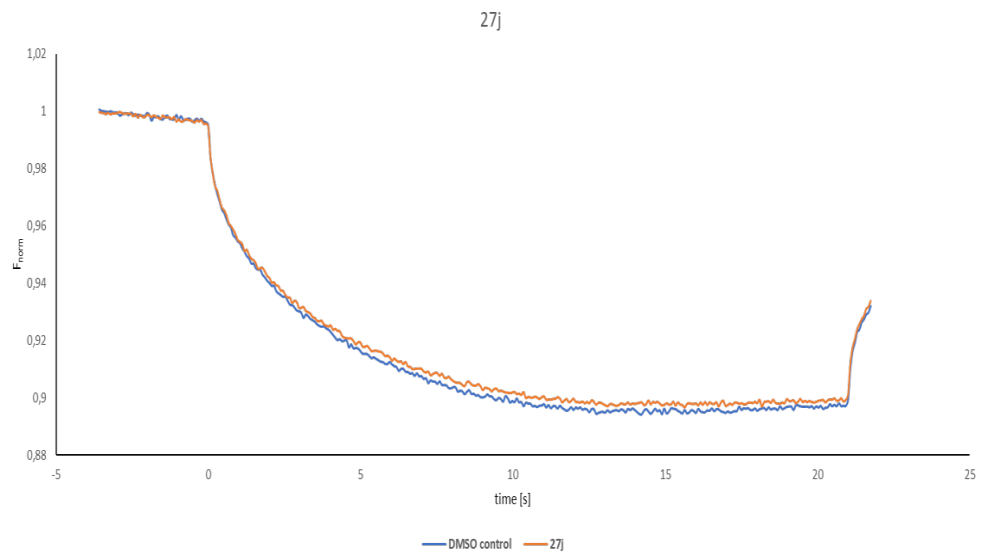


Figure S224. MST curve of 27j.

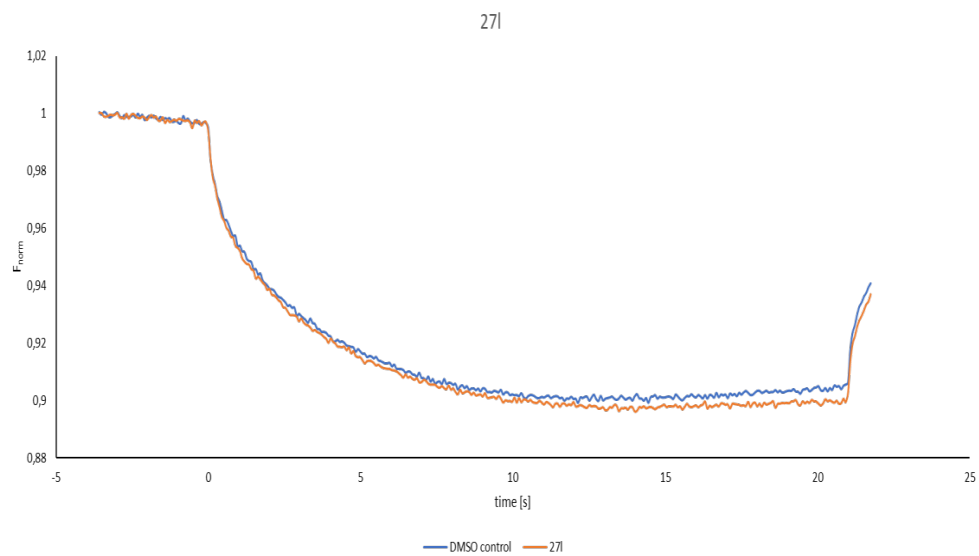


Figure S225. MST curve of 27l.

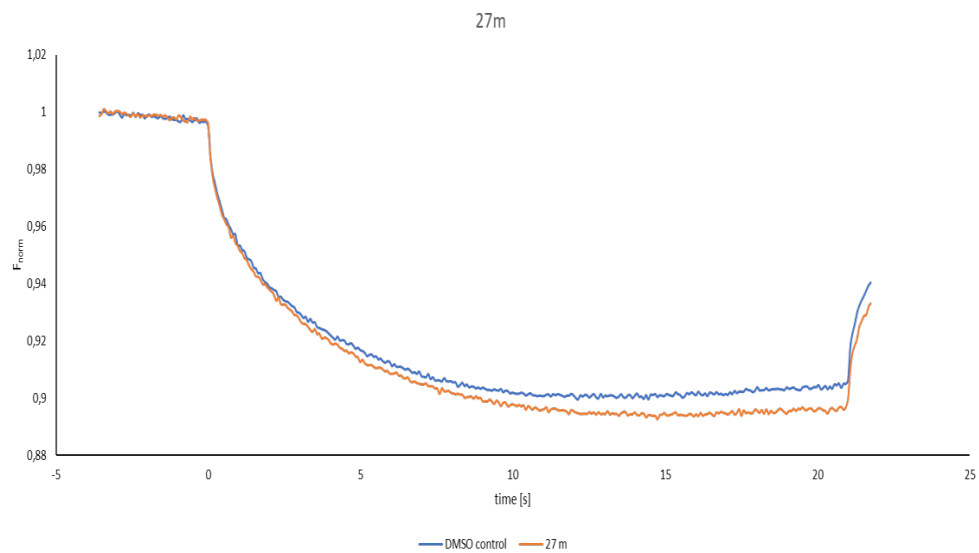


Figure S226. MST curve of 27m.

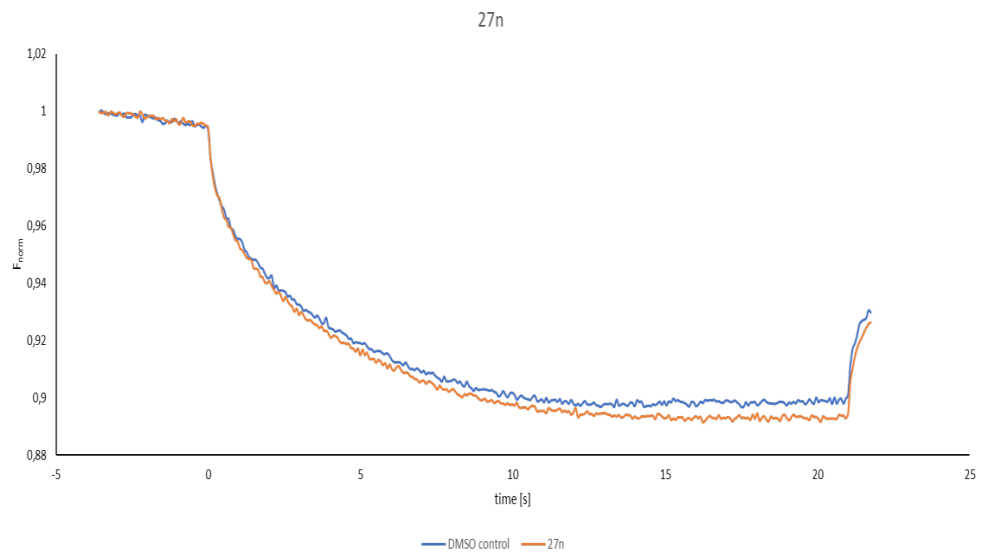


Figure S227. MST curve of **27n**.

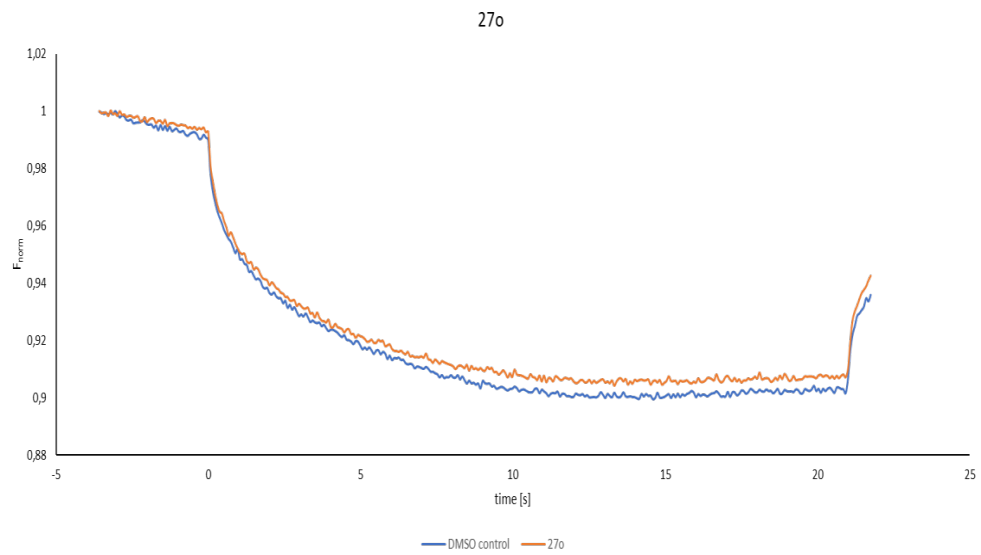


Figure S228. MST curve of **27o**.

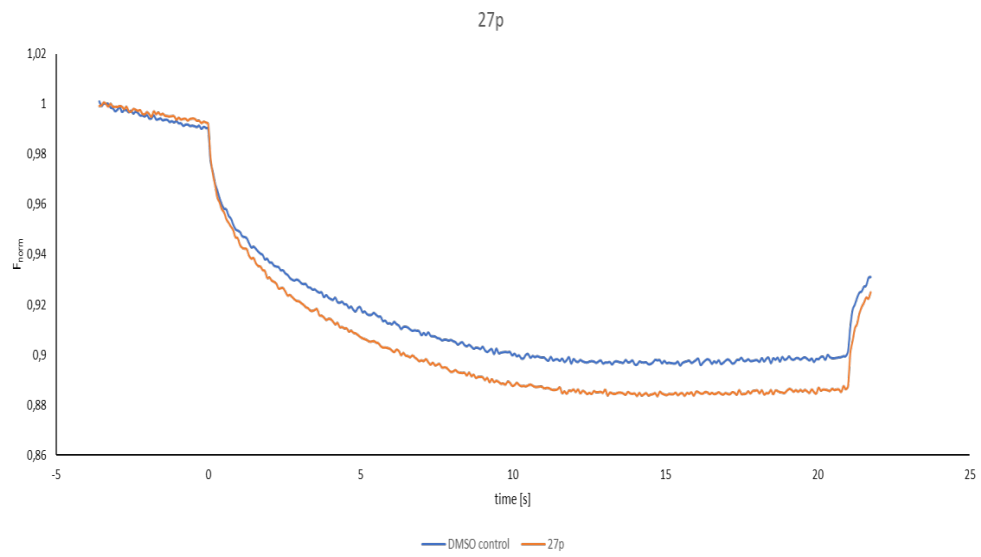


Figure S229. MST curve of 27p.

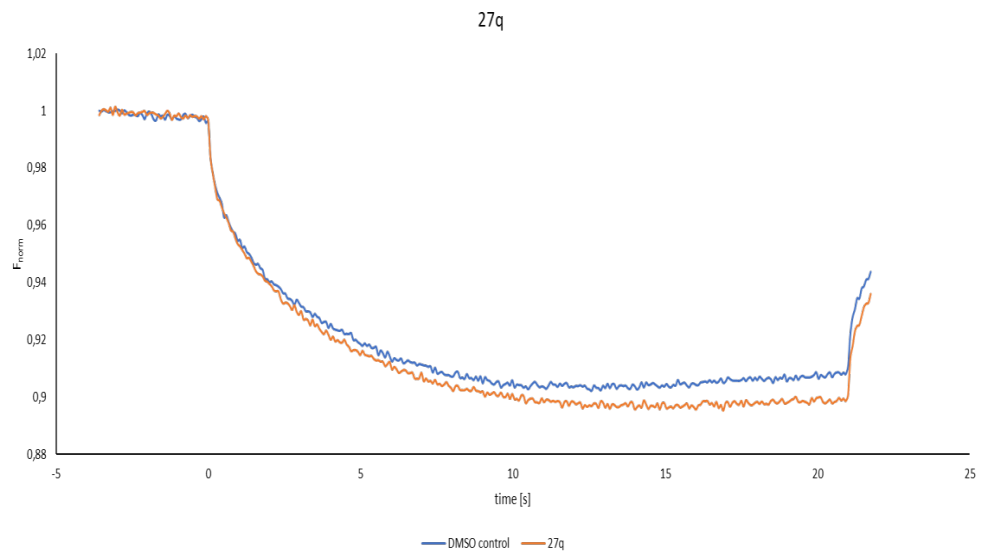


Figure S230. MST curve of 27q.

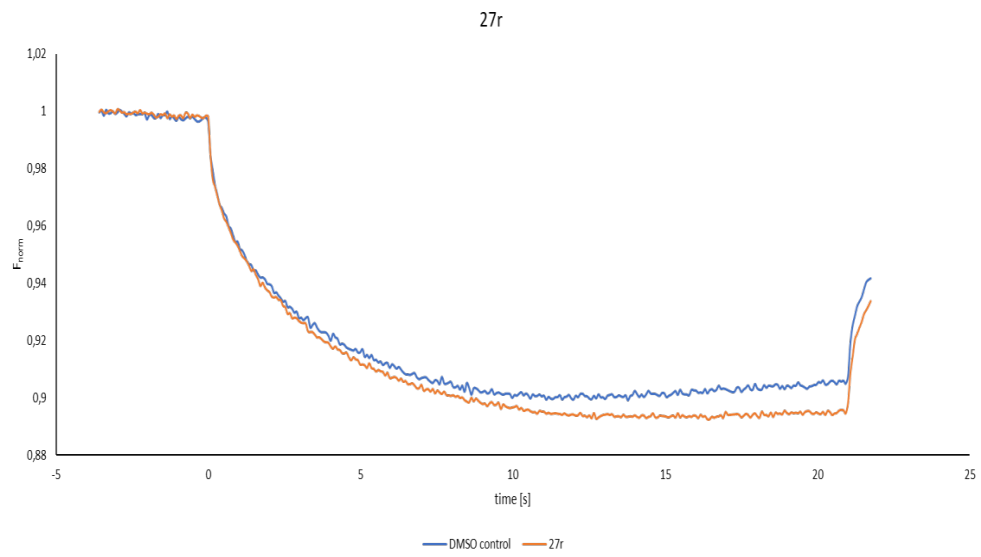


Figure S231. MST curve of 27r.

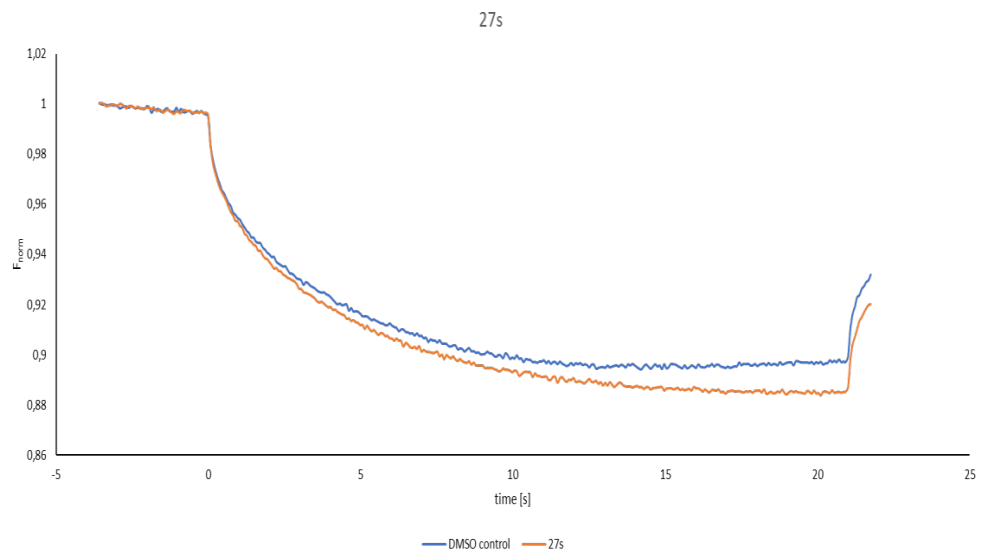


Figure S232. MST curve of 27s-A/B.

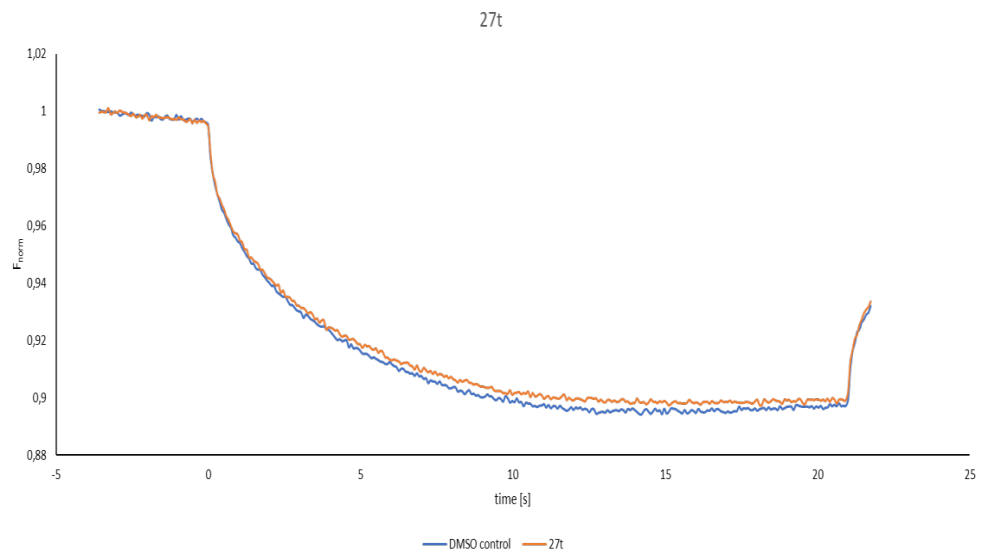


Figure S233. MST curve of 27t.

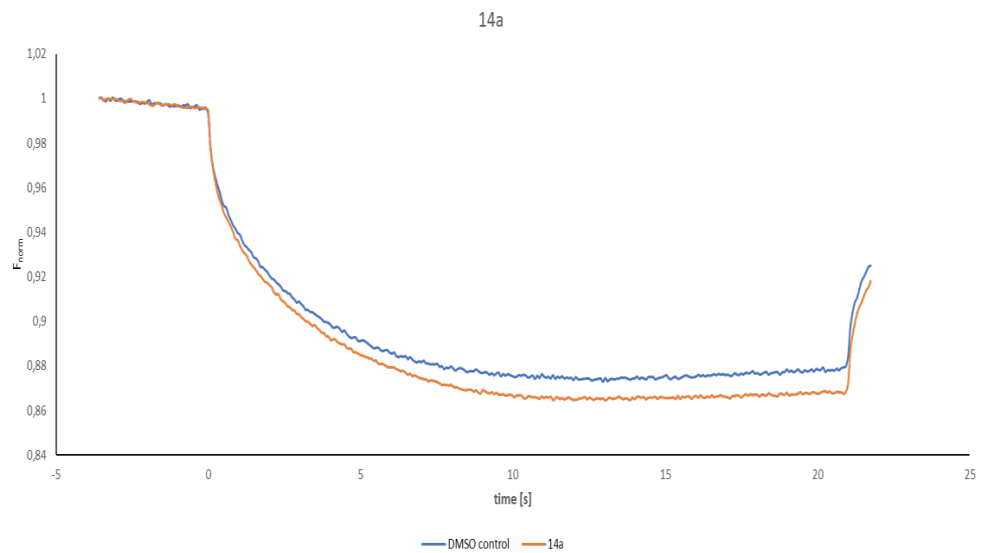


Figure S234. MST curve of 14a.

Determination of Z'-factors

Z'-factors for the MST pre-screening assay were determined for the known pan-methyltransferase inhibitor SFG and **27s-A/B**, which showed the highest affinity within the set of inhibitors against DNMT2. Therefore, DNMT2 was fluorescence-labeled as described above. Measurements were performed according to the method described above, but in septets for both SFG and **27s-A/B** against a DMSO control. Z'-factors were calculated as described in literature by Zhang *et al.*, *J. Biomol. Screen.* **1999**, *4*, 67–73.

$$Z' = 1 - \frac{(3\sigma_{c+} + 3\sigma_{c-})}{|\mu_{c+} - \mu_{c-}|}$$

	Measurement 1		Measurement 2		Measurement 3		Measurement 4	
	DMSO	SFG	DMSO	SFG	DMSO	SFG	DMSO	SFG
F _{norm}	902,19	888,05	901,93	881,65	903,89	883,27	901,37	886,47
	903,54	888,72	902,25	882,60	903,55	883,44	901,39	886,56
	903,98	889,29	901,91	881,71	903,44	884,08	898,49	886,68
	902,94	889,35	900,22	880,99	903,46	883,11	898,79	886,93
	903,03	889,19	902,49	883,19	903,09	884,06	899,27	887,46
	903,06	890,59	902,61	882,12	903,88	884,22	900,48	887,19
	901,94	890,06	902,24	883,20	903,60	884,98	899,27	887,78
μ	902,95	889,32	901,95	882,21	903,56	883,88	899,87	887,01
σ	0,71	0,83	0,81	0,83	0,26	0,65	1,21	0,49
Z'	0,66		0,75		0,86		0,60	

	Measurement 1		Measurement 2		Measurement 3		Measurement 4	
	DMSO	27s	DMSO	27s	DMSO	27s	DMSO	27s
F _{norm}	891.19	874.97	898,14	876,95	897,88	878,57	876,95	898,14
	891.79	874.82	898,17	877,79	897,17	879,02	877,79	898,17
	892.05	874.82	897,39	877,16	897,91	878,65	877,16	897,39
	891.88	876.26	896,93	877,69	897,72	878,67	877,69	896,93
	891.56	875.69	897,62	879,15	898,62	879,07	879,15	897,62
	892.30	876.15	897,19	878,67	899,21	878,80	878,67	896,11
	892.34	877.59	898,82	879,47	897,39	880,07	879,47	897,19
μ	891.87	875.76	897,75	878,12	897,98	878,98	897,36	878,12
σ	0.41	1.01	0,66	0,98	0,71	0,52	0,72	0,98
Z'	0,74		0,75		0,81		0,74	

ITC Curves

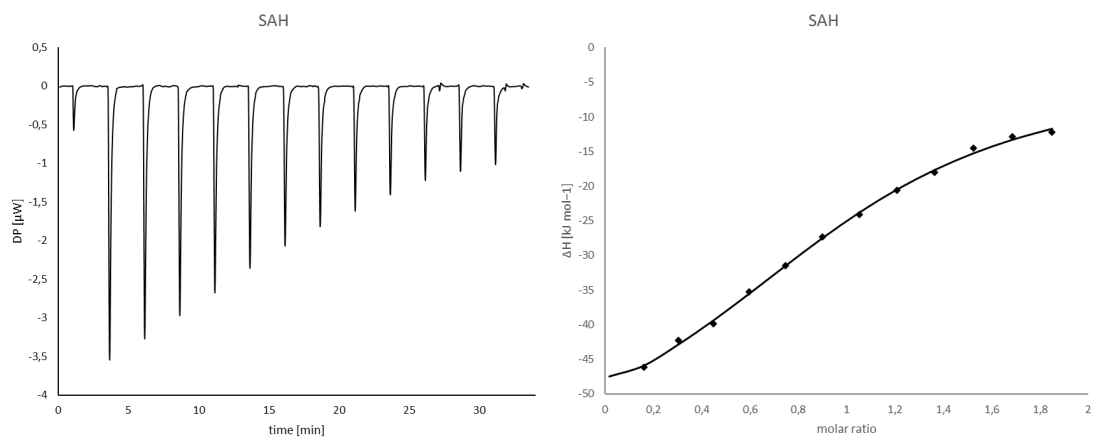


Figure S235. ITC curve of SAH.

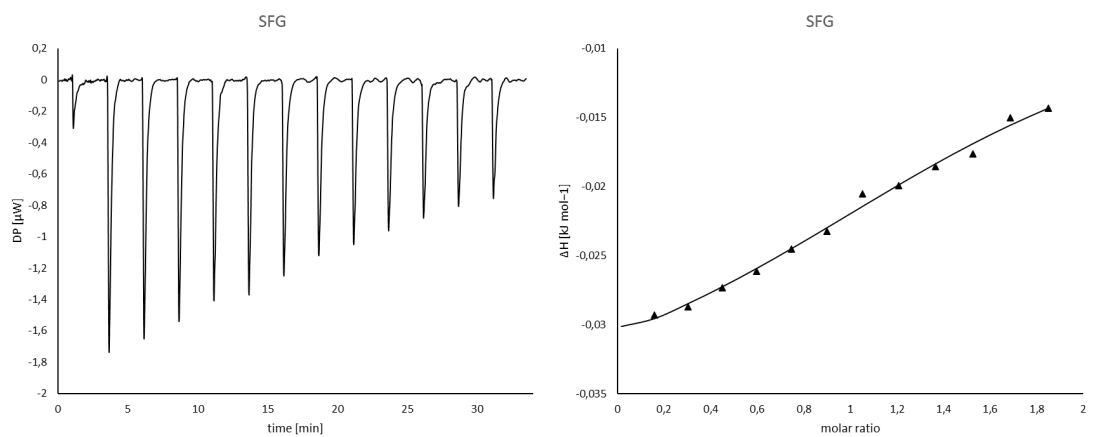


Figure S236. ITC curve of Sinefungin.

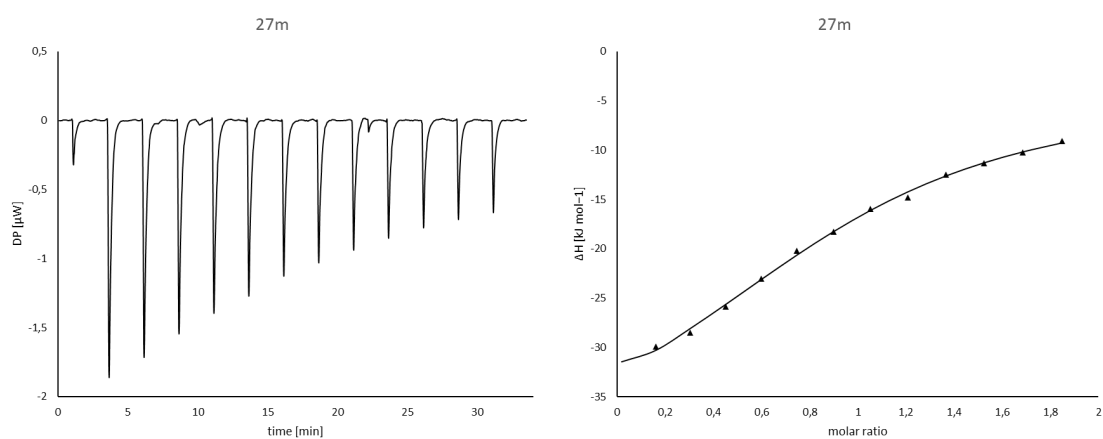


Figure S237. ITC curve of 27m.

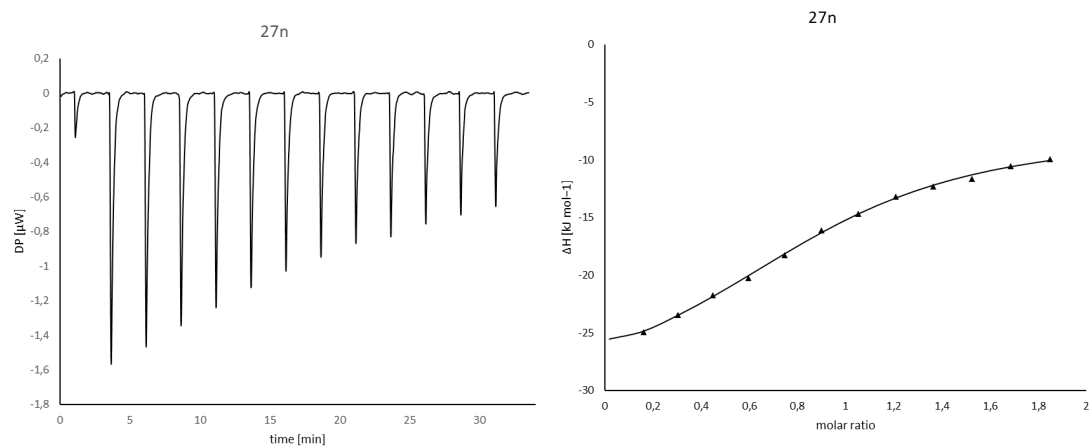


Figure S238. ITC curve of 27n.

Docking

Table S1: Molecular docking results sorted by FlexX-score. ^aMolecules were classified as binders when MST-shift or at least 10% inhibition at a concentration of 100 μ M in the inhibition assay was observed.

^bRe-docking RMSD of SAH: 0.77 Å

Cpd.	binder / non-binder ^a	FlexX-score (kJ mol ⁻¹)
14d	non-binder	-51.95
21b	non-binder	-51.10
14b	non-binder	-49.84
21c	non-binder	-48.99
Sinefungin	binder	-48.33
14a	binder	-44.47
27m	binder	-44.23
27q	binder	-43.18
27a	binder	-42.92
27r	binder	-42.34
27j	binder	-42.21
8a	non-binder	-42.13
SAH ^b	binder	-42.02
27p	binder	-41.43
21a	non-binder	-41.38
27o	binder	-41.17
17d	non-binder	-40.17
27l	binder	-40.10
27e	non-binder	-40.09
27i	binder	-39.98
27c	non-binder	-39.91
27b	binder	-39.79
27h	binder	-39.75
27n	binder	-39.21
17e	non-binder	-38.65
27f	non-binder	-38.48
27d	binder	-38.33
17c	non-binder	-38.30
17b	non-binder	-37.41
27s (<i>R</i>)	binder	-37.00
14c	non-binder	-36.40
21d	non-binder	-35.66
27k	non-binder	-35.55
19	non-binder	-35.25
27s (<i>S</i>)	binder	-34.52
17a	non-binder	-33.05
8b	non-binder	-30.45
27g	non-binder	-28.51
27t	binder	-24.86

Table S2: 3D-RISM results for hydration sites within 4 Å of SAH for the SAH-DNMT2 complex crystal structure PDB-ID 1G55. Bold letters indicate hydration sites discussed in the main manuscript. *Hydration site ID-247 has no corresponding crystallographic water molecule. Water molecule 656 can be linked to hydration site ID-244 (RMSD 0.75Å).

ID	Occupancy	dG	Vol	Aniso	HB Tot	HB Rec	HB		Dist	System
							Lig	Xtal		
193	0.02	8.09	1.06	0	4.38	4.38	0			Cplx
199	0.43	4.16	1.89	0.42	-4.03	-5.46	1.43	HOH459	1.91	Cplx
241	0.52	-2.9	3.14	0.68	-4.05	-2.55	-1.5	HOH642	1.77	Cplx
203	0.54	3.65	0.76	0	-3.69	-3.69	0	HOH471	1.64	Cplx
189	0.57	-10.78	1.11	0.06	-14.25	-6.89	-7.36	HOH413	0.73	Cplx
183	0.59	-3.65	1.47	0.26	-1.35	-1.35	0	HOH644	1.75	Cplx
196	0.59	4.46	0.76	0	-1.61	-1.01	-0.6			Cplx
250	0.61	1.15	0.79	0.01	-3.75	-2.12	-1.64	HOH659	0.61	Cplx
194	0.62	-9.97	1.93	0.44	-5.01	-5.01	0			Cplx
239	0.62	10.23	0.79	0.01	-1.33	-0.04	-1.29	HOH571	1	Cplx
197	0.64	-7.22	1.61	0.32	-14.11	-6.37	-7.74	HOH459	0.16	Cplx
247	0.66	3.25	0.76	0	-4.97	-3.01	-1.96	HOH656	2.27^a	Cplx
225	0.68	8.53	1	0.09	-2.91	-0.53	-2.38	HOH644	1.35	Cplx
296	0.69	3.77	1.64	0.33	-10.12	-10.12	0	HOH658	1.05	Cplx
191	0.71	-4.37	1.78	0.38	-4.28	-4.28	0	HOH642	2.01	Cplx
192	0.71	5.07	1.05	0.11	-5.84	-4.74	-1.1	HOH414	0.51	Cplx
231	0.71	7.71	0.76	0	-1.74	-0.24	-1.5	HOH657	1.2	Cplx
284	0.74	5.32	1.06	0	-0.5	-0.13	-0.37			Cplx
222	0.75	-5.17	0.76	0	-3.28	-3.28	0	HOH657	3.13	Cplx
228	0.79	7.42	1.62	0.32	-4.39	-3.93	-0.47	HOH642	3	Cplx
291	0.79	4.86	1.06	0	-0.72	-0.12	-0.59			Cplx
244	0.86	5.22	1.06	0	-2.12	0	-2.12	HOH656	0.75	Cplx
186	0.91	0.61	1.34	0.22	-4.37	-1.03	-3.34	HOH495	0.93	Cplx

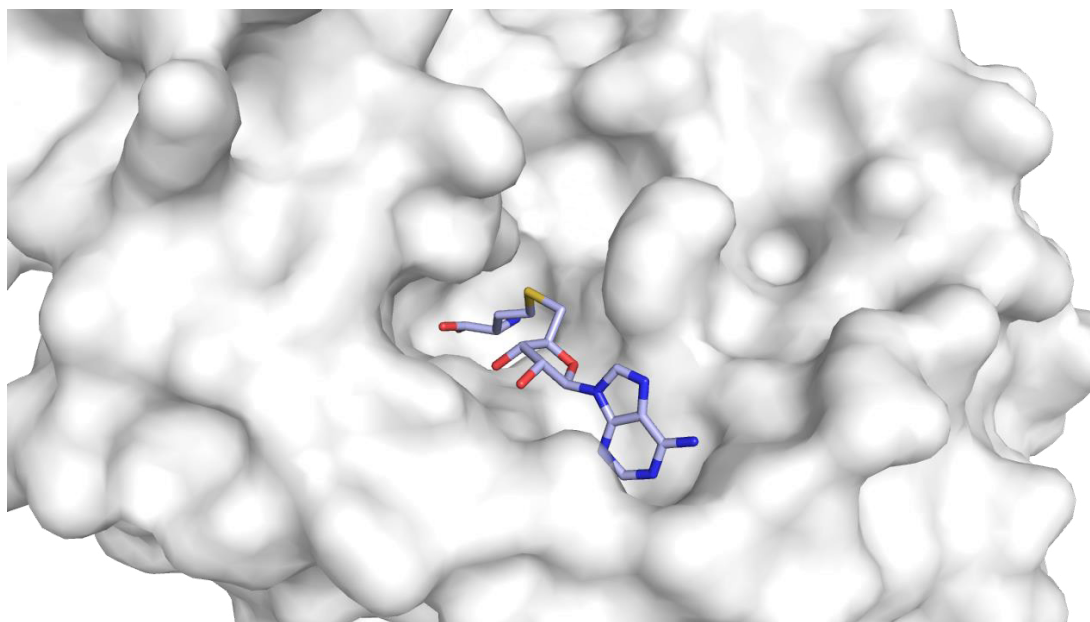


Figure S239. SAH (light blue carbon atoms) in complex with DNMT2 (PDB-ID 1G55).

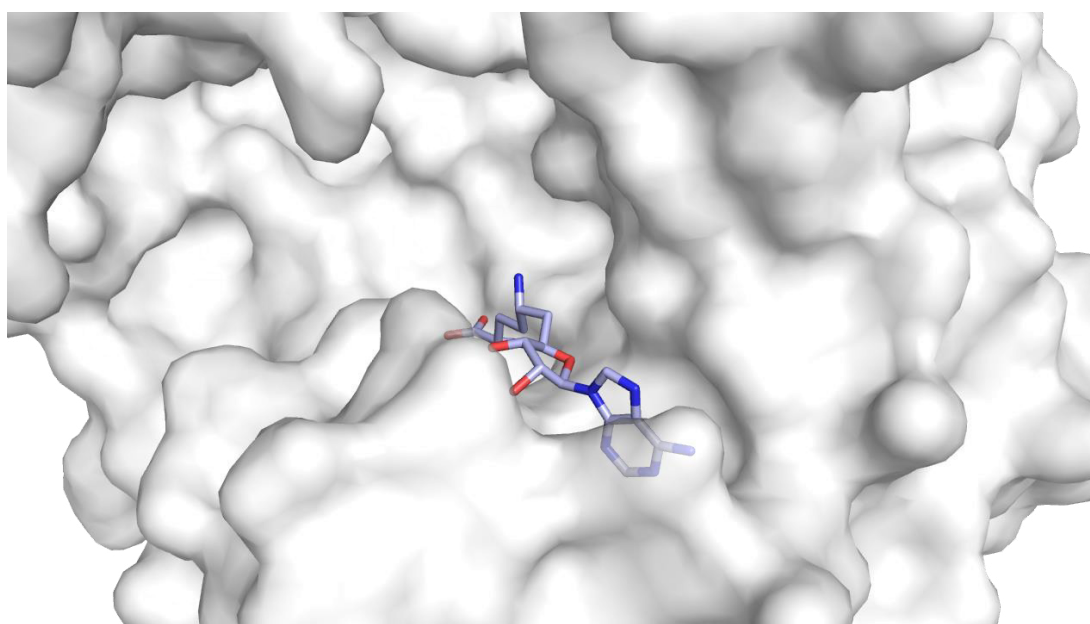


Figure S240. Sinefungin (light blue carbon atoms) in complex with NSUN6 (PDB-ID 5WWR).

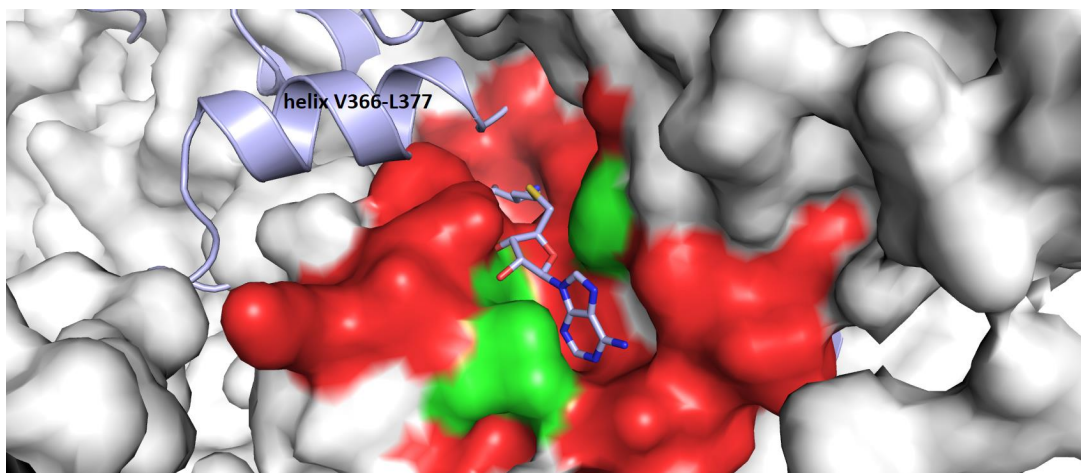


Figure S241. Surface of NSUN2 AlphaFold homology model in superposition with the DNMT2-SAH complex (light blue ligand and cartoon, PDB-ID 1G55). Green surface patches illustrate identical residues, red patches different. An alpha-helix forming the cytidine binding site in DNMT2 (residues 366–377) is also missing in NSUN2.

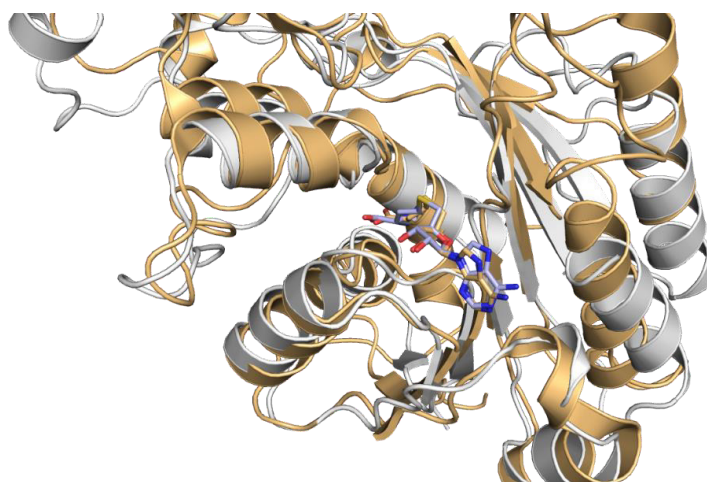


Figure S242. Overall structure comparison of DNMT2-SAH complex (PDB-ID 1G55, white cartoon and light blue ligand) and DNMT3a-SAH complex (PDB-ID 6W8B, light orange cartoon and ligand).

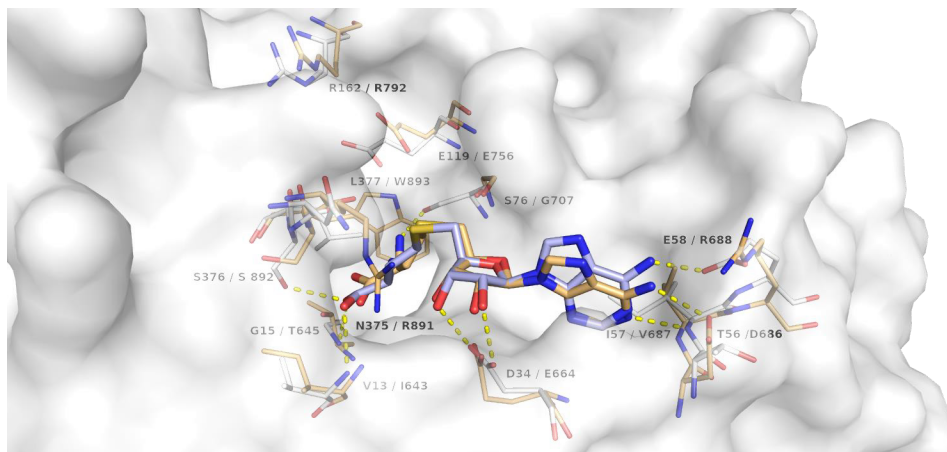


Figure S243. Superposition of DNMT2 (white carbon atoms, surface and light blue ligand) and DNMT3a (light orange binding site and ligand) binding sites. Residues are labelled as DNMT2/DNMT3a.

CaCo-2 Cell Permeability Assay: Chromatograms

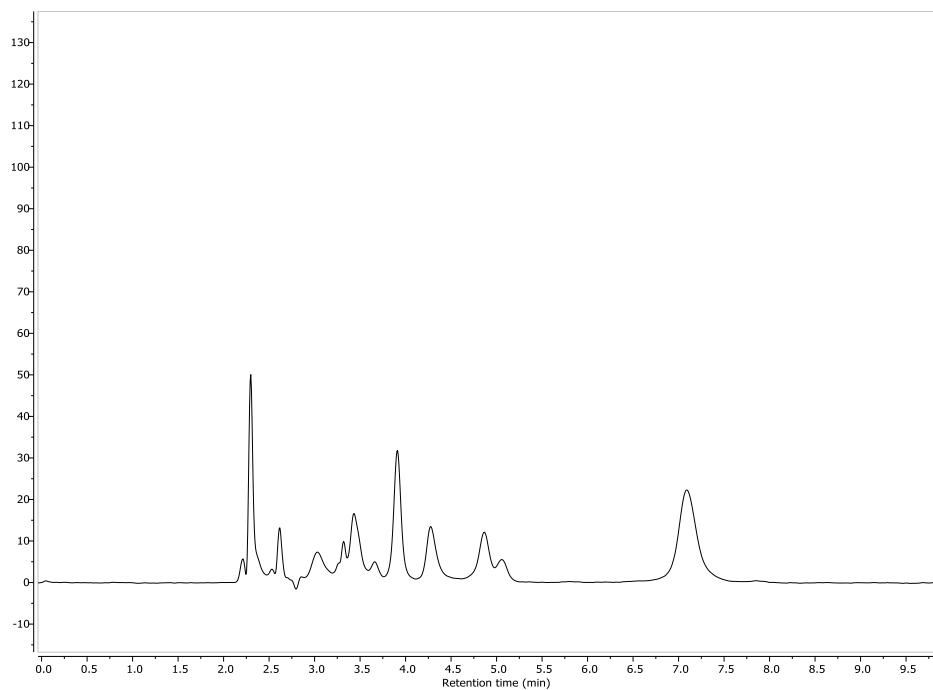


Figure S244. DMSO control, MeCN/H₂O = 5:95 + 0.1% HCOOH, the chromatogram shows the peaks of the medium used for the assays.

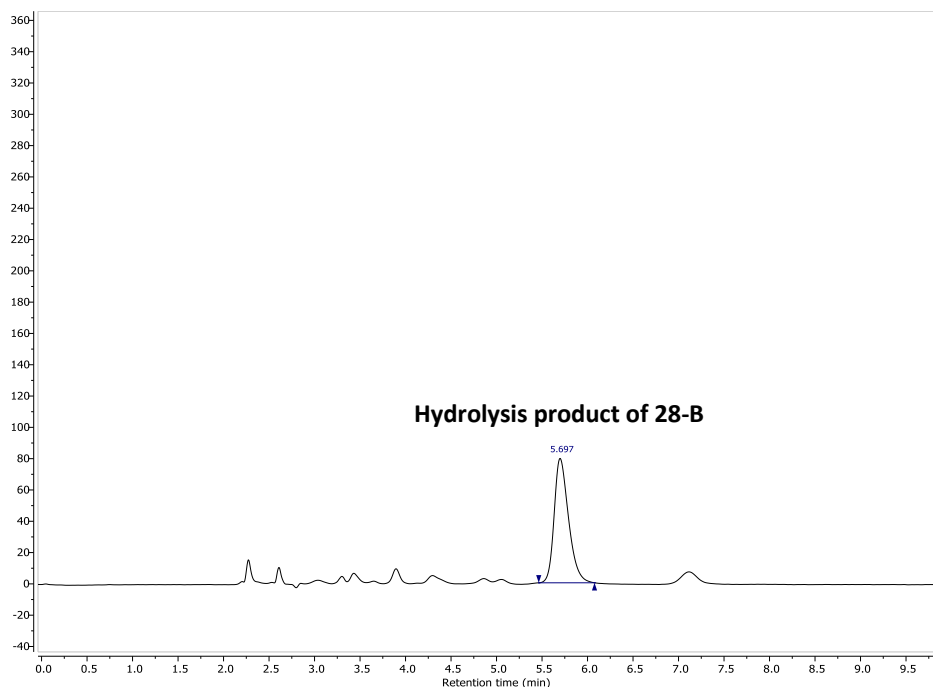


Figure S245. **28-B**, MeCN/H₂O = 5:95 + 0.1% HCOOH, apical compartment; the chromatogram shows that the ester **28-B** is hydrolyzed in the medium.

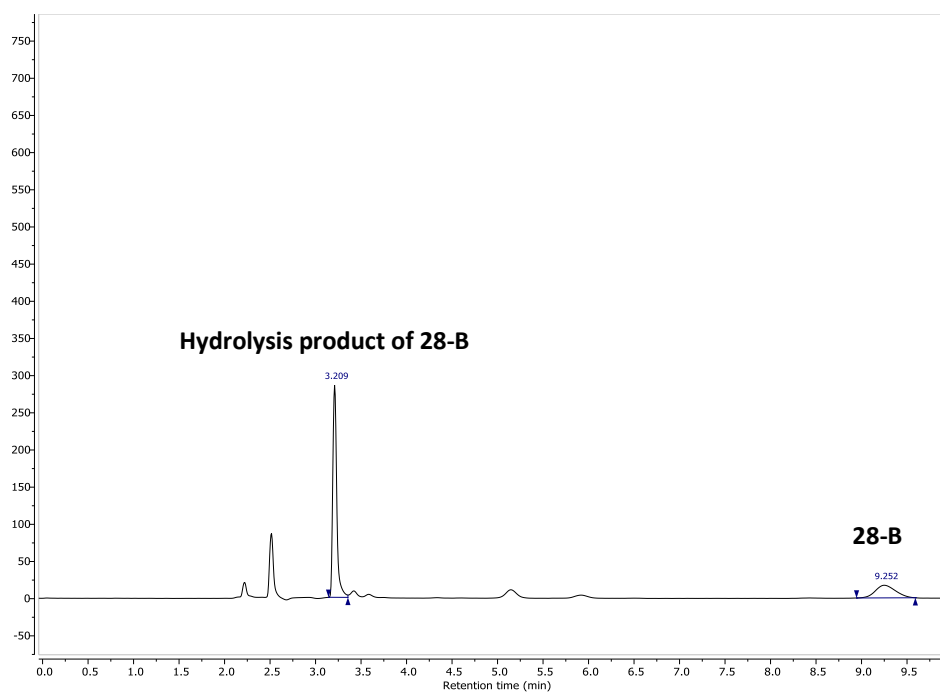


Figure S246. **28-B**, MeCN/H₂O = 10:90 + 0.1% HCOOH, apical compartment; the chromatogram shows that the ester **28-B** is hydrolyzed in the medium yielding the respective acid **27**; only minor amounts of unhydrolyzed ester are found.

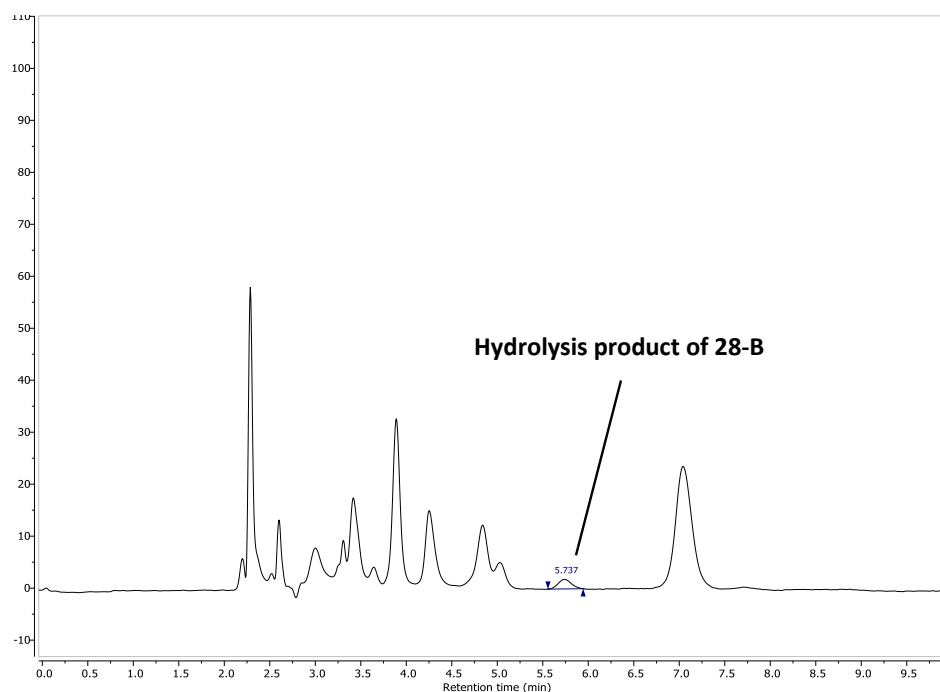


Figure S247. **28-B**, MeCN/H₂O = 5:95 + 0.1% HCOOH, basolateral compartment; only the peak for the hydrolysis product is observed.

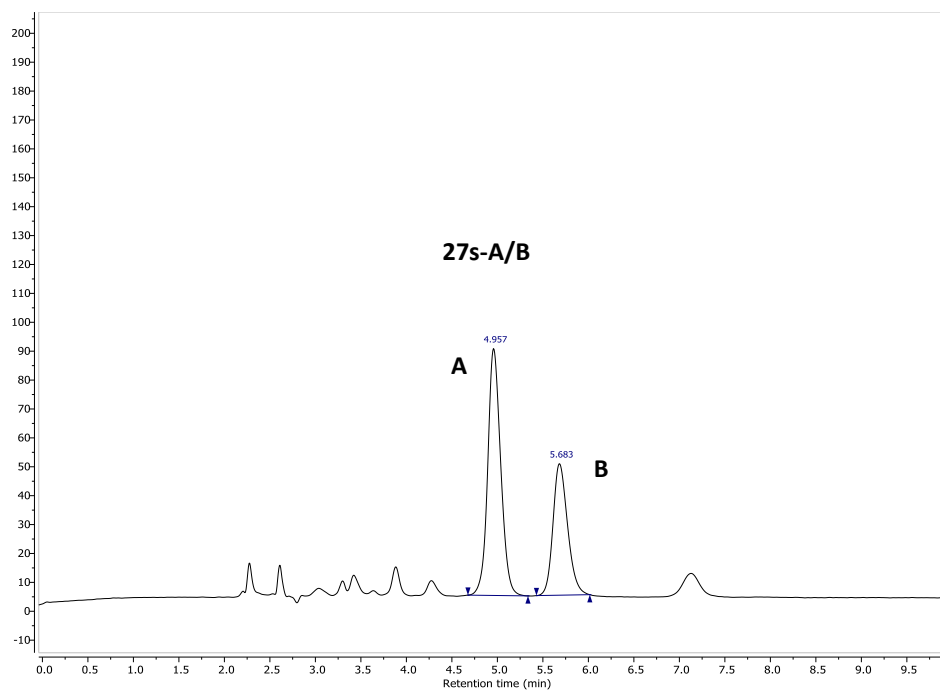


Figure S248. **27s-A/B**, MeCN/H₂O = 5:95 + 0.1% HCOOH, apical compartment; the chromatogram shows the peaks for both epimers **27s-A** and **27s-B**

An Optimized Microscale Thermophoresis Method for High-Throughput Screening of DNA Methyltransferase 2 Ligands.

Project summary and own contributions

In our previous study, the high predictive value of microscale thermophoresis (MST) as a screening method for DNMT2 could be shown. Unfortunately, no affinity determinations could be conducted successfully due to the limitations of the established method. This was foremost caused by a small signal-to-noise ratio, little changes in thermophoresis induced by the compounds, and a lack of compound solubility in the high concentrations needed to achieve complete protein saturation. Also, the fact that results for different compounds obtained from a screening performed at one single concentration have not been comparable seemed disadvantageous. It was assumed that various factors were responsible for the shortcomings of this method. Since DNMT2 exceeds the mass of the small molecular compounds within a screening by approximately two orders of magnitude, it was assumed that binding alters the thermophoresis behavior of the protein-ligand complex only slightly. This would probably lead to the small changes observed in MST experiments and also to the poor signal-to-noise ratios detected. Moreover, the high concentrations of compound needed in the established method might cause unspecific binding, which would increase the number of false positive hits in a screening. The lack of transferability of single point measurement had been inherent to the established MST method, probably due to the fact that the observed differences in thermophoresis, which are caused by the respective ligands, did not necessarily correlate with their affinity towards DNMT2.

In a previously published article by LUAN *et al.*,¹⁴⁹ a fluorescence polarization (FP) method was described for the investigation of the methyltransferase MLL1. According to their description, an FP assay for DNMT2 was established. Afterward, their fluorescent dye, which was derived from SAH, was used to develop an MST method that circumvents most of the above-mentioned disadvantages. In this new method, DNMT2 is not labeled at the His-tag but with a fluorescent probe that is bound to the active site of DNMT2. Displacement of the fluorescent dye by other ligands will alter the thermophoresis behavior of the small-molecular dye drastically. This led to improved signal-to-noise ratios. Furthermore, this displacement assay was more sensitive and required smaller compound concentrations, which allowed reproducible affinity determinations. Moreover, one-point screening results with this method were transferable. In previous experiments, this had not been the case since different protein-ligand complexes presented incomparable thermophoresis behaviors. In this optimized method, only the complex of the fluorescent dye with DNMT2 is detected. Thus, the measurements indicate how much fluorescent dye is bound or unbound, which gives the screening method a certain comparability. It also allows semi-quantitative statements on the basis of one-point

measurements. Unfortunately, the method was not suited for other methyltransferases of interest such as NSUN2 or NSUN6, due to the low affinity of the fluorescent dye to these proteins.

Own contribution: expression and purification of protein with support from [REDACTED]; assay development; performing of FP assay and MST assay; writing of the manuscript together with [REDACTED].

Contributions from other authors: synthesis of the fluorescent dye; providing compounds from publication (1) for measurements.

This work has been published in: ACS Pharmacology & Translational Sciences (CiteScore: 5.1)

Reprinted with permission from: *ACS Pharmacol. Transl. Sci.* 2022, 5, 11, 1079–1085. “An Optimized Microscale Thermophoresis Method for High-Throughput Screening of DNA Methyltransferase 2 Ligands” Copyright © 2022 American Chemical Society

An Optimized Microscale Thermophoresis Method for High-Throughput Screening of DNA Methyltransferase 2 Ligands

Robert Alexander Zimmermann,[‡] Marvin Schwickert,[‡] J. Laurenz Meidner,[‡] Zarina Nidoieva, Mark Helm, and Tanja Schirmeister*Cite This: *ACS Pharmacol. Transl. Sci.* 2022, 5, 1079–1085

Read Online

ACCESS |

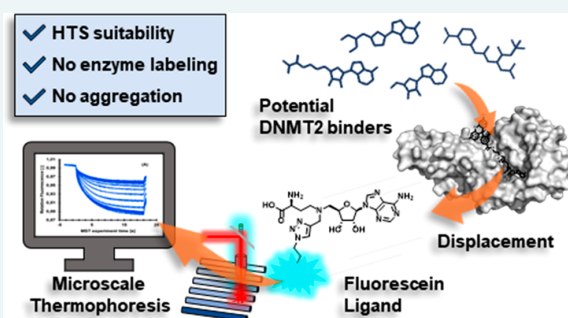
Metrics & More

Article Recommendations

Supporting Information

ABSTRACT: Developing methyltransferase inhibitors is challenging, since most of the currently used assays are time-consuming and cost-intensive. Therefore, efficient, fast, and reliable methods for screenings and affinity determinations are of utmost importance. Starting from a literature-known fluorescent S-adenosylhomocysteine derivative, 5-FAM-triazolyl-adenosyl-Dab, developed for a fluorescence polarization assay to investigate the histone methyltransferase mixed-lineage leukemia 1, we herein describe the applicability of this compound as a fluorescent tracer for the investigation of DNA-methyltransferase 2 (DNMT2), a human RNA methyltransferase. Based on these findings, we established a microscale thermophoresis (MST) assay for DNMT2. This displacement assay can circumvent various problems inherent to this method. Furthermore, we optimized a screening method via MST which even indicates if the detected binding is competitive and gives the opportunity to estimate the potency of a ligand, both of which are not possible with a direct binding assay.

KEYWORDS: Drug discovery, High-throughput-screening, Microscale thermophoresis, RNA methyltransferase DNMT2, Fluorescein-labeling



Originally the human DNA methyltransferase 2 (DNMT2) was considered to be a DNA-modifying enzyme, as it shares most of its sequence with other members of the DNMT family (DNMT1, DNMT3A, DNMT3B).^{1,2} However, in 2006, Goll et al. discovered that the main substrate of DNMT2 is tRNA. DNMT2 catalyzes the methylation of a cytosine at position 38 in the anticodon loop of tRNA^{Asp}. During this modification, the cofactor S-adenosylmethionine (SAM) is converted to S-adenosylhomocysteine (SAH), a known product inhibitor of DNMT2.³ Subsequently, tRNA^{Val} and tRNA^{Gly} were also found to be substrates of DNMT2, underlining its role as an RNA methyltransferase, especially in humans.⁴ Since then, a lot of possible physiological roles of DNMT2 were discussed. It was proven that DNMT2 together with other RNA-methyltransferases like NSUN2 has a critical influence on tRNA stability and protein translation in cells.^{5–7} During oxidative stress, an up-regulation of DNMT2 could be detected, leading to the assumption that DNMT2 also helps cells coping with exogenous stress factors.^{8–10} DNMT2 was as well found to be overexpressed in cancer cells, where mutations on DNMT2 are assumed to play a functional role in tumorigenesis.^{11,12} Furthermore, DNMT2 is also involved in the epigenetic inheritance process.¹³ Taken all this into

account, DNMT2 appears to be a promising drug target for medicinal chemistry. Therefore, reliable methods to identify potent binders are required.

Tritium incorporation assays using ³H-SAM are still the most reliable and therefore often used methods to assay methyltransferases like DNMT2, despite all the disadvantages, such as time consumption and high costs.^{14,15} Other methods, like LC-MS, still require a lot of working steps and time.¹⁶ Therefore, fast, reliable, and cost-efficient screening methods are needed to reduce the number of compounds subjected to tritium incorporation or LC-MS assays to a minimum. At present, various biophysical methods are available for affinity-based screening assays such as isothermal titration calorimetry (ITC),¹⁷ differential scanning fluorimetry (DSF),¹⁸ surface plasmon resonance (SPR),¹⁹ or microscale thermophoresis (MST).²⁰ All have their advantages but also their disadvantages. ITC measurements not only determine ligand affinities,

Received: August 26, 2022

Published: October 19, 2022



ACS Publications

© 2022 American Chemical Society

1079

<https://doi.org/10.1021/acspsci.2c00175>
ACS Pharmacol. Transl. Sci. 2022, 5, 1079–1085

by measuring the binding enthalpy, but also reveal thermodynamic data of the binding as well as binding stoichiometry. Although this is a very robust method, the enormous amounts of protein and ligand needed can be a major obstacle.^{21–23} DSF is a fast-screening method based on the measurement of protein melting curves in the presence of a fluorescent dye.^{18,24,25} A disadvantage is the fact that some ligands induce only small thermal shifts, leading to a false negative result in a screening campaign.²⁶ Today, SPR is one key technology applied in pharmaceutical research.²⁷ Although it offers several advantages, such as fast, reliable, and label-free measurements, one cannot ignore that the necessity of surface immobilization remains a major challenge. Besides SPR, the significance of MST also emerges.^{28–31} In contrast to SPR or ITC, thermodynamic properties cannot be analyzed using MST with a single measurement but require several measurements at different temperatures.³² However, especially in early drug discovery, this sample-saving method can be of great benefit. It is based on the principle that molecules migrate in a temperature gradient. This so-called thermophoresis is reproducible at given conditions, but even small changes such as ligand binding can alter that behavior.³² Furthermore, the change in the thermophoresis behavior correlates with the extent of this interaction. This allows an affinity determination of a protein–ligand interaction by observing fluorescence changes.^{20,32,33} Besides thermophoresis, other effects can cause these changes, e.g., temperature differences and changes in the local environment of the fluorophore.^{34,35} The advantages of this method are certainly its sensitivity and scalability, but also the fact that screenings can be performed directly with cell lysates or blood sera, which makes it a powerful method for drug discovery.^{20,26,32,36–40} Determining binding affinity by MST, however, comes with some inherent problems. In most cases, the protein of interest must be fluorescently labeled, either in a covalent manner, by thiol or amide coupling, or in a non-covalent manner, by His-tag labeling with a fluorescent dye.^{32,33} Direct measuring of protein–ligand interactions by MST only shows binding events but cannot reveal if the detected binding is competitive with respect to the active site of the protein, or if the ligand binding occurs on an allosteric site. It can also be very challenging to reach saturation conditions for the bound protein–ligand complex, especially if ligands only have binding affinities in the low single-digit micromolar range like the currently known inhibitors of DNMT2. Achieving saturation conditions often needs high protein and ligand concentrations resulting in protein and/or ligand aggregation and/or unspecific binding. Furthermore, the maximal effect of a ligand on the thermophoresis behavior of the protein–ligand complex is not predictable. Therefore, it is not uncommon, that low-affinity ligands have a stronger influence on the thermophoresis behavior than high-affinity ones.

The main cause of these problems is notably due to the necessity of fluorescent-labeling of the protein. If the fluorescent dye is not attached to the enzyme but rather a known ligand (fluorescence tracer)—especially one with a strong thermophoresis behavior—a displacement assay could be established to circumvent a lot of this problems. In this paper, we introduce an optimized MST method with excellent suitability for high-throughput-screening of DNMT2 ligands. We developed a displacement assay, using a literature-known fluorescein-based tool compound 5-FAM-triazolyl-adenosyl-Dab (**6**, FTAD, see Scheme 1), that originally was applied by

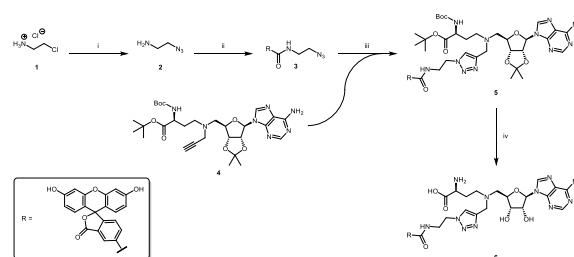
Luan et al. in a fluorescence polarization (FP) assay for the histone methyltransferase mixed-lineage leukemia 1 (MLL1).⁴¹ Our method circumvents the inherent problems previously described, and provides the following improvements:

- reduced aggregation due to lower concentrations of ligand
- half-quantitative screenings outcomes
- determination of active site interactions
- no enzyme labeling required

RESULTS AND DISCUSSION

Chemistry. For the preparation of the tool compound, we followed a synthetic procedure similar to the one used by Luan et al. (Scheme 1).⁴¹ First the azide **2** was prepared in a

Scheme 1. Synthesis of FTAD (6**)^a**



^aReagents and conditions: (i) NaN₃, H₂O, 85 °C, 24 h, 67%; (ii) 5-FAM, TPTU, DIPEA, DMF, 0–20 °C, 48 h, 96%; (iii) CuSO₄, sodium ascorbate, MeOH/H₂O, 16 h, 61%; (iv) 1. TFA, DCM, 5 °C; 2. TFA, H₂O, 5 °C, 99%.

nucleophilic substitution reaction of 2-chloroethylamine hydrochloride **1** and sodium azide. This product was then coupled to 5-carboxyfluorescein (5-FAM) using *O*-(2-oxo-1(2*H*)pyridyl)-*N,N,N',N'*-tetramethyluronium tetrafluoroborate (TPTU) and *N*-ethyl-diisopropylamine (DIPEA), yielding compound **3**. In the subsequent copper(I)-catalyzed azide–alkyne cycloaddition (CuAAC), the alkyne **4** was connected to the azide **3**, forming the triazole product **5**. The synthesis of building block **4** was carried out according to literature.⁴² In the final step, all protecting groups were cleaved using a two-step procedure. First, 50% (v/v) trifluoroacetic acid (TFA in DCM) was used at 5 °C, then 14% TFA in water at 5 °C to finally yield FTAD (**6**) as its trifluoroacetate salt.

Establishment of DNMT2 Fluorescence Polarization Assay. Binding affinity of FTAD (**6**) to DNMT2 was investigated using the fluorescence polarization assay protocol described for the histone methyltransferase MLL1.⁴¹ Therefore, a saturation curve was measured, which resulted in a *K_D* value of 2.4 μM. These results indicated that this fluorescent probe is not only suitable to assay MLL1 but also DNMT2. To check the quality of this assay, the *Z*-factor was evaluated. The obtained value of 0.92 for the *Z*-factor is very good and sufficient to establish an assay for the determination of binding affinities.⁴³ Next, the literature known binding affinities of *S*-adenosylhomocysteine (**7**, SAH) and simefungin (**8**, SFG) could be confirmed. *K_D* values of 12.2 μM and 6.5 μM for SAH and SFG were measured, which are quite similar to reported values from literature (*K_D* = 13.6 μM and *K_D* = 7.5 μM).⁴² Furthermore, the binding affinity of a recently published DNMT2 inhibitor (**9**) was determined, revealing a *K_D* of 7.8

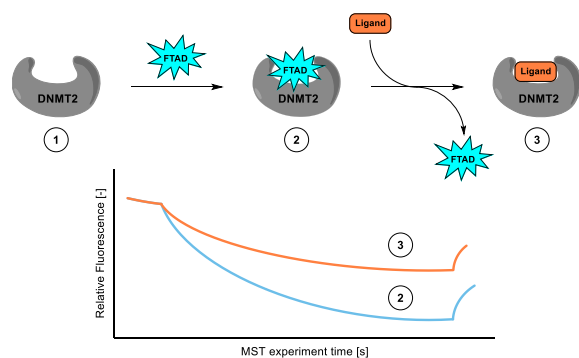
μM which was also found to fit to the published value of $8.1 \mu\text{M}$.⁴²

To investigate if this tool compound may be suitable for pan-methyltransferase assays, binding toward the human tRNA methyltransferases NSUN2 and NSUN6 as well as the histone methyltransferase EHMT2 of the KMT family was tested. Unfortunately, FTAD showed only weak affinities to those methyltransferases with approximate K_D values in the higher two-digit or the three-digit micromolar range (data not shown).

Nevertheless, these findings proved that this tool compound which originally was designed to assay MLL1 via FP was also suitable for DNMT2.

Establishment of DNMT2 Microscale Thermophoresis Assay. In a next step, FTAD (6) was used as a fluorescence tracer for a microscale thermophoresis (MST) displacement assay. The assay is based on the formation of a FTAD-DNMT2 complex, which allows fluorescence tracing. By adding a ligand of interest FTAD is displaced, which results in an altered fluorescence signal, since FTAD is no longer bound to DNMT2 (Scheme 2). Excitation and emission

Scheme 2. Establishment of DNMT2 Microscale Thermophoresis Assay⁴



⁴Steps: (1) Unlabeled DNMT2 cannot be observed by MST. (2) DNMT2 is pre-incubated with FTAD; the FTAD-DNMT2 complex can be observed by MST. (3) Displacement of FTAD with ligand of interest; free FTAD can be observed by MST.

wavelengths of FTAD were sufficient for MST measurements with blue light settings (excitation: 465–490 nm and emission: 500–550 nm). At first, an assay concentration for FTAD was evaluated, starting with 50 nM, as described in the FP protocol. Since the fluorescence signal was not optimal, the concentration was increased. Finally, a concentration of 100 nM was chosen, which allowed measurements with sufficient fluorescence signal, at the lowest possible concentration. Furthermore, no surface absorption or bleaching was detected in standard capillaries. In a dilution series of DNMT2 at constant FTAD concentrations, binding affinity of FTAD against DNMT2 was investigated using MST, revealing a K_D value of $1.8 \mu\text{M}$, which is in very good accordance with the binding affinity determined using FP (Figure 1A,B). Furthermore, a Z-factor of 0.90 (Figure 1C) for this assay indicated that this assay had a very good quality. In the next step, the binding affinities of SAH and SFG were verified by MST. Since displacement assays only provide EC_{50} values, those results were corrected for the binding competition with the fluorescence tracer according to the instructions of

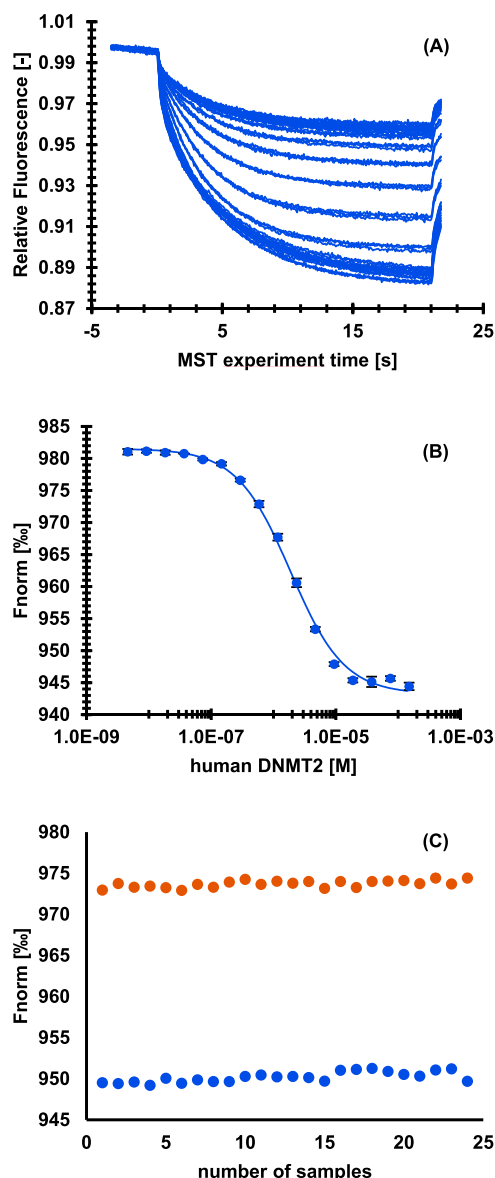
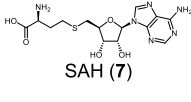
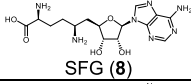
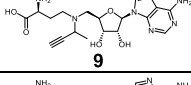
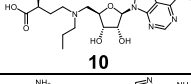
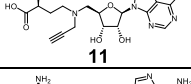
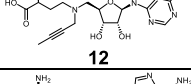
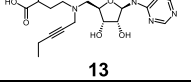


Figure 1. Microscale thermophoresis assay for FTAD against a dilution series of human DNMT2. (A) Raw traces of runs. (B) Normalized fluorescence plotted against concentration of human DNMT2. Data is given as mean \pm SD of triplicates. K_D of FTAD against DNMT2 was found to be $1.8 \mu\text{M} \pm 0.1 \mu\text{M}$. (C) Z-factor determination of microscale thermophoresis assay. In orange, free FTAD without DNMT2; in blue, FTAD in the presence of $2 \mu\text{M}$ human DNMT2.

Nanotemper Technologies to receive K_D values. For SAH, $K_D = 6.5 \mu\text{M}$ was determined, while for SFG, $K_D = 9.2 \mu\text{M}$ was found. Both values were in high accordance with literature, where K_D values of $13.6 \mu\text{M}$ and $7.5 \mu\text{M}$, respectively, were described (Table 1). For compound 9, a K_D value of $5.2 \mu\text{M}$ was found, which correlates quite well with the literature value ($K_D = 8.1 \mu\text{M}$ ⁴²). Interestingly, also for compound 10, a literature known non-inhibitor of DNMT2,⁴² a very slight protein–ligand interaction could be detected in this assay with

Table 1. Binding Affinities of Different Ligands toward DNMT2 Measured by Orthogonal Biophysical Methods

Compound	ITC ^a / μM	FP ^c / μM	MST ^d / μM
 SAH (7)	13.6 \pm 4.4 ^b	12.2 \pm 0.9	6.5 \pm 1.4
 SFG (8)	7.5 \pm 3.5	6.5 \pm 0.5	9.2 \pm 0.5
 9	8.1 \pm 1.4	7.8 \pm 1.1	5.2 \pm 0.6
 10	n.d.*	n.d.	> 70
 11	11.4 \pm 2.4	n.d.	15.3 \pm 3.1
 12	10.2 \pm 2.2	n.d.	11.3 \pm 0.8
 13	10.5 \pm 3.3	n.d.	11.0 \pm 1.1

^a K_D values from ITC experiments; shown are mean values \pm SD of $n = 3$ experiments. ^bMean values \pm SD of $n = 6$ experiments. ^c K_D values from FP assays; shown are mean values \pm SD of $n = 3$ experiments. ^d K_D values from MST displacement assays; shown are mean values \pm SD of $n = 4$ experiments. *n.d. = could not be determined due to the high concentrations of enzyme and ligand required to quantify low-affinity binding.

an EC_{50} of $>100 \mu\text{M}$, this indicates that the method is even capable to identify very low affinity binders if needed. To further confirm the potential of this assay for affinity determination, three additional SAH-derived DNMT2 inhibitors, 11–13,⁴² were selected and the K_D values were determined by the MST displacement assay and by ITC as an orthogonal method.

The data are in very good agreement, proving the reliability of the assay. Moreover, in comparison to the ITC method, the amounts of samples, especially of protein, are much lower.

One of the most considerable findings was the fact that with this displacement method the plateaus for total unbound and bound protein could be resolved very well (Figure 2). Since the maxima of the shifts can easily be measured by control runs, the fits derived from those measurements are far more reliable than those of direct binding assays based on MST. Aggregation, up to concentrations needed to reach a plateau, was not observed in any run. Furthermore, the signal-to-noise ratio was highly increased compared to direct measurements of labeled DNMT2. This may derive from the largely increased shift, which is probably due to the fact, that the large DNMT2 molecule influences the thermophoresis behavior of the small fluorescence tracer much more, than vice versa a small molecular ligand a >40 kDa protein like DNMT2.

MST can be used as a fast and efficient screening method.⁴² Although common MST assays using labeled protein are highly

sensitive screening methods that can detect binders with almost negligible affinity, there remain some problems. One is for sure the comparability of the detected shifts. The extent of the included shifts in thermophoresis does not correlate very well with the affinity of different ligands; i.e., a less affine ligand can induce a larger shift than a ligand with higher affinity. In our recently published structure–activity relationship (SAR) study for SAH-derived DNMT2 inhibitors, MST was used as an initial screening method. Some ligands were found to induce noteworthy shifts in the thermophoretic behavior, but a tritium incorporation assay revealed that a lot of those ligands showed only poor inhibitory properties.⁴² By plotting the induced shifts against the found inhibition, no correlation could be detected (Figure 3A).

Therefore, a screening with our novel displacement method was performed for a set of binders and non-binders of this SAR study. A ligand concentration of $20 \mu\text{M}$ was found to be suitable for this screening. Since for a displacement assay the detectable shift is known from the beginning and depends only on the fraction of bound and unbound fluorescence tracer, this seemed to open the possibility to achieve a correlation between the thermophoresis shifts and the actual inhibition of DNMT2. Indeed, a correlation between the thermophoresis shifts in this displacement assay and the measured inhibition from the tritium incorporation assay could be found (Figure 3B). This led to the conclusion that ligands inducing a thermophoretic shift $<5\%$ should not be considered for further measurements, while ligands inducing shifts $\sim 10\%$ and higher are likely to be very promising DNMT2 inhibitors. The displacement assay not only allows researchers to discriminate good and poor binders. Given the fact that FTAD binds to the active site of DNMT2, this assay also indicates if the ligand is active-site directed, which can be very helpful for the screening of DNMT2 inhibitors that structurally do not resemble the natural ligand. It is noteworthy that the displacement assay can be performed at decreased ligand concentrations in a range of $20 \mu\text{M}$ instead of $100 \mu\text{M}$, which can prevent unspecific binding to the protein and therefore misleading hits from the beginning.

CONCLUSION

Within this study we present a novel method for a fast and reliable ligand screening for the human RNA methyltransferase DNMT2 using microscale thermophoresis. The assay can easily be extended to a high-throughput screening. This displacement assay allows screenings at low ligand, dye, and protein concentrations. Together with the small volumes required for microscale thermophoresis, this results in a cost-effective but still robust method. Under the conditions described, no adsorption, bleaching, or aggregation was detected, which usually can cause severe interferences in direct microscale thermophoresis assays. Furthermore, this assay reveals accurate screening results, which facilitates early-stage drug discovery in the field of DNMT2. Due to the fact that the fluorescence tracer is bound to the active site of DNMT2, thermophoresis shifts detected by this method always indicate active-site targeting, making further binding-site verification unnecessary. As a result of the increased thermophoresis shifts compared to direct microscale thermophoresis assays with labeled protein, this method can be used for reliable binding affinity determination up to the low micromolar range. In summary, we are highly convinced that this method can be a

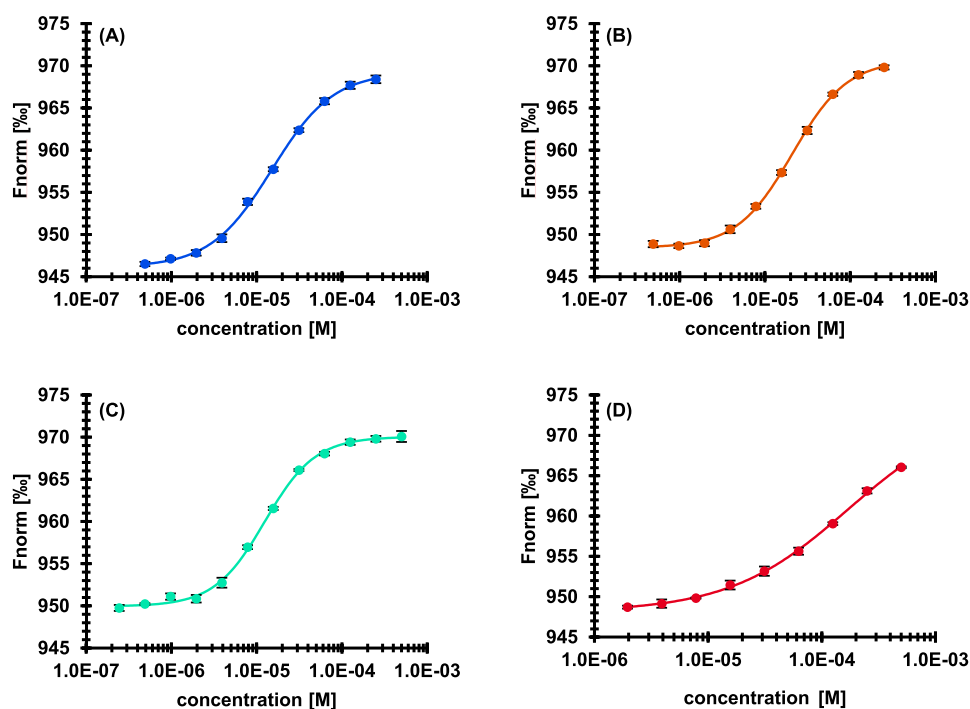


Figure 2. Displacement of FTAD by literature known inhibitors in a microscale thermophoresis assay. Data is given as mean \pm SD of quadruplicates. (A) SAH (7), $EC_{50} = 15.0 \pm 0.7 \mu\text{M}$; (B) SFG (8), $EC_{50} = 20.9 \pm 0.7 \mu\text{M}$; (C) compound 9, $EC_{50} = 12.4 \pm 0.5 \mu\text{M}$; and (D) compound 10, $EC_{50} > 100 \mu\text{M}$.

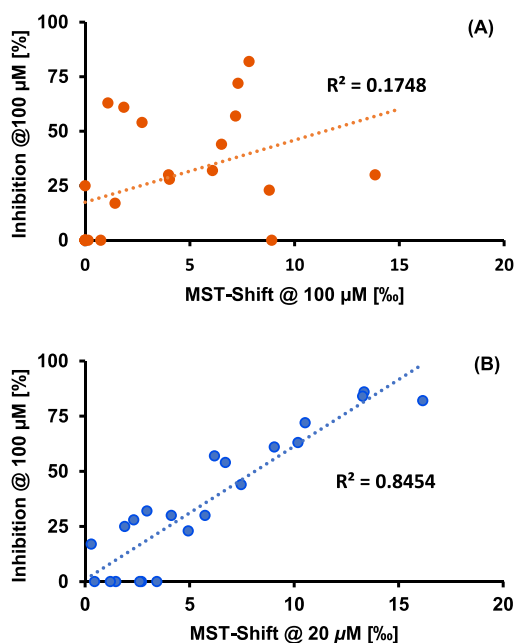


Figure 3. Correlation of MST shifts at $20 \mu\text{M}$ compound concentrations and inhibition at $100 \mu\text{M}$ in a tritium incorporation assay for literature-known compounds: (A) for direct MST assay and (B) for MST displacement assay.

powerful tool accelerating the search for potent DNMT2 inhibitors.

■ ASSOCIATED CONTENT

Supporting Information

The Supporting Information is available free of charge at <https://pubs.acs.org/doi/10.1021/acspsci.2c00175>.

Microscale thermophoresis raw traces, NMR spectra, and chromatograms (PDF)

■ AUTHOR INFORMATION

Corresponding Author

Tanja Schirmeister – Institute of Pharmaceutical and Biomedical Sciences, Johannes Gutenberg University Mainz, D-55128 Mainz, Germany; Email: schirmei@uni-mainz.de

Authors

Robert Alexander Zimmermann – Institute of Pharmaceutical and Biomedical Sciences, Johannes Gutenberg University Mainz, D-55128 Mainz, Germany; orcid.org/0000-0002-5330-9234

Marvin Schwickert – Institute of Pharmaceutical and Biomedical Sciences, Johannes Gutenberg University Mainz, D-55128 Mainz, Germany; orcid.org/0000-0002-1385-1416

J. Laurenz Meidner – Institute of Pharmaceutical and Biomedical Sciences, Johannes Gutenberg University Mainz, D-55128 Mainz, Germany; orcid.org/0000-0001-5488-0646

Zarina Nidoieva – Institute of Pharmaceutical and Biomedical Sciences, Johannes Gutenberg University Mainz, D-55128 Mainz, Germany; orcid.org/0000-0001-5364-7527

Mark Helm – Institute of Pharmaceutical and Biomedical Sciences, Johannes Gutenberg University Mainz, D-55128 Mainz, Germany; orcid.org/0000-0002-0154-0928

Complete contact information is available at: <https://pubs.acs.org/10.1021/acspsci.2c00175>

Author Contributions

[‡]R.A.Z., M.S., and J.L.M. contributed equally to the project.

Funding

Financial support by the DFG (Deutsche Forschungsgemeinschaft) in the framework of the Transregio Collaborative Research Center TRR 319 (RMaP, RNA Modification and Processing), projects A01 (T.S.), C01, and C03 (M.H.), is gratefully acknowledged. Z.N. gratefully acknowledges financial support by the Volkswagen Stiftung.

Notes

The authors declare no competing financial interest.

ABBREVIATIONS

CCR2, CC chemokine receptor 2; CCL2, CC chemokine ligand 2; CCR5, CC chemokine receptor 5; Dab, 2,4-diaminobutyric acid; 5-FAM, 5-carboxyfluorescein; FTAD, 5-FAM-triazolyl-adenosyl-Dab; TLC, thin-layer chromatography

REFERENCES

- (1) Van den Wyngaert, I.; Sprengel, J.; Kass, S. U.; Luyten, W. H. Cloning and Analysis of a Novel Human Putative DNA Methyltransferase. *FEBS Lett.* **1998**, *426* (2), 283–289.
- (2) Dong, A. Structure of Human DNMT2, an Enigmatic DNA Methyltransferase Homolog That Displays Denaturant-Resistant Binding to DNA. *Nucleic Acids Res.* **2001**, *29* (2), 439–448.
- (3) Goll, M. G.; Kirpekar, F.; Maggert, K. A.; Yoder, J. A.; Hsieh, C. L.; Zhang, X.; Golic, K. G.; Jacobsen, S. E.; Bestor, T. H. Methylation of TRNA^{Asp} by the DNA Methyltransferase Homolog Dnmt2. *Science* **2006**, *311* (5759), 395–398.
- (4) Schaefer, M.; Pollex, T.; Hanna, K.; Tuorto, F.; Meusburger, M.; Helm, M.; Lyko, F. RNA Methylation by Dnmt2 Protects Transfer RNAs against Stress-Induced Cleavage. *Genes Dev.* **2010**, *24* (15), 1590–1595.
- (5) Tuorto, F.; Liebers, R.; Musch, T.; Schaefer, M.; Hofmann, S.; Kellner, S.; Frye, M.; Helm, M.; Stoecklin, G.; Lyko, F. RNA Cytosine Methylation by Dnmt2 and NSun2 Promotes TRNA Stability and Protein Synthesis. *Nat. Struct. Mol. Biol.* **2012**, *19* (9), 900–905.
- (6) Shanmugam, R.; Fierer, J.; Kaiser, S.; Helm, M.; Jurkowski, T. P.; Jeltsch, A. Cytosine Methylation of TRNA-Asp by DNMT2 Has a Role in Translation of Proteins Containing Poly-Asp Sequences. *Cell Discovery* **2015**, *1*, 15010.
- (7) Tuorto, F.; Herbst, F.; Alerasool, N.; Bender, S.; Popp, O.; Federico, G.; Reitter, S.; Liebers, R.; Stoecklin, G.; Gröne, H.; Dittmar, G.; Glimm, H.; Lyko, F. The TRNA Methyltransferase Dnmt2 Is Required for Accurate Polypeptide Synthesis during Haematopoiesis. *EMBO J.* **2015**, *34* (18), 2350–2362.
- (8) Becker, M.; Müller, S.; Nellen, W.; Jurkowski, T. P.; Jeltsch, A.; Ehrenhofer-Murray, A. E. Pmt1, a Dnmt2 Homolog in *Schizosaccharomyces Pombe*, Mediates TRNA Methylation in Response to Nutrient Signaling. *Nucleic Acids Res.* **2012**, *40* (22), 11648–11658.
- (9) Lin, M.-J.; Tang, L.-Y.; Reddy, M. N.; Shen, C.-K. J. DNA Methyltransferase Gene DDnmt2 and Longevity of *Drosophila*. *J. Biol. Chem.* **2005**, *280* (2), 861–864.
- (10) Kaul, G.; Thippeswamy, H. Role of Heat Shock Proteins in Diseases and Their Therapeutic Potential. *Indian J. Microbiol.* **2011**, *51* (2), 124–131.
- (11) Forbes, S. A.; Beare, D.; Gunasekaran, P.; Leung, K.; Bindal, N.; Boutselakis, H.; Ding, M.; Bamford, S.; Cole, C.; Ward, S.; Kok, C. Y.; Jia, M.; De, T.; Teague, J. W.; Stratton, M. R.; McDermott, U.; Campbell, P. J. COSMIC: Exploring the World's Knowledge of

Somatic Mutations in Human Cancer. *Nucleic Acids Res.* **2015**, *43*, D805–811.

(12) Elhardt, W.; Shanmugam, R.; Jurkowski, T. P.; Jeltsch, A. Somatic Cancer Mutations in the DNMT2 TRNA Methyltransferase Alter Its Catalytic Properties. *Biochimie* **2015**, *112*, 66–72.

(13) Zhang, Y.; Zhang, X.; Shi, J.; Tuorto, F.; Li, X.; Liu, Y.; Liebers, R.; Zhang, L.; Qu, Y.; Qian, J.; Pahima, M.; Liu, Y.; Yan, M.; Cao, Z.; Lei, X.; Cao, Y.; Peng, H.; Liu, S.; Wang, Y.; Zheng, H.; Woolsey, R.; Quilici, D.; Zhai, Q.; Li, L.; Zhou, T.; Yan, W.; Lyko, F.; Zhang, Y.; Zhou, Q.; Duan, E.; Chen, Q. Dnmt2 Mediates Intergenerational Transmission of Paternally Acquired Metabolic Disorders through Sperm Small Non-Coding RNAs. *Nat. Cell Biol.* **2018**, *20* (5), 535–540.

(14) Jurkowski, T. P.; Meusburger, M.; Phalke, S.; Helm, M.; Nellen, W.; Reuter, G.; Jeltsch, A. Human DNMT2 Methylates TRNA(Asp) Molecules Using a DNA Methyltransferase-like Catalytic Mechanism. *RNA* **2008**, *14* (8), 1663–1670.

(15) Müller, S.; Windhof, I. M.; Maximov, V.; Jurkowski, T.; Jeltsch, A.; Förstner, K. U.; Sharma, C. M.; Gräf, R.; Nellen, W. Target Recognition, RNA Methylation Activity and Transcriptional Regulation of the Dictyostelium Discoideum Dnmt2-Homologue (DnmA). *Nucleic Acids Res.* **2013**, *41* (18), 8615–8627.

(16) Salyan, M. E. K.; Pedicord, D. L.; Bergeron, L.; Mintier, G. A.; Hunihan, L.; Kuit, K.; Balanda, L. A.; Robertson, B. J.; Feder, J. N.; Westphal, R.; Shipkova, P. A.; Blat, Y. A General Liquid Chromatography/Mass Spectroscopy-Based Assay for Detection and Quantitation of Methyltransferase Activity. *Anal. Biochem.* **2006**, *349* (1), 112–117.

(17) Szlag, V. M.; Jung, S.; Rodriguez, R. S.; Bourgeois, M.; Bryson, S.; Schatz, G. C.; Reineke, T. M.; Haynes, C. L. Isothermal Titration Calorimetry for the Screening of Aflatoxin B1 Surface-Enhanced Raman Scattering Sensor Affinity Agents. *Anal. Chem.* **2018**, *90* (22), 13409–13418.

(18) Gao, K.; Oerlemans, R.; Groves, M. R. Theory and Applications of Differential Scanning Fluorimetry in Early-Stage Drug Discovery. *Biophys. Rev.* **2020**, *12* (1), 85–104.

(19) Olaru, A.; Bala, C.; Jaffrezic-Renault, N.; Aboul-Enein, H. Y. Surface Plasmon Resonance (SPR) Biosensors in Pharmaceutical Analysis. *Crit. Rev. Anal. Chem.* **2015**, *45* (2), 97–105.

(20) Jerabek-Willemsen, M.; Wienken, C. J.; Braun, D.; Baaske, P.; Duhr, S. Molecular Interaction Studies Using Microscale Thermophoresis. *Assay Drug Dev. Technol.* **2011**, *9* (4), 342–353.

(21) Bastos, M.; Velazquez-Campoy, A. Isothermal Titration Calorimetry (ITC): A Standard Operating Procedure (SOP). *Eur. Biophys. J.* **2021**, *50* (3–4), 363–371.

(22) Baranauskienė, L.; Kuo, T.-C.; Chen, W.-Y.; Matulis, D. Isothermal Titration Calorimetry for Characterization of Recombinant Proteins. *Curr. Opin. Biotechnol.* **2019**, *55*, 9–15.

(23) Kabiri, M.; Unsworth, L. D. Application of Isothermal Titration Calorimetry for Characterizing Thermodynamic Parameters of Biomolecular Interactions: Peptide Self-Assembly and Protein Adsorption Case Studies. *Biomacromolecules* **2014**, *15* (10), 3463–3473.

(24) Niesen, F. H.; Berglund, H.; Vedadi, M. The Use of Differential Scanning Fluorimetry to Detect Ligand Interactions That Promote Protein Stability. *Nat. Protoc.* **2007**, *2* (9), 2212–2221.

(25) Zhang, R.; Monsma, F. Fluorescence-Based Thermal Shift Assays. *Curr. Opin. Drug Discovery Devel.* **2010**, *13* (4), 389–402.

(26) Linke, P.; Amaning, K.; Maschberger, M.; Vallee, F.; Steier, V.; Baaske, P.; Duhr, S.; Breitsprecher, D.; Rak, A. An Automated Microscale Thermophoresis Screening Approach for Fragment-Based Lead Discovery. *J. Biomol. Screen.* **2016**, *21* (4), 414–421.

(27) Hinman, S. S.; McKeating, K. S.; Cheng, Q. Surface Plasmon Resonance: Material and Interface Design for Universal Accessibility. *Anal. Chem.* **2018**, *90* (1), 19–39.

(28) Rainard, J. M.; Pandarakalam, G. C.; McElroy, S. P. Using Microscale Thermophoresis to Characterize Hits from High-Throughput Screening: A European Lead Factory Perspective. *SLAS Discovery Adv. life Sci. R D* **2018**, *23* (3), 225–241.

(29) Milite, C.; Feoli, A.; Horton, J. R.; Rescigno, D.; Cipriano, A.; Pisapia, V.; Viviano, M.; Pepe, G.; Amendola, G.; Novellino, E.; Cosconati, S.; Cheng, X.; Castellano, S.; Sbardella, G. Discovery of a Novel Chemotype of Histone Lysine Methyltransferase EHMT1/2 (GLP/G9a) Inhibitors: Rational Design, Synthesis, Biological Evaluation, and Co-Crystal Structure. *J. Med. Chem.* **2019**, *62* (5), 2666–2689.

(30) Kozielski, F.; Sele, C.; Talibov, V. O.; Lou, J.; Dong, D.; Wang, Q.; Shi, X.; Nyblom, M.; Rogstam, A.; Krojer, T.; Fisher, Z.; Knecht, W. Identification of Fragments Binding to SARS-CoV-2 Nsp10 Reveals Ligand-Binding Sites in Conserved Interfaces between Nsp10 and Nsp14/Nsp16. *RSC Chem. Biol.* **2022**, *3* (1), 44–55.

(31) Feoli, A.; Pisapia, V.; Viviano, M.; Castellano, S.; Bartoschik, T.; Sbardella, G. Development of a Microscale Thermophoresis-Based Method for Screening and Characterizing Inhibitors of the Methyl-Lysine Reader Protein MRG15. *SLAS Discovery Adv. Life Sci. R D* **2021**, *26* (1), 77–87.

(32) Seidel, S. A. I.; Dijkman, P. M.; Lea, W. A.; van den Bogaart, G.; Jerabek-Willemsen, M.; Lazic, A.; Joseph, J. S.; Srinivasan, P.; Baaske, P.; Simeonov, A.; Katritch, I.; Melo, F. A.; Ladbury, J. E.; Schreiber, G.; Watts, A.; Braun, D.; Duhr, S. Microscale Thermophoresis Quantifies Biomolecular Interactions under Previously Challenging Conditions. *Methods* **2013**, *59* (3), 301–315.

(33) Bartoschik, T.; Gupta, A.; Kern, B.; Hitchcock, A.; Adams, N. B. P.; Tschammer, N. Quantifying the Interaction of Phosphite with ABC Transporters: MicroScale Thermophoresis and a Novel His-Tag Labeling Approach. *Methods Mol. Biol.* **2020**, *2168*, 51–62.

(34) López-Méndez, B.; Uebel, S.; Lundgren, L. P.; Sedivy, A. Microscale Thermophoresis and Additional Effects Measured in NanoTemper Monolith Instruments. *Eur. Biophys. J.* **2021**, *50* (3–4), 653–660.

(35) Royer, C. A. Probing Protein Folding and Conformational Transitions with Fluorescence. *Chem. Rev.* **2006**, *106* (5), 1769–1784.

(36) Wienken, C. J.; Baaske, P.; Rothbauer, U.; Braun, D.; Duhr, S. Protein-Binding Assays in Biological Liquids Using Microscale Thermophoresis. *Nat. Commun.* **2010**, *1*, 100.

(37) Seidel, S. A. I.; Wienken, C. J.; Geissler, S.; Jerabek-Willemsen, M.; Duhr, S.; Reiter, A.; Trauner, D.; Braun, D.; Baaske, P. Label-Free Microscale Thermophoresis Discriminates Sites and Affinity of Protein-Ligand Binding. *Angew. Chem., Int. Ed. Engl.* **2012**, *51* (42), 10656–10659.

(38) Jerabek-Willemsen, M.; André, T.; Wanner, R.; Roth, H. M.; Duhr, S.; Baaske, P.; Breitsprecher, D. MicroScale Thermophoresis: Interaction Analysis and Beyond. *J. Mol. Struct.* **2014**, *1077*, 101–113.

(39) Bartoschik, T.; Galinec, S.; Kleusch, C.; Walkiewicz, K.; Breitsprecher, D.; Weigert, S.; Müller, Y. A.; You, C.; Piehler, J.; Vercauteren, T.; Daelemans, D.; Tschammer, N. Near-Native, Site-Specific and Purification-Free Protein Labeling for Quantitative Protein Interaction Analysis by MicroScale Thermophoresis. *Sci. Rep.* **2018**, *8* (1), 4977.

(40) Magnez, R.; Thiroux, B.; Taront, S.; Segoula, Z.; Quesnel, B.; Thuru, X. PD-1/PD-L1 Binding Studies Using Microscale Thermophoresis. *Sci. Rep.* **2017**, *7* (1), 17623.

(41) Luan, Y.; Blazer, L. L.; Hu, H.; Hajian, T.; Zhang, J.; Wu, H.; Houliston, S.; Arrowsmith, C. H.; Vedadi, M.; Zheng, Y. G. Design of a Fluorescent Ligand Targeting the S-Adenosylmethionine Binding Site of the Histone Methyltransferase MLL1. *Org. Biomol. Chem.* **2016**, *14* (2), 631–638.

(42) Schwickert, M.; Fischer, T. R.; Zimmermann, R. A.; Hoba, S. N.; Meidner, J. L.; Weber, M.; Weber, M.; Stark, M. M.; Koch, J.; Jung, N.; Kersten, C.; Windbergs, M.; Lyko, F.; Helm, M.; Schirmeister, T. Discovery of Inhibitors of DNA Methyltransferase 2, an Epitranscriptomic Modulator and Potential Target for Cancer Treatment. *J. Med. Chem.* **2022**, *65* (14), 9750–9788.

(43) Zhang, J. H.; Chung, T. D.; Oldenburg, K. R. A Simple Statistical Parameter for Use in Evaluation and Validation of High Throughput Screening Assays. *J. Biomol. Screen.* **1999**, *4* (2), 67–73.

Recommended by ACS

Targeted Degradation of Androgen Receptor for the Potential Treatment of Prostate Cancer

Robert B. Kargbo.

SEPTEMBER 20, 2022
ACS MEDICINAL CHEMISTRY LETTERS

READ 

Structure of a 14-3-3ε:FOXO3a^{pS253} Phosphopeptide Complex Reveals 14-3-3 Isoform-Specific Binding of Forkhead Box Class O Transcription Factor (FOXO) Pho...

Subashini Mathivanan, Neelagandan Kamariah, *et al.*

JULY 05, 2022
ACS OMEGA

READ 

Ultrasensitive and Label-Free Detection of Multiple DNA Methyltransferases by Asymmetric Nanopore Biosensor

Siqi Zhang, Jing-Juan Xu, *et al.*

MARCH 02, 2022
ANALYTICAL CHEMISTRY

READ 

An Isothermal Autocatalytic Hybridization Reaction Circuit for Sensitive Detection of DNA Methyltransferase and Inhibitors Assay

Fengzhe Li, Fuan Wang, *et al.*

MARCH 02, 2022
ANALYTICAL CHEMISTRY

READ 

Get More Suggestions >

Supporting Information

An Optimized Microscale Thermophoresis Method for High-Throughput-Screening of DNA methyltransferase 2 Ligands

Robert Alexander Zimmermann,^{‡,[a]} Marvin Schwickert,^{‡,[a]} J. Laurenz
Meidner,^{‡,[a]} Zarina Nidoieva,^[a] Mark Helm^[a] and Tanja Schirmeister^{*,[a]}

^[a]Institute of Pharmaceutical and Biomedical Sciences, Johannes Gutenberg University
Mainz, Staudinger Weg 5, D-55128 Mainz, Germany.

[‡]These authors contributed equally.

*Corresponding author:

Prof. Dr. Tanja Schirmeister, Phone: +49 6131 39-25742, E-Mail: schirmei@uni-mainz.de.

Content

Experimental Section	3
Spectra and chromatograms	6
FP diagrams	11
MST diagrams	12

Experimental Section

Expression of full-length human DNMT2

Plasmid coding for the full length human DNMT2 was generously gifted by Albert Jeltsch (University of Stuttgart, Germany). Protein expression in *E. coli* and isolation was performed as described previously (Schwickert *et al.*, *J. Med. Chem.* **2022**, 65 (14), 9750–9788).

Establishing of Fluorescence polarization (FP) assay

Determination of K_D value for FTAD

Evaluation of a K_D for FTAD against DNMT2 was conducted by measuring a saturation curve with increasing DNMT2 concentrations until a maximum of response was reached. Therefore, DNMT2 was concentrated in storage buffer (50 mM NaPi pH 8.0, 300 mM NaCl, 1 mM EDTA, 2 mM DTT, 0.1 % PS-20) using centrifugal filters. The mentioned buffer was chosen to ensure protein stability up to concentrations needed to observe a maximum in the binding behaviour. Finally, a dilution series was prepared to cover a concentration range from 150 μ M to 4.6 nM DNMT2. Each sample was incubated with 50 nM FTAD for 15 minutes prior to measurement to form protein-fluorophore complexes. Measurements were performed in triplicates on a Tecan Infinite F200 Pro fluorimeter in black 96-well half-area plates at room temperature. For excitation a wavelength of 485 nm was chosen, and emission was detected at 535 nm.

Determination of Z factor

For positive control FTAD was diluted to 50 nM in assay buffer (50 mM Hepes pH 7.5, 150 mM NaCl, 1 mM DTT, 0.1% PEG-8000, 0.05% PS-20) and DNMT2 was added in a final concentration of 2 μ M to a final volume of 50 μ L. As a negative control for this assay FTAD was diluted to a final concentration of 50 nM in assay buffer, then storage buffer of DNMT2 was added to a final volume of 50 μ L. Storage buffer of DNMT2 was added to match the buffers of the negative and the positive controls. This was done for 27 replicates of each control, the samples were then incubated for 15 minutes at room temperature prior to measurement. The reader settings were the same as described above, data was processed using Microsoft Excel Version 2206 Build 16.0.15330.20260 finally a Z-factor was calculated as described by Zhang *et al.* (Zhang *et al.*, *J. Biomol. Screen.* **1999**, 4 (2), 67–73).

Fluorescence polarization (FP) assay

All experiments were performed in black 96-well half area plates, at room temperature in triplicates using a Tecan Infinite F200 Pro fluorimeter. SAH, SFG and compound **9** were obtained as 25 mM DMSO stocks, and seven 1:1 dilutions in DMSO were prepared for each compound. DNMT2 and FTAD were diluted to a final concentration of 2 μ M and 50 nM respectively in assay buffer. Finally, 2.5 μ L DMSO stock was added to obtain a final volume of 50 μ L, resulting in a concentration range from 250 μ M to 1.95 μ M for each compound. All samples were incubated for 15 minutes at room temperature prior to measurement. Reader settings were as described above, data was processed using GraFit5 v0.13. K_D values of measured EC_{50} values were calculated with the following formula as proposed by Munson *et al.* (Munson *et al.*, *J. Recept. Res.* **1988**, 8 (1–4), 533–546).

$$K_D^{Ligand} = \frac{EC_{50}}{1 + \frac{L_T(y_0 + 2)}{2 * K_D^{Dye}(y_0 + 1)} + y_0} - K_D^{Dye} \left(\frac{y_0}{y_0 + 2} \right)$$

Establishing of microscale thermophoresis (MST) assay

Determination of K_D value for FTAD

Optimal assay conditions for DNMT2 were evaluated previously (Schwickert *et al.*, *J. Med. Chem.* **2022**, 65 (14), 9750–9788), these conditions were also used for all following measurements. To determine an optimal concentration of FTAD several concentrations of FTAD were screened in assay buffer. A concentration of 100 nM FTAD showed sufficient fluorescence counts at 30% excitation power with blue light. To determine a K_D for FTAD binding to DNMT2 a saturation curve was measured. Therefore, DNMT2 was concentrated as described for the FP assay. Finally, a dilution series was prepared to cover a concentration range from 150 μ M to 4.6 nM DNMT2. Each sample was incubated with 100 nM FTAD for 15 minutes prior to measurement to form protein-fluorophore complexes. Measurements were performed using a Monolith NT115 (Nanotemper Technologies, Muenchen, Germany) and standard capillaries (Nanotemper Technologies, Muenchen, Germany). For excitation blue light was chosen with an excitation power of 30% at 25°C and medium MST power. All measurements were performed in triplicates. Data obtained from those measurements was processed using the MO. Affinity Analysis software v2.3.(Nanotemper Technologies, Muenchen, Germany).

Determination of Z factor

For positive control FTAD was diluted to 100 nM in assay buffer and DNMT2 was added in a final concentration of 2 μ M. As a negative control for this assay FTAD was diluted to a final concentration of 100 nM in assay buffer, then storage buffer of DNMT2 was added. Storage buffer of DNMT2 was added to match the buffers of the negative and the positive controls. This was done for 24 replicates of each control, the samples were then incubated for 15 minutes at room temperature prior to measurement. All measurements were performed

on a Monolith NT115 (Nanotemper Technologies, Muenchen, Germany) with standard capillaries (Nanotemper Technologies, Muenchen, Germany). Settings were the same as described above, data was processed using the MO. Affinity Analysis software v2.3. (Nanotemper Technologies, Muenchen, Germany), finally a Z-factor was calculated as described by Zhang *et al.* (Zhang *et al.*, *J. Biomol. Screen.* **1999**, 4 (2), 67–73).

Microscale thermophoresis (MST) assay

All measurements were performed on a Monolith NT 115 (Nanotemper Technologies, Muenchen, Germany) and for each measurement a total volume of 10 μL was loaded into standard capillaries (Nanotemper Technologies, Muenchen, Germany). SAH, SFG and compounds **9–13** were obtained as 25 mM stocks in DMSO, dilution series were prepared on this basis. Prior to measurements DNMT2 was diluted into assay-buffer and FTAD was added to form fluorophore-protein complexes. After 5 minutes SAH, SFG or compounds **9–13** were added resulting in the following final concentrations: 2 μM DNMT2, 100 nM FTAD and 1% DMSO stock (250 μM – 1.95 μM). Incubation time was again 10 minutes, after that measurements were performed immediately using the same settings as described above. All data received was processed using the MO. Affinity Analysis software v2.3. (Nanotemper Technologies, Muenchen, Germany)

Calculations for determination of K_D -values

EC_{50} -values were obtained using the MO. Affinity Analysis software v2.3. (Nanotemper Technologies, Muenchen, Germany). To receive a K_D -value, which is corrected by the binding competition of fluorescence trace and ligand the following formulas were used, which were provided by Nanotemper Technologies.

$$K_D^{Ligand} = K_D^{Dye} * \frac{\gamma}{2 - \gamma} * \left(\frac{EC_{50}}{[T]_t K_D^{Dye} * \frac{\gamma}{2 - \gamma} - 0.5 * \gamma * [F]_t} - 1 \right)$$

$$\gamma = \frac{[T]_t + [F]_t + K_d - \sqrt{([T]_t + [F]_t + K_d)^2 - [T]_t[F]_t}}{2[F]_t}$$

$[T]_t$ gives the concentration of protein, $[F]_t$ gives the concentration of fluorescence tracer and K_D indicating the binding affinity of the fluorescence tracer towards DNMT2 as determined by microscale thermophoresis.

Microscale thermophoresis (MST) screening assay

All compounds were provided as 25 mM stocks in DMSO. All stocks were diluted to a concentration of 40 μM with assay buffer. DNMT2 was diluted to a concentration of 4 μM in assay buffer, FTAD was added to a final concentration of 200 nM. Fluorescence probed DNMT2 was then diluted 1:1 with the diluted compounds resulting in the following concentrations: 2 μM DNMT2, 100 nM FTAD, 20 μM compound. This mixture was incubated for 15 minutes at room temperature prior to measurement. Measurements were performed on a Monolith NT 115 (Nanotemper Technologies, Muenchen, Germany) using standard capillaries (Nanotemper Technologies, Muenchen, Germany). Data was processed using the MO. Affinity Analysis software v2.3. (Nanotemper Technologies, Muenchen, Germany)

Synthetic procedures

General

Reagents and solvents were of commercial quality and were used without further purification. Reaction progress was monitored by thin-layer chromatography using Alugram Xtra F254 silica plates from Machery-Nagel. For compound purification by column chromatography silica gel (40–63 μm) from Machery-Nagel was used. NMR spectra were recorded at 300 MHz on a Bruker Fourier 300 and at 600 MHz on a Bruker Avance III 600. Chemical shifts are indicated in parts per million (ppm), using the solvent resonance (CDCl_3 , $\text{DMSO-}d_6$ or CD_3OD from Deutero GmbH) as internal standard. The identity and purity of the final compound was determined by combined HPLC/ESI-MS analysis using an Agilent 1100 series HPLC system with an Agilent Zorbax SB-Aq (4.6 x 150 mm; mobile phase: $\text{MeCN}/\text{H}_2\text{O} = 30:70 + 0.1\% \text{HCOOH}$; flow rate: 0.7 mL/min) column. The sample was applied using 5 μL injection with quantitation by AUC at 210 nm, 254 nm, and 280 nm. Fourier-transformed ATR-corrected IR spectra were measured on an Avatar 330 single crystal spectrometer from Thermo Nicolet. Melting points (uncorrected) were measured by an MPM-H3 using semi-open capillaries. Specific rotations were determined by a Krüss P3000 polarimeter and are given in $\text{deg cm}^3 \text{g}^{-1} \text{dm}^{-1}$. The purity of all compounds tested in the described biological assays was $\geq 95\%$ as determined by LC-MS.

2-Azidoethan-1-amine (2)

The product was synthesized according to a procedure by Fang *et al.* (Fang *et al. Org. Biomol. Chem.* **2019**, 17, 10013–10019).

2-Chloroethylamine hydrochloride (1.50 g, 12.9 mmol, 1 equiv) and sodium azide (2.52 g, 38.8 mmol, 3 equiv) were dissolved in water and stirred for 24 h at 80–90 °C. Aqueous KOH solution (4 mL, 15 wt-%) was added at room temperature followed by the extraction with diethyl ether (4 x 10 mL). The combined organic layers were dried over anhydrous sodium sulfate, filtered, and concentrated in vacuo to give the

product as a colorless oil (1.06 g, 8.62 mmol, 67%). ¹H NMR (300 MHz, CDCl₃): δ/ppm = 3.37 (t, *J* = 5.7 Hz, 1H), 2.88 (t, *J* = 5.7 Hz, 1H), 1.48 (s, 2H). ¹³C NMR (75.5 MHz, CDCl₃): δ/ppm = 54.7, 41.5. FT-IR: ν/cm⁻¹ = 3362, 2968, 2931, 2871, 2098, 1599, 1466, 1377, 1342, 1288, 1160, 1129, 1107, 1042, 952, 869, 816.

N-(2-Azidoethyl)-3',6'-dihydroxy-3-oxo-3*H*-spiro[isobenzofuran-1,9'-xanthen]-5-carboxamide (**3**)

A solution of 5-FAM (200 mg, 0.53 mmol, 1 equiv) in DMF (6 ml) was cooled to 0 °C in an ice bath. DIPEA (316 μL, 1.86 mmol, 3.5 equiv) was added dropwise while stirring, followed by the addition of TPTU (236 mg, 0.78 mmol, 1.5 equiv). After stirring for 20 min at 0 °C 2-azidoethan-1-amine (68.6 mg, 0.80 mmol, 1.5 equiv) was added and stirring was continued at 0 °C for 1 h and subsequently for 48 h at room temperature. The solvent was evaporated under reduced pressure and the residue was purified by column chromatography (DCM/MeOH = 9:1 + 0.1% TFA) yielding the desired product as an orange solid (226 mg, 0.51 mmol, 96%). ¹H NMR (300 MHz, CD₃OD): δ/ppm = 8.44 (d, *J* = 1.6 Hz, 1H), 8.20 (dd, *J* = 8.0, 1.6 Hz, 1H), 7.31 (d, *J* = 8.0 Hz, 1H), 6.71 (d, *J* = 2.3 Hz, 2H), 6.63 (d, *J* = 8.7 Hz, 2H), 6.56 (dd, *J* = 8.7, 2.3 Hz, 2H), 3.65–3.57 (m, 2H), 3.57–3.49 (m, 2H). ¹³C NMR (75 MHz, CD₃OD): δ/ppm = 169.7, 168.6, 164.2, 155.7, 137.7, 134.8, 131.1, 129.6, 127.2, 126.5, 115.6, 112.5, 103.6, 51.4, 40.8, 30.7, 24.2. FT-IR: ν/cm⁻¹ = 3330, 2978, 2359, 1639, 1506, 1455, 1369, 1248, 1203, 1179, 1153, 1112, 995, 847, 798, 721, 668. mp: 190 °C (decomposition).

tert-Butyl(S)-4-(((3*aR*,4*R*,6*R*,6*aR*)-6-(6-amino-9*H*-purin-9-yl)-2,2-dimethyltetrahydrofuro[3,4-*c*][1,3]dioxol-4-yl)methyl)((1-(2-(3',6'-dihydroxy-3-oxo-3*H*-spiro[isobenzofuran-1,9'-xanthen]-5-carboxamido)ethyl)-1*H*-1,2,3-triazol-4-yl)methyl)amino)-2-((*tert*-butoxycarbonyl)amino)butanoate (**5**)

Compound **4** (230 mg, 0.38 mmol, 1 equiv), compound **3** (170 mg, 0.38 mmol, 1 equiv) and copper(II) sulfate pentahydrate (28.6 mg, 0.11 mmol, 0.3 equiv) were suspended in MeOH (12 mL). A solution of sodium ascorbate (37.9 mg, 0.19 mmol, 0.5 equiv) in water (4 mL) was added and the resulting mixture was stirred overnight. The solvents were removed under reduced pressure and the residue was purified by column chromatography (DCM/MeOH 9:1 + 0.1 % HCOOH) yielding the desired product as a yellow solid (246 mg, 0.24 mmol, 61%). ¹H NMR (300 MHz, CDCl₃): δ/ppm = 9.05–8.94 (m, 1H), 8.40 (d, *J* = 1.4 Hz, 1H), 8.28 (s, 1H), 8.21–8.17 (m, 1H), (8.17–8.12 (m, 2H), 7.87 (s, 1H), 7.33 (d, *J* = 8.0 Hz, 1H), 7.25 (s, 1H), 6.98 (d, *J* = 7.8 Hz, 1H), 6.73 (d, *J* = 1.7 Hz, 2H), 6.56 (s, 4H), 6.15 (d, *J* = 2.4 Hz, 1H), 5.49–5.37 (m, 1H), 5.02–4.92 (m, 1H), 4.55 (t, *J* = 5.9 Hz, 2H), 4.39–4.29 (m, 1H), 4.03–3.87 (m, 1H), 3.83–3.71 (m, 4H), 3.64 (s, 1H) 2.92–2.74 (m, 1H), 2.67–2.53 (m, 2H), 2.47–2.35 (m, 1H), 1.96–1.80 (m, 1H), 1.77–1.61 (m, 1H), 1.53 (s, 3H), 1.36 (s, 18H), 1.31 (s, 3H). ¹³C NMR (75.5 MHz, CDCl₃): δ/ppm = 171.89, 168.22, 165.17, 163.15, 159.82, 156.16, 155.62, 154.92, 152.66, 151.90, 148.83, 141.97, 140.28, 135.97, 134.72, 129.13, 126.55, 124.33, 123.43, 119.39, 113.36, 112.83, 109.02, 102.41, 89.34, 84.04, 83.47, 83.07, 82.94, 80.34, 78.14, 54.61, 53.50, 52.48, 51.37, 50.14, 48.74, 48.13, 28.23, 27.99, 27.65, 27.05, 25.34. FT-IR: ν/cm⁻¹ = 3335, 2980, 2361, 1641, 1506, 1455, 1369, 1248, 1203, 1181, 1153, 1114, 850, 799, 721. mp: 225 °C (decomposition). [α]_D²⁰ = +5 (10 mg/mL; MeOH).

(S)-2-Amino-4-(((2*R*,3*S*,4*R*,5*R*)-5-(6-amino-9*H*-purin-9-yl)-3,4-dihydroxytetrahydrofuran-2-yl)methyl)((1-(2-(3',6'-dihydroxy-3-oxo-3*H*-spiro[isobenzofuran-1,9'-xanthen]-5-carboxamido)ethyl)-1*H*-1,2,3-triazol-4-yl)methyl)amino)butanoic acid Trifluoroacetate salt (**6**, **FTAD**)

To a solution of compound **5** (182 mg, 0.17 mmol) in DCM (4 mL) at 5 °C was added TFA (4 mL). The solution was kept at 5 °C for 24 h. After the mixture was diluted and co-distilled with DCM (3x 40 mL), the residue was dissolved in H₂O (3 mL) and cooled to 5 °C. TFA (0.5 mL) was added, and the solution was kept at 5 °C for 5 d. The mixture was diluted with water (12 mL) and dried by lyophilization to give FTAD (**6**, 194 mg, 0.17 mmol, 99%, 2.3 equiv TFA) as an orange trifluoroacetate salt. ¹H NMR (600 MHz, CD₃OD): δ/ppm = 8.31–8.19 (m, 3H), 8.16–8.11 (m, 1H), 8.08–8.03 (m, 1H), 7.23 (d, *J* = 8.0 Hz, 1H), 6.65–6.62 (m, 2H), 6.53–6.44 (m, 4H), 6.05–5.98 (m, 1H), 4.69–4.58 (m, 3H), 4.51–4.43 (m, 1H), 4.38–4.25 (m, 3H), 3.89–3.79 (m, 3H), 3.48–3.40 (m, 1H), 3.36–3.27 (m, 2H), 2.36–2.25 (m, 1H), 2.13–2.01 (m, 1H), 1.33–1.29 (m, 1H). ¹³C NMR (150 MHz, CD₃OD): δ/ppm = 168.4, 166.5, 159.3, 154.5, 151.8, 147.8, 140.9, 135.3, 133.3, 128.0, 126.4, 125.5, 123.6, 122.8, 111.6, 108.5, 101.4, 89.2, 79.1, 72.5, 71.3, 55.3, 54.4, 53.6, 52.1, 50.9, 49.1, 45.7, 39.1, 24.5, 16.5, 15.1. FT-IR: ν/cm⁻¹ = 3090, 2609, 1742, 1670, 1506, 1452, 1317, 1248, 1178, 1128, 994, 836, 798, 761, 720. mp: 67 °C (decomposition). [α]_D²⁰ = +17 (10 mg/mL; MeOH). ESI-MS: calcd for C₄₀H₃₉N₁₁O₁₁ m/z [M+2H]²⁺ = 425.65; found: 425.57. Purity: 95% (HPLC, MeCN/H₂O = 30:70 + 0.1% HCOOH); t_R = 2.38 min.

Spectra and chromatograms

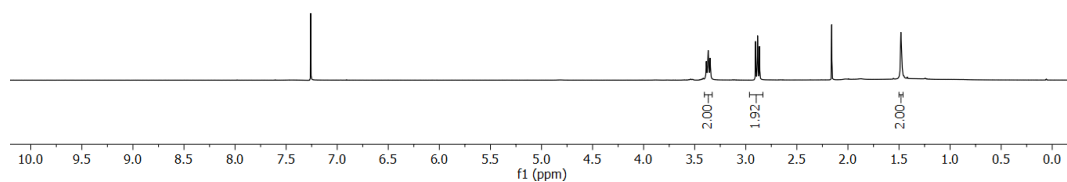


Figure S1. ¹H NMR of compound 2.

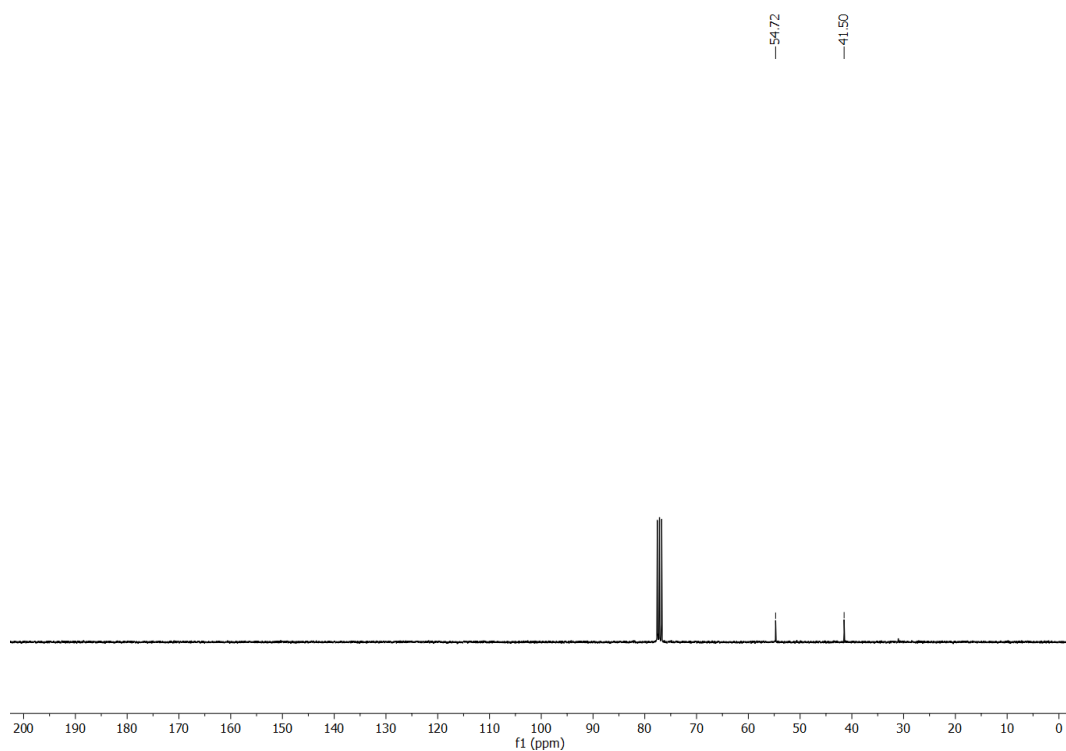


Figure S2. ¹³C NMR of compound 2.

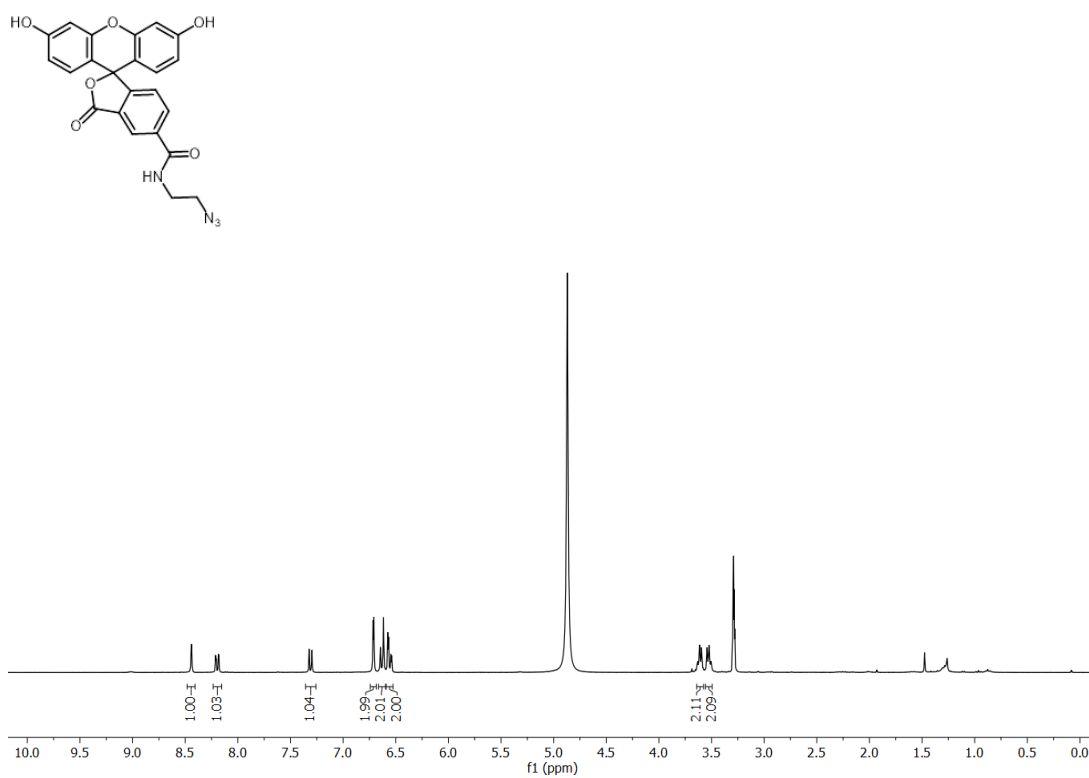


Figure S3. ¹H NMR of compound 3.

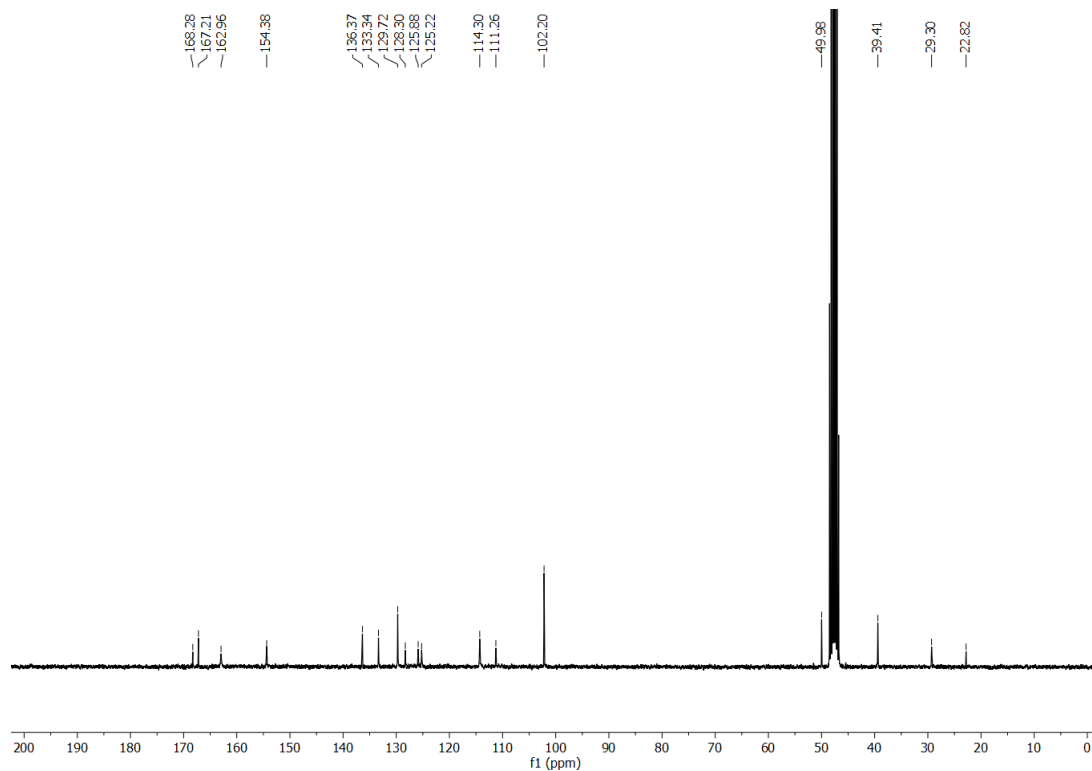


Figure S4. ¹³C NMR of compound 3.

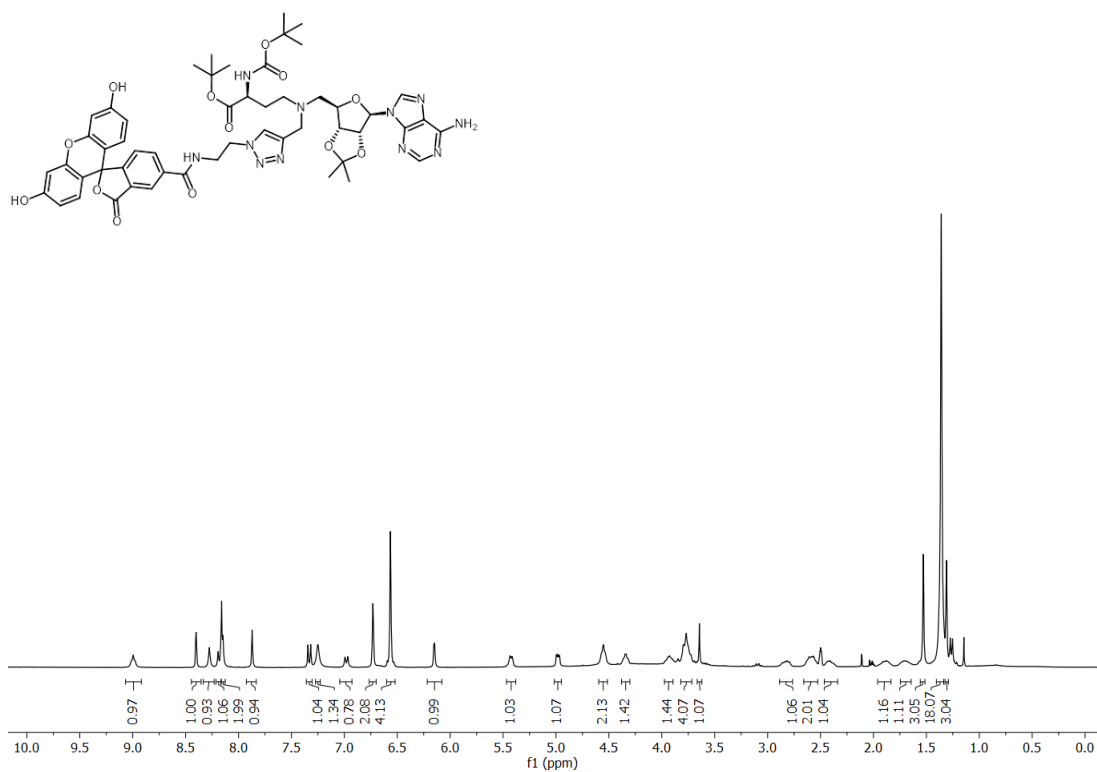


Figure S5. ^1H NMR of compound 5.

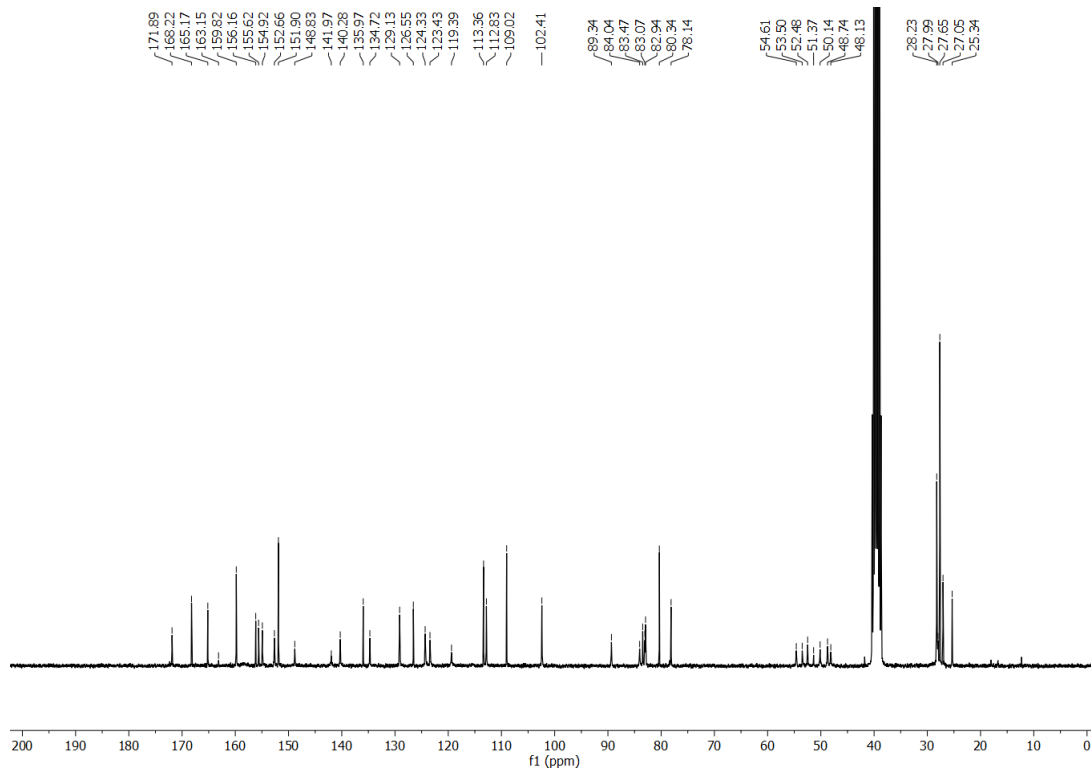


Figure S6. ^{13}C NMR of compound 5.

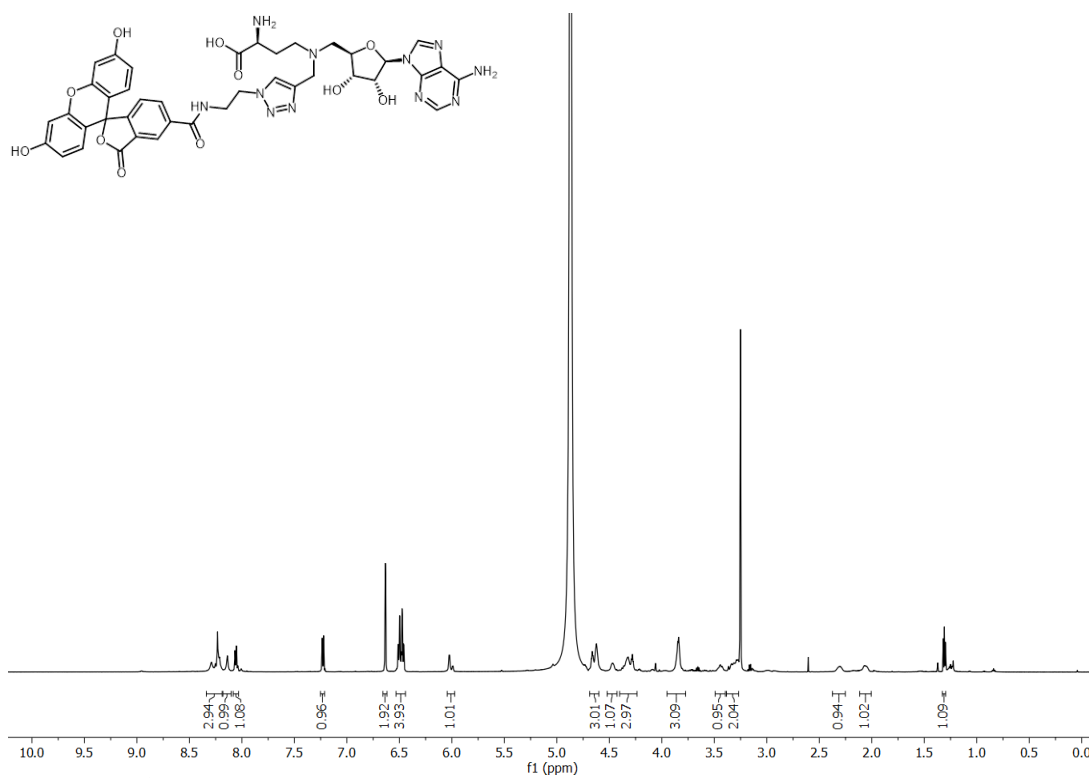


Figure S7. ¹H NMR of FTAD (compound 6).

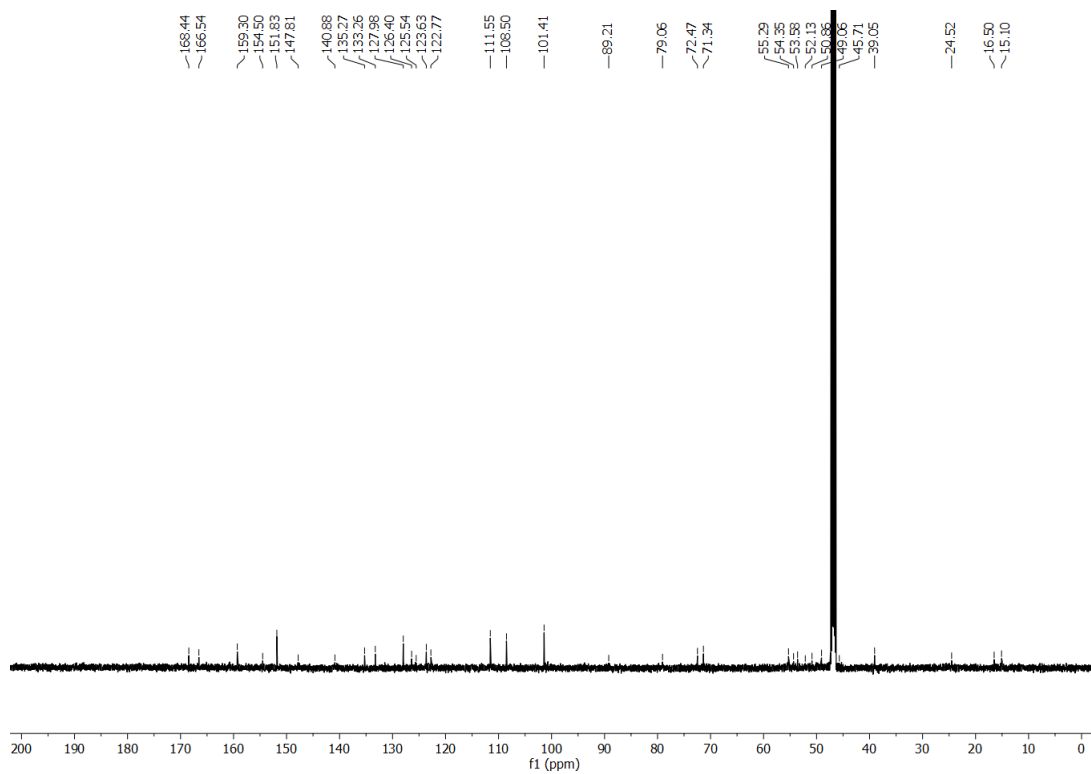


Figure S8. ¹³C NMR of FTAD (compound 6).

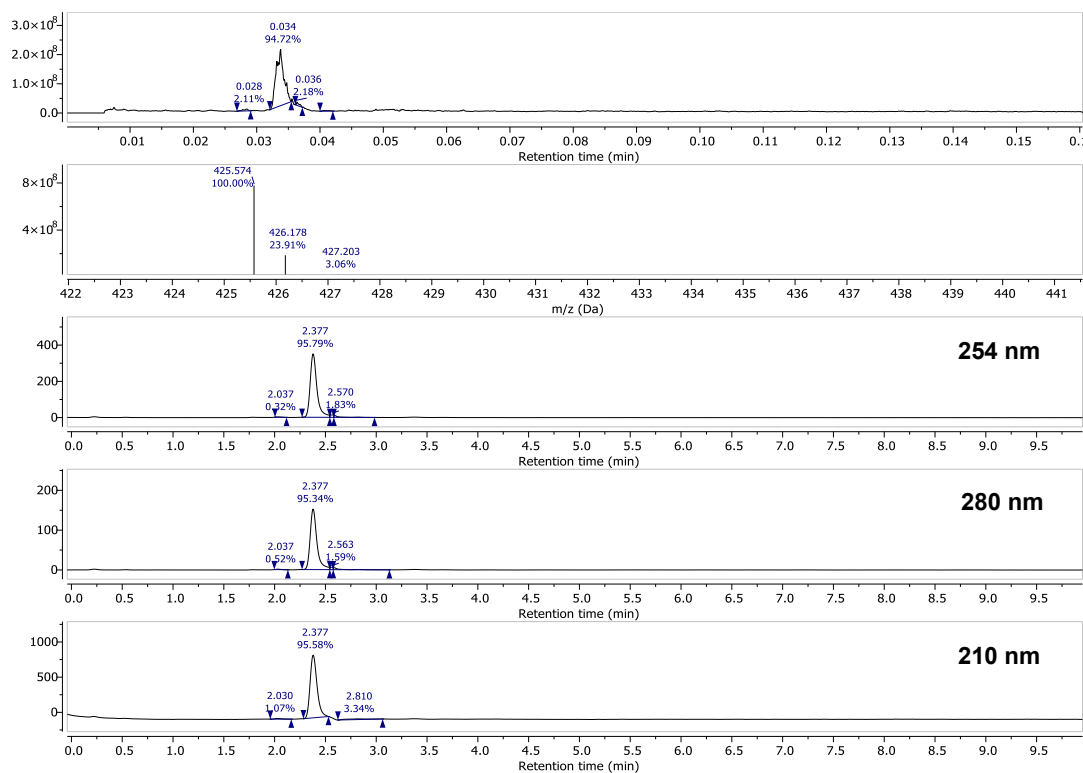


Figure S8. TIC, mass spectrum and chromatograms () of FTAD (compound **6**).

FP Diagrams

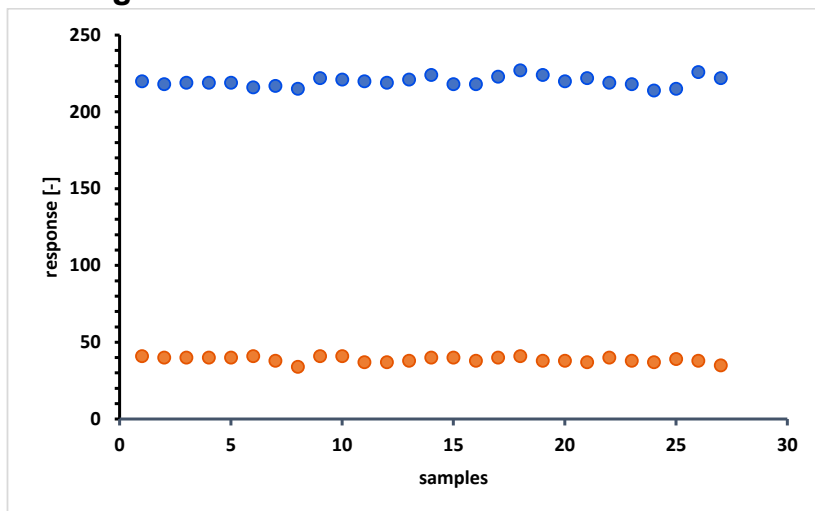


Figure S9: Determination of Z-factor for Fluorescence Polarization Assay

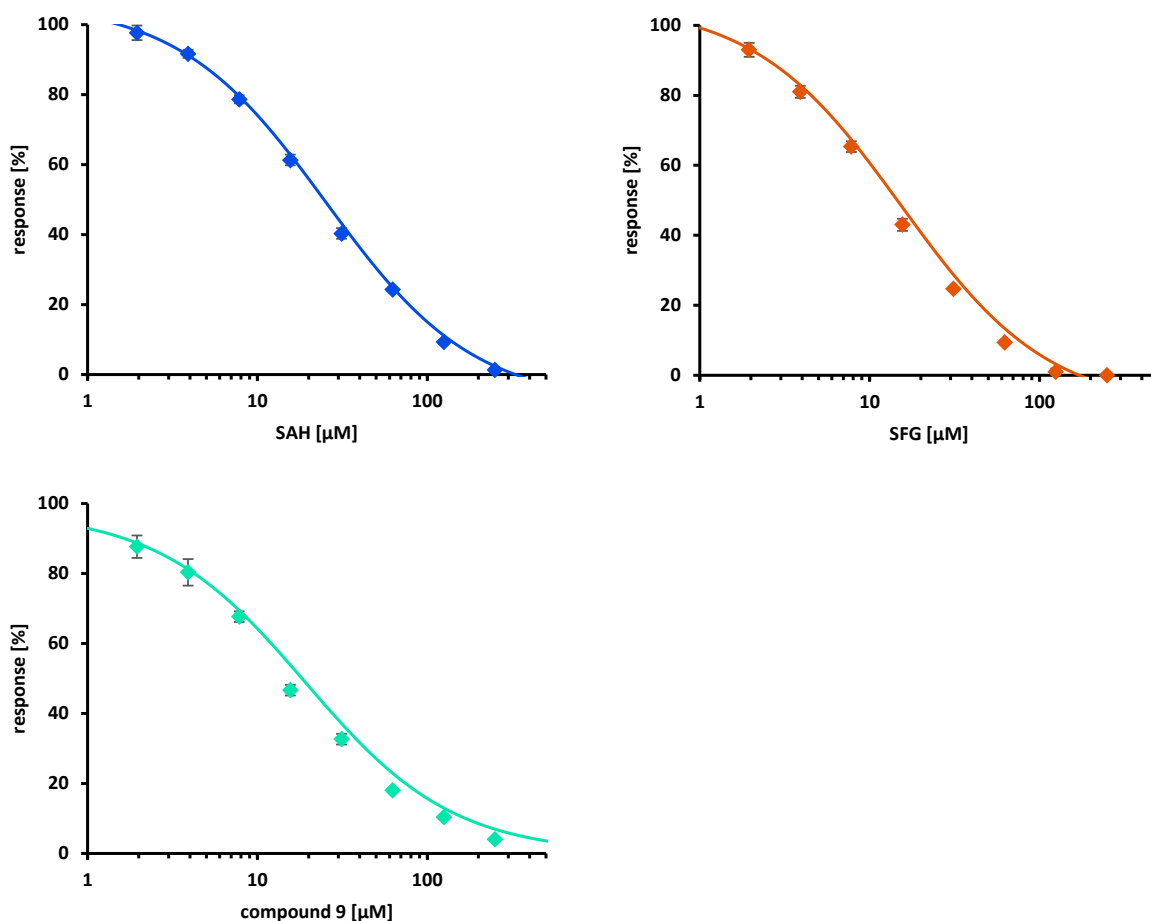


Figure S10: Raw data of fluorescence polarization assays for SAH, SFG and compound **9**. Shown is mean \pm SD of three experiments

MST Diagrams

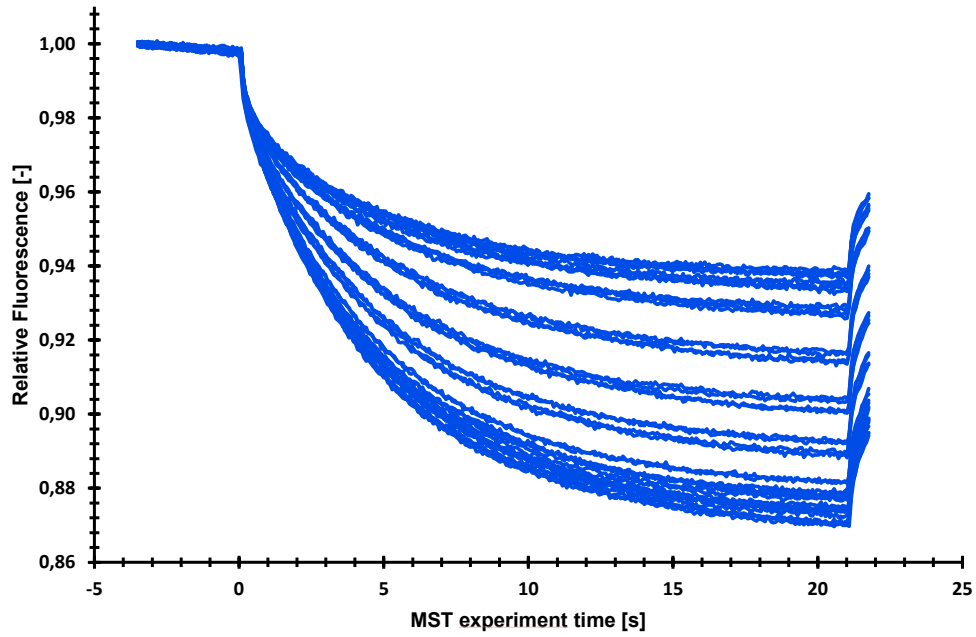


Figure S11. Raw traces for MST assay of SAH. Data of n=4 experiments.

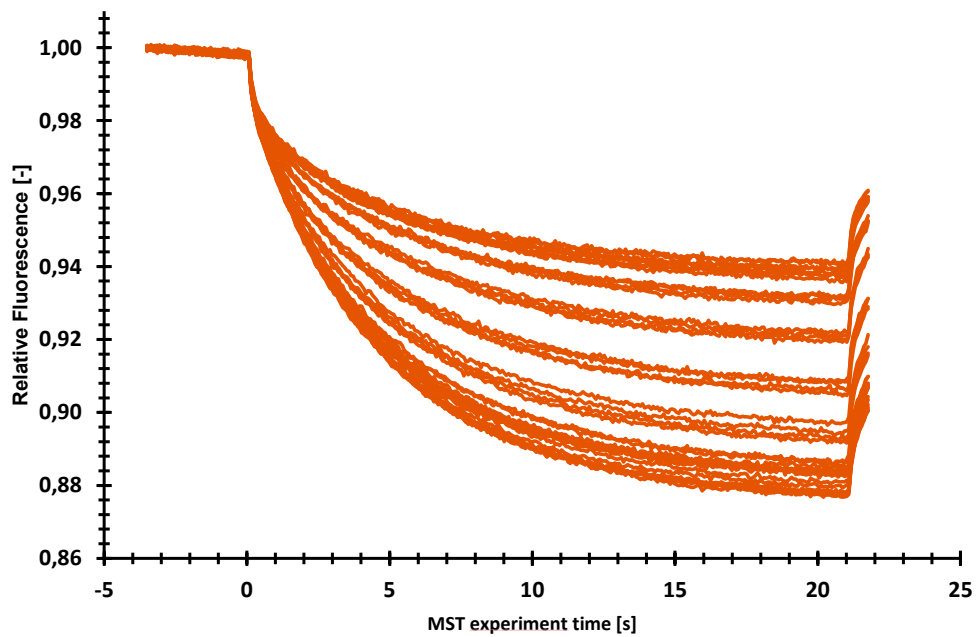


Figure S12. Raw traces of MST assay of SFG. Data of n=4 experiments.

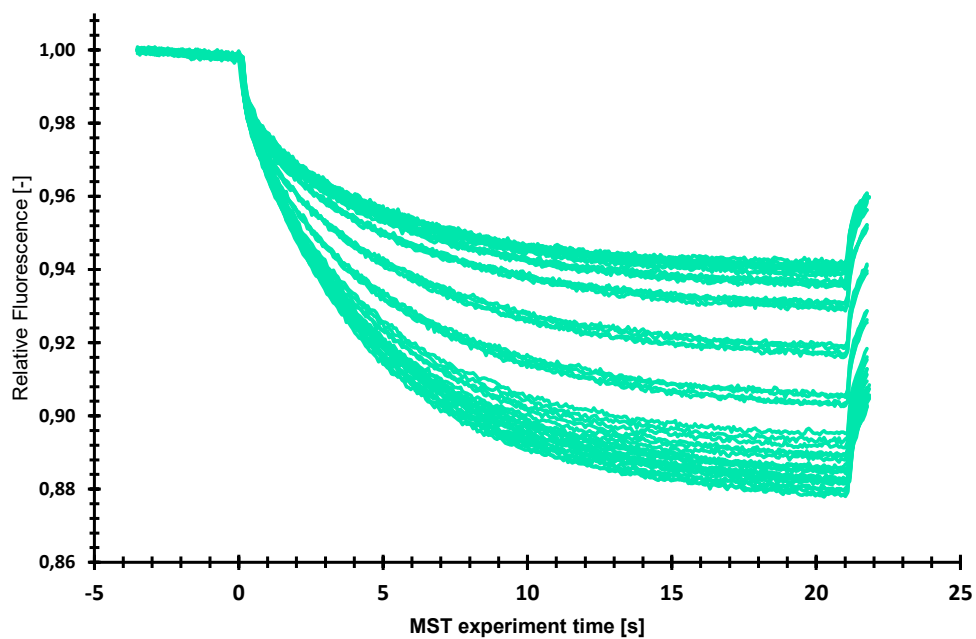


Figure S13. Raw traces of MST assay for compound **9**. Data of n=4 experiments.

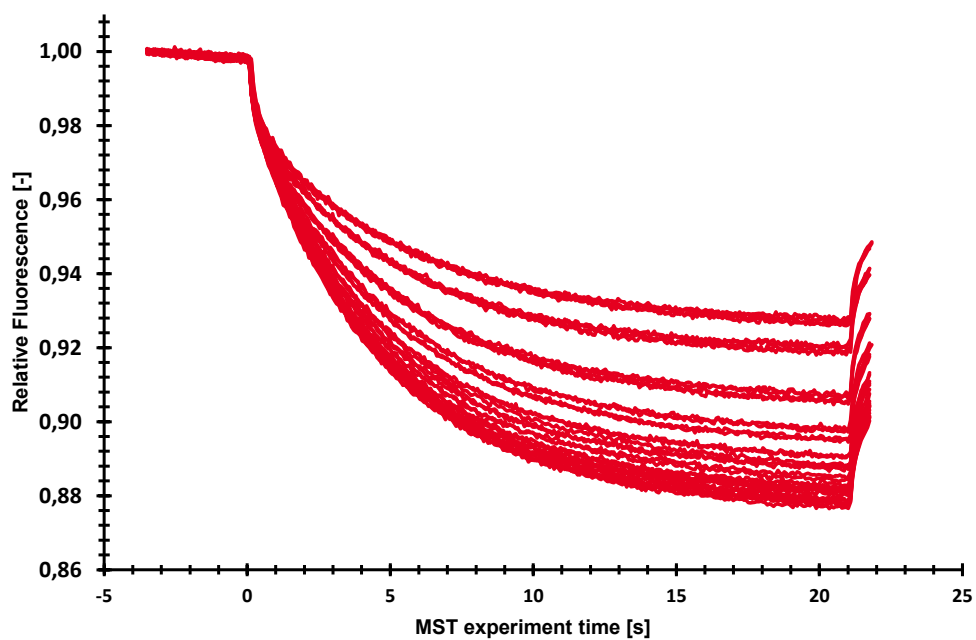


Figure S14. Raw traces of MST assay for compound **10**. Data of n=4 experiments.

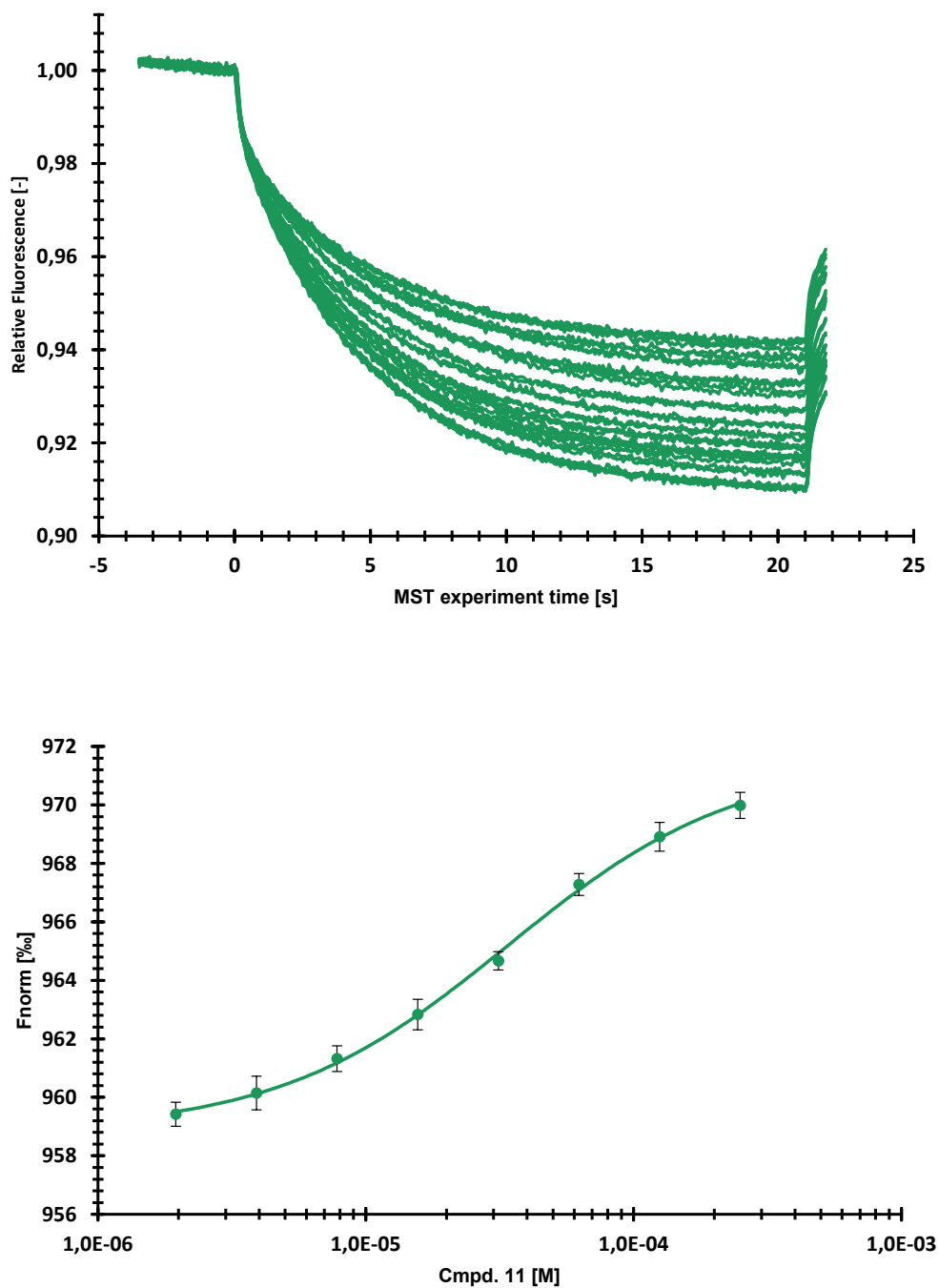


Figure S15: top) raw trace of MST assay of compound 11. Data of n = 4 experiments; bottom) EC₅₀ fit of compound 11. Shown are means and errors.

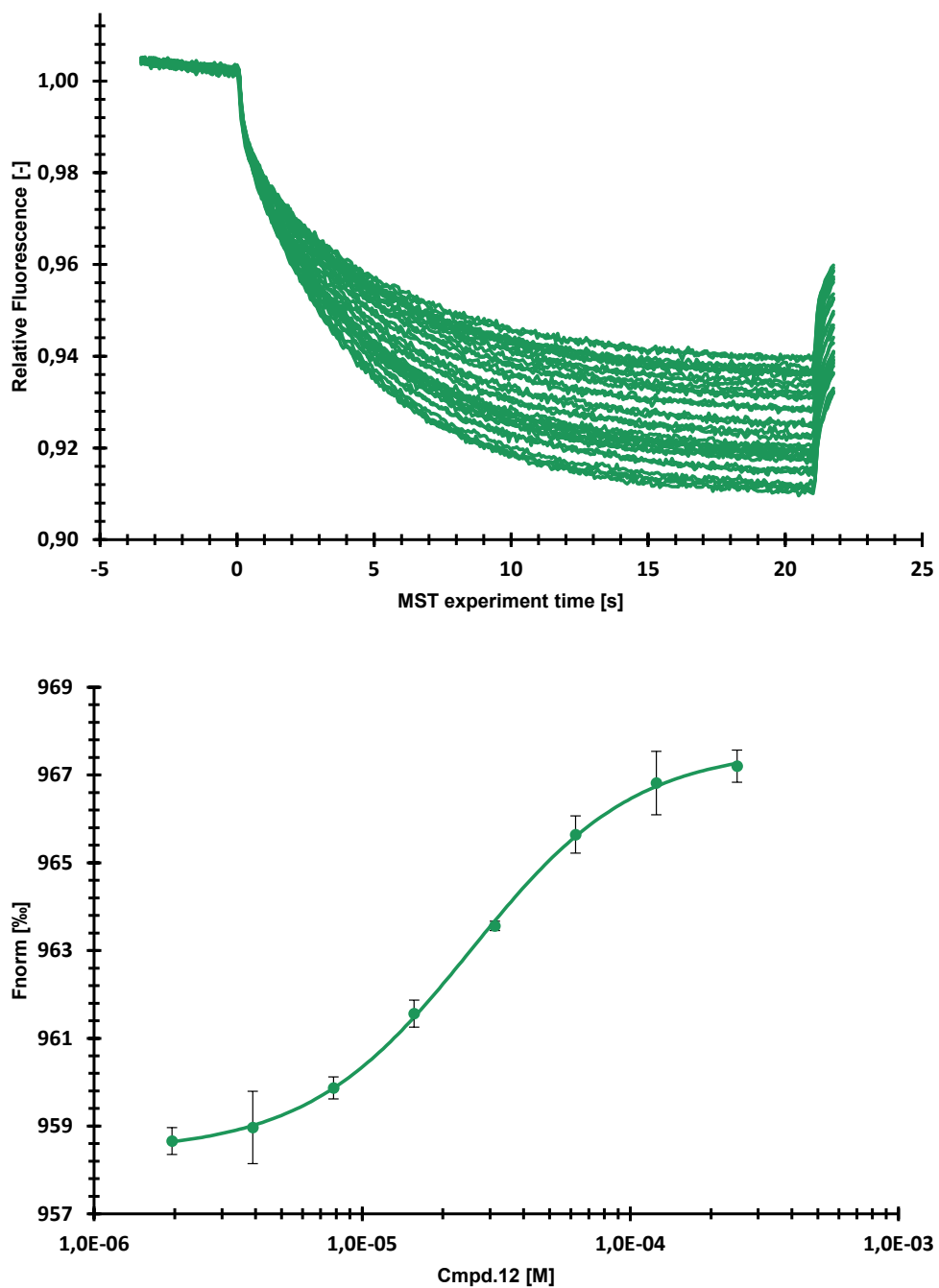


Figure S16: top) raw trace of MST assay of compound **12**. Data of n = 4 experiments; bottom) EC₅₀ fit of compound **12**. Shown are means and errors

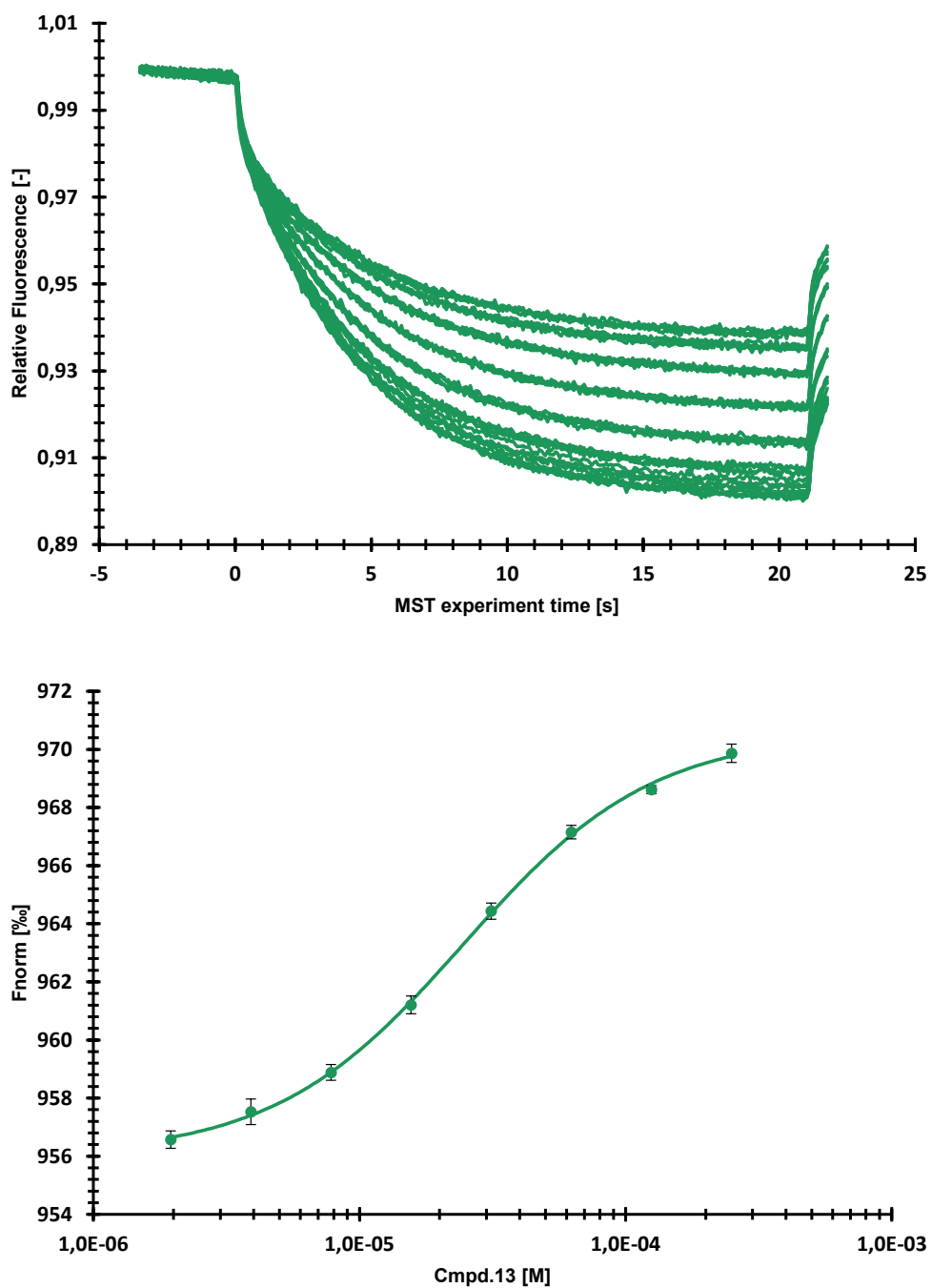


Figure S17: top) raw trace of MST assay of compound **13**. Data of n = 4 experiments; **bottom)** EC₅₀ fit of compound **13**. Shown are means and errors

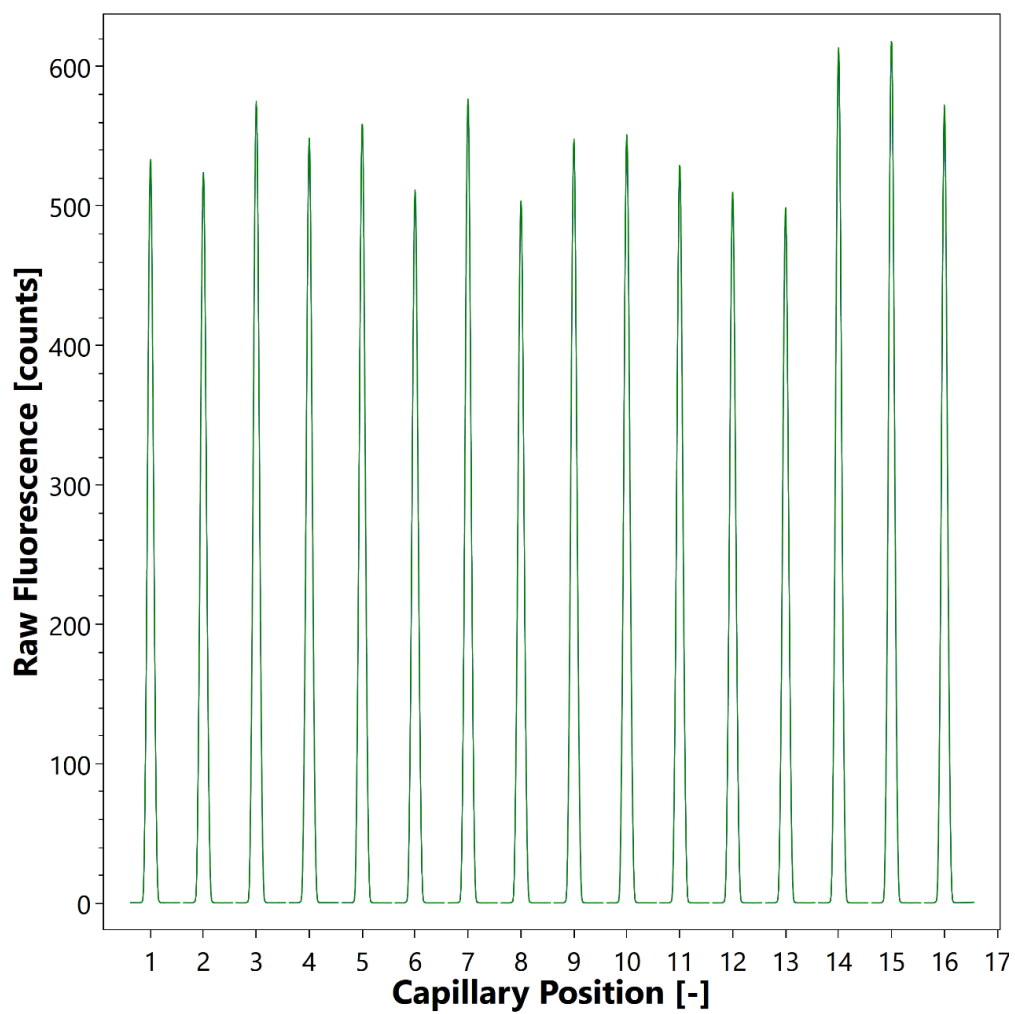


Figure S18: Exemplary image of a capillary scan. Shown a capillary scan of the affinity determination of SAH.

Chemical Space Virtual Screening against Hard-to-Drug RNA Methyltransferases DNMT2 and NSUN6.

Project summary and own contributions

One possibility to increase the selectivity of methyltransferase inhibitors might be the design of non-SAH-like scaffolds. There are different approaches to achieving this goal. For example, a high throughput screening or a fragment-based screening could help to find promising non-SAH-like hits. Unfortunately, these approaches require large compound libraries and an enormous screening capacity. Alternatively, there are computer-based virtual screening approaches that help to preselect promising compounds. Currently, the number of crystal structures of DNMT2 and NSUN6 is very limited, which makes a virtual screening for these proteins very challenging, and it could also have a negative impact on the quality of the results obtained. Nevertheless, this *in silico* approach should limit the number of compounds to be tested in an *in vitro* test drastically. Using the commercial make-on-demand *REAL Space* library of ENAMINE LTD., a virtual screening for DNMT2 and NSUN6 was performed. The virtual screening for DNMT2 consisted of over 700 million compounds, whereas the virtual screening for NSUN6 consisted of over 14 billion compounds. Finally, 21 compounds for DNMT2 and 17 compounds for NSUN6 were selected. Since it was the aim of this study to leave the SAH scaffold behind, all selected compounds did not show a SAH-like scaffold. Finally, the synthesis of the selected compounds was ordered at ENAMINE LTD., and they were able to synthesize 18 of 21 selected compounds for DNMT2 and 12 of 17 selected compounds for NSUN6. The binding of the compounds was tested in a microscale thermophoresis assay at three concentrations to detect concentration-dependent binding. Compounds that had shown a concentration-dependent binding were tested again in a half-logarithmic dilution series to determine binding affinity. Furthermore, cross-testing of the compounds with the respective other protein was performed to estimate if some selectivity had been achieved by the virtual screening. Five hits each have been found for DNMT2 and NSUN6, of which each three showed some selectivity towards the respective other protein. Unfortunately, their affinity was only in the mid-two-digit or even three-digit micromolar range. The hits for DNMT2 also did not show any inhibition in the tritium-incorporation assay, probably due to their lack of affinity. Nevertheless, these compounds are a starting point for further studies to design and synthesize non-SAH-like inhibitors of DNMT2 and NSUN6.

Own contribution: expression and purification of protein with support from [REDACTED], conducting the MST experiments, writing of the manuscript together with [REDACTED].

Contributions from other authors: virtual screening for DNMT2 and NSUN6; selection of compounds; mass spectrometric verification of compounds; tritium incorporation assay.

This work has been published in: International Journal of Molecular Sciences (Impact factor: 6.208)

Reprinted with permission from: Copyright © 2023 by the authors. Licensee MDPI, Basel, Switzerland.

This article is an open access article distributed under the terms and conditions of the Creative Commons Attribution (CC BY) license (<https://creativecommons.org/licenses/by/4.0/>).



Article

Chemical Space Virtual Screening against Hard-to-Drug RNA Methyltransferases DNMT2 and NSUN6

Robert A. Zimmermann , Tim R. Fischer, Marvin Schwickert , Zarina Nidoieva, Tanja Schirmeister and Christian Kersten *

Institute of Pharmaceutical and Biomedical Sciences, Johannes Gutenberg-University, Staudingerweg 5, 55128 Mainz, Germany

* Correspondence: kerstec@uni-mainz.de

Abstract: Targeting RNA methyltransferases with small molecules as inhibitors or tool compounds is an emerging field of interest in epitranscriptomics and medicinal chemistry. For two challenging RNA methyltransferases that introduce the 5-methylcytosine (m^5C) modification in different tRNAs, namely DNMT2 and NSUN6, an ultra-large commercially available chemical space was virtually screened by physicochemical property filtering, molecular docking, and clustering to identify new ligands for those enzymes. Novel chemotypes binding to DNMT2 and NSUN6 with affinities down to $K_{D,app} = 37 \mu M$ and $K_{D,app} = 12 \mu M$, respectively, were identified using a microscale thermophoresis (MST) binding assay. These compounds represent the first molecules with a distinct structure from the cofactor SAM and have the potential to be developed into activity-based probes for these enzymes. Additionally, the challenges and strategies of chemical space docking screens with special emphasis on library focusing and diversification are discussed.

Keywords: RNA methyltransferases; DNMT2; NSUN6; virtual screening; ultra-large molecular libraries; molecular docking; chemical spaces



Citation: Zimmermann, R.A.; Fischer, T.R.; Schwickert, M.; Nidoieva, Z.; Schirmeister, T.; Kersten, C. Chemical Space Virtual Screening against Hard-to-Drug RNA Methyltransferases DNMT2 and NSUN6. *Int. J. Mol. Sci.* **2023**, *24*, 6109. <https://doi.org/10.3390/ijms24076109>

Academic Editor: Giulio Vistoli

Received: 20 January 2023

Revised: 20 February 2023

Accepted: 22 March 2023

Published: 24 March 2023



Copyright: © 2023 by the authors. Licensee MDPI, Basel, Switzerland. This article is an open access article distributed under the terms and conditions of the Creative Commons Attribution (CC BY) license (<https://creativecommons.org/licenses/by/4.0/>).

1. Introduction

1.1. RNA Methyltransferases as a Target

RNA modifications play an important role in an abundance of both physiological and pathophysiological biochemical pathways [1–4]. Among over 170 known RNA modifications [5–7], one of the most significant ones is methylation, which is introduced by methyltransferases. One prominent example of interfering with RNA modifying enzymes as a therapeutic strategy is the methyltransferase 3 (METTL3, also called N^6 -adenosine-methyltransferase) inhibitor STM2457, which is under investigation for the treatment of acute myeloid leukemia (AML) [8]. Examination of other RNA methyltransferases as possible drug targets is still in its infancy, which is also reflected in the literature [9]. However, in recent times, research in this area has started to accelerate. In this emerging field, the 5-methylcytosine (m^5C) modification, which is catalyzed by various members of the Nol1/Nop2/SUN (NSUN) family, but also by the DNA methyltransferase 2 (DNMT2), is of special interest in different human diseases [10].

Due to its high structural similarity to DNMT1 and DNMT3, DNMT2 was classified as a member of the DNMT family, but it was found that the main substrate of DNMT2 is RNA. The first reported RNA substrate of DNMT2 was tRNA^{Asp} [11–13]. Meanwhile, tRNA^{Val} and tRNA^{Gly} were identified as substrates of DNMT2 as well [14,15]. The m^5C modification introduced by DNMT2 in position C-38 of the anticodon loop of tRNA^{Asp} increases the stability of the tRNA and therefore affects protein translation [16–18]. The influence of DNMT2 involves epigenetic but also pathogenic pathways, especially in carcinogenesis and inheritance of metabolic disorders [19–21]. Besides azacytidine and zebularine, which both have to be incorporated into the substrate tRNA to inhibit DNMT2 [22,23], several

derivatives of the enzyme's cofactor *S*-adenosyl-L-methionine (SAM, Figure 1) and the autoinhibitory reaction product *S*-adenosyl-L-homocysteine (SAH) and the well-known natural product pan-methyltransferase inhibitor sinefungin (SFG) were identified to inhibit DNMT2 [24,25].

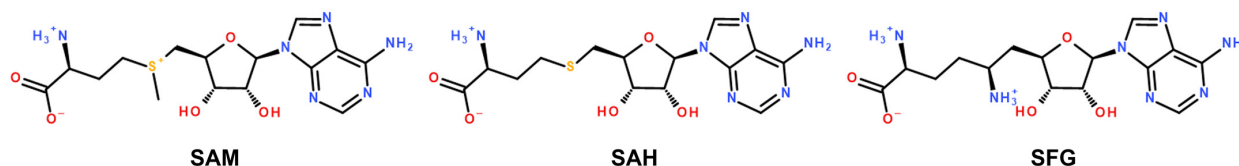


Figure 1. Molecular structures of the DNMT2 and NSUN6 cofactor SAM, the reaction product and auto-inhibitor SAH and the pan-methyltransferase inhibitor SFG.

NSUN6 is a member of the NSUN family and methylates C-72 in tRNA^{Cys} and tRNA^{Thr}, as well as several mRNAs [26,27]. NSUN6 was claimed to be involved in bone metastasis [28], but its complete physiological role remains elusive [29]. Besides SAH, sinefungin, and derivatives, to the best of our knowledge, no drug-like inhibitors designed for NSUN6 have been reported in the literature so far. Although NSUN6 and DNMT2 may not be potential drug targets in the first place, the development of activity-based probes (ABPs) [30,31] for RNA methyltransferases aims to improve our understanding of the biological impact of RNA methylation in general via chemical knock-out in cellular models. Therefore, the requirements for ABPs can be less strict in terms of drug metabolism and pharmacokinetics than for actual drug candidates while still requiring high affinity and selectivity.

1.2. Ultra-Large Library Docking

With the advance of commercial, combinatorial make-on-demand chemical spaces, structure-based virtual screening faces new opportunities and challenges. With the knowledge of robust reactions and available building blocks, new molecular entities become available for ultra-large library (also called chemical spaces) virtual screenings while being likely to be synthetically accessible at the same time. These chemical spaces hold the promise that included novel chemotypes can bind to so-far-undrugged targets. Current make-on-demand spaces are far beyond the size of in-stock compounds. While the curated ZINC20 library [32] covers around 8.1 million drug-like [33] in-stock molecules (molecular weight ≤ 500 g/mol, $\log P \leq 5$, reactivity: anodyne) from a plethora of different supplier catalogs, current commercial chemical spaces overshadow these by three (e.g., WuXi LabNetworks's GalaXi, 8×10^9 molecules) to almost four orders of magnitude (e.g., Enamine's REALspace, 3.4×10^{10} , values from December 2022) [34,35]. While exhaustive molecular docking screens (in the following referred to as 'brute-force docking') can be feasible up to many millions to a few billion molecules, they demonstrated impressive hit rates and identified potent binders previously (Table 1) [36–39], increasing sizes of chemical spaces will make this approach (computationally) too expensive if not impossible [40]. This especially holds true if proprietary chemical spaces are considered, such as Merck MASSIV 2018 (10^{20} molecules) or GSK XXL 2020 (10^{26} molecules) [34,41]. Subsequently, even though 'bigger is better' [42] is usually valid for virtual screening libraries, new strategies for structure-based screenings are required to focus libraries prior to docking [43,44]. One approach is the docking of a diverse subset. However, even though this speeds up the docking time, it cannot be known a priori if the diverse cluster representatives are suitable for the target of interest. Eventually, complete clusters of likely binders are discarded if the cluster representative does not match a required interaction pattern [36]. This likewise accounts for random subsets, but in combination with a machine-learning (ML) model to quickly estimate docking scores, this strategy yielded some promising results for speeding up the process while maintaining high hit rates recently [40]. Alternatively, taking advantage of target knowledge can be a promising route to design its own focused

chemical spaces, as demonstrated in an exclusive series of tetrahydropyridines as potential serotonin (5-hydroxytryptamine, 5-HT) receptor ligands [45]. Another approach is based on fragment-based drug design (FBDD), either physically by generating a chemical space upon crystallographically known fragment substructures and corresponding building blocks [46,47] or starting with pure fragment docking [48,49]. While both strategies rely on the placement of initial virtual ‘synthons’, a crystallographic fragment screening as a first step can support the docking process using the experimental binding mode for template docking, whereas the latter is defined by general limitations of fragment docking. The limitation that probably requires the most attention in this regard is that scoring functions might be unable to distinguish the correct binding mode from incorrect ones due to the intrinsically low number of interactions of fragments requiring proper additional re-scoring methods or pharmacophore constraints [47,49–51].

While for the described virtual screening strategies, several success stories are reported with both high hit rates and very potent ligands (Table 1), those virtual screenings were usually performed for very well-described targets such as kinases and G-protein-coupled receptors (GPCRs) with several crystal structures and known ligands available. However, virtual chemical spaces hold the promise to contain novel chemotypes not (yet) present in conventional in-stock libraries as suitable ligands for so-far-undrugged and considered undruggable or hard-to-drug targets. In our study, we applied the virtual screening strategy on targets of interest DNMT2 and NSUN6 with only a few known ligands, a small number of crystal structures, and rather low predicted druggability, where hit rates tend to be lower (Table 1) [52–55]. Reported ligands for DNMT2 and NSUN6 are either close homologs of the native cofactor SAM with poor physicochemical properties, low drug-likeness, and limited selectivity over other SAM-dependent enzymes [25] or require incorporation into the substrate tRNA-like 5-azacytidine [23]. Likewise, the drug-candidate inhibitor of the structurally closely related DNMT1, GSK3685032, was recently shown to bind primarily to the DNA rather than to the enzyme [56]. This molecule was optimized from only one hit series of a 1.8 million compound high-throughput screening (HTS; most other initial hits were not followed up due to inactivity after purification or non-specific binding). This is a further hint for the low druggability of DNMTs, which eventually requires novel chemotypes to identify new ligands. As another consequence of the low number of known ligands for the m⁵C-RNA methyltransferases of interest, also model validation is considered best practice [37], which includes binder vs. non-binder/decoy discrimination offered limited possibilities.

Table 1. Recent examples of (ultra-)large library structure-based virtual screenings and results from this work.

Target	Reported Ligands ^a	PDB-Entries ^b	PDB-ID	Predicted Druggability ^c	VS Strategy	VS Library Size	Synthesis Success Rate	Hit Rate	Most Potent Hit (→ Improved Lead Compound)	References
D ₄	4457	96	5WIU	0.74	Brute force	138 million	549/589 (93%)	58/238 (24%)	EC ₅₀ = 180 pM	[36]
AmpC	62,046	123	1L2S	0.40	Brute force	99 million	44/51 (86%)	5/44 (11%)	K _i = 1.3 μM	[36]
MT1	1334 (MT1A)	12	6ME3	0.67	Brute force	150 million	38/40 (95%)	15/38 (39%)	EC ₅₀ = 470 pM	[38]
KEAP1	704 (KEAP1/NRF2)	125	5FNQ/4IFL	0.61/0.47	Brute force	1.3 billion	n.a.	69/590 (12%)	K _D = 114 nM	[39]
5-HT _{2A}	5-HT _{2A} : 7568 5-HT _{2B} : 3616	5-HT _{2A} : 12 5-HT _{2B} : 97	homology model ^d 5TVN	0.67	Brute force, focused library	75 million (tetrahydropyridines)	n.a.	4/17 (24%)	K _i = 0.67 μM (→ EC ₅₀ = 41 nM)	[45]
PKA	2500	343	5N3J	0.55	X-ray fragment screening, synthon-based	208 thousand fragments as synthons, 2.7 billion <0.1% of 11 billion,	93/106 (88%)	30/75 ^e (40%)	K _i = 0.74 μM	[47]
CB ₁	10,090	4	5ZTY	0.96	Synthon-based	600 thousand minimal synthons, 1.5 million <0.1% of 11 billion,	60/80 (75%)	21/60 (35%)	K _i = 0.28 μM (→ K _i = 0.9 nM)	[48]
ROCK1	3552	26	2ETR	0.53	Synthon-based	600 thousand minimal synthons, 1 million superstructures	21/24 (88%)	6/21 (29%)	IC ₅₀ = 6.3 nM	[48]
ROCK1	3552	26	2ETR	0.53	Synthon-based	137 thousand fragment-sized building blocks, 5.2 million superstructures	n.a.	27/69 (39%)	K _i = 38 nM	[49]

Table 1. Cont.

Target	Reported Ligands ^a	PDB-Entries ^b	PDB-ID	Predicted Druggability ^c	VS Strategy	VS Library Size	Synthesis Success Rate	Hit Rate	Most Potent Hit (→ Improved Lead Compound)	References
SARS-CoV-2 M ^{Pro}	201 (1765) [57]	774	6W63/5RF7	0.15/0.12	Brute force; focused (fragment)	235 million; 2 million	n.a.	19/100 (19%); 21/93 (23%) ^f	K _D = 23 μM; K _D = 7.2 μM	[52]
SARS-CoV-2 M ^{Pro}	201 (1765) [57]	774	4MDS	0.23	Brute force; deep learning	1.3 billion	0/0 n.a.	0/0 1/32 (3%)	0 IC ₅₀ = 0.8 mM ^g	[53–55]
DNMT2	1 (16) ^h	1	1G55	0.44	Filtering, brute force	720 million filtered to 3.4 million 21.4 million	18/21 (86%)	5/18 (28%)	K _{D,app} = 37 μM	This work
NSUN6	1 (5) ^h	4	5WWR	0.33	Filtering, diversity subset	400 thousand, analog search in 14 billion	12/17 (71%)	5/12 (42%)	K _{D,app} = 12 μM	This work

^a According to ChEMBL (<https://www.ebi.ac.uk/chembl/>, accessed on 15 December 2022). ^b With 95% sequence identity to the entry used for docking (<https://www.rcsb.org/>, accessed on 15 December 2022). ^c Calculated with the DogSiteScorer [58,59] implementation of SeeSAR-12.0.1 for the PDB-ID used in the reported VS. Values between 0 and 1 with higher numbers indicating higher druggability. ^d The used template structure 5-HT_{2B} receptor (PDB-ID 5TVN) shares 67% sequence identity and 80% sequence similarity with the 5-HT_{2A} receptor. ^e 18 of 93 compounds were not sufficiently soluble for testing. ^f Hit rate in SPR binding assay. M^{Pro} was inhibited by 3 and 5 compounds, respectively (hit rates of 3% and 5%). ^g In the original publication [55], no in vitro validation was performed. Re-scoring and testing was conducted by Rossetti et al. [53]. ^h Recently, 16 SAM-analog inhibitors of DNMT2 and 5 of NSUN6 that are not yet available in ChEMBL were discovered [25]. n.a.: Information on synthesis success rates are not available; D₄, dopamine receptor type 4; AmpC, β-lactamase; MT1, melatonin receptor type 1; KEAP1, Kelch-like ECH-associated protein 1; 5-HT_{2A}, serotonin receptor type 2A; PKA, protein kinase A; CB₁, cannabinoid receptor type 1; SARS-CoV-2 M^{Pro}, severe acute respiratory syndrome coronavirus-2 main protease.

2. Results

2.1. Virtual Screening

In order to identify new chemotypes as DNMT2 and NSUN6 inhibitors distinct from the native ligand SAM, virtual screenings of the Enamine Ltd. readily accessible (REAL) chemical space were performed. For the DNMT2 virtual screening (Figure 2A), REAL Space consisted of 719,205,874 compounds, which was too large for a brute-force docking approach and required rather strict physicochemical property filtering (Table S1). Besides the removal of reactive or pan-assay interference compounds (PAINS) [60,61] and consideration of typical drug-like criteria according to the Lipinski rule of five (RO5) [33] and Oprea lead-likeness [62], additional truncation was performed based on the native ligand SAM, which is moderately large and very polar. By the application of upper and lower limits on molecular weight, rotatable bonds, charge, ring number and size, polar surface area (PSA), and chiral centers to reduce chemical complexity for future optimization, the screening library was reduced to a computationally feasible number. The remaining 3,447,976 molecules were docked against the DNMT2-SAH complex structure (PDB-ID 1G55) [63]. Among the 300 best-scoring compounds, which were visually inspected, several close analogs were observed. Subsequently, the top 20,000 molecules were also clustered prior to the final selection of 21 structurally diverse ligands from the top 300 clusters for testing (compounds 1.1–1.21, Table S2). A total of 18 of these 21 were successfully synthesized by Enamine Ltd. (Kyiv, Ukraine) with the company's robust internal procedures.

Differently from the DNMT2 virtual screening procedure (Figure 2B), instead of starting from the whole REAL Space (at the time over 14 billion molecules), the subset REAL diversity (Tanimoto similarity between compounds of less than 0.65 using the Morgan 2, 512 bit fingerprint according to Enamine Ltd.) of 21,441,180 compounds was subjected to physicochemical filtering (Table S1), resulting in only 400,306 molecules for docking against the NSUN6-SFG complex structure (PDB-ID 5WWR, tRNA present in the crystal structure was removed prior to docking) [64]. After visual inspection of the top 300 hits by docking score, for 15 selected compounds, 99 analogs per molecule were searched by structural similarity in the complete REAL Space and subsequently docked. Notably, only four analog series molecules with better scores compared to the initial hits were found. This and the overall lower fraction of very high-scoring molecules hinted to the previously described hypothesis [36] that while hits are among the best of their respective

clusters, other promising scaffolds with a worse scoring representative got lost during this process. The final hit selection consisted of nine initial hits from the diversity subset and four initial hit + analog pairs. Syntheses by Enamine Ltd. were successful for 12 of these 17 molecules (compounds 2.1–2.17, Table S3).

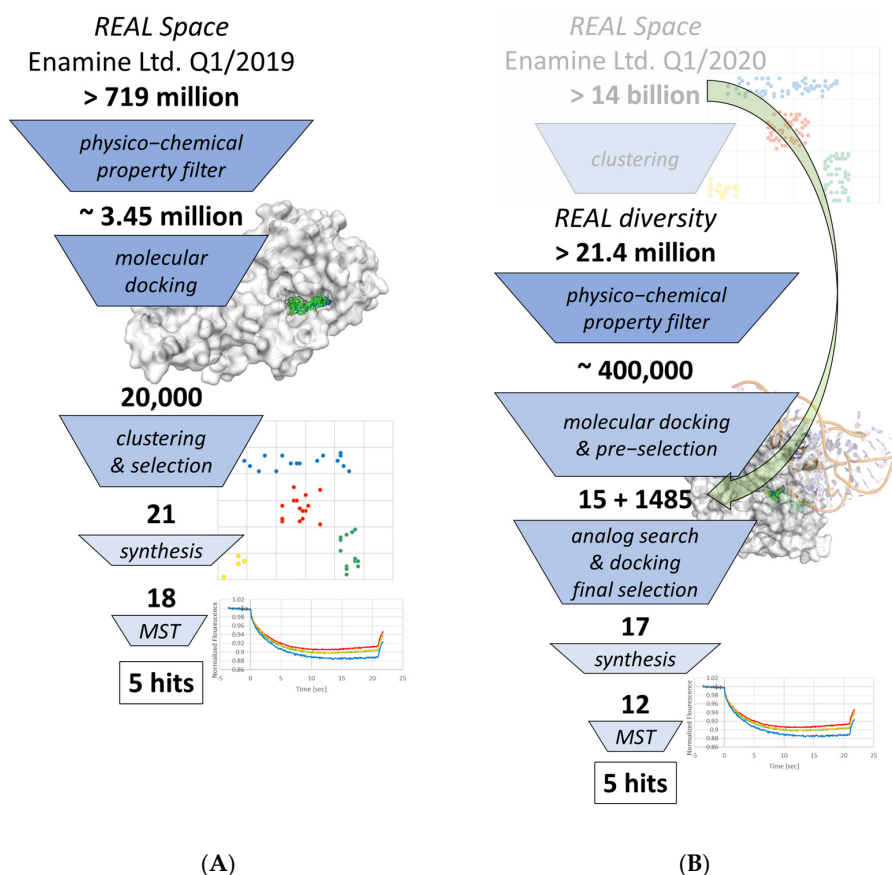


Figure 2. Virtual screening workflow for DNMT2 performing first molecular docking and then clustering (A), and NSUN6 starting from a diversity subset (first clustering) followed by docking and analog search in the whole chemical space (indicated by the green arrow) prior hit selection and testing (B).

Even though the two virtual screenings were performed independently and separated in time, the hit selection criteria for both DNMT2 and NSUN6 were similarly based on the docking score as a first filtering step and the resembling of the crystallographic ligands' interactions with the RNA methyltransferases. Special emphasis was put on molecules to not have peculiar internal torsion strain and being deeply burrowed in the SAM amino acid-moiety sub-pocket to result in H-bond interactions with the Gly-15 and Val-13 backbone as well as the Ser-376 sidechain in DNMT2 (Figure 3A) or Gly-245, Lys-248 backbone, and Ser-223 and additionally Lys-248 sidechain in NSUN6, respectively (Figure 3B). Followed by an eventually rigidified cyclic-aliphatic or aromatic linker that was allowed to enter the binding site of Cyt-38 in DNMT2 or Cyt-72 in NSUN6 (docking was performed without the tRNA present in the crystal structure), a mimic of the ribose vicinal diol interaction with Asp-34 or Asp-266, respectively, was prioritized. Lastly, substructures resembling the interactions of the adenine moiety of SAH and SFG, namely an H-bond donor to Glu-58/Asp-293, and H-bond acceptors for the backbone of Ile-57/Gly-294 and Val-35/Lys-267

(enumeration DNMT2/NSUN6) incorporated in or attached to an aromatic ring system, were favored.

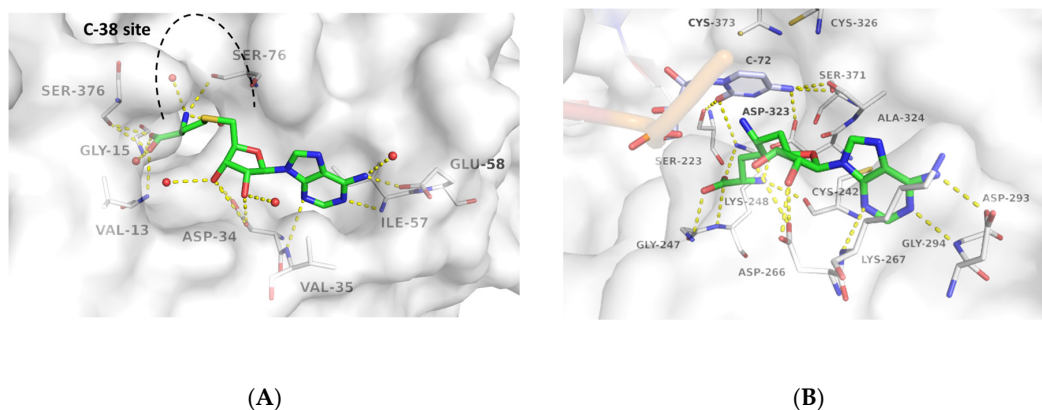


Figure 3. Binding modes of SAH-bound to DNMT2 (A) (PDB-ID 1G55) and SFG bound to NSUN6 (B) (PDB-ID 5WWR). Enzymes are shown with white surface and carbon atoms, ligands with green carbon atoms. Polar contacts are shown as yellow dashed lines, water molecules as red spheres. For clear view only residues forming polar contacts with the ligands are shown as lines and labeled as well as C-72 (light blue carbon atoms) and the catalytic Cys-residues 326 and 373 in the NSUN6-tRNA-SFG complex (B).

2.2. Binding Assay and Structure–Affinity Relationship

Due to previous library filtering (Table S1), none of the obtained compounds was flagged as PAINS [61], potential aggregators, or reactive species. All virtual screening hits were subjected to a microscale thermophoresis (MST) pre-screening at three different concentrations of 300, 100, and 33.3 μM (Tables S2 and S3). MST proved to be especially suitable as a primary binding assay due to its high sensitivity and robustness that allowed the application for very weak binders or even fragments [65] and was demonstrated to be highly accurate for DNMT2 and NSUN6 ligand identification, previously [25,66]. For the literature known reference ligand SAH, K_D values of 11.8 μM and 9.1 μM for DNMT2 and NSUN6, respectively, were determined (Table 2). Virtual screening hits showing a dose-dependent shift of thermophoresis (Tables S2 and S3) were measured at additional concentrations to obtain K_D values. However, due to limited solubility, this was not always achieved when the upper plateau of MST dose–response curves could not be reached. Subsequently, apparent K_D values ($K_{D,app}$) are presented when possible as a lower limit (indicated as $K_{D,app} \geq$ fitted value).

From the DNMT2 virtual screening, five hits could be identified as binders via MST (Table 2). The strongest binder of DNMT2 was **1.4** with $K_{D,app} = 37 \mu\text{M}$, while for **1.14** a $K_{D,app} \geq 67 \mu\text{M}$ could be determined. **1.6**, **1.17**, and **1.18** showed a reproducible, dose-dependent shift of thermophoresis in the dose–response curve and, thus, also binding. However, a $K_{D(app)}$ value could not be determined clearly and is estimated to be in the high micromolar to millimolar range.

MST confirmed five ligands out of the NSUN6 virtual screening as well. $K_{D,app}$ values of 16.4 μM , 42 μM , $\geq 72 \mu\text{M}$, $\geq 83 \mu\text{M}$ and $\geq 369 \mu\text{M}$ could be determined for **2.4**, **2.8**, **2.5**, **2.2**, and **2.1**, respectively (Table 3).

Table 2. MST results of SAH and newly identified DNMT2-ligands derived from the DNMT2 virtual screening. Measured normalized fluorescence values (F_{norm} [%]) are mean with standard error of at least duplicate determination. Apparent K_D values ($K_{D,app}$) are indicated as a lower limit (via the \geq symbol) if the upper plateau of the dose–response curve was not completely reached. In case a dose-dependent shift in thermophoresis was observed, which indicates binding, but the curve could not be fitted with sufficient accuracy (**1.6**, **1.17**, **1.18**), $K_{D,app}$ was not determined (n.d.). Molecules are depicted in their docked stereoisomers, protomers, and tautomers; however, for **1.6**, **1.17**, and **1.18**, racemic mixtures were obtained for testing. All molecules are drawn in the same orientation as SAH, with left side: amino acid mimetic, central part: ribose replacement, right side: adenine mimetic.

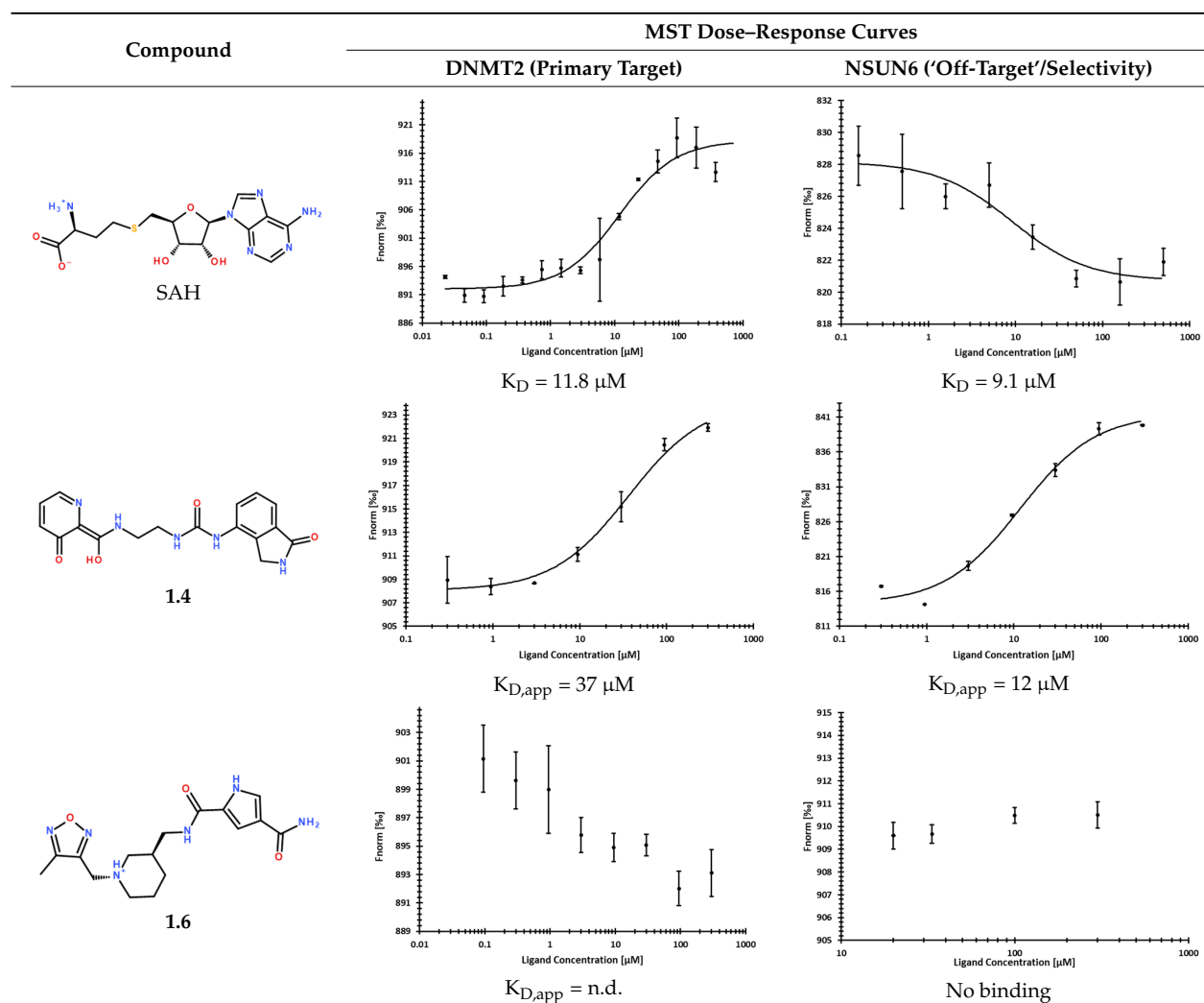
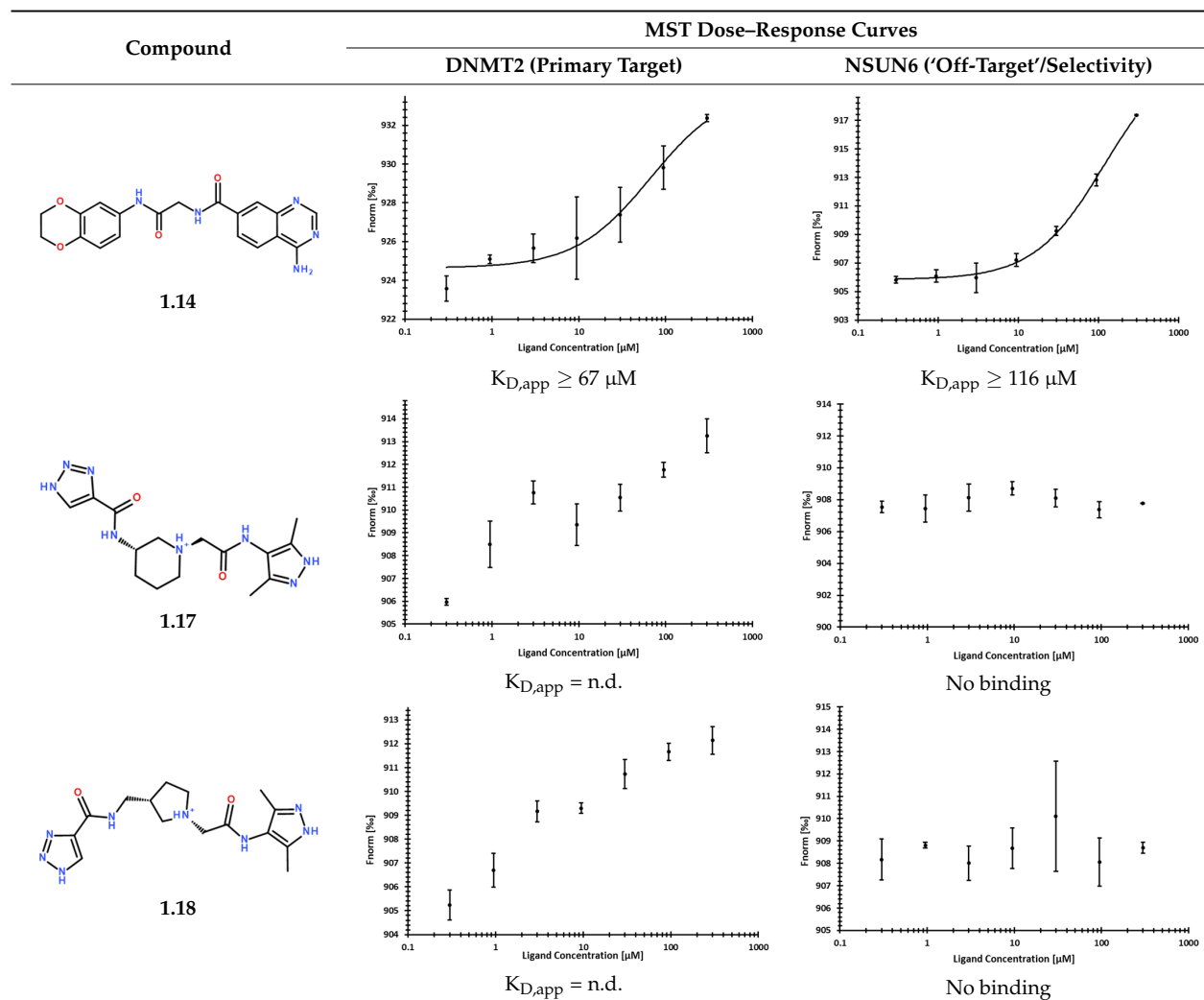


Table 2. Cont.



For DNMT2 hits (Table 2), regularly observed features in predicted binding modes were mimics of the H-bond acceptor profile of SAM's methionine amino acid carboxylate sub-structure. While not necessarily being charged, for **1.4** (Figure 4A), instead of the docked and depicted protomer, a phenolate anion also seems reasonable due to the vinylogous acid with a predicted pK_a of 7.04 (calculated with MOE). More often, H-bond acceptors were found in a heterocycle-like triazine (**1.17** and **1.18**) or oxadiazole (**1.6**). A mimic of the native ligand's basic, primary amine, however, was not found in the virtual screening hits. Connected by different types of linkers, the ribose hydroxy groups are replaced by either a urea (**1.4**, Figure 4A), an amide (**1.6**, **1.14**), or a basic nitrogen (**1.17**, **1.18**, Figure 4B) to interact with Asp-34. Lastly, the natural ligand's adenine moiety and its H-bond interaction profile with Glu-58 and Ile-57 (Figure 3A) can be mimicked by an analog 4-amino quinazoline (**1.14**), an amide either attached to (**1.6**) or part of (**1.4**, Figure 4A) a ring system, or by a 3,5-dimethyl-1*H*-pyrazole (**1.17**, **1.18**, Figure 4B).

Table 3. MST results of newly identified NSUN6-ligands derived from the NSUN6 virtual screening. Measured normalized fluorescence values (F_{norm} [%]) are mean with standard error of at least duplicate determination. Apparent K_D values ($K_{D,\text{app}}$) are indicated as a lower limit (via the \geq symbol) if the upper plateau of the dose–response curve was not completely reached. In case a dose-dependent shift in thermophoresis was observed, which indicates binding, but the curve could not be fitted with sufficient accuracy, $K_{D,\text{app}}$ was not determined (n.d.). Molecules are depicted in their docked stereoisomers, protomers, and tautomers; however, for 2.1 and 2.4, racemic mixtures were obtained for testing. All molecules are drawn in the same orientation as SAH, with left side: amino acid mimetic, central part: ribose replacement, right side: adenine mimetic.

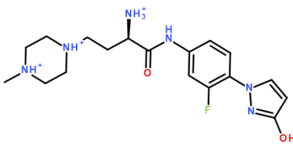
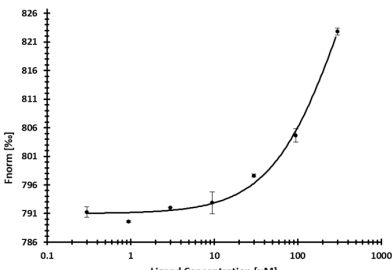
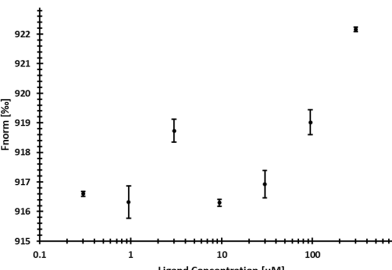
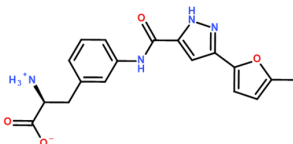
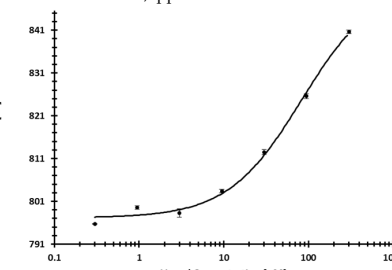
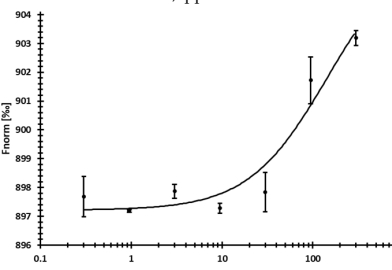
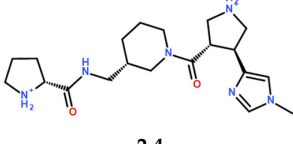
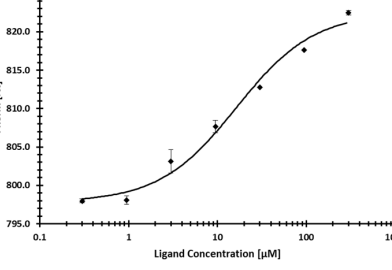
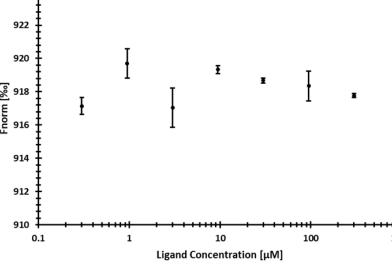
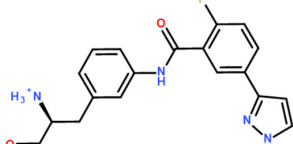
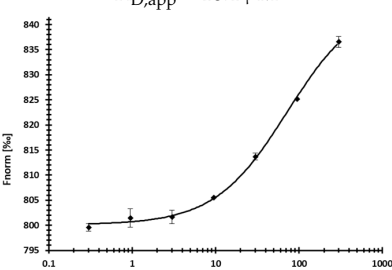
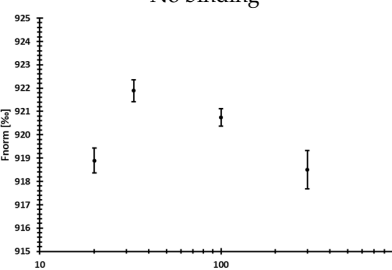
Compound	MST Results	
	NSUN6 (Primary Target)	DNMT2 ('Off-Target'/Selectivity)
 2.1	 $K_{D,\text{app}} \geq 369 \mu\text{M}$	 $K_{D,\text{app}} = \text{n.d.}$
 2.2	 $K_{D,\text{app}} \geq 83 \mu\text{M}$	 $K_{D,\text{app}} \geq 145 \mu\text{M}$
 2.4	 $K_{D,\text{app}} = 16.4 \mu\text{M}$	 No binding
 2.5	 $K_{D,\text{app}} \geq 72 \mu\text{M}$	 No binding

Table 3. Cont.

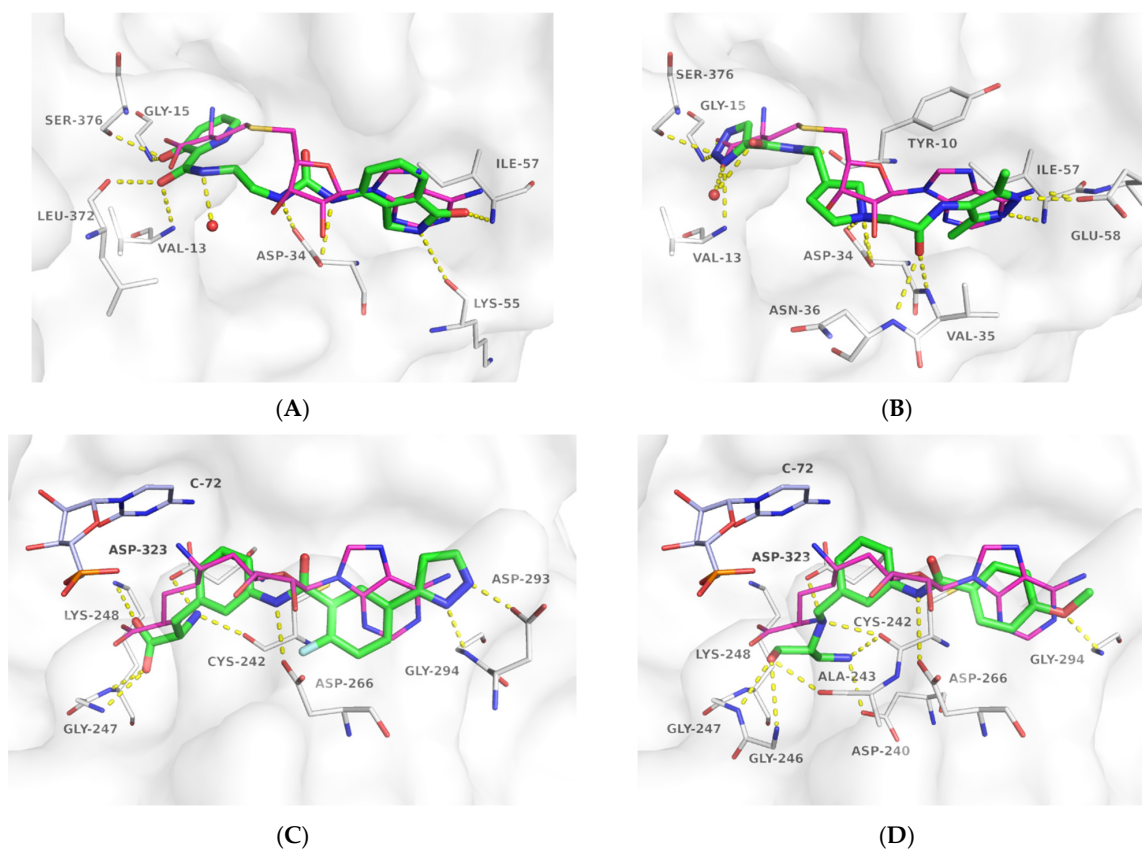
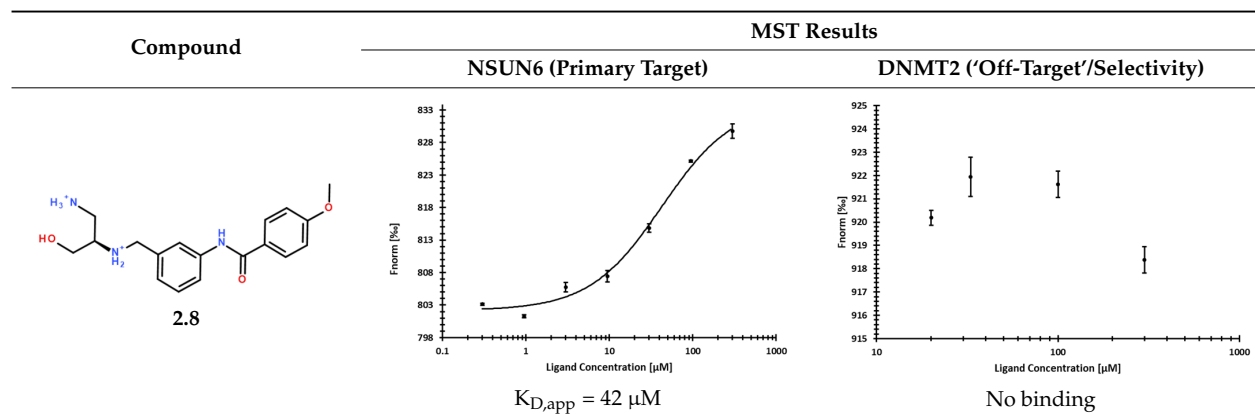


Figure 4. Predicted binding modes of **1.4** in complex with DNMT2 (A), **1.18** in complex with DNMT2 (B), **2.5** in complex with NSUN6 (C), and **2.8** in complex with NSUN6 (D). Docking poses are depicted with green carbon atoms, enzymes with white carbon atoms, and transparent surfaces. For a clear view, only residues forming polar interactions (yellow dashed lines) are shown and labeled. For orientation, the crystallographic reference ligands SAH (DNMT2, PDB-ID 1G55) and SFG (NSUN6, PDB-ID 5WWR) are shown with magenta carbon atoms. In NSUN6, C-72 is depicted with light blue carbon atoms for orientation, but tRNA was removed during molecular docking.

Differently from the DNMT2 hits where only mimetics of the acid were found, binders of NSUN6 feature the complete amino acid sub-structure (2.2, 2.5, Figure 4C, Table 3) or a basic nitrogen alone (2.1, 2.4), or even an additional positively charged group as in 2.8, which interacts with Asp 240 (Figure 4D). In 2.2, 2.5, and 2.8, a meta-substituted benzene linker was found as a common feature attached to an amide, which acts as an H-bond donor for Asp-266 replacing the interaction of one of the ribose hydroxyls according to the docking predictions (Figure 4C,D). As the adenine replacement, a variety of different one- or two-ring systems was found.

One intention of the virtual screening was the identification of novel chemotypes distinct from the native ligand SAM and eventually improved selectivity for the target RNA methyltransferase. Even though there are some differences in sequence identity and similarity within the SAM-binding sites (17% identity, 31% similarity), interaction profiles are highly conserved between DNMT2 and NSUN6 (Figure 3A,B). Testing of hits from the DNMT2 virtual screening against NSUN6 and vice versa, however, showed selectivity for 1.6, 1.17, 1.18 for DNMT2 and 2.4, 2.5, and 2.8 for NSUN6 as intended (Tables 2 and 3, right column). Molecules were defined to be selective when no MST shift was observed for the other ('off-target') enzyme at a ligand concentration of up to 300 μM . Notably, non-selective NSUN6 ligands 2.1 and 2.2 (Table 3) contain an amino acid or only the basic moiety, a feature not found in the DNMT2 virtual screening. This indicates that the presence of the basic nitrogen is underestimated in the DNMT2 docking, which was observed previously when for SAM-analog DNMT2 inhibitors, a drastic loss of potency was observed upon removal of the positively charged nitrogen from a SAH-scaffold [25]. It was hypothesized that this basic amine is involved in an H-bond network with several water molecules not captured by the docking protocol. Further, 1.4 (DNMT2 $K_{D,app} = 37 \mu\text{M}$) turned out to be the strongest binder of NSUN6 ($K_{D,app} = 12 \mu\text{M}$) even though derived from the DNMT2- and not the NSUN6-virtual screening. Likewise, 1.14 was not selective over NSUN6 with a $K_{D,app} \geq 116 \mu\text{M}$ (DNMT2 $K_{D,app} \geq 67 \mu\text{M}$), and for 2.2 from the NSUN6 docking, a DNMT2 $K_{D,app} \geq 145 \mu\text{M}$ was determined.

Lastly, compounds 1.4, 1.6, 1.14, 1.17, and 1.18 were subjected to a DNMT2 tritium incorporation activity assay at a concentration of 100 μM . However, the low binding affinity in the mid-micromolar to presumably millimolar range did not effectively translate into significant enzyme inhibition (Figure S1). Based on crystal structure analysis, there is no evidence for an allosteric druggable binding site. Eventually, the presence of substrate tRNA might induce conformational changes in the catalytic loop [67] of the enzyme-altering ligand binding strength and behavior compared to the tRNA-free MST binding assay. Another hypothesis, even though rather speculative and to be taken with caution, is that the free energy of ligand binding is spent to 'flip-out' C-38 of tRNA^{ASP} for methylation [68], forming a more stable ternary DNMT2-tRNA-inhibitor complex compared to the DNMT2-inhibitor complex alone. However, the required structural, thermodynamic, and, eventually, kinetic characterization of these complex formations is beyond the scope of this manuscript and likely requires more potent ligands for in-depth elucidation.

3. Discussion

The advance of commercial chemical spaces allows virtual screenings of a novel yet synthetically accessible chemical matter for targets of interest. Applying two different strategies of chemical space docking screens led to the identification of novel binders with $K_{D,app}$ values down to 12 μM for RNA methyltransferases that have low predicted druggability, DNMT2 and NSUN6 (Tables 2 and 3). While for both targets, the virtual screening strategy included strict physicochemical property filtering (Table S1) based on known ligands' parameters to reduce the library size to a computationally feasible number of molecules, different methods of diversification were applied (Figure 2). While for DNMT2, a larger library of 3.4 million molecules was docked and clustered afterward ('first dock, then cluster'), for NSUN6, a diversity subset was used as a starting point for filtering and docking followed by an analog search ('first cluster, then dock'). Interestingly, hit numbers

were similar for both strategies, with 5 of 18 for DNMT2 and 5 of 12 for NSUN6, respectively, even though it is hypothesized that diversity subsets might lose complete clusters of potential ligands if the cluster representatives do not resemble favorable interaction profiles [36]. This was indirectly hinted during the hit selection process when initial virtual screening hits from the REAL diversity subset for NSUN6 usually showed lower scores than their analogs from REAL Space (Table S3). However, handling the increasing size of commercial (and proprietary) [41] chemical spaces will require new strategies to focus libraries prior to computationally more expensive molecular docking screens [43–45] or improvements in fragment docking and scoring [50,51] to enhance synthon-based chemical space design within the binding site [47–49]. In this study, both DNMT2 and NSUN6 binders showed affinities in the mid-micromolar to presumably millimolar range in an MST binding assay. **1.4** and **1.14** were the strongest identified binders of DNMT2 with $K_{D,app} = 37 \mu\text{M}$ and $\geq 67 \mu\text{M}$, respectively. For NSUN6, the highest affinity was found for **2.4** ($K_{D,app} = 16.4 \mu\text{M}$) and **2.8** ($K_{D,app} = 42 \mu\text{M}$). However, selectivity between the two methyltransferases was not always achieved, as seen, for example, in compound **1.4**, which originates from the DNMT2 virtual screening but is also the strongest binder of NSUN6 with a $K_{D,app}$ of $12 \mu\text{M}$. Hence, the identified compounds can be considered initial hits as starting points for further hit-to-lead optimization. While no analogs of these novel chemotypes are available in commercial in-stock libraries, their origin from REAL Space still allows fast and easy derivatization either by the combination of the available building blocks or a direct SAR-by-catalog approach to improving the inhibitory potency and selectivity for the development of DNMT2 and NSUN6 ABPs in the future.

4. Materials and Methods

4.1. Virtual Screening

The virtual, combinatoric synthesis molecule libraries REAL Space and REAL diversity were obtained from the supplier's homepage (Enamine Ltd., <https://enamine.net/compound-collections/real-compounds/> accessed on 14 January 2019 for REAL Space and 10 August 2020 for REAL diversity) in SMILES format. Physicochemical property-filters (Table S1) to reduce library sizes were applied with MOE (Molecular Operating Environment (MOE), 2018.0101 Chemical Computing Group ULC, 1010 Sherbooke St. West, Suite #910, Montreal, QC, Canada, H3A 2R7, 2018.) and FILTER (FILTER part of OMEGA 3.1.0.3: OpenEye Scientific Software, Santa Fe, NM, USA, <http://www.eyesopen.com>, 2018). Energetically favorable 3D conformers for docking were generated using OMEGA [69].

For DNMT2 virtual screening, the DNMT2-SAH complex structure (PDB-ID 1G55) [63] and the FlexX-3.0 [70] (BiosolveIT GmbH, FlexX v.3.0 Sankt Augustin, Germany, 2018) as the docking engine were used. The docking setup was validated by re-docking of the crystallographic reference ligand SAH (FlexX-score: -38.08 kJ/mol , RMSD: 0.997 \AA). The filtered 3.45 million compound library derived from REAL Space was docked under these conditions. Top-scoring molecules of rank 1–300 were visually inspected for hit selection. Additionally, the top 20,000 molecules were clustered using MACCS fingerprints and the Tanimoto coefficient similarity metric (max. 0.65) within MOE. The top 300 clusters were also considered during hit selection for testing (Table S2).

For docking setup validation of the NSUN6 virtual screening with FlexX-4.1 (BiosolveIT GmbH, FlexX v.4.1 Sankt Augustin, Germany, 2019), re- and cross-docking of SAM and SFG from PDB-IDs 5WWR and 5WWS were performed for chains A and B in presence and absence of the tRNA present in the crystal structure, respectively [64]. Additionally, scoring was evaluated by docking SAM, SFG, and SAH and 150 decoys derived from the database of useful decoys-enhanced (DUD-E) [71] with similar physicochemical properties but distinct structural features. Even though FlexX is suitable for RNA-ligand docking [72], a docking setup without the tRNA present in the crystal structure was selected to allow potential ligands to not only bind to the SAM-, but also the Cyt-72 sub-pocket as demonstrated previously [25]. Additional interactions within this site hold the potential of improved binding affinity and selectivity while also interfering with tRNA binding. The

NSUN6 docking screen was subsequently performed with PDB-ID 5WWR, chain B, which showed reasonable posing and scoring for SFG re-docking (FlexX-score: -43.63 kJ/mol, rank: 2/153, RMSD: 1.09 Å), SAM cross-docking (FlexX-score: -46.32 kJ/mol, rank: 1/153, RMSD: 0.93 Å) and SAH docking (FlexX-score: -36.71 kJ/mol, rank: 18/153). Docking of the filtered REAL diversity library of around 400,000 molecules was performed under the same conditions. After visual inspection of the 300 top-scoring molecules, analogs of 15 molecules were searched in the complete REAL Space (at the time over 14 billion molecules) using infiniSee-1.2 [73,74] (BiosolveIT GmbH, infiniSee v.1.2 Sankt Augustin, Germany, 2019) and 99 analogs for each of the 15 initial molecules were also docked prior final compound selection for testing.

Molecules were ordered from Enamine Ltd. Custom synthesis based on the company's internal procedures was successful for 18 out of 21 compounds from the DNMT2 virtual screening (86% synthesis success rate) and 12 of 17 for the NSUN6 virtual screening (71% synthesis success rate), respectively. Identity and purity $> 90\%$ of obtained compounds were guaranteed by the supplier and confirmed for MST hits using in-house LC/ESI-MS analysis (Tables S2 and S3). HPLC/ESI-MS analysis was performed using an Agilent 1100 series HPLC system with an Agilent Poroshell 120 EC-C₁₈ (150×2.10 mm) or an Agilent Zorbax SB-Aq (4.6×150 mm) column (both at 40 °C oven temperature) with MeCN/H₂O + 0.1% HCOOH = 10:90 \rightarrow 100:0 as a mobile phase at a flow rate of 0.7 mL/min. Samples were applied using 5 μ L injection with quantitation by AUC at 254 nm or 210 nm. Electrospray ionization (ESI) mass spectra were recorded on an Agilent 1100 series LC/MSD Ion trap spectrometer in the positive ion mode.

Figures are made with PyMOL (The PyMOL Molecular Graphics System, Version 2.4.0 Schrödinger, LLC.). The background of the TOC figure was generated with craiyon (<https://www.craiyon.com/> accessed on 15 December 2022).

4.2. Protein Expression and Purification

The plasmid containing genes for DNMT2 was kindly provided by Albert Jeltsch (University of Stuttgart, Stuttgart, Germany). Expression and purification were performed as described previously with minor adaptations [25]. In brief, the concentration of sodium chloride in the buffers used for immobilized metal affinity chromatography was increased to 500 mM to remove more unspecific bound impurities from DNMT2; therefore, ion-exchange chromatography was skipped. A plasmid for the expression of NSUN6 was designed and synthesized as described previously [25] (made available via Addgene, ID: #188060, <https://www.addgene.org>). Expression and purification were performed according to the literature. Plasmids coding for each enzyme were separately transformed into *E. coli* Rosetta2 cells. These were grown in LB medium at 30 °C overnight. The next day, 1 L TB medium was inoculated with 20 mL overnight culture. Cells were grown at 37 °C until an OD₆₀₀ of ~ 0.8 was reached, then the temperature was reduced to 20 °C for DNMT2 and 16 °C for NSUN6, respectively. Overexpression of the proteins was induced by adding isopropyl- β -D-thiogalactopyranoside (IPTG) to a final concentration of 500 μ M. Overexpression was maintained overnight. Cells were harvested by centrifugation. After cell lysis by sonication, cell debris was removed by centrifugation, and the supernatant was subjected to immobilized metal affinity chromatography (Ni²⁺-NTA, HisTrap HP, 5 mL) for further purification a size-exclusion chromatography (Superdex 16/600 75 PG) was performed using an ÄKTA Start (GE Healthcare, Chicago, IL, USA). Glycerol concentrations were adjusted to allow liquid storage of proteins at -20 °C until further use.

4.3. Microscale Thermophoresis

Since the constructs of DNMT2 and NSUN6 contain hexa-histidine tags, proteins were labeled using a Monolith His-Tag Labeling Kit RED-Tris-NTA 2nd generation according to the manufacturer's instructions. This labeling strategy was chosen since it should prevent any interference with the actual binding site of the proteins. Labeled protein was diluted to a concentration of 20 nM into MST buffer (50 mM Hepes, pH 7.5, 150 mM NaCl, 10 mM

MgCl₂, 1 mM DTT, 0.05% polysorbate-20, 0.1% PEG-8000). All compounds were prepared as stocks dissolved in DMSO to a concentration of 50 mM. For all compounds, dilutions in MST buffer to concentrations of 600 μM, 200 μM, and 66.7 μM, respectively, were prepared. Labeled protein was then mixed 1:1 with the dilution series of each compound (final concentrations: 10 nM protein, ligands 300, 100, and 33.3 μM, respectively) and incubated for 5 min at room temperature. All measurements were performed on a Monolith Pico instrument (NanoTemper Technologies, Muenchen, Germany) with red light. To induce thermophoresis, medium MST power was selected for DNMT2 and high MST power for NSUN6. All experiments were performed in quadruplicates. For all compounds that showed a concentration-dependent thermophoresis behavior, a half-logarithmic dilution series was prepared to cover a range from 600 μM to 600 nM. Obtained dilutions were then mixed 1:1 with labeled protein (20 nM) and incubated for 5 min at room temperature prior to measurement. Experiments were performed in duplicates. All data received were analyzed using the MO. Affinity Analysis software version 2.3 (NanoTemper Technologies, Muenchen, Germany).

4.4. Tritium Incorporation Assay

DNMT2 activity assays were carried out in 20 μL containing 100 mM Tris-HCl, pH 8, 100 mM NH₄OAc, 0.1 mM EDTA, 10 mM MgCl₂, and 10 mM DTT. The amount of DMSO in the reaction mixture was adjusted to 5%, while tRNA^{Asp} was added to a final concentration of 5 μM after heating it to 75 °C for 5 min and slowly cooling it to room temperature. To this, SAM was added as a mixture of cold SAM (New England Biolabs GmbH, Ipswich, MA, USA) and ³H-SAM (Hartmann Analytics, Braunschweig, Germany) to final concentrations of 0.9 μM and 0.025 μCi μL⁻¹. DNMT2 was added last to a concentration of 250 nM, and enzymatic reactions were run at 37 °C. Aliquots of 8 μL were taken out of the reaction mixture at 0 and 20 min, spotted on Whatman[®] glass microfiber filters (GF/C, 25 mm), and transferred into an ice-cold trichloroacetic acid (TCA) solution (5%) where they were kept for at least 15 min. Subsequently, two washing steps with the TCA solution (5%) for 20 and 10 min and one with EtOH for 10 min were carried out at room temperature. The filters were dried and placed into scintillation vials. A total of 3 mL of Gold MV liquid scintillation cocktail (PerkinElmer, Waltham, MA, USA) was added before scintillation was measured for 1 min on a scintillation counter (TriCarb[®] Liquid Scintillation Analyzer 4810TR, PerkinElmer, Waltham, MA, USA). For the inhibition assay, compounds were present at a final concentration of 100 μM during the enzymatic reaction, and inhibition in percent was calculated by referencing the scintillation signal to a positive control without compound. All experiments were carried out in biological triplicates, while errors refer to the obtained standard deviation.

Supplementary Materials: The following supporting information can be downloaded at: <https://www.mdpi.com/article/10.3390/ijms24076109/s1>. References [33,61,62,75] are cited in Supplementary Materials.

Author Contributions: Conceptualization, C.K.; methodology, R.A.Z., T.R.F., M.S. and C.K.; software, C.K.; validation, R.A.Z. and C.K.; formal analysis, T.S. and C.K.; investigation, R.A.Z., T.R.F., M.S., Z.N. and C.K.; resources, T.S.; data curation, R.A.Z. and C.K.; writing—original draft preparation, R.A.Z. and C.K.; writing—review and editing, R.A.Z., T.S. and C.K.; visualization, R.A.Z. and C.K.; supervision, T.S. and C.K.; project administration, T.S. and C.K.; funding acquisition, T.S. All authors have read and agreed to the published version of the manuscript.

Funding: Financial support by the DFG (Deutsche Forschungsgemeinschaft) in the framework of the Transregio Collaborative Research Center TRR 319 (RMaP, RNA Modification, and Processing), projects A01 (T.S.), and by the Volkswagen Stiftung (Z.N.), is gratefully acknowledged. The MST instrument was provided by the Bundesministerium für Bildung und Forschung (BMBF) to Mark Helm, who is gratefully acknowledged for access to the instrument and scientific discussion (BMBF/01ED1804).

Institutional Review Board Statement: Not applicable.

Informed Consent Statement: Not applicable.

Data Availability Statement: Not applicable.

Acknowledgments: Parts of this research were conducted using the supercomputer MOGON and/or advisory services offered by Johannes Gutenberg University Mainz (hpc.uni-mainz.de), which is a member of the AHRP (Alliance for High-Performance Computing in Rhineland Palatinate, www.ahrp.info) and the Gauss Alliance e.V. The authors gratefully acknowledge the computing time granted on the supercomputer Mogon at Johannes Gutenberg University Mainz (hpc.uni-mainz.de). We further thank OpenEye Scientific (<https://www.eyesopen.com/>) for free academic software licenses. We additionally thank Chloé Astrid Walter, Wenyu Eva Zhu, and Zahra Riazimand for their support in the lab.

Conflicts of Interest: The authors declare no conflict of interest.

Abbreviations

ABP, activity-based probe; AML, acute myeloid leukemia; AmpC, β -lactamase; CB₁, cannabinoid receptor type 1; D₄, dopamine receptor type 4; DNMT2, RNA methyltransferase 2; GPCR, G-protein-coupled receptor; 5-HT_{2A}, serotonin receptor type 2A; HTS, high-throughput screening; IPTG, isopropyl- β -D-thiogalactopyranoside; KEAP1, Kelch-like ECH-associated protein 1; m5C, 5-methylcytosine; METTL3, methyltransferase 3; ML, machine learning; MST, microscale thermophoresis; MT1, melatonin receptor type 1; NSUN6, Nol1/Nop2/SUN 6; PDB, protein data bank; PKA, protein kinase A; PSA, polar surface area; REAL, readily accessible; SAH, S-adenosyl homocysteine; SAM, S-adenosyl methionine; SARS-CoV-2 Mpro, severe acute respiratory syndrome coronavirus-2 main protease; SFG, simefungin; SMILES, simplified molecular input line entry specification; TCA, trichloroacetic acid.

References

- Jung, Y.; Goldman, D. Role of RNA Modifications in Brain and Behavior. *Genes Brain Behav.* **2018**, *17*, e12444. [[CrossRef](#)] [[PubMed](#)]
- Boo, S.H.; Kim, Y.K. The Emerging Role of RNA Modifications in the Regulation of mRNA Stability. *Exp. Mol. Med.* **2020**, *52*, 400–408. [[CrossRef](#)] [[PubMed](#)]
- Barbieri, I.; Kouzarides, T. Role of RNA Modifications in Cancer. *Nat. Rev. Cancer* **2020**, *20*, 303–322. [[CrossRef](#)]
- Thompson, M.G.; Sacco, M.T.; Horner, S.M. How RNA Modifications Regulate the Antiviral Response. *Immunol. Rev.* **2021**, *304*, 169–180. [[CrossRef](#)]
- Dunin-Horkawicz, S.; Czerwoniec, A.; Gajda, M.J.; Feder, M.; Grosjean, H.; Bujnicki, J.M. MODOMICS: A Database of RNA Modification Pathways. *Nucleic Acids Res.* **2006**, *34*, 145–149. [[CrossRef](#)] [[PubMed](#)]
- Boccalletto, P.; MacHnicka, M.A.; Purta, E.; Pitkowski, P.; Baginski, B.; Wirecki, T.K.; De Crécy-Lagard, V.; Ross, R.; Limbach, P.A.; Kotter, A.; et al. MODOMICS: A Database of RNA Modification Pathways. 2017 Update. *Nucleic Acids Res.* **2018**, *46*, D303–D307. [[CrossRef](#)]
- Boccalletto, P.; Stefaniak, F.; Ray, A.; Cappannini, A.; Mukherjee, S.; Purta, E.; Kurkowska, M.; Shirvanizadeh, N.; Destefanis, E.; Groza, P.; et al. MODOMICS: A Database of RNA Modification Pathways. 2021 Update. *Nucleic Acids Res.* **2022**, *50*, D231–D235. [[CrossRef](#)]
- Yankova, E.; Blackaby, W.; Albertella, M.; Rak, J.; De Braekeleer, E.; Tsagkogeorga, G.; Pilka, E.S.; Aspris, D.; Leggate, D.; Hendrick, A.G.; et al. Small-Molecule Inhibition of METTL3 as a Strategy against Myeloid Leukaemia. *Nature* **2021**, *593*, 597–601. [[CrossRef](#)]
- Fischer, T.R.; Meidner, L.; Schwickert, M.; Weber, M.; Zimmermann, R.A.; Kersten, C.; Schirmeister, T.; Helm, M. Chemical Biology and Medicinal Chemistry of RNA Methyltransferases. *Nucleic Acids Res.* **2022**, *50*, 4216–4245. [[CrossRef](#)]
- Popis, M.C.; Blanco, S.; Frye, M. Posttranscriptional Methylation of Transfer and Ribosomal RNA in Stress Response Pathways, Cell Differentiation, and Cancer. *Curr. Opin. Oncol.* **2016**, *28*, 65–71. [[CrossRef](#)]
- Goll, M.G.; Kirpekar, F.; Maggert, K.A.; Yoder, J.A.; Hsieh, C.L.; Zhang, X.; Golic, K.G.; Jacobsen, S.E.; Bestor, T.H. Methylation of TRNA^{Asp} by the DNA Methyltransferase Homolog Dnmt2. *Science* **2006**, *311*, 395–398. [[CrossRef](#)] [[PubMed](#)]
- Jeltsch, A.; Nellen, W.; Lyko, F. Two Substrates Are Better than One: Dual Specificities for Dnmt2 Methyltransferases. *Trends Biochem. Sci.* **2006**, *31*, 306–308. [[CrossRef](#)]
- Jeltsch, A.; Ehrenhofer-Murray, A.; Jurkowski, T.P.; Lyko, F.; Reuter, G.; Ankri, S.; Nellen, W.; Schaefer, M.; Helm, M. Mechanism and Biological Role of Dnmt2 in Nucleic Acid Methylation. *RNA Biol.* **2017**, *14*, 1108–1123. [[CrossRef](#)]
- Schaefer, M.; Lyko, F. Solving the Dnmt2 Enigma. *Chromosoma* **2010**, *119*, 35–40. [[CrossRef](#)]
- Schaefer, M.; Pollex, T.; Hanna, K.; Tuorto, F.; Meusburger, M.; Helm, M.; Lyko, F. RNA Methylation by Dnmt2 Protects Transfer RNAs against Stress-Induced Cleavage. *Genes Dev.* **2010**, *24*, 1590–1595. [[CrossRef](#)]

16. Tuorto, F.; Liebers, R.; Musch, T.; Schaefer, M.; Hofmann, S.; Kellner, S.; Frye, M.; Helm, M.; Stoecklin, G.; Lyko, F. RNA Cytosine Methylation by Dnmt2 and NSun2 Promotes TRNA Stability and Protein Synthesis. *Nat. Struct. Mol. Biol.* **2012**, *19*, 900–905. [[CrossRef](#)]
17. Tuorto, F.; Herbst, F.; Alerasool, N.; Bender, S.; Popp, O.; Federico, G.; Reitter, S.; Liebers, R.; Stoecklin, G.; Gröne, H.; et al. The TRNA Methyltransferase Dnmt2 Is Required for Accurate Polypeptide Synthesis during Haematopoiesis. *EMBO J.* **2015**, *34*, 2350–2362. [[CrossRef](#)] [[PubMed](#)]
18. Shanmugam, R.; Fierer, J.; Kaiser, S.; Helm, M.; Jurkowski, T.P.; Jeltsch, A. Cytosine Methylation of TRNA-Asp by DNMT2 Has a Role in Translation of Proteins Containing Poly-Asp Sequences. *Cell Discov.* **2015**, *1*, 15010. [[CrossRef](#)]
19. Elhardt, W.; Shanmugam, R.; Jurkowski, T.P.; Jeltsch, A. Somatic Cancer Mutations in the DNMT2 TRNA Methyltransferase Alter Its Catalytic Properties. *Biochimie* **2015**, *112*, 66–72. [[CrossRef](#)]
20. Forbes, S.A.; Beare, D.; Gunasekaran, P.; Leung, K.; Bindal, N.; Boutselakis, H.; Ding, M.; Bamford, S.; Cole, C.; Ward, S.; et al. COSMIC: Exploring the World’s Knowledge of Somatic Mutations in Human Cancer. *Nucleic Acids Res.* **2015**, *43*, D805–D811. [[CrossRef](#)] [[PubMed](#)]
21. Zhang, Y.; Zhang, X.; Shi, J.; Tuorto, F.; Li, X.; Liu, Y.; Liebers, R.; Zhang, L.; Qu, Y.; Qian, J.; et al. Dnmt2 Mediates Intergenerational Transmission of Paternally Acquired Metabolic Disorders through Sperm Small Non-Coding RNAs. *Nat. Cell Biol.* **2018**, *20*, 535–540. [[CrossRef](#)] [[PubMed](#)]
22. Zhou, L.; Cheng, X.; Connolly, B.A.; Dickman, M.J.; Hurd, P.J.; Hornby, D.P. Zebularine: A Novel DNA Methylation Inhibitor That Forms a Covalent Complex with DNA Methyltransferases. *J. Mol. Biol.* **2002**, *321*, 591–599. [[CrossRef](#)] [[PubMed](#)]
23. Schaefer, M.; Hagemann, S.; Hanna, K.; Lyko, F. Azacytidine Inhibits RNA Methylation at DNMT2 Target Sites in Human Cancer Cell Lines. *Cancer Res.* **2009**, *69*, 8127–8132. [[CrossRef](#)] [[PubMed](#)]
24. Halby, L.; Marechal, N.; Pechalrieu, D.; Cura, V.; Franchini, D.M.; Faux, C.; Alby, F.; Troffer-Charlier, N.; Kudithipudi, S.; Jeltsch, A.; et al. Hijacking DNA Methyltransferase Transition State Analogues to Produce Chemical Scaffolds for Prmt Inhibitors. *Philos. Trans. R. Soc. B Biol. Sci.* **2018**, *373*, 20170072. [[CrossRef](#)]
25. Schwickert, M.; Fischer, T.R.; Zimmermann, R.A.; Hoba, S.N.; Meidner, J.L.; Weber, M.; Weber, M.; Stark, M.M.; Koch, J.; Jung, N.; et al. Discovery of Inhibitors of DNA Methyltransferase 2, an Epitranscriptomic Modulator and Potential Target for Cancer Treatment. *J. Med. Chem.* **2022**, *65*, 9750–9788. [[CrossRef](#)]
26. Haag, S.; Warda, A.S.; Kretschmer, J.; Günnigmann, M.A.; Höbartner, C.; Bohnsack, M.T. NSUN6 Is a Human RNA Methyltransferase That Catalyzes Formation of M5C72 in Specific TRNAs. *RNA* **2015**, *21*, 1532–1543. [[CrossRef](#)]
27. Selmi, T.; Hussain, S.; Dieltmann, S.; Heiß, M.; Borland, K.; Flad, S.; Carter, J.M.; Dennison, R.; Huang, Y.L.; Kellner, S.; et al. Sequence- And Structure-Specific Cytosine-5 MRNA Methylation by NSUN6. *Nucleic Acids Res.* **2021**, *49*, 1006–1022. [[CrossRef](#)]
28. Li, C.; Wang, S.; Xing, Z.; Lin, A.; Liang, K.; Song, J.; Hu, Q.; Yao, J.; Chen, Z.; Park, P.K.; et al. A ROR1-HER3-LncRNA Signalling Axis Modulates the Hippo-YAP Pathway to Regulate Bone Metastasis. *Nat. Cell Biol.* **2017**, *19*, 106–119. [[CrossRef](#)]
29. Wang, W.; Huang, H.; Jiang, H.; Tian, C.; Tang, Y.; Gan, D.; Wen, X.; Song, Z.; He, Y.; Ou, X.; et al. A Cross-Tissue Investigation of Molecular Targets and Physiological Functions of Nsun6 Using Knockout Mice. *Int. J. Mol. Sci.* **2022**, *23*, 6584. [[CrossRef](#)]
30. Arrowsmith, C.H.; Audia, J.E.; Austin, C.; Baell, J.; Bennett, J.; Blagg, J.; Bountra, C.; Brennan, P.E.; Brown, P.J.; Bunnage, M.E.; et al. The Promise and Peril of Chemical Probes. *Nat. Chem. Biol.* **2015**, *11*, 536–541. [[CrossRef](#)]
31. Lee, J.; Schapira, M. The Promise and Peril of Chemical Probe Negative Controls. *ACS Chem. Biol.* **2021**, *16*, 579–585. [[CrossRef](#)]
32. Irwin, J.J.; Tang, K.G.; Young, J.; Dandarchuluun, C.; Wong, B.R.; Khurelbaatar, M.; Moroz, Y.S.; Mayfield, J.; Sayle, R.A. ZINC20—A Free Ultralarge-Scale Chemical Database for Ligand Discovery. *J. Chem. Inf. Model.* **2020**, *60*, 6065–6073. [[CrossRef](#)]
33. Lipinski, C.A.; Lombardo, F.; Dominy, B.W.; Feeney, P.J. Experimental and Computational Approaches to Estimate Solubility and Permeability in Drug Discovery and Development Settings. *Adv. Drug Deliv. Rev.* **2001**, *46*, 3–26. [[CrossRef](#)] [[PubMed](#)]
34. Hoffmann, T.; Gastreich, M. The next Level in Chemical Space Navigation: Going Far beyond Enumerable Compound Libraries. *Drug Discov. Today* **2019**, *24*, 1148–1156. [[CrossRef](#)] [[PubMed](#)]
35. Bellmann, L.; Penner, P.; Gastreich, M.; Rarey, M. Comparison of Combinatorial Fragment Spaces and Its Application to Ultralarge Make-on-Demand Compound Catalogs. *J. Chem. Inf. Model.* **2022**, *62*, 553–566. [[CrossRef](#)] [[PubMed](#)]
36. Lyu, J.; Wang, S.; Balius, T.E.; Singh, I.; Levit, A.; Moroz, Y.S.; O’Meara, M.J.; Che, T.; Alga, E.; Tolmachova, K.; et al. Ultra-Large Library Docking for Discovering New Chemotypes. *Nature* **2019**, *566*, 224–229. [[CrossRef](#)] [[PubMed](#)]
37. Bender, B.J.; Gahbauer, S.; Lutten, A.; Lyu, J.; Webb, C.M.; Stein, R.M.; Fink, E.A.; Balius, T.E.; Carlsson, J.; Irwin, J.J.; et al. A Practical Guide to Large-Scale Docking. *Nat. Protoc.* **2021**, *16*, 4799–4832. [[CrossRef](#)]
38. Stein, R.M.; Kang, H.J.; McCorvy, J.D.; Glatfelter, G.C.; Jones, A.J.; Che, T.; Slocum, S.; Huang, X.P.; Savych, O.; Moroz, Y.S.; et al. Virtual Discovery of Melatonin Receptor Ligands to Modulate Circadian Rhythms. *Nature* **2020**, *579*, 609–614. [[CrossRef](#)]
39. Gorgulla, C.; Boeszoemenyi, A.; Wang, Z.F.; Fischer, P.D.; Coote, P.W.; Padmanabha Das, K.M.; Malets, Y.S.; Radchenko, D.S.; Moroz, Y.S.; Scott, D.A.; et al. An Open-Source Drug Discovery Platform Enables Ultra-Large Virtual Screens. *Nature* **2020**, *580*, 663–668. [[CrossRef](#)]
40. Yang, Y.; Yao, K.; Repasky, M.P.; Leswing, K.; Abel, R.; Shoichet, B.K.; Jerome, S.V. Efficient Exploration of Chemical Space with Docking and Deep Learning. *J. Chem. Theory Comput.* **2021**, *17*, 7106–7119. [[CrossRef](#)]
41. Warr, W.A.; Nicklaus, M.C.; Nicolaou, C.A.; Rarey, M. Exploration of Ultralarge Compound Collections for Drug Discovery. *J. Chem. Inf. Model.* **2022**, *62*, 2021–2034. [[CrossRef](#)]
42. Gloriam, D.E. Bigger Is Better in Virtual Drug Screens. *Nature* **2019**, *566*, 193–194. [[CrossRef](#)]

43. Clark, D.E. Virtual Screening: Is Bigger Always Better? Or Can Small Be Beautiful? *J. Chem. Inf. Model.* **2020**, *60*, 4120–4123. [[CrossRef](#)]
44. Grebner, C.; Malmerberg, E.; Shewmaker, A.; Batista, J.; Nicholls, A.; Sadowski, J. Virtual Screening in the Cloud: How Big Is Big Enough? *J. Chem. Inf. Model.* **2020**, *60*, 4274–4282. [[CrossRef](#)] [[PubMed](#)]
45. Kaplan, A.L.; Confair, D.N.; Kim, K.; Barros-Álvarez, X.; Rodriguiz, R.M.; Yang, Y.; Kweon, O.S.; Che, T.; McCorvy, J.D.; Kamber, D.N.; et al. *Bespoke Library Docking for 5-HT_{2A} Receptor Agonists with Antidepressant Activity*; Springer: New York, NY, USA, 2022; Volume 610, ISBN 4158602205258.
46. Metz, A.; Wollenhaupt, J.; Glöckner, S.; Messini, N.; Huber, S.; Barthel, T.; Merabet, A.; Gerber, H.D.; Heine, A.; Klebe, G.; et al. Frag4Lead: Growing Crystallographic Fragment Hits by Catalog Using Fragment-Guided Template Docking. *Acta Crystallogr. Sect. D Struct. Biol.* **2021**, *77*, 1168–1182. [[CrossRef](#)] [[PubMed](#)]
47. Müller, J.; Klein, R.; Tarkhanova, O.; Gryniukova, A.; Borysko, P.; Merkl, S.; Ruf, M.; Neumann, A.; Gastreich, M.; Moroz, Y.S.; et al. Magnet for the Needle in Haystack: “Crystal Structure First” Fragment Hits Unlock Active Chemical Matter Using Targeted Exploration of Vast Chemical Spaces. *J. Med. Chem.* **2022**, *65*, 15663–15678. [[CrossRef](#)]
48. Sadybekov, A.A.; Sadybekov, A.V.; Liu, Y.; Iliopoulos-Tsoutsouvas, C.; Huang, X.P.; Pickett, J.; Houser, B.; Patel, N.; Tran, N.K.; Tong, F.; et al. Synthon-Based Ligand Discovery in Virtual Libraries of over 11 Billion Compounds. *Nature* **2022**, *601*, 452–459. [[CrossRef](#)]
49. Beroza, P.; Crawford, J.J.; Ganichkin, O.; Gendele, L.; Harris, S.F.; Klein, R.; Miu, A.; Steinbacher, S.; Klingler, F.M.; Lemmen, C. Chemical Space Docking Enables Large-Scale Structure-Based Virtual Screening to Discover ROCK1 Kinase Inhibitors. *Nat. Commun.* **2022**, *13*, 6447. [[CrossRef](#)]
50. Verdonk, M.L.; Giangreco, I.; Hall, R.J.; Korb, O.; Mortenson, P.N.; Murray, C.W. Docking Performance of Fragments and Druglike Compounds. *J. Med. Chem.* **2011**, *54*, 5422–5431. [[CrossRef](#)] [[PubMed](#)]
51. Chachulski, L.; Windshügel, B. LEADS-FRAG: A Benchmark Data Set for Assessment of Fragment Docking Performance. *J. Chem. Inf. Model.* **2020**, *60*, 6544–6554. [[CrossRef](#)] [[PubMed](#)]
52. Luttns, A.; Gullberg, H.; Abdurakhmanov, E.; Vo, D.D.; Akaberi, D.; Talibov, V.O.; Nekhotiaeva, N.; Vangeel, L.; De Jonghe, S.; Jochmans, D.; et al. Ultralarge Virtual Screening Identifies SARS-CoV-2 Main Protease Inhibitors with Broad-Spectrum Activity against Coronaviruses. *J. Am. Chem. Soc.* **2022**, *144*, 2905–2920. [[CrossRef](#)] [[PubMed](#)]
53. Rossetti, G.G.; Ossorio, M.A.; Rempel, S.; Kratzel, A.; Dionellis, V.S.; Barriot, S.; Tropia, L.; Gorgulla, C.; Arthanari, H.; Thiel, V.; et al. Non-Covalent SARS-CoV-2 Mpro Inhibitors Developed from in Silico Screen Hits. *Sci. Rep.* **2022**, *12*, 2505. [[CrossRef](#)] [[PubMed](#)]
54. Cerón-Carrasco, J.P. When Virtual Screening Yields Inactive Drugs: Dealing with False Theoretical Friends. *ChemMedChem* **2022**, *17*, e202200278. [[CrossRef](#)] [[PubMed](#)]
55. Ton, A.T.; Gentile, F.; Hsing, M.; Ban, F.; Cherkasov, A. Rapid Identification of Potential Inhibitors of SARS-CoV-2 Main Protease by Deep Docking of 1.3 Billion Compounds. *Mol. Inform.* **2020**, *39*, e2000028. [[CrossRef](#)] [[PubMed](#)]
56. Pappalardi, M.B.; Keenan, K.; Cockerill, M.; Kellner, W.A.; Stowell, A.; Sherk, C.; Wong, K.; Pathuri, S.; Briand, J.; Steidel, M.; et al. Discovery of a First-in-Class Reversible DNMT1-Selective Inhibitor with Improved Tolerability and Efficacy in Acute Myeloid Leukemia. *Nat. Cancer* **2021**, *2*, 1002–1017. [[CrossRef](#)]
57. Macip, G.; Garcia-segura, P.; Mestres-truyol, J.; Saldívar-espinoza, B.; Pujadas, G.; Garcia-Vallvé, S. A Review of the Current Landscape of SARS-CoV-2 Main Protease Inhibitors: Have We Hit the Bullseye Yet? *Int. J. Mol. Sci.* **2022**, *23*, 259. [[CrossRef](#)]
58. Volkamer, A.; Griewel, A.; Grombacher, T.; Rarey, M. Analyzing the Topology of Active Sites: On the Prediction of Pockets and Subpockets. *J. Chem. Inf. Model.* **2010**, *50*, 2041–2052. [[CrossRef](#)]
59. Volkamer, A.; Kuhn, D.; Grombacher, T.; Rippmann, F.; Rarey, M. Combining Global and Local Measures for Structure-Based Druggability Predictions. *J. Chem. Inf. Model.* **2012**, *52*, 360–372. [[CrossRef](#)]
60. Baell, J.B.; Holloway, G.A. New Substructure Filters for Removal of Pan Assay Interference Compounds (PAINS) from Screening Libraries and for Their Exclusion in Bioassays. *J. Med. Chem.* **2010**, *53*, 2719–2740. [[CrossRef](#)]
61. Baell, J.; Walters, M.A. Chemistry: Chemical Con Artists Foil Drug Discovery. *Nature* **2014**, *513*, 481–483. [[CrossRef](#)]
62. Oprea, T.I. Property Distribution of Drug-Related Chemical Databases. *J. Comput. Aided Mol. Des.* **2000**, *14*, 251–264. [[CrossRef](#)]
63. Dong, A.; Yoder, J.A.; Zhang, X.; Zhou, L.; Bestor, T.H.; Cheng, X. Structure of Human DNMT2, an Enigmatic DNA Methyltransferase Homolog That Displays Denaturant-Resistant Binding to DNA. *Nucleic Acids Res.* **2001**, *29*, 439–448. [[CrossRef](#)] [[PubMed](#)]
64. Liu, R.-J.; Long, T.; Li, J.; Li, H.; Wang, E.-D. Structural Basis for Substrate Binding and Catalytic Mechanism of a Human RNA:M⁵C Methyltransferase NSun6. *Nucleic Acids Res.* **2017**, *45*, 6684–6697. [[CrossRef](#)] [[PubMed](#)]
65. Linke, P.; Amaning, K.; Maschberger, M.; Vallee, F.; Steier, V.; Baaske, P.; Duhr, S.; Breitsprecher, D.; Rak, A. An Automated Microscale Thermophoresis Screening Approach for Fragment-Based Lead Discovery. *J. Biomol. Screen.* **2016**, *21*, 414–421. [[CrossRef](#)]
66. Zimmermann, R.A.; Schwickert, M.; Meidner, J.L.; Nidoieva, Z.; Helm, M.; Schirmeister, T. An Optimized Microscale Thermophoresis Method for High-Throughput Screening of DNA Methyltransferase 2 Ligands. *ACS Pharmacol. Transl. Sci.* **2022**, *5*, 1079–1085. [[CrossRef](#)]
67. Li, S.; Du, J.; Yang, H.; Yin, J.; Ding, J.; Zhong, J. Functional and Structural Characterization of DNMT2 from Spodoptera Frugiperda. *J. Mol. Cell Biol.* **2013**, *5*, 64–66. [[CrossRef](#)]

68. Li, H.; Zhu, D.; Wu, J.; Ma, Y.; Cai, C.; Chen, Y.; Qin, M.; Dai, H. New Substrates and Determinants for TRNA Recognition of RNA Methyltransferase DNMT2/TRDMT1. *RNA Biol.* **2021**, *18*, 2531–2545. [[CrossRef](#)]
69. Hawkins, P.C.D.; Skillman, A.G.; Warren, G.L.; Ellingson, B.A.; Stahl, M.T. Conformer Generation with OMEGA: Algorithm and Validation Using High Quality Structures from the Protein Databank and Cambridge Structural Database. *J. Chem. Inf. Model.* **2010**, *50*, 572–584. [[CrossRef](#)]
70. Rarey, M.; Kramer, B.; Lengauer, T.; Klebe, G. A Fast Flexible Docking Method Using an Incremental Construction Algorithm. *J. Mol. Biol.* **1996**, *261*, 470–489. [[CrossRef](#)] [[PubMed](#)]
71. Mysinger, M.M.; Carchia, M.; Irwin, J.J.; Shoichet, B.K. Directory of Useful Decoys, Enhanced (DUD-E): Better Ligands and Decoys for Better Benchmarking. *J. Med. Chem.* **2012**, *55*, 6582–6594. [[CrossRef](#)]
72. Kallert, E.; Fischer, T.R.; Schneider, S.; Grimm, M.; Helm, M.; Kersten, C. Protein-Based Virtual Screening Tools Applied for RNA-Ligand Docking Identify New Binders of the PreQ1-Riboswitch. *J. Chem. Inf. Model.* **2022**, *62*, 4134–4148. [[CrossRef](#)] [[PubMed](#)]
73. Rarey, M.; Dixon, J.S. Feature Trees: A New Molecular Similarity Measure Based on Tree Matching. *J. Comput. Aided. Mol. Des.* **1998**, *12*, 471–490. [[CrossRef](#)] [[PubMed](#)]
74. Rarey, M.; Stahl, M. Similarity Searching in Large Combinatorial Chemistry Spaces. *J. Comput. Aided. Mol. Des.* **2001**, *15*, 497–520. [[CrossRef](#)] [[PubMed](#)]
75. Wang, R.; Fu, Y.; Lai, L. A New Method for Calculating Partition Coefficients of Organic Compounds. *Acta Phys.-Chim. Sin.* **1997**, *13*, 615–621. [[CrossRef](#)]

Disclaimer/Publisher's Note: The statements, opinions and data contained in all publications are solely those of the individual author(s) and contributor(s) and not of MDPI and/or the editor(s). MDPI and/or the editor(s) disclaim responsibility for any injury to people or property resulting from any ideas, methods, instructions or products referred to in the content.

Chemical Space Virtual Screening against Hard-to-Drug RNA Methyltransferases DNMT2 and NSUN6

*Robert A. Zimmermann¹, Tim R. Fischer¹, Marvin Schwickert¹, Zarina Nidoieva¹, Tanja Schirmeister¹, Christian Kersten¹ **

¹Institute of Pharmaceutical and Biomedical Sciences, Johannes Gutenberg-University, Staudingerweg 5, 55128 Mainz, Germany

*correspondence: Christian Kersten, E-mail: kerstec@uni-mainz.de

Content:

Tables S1-S3

Figure S1

References

Table S1: Physicochemical property filtering criteria.

parameter
no PAINS [1]
non-reactive
no predicted aggregators
predicted water solubility: <i>poor</i> or better [2]
allowed elements: H,C,N,O,F,P,S,Cl,Br,I
RO5 [3] violations: 0
rotatable bonds < 11
molecular weight: 325-400 g/mol
sum of formal charges: 3
formal charge: -2 – +2 ^a
rings: 2-4
max. ring size: 11 atoms
max. connected non-ring: 19 atoms
2D PSA: 100-150 Å ²
max. chiral centers: 1 ^b

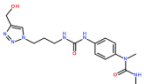
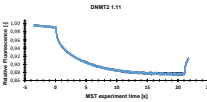
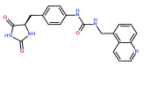
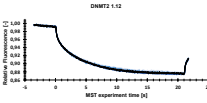
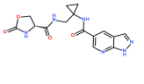
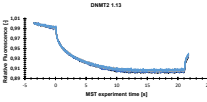
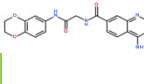
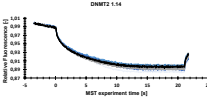
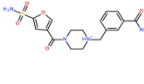
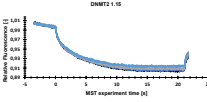
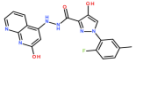
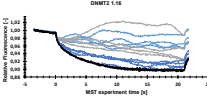
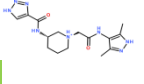
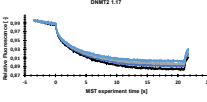
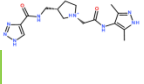
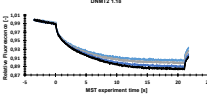
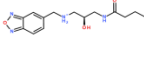
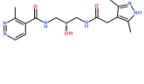
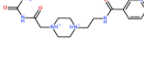
^aFor dominant protomer at pH = 7. ^bNumber of chiral centers was limited to reduce chemical complexity and simplify subsequent chemical derivatization of potential hit scaffolds.

Development of selective inhibitors for the human methyltransferases DNMT2 and NSUN6

Table S2: DNMT2 molecular docking and MST pre-screening results of tested virtual screening hits. Molecules are depicted as stereoisomers, protomers and tautomers according to their docking poses even though racemic mixtures (rac.) were purchased. Hits of the MST assay are highlighted in green. CoA: cofactor of analysis; C₁₈: HPLC column Agilent Poroshell 120 EC-C18 (150 × 2.10 mm), Zorb HPLC column Agilent Zorbex SB-Aq (4.6 × 150 mm)

Compound	Structure	SMILES	FlexX docking score [kcal/mol]	FlexX docking rank (out of 3.45 M)	LC-MS analytic: mass calc. [g/mol]; mass found [g/mol]; purity; (vendor)	MST pre-screening (ligand concentration: 0 μM (black, DMSO control), 33 μM (light blue), 100 μM (grey), 300 μM (dark blue))
1.1		<chem>S(=O)(=O)C1=CC=CC=C1C(=O)N2C(F)C(=O)N2C2=CC=C1</chem>	-48.20	808	366.08; 366.37; >99% (vendor CoA)	
1.2		<chem>O=C(Nc1c(C)[nH]c1C)N[C@@H]1CCN(C1=O)C2=CC(=O)N2C2=CC=C1</chem>	-53.16	17	390.16; 391.46; >99% (vendor CoA)	
1.3		<chem>O=C(NC)C1=CC=C(C=C1)N2C(=O)C3=CC(=O)N2C3=CC=C1</chem>	-50.55	135	384.2; 384.43; 97% (vendor CoA)	
1.4		<chem>O=C(NCCN(C)O)C1=CC(=O)C=CC=N1N1C1=CC(=O)N2C2=CC=C1</chem>	-48.03	909	355.13; 355.35; 99% (vendor CoA) / [M+H] ⁺ 356.1; 356.2; 95% (re-determined, ESI-MS, C ₁₈)	
1.5		<chem>O=C(NC)C1=CC=C(C=C1)N2C(=O)C3=CC(=O)N2C3=CC=C1</chem>	-50.55	134	384.2; 384.43; >99% (vendor CoA)	
1.6		<chem>O=C(NC)C1=CC=C(C=C1)N2C(=O)C3=CC(=O)N2C3=CC=C1</chem>	-49.77	242	346.19; 346.38; 98% (vendor CoA) / [M+H] ⁺ 347.2; 347.11; 98% (re-determined, ESI-MS, Zorb)	
1.7		<chem>S(=O)(=O)N1=CC=C(C=C1)C(=O)N2C3=CC(=O)N2C3=CC=C1</chem>	-52.49	31	387.15; 387.46; 98% (vendor CoA)	
1.8		<chem>S(=O)(=O)N1=CC=C(C=C1)C(=O)N2C3=CC(=O)N2C3=CC=C1</chem>	-53.33	14	373.13; 373.43; >99% (vendor CoA)	
1.9		<chem>Fc1c(C=O)N2C(=O)N[C@@H]2C3=CC(=O)N2C3=CC=C1</chem>	-52.45	32	386.15; 386.38; >99% (vendor CoA)	
1.10		<chem>O=C(NC)C1=CC=C(C=C1)N2C(=O)C3=CC(=O)N2C3=CC=C1</chem>	-52.05	47	¹ H-NMR identity confirmed; >99% (vendor CoA)	

Development of selective inhibitors for the human methyltransferases DNMT2 and NSUN6

1.11		<chem>O=C(NC)C(=O)N(C)C(=O)NCCC(=O)N(C)C(=O)N(C)C</chem>	-48.29	759	361.2; 361.4; >99% (vendor CoA)		no concentration-dependent MST-shift (no binding)
1.12		<chem>O=C(NC)C(=O)N(C)C(=O)NCCC(=O)N(C)C(=O)N(C)C</chem>	-49.53	281	389.16; 389.41; >99% (vendor CoA)		no concentration-dependent MST-shift (no binding)
1.13		<chem>O=C(NC)C(=O)N(C)C(=O)NCCC(=O)N(C)C(=O)N(C)C</chem>	-50.31	179	>90% (vendor)		no concentration-dependent MST-shift (no binding)
1.14		<chem>O=C(N)C(=O)N(C)C(=O)NCCC(=O)N(C)C(=O)N(C)C</chem>	-49.41	318	>90% (vendor) / [M+H] ⁺ 380.1; 380.1; >99% (re-determined, ESI-MS, C ₁₄)		concentration-dependent MST-shift (binding)
1.15		<chem>S(=O)(=O)N(C)C(=O)NCCC(=O)N(C)C(=O)N(C)C</chem>	-50.54	141	>90% (vendor)		no concentration-dependent MST-shift (no binding)
1.16		<chem>Fc1c(O)nc(O)nc(O)c1</chem>	-49.40	319	>90% (vendor)		no concentration-dependent MST-shift (no binding)
1.17		<chem>O=C(N)C(=O)N(C)C(=O)NCCC(=O)N(C)C(=O)N(C)C</chem>	-52.19	40	>90% (vendor) / [M+H] ⁺ 347.2; 347.1; 91% (re-determined, ESI-MS, Zn ²⁺ , gradient)		concentration-dependent MST-shift (binding)
1.18		<chem>O=C(N)C(=O)N(C)C(=O)NCCC(=O)N(C)C(=O)N(C)C</chem>	-52.74	25	>90% (vendor) / [M+H] ⁺ 347.19; 347.11; >99% (re-determined, ESI-MS, Zn ²⁺)		concentration-dependent MST-shift (binding)
1.19		<chem>O=C(N)C(=O)N(C)C(=O)NCCC(=O)N(C)C(=O)N(C)C</chem>	-54.95	3	synthesis not successful		
1.20		<chem>O=C(N)C(=O)N(C)C(=O)NCCC(=O)N(C)C(=O)N(C)C</chem>	-50.45	148	synthesis not successful		
1.21		<chem>O=C(N)C(=O)N(C)C(=O)NCCC(=O)N(C)C(=O)N(C)C</chem>	-55.59	2	synthesis not successful		

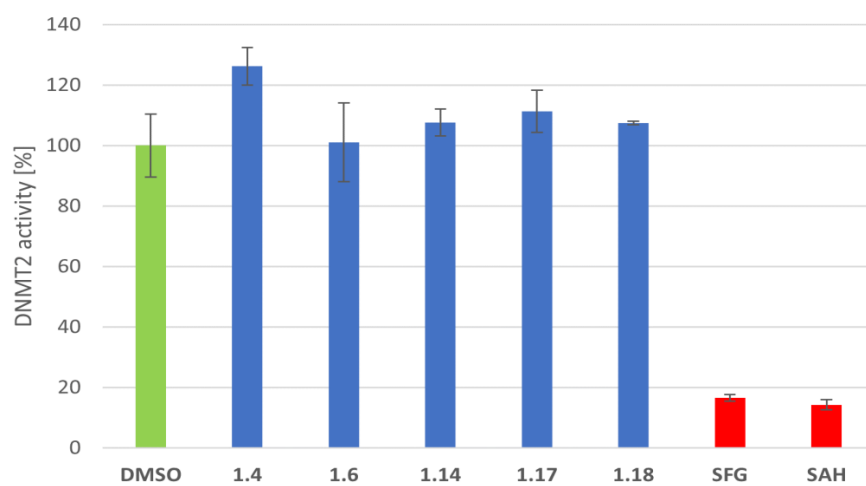


Figure S1. DNMT2 tritium incorporation enzyme activity assay results in absence and presence of ligands at a concentration of 100 μ M. Values represent average values with standard error of triplicate determinations normalized to the DMSO control.

References

- 1 Baell, J.; Walters, M. A. Chemistry: Chemical Con Artists Foil Drug Discovery. *Nature* **2014**, *513*, 481–483. <https://doi.org/10.1038/513481a>.
- 2 Wang, R.; Fu, Y.; Lai, L. A New Method for Calculating Partition Coefficients of Organic Compounds. *Acta Phys. - Chim. Sin.* **1997**, *13* (1), 615–621. <https://doi.org/10.3866/pku.whxb19970101>.
- 3 Lipinski, C. A.; Lombardo, F.; Dominy, B. W.; Feeney, P. J. Experimental and Computational Approaches to Estimate Solubility and Permeability in Drug Discovery and Development Settings. *Adv. Drug Deliv. Rev.* **2001**, *46*, 3–26. <https://doi.org/10.1016/j.addr.2012.09.019>.

Covalent S-adenosylhomocysteine-based DNA methyltransferase 2 inhibitors with a new type of aryl warhead.

Project summary and own contributions

The main aim of this study was to improve the results from publication (1). Starting from a branched SAH-like scaffold with a benzylic moiety, which showed moderate affinity, a diverse set of aromatic derivatives has been synthesized. Therefore, the so-called “Topliss scheme” was applied to design improved DNMT2 inhibitors. The synthesized compounds were tested using the optimized MST method from publication (2), and depending on the results, new compounds have been synthesized according to the “Topliss scheme”. Besides this approach, some inhibitors beyond the “Topliss scheme” have been synthesized. To verify the outcome of the MST screening, a ^3H assay was used to determine the inhibitory effect of the compounds. Furthermore, the thermodynamics of the most promising compounds was investigated with ITC experiments. Interestingly for some very electrophilic inhibitors, there has been a large difference in affinity determined by MST and inhibition determined in the ^3H -assay. Further experiments revealed that some of the compounds react with DTT at high concentrations, which are required in the ^3H assay to maintain reducing conditions. Thus, the experiments were performed again with TCEP as a reducing agent, which is far less nucleophilic than DTT. And indeed, the results from this adjusted ^3H -assay were in high accordance with the affinity determined in the MST screening. These results lead to the hypothesis that the electrophilic compounds would also react covalently with exposed cysteines of DNMT2. To investigate the binding mode of the inhibitors, native and denatured protein mass spectrometry was applied for a set of electrophilic compounds, as well as some negative controls without electrophilic moieties. The results showed that several of the electrophilic compounds formed covalent bonds. Tryptic digest of DNMT2 showed that the inhibitors mainly bound the cysteine in the active site of DNMT2. Furthermore, some compounds formed a second covalent bond beyond the active site. These findings present valuable insights into which exact electrophilicity is needed to target the active site cysteine only. Finally, the selectivity of the most promising compounds was measured towards NSUN2 and NSUN6, which both methylate tRNA like DNMT2. Fortunately, some of the DNMT2 inhibitors showed remarkable selectivity, although they hold quite electrophilic moieties. To the best of our knowledge, the compounds presented in this study are the first SAH-like inhibitors that inhibit DNMT2 in a covalent manner while maintaining selectivity towards other tRNA methyltransferases like NSUN2 and NSUN6. These results are an important step toward potent yet selective inhibition of the human methyltransferase DNMT2.

Own contribution: expression and purification of protein with support from [REDACTED], conducting the MST and ITC experiments; preliminary works for protein mass spectrometry, writing of the manuscript together with [REDACTED]

Contributions from other authors: design and synthesis of compounds, stability testing of compounds; conducting the ³H-assay; conducting the protein mass spectrometry.

This work has been published in: ACS Medicinal Chemistry Letters (Impact factor: 4.632/CiteScore: 6.6)

Reprinted (adapted) with permission from: *ACS Med. Chem. Lett.* 2023, Article ASAP. "Covalent S-Adenosylhomocysteine-Based DNA Methyltransferase 2 Inhibitors with a New Type of Aryl Warhead"
Copyright 2023 American Chemical Society."

Covalent S-Adenosylhomocysteine-Based DNA Methyltransferase 2 Inhibitors with a New Type of Aryl Warhead

Marvin Schwickert,[§] Robert A. Zimmermann,[§] Tanja Habeck, Sabrina N. Hoba, Zarina Nidoieva, Tim R. Fischer, Martin M. Stark, Christian Kersten, Frederik Lermyte, Mark Helm,^{*} and Tanja Schirmeister^{*}Cite This: <https://doi.org/10.1021/acsmchemlett.3c00062>

Read Online

ACCESS |

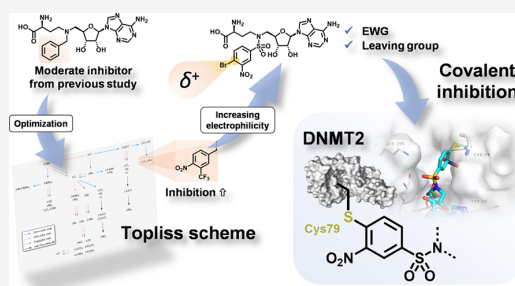
Metrics & More

Article Recommendations

Supporting Information

ABSTRACT: The DNA methyltransferase 2 (DNMT2) is an RNA modifying enzyme associated with pathophysiological processes, such as mental and metabolic disorders or cancer. Although the development of methyltransferase inhibitors remains challenging, DNMT2 is not only a promising target for drug discovery, but also for the development of activity-based probes. Here, we present covalent SAH-based DNMT2 inhibitors decorated with a new type of aryl warhead. Based on a noncovalent DNMT2 inhibitor with *N*-benzyl substituent, the *Topliss* scheme was followed for optimization. The results showed that electron-deficient benzyl moieties highly increased affinity. By decorating the structures with strong electron-withdrawing moieties and leaving groups, we adjusted the electrophilicity to create covalent DNMT2 inhibitors. A 4-bromo-3-nitrophenylsulfonamide-decorated SAH derivative (**80**) turned out to be the most potent ($IC_{50} = 1.2 \pm 0.1 \mu M$) and selective inhibitor. Protein mass spectrometry confirmed the covalent reaction with the catalytically active cysteine-79.

KEYWORDS: DNMT2, covalent SAH-based inhibitors, aryl warhead, *Topliss* scheme, microscale thermophoresis, protein mass spectrometry



RNA and its modifications play a significant role in epigenetic inheritance.^{1,2} Studies revealed that some RNA modifications are linked to mental³ and metabolic disorders.⁴ Inheritance of metabolic disorders has been found to be caused by increased levels of m²G and m⁵C modifications.⁵ The human DNA methyltransferase 2 (hDNMT2), which among others is responsible for m⁵C modifications, is involved in this process.⁶ Due to its similar sequence and structure, hDNMT2 is part of the DNA methyltransferase family, but its main substrate is tRNA at position C38.^{7,8} hDNMT2 plays a role in different physiological processes but is also linked to cancer.⁸

To transfer a methyl group to tRNA, hDNMT2 requires S-adenosyl-L-methionine (SAM) as a cofactor, releasing m⁵C38-tRNA^{Asp} and S-adenosyl-L-homocysteine (SAH) as a by-product.⁷ Besides the natural inhibitors SAH and sinefungin (SFG),⁹ the chemotherapeutic agents 5-azacytidine, decitabine, and zebularine are known to inactivate DNMTs.¹⁰

Methyltransferases are hard-to-drug targets, especially due to the high cellular concentration of SAM¹¹ that competes with a potential inhibitor. Furthermore, most of the over 200 different methyltransferases (MTases)¹² in humans are SAM-dependent, which increases the challenge to find selective SAH-based inhibitors. Because covalent inhibitors are capable of competing with high natural ligand concentrations,¹³ these issues can be overcome with a warhead-decorated SAH derivative. Moreover,

high selectivity can be achieved by targeting the catalytically active cysteines found in the hDNMT¹⁴ or NOL1/NOP2/sun domain (NSUN)¹⁵ families since various other MTases follow different mechanisms.¹⁶ Such covalent modifiers can also be a suitable basis for the development of fluorescently labeled activity-based probes (ABPs),¹⁷ which can be used to improve the understanding of RNA methyltransferases and their RNA modifications.

Here, we present covalent SAH-based hDNMT2 inhibitors with 4-halo-3-nitrophenylsulfonamide warheads. This warhead class represents a well-fitting substructure for the cytidine binding site of the enzyme, as it not only mimics the cytidine residue of tRNA but also provides proper orientation and length to reach the catalytically active cysteine-79. Recently, we published hDNMT2 inhibitors based on the SAH scaffold.⁹ We replaced the sulfur atom with various *N*-alkylated substructures, and the *N*-but-3-yn-2-yl derivative **1** turned out

Received: February 22, 2023

Accepted: May 2, 2023

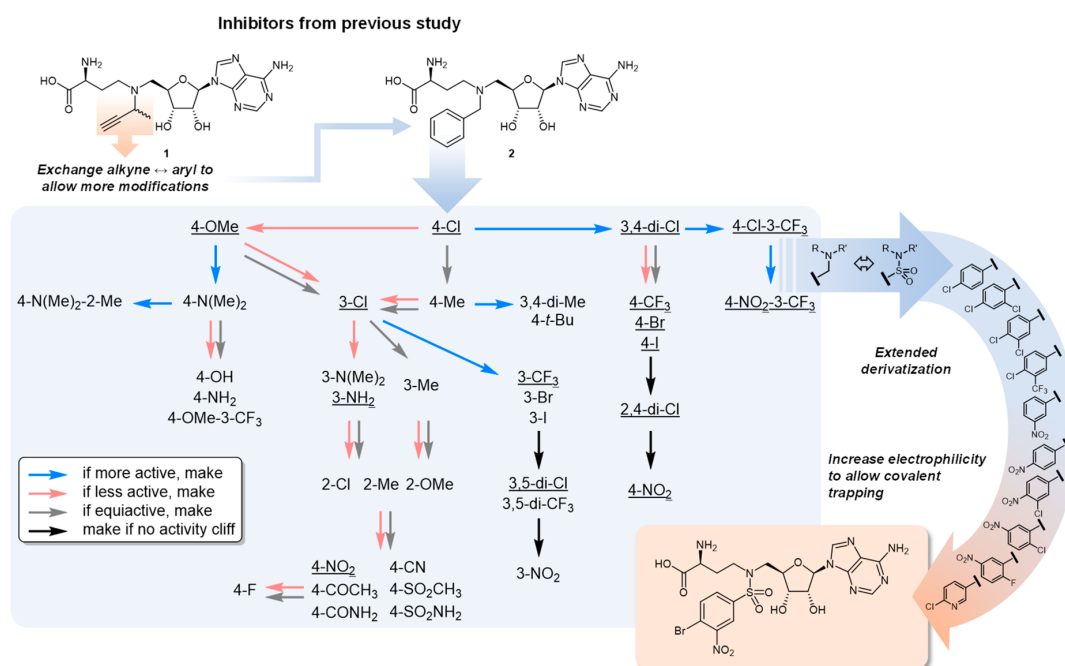
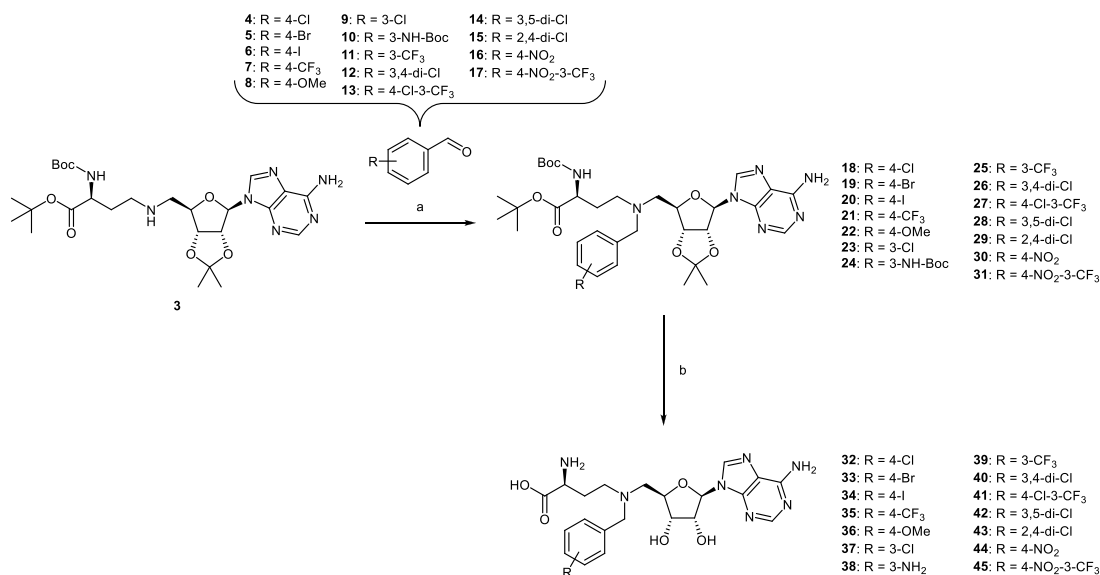


Figure 1. Derivatization of the benzylamine derivative **2** according to the *Topliss* scheme. Based on the 4-chloro-3-trifluoromethyl and the 4-nitro-3-trifluoromethyl derivatives, an additional SAR study was conducted. First, the aminomethyl substructure was exchanged with a sulfonamide unit to increase the electrophilicity. The aryl moiety was decorated with electron-withdrawing groups and leaving groups to allow a potential covalent reaction with the catalytically active cysteine of hDNMT2.

Scheme 1. Synthesis of Benzylamine Derivatives **32–45**^a

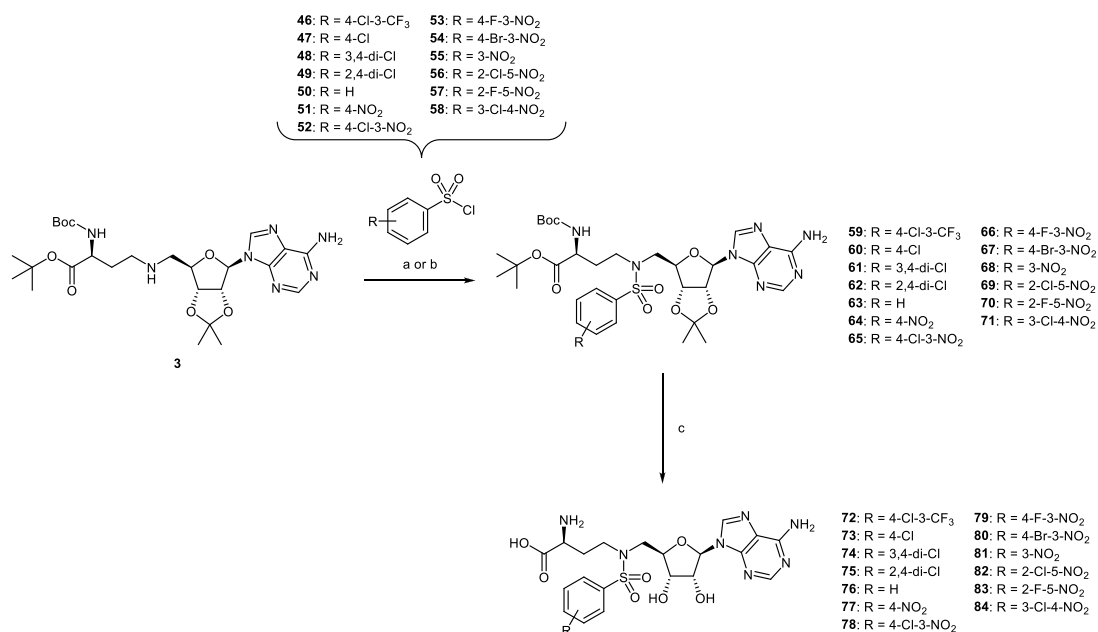


^aReagents and conditions: (a) NaBH(OAc)₃, HOAc, 1,2-DCE, 0 °C to rt, overnight, 37–96%; (b) (1) TFA/DCM (1:1 v/v), 5 °C; (2) TFA/H₂O (1:6 v/v), 5 °C, 99%.

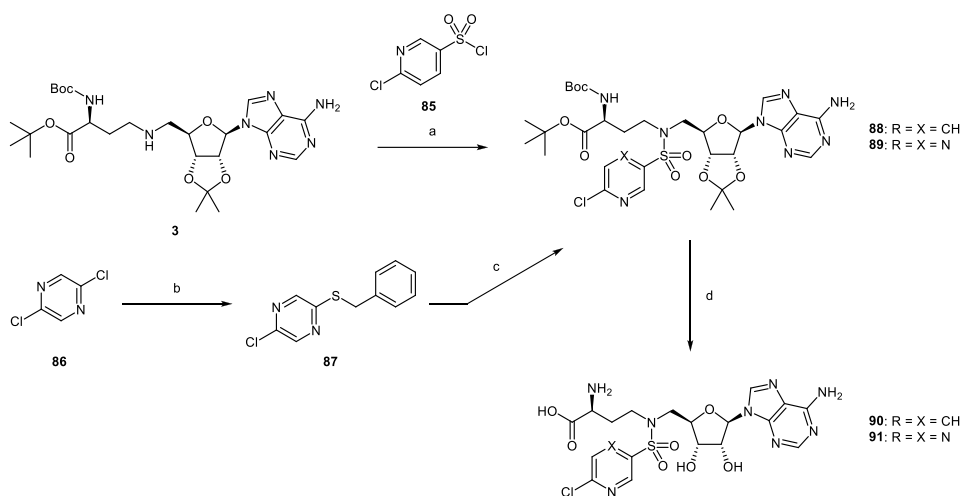
to be the most potent inhibitor of hDNMT2 in a tritium-incorporation assay (³H-assay) (IC₅₀ = 12.9 ± 1.9 μM). We also tested the *N*-benzylated derivative **2**, which showed moderate affinity (57% at 100 μM). Because the phenyl moiety allows a

huge space for modifications, we considered the scaffold as a basis for optimization.

Starting from this structure, we developed *N*-benzyl containing compounds according to the *Topliss* scheme (Figure 1). This is an operational scheme in drug design for the

Scheme 2. Synthesis of Sulfonamide Derivatives 72–84^a

^aReagents and conditions: (a) NEt₃, DCM, Δ, 2 h, 52–73%; (b) NaHCO₃, H₂O, DCM, rt, overnight, 43–82%; (c) (1) TFA/DCM (1:1 v/v), 5 °C; (2) TFA/H₂O (1:6 v/v), 5 °C, 99%.

Scheme 3. Synthesis of the Heterocycles 90 and 91^a

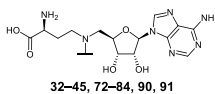
^aReagents and conditions: (a) NEt₃, DCM, Δ, 2 h, 62%; (b) benzyl mercaptan, NaH, THF, 1 h at 0 °C, 16 h at rt, 91%; (c) (1) sulfonyl chloride, –5 °C, 2 h; (2) 3, NaHCO₃, H₂O, DCM, rt, overnight, 34%; (d) (1) TFA/DCM (1:1 v/v), 5 °C; (2) TFA/H₂O (1:6 v/v), 5 °C, 99%.

derivatization of aromatic compounds considering hydrophobic (π), electronic (σ), and steric (E_s) values of different substituents.¹⁸ Starting from an unsubstituted phenyl moiety, the 4-chloro analogue is initially proposed as it increases the π value. Subsequently, we followed the scheme suggestions depending on the inhibitory effects. Selected derivatives of nonproposed paths were also tested for comparison.

We performed an additional structure–activity relationship study based on the scaffold that exhibited the highest activity. The methylenamine substructure of the *N*-benzyl moiety was

replaced with a sulfonamide to test the influence of an additional –I and –M effect. To allow a covalent reaction with the catalytically active cysteine in the cytidine site, electron-deficient aryls with halogen leaving groups were designed to increase electrophilicity. To confirm the covalent reaction between ligand and hDNMT2, protein mass spectrometric experiments were conducted.

Chemistry. The benzyl derivatives were synthesized by reductive amination using protected adenosyl-2,4-diaminobutyric acid (adenosyl-Dab)⁹ 3 and substituted benzaldehydes 4–

Table 1. Binding of Compounds to hDNMT2 as Determined by MST and Inhibition of hDNMT2 as Determined in the ³H-Assays^a

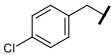
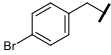
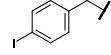
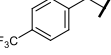
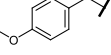
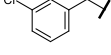
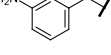
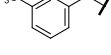
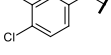
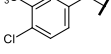
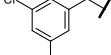
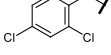
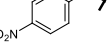
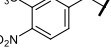
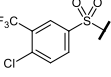
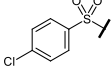
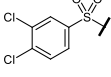
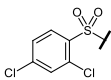
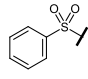
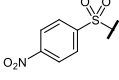
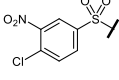
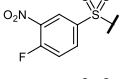
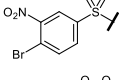
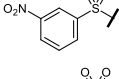
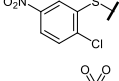
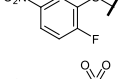
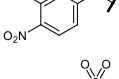
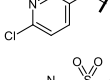
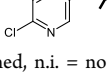
Compound	MST		ITC	³ H-assay		
	Shift at 20 μM / %	K _D ^{app} / μM	K _D ^{app} / μM	% inhibition at 100 μM	IC ₅₀ / μM	
SFG	13.3	20.9 ± 0.7 ²⁰	7.5 ± 3.5 ⁹	83.5 ± 1.1 ⁹	13.2 ± 0.8 ⁹	
32		10.7	28.2 ± 1.4	32.1 ± 8.4	72.3 ± 3.1	62.8 ± 3.0
33		8.5	n. d.	n. d.	67.3 ± 3.4	n. d.
34		10.8	18.1 ± 1.0	n. d.	75.5 ± 0.8	n. d.
35		11.3	23.7 ± 1.0	n. d.	51.1 ± 6.6	n. d.
36		6.2	55.8 ± 4.9	n. d.	64.0 ± 3.1	n. d.
37		9.8	n. d.	n. d.	67.2 ± 3.4	n. d.
38		6.3	n. d.	n. d.	n. i.	n. d.
39		8.9	45.1 ± 2.3	n. d.	60.6 ± 3.0	n. d.
40		11.3	17.9 ± 0.9	n. d.	73.8 ± 3.5	n. d.
41		14.2	10.4 ± 0.4	6.0 ± 0.7	86.2 ± 3.0	18.3 ± 4.0
42		8.5	n. d.	n. d.	59.6 ± 4.6	n. d.
43		6.9	n. d.	n. d.	47.0 ± 3.2	n. d.
44		11.8	14.8 ± 0.6	n. d.	65.5 ± 4.0	n. d.
45		17.1	4.2 ± 0.3	0.9 ± 0.1	94.0 ± 2.1	2.5 ± 0.2
72		11.7	19.5 ± 1.4	n. d.	54.3 ± 3.7	n. d.
73		2.9	n. d.	n. d.	n. i.	n. d.
74		7.9	n. d.	n. d.	27.8 ± 17.0	n. d.

Table 1. continued

Compound	MST		ITC	³ H-assay	
	Shift at 20 μM / %	K _D ^{app} / μM	K _D ^{app} / μM	% inhibition at 100 μM	IC ₅₀ / μM
75 	0.8	n. d.	n. d.	n. d.	n. d.
76 	1.2	n. d.	n. d.	n. d.	n. d.
77 	2.5	n. d.	n. d.	n. d.	n. d.
78 	18.0	2.5 ± 0.1	4.3 ± 0.2	98.2 ± 1.6	2.3 ± 0.5
79 	16.3	11.2 ± 0.6	17.3 ± 3.6	92.8 ± 3.7	8.5 ± 1.3
80 	18.3	2.3 ± 0.1	4.9 ± 0.4	98.7 ± 1.1	1.2 ± 0.1
81 	1.4	n. d.	n. d.	n. i.	n. d.
82 	0.2	n. d.	n. d.	n. d.	n. d.
83 	2.0	n. d.	n. d.	n. d.	n. d.
84 	10.9	22.7 ± 0.9	n. d.	67.0 ± 1.6	n. d.
90 	4.1	n. d.	n. d.	33.2 ± 1.9	n. d.
91 	17.2	2.6 ± 0.2	1.9 ± 0.3	100.0 ± 6.4	1.1 ± 0.2

^an.d. = not determined, n.i. = no inhibition.

17 (Scheme 1). For this, sodium triacetoxyborohydride and acetic acid were used as reagents in 1,2-dichloroethane. The building block 3 was prepared according to a previously described procedure.⁹ In the final step, the protecting groups were removed by treatment with 50% (v/v) TFA in dichloromethane at 5 °C, followed by treatment with 14% (v/v) TFA in water at 5 °C. To further increase the electrophilicity of the aromatic ring, the methylenamine substructure of the benzyl moiety was exchanged by a sulfonamide group. With its -I and -M effects, this compound class shows interesting properties as electron-withdrawing substituents seemed to increase the affinity for hDNMT2. Electron-withdrawing groups which can potentially act as leaving groups, such as halides, were chosen as substituents to enable a possible covalent reaction with the catalytically active cysteine of hDNMT2. To obtain the sulfonamide-based inhibitors, building block 3 was brought to reaction with substituted phenylsulfonyl chlorides 46–58 either

in the presence of triethylamine in DCM under reflux or using a two-phase system consisting of DCM and saturated NaHCO₃ solution at room temperature (Scheme 2). In the final step, the resulting precursors 59–71 were deprotected using 50% (v/v) TFA in dichloromethane at 5 °C, followed by treatment with 14% (v/v) TFA in water at 5 °C to give the inhibitors 72–84. To investigate the effect of intracyclic nitrogens as replacements for the nitro groups, pyridine and pyrazine derivatives decorated with chlorine were synthesized (Scheme 3). The pyridine derivative 90 was prepared by combining the building block 3 and 6-chloropyridine-3-sulfonyl chloride 85 with triethylamine in DCM under reflux to yield the protected precursor 88. For the synthesis of the pyrazine derivative 91, 2,5-dichloropyrazine 86 was substituted with benzyl mercaptan in the presence of sodium hydride in THF to give 87. In the next step, 87 was treated with sulfuryl chloride¹⁹ and was reacted with the building block 3 using a two-phase system consisting of DCM and

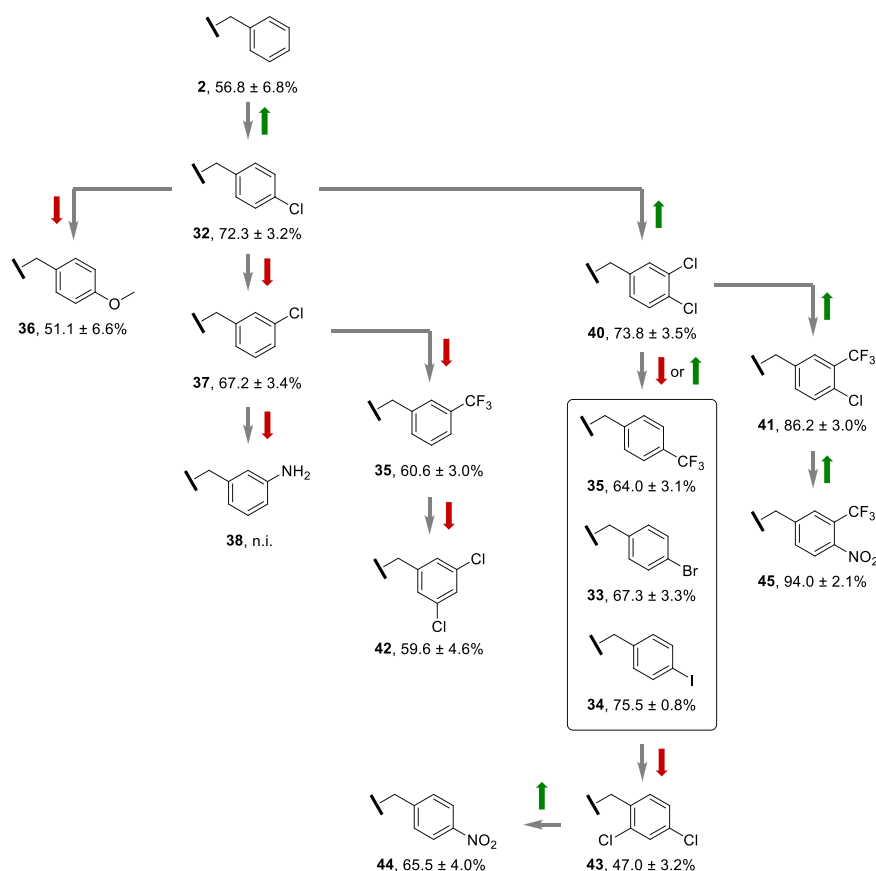


Figure 2. Synthesized compounds and corresponding results with depiction of positions in the *Topliss* scheme. Arrows indicate either increase (green) or decrease (red) in inhibition.

saturated NaHCO_3 solution at room temperature to yield the protected pyrazine derivative **89**. The precursors **88** and **89** were finally deprotected using 50% (*v/v*) TFA in dichloromethane at 5 °C, followed by treatment with 14% (*v/v*) TFA in water at 5 °C to yield the inhibitors **90** and **91**. A 2-chloropyrimidine derivative was also to be synthesized, but due to its high reactivity already with weak nucleophiles such as methanol and water, which led to substitution of chlorine, it was not further pursued.

Biological Evaluation: hDNMT2 Binding and Inhibition. To determine the binding affinity of the compounds toward hDNMT2, a screening was performed with full-length hDNMT2 (if not described otherwise, full-length protein was used) based on a microscale thermophoresis (MST) displacement method using the fluorescent ligand FTAD.²⁰ Potent binders were defined as compounds that were able to displace FTAD approximately to the same extent as SFG (MST shift $\geq 13\%$; cut-off $\geq 10\%$). For all potent binders an apparent K_D value (K_D^{app}) was determined using MST. All other compounds were not further evaluated. Ligands with the highest affinity toward hDNMT2 (**41**, **45**, **78–80**, and **91**; **32** for comparison), were subjected to isothermal titration calorimetry (ITC), which served as an orthogonal method to quantify the binding affinity of those ligands. The results from ITC measurements confirmed the data of the MST measurements, as the results of both methods showed a high consistency. Finally, to investigate their actual inhibitory effect, the most potent binders and some

selected weak binders were evaluated using a ^3H -assay. The assay was performed with tRNA^{Asp} as substrate and tritium-labeled SAM (^3H -SAM) as cosubstrate at a compound concentration of 100 μM . For the most potent inhibitors IC_{50} values were determined. All results are summarized in Table 1. Within the benzyl series, 7 out of 14 compounds (**32**, **34**, **35**, **40**, **41**, **44**, and **45**) could be classified as promising binders, as they caused an MST shift $\geq 10\%$. Starting with the 4-chloro substituent **32** in the *Topliss* scheme, an increase in inhibition from 57% to 72% was achieved. According to the scheme, the proposed modification in this case is the 3,4-dichloro substitution (**40**). With an inhibition of 74%, it did not show a significant increase in potency, resulting in the proposed modifications 4- CF_3 , 4-Br, and 4-I. While the 4-bromo (**33**) and 4-trifluoro (**35**) derivatives showed reduced inhibition (67% and 51%, respectively), the 4-iodo modification (**34**) was equipotent (75%). Based on alternative modifications in this branch, we tested the 2,4-dichloro derivative **43**, which further reduced inhibition to 47%. Because the proposed modifications of this branch did not significantly improve inhibition, we followed the branch proposed if the 3,4-dichloro substitution (**40**) would be classified as more potent (73.8 ± 3.5% vs 72.3 ± 3.1%) than the 4-chloro modification (**32**) after all. As a result, the proposed modification 4-chloro-3-trifluoromethyl **41** was tested and exhibited a significant increase in inhibition of up to 86%. Based on this result, the scheme proposed the 4-nitro-3-trifluoromethyl derivative **45** as a final modification. Notably, an

even higher inhibition of 94% ($IC_{50} = 2.5 \pm 0.2 \mu M$) was achieved. To identify potential inhibitors that were likely omitted due to incorrect prediction of the scheme we selected different structures of the remaining branches: 4-OMe (**36**), 3-Cl (**37**), 3-NH₂ (**38**), 3-CF₃ (**39**), 3,5-diCl (**42**), and 4-NO₂ (**44**). The tests revealed that the derivatives **36**, **37**, **39**, and **42** showed moderate inhibition of 59–67%, whereas the 3-amino structure **38** was inactive. Interestingly, the nitro derivative **44** showed a significant increase in inhibition compared to its direct branch precursor **43** (66% vs 47%). However, its inhibition was still lower than that of compounds **33–35** of the same branch. Evaluation of the inhibition of hDNMT2 in correlation with the substituent effects revealed that the results were in high accordance with the *Topliss* scheme suggestions (Figure 2). It could be observed that the more electron-withdrawing groups were introduced, the stronger was the inhibition of hDNMT2, which was demonstrated by the following branch: 4-Cl (**32**) → 3,4-diCl (**40**) → 4-Cl-3-CF₃ (**41**) → 4-NO₂-3-CF₃ (**45**) with increasing inhibition of 72% → 74% → 86% → 94%, respectively. While substituents in position 2 significantly reduced inhibition, probably due to steric hindrance within the binding pocket, introduction of several groups at position 3 was tolerated. However, the potency compared to the phenyl derivative **2** was only slightly increased from 56% to 67% by introducing the 3-Cl substituent (**37**). Position 4 also allowed several substituents, e.g., 4-Cl (**32**), 4-Br (**33**), 4-I (**34**), 4-CF₃ (**35**), 4-OMe (**36**), and 4-NO₂ (**44**), all of which increased the potency compared to the unsubstituted inhibitor **2**. A significant increase in inhibition was achieved with the 4-Cl (72%) and the 4-I (75%) substituents. Interestingly, they differ in electro-negativity and volume, yet they showed equipotent inhibition of hDNMT2. So far, a disubstituted, electron-deficient benzyl group appeared to be most effective at enhancing inhibition.

To further increase electrophilicity of the aromatic ring, we replaced the methylenamine substructure of the *N*-benzyl moiety with a sulfonamide that introduces additional $-I$ and $-M$ effects. Based on this modification, a subsequent structure–activity relationship (SAR) study was conducted using different aryl sulfonyl moieties with strong electron-withdrawing groups such as NO₂ and CF₃ as well as intracyclic nitrogen atoms. To enable a possible covalent reaction with the catalytically active cysteine, the aromatic rings were decorated with halogen leaving groups. First, we started with the 4-chloro-3-trifluoromethyl analogue **72** for comparison with one of the most active compounds (**41**). With an inhibition of 54%, it showed a significantly lower inhibition than **41** with 86%, which indicates a negative effect of the sulfonamide group. The same holds true for **73** (4-Cl, no inhibition), **74** (3,4-diCl, 28% inhibition), **75** (2,4-diCl, no inhibition), **76** (unsubstituted, no inhibition), and **77** (4-NO₂, no inhibition), which caused significantly lower inhibition compared to their corresponding benzyl derivatives. Interestingly, the 4-chloro-3-nitro derivative **78** had the highest inhibitory activity of 98% ($IC_{50} = 2.3 \pm 0.5 \mu M$). Given **78** as the new lead structure, we analyzed changes in the substitution pattern. For the 4-F-3-NO₂ modification (**79**), a slightly lower inhibition of 93% ($IC_{50} = 8.5 \pm 1.3 \mu M$) was observed, while the 4-Br-3-NO₂ derivative **80** was found to be equipotent with an inhibition of 99% ($IC_{50} = 1.2 \pm 0.1 \mu M$). Other structural changes such as 3-NO₂ (**81**), 2-Cl-5-NO₂ (**82**), and 2-F-5-NO₂ (**83**) did not lead to inhibition of hDNMT2. The 3-Cl-4-NO₂ derivative **84** showed only moderate inhibition of 67%. Replacing the 3-nitro group of **78** with an intracyclic nitrogen (**90**) atom resulted in a strong reduction of inhibition to 33%.

However, a second intracyclic nitrogen located in the opposite position, as found in pyrazine moieties, increased the inhibition to 100% (**91**, $IC_{50} = 1.1 \pm 0.2 \mu M$). Comparing the benzyl derivatives with the sulfonamide-based compounds, an obvious trend is observable. The sulfonamide derivatives showed significantly lower inhibition compared to their benzyl analogues, e.g., **32** vs **73** (4-Cl), **40** vs **74** (3,4-diCl), and **41** vs **72** (4-Cl-3-CF₃). Yet the 4-Cl/Br-3-NO₂ substituted sulfonamide-based derivatives **78** and **80** as well as the 4-chloropyrazine derivative **91** showed the highest inhibition ($IC_{50} < 2.5 \mu M$). The results also highlight the quality of our FTAD-based MST screening method²⁰ because the screening results showed high consistency with the measured inhibition in the ³H-assay.

Warhead Stability in the Presence of DTT. We found that the inhibition of hDNMT2 by compound **79** was highly dependent on the presence of the reducing agent used in the assays. While inhibition of 93% ($IC_{50} = 8.5 \pm 1.3 \mu M$) was measured in the presence of TCEP, no inhibition could be observed in the presence of DTT. These findings strongly suggest a covalent reaction of the thiol-based agent with the electrophilic inhibitor. For this reason, we conducted stability tests with DTT and the inhibitors **78–80** in TRIS buffer pH = 8.0 at room temperature under assay-like conditions. The inactivation was determined by LC-MS after 2 min followed by 15 min intervals (Figure 3).

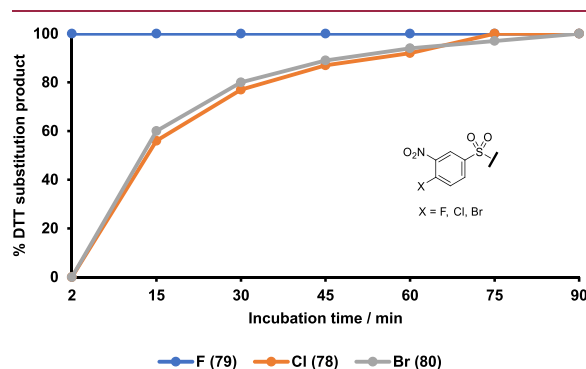


Figure 3. Stability test of inhibitors **78–80** in the presence of DTT under assay-like conditions. Percent inactivation was determined initially after 2 min and then at 15 min intervals.

LC-MS measurements confirmed the formation of a DTT substitution product in all three cases. Figure 3 shows that **79** already completely reacted with DTT after 2 min. **78** reacts with a rate comparable to **80**, but much slower than **79**. In the first 15 min, both react very quickly until a conversion of ca. 60% was reached. A full conversion was observed after 90 min, respectively.

Protein Mass Spectrometry. To investigate the binding of the ligands **45**, **78–80**, and **91** to hDNMT2, we used intact-protein LC-MS under denaturing conditions, which only preserve covalently bound ligands. Additionally, direct infusion nano-electrospray ionization experiments were performed under non-denaturing conditions, which allow preservation of non-covalent binding. hDNMT2 harbors a flexible loop (residues 191–237) that decreases protein stability and prevents crystallization. However, a construct without this loop was cocrystallized with SAH (PDB 1G55). Based on this construct, a deletion mutant without residues 191–237 (hDNMT2Δ) was

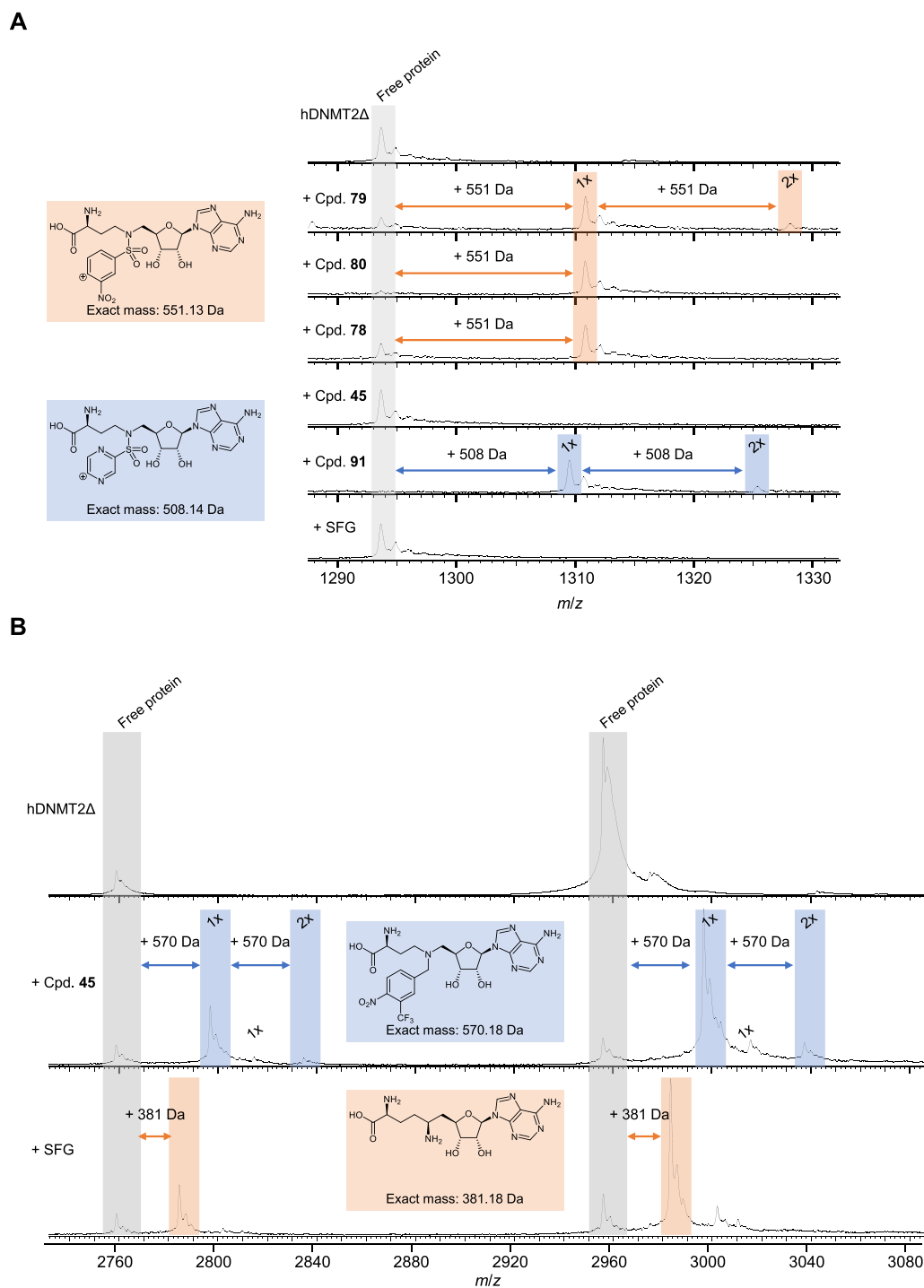


Figure 4. (A) LC-MS of intact, denatured hDNMT2Δ with and without ligands. Corresponding peak for free protein signal is highlighted in gray (32+ charge state). For 45 and SFG, no binding was detected under denaturing conditions. Binding to 78–80 all led to addition of the same 551 Da moiety (mass shift and corresponding structure shown in orange). Binding to 91 led to addition of a 508 Da moiety (structure and mass shift shown in blue). (B) Native MS of hDNMT2Δ in complex with 45 and SFG. Peaks corresponding to free protein signal (charge states 14+ and 15+) are highlighted in gray. Binding to 45 (two binding events) and SFG (one event) are highlighted in blue and orange, respectively.

designed, which was better suited for mass spectrometry than hDNMT2.

hDNMT2Δ showed decreased but measurable activity in the ³H-assay, which supports the hypothesis that hDNMT2Δ binds

H

<https://doi.org/10.1021/acsmchemlett.3c00062>
ACS Med. Chem. Lett. XXXX, XXX, XXX–XXX

SAH. For all experiments, the known noncovalent ligand SFG was used as a control. All LC-MS spectra exhibited the broad charge state distribution and high charge states typical for denatured proteins. In Figure 4A, the results of these measurements, zoomed in on the region around charge state 32+ (m/z 1293), are shown. For 78–80, the same mass shift of 551 Da, corresponding to addition of the structure highlighted in orange, was observed. This indicates loss of the halogen substituent and the formation of a covalent bond between the protein and ligand. A second addition of ligand 79 was detected, which suggests the existence of two potential binding sites of this ligand and therefore a less specific binding of the desired target cysteine. A comparable result was observed with ligand 91, where two mass shifts of 508 Da, corresponding to the blue-highlighted structure, were detected. Here, a very low amount of remaining free protein signal was observed, which indicates a fast and favorable reaction of this ligand with hDNMT2 Δ . For 45 and the known noncovalent ligand SFG, no mass shift and thus no covalent irreversible binding was demonstrated. A table with observed and calculated masses, mass errors, and intensities can be found in the Supporting Information. Additional measurements under near-native conditions were performed with SFG and 45 (Figure 4B). As is typical in native MS, these spectra show a narrow charge state distribution with low charge states. For both ligands, a shift by the corresponding mass was detected (570 Da for 45; 381 Da for SFG). Furthermore, a second binding event of ligand 45 was observed. This demonstrates the noncovalent binding of 45 and SFG to hDNMT2 Δ . This second, but weaker binding event observed for 45 and 74 could also explain the increased binding stoichiometry determined in the ITC experiments (1.37 ± 0.01 and 1.34 ± 0.04 , respectively). On the other hand, for 91, a decreased binding stoichiometry (0.84 ± 0.01) was measured, leading to the assumption that this compound is too reactive and therefore could cause partial protein aggregation. All other compounds investigated with ITC showed binding stoichiometries in the range from 0.9 to 1.1 toward hDNMT2 Δ , which correlates nicely with data obtained from protein MS. We determined the binding sites of the covalent ligands with a tryptic digest followed by bottom-up LC-MS/MS. A high sequence coverage of over 80% was achieved for all samples. For 78–80, binding to Cys79, which is known to be the catalytically active cysteine, was detected. In agreement with the denatured intact mass measurements, which indicated a second binding site for 79, an additional modified peptide containing the cysteine residue corresponding to Cys287 in the wild-type protein was detected. Similarly, binding of 91 was also observed at Cys79 and Cys287. As expected, no modified peptides were detected for 45 and SFG, which is consistent with a noncovalent binding mode. These findings indicated two covalent binding sites for 79 and 91, and the binding to only the desired target Cys79 for 78 and 80. Given that four surface-exposed cysteines can be found in the crystal structure of hDNMT2 (PDB 1G55), the results highlight the nonpromiscuous binding behavior of compounds 78 and 80, which only reacted with the catalytically active Cys79. A detailed overview of the results is shown in the Supporting Information.

Selectivity. Selectivity of the most promising inhibitors (45, 78–80, and 91) toward other tRNA modifying m⁵C MTases (NSUN2 and NSUN6) was measured in a ³H-assay at 100 μ M (Figure 5). All selected inhibitors showed higher selectivity compared to SFG,⁹ with compound 80 being the most selective one as it did not inhibit NSUN2 and NSUN6. Compounds 78 and 91 appeared to be highly selective as they showed only slight

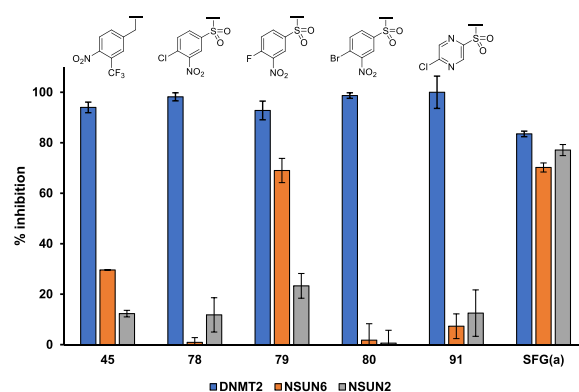


Figure 5. Inhibition of different RNA methyltransferases by most potent DNMT2 inhibitors at 100 μ M. Triplicates \pm SD are given. (a) Data from previous study.

inhibition of NSUN2 ($12 \pm 6.8\%$ and $13 \pm 9.2\%$) and NSUN6 (n.i. and $7 \pm 4.9\%$). Lower selectivity was observed for 45 ($12 \pm 1.3\%$ for NSUN2; $30 \pm 0.1\%$ for NSUN6) and 79 ($23 \pm 4.9\%$ for NSUN2; $69 \pm 4.8\%$ for NSUN6). Given that 79 is highly reactive, a lack of selectivity was expected. Furthermore, detection of beyond active site binding to hDNMT2 Δ for 45 and 79 via LC-MS already indicated a promiscuous binding behavior of those compounds. To investigate a concentration range more common in biochemical assays, the selectivity was also determined at 10 μ M inhibitor concentration (Supporting Information). All tested inhibitors except 79 have been found to be highly selective yet potent hDNMT2 inhibitors at 10 μ M.

Docking Studies Confirm Proper Orientation Allowing Covalent Reaction. To investigate the binding mode of compounds 45, 78–80, and 91 and confirm a proper orientation that enables a covalent reaction, docking studies using FlexX²¹ and MOE (Molecular Operating Environment, 2022.02 Chemical Computing Group ULC, Montreal, Canada, 2023) were performed (Supporting Information). Because the catalytic loop (residues 79–96) is not resolved in the crystal structure of hDNMT2 (PDB 1G55), it was introduced using the “Loop Modeler” functionality within MOE.

Based on the docking-predicted binding modes, the benzyl derivative 45 as well as the aromatic sulfonamides 78–80 and 91 expand from the SAM site toward the cytidine binding site. Figure 6 shows the binding poses of compound 80 as an example. The proximity of the electrophilic carbon atoms to the nucleophilic sulfur atom of the catalytic Cys79 of 3.9–4.2 Å (Table S3) indicated high likelihood of a covalent reaction.

Conclusion. In this letter, we presented covalent SAH-based hDNMT2 inhibitors with a new type of aryl warhead. By successfully applying the *Topliss* scheme to the moderate inhibitor *N*-benzyl-adenosyl-Dab 2,⁹ electron-deficient benzyl derivatives (4-Cl-3-CF₃ 41, 4-NO₂-3-CF₃ 45) exhibiting stronger hDNMT2 inhibition were identified. Based on these findings, the electrophilicity was further increased by replacing the methylenamine substructure with a sulfonamide function. We performed a subsequent SAR study using different aryl sulfonyl building blocks with strong electron-withdrawing groups such as NO₂ and CF₃ as well as intracyclic nitrogen atoms. By attaching halogen leaving groups, the aromatic rings were adjusted to enable a covalent reaction with the catalytically active cysteine of hDNMT2. Protein mass spectrometry revealed that the 4-halogen-3-NO₂-decorated phenylsulfona-

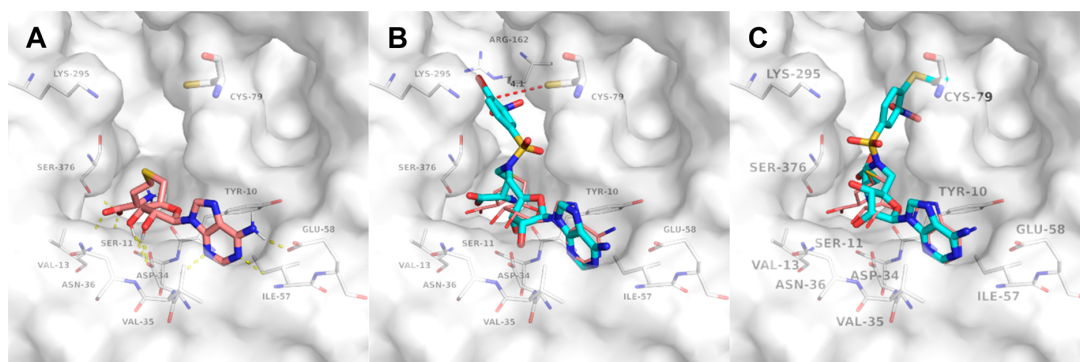


Figure 6. Noncovalent and covalent docking of compound **80** (cyan) with SAH as reference (salmon). (A) Crystal structure of SAH (PDB 1G55). (B) Noncovalent docking of compound **80**. The distance of the electrophilic carbon to Cys79 is indicated with a red dotted line. (C) Covalent docking of compound **80**.

imide derivatives **78–80** and the 2-chloropyrazine structure **91** reacted covalently with the catalytically active Cys79 in the cytidine site of hDNMT2. However, compounds **79** and **91** exhibited too high reactivity as they also bound to Cys287 on the protein surface. Furthermore, a stability test showed that **79** was quickly inactivated by reaction with DTT (Figure 3). Our results highlighted the nonpromiscuous binding behavior of compounds **78** and **80**, which exclusively reacted with the catalytically active Cys79, although four solvent-exposed cysteines can be found in the hDNMT2 crystal structure. The most promising covalent inhibitor turned out to be the 4-Br-3-NO₂-phenylsulfonamide derivative **80**, with an IC₅₀ value of 1.2 ± 0.1 μM resulting in an improvement of 1 order of magnitude compared to our previously published inhibitors.⁹ Therefore, it outclasses the natural ligands SAH and SFG. Moreover, compound **80** showed high selectivity toward NSUN2 and NSUN6 (Figure 5). With the discovery of covalent hDNMT2 inhibitors, this study provides a suitable basis for the development of fluorescently ABPs. Such tool compounds can be used for future studies to improve the understanding of RNA methyltransferases and the biological impact of their RNA modifications.

■ ASSOCIATED CONTENT

Supporting Information

The Supporting Information is available free of charge at <https://pubs.acs.org/doi/10.1021/acsmchemlett.3c00062>.

Synthesis protocols and analytical data of all compounds, NMR spectra, LC-MS chromatograms of all tested compounds, MST traces, ITC curves, molecular docking results (PDF)

■ AUTHOR INFORMATION

Corresponding Authors

Tanja Schirmeister – Institute of Pharmaceutical and Biomedical Sciences, Johannes Gutenberg University Mainz, D-55128 Mainz, Germany; Phone: +49 6131 39-25742; Email: schirmei@uni-mainz.de

Mark Helm – Institute of Pharmaceutical and Biomedical Sciences, Johannes Gutenberg University Mainz, D-55128 Mainz, Germany; orcid.org/0000-0002-0154-0928; Phone: +49 6131 39-25731; Email: mhelm@uni-mainz.de

Authors

Marvin Schwickert – Institute of Pharmaceutical and Biomedical Sciences, Johannes Gutenberg University Mainz, D-55128 Mainz, Germany; orcid.org/0000-0002-1385-1416

Robert A. Zimmermann – Institute of Pharmaceutical and Biomedical Sciences, Johannes Gutenberg University Mainz, D-55128 Mainz, Germany; orcid.org/0000-0002-5330-9234

Tanja Habeck – Technical University of Darmstadt, D-64287 Darmstadt, Germany

Sabrina N. Hoba – Institute of Pharmaceutical and Biomedical Sciences, Johannes Gutenberg University Mainz, D-55128 Mainz, Germany

Zarina Nidoieva – Institute of Pharmaceutical and Biomedical Sciences, Johannes Gutenberg University Mainz, D-55128 Mainz, Germany; orcid.org/0000-0001-5364-7527

Tim R. Fischer – Institute of Pharmaceutical and Biomedical Sciences, Johannes Gutenberg University Mainz, D-55128 Mainz, Germany

Martin M. Stark – Institute of Pharmaceutical and Biomedical Sciences, Johannes Gutenberg University Mainz, D-55128 Mainz, Germany

Christian Kersten – Institute of Pharmaceutical and Biomedical Sciences, Johannes Gutenberg University Mainz, D-55128 Mainz, Germany; orcid.org/0000-0001-9976-7639

Frederik Lermyte – Technical University of Darmstadt, D-64287 Darmstadt, Germany

Complete contact information is available at: <https://pubs.acs.org/doi/10.1021/acsmchemlett.3c00062>

Author Contributions

§M.S. and R.A.Z. contributed equally.

Notes

The authors declare the following competing financial interest(s): Mark Helm is a consultant for Moderna Inc.

■ ACKNOWLEDGMENTS

Financial support by the Deutsche Forschungsgemeinschaft (DFG, German Research Foundation), project numbers 439669440 TRR319 RMaP TP A01 (T.S.), C01, and C03 (M.H.) is gratefully acknowledged. Z.N. gratefully acknowledges financial support by the Volkswagen Stiftung. Financial

support for F.L. was provided by LOEWE project TRABITA funded by the Hessian Ministry of Higher Education, Research, and the Arts (HMWK). The Synapt XS instrument was partially funded through project number 461372424 of the German Research Foundation (DFG). Additional support by the Fonds der Chemischen Industrie (Sachkostenzuschuss to F.L.) is gratefully acknowledged. We thank Rebecca Federkiel (University of Mainz) for her practical support with the MST experiments.

■ ABBREVIATIONS

ABP, activity-based probe; 5-FAM, 5-carboxyfluorescein; Dab, 2,4-diaminobutyric acid; DCE, dichloroethane; DCM, dichloromethane; DNMT, DNA N-methyltransferase; DTT, dithiothreitol; FTAD, 5-FAM-triazolyl-adenosyl-Dab; ITC, isothermal titration calorimetry; MST, microscale thermophoresis; MTase, methyltransferase; NSUN, NOL1/NOP2/sun domain; RMSD, root-mean-square deviation; SAH, S-adenosylhomocysteine; SAM, S-adenosylmethionine; SFG, sinefungin; TCEP, tris(2-carboxyethyl)phosphine; TFA, trifluoroacetic acid; THF, tetrahydrofuran; TRIS, tris(hydroxymethyl)aminomethane

■ REFERENCES

- (1) Jonkhout, N.; Tran, J.; Smith, M. A.; Schonrock, N.; Mattick, J. S.; Novoa, E. M. The RNA Modification Landscape in Human Disease. *RNA* **2017**, *23* (12), 1754–1769.
- (2) Liebers, R.; Rassoulzadegan, M.; Lyko, F. Epigenetic Regulation by Heritable RNA. *PLoS Genet.* **2014**, *10*, e1004296.
- (3) Wang, Y.; Chen, Z.-P.; Hu, H.; Lei, J.; Zhou, Z.; Yao, B.; Chen, L.; Liang, G.; Zhan, S.; Zhu, X.; Jin, F.; Ma, R.; Zhang, J.; Liang, H.; Xing, M.; Chen, X.-R.; Zhang, C.-Y.; Zhu, J.-N.; Chen, X. Sperm MicroRNAs Confer Depression Susceptibility to Offspring. *Sci. Adv.* **2021**, *7*, eabd7605.
- (4) Zhang, Y.; Shi, J.; Rassoulzadegan, M.; Tuorto, F.; Chen, Q. Sperm RNA Code Programmes the Metabolic Health of Offspring. *Nat. Rev. Endocrinol.* **2019**, *15* (8), 489–498.
- (5) Chen, Q.; Yan, M.; Cao, Z.; Li, X.; Zhang, Y.; Shi, J.; Feng, G.; Peng, H.; Zhang, X.; Zhang, Y.; Qian, J.; Duan, E.; Zhai, Q.; Zhou, Q. Sperm TsRNAs Contribute to Intergenerational Inheritance of an Acquired Metabolic Disorder. *Science* **2016**, *351* (6271), 397–400.
- (6) Zhang, Y.; Zhang, X.; Shi, J.; Tuorto, F.; Li, X.; Liu, Y.; Liebers, R.; Zhang, L.; Qu, Y.; Qian, J.; Pahima, M.; Liu, Y.; Yan, M.; Cao, Z.; Lei, X.; Cao, Y.; Peng, H.; Liu, S.; Wang, Y.; Zheng, H.; Woolsey, R.; Quilici, D.; Zhai, Q.; Li, L.; Zhou, T.; Yan, W.; Lyko, F.; Zhang, Y.; Zhou, Q.; Duan, E.; Chen, Q. Dnmt2 Mediates Intergenerational Transmission of Paternally Acquired Metabolic Disorders through Sperm Small Non-Coding RNAs. *Nat. Cell Biol.* **2018**, *20* (5), 535–540.
- (7) Goll, M. G.; Kirpekar, F.; Maggert, K. A.; Yoder, J. A.; Hsieh, C. L.; Zhang, X.; Golic, K. G.; Jacobsen, S. E.; Bestor, T. H. Methylation of TRNA^{Asp} by the DNA Methyltransferase Homolog Dnmt2. *Science* (80-) **2006**, *311* (5759), 395–398.
- (8) Jeltsch, A.; Ehrenhofer-Murray, A.; Jurkowski, T. P.; Lyko, F.; Reuter, G.; Ankri, S.; Nellen, W.; Schaefer, M.; Helm, M. Mechanism and Biological Role of Dnmt2 in Nucleic Acid Methylation. *RNA Biol.* **2017**, *14* (9), 1108–1123.
- (9) Schwickert, M.; Fischer, T. R.; Zimmermann, R. A.; Hoba, S. N.; Meidner, J. L.; Weber, M.; Weber, M.; Stark, M. M.; Koch, J.; Jung, N.; Kersten, C.; Windbergs, M.; Lyko, F.; Helm, M.; Schirmeister, T. Discovery of Inhibitors of DNA Methyltransferase 2, an Epitranscriptomic Modulator and Potential Target for Cancer Treatment. *J. Med. Chem.* **2022**, *65*, 9750.
- (10) Ganesan, A.; Arimondo, P. B.; Rots, M. G.; Jeronimo, C.; Berdasco, M. The Timeline of Epigenetic Drug Discovery: From Reality to Dreams. *Clin. Epigenetics* **2019**, *11* (1), 174.
- (11) Fontecave, M.; Atta, M.; Mulliez, E. S-Adenosylmethionine: Nothing Goes to Waste. *Trends Biochem. Sci.* **2004**, *29* (5), 243–249.
- (12) Petrossian, T. C.; Clarke, S. G. Uncovering the Human Methyltransferasome. *Mol. Cell. Proteomics* **2011**, *10*, M110.000976.
- (13) De Cesco, S.; Kurian, J.; Dufresne, C.; Mittermaier, A. K.; Moitessier, N. Covalent Inhibitors Design and Discovery. *Eur. J. Med. Chem.* **2017**, *138*, 96–114.
- (14) Lyko, F. The DNA Methyltransferase Family: A Versatile Toolkit for Epigenetic Regulation. *Nat. Rev. Genet.* **2018**, *19* (2), 81–92.
- (15) Bohnsack, K. E.; Höbartner, C.; Bohnsack, M. T. Eukaryotic 5-Methylcytosine (M⁵C) RNA Methyltransferases: Mechanisms, Cellular Functions, and Links to Disease. *Genes (Basel)* **2019**, *10*, 102.
- (16) Sun, Q.; Huang, M.; Wei, Y. Diversity of the Reaction Mechanisms of SAM-Dependent Enzymes. *Acta Pharm. Sin. B* **2021**, *11* (3), 632–650.
- (17) Lee, J.; Schapira, M. The Promise and Peril of Chemical Probe Negative Controls. *ACS Chem. Biol.* **2021**, *16*, 579–585.
- (18) Topliss, J. G. Utilization of Operational Schemes for Analog Synthesis in Drug Design. *J. Med. Chem.* **1972**, *15* (10), 1006–1011.
- (19) Cooper, M.; Miller, D.; Macleod, A.; Van Wiltenburg, J.; Thom, S.; St-Gallay, S.; Shannon, J.; Alanine, T.; Onions, S.; Strutt, I. Novel Sulfonamide Carboxamide Compounds. WO2019/8025A1, 2019.
- (20) Zimmermann, R. A.; Schwickert, M.; Meidner, J. L.; Nidoieva, Z.; Helm, M.; Schirmeister, T. An Optimized Microscale Thermophoresis Method for High-Throughput Screening of DNA Methyltransferase 2 Ligands. *ACS Pharmacol. Transl. Sci.* **2022**, *5* (11), 1079–1085.
- (21) Rarey, M.; Kramer, B.; Lengauer, T.; Klebe, G. A Fast Flexible Docking Method Using an Incremental Construction Algorithm. *J. Mol. Biol.* **1996**, *261* (3), 470–489.

Supporting Information

Covalent *S*-Adenosylhomocysteine-Based DNA Methyltransferase 2 Inhibitors with a New Type of Aryl Warhead

Marvin Schwickert,^{‡,#} Robert A. Zimmermann,^{‡,#} Tanja Habeck,[†] Sabrina N. Hoba,[#] Zarina Nidoieva,[#] Tim R. Fischer,[#] Martin M. Stark,[#] Christian Kersten,[#] Frederik Lermyte,[†] Mark Helm^{#*} and Tanja Schirmeister^{#*}

[#]Institute of Pharmaceutical and Biomedical Sciences, Johannes Gutenberg University Mainz, Staudinger Weg 5, D-55128 Mainz, Germany

[†]Technical University of Darmstadt, Alarich-Weiss-Str. 4, D-64287 Darmstadt, Germany

*Corresponding authors:

Prof. Dr. Tanja Schirmeister, Phone: +49 6131 39-25742, E-Mail: schirmei@uni-mainz.de.

Prof. Dr. Mark Helm, Phone: +49 6131 39-25731, E-Mail: mhelm@uni-mainz.de

[‡]These authors contributed equally.

TABLE OF CONTENT

SYNTHESES	3
NMR SPECTRA AND CHROMATOGRAMS	32
ENZYME EXPRESSION AND PURIFICATION	106
MICROSCALE THERMOPHORESIS (MST)	108
MST PLOTS	109
ISOTHERMAL TITRATION CALORIMETRY (ITC)	117
ITC THERMOGRAMS	118
TRITIUM INCORPORATION ASSAY (³ H-ASSAY)	139
PROTEIN MASS SPECTROMETRY	140
MOLECULAR DOCKING	149
REFERENCES	150

ENZYME EXPRESSION AND PURIFICATION

Bacterial Expression and Purification of Human Full-Length DNMT2 (hDNMT2)

Plasmid coding for the full-length human DNMT2 was kindly provided by Albert Jeltsch (University of Stuttgart, Germany). Expression was performed as described previously in literature.² The purification was conducted similar with some adjustments. Cells were disrupted in lysis buffer (50 mM sodium phosphate pH 8.0, 500 mM NaCl, 25 mM imidazole, 0.1% polysorbate-20) and centrifuged at 17,500g for 60 min at 4 °C to remove the cell debris. Clear supernatant was loaded on a HisTrap HP 5 mL column using an ÄKTA start system. To remove unspecific bound impurities, the column was washed with several column volume of lysis buffer and afterwards with several column volumes of a mixture of 96% lysis buffer and 4% elution buffer (50 mM sodium phosphate pH 8.0, 500 mM NaCl, 800 mM imidazole, 0.1% polysorbate-20). The protein was finally eluted in a mixture of 30% lysis buffer and 70% elution buffer. The increased sodium chloride concentration in this buffer allowed to skip a further ion exchange chromatography step prior to size exclusion chromatography (SEC). SEC was performed on a Superdex 16/600 75 µg column equilibrated in SEC buffer (50 mM sodium phosphate pH 8.0, 300 mM NaCl, 1 mM EDTA, 2 mM DTT, 0.1% polysorbate-20). Protein was concentrated in Amicon Ultra 15 mL centrifugal filters with a 10 kDa cut-off (EMD, Darmstadt, Germany) and was then mixed 1:4 with storage buffer (50 mM sodium phosphate pH 8.0, 300 mM NaCl, 1 mM EDTA, 2 mM DTT, 0.1% polysorbate-20, 60% glycerol). Protein was stored liquid at -20°C until further use.

Bacterial Expression and Purification of Human DNMT2 Deletion Mutant (hDNMT2Δ)

Due to a lack of stability of full-length DNMT2 in some buffer conditions a deletion mutant was designed according to a published crystal structure of DNMT2 (PDB ID: 1G55).³ This sequence lacks the amino acids 191–237 the remaining sequence was synthesised and inserted in a pET-28a(+)-vector between the NdeI and XhoI restriction sites by Genscript. The sequence was verified by Eurofins Genomics Europe. The plasmid is made available at Addgene (Addgene ID: 198382). Competent *E. coli* Rosetta 2 (DE3) pLysS cells were transformed and grown overnight in LB medium at 30 °C. 1 L of TB medium was inoculated with 20 mL of pre-culture each and was grown at 37 °C until the optical density at 600 nm of 0.7 was reached. Temperature was reduced to 20 °C, overexpression was induced with IPTG in a final concentration of 500 µM and was maintained overnight. Cells were harvested by centrifugation and were washed with lysis buffer (50 mM sodium phosphate pH 8.0, 500 mM NaCl, 25 mM imidazole, 0.1% polysorbate-20), afterwards cells were resuspended in lysis buffer again and incubated for ~ 30 min with lysozyme and DNase I on ice prior to sonication. Cells were disrupted on ice in 12 x 45 s intervals at 50% sonication power. Debris was removed by centrifugation and clear supernatant was loaded on a HisTrap HP 5 mL column. Purification was then performed as described above, with some adjustments to the SEC run. A Superdex 16/600 75 µg column equilibrated with storage buffer (200 mM ammonium acetate pH 7.1, 2 mM TCEP) was used for size exclusion chromatography, eluted protein was concentrated in Amicon Ultra 15 mL centrifugal filters with a 10 kDa cut-off (EMD, Darmstadt, Germany) to a concentration of 15 µM and was flash-frozen in liquid nitrogen. Protein was stored at -20 °C until further use.

Bacterial Expression and Purification of Human Full-Length NSUN2

Expression and purification were performed as described previously in literature.² Plasmid used for overexpression is available at Addgene (Addgene ID: 188059). Transformed *E. coli* Rosetta (DE3) pLysS cells were grown and overexpression was induced as described above. Deviating from the purification procedure described above cells were disrupted in lysis buffer (50 mM sodium phosphate pH 8.0, 300 mM NaCl, 10 mM imidazole, 0.1% polysorbate-20), and were loaded on a HisTrap HP 5 mL column. The column was washed with several column volumes of lysis buffer to remove unspecific bound impurities. Subsequently, protein was eluted in elution buffer (50 mM sodium phosphate pH 8.0, 300 mM NaCl, 500 mM imidazole, 0.1% polysorbate-20) and was further purified using a Superdex 16/600 75 pg column equilibrated with SEC buffer (50 mM sodium phosphate pH 8.0, 300 mM NaCl, 1 mM EDTA, 2 mM DTT, 0.1% polysorbate-20). Protein was concentrated using Amicon Ultra 15 mL centrifugal filters with a 10 kDa cut-off (EMD, Darmstadt, Germany) and was diluted 1:4 with storage buffer (50 mM sodium phosphate pH 8.0, 300 mM NaCl, 1 mM EDTA, 2 mM TCEP, 0.1% polysorbate-20, 60% glycerol) to allow liquid storage at -20°C until further use. Protein should be used within 2 weeks after preparation, to avoid drastic activity loss.

Bacterial Expression and Purification of Human Full-Length NSUN6

Expression and purification were performed as described previously in literature.² Plasmid used for overexpression is available at Addgene (Addgene ID: 188060). Transformed *E. coli* Rosetta (DE3) pLysS cells were grown and overexpression was induced as described above. Deviating from the purification procedure described above cells were disrupted in lysis buffer (50 mM sodium phosphate pH 7.5, 150 mM NaCl, 10 mM imidazole, 0.1% polysorbate-20), and were loaded on a HisTrap HP 5 mL column. The column was washed with several column volumes of lysis buffer to remove unspecific bound impurities. Subsequently, protein was eluted in elution buffer (50 mM sodium phosphate pH 7.5, 150 mM NaCl, 500 mM imidazole, 0.1% polysorbate-20) and was further purified using a Superdex 16/600 75 pg column equilibrated with SEC buffer (25 mM Hepes pH 7.5, 300 mM NaCl, 1 mM TCEP, 0.1% polysorbate-20, 10% glycerol). Protein was concentrated using Amicon Ultra 15 mL centrifugal filters with a 10 kDa cut-off (EMD, Darmstadt, Germany) and was diluted 1:4 with storage buffer (25 mM Hepes pH 7.5, 300 mM NaCl, 1 mM TCEP, 0.1% polysorbate-20, 60% glycerol) to allow liquid storage at -20°C until further use. Protein should be used within 2 weeks after preparation, to avoid drastic activity loss.

MICROSCALE THERMOPHORESIS (MST)

Screening

This assay was described previously in literature.⁴ Compounds were provided as 50 mM stocks in DMSO and were diluted to a concentration of 40 μ M in MST buffer (50 mM Hepes pH 7.5, 150 mM NaCl, 10 mM MgCl₂, 1 mM DTT, 0.05% polysorbate-20, 0.1% PEG-8000). Protein was mixed with 50 mM 5-FAM-triazolyl-adenosyl-Dab (FTAD) in MST buffer to receive a concentration of 4 μ M and 200 nM respectively. Diluted compound and protein were then mixed 1:1 to a final compound concentration of 20 μ M. The mixtures were incubated for 10 min at room temperature and were then loaded in standard capillaries (NanoTemper Technologies, Munich, Germany). Measurements were performed on a Monolith NT.115 with blue light settings, medium MST-power, 30% excitation power and 25 °C. Experiments were performed as duplets and data was processed using the MO. analysis software (NanoTemper Technologies, Munich, Germany). Read-out was done after 2.5 s MST-time and exported to Microsoft Excel. Normalized fluorescence after 2.5 s for every compound was compared to a DMSO control and shifts in the normalized fluorescence were calculated.

Affinity Determination

Protein was prepared as described above. Compounds were prediluted in 8 semi-logarithmic steps in DMSO, afterwards each dilution was diluted again in MST buffer to obtain a dilution series from 1 mM–100 nM. Those dilutions were mixed 1:1 with FTAD-labelled DNMT2, so a final dilution series from 500 μ M–50 nM was obtained. For less affine compounds the final dilutions series was from 750 μ M–75 nM. For every measurement a negative control with DMSO and a positive control without DNMT2 was done. Experiments were performed in triplicates with the same settings as described above. Data was processed using the MO. analysis software (NanoTemper Technologies, Munich, Germany). As MST-time 2.5 s was chosen and data points were fitted using the Hill Model.

MST PLOTS

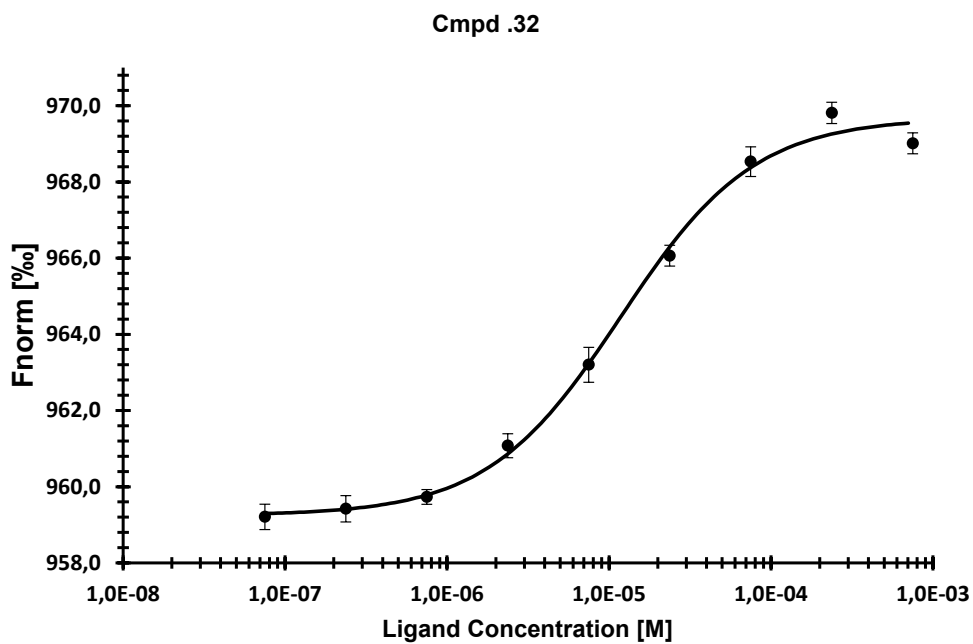


Figure S148: Binding affinity of **32** towards DNMT2 determined by MST displacement assay. Average of three experiments \pm SD is given.

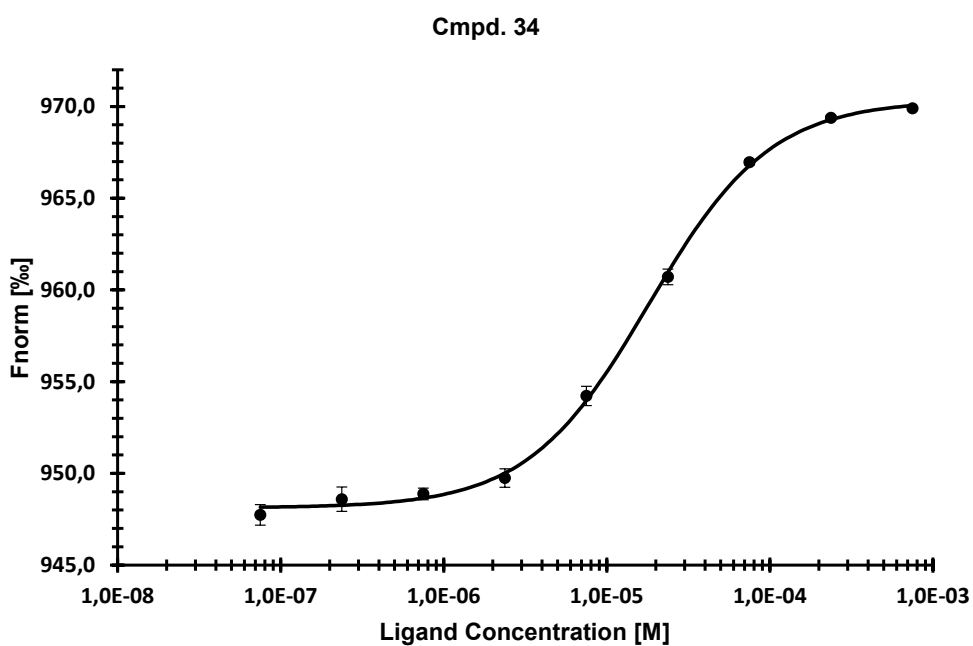


Figure S149: Binding affinity of **34** towards DNMT2 determined by MST displacement assay. Average of three experiments \pm SD is given.

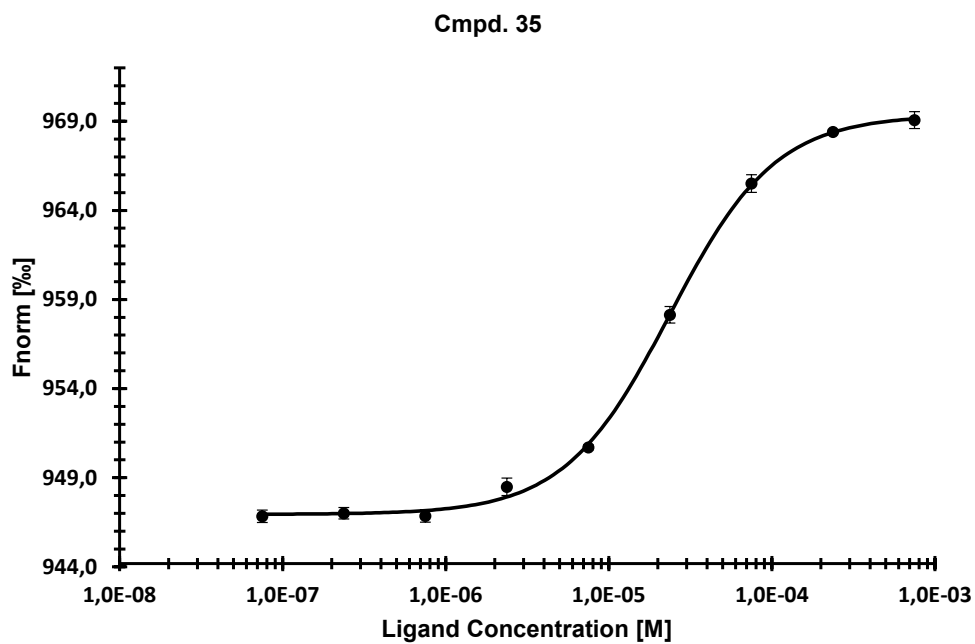


Figure S150: Binding affinity of **35** towards DNMT2 determined by MST displacement assay. Average of three experiments \pm SD is given.

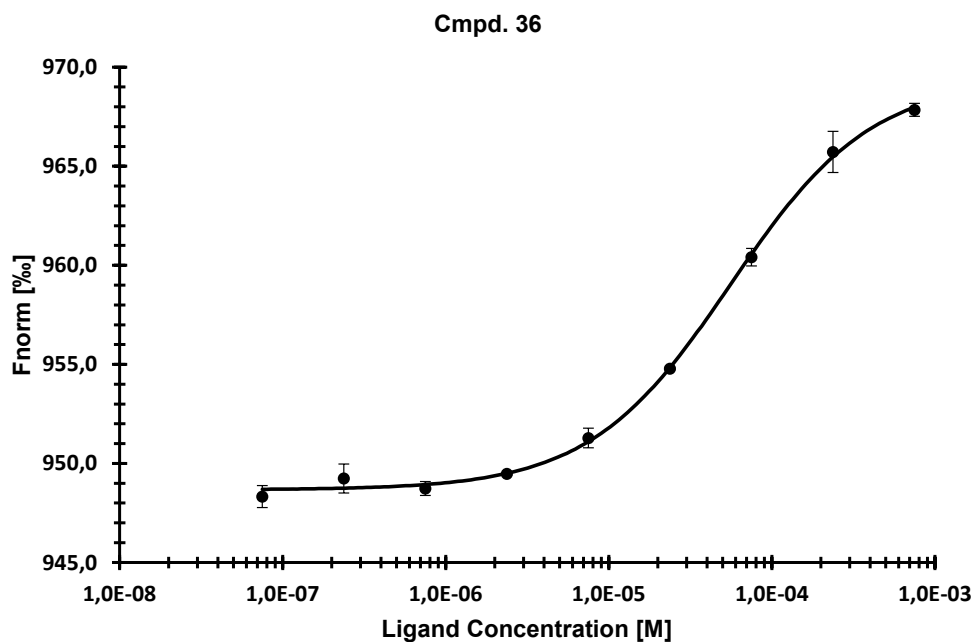


Figure S151: Binding affinity of **36** towards DNMT2 determined by MST displacement assay. Average of three experiments \pm SD is given.

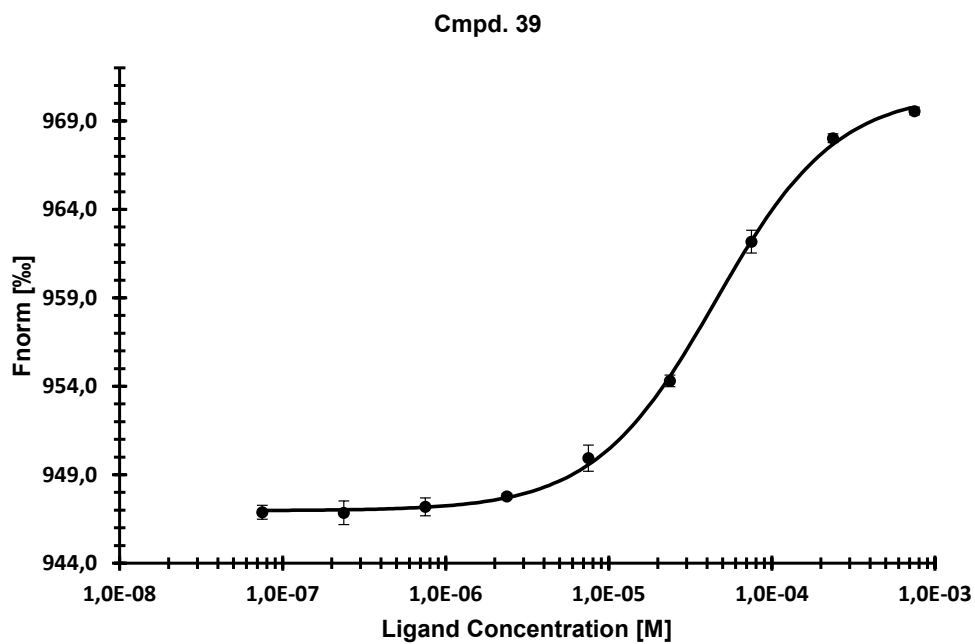


Figure S152: Binding affinity of **39** towards DNMT2 determined by MST displacement assay. Average of three experiments \pm SD is given.

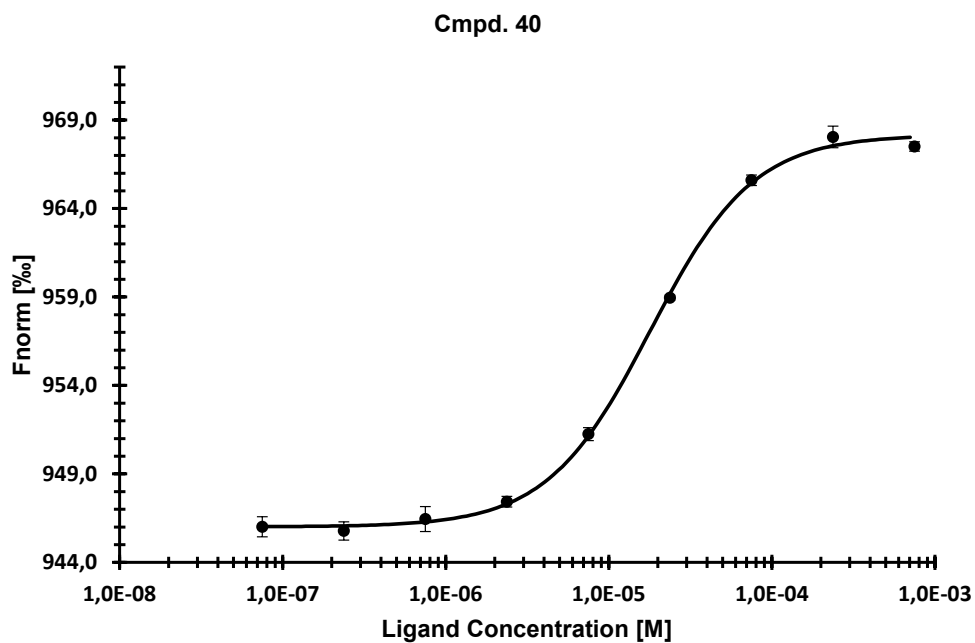


Figure S153: Binding affinity of **40** towards DNMT2 determined by MST displacement assay. Average of three experiments \pm SD is given.

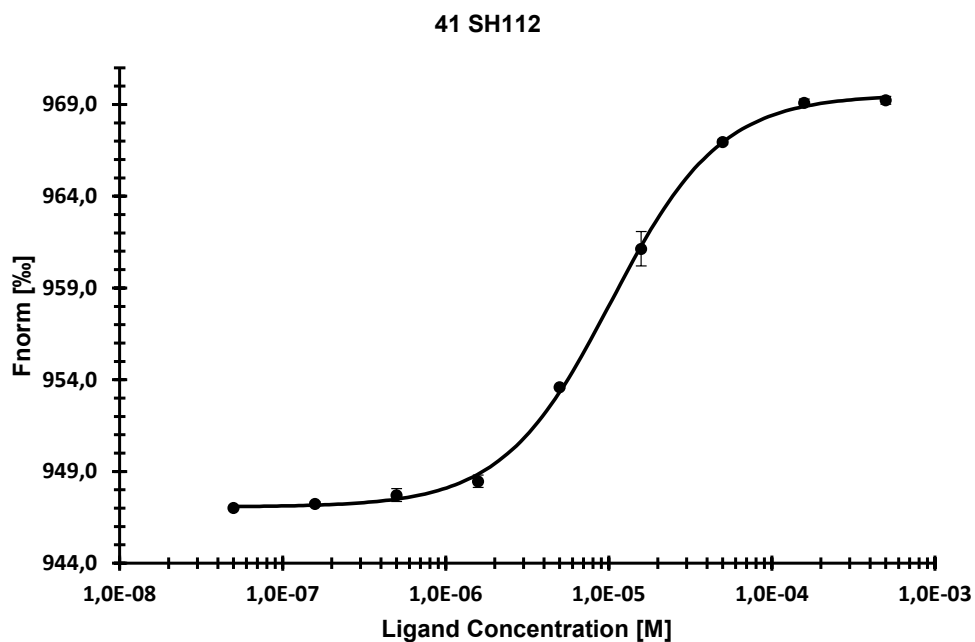


Figure S154: Binding affinity of **41** towards DNMT2 determined by MST displacement assay. Average of three experiments \pm SD is given.

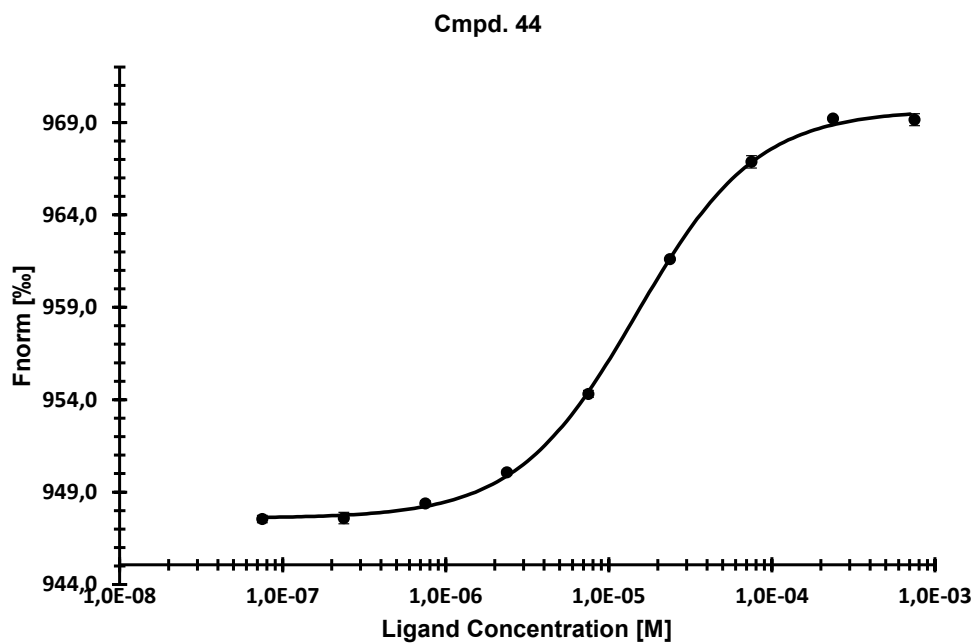


Figure S155: Binding affinity of **44** towards DNMT2 determined by MST displacement assay. Average of three experiments \pm SD is given.

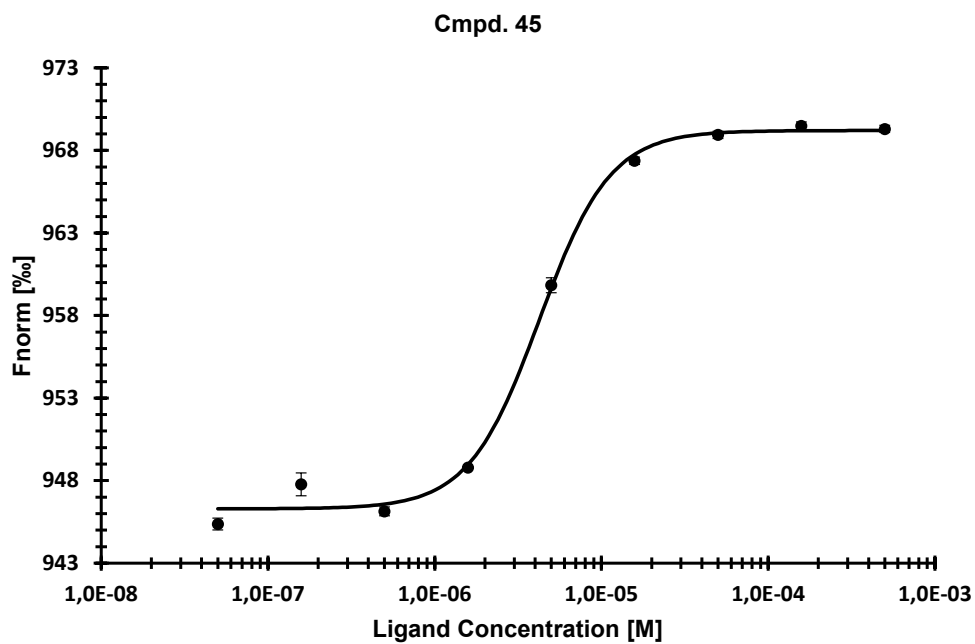


Figure S156: Binding affinity of **45** towards DNMT2 determined by MST displacement assay. Average of three experiments \pm SD is given.

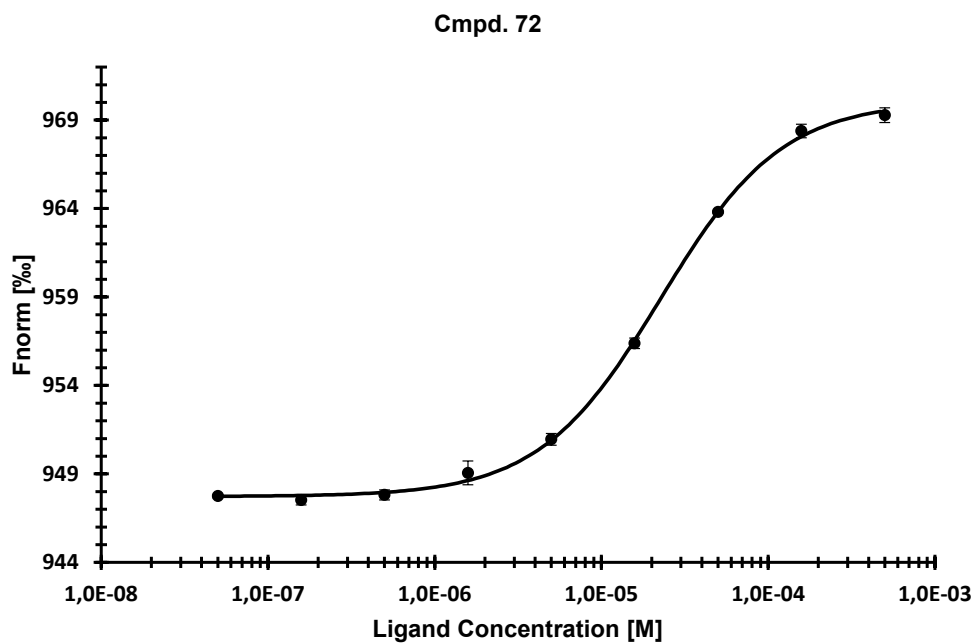


Figure S157: Binding affinity of **72** towards DNMT2 determined by MST displacement assay. Average of three experiments \pm SD is given.

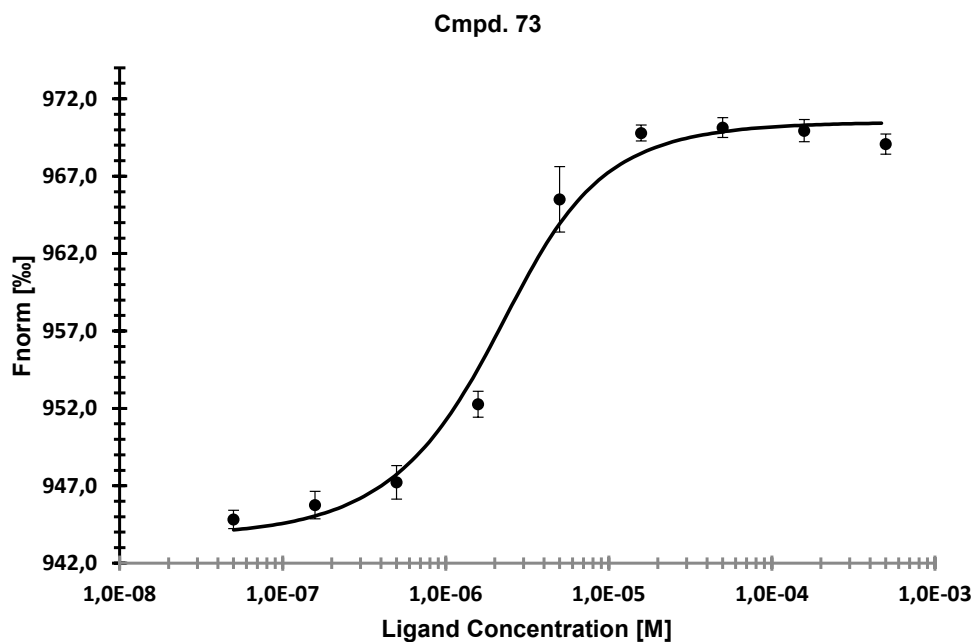


Figure S158: Binding affinity of **73** towards DNMT2 determined by MST displacement assay. Average of three experiments \pm SD is given.

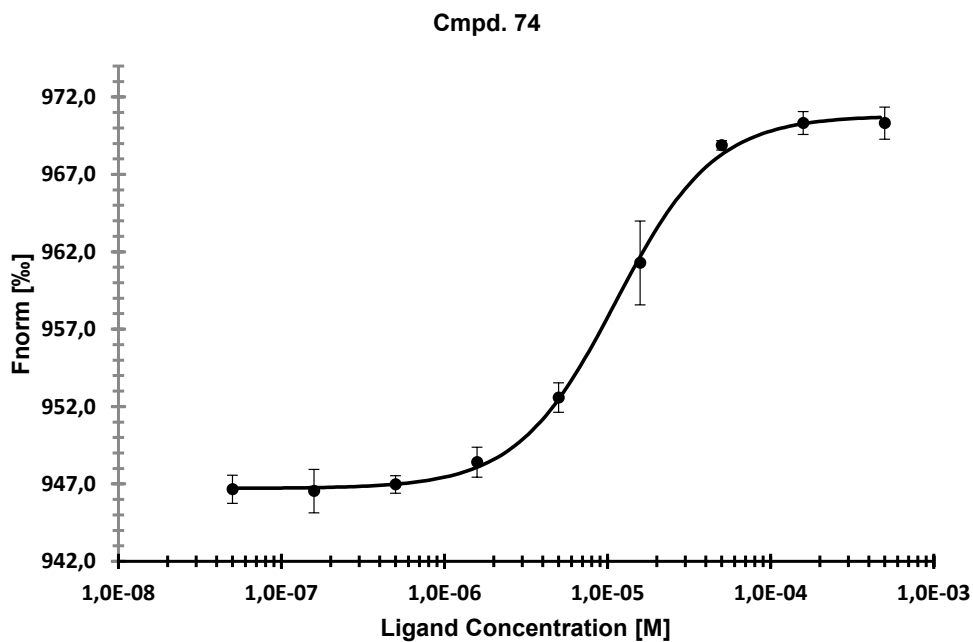


Figure S159: Binding affinity of **74** towards DNMT2 determined by MST displacement assay. Average of three experiments \pm SD is given.

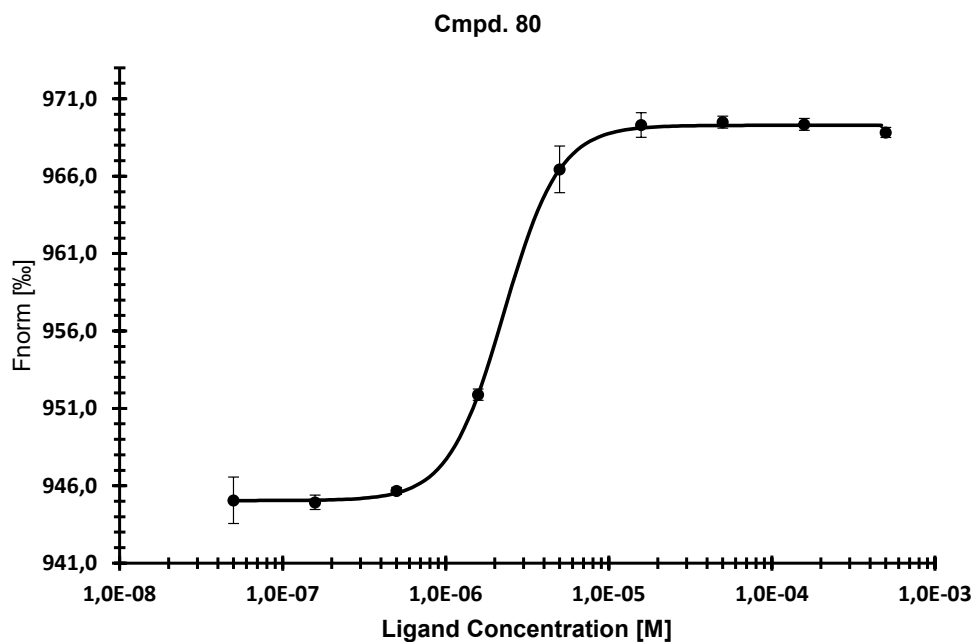


Figure S160: Binding affinity of **80** towards DNMT2 determined by MST displacement assay. Average of three experiments \pm SD is given.

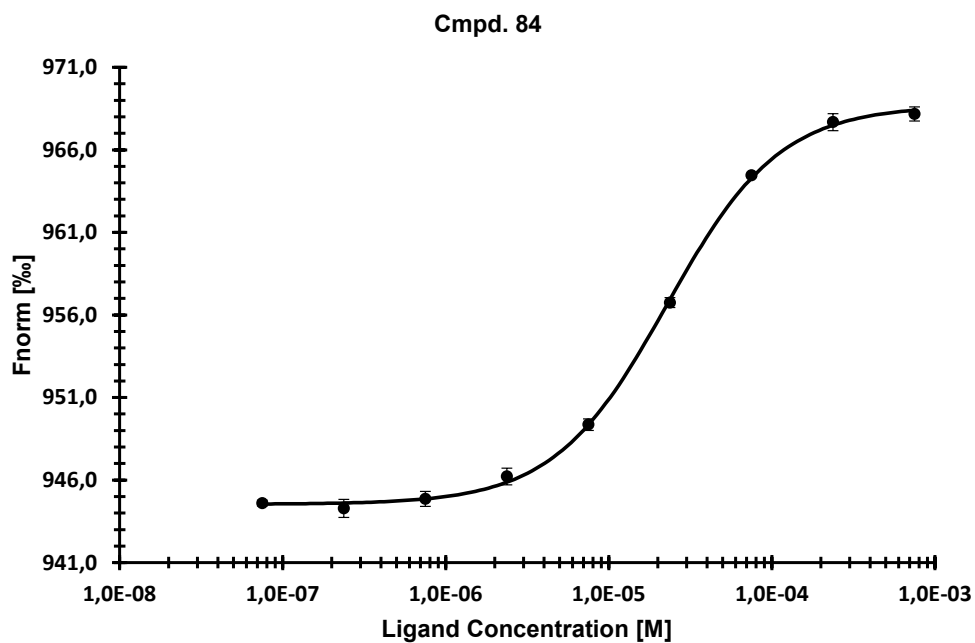


Figure S161: Binding affinity of **84** towards DNMT2 determined by MST displacement assay. Average of three experiments \pm SD is given.

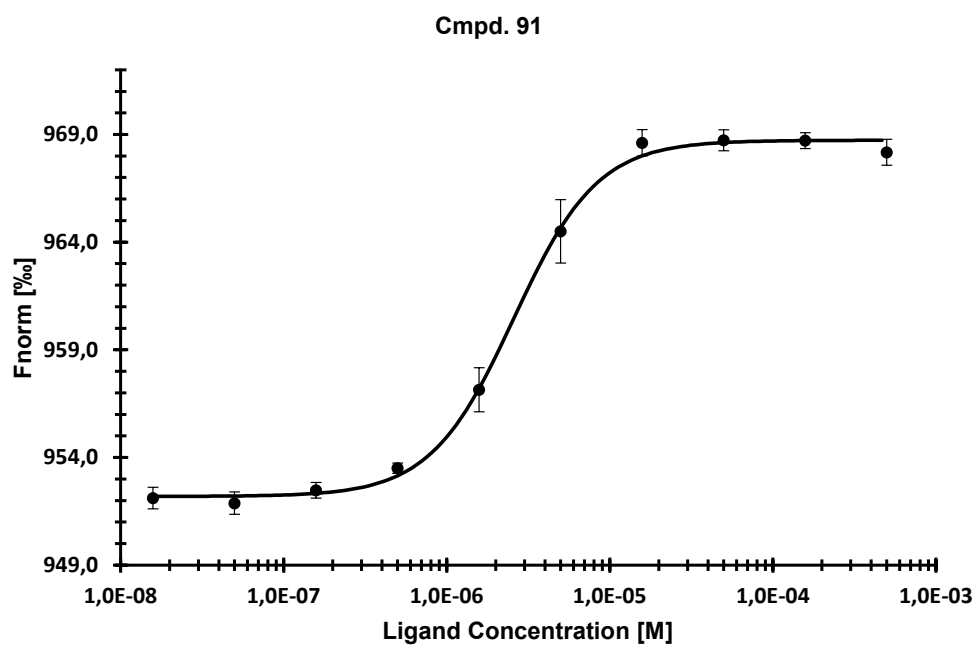


Figure S162: Binding affinity of 91 towards DNMT2 determined by MST displacement assay. Average of three experiments \pm SD is given.

ISOTHERMAL TITRATION CALORIMETRY (ITC)

Affinity Determination

Human full-length DNMT2 was buffer exchanged using a Superdex 16/600 75 μ g size-exclusion chromatography column equilibrated in ITC buffer (50 mM sodium phosphate pH 7.5, 300 mM NaCl, 0.5 EDTA, 1 mM TCEP, 0.05% polysorbate-20) and concentrated using Amicon Ultra 15 mL centrifugal filters with a 10 kDa cut-off (EMD, Darmstadt, Germany). Compounds were provided as 50 mM stocks in DMSO and were diluted in ITC buffer to a final concentration of 500 μ M (1% DMSO). Protein was diluted and buffer matched with 1% DMSO to a final protein concentration of 30 μ M. All experiments were performed using a MicroPEAK-ITC Automated (Malvern Panalytical, Malvern, UK). Measurements were performed in 13 injections at 25 °C in triplicates. Data was analyzed and fitted using MicroCal PEAQ-ITC Analysis Software 1.21. (Malvern Panalytical, Malvern, UK). Considering the low ionization heat of phosphate buffers the values were not buffer corrected.

ITC THERMOGRAMS

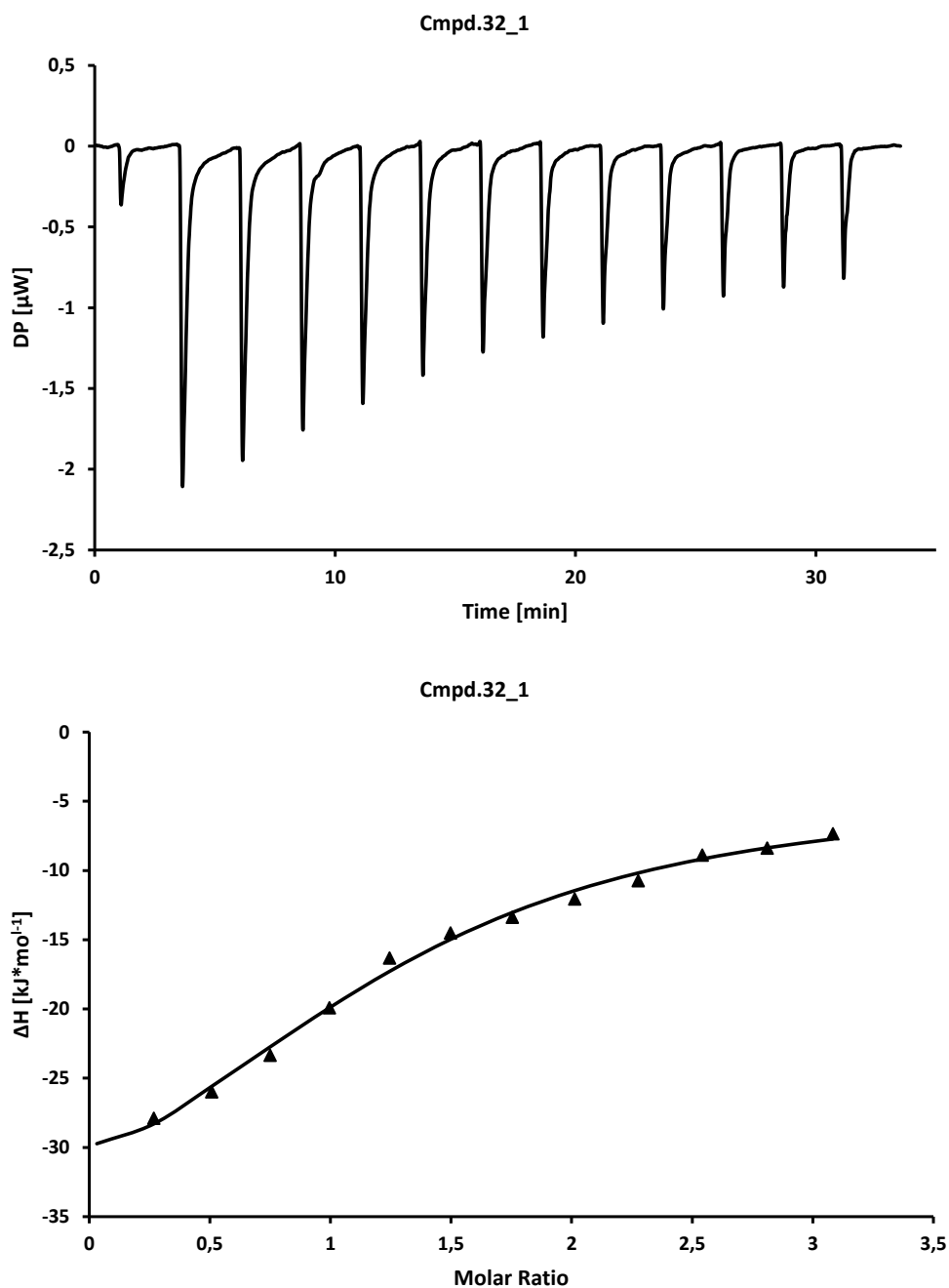


Figure S163: Binding affinity of **32** towards DNMT2 determined by Isothermal Titration Calorimetry. Above) raw ITC data of the first run. below) integrated and fitted ITC data of the first run.

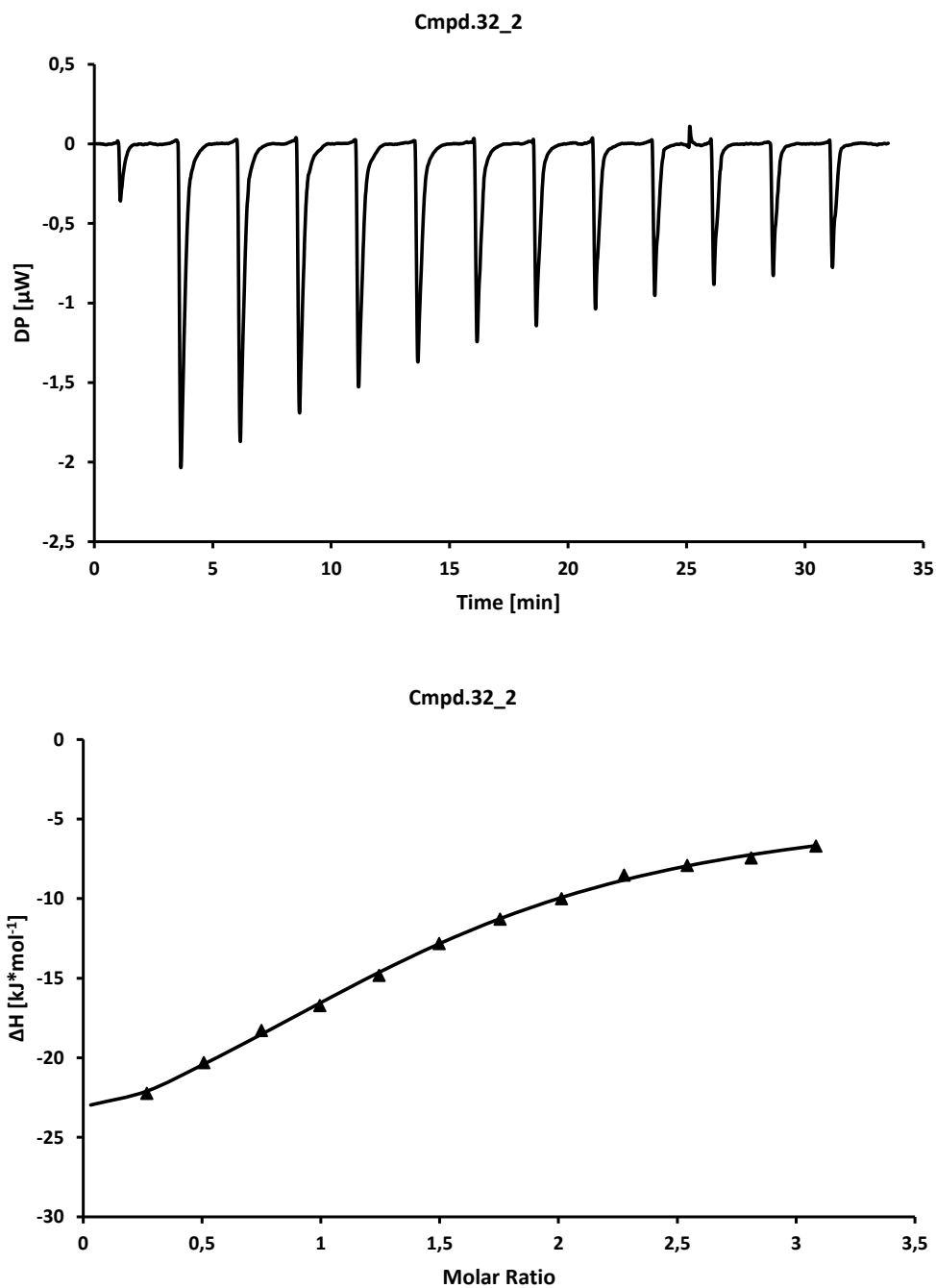


Figure S164: Binding affinity of **32** towards DNMT2 determined by Isothermal Titration Calorimetry. Above) raw ITC data of the second run. below) integrated and fitted ITC data of the second run.

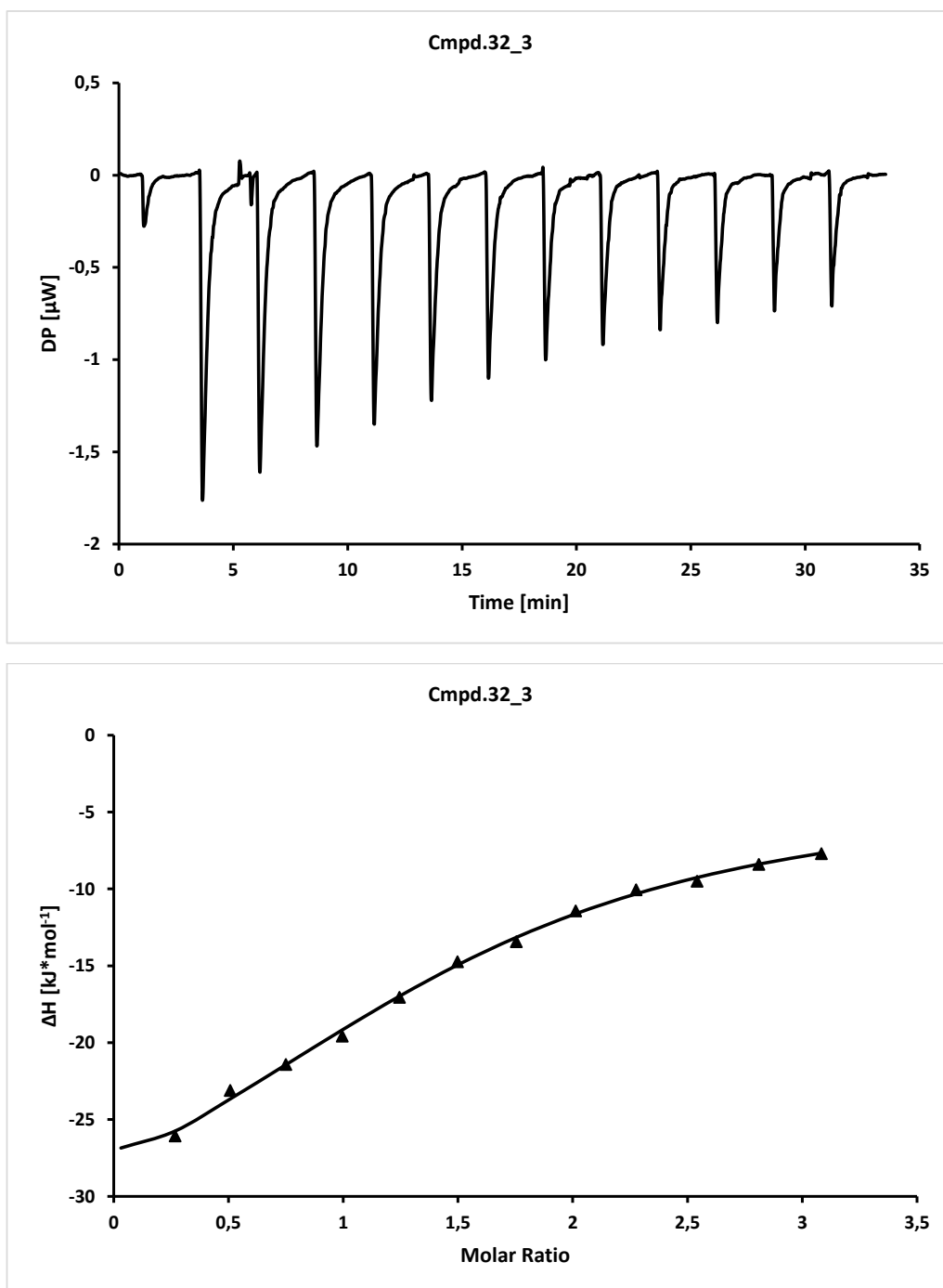


Figure S165: Binding affinity of **32** towards DNMT2 determined by Isothermal Titration Calorimetry. Above) raw ITC data of the third run. below) integrated and fitted ITC data of the third run.

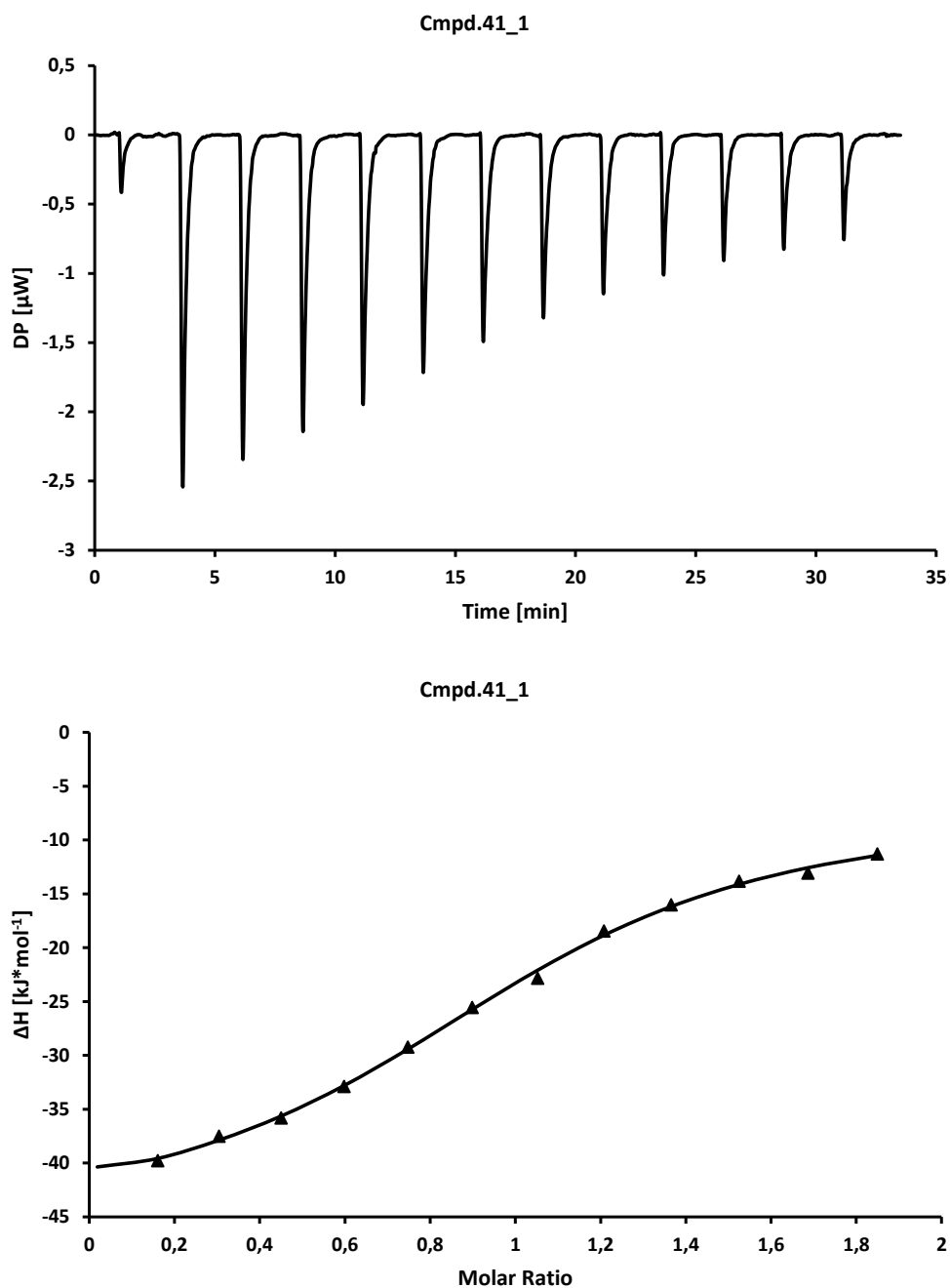


Figure S166: Binding affinity of **41** towards DNMT2 determined by Isothermal Titration Calorimetry. Above) raw ITC data of the first run. below) integrated and fitted ITC data of the first run.

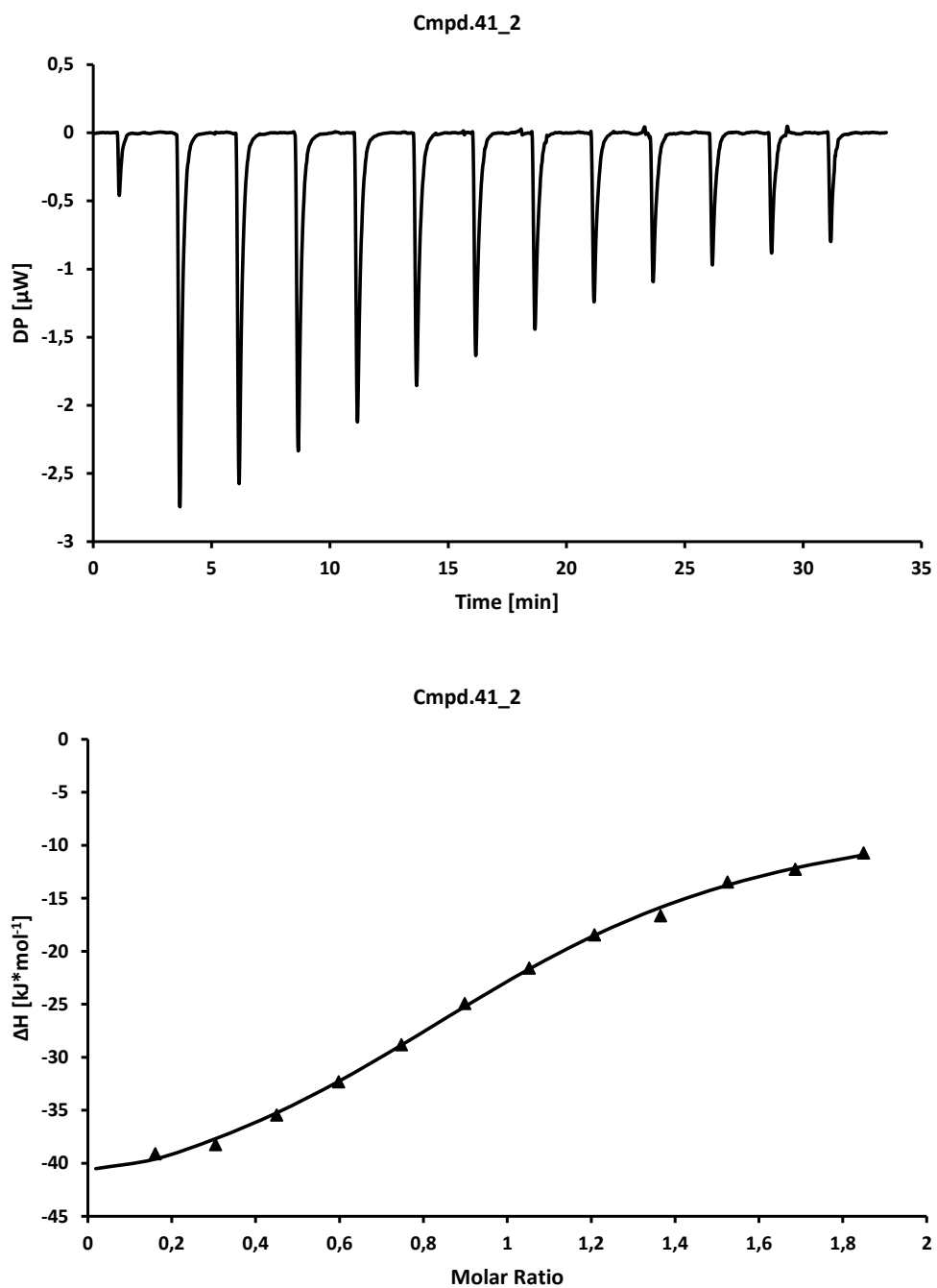


Figure S167: Binding affinity of **41** towards DNMT2 determined by Isothermal Titration Calorimetry. Above) raw ITC data of the second run. below) integrated and fitted ITC data of the second run.

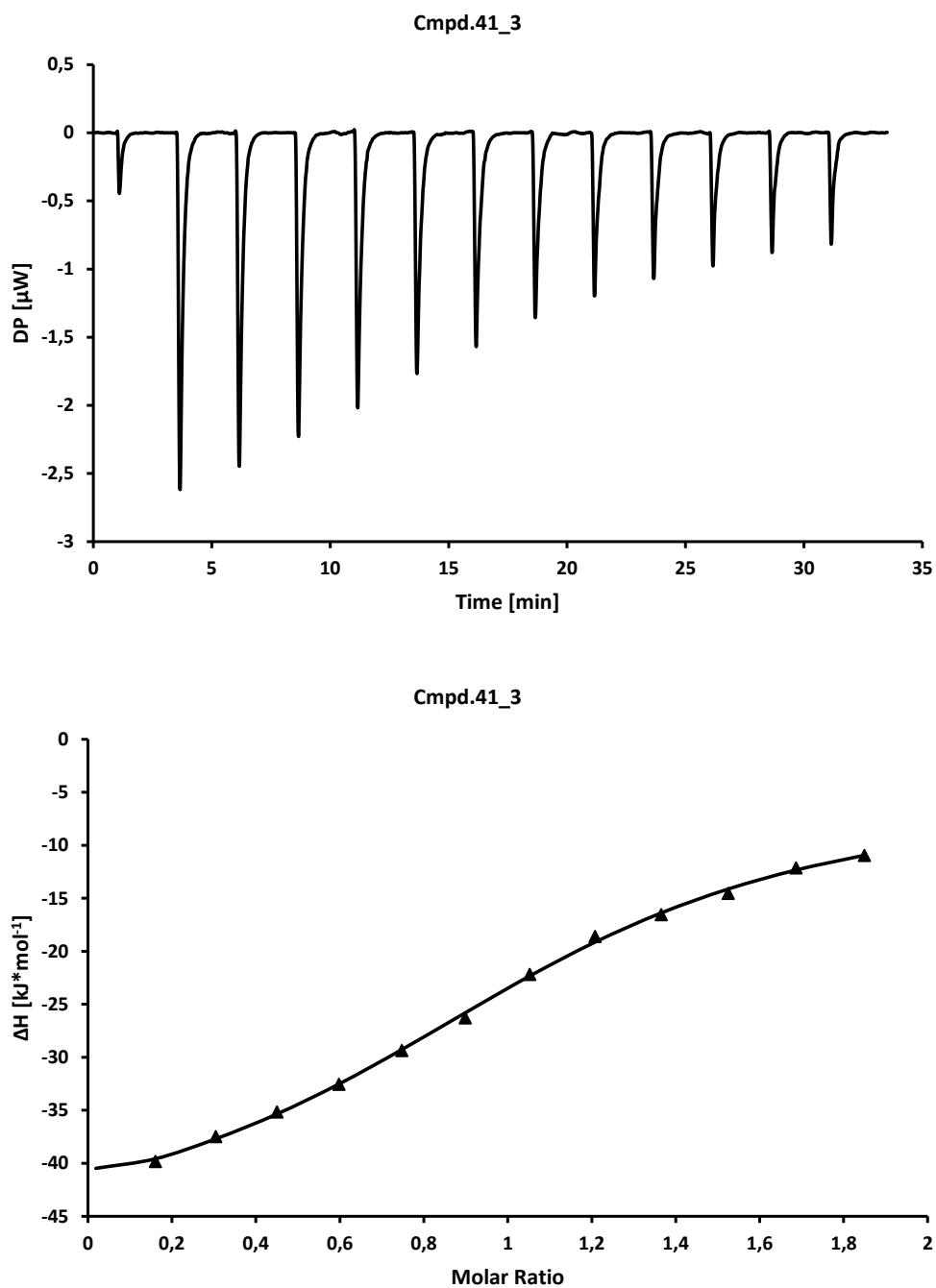


Figure S168: Binding affinity of **41** towards DNMT2 determined by Isothermal Titration Calorimetry. Above) raw ITC data of the third run. below) integrated and fitted ITC data of the third run.

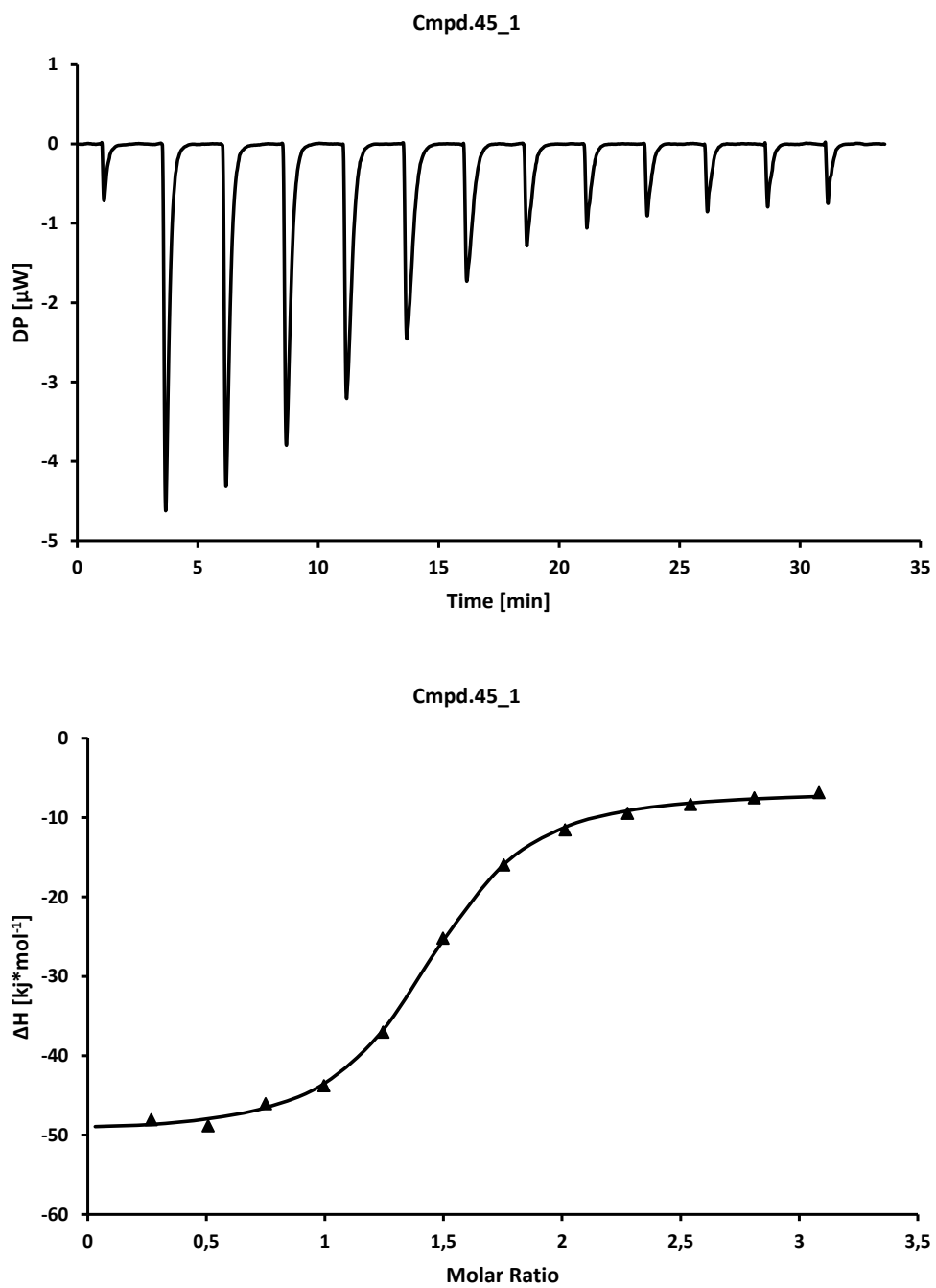


Figure S169: Binding affinity of 45 towards DNMT2 determined by Isothermal Titration Calorimetry. Above) raw ITC data of the first run. below) integrated and fitted ITC data of the first run.

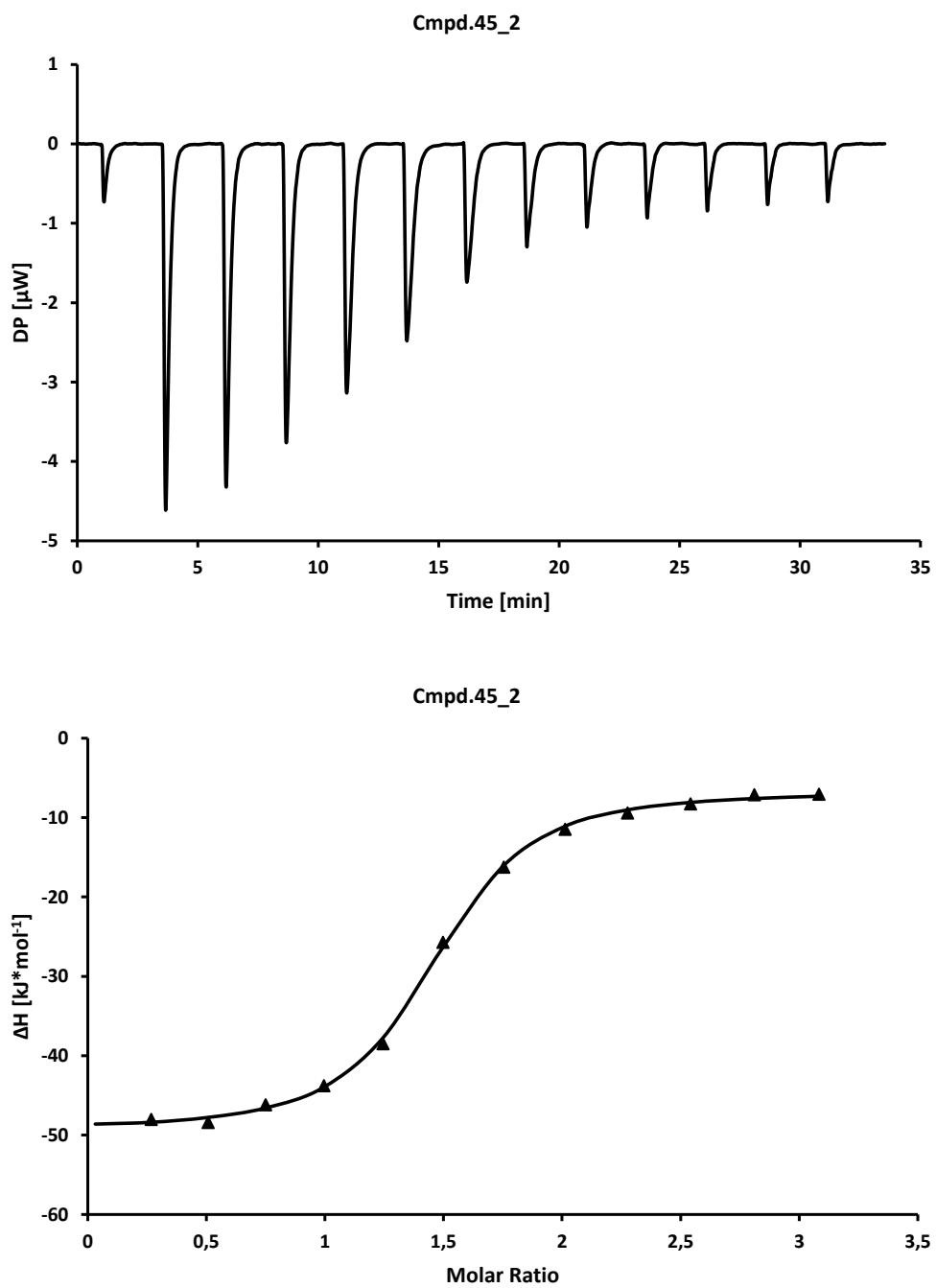


Figure S170: Binding affinity of 45 towards DNMT2 determined by Isothermal Titration Calorimetry. Above) raw ITC data of the second run. below) integrated and fitted ITC data of the second run.

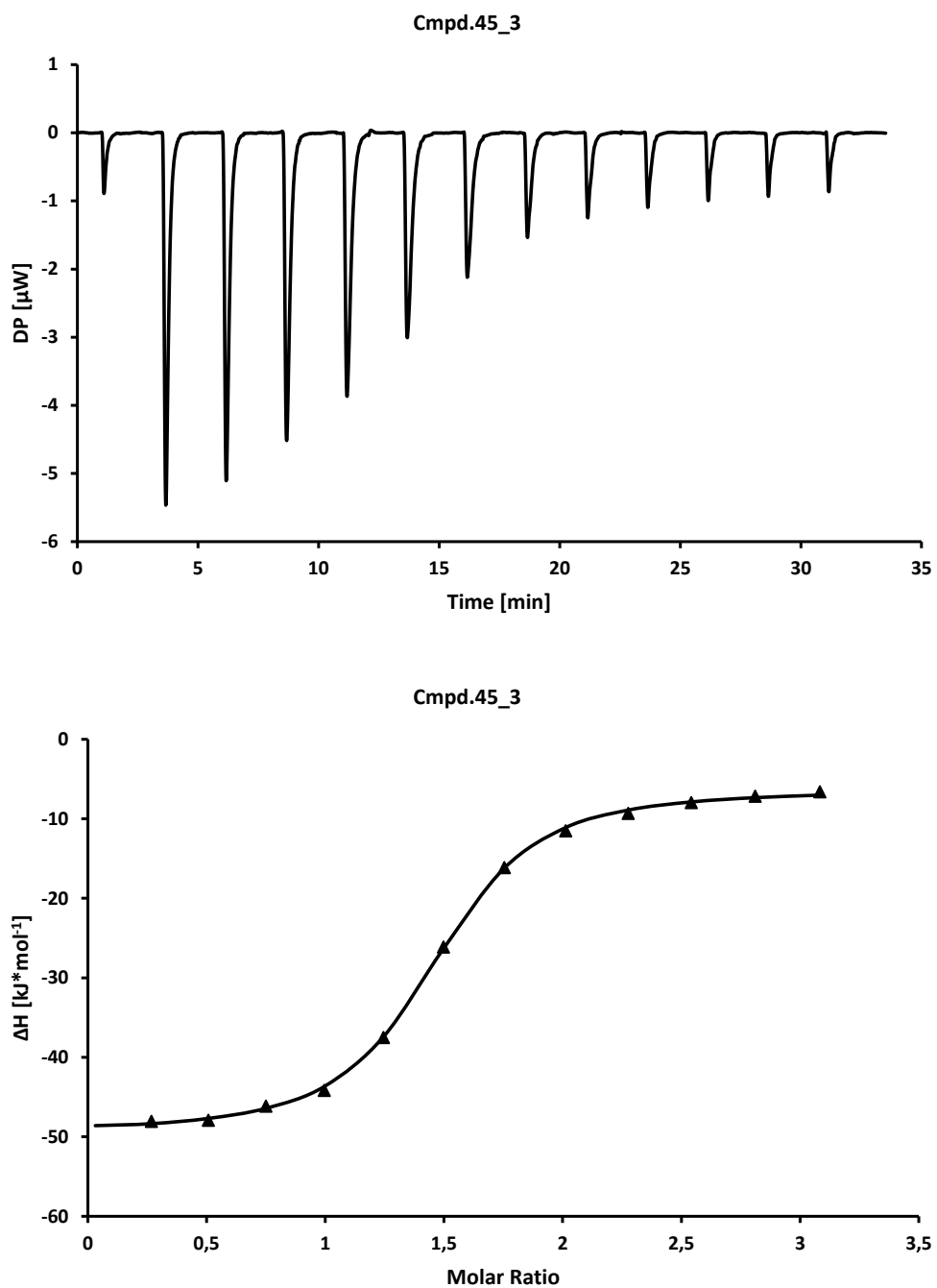


Figure S171: Binding affinity of 45 towards DNMT2 determined by Isothermal Titration Calorimetry. Above) raw ITC data of the third run. below) integrated and fitted ITC data of the third run.

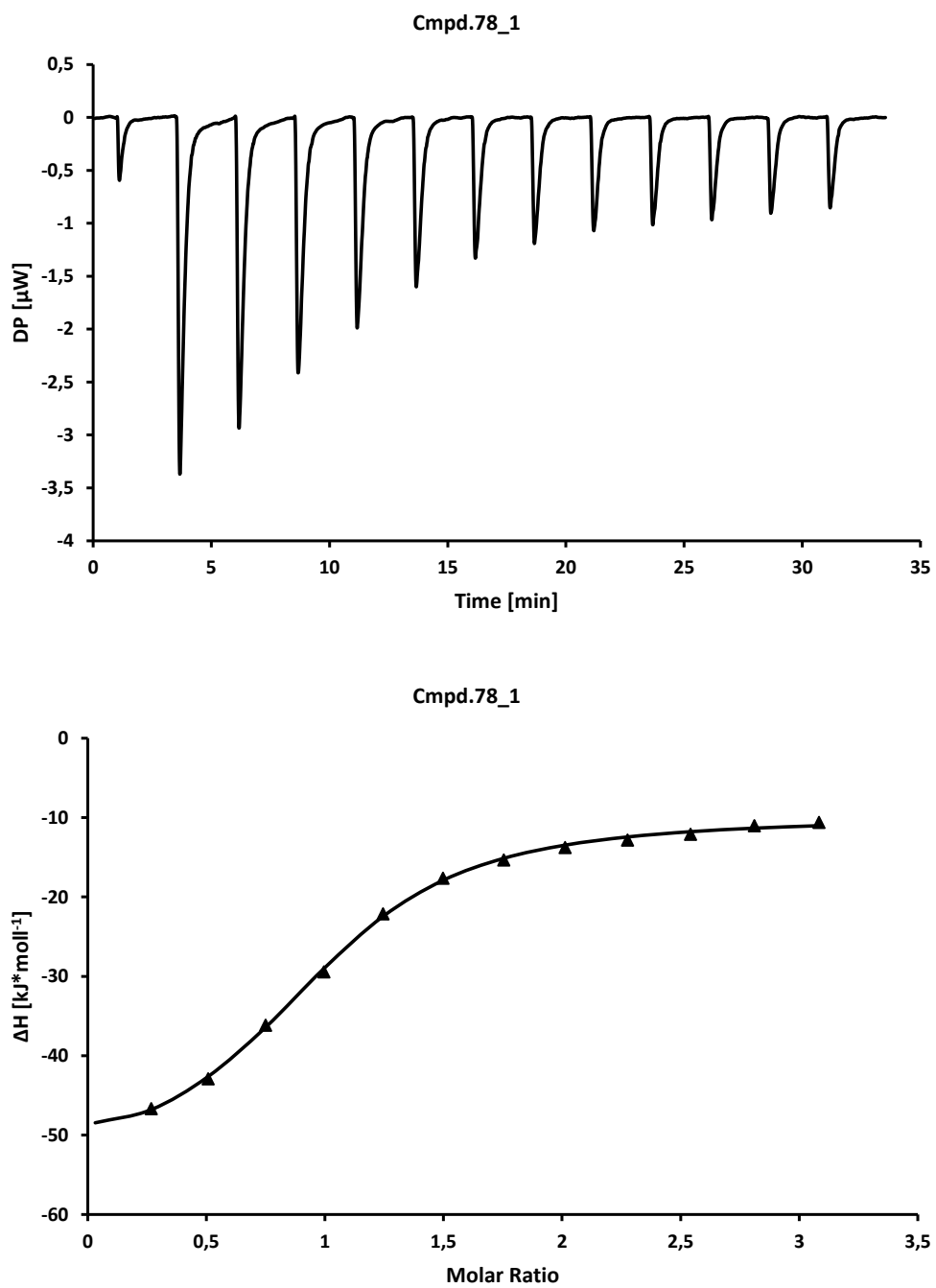


Figure S172: Binding affinity of **78** towards DNMT2 determined by Isothermal Titration Calorimetry. Above) raw ITC data of the first run. below) integrated and fitted ITC data of the first run.

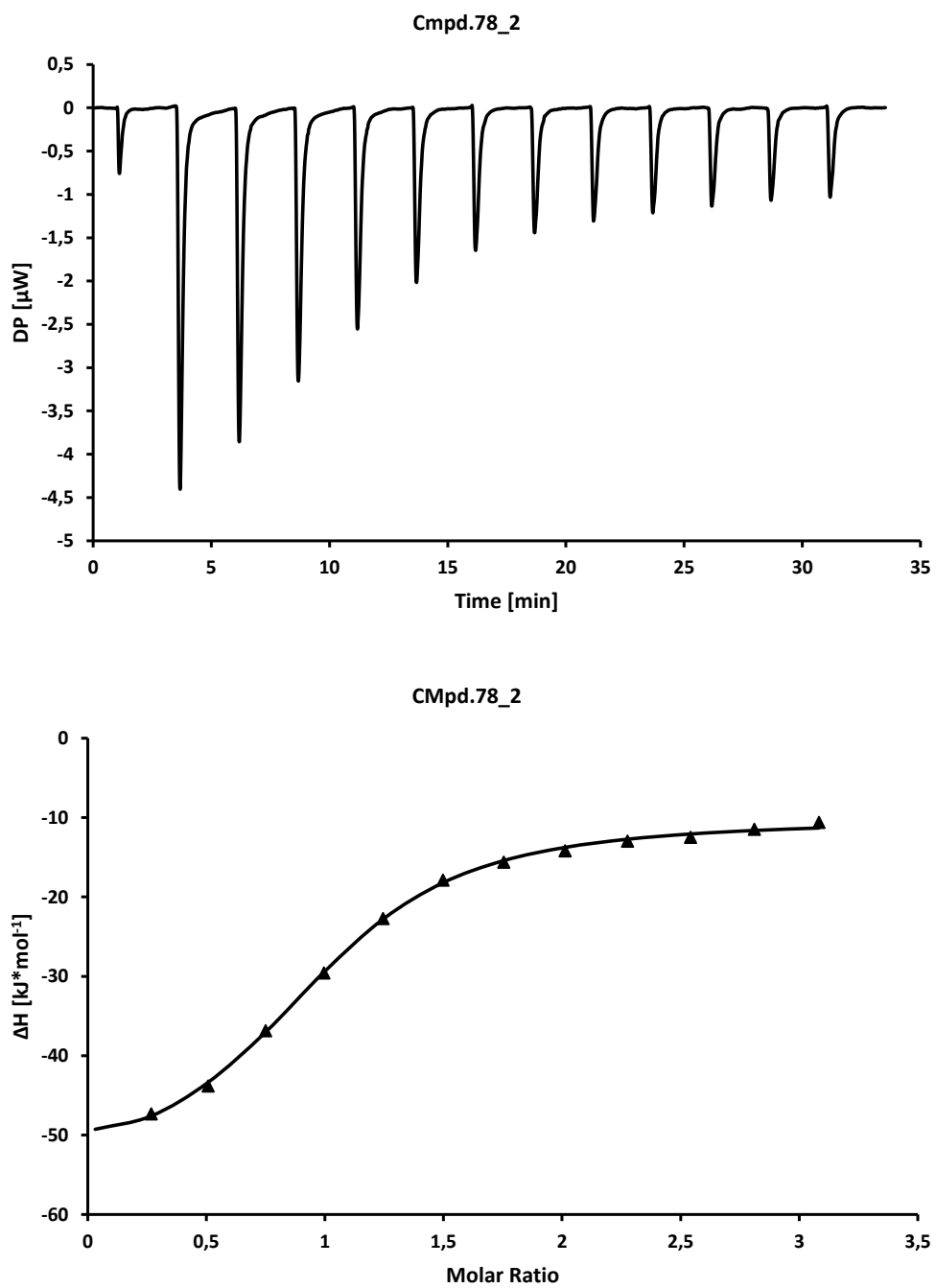


Figure S173: Binding affinity of **78** towards DNMT2 determined by Isothermal Titration Calorimetry. Above) raw ITC data of the second run. below) integrated and fitted ITC data of the second run.

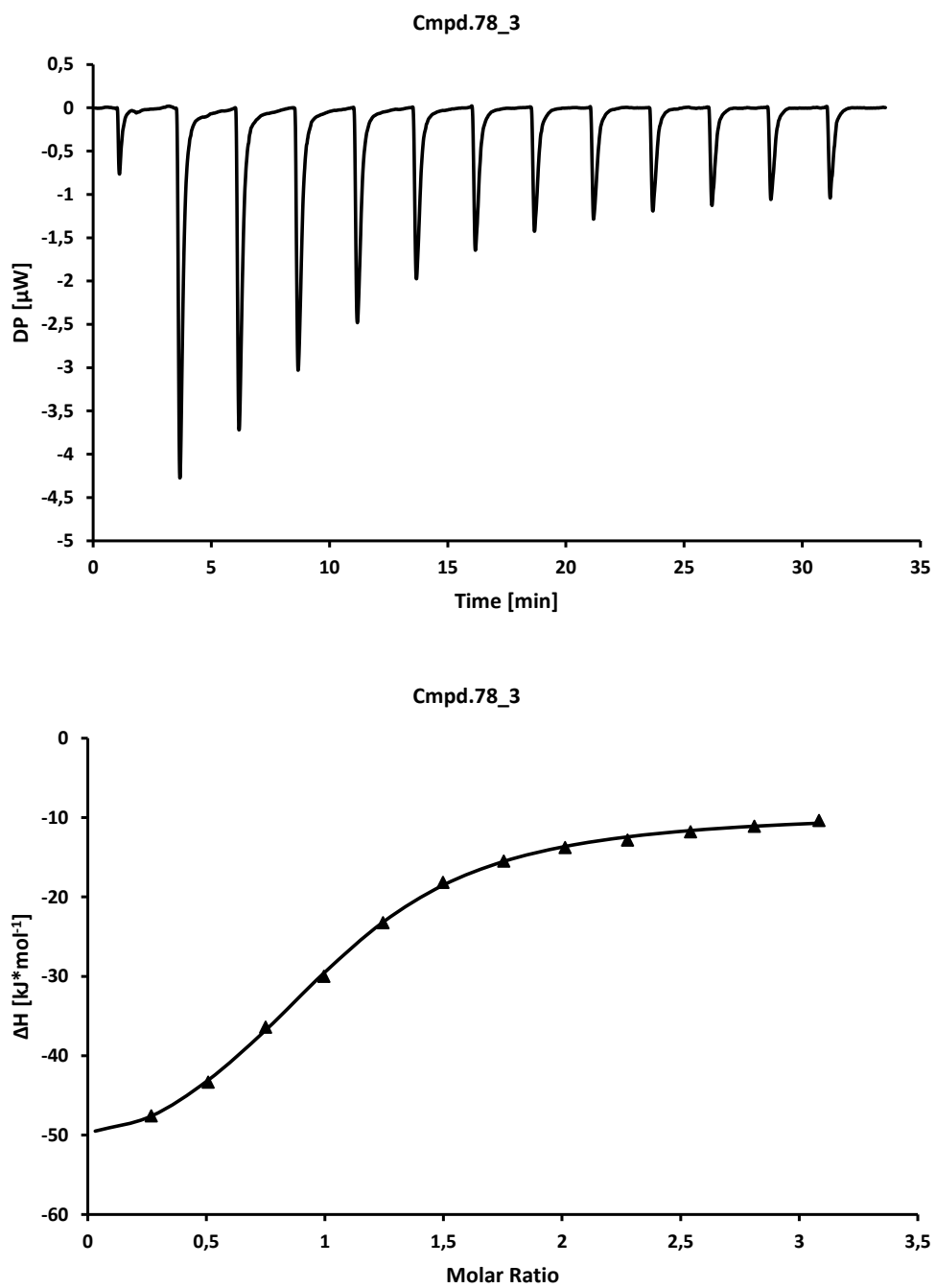


Figure S174: Binding affinity of **78** towards DNMT2 determined by Isothermal Titration Calorimetry. Above) raw ITC data of the third run. below) integrated and fitted ITC data of the third run.

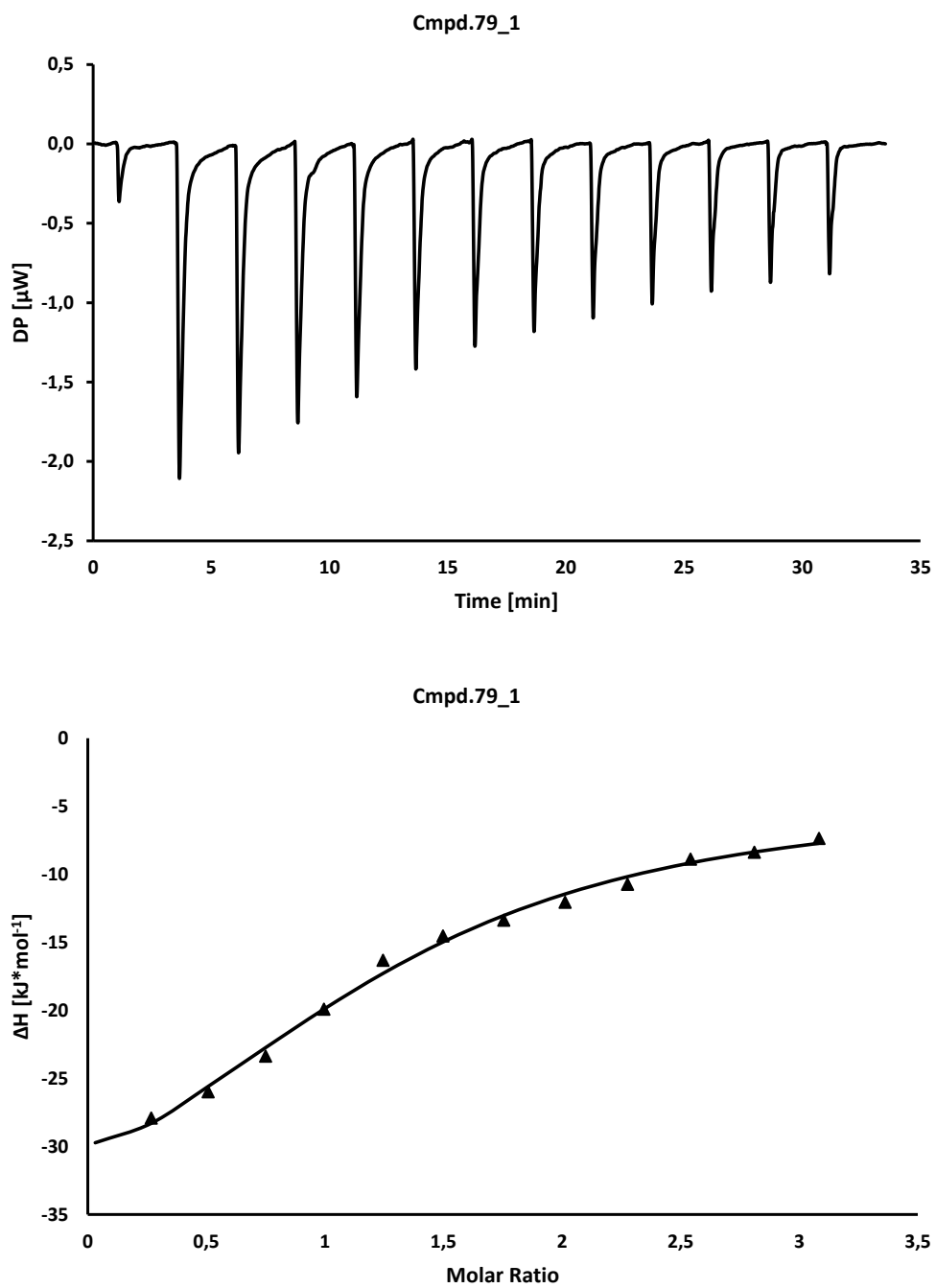


Figure S175: Binding affinity of **79** towards DNMT2 determined by Isothermal Titration Calorimetry. Above) raw ITC data of the first run. below) integrated and fitted ITC data of the first run.

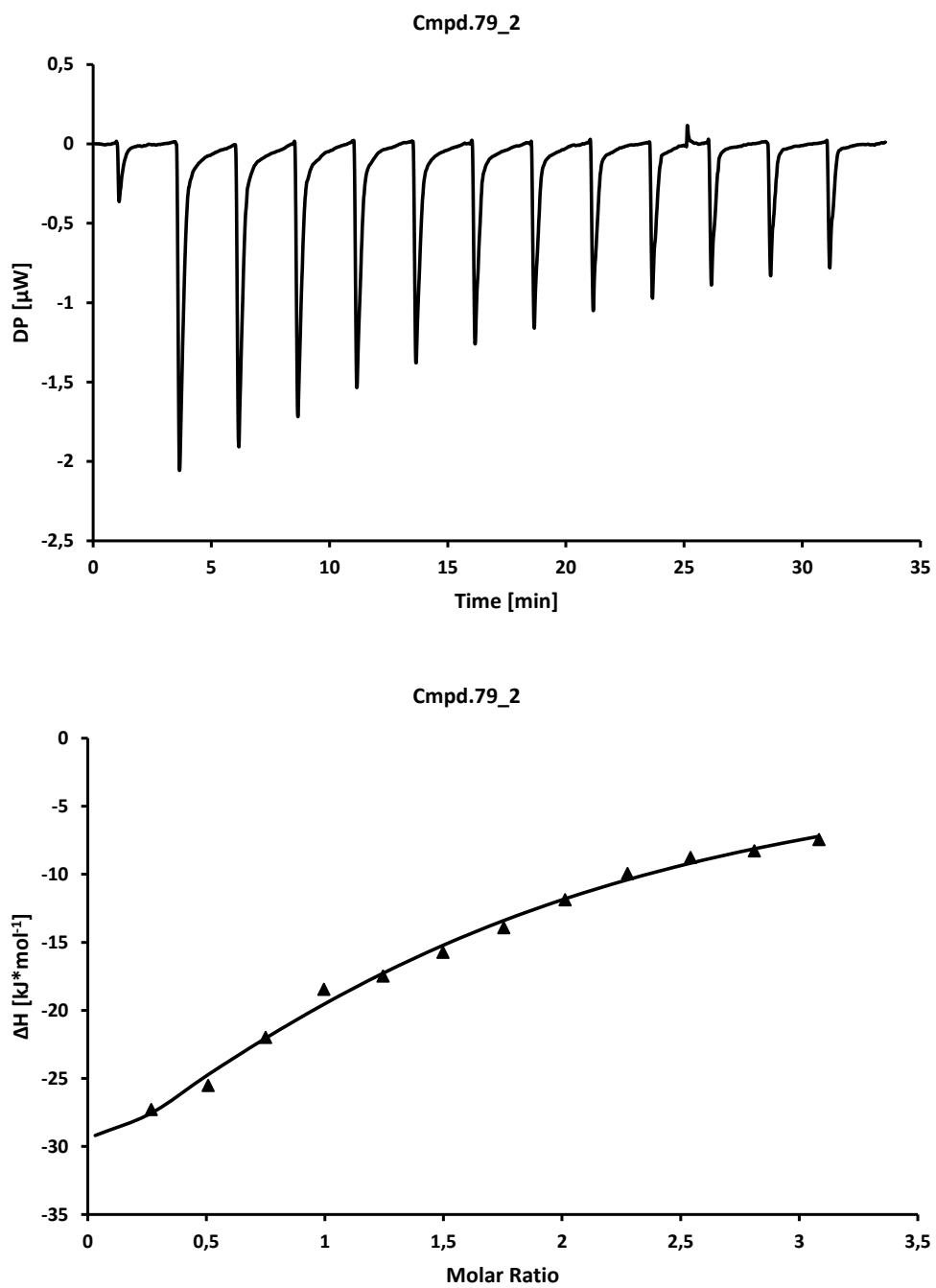


Figure S176: Binding affinity of **79** towards DNMT2 determined by Isothermal Titration Calorimetry. Above) raw ITC data of the second run. below) integrated and fitted ITC data of the second run.

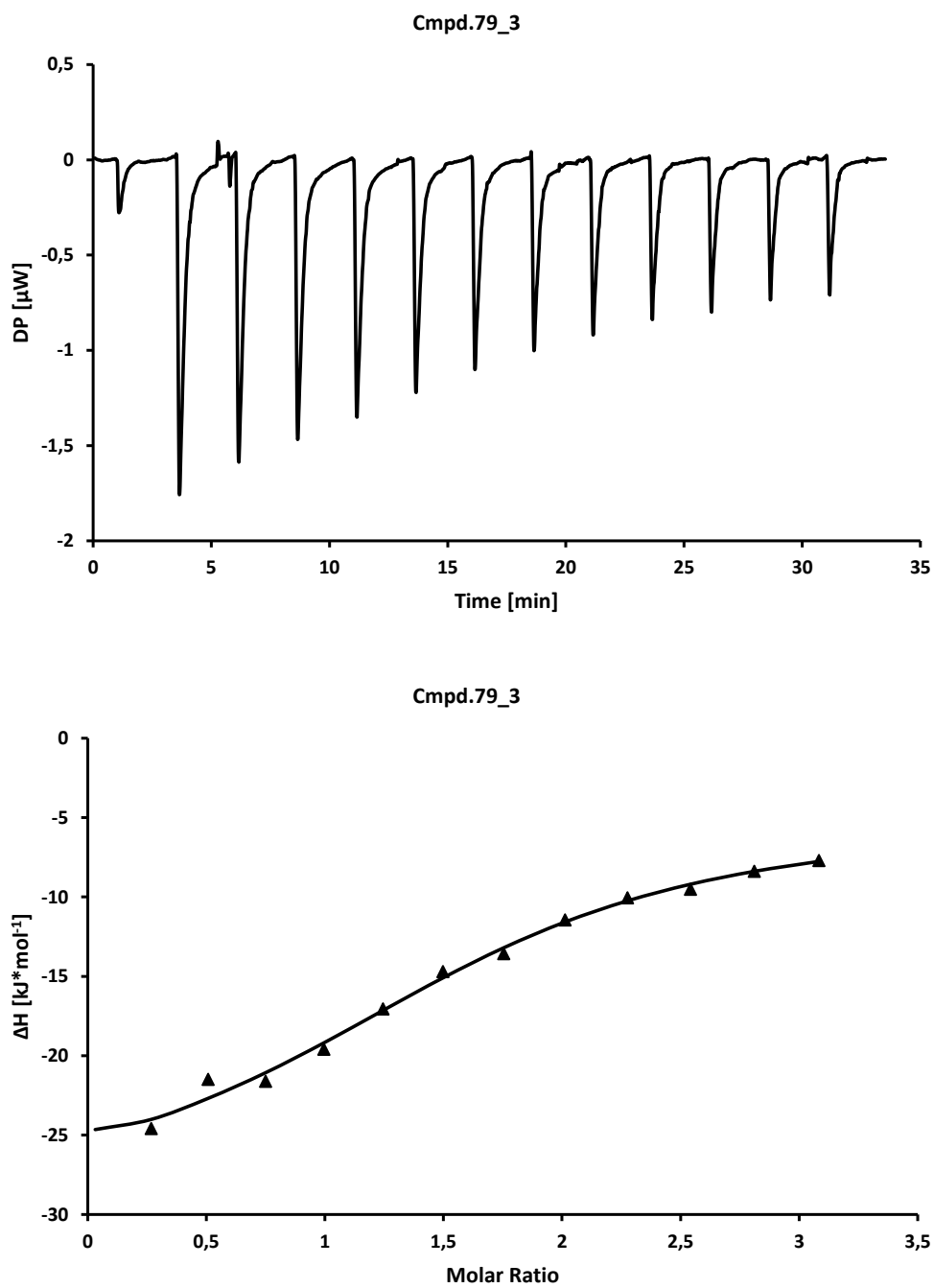


Figure S177: Binding affinity of **79** towards DNMT2 determined by Isothermal Titration Calorimetry. Above) raw ITC data of the third run. below) integrated and fitted ITC data of the third run.

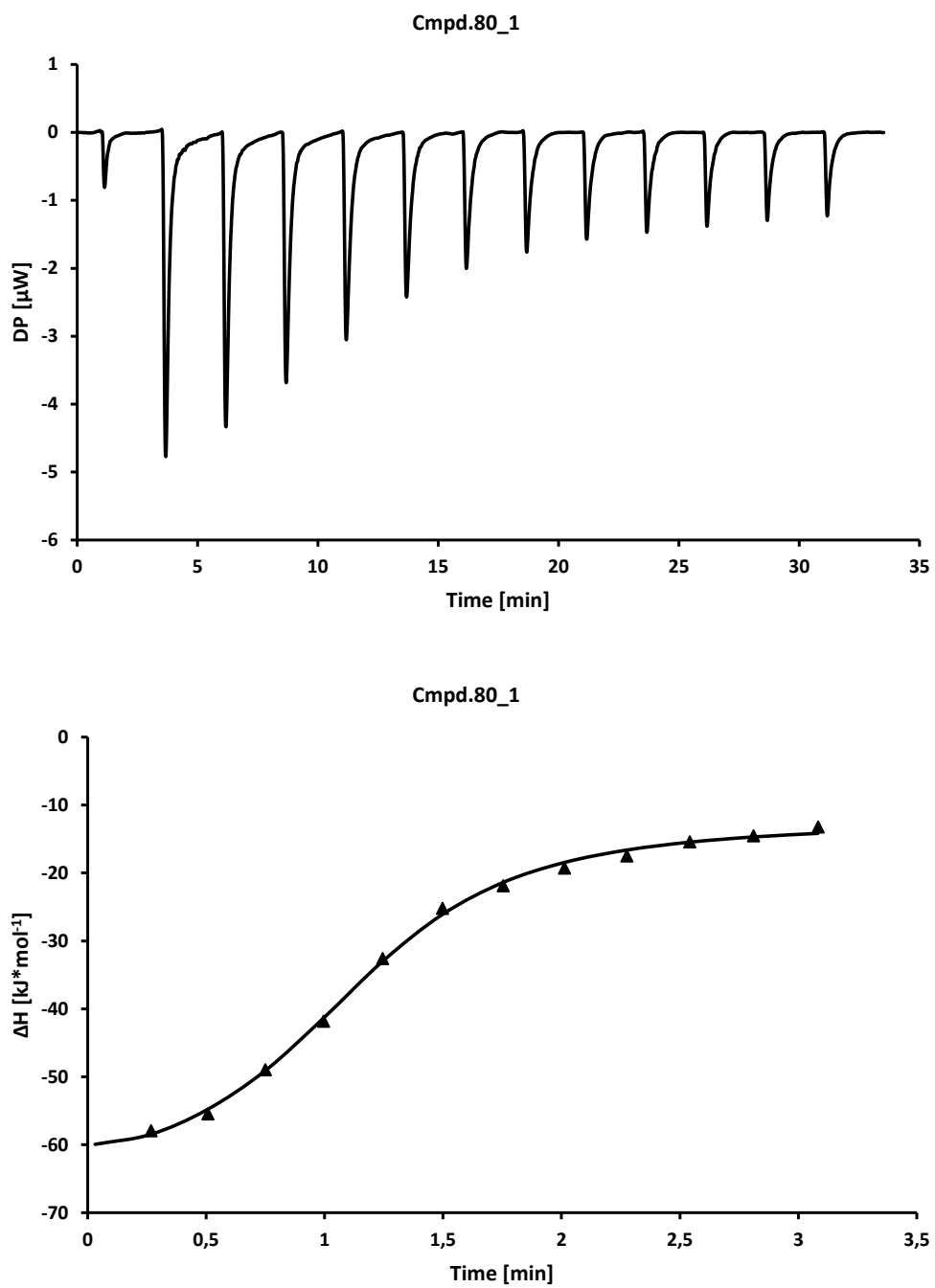


Figure S178: Binding affinity of **80** towards DNMT2 determined by Isothermal Titration Calorimetry. Above) raw ITC data of the first run. below) integrated and fitted ITC data of the first run.

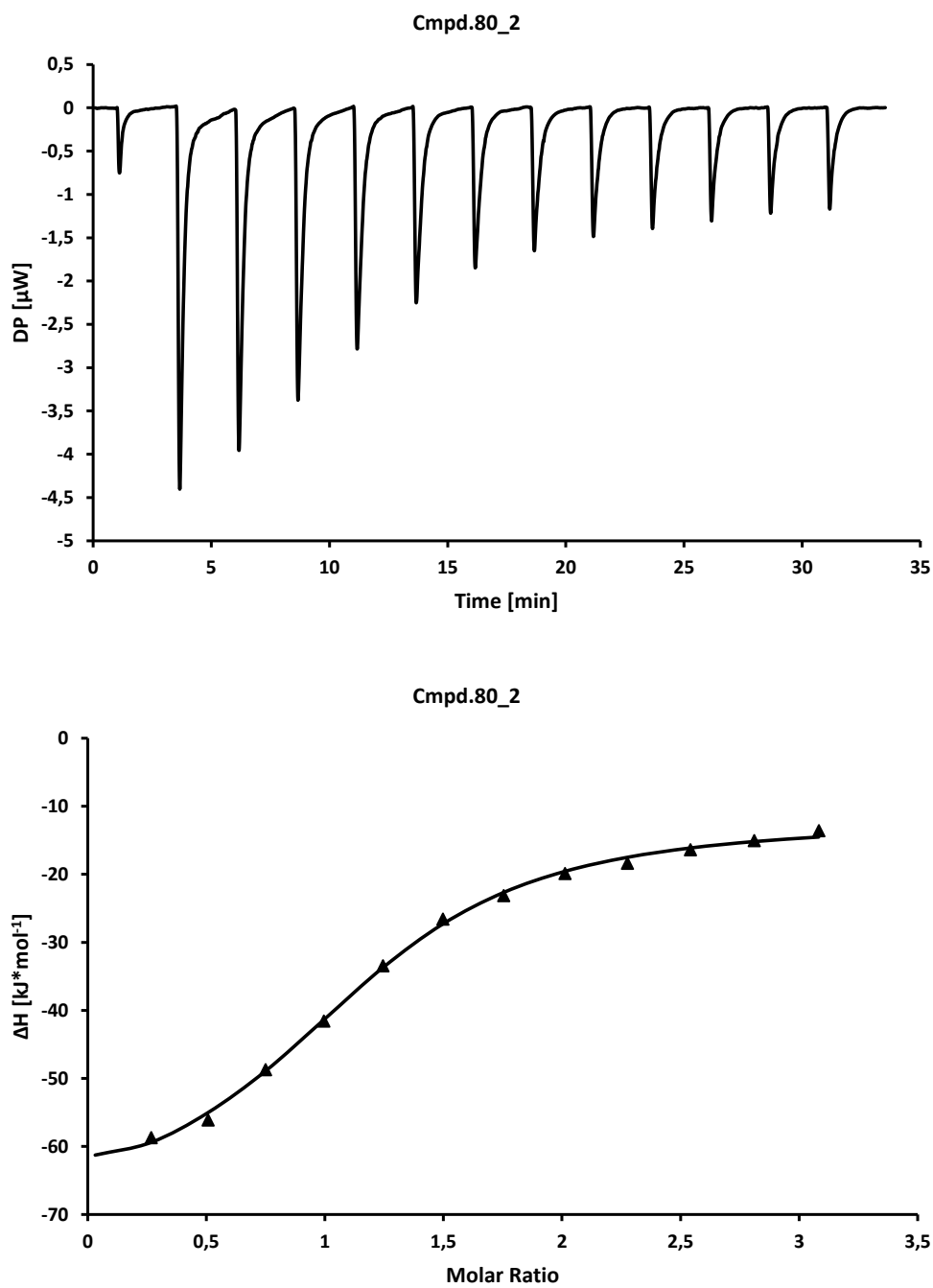


Figure S179: Binding affinity of **80** towards DNMT2 determined by Isothermal Titration Calorimetry. Above) raw ITC data of the second run. below) integrated and fitted ITC data of the second run.

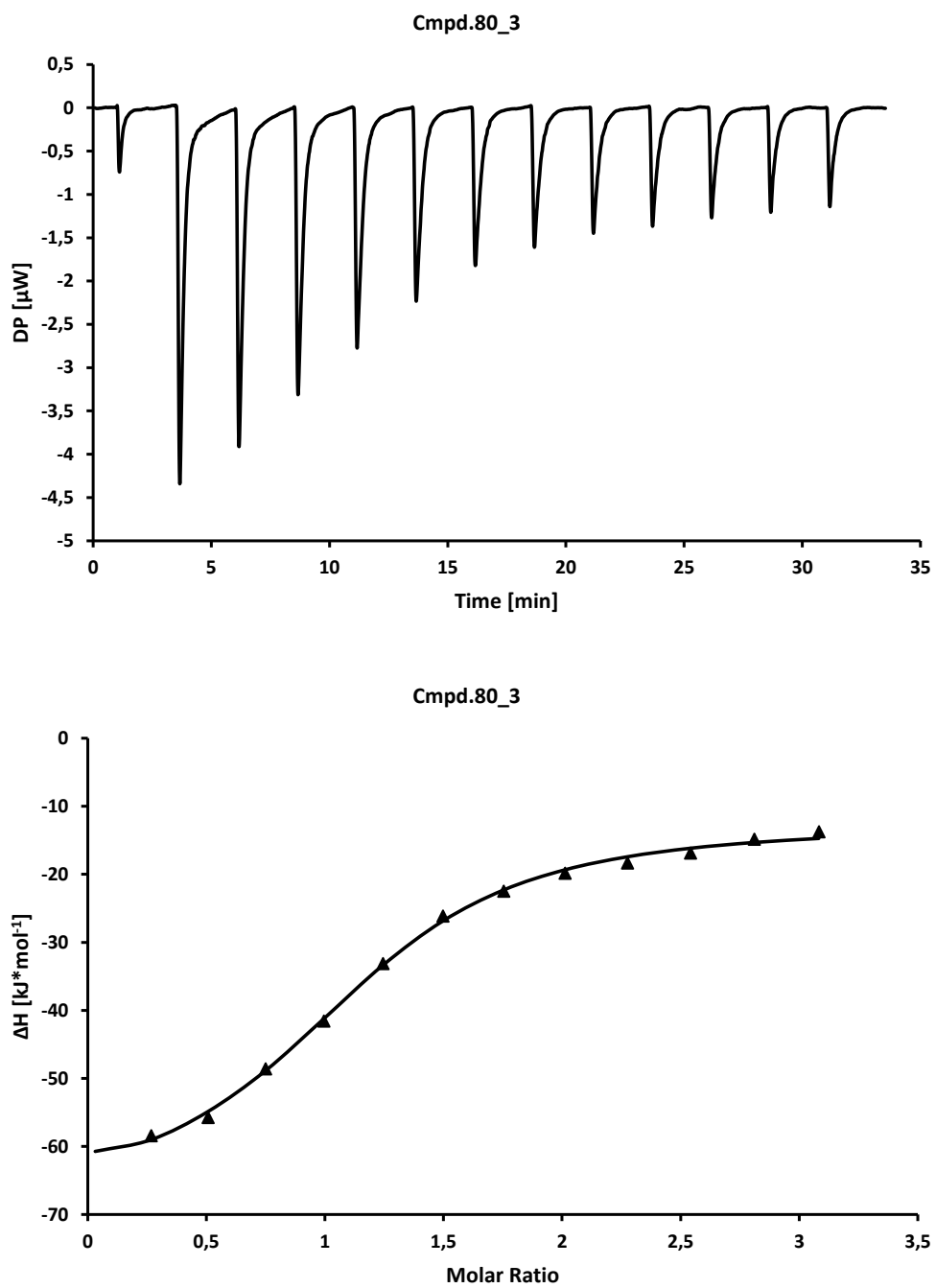


Figure S180: Binding affinity of **80** towards DNMT2 determined by Isothermal Titration Calorimetry. Above) raw ITC data of the third run. below) integrated and fitted ITC data of the third run.

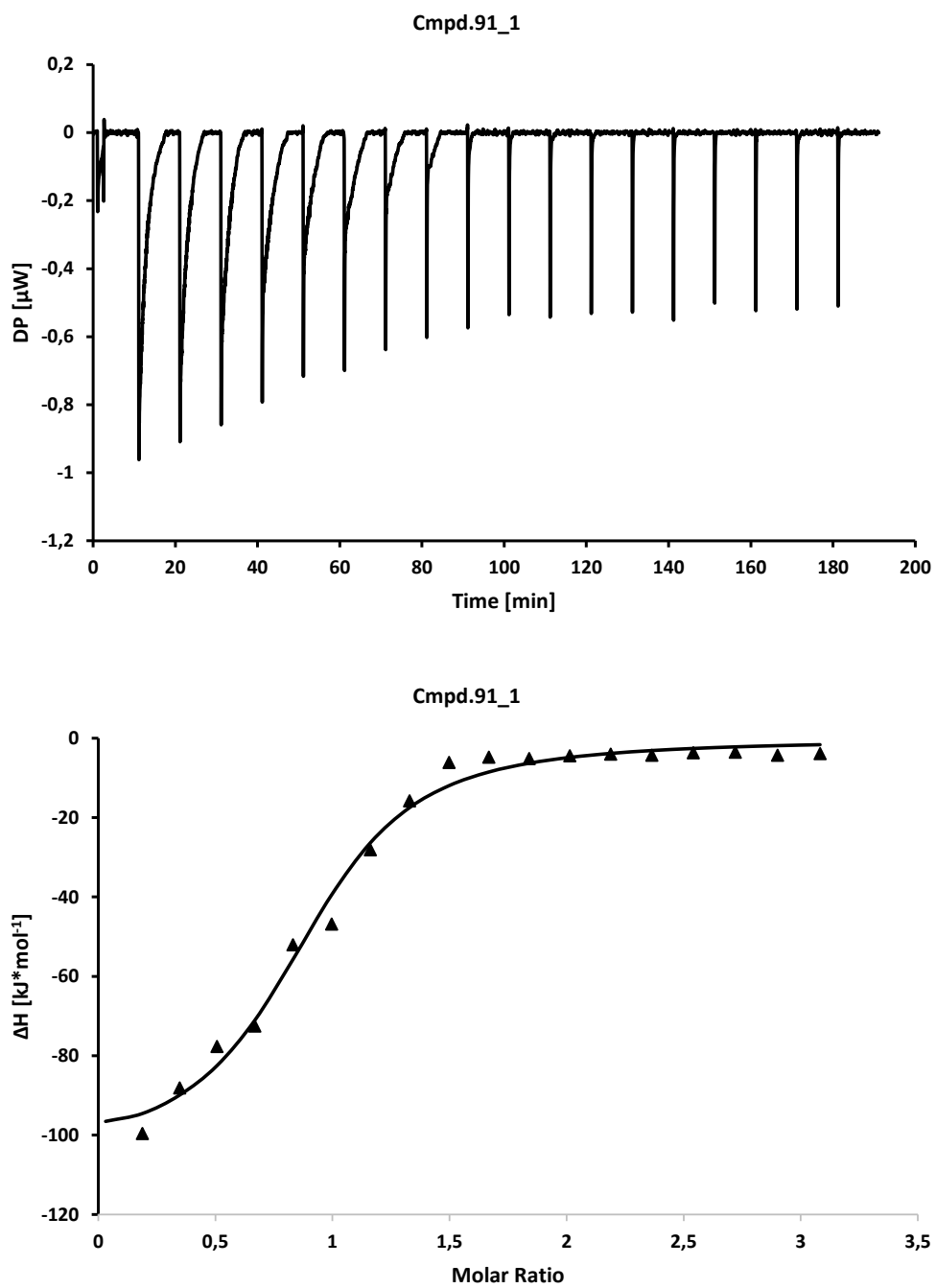


Figure S181: Binding affinity of **91** towards DNMT2 determined by Isothermal Titration Calorimetry. Above) raw ITC data of the first run. below) integrated and fitted ITC data of the first run.

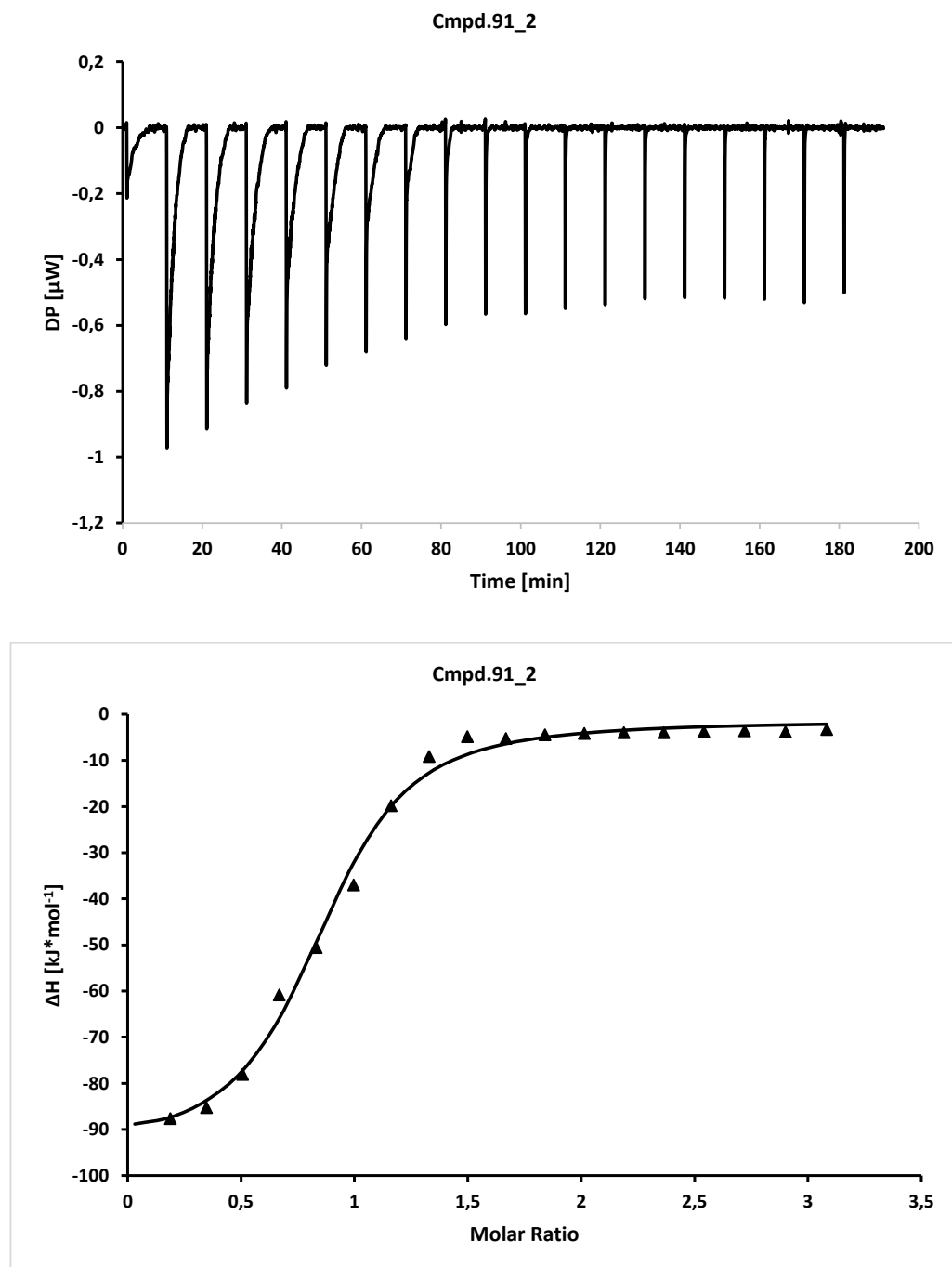


Figure S182: Binding affinity of **91** towards DNMT2 determined by Isothermal Titration Calorimetry. Above) raw ITC data of the second run. below) integrated and fitted ITC data of the second run.

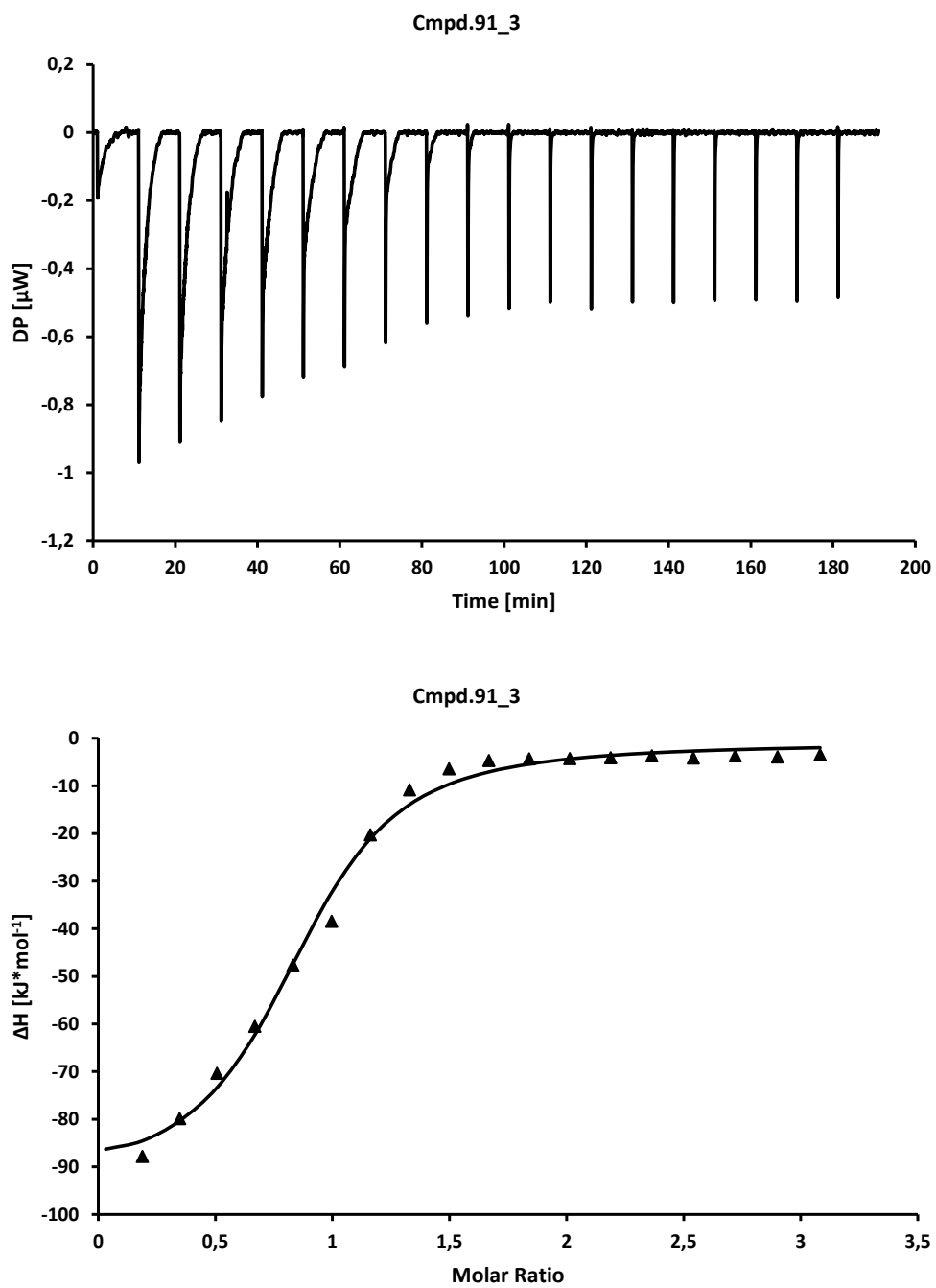


Figure S183: Binding affinity of **91** towards DNMT2 determined by Isothermal Titration Calorimetry. Above) raw ITC data of the third run. below) integrated and fitted ITC data of the third run.

Table S1. Overview of results from ITC measurements. Average \pm SD from three experiments each is given.

Cpd.	K_D [μ M]	ΔH [$\text{kJ} \cdot \text{mol}^{-1}$]	ΔG [$\text{kJ} \cdot \text{mol}^{-1}$]	$-\Delta S$ [$\text{kJ} \cdot \text{mol}^{-1}$]	N
32	32.1 \pm 8.4	-42.7 \pm 11.7	-25.7 \pm 0.6	17.0 \pm 12.4	0.92 \pm 0.09
41	6.0 \pm 0.7	-42.0 \pm 1.7	-29.8 \pm 0.3	12.1 \pm 2.0	1.04 \pm 0.02
79	17.3 \pm 3.6	-32.5 \pm 3.6	-27.2 \pm 0.5	5.3 \pm 4.1	1.34 \pm 0.04
80	4.9 \pm 0.4	-55.8 \pm 3.9	-30.3 \pm 0.2	25.5 \pm 1.5	1.08 \pm 0.01
45	0.94 \pm 0.05	-43.2 \pm 0.3	-34.4 \pm 0.1	8.8 \pm 0.5	1.37 \pm 0.01
78	4.3 \pm 0.2	-45.6 \pm 0.8	-30.6 \pm 0.1	14.9 \pm 0.9	0.93 \pm 0.01
91	1.9 \pm 0.3	-32.7 \pm 0.4	-96.7 \pm 2.9	64.0 \pm 3.3	0.84 \pm 0.01

TRITIUM INCORPORATION ASSAY (^3H -ASSAY)

The assay was performed as described before² with minor changes. For compounds **78**, **79**, and **91** TCEP was used as reducing agent since DTT caused inactivation of the inhibitors. TCEP concentration in buffer was adjusted to 2 mM, 1 mM, and 0,6 mM for DNMT2, NSUN6, and NSUN2, respectively.

Additionally to the screening at 100 μ M compound concentration, a screening at 10 μ M compound concentration was conducted. Table S2 shows the screening results at 10 μ M compound concentrations towards different RNA methyltransferases.

Table S2. Selectivity determination. Enzyme inhibition \pm error at 10 μ M compound concentration towards DNMT2, NSUN6, and NSUN2 are given. Measurements were performed in triplicates.

Cpd.	DNMT2	NSUN6	NSUN2
45	80.2 \pm 2.4	0 \pm 2.1	4.9 \pm 0.3
78	82.5 \pm 0.5	6.8 \pm 3.3	0 \pm 1,3
79	40.1 \pm 4.8	46.5 \pm 5.5	19.9 \pm 2.3
80	97.7 \pm 6.4	0 \pm 2.6	0.6 \pm 1.0
91	82.7 \pm 2.8	0 \pm 3.6	0 \pm 3.3

PROTEIN MASS SPECTROMETRY

A Waters Synapt XS instrument was used for all experiments. For LC, a Waters Acquity HPLC M-Class with a CTC PAL injection system was used.

For the denatured intact mass measurement, the protein was diluted to 1 μM in 200 mM aqueous ammonium acetate and 5 mM TCEP and mixed with a 10-fold excess of the respective ligand (**45**, **78–80**, **91**, or SFG). Samples were then incubated on ice for one hour before the injection into the LC system. The LC separation was performed on a C4 column (Waters Acquity BEH C4 2.1 x 50 mm) with a water-acetonitrile gradient for 15 minutes. The injection volume was 50 μl and a flow rate of 80 $\mu\text{l}/\text{min}$ was used. MassLynx (V4.2) and UniDec were used for data analysis.⁵

Native MS was performed using a nano-electrospray ionization setup for direct infusion with in-house pulled emitters. For these measurements, 5 μl of a 40 μM protein solution in 200 mM aqueous ammonium acetate and 5 mM TCEP were used, and a 10-fold excess of ligand (**45** or SFG) was added. Measurements were performed after one hour of incubation of the samples on ice. Data analysis was performed manually using MassLynx (V4.2).

For the binding site determination, a standard bottom-up approach with a tryptic digest followed by LC-MS/MS measurement was used. The different ligands were again mixed in 10-fold excess with the protein and were incubated for one hour on ice. Afterwards the 40 μM protein solutions were diluted to 10 μM using a urea lysis buffer (8 M urea, 100 mM NaCl, 50 mM triethylammonium bicarbonate TEAB) to fully denature the protein. Subsequently, 30 mM iodoacetamide (IAA) was added and the mixture was incubated for 30 min in the dark to alkylate the free cysteines. Dithiothreitol (DTT; 10 mM) was added and incubated for 15 min in the dark to quench unreacted IAA. This mixture was diluted 1:5 with 50 mM TEAB to reduce the urea concentration. Trypsin was added in 1:50 enzyme:protein ratio and the digestion was performed overnight at 37 °C and then stopped by adding 0.2% trifluoroacetic acid. For LC-MS/MS analysis, 50 μl of the sample was injected. A standard water:acetonitrile gradient and a C18 column (Waters Acquity BEH C18 1 x 100 mm) were used to separate the peptides. The MS/MS measurement was performed in data independent acquisition mode using ion mobility separation; this method is also referred to as HDMSe. ProteinLynx Global Server (Waters) was used for data analysis. The used database consisted of the known sequences of DNMT2 Δ and trypsin (porcine) supplemented by the potential modifications due to the ligands.

Table S3. Deconvoluted data of the denatured intact mass measurement. The mass spectra were copied to UniDec for deconvolution. Centroid mass, uncertainty and intensity values are direct results from UniDec using the presets for denatured measurements on a QTOF. All intensity values are normalized to the highest peak in the respective measurement which corresponds to the 100% value.

	Centroid mass / Da	Intensity / %	Theoretical mass / Da	mass error / ppm
DNMT2Δ	41364.572	100	41364.335	5.737
DNMT2Δ + Cpd. 79				
free	41364.064	31.6	41364.335	-6.544
1 × bound	41914.627	100	41914.837	-5.017
2 × bound	42465.108	20.04	42465.339	-5.447
DNMT2Δ + Cpd. 80				
free	41364.817	6.72	41364.335	11.653
1 × bound	41914.598	100	41914.837	-5.712
DNMT2Δ + Cpd. 45				
free	41364.063	100	41364.335	-6.585
DNMT2Δt + Cpd. 78				
free	41364.683	39.32	41364.335	8.406
1 × bound	41914.549	100	41914.837	-6.878
DNMT2Δ + Cpd. 91				
free	41364.730	0.91	41364.335	9.537
1 × bound	41871.474	100	41871.815	-8.153
2 × bound	42378.989	19.93	42379.296	-7.256
DNMT2Δ + SFG				
free	41363.997	100	41364.335	-8.166

Development of selective inhibitors for the human methyltransferases DNMT2 and NSUN6

```

      10      20      30      40      50      60
MEPLRVLELY SGVGGMHHAL RESCIPAQVV AAIDVNTVAN EVYKYNFPHT QLLAKTIEGI
      70      80      90     100     110     120
TLEEFDRLSF DMILMSPPCQ PFTRIGRQGD MTDSTRNSFL HILDILPRLQ KLPKYILLEN
      130     140     150     160     170     180
VKGFEVSSSTR DLIQTIENC GFOYQEFLLS PTLGIPNSR LRYFLIAKIQ SEPLPFQAPG
      190     200     210     220     230     240
QVLMEFPKIE -----IHR
      250     260     270     280     290     300
KNQQSDLSV KMLKDFLEDD TDVNQYLLPE KSLLR YALL DIVQPTCRS VCFTK GYGSY
      310     320     330     340     350     360
IEGTGSVLQT AEDVQVENIY KSLTNLSQEE QITKLLILK L RYFTPK EIAN LLGFPPEFGF
      370     380     390
PEKITVKQR Y RLLGNSLVH VVAKLIKILY E

```

Figure S184: Bottom-up results for DNMT2Δ without ligand. Sequence regions covered by detected peptides are highlighted in green (sequence coverage = 86.8 %). The flexible loop, that has been deleted is highlighted in grey.

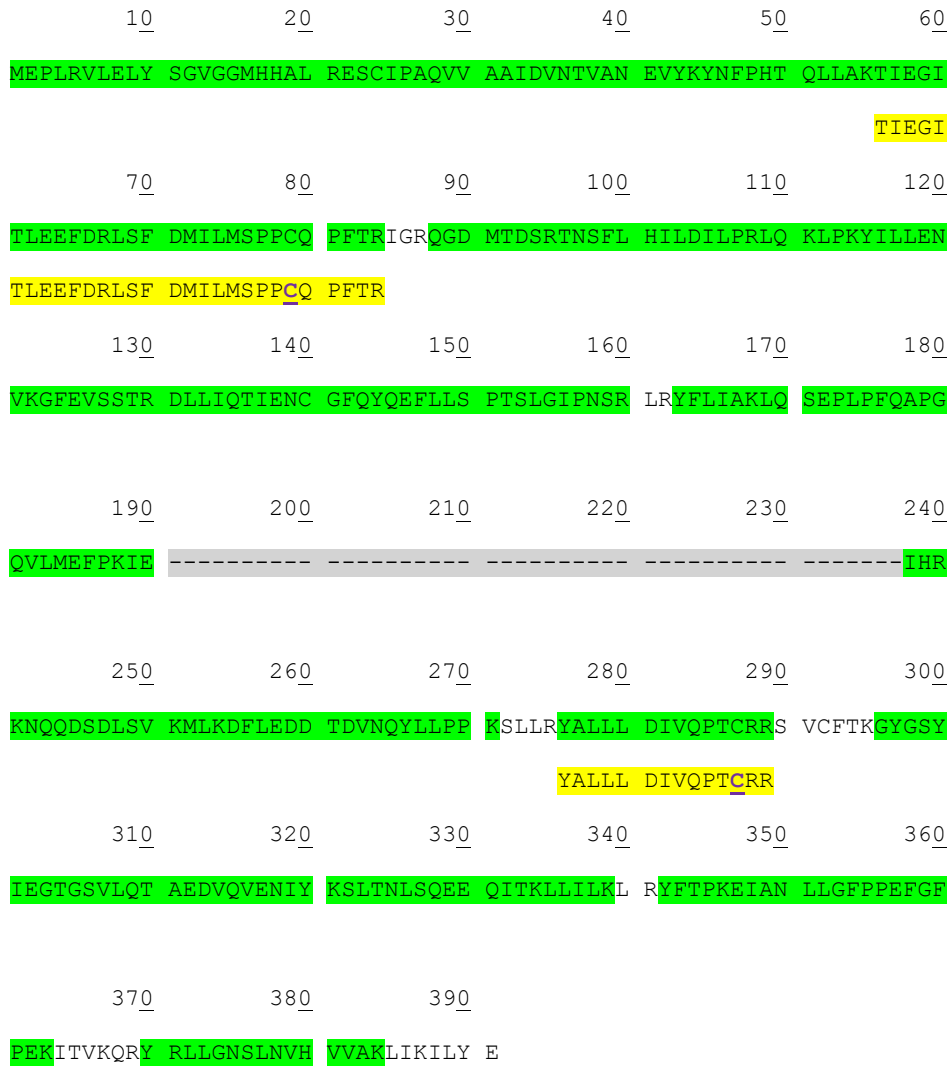


Figure S185: Bottom-up results for DNMT2Δ bound to covalent ligand 79. Sequence regions covered by detected peptides are highlighted in green (sequence coverage = 92.8 %). The flexible loop, that has been deleted is highlighted in grey. The yellow highlights indicate peptides that were bound to the ligand, and cysteine residues involved in binding are indicated in underlined purple text.

Development of selective inhibitors for the human methyltransferases DNMT2 and NSUN6



Figure S186: Bottom-up results for DNMT2A bound to covalent ligand **80**. Sequence regions covered by detected peptides are highlighted in green (sequence coverage = 79.9 %). The flexible loop, that has been deleted is highlighted in grey. The yellow highlights indicate peptides that were bound to the ligand, and the cysteine residue involved in binding is indicated in underlined purple text.

Development of selective inhibitors for the human methyltransferases DNMT2 and NSUN6



Figure S188: Bottom-up results for DNMT2A bound to covalent ligand **91**. Sequence regions covered by detected peptides are highlighted in green (sequence coverage = 90.4 %). The flexible loop, that has been deleted is highlighted in grey. The yellow highlights indicate peptides that were bound to the ligand, and cysteine residues involved in binding are indicated in underlined purple text.

Development of selective inhibitors for the human methyltransferases DNMT2 and NSUN6

10 20 30 40 50 60
 MEPLRVLELY SGVGGMHHAL RESCIQAQVV AAIDVNTVAN EVYKYNFPHT QLLAKTIEGI
 70 80 90 100 110 120
 TLEEFDRLSF DMILMSPPCQ PFTRIGRQGD MDSRTNSFL HILDILPRLQ KLPKYILLEN
 130 140 150 160 170 180
 VKGFEVSSSTR DLIQTIENC GFOYQEFLLS PTLGIPNSR LRYFLIAKLQ SEPLPFQAPG
 190 200 210 220 230 240
 QVLMFEPKIE -----IHR
 250 260 270 280 290 300
 KNQQSDLSV KMLKDFLEDD TDVNQYLLPE KSLLR YALL DIVQPTCRRS VCFTK GYGSY
 310 320 330 340 350 360
 IEGTGSVLQT AEDVQVENIY KSLTNLSQEE QITKLLILKL RYFTPK EIAN LLGFPPEFGH
 370 380 390
 PEKITVKQR Y RLLGNLSNVH VVAKLIKILY E

Figure S189. Bottom-up results for DNMT2Δ bound to non-covalent ligand 45. Sequence regions covered by detected peptides are highlighted in green (sequence coverage = 91.5 %). The flexible loop, that has been deleted is highlighted in grey. As expected, no ligand-bound peptides were detected as ligand binding was lost during the denaturation step.

Development of selective inhibitors for the human methyltransferases DNMT2 and NSUN6

10 20 30 40 50 60
 MEPLRVLELY SGVGGMHHAL RESCIPAQVV AAIDVNTVAN EVYKYNFPHT QLLAKTIEGI

 70 80 90 100 110 120
 TLEEFDRLSF DMILMSPPCQ PFTRIGRQGD MDSRTNSFL HILDILPRLQ KLPKYILLEN

 130 140 150 160 170 180
 VKGFVSSSTR DLIQTIENC GFQYQEFLLS PTLGIPNSR LRYFLIAKLQ SEPLPFQAPG

 190 200 210 220 230 240
 QVLMFEPKIE -----IHR

 250 260 270 280 290 300
 KNQQSDLSV KMLKDFLEDD TDVNQYLLPE KSLLR YALL DIVQPTCRRS VCFTK GYGSY

 310 320 330 340 350 360
 IEGTGSVLQT AEDVQVENIY KSLTNLSQEE QITKLLILKL RYFTPK EIAN LLGFPEFGE

 370 380 390
 PEKITVKQR Y RLLGNLNVH VVAKLIKILY E

Figure S190: Bottom-up results for DNMT2Δ bound to non-covalent ligand sinefungin. Sequence regions covered by detected peptides are highlighted in green (sequence coverage = 93.4%). The flexible loop, that has been deleted is highlighted in grey. As expected, no ligand-bound peptides were detected as ligand binding was lost during the denaturation step.

MOLECULAR DOCKING

The lacking catalytic loop (residues 79–96) in the crystal structure of human DNMT2 (PDB-ID 1G55)³ was introduced using the ‘Loop Modeler’ functionality within MOE (Molecular Operating Environment (MOE), 2022.02 Chemical Computing Group ULC, 1010 Sherbooke St. West, Suite #910, Montreal, QC, Canada, H3A 2R7, 2023.) using the PDB-similarity and de novo loop search. From the PDB a suitable loop from PDB-ID 2D0I was identified and used for model building.⁶ The DNMT2 structure including the modelled loop 79–96 is provided as PDB file. From this structure the binding site was defined using the DogSiteScorer^{7,8} functionality within SeeSAR (SeeSAR version 12.1.0; BioSolveIT GmbH, Sankt Augustin, Germany, 2022, www.biosolveit.de/SeeSAR) covering 38 residues of the combined SAM- and cytidine-binding sites. The docking setup was validated by re-docking of the crystallographic reference ligand SAH (FlexX-score: –10.00 kcal/mol, RMSD: 1.05 Å) using FlexX (FlexX version 5.1.0; BioSolveIT GmbH, Sankt Augustin, Germany, 2022, www.biosolveit.de/SeeSAR)⁹ in command-line mode. 3D conformers of compounds **45**, **78–80**, and **91** were generated using OMEGA classic (OMEGA 4.2.1.1: OpenEye Scientific Software, Santa Fe, NM, USA. <http://www.eyesopen.com>, 2019)¹⁰ and docked with FlexX using identical parameters. Non-covalent and covalent docking with MOE was performed using pharmacophore constraints on the basic nitrogen (cationic/H-bond donor) and adenine (aromatic) of SAH to enrich SAH-like orientation within the binding site. For covalent docking Cys79 as the attachment point for covalent reaction was selected. 70 initially generated binding modes were refined using the induced fit method and ‘London ΔG’ re-scoring. Top 15 poses were visually inspected for interaction profiles with the SAM- and cytidine binding sites.

Table S4. Results of non-covalent and covalent docking.

Compound	FlexX (non-covalent docking)		MOE		
	Score [kcal/mol]	Distance Cys (S)–ligand (electrophilic C) [Å]	Score non-covalent [kcal/mol]	Distance Cys (S)–ligand (electrophilic C) [Å]	Score covalent [kcal/mol]
SAH (redocking)	–10.00 (RMSD: 1.05 Å)	-	–14.10 (RMSD: 0.57 Å)	-	-
79	–12.53	3.9	–19.40	3.5	
78	–12.61	3.9	–18.68	3.7	–15.98 ^a
80	–12.15	3.9	–17.71	3.8	
91	–9.42	4.2	–17.06	3.5	–14.46
41	–11.45	-	–17.52	-	-
45	–12.55	-	–18.86	-	-

^a**78–80** result in the same covalent adduct.

REFERENCES

- (1) Cooper, M.; Miller, D.; Macleod, A.; Van Wiltenburg, J.; Thom, S.; St-Gallay, Stephen Shannon, J.; Alanine, T.; Onions, S.; Strutt, I. Novel Sulfonamide Carboxamide Compounds. WO2019/8025 A1, 2019.
- (2) Schwickert, M.; Fischer, T. R.; Zimmermann, R. A.; Hoba, S. N.; Meidner, J. L.; Weber, M.; Weber, M.; Stark, M. M.; Koch, J.; Jung, N.; Kersten, C.; Windbergs, M.; Lyko, F.; Helm, M.; Schirmeister, T. Discovery of Inhibitors of DNA Methyltransferase 2, an Epitranscriptomic Modulator and Potential Target for Cancer Treatment. *J. Med. Chem.* **2022**. <https://doi.org/10.1021/acs.jmedchem.2c00388>.
- (3) Dong, A.; Yoder, J. A.; Zhang, X.; Zhou, L.; Bestor, T. H.; Cheng, X. Structure of Human DNMT2, an Enigmatic DNA Methyltransferase Homolog That Displays Denaturant-Resistant Binding to DNA. *Nucleic Acids Res.* **2001**, *29* (2), 439–448. <https://doi.org/10.1093/nar/29.2.439>.
- (4) Zimmermann, R. A.; Schwickert, M.; Meidner, J. L.; Nidoieva, Z.; Helm, M.; Schirmeister, T. An Optimized Microscale Thermophoresis Method for High-Throughput Screening of DNA Methyltransferase 2 Ligands. *ACS Pharmacol. Transl. Sci.* **2022**, *5* (11), 1079–1085. <https://doi.org/10.1021/acspsci.2c00175>.
- (5) Marty, M. T.; Baldwin, A. J.; Marklund, E. G.; Hochberg, G. K. A.; Benesch, J. L. P.; Robinson, C. V. Bayesian Deconvolution of Mass and Ion Mobility Spectra: From Binary Interactions to Polydisperse Ensembles. *Anal. Chem.* **2015**, *87* (8), 4370–4376. <https://doi.org/10.1021/acs.analchem.5b00140>.
- (6) Lokanath, N.K., Terao, Y., Kunishima, N., R. S. G. I. (RSGI). Crystal Structure PH0520 Protein from *Pyrococcus Horikoshii* OT3. **2005**. <https://doi.org/10.2210/pdb2D0I/pdb>.
- (7) Volkamer, A.; Griewel, A.; Grombacher, T.; Rarey, M. Analyzing the Topology of Active Sites: On the Prediction of Pockets and Subpockets. *J. Chem. Inf. Model.* **2010**, *50* (11), 2041–2052. <https://doi.org/10.1021/ci100241y>.
- (8) Volkamer, A.; Kuhn, D.; Grombacher, T.; Rippmann, F.; Rarey, M. Combining Global and Local Measures for Structure-Based Druggability Predictions. *J. Chem. Inf. Model.* **2012**, *52* (2), 360–372. <https://doi.org/10.1021/ci200454v>.
- (9) Rarey, M.; Kramer, B.; Lengauer, T.; Klebe, G. A Fast Flexible Docking Method Using an Incremental Construction Algorithm. *J. Mol. Biol.* **1996**, *261* (3), 470–489. <https://doi.org/10.1006/jmbi.1996.0477>.
- (10) Hawkins, P. C. D.; Skillman, A. G.; Warren, G. L.; Ellingson, B. A.; Stahl, M. T. Conformer Generation with OMEGA: Algorithm and Validation Using High Quality Structures from the Protein Databank and Cambridge Structural Database. *J. Chem. Inf. Model.* **2010**, *50* (4), 572–584. <https://doi.org/10.1021/ci100031x>.

Outlook

Within this project, we have been able to design potent and, to a certain extent also, selective inhibitors for DNMT2. This includes, to the best of our knowledge, the first inhibitors, which display a covalent binding towards DNMT2. Additionally, we were able to develop an optimized MST method for DNMT2, which will facilitate the search for novel inhibitors.

The following steps should aim to improve our assay capacities. At the current stage, the optimized MST method can only be used to screen DNMT2. A broader panel of fluorescent probes could help to adapt this method to other methyltransferases of interest, for example, NSUN2 or NSUN6. This would open the possibility of fast, reliable, and material-saving screenings and affinity determination. Moreover, it would simplify the determination of the inhibitors' selectivity tremendously. Currently, ██████████ and his coworkers are aiming to develop tool compounds that can be used as fluorescent probes for several methyltransferases. An alternative approach could be to implement thermal shift assays like nanoDSF as another biophysical method. One of the main advantages of this method is the fact that it does not require any labeling. It would be nicely suited as an orthogonal method for MST since the physical principles behind those methods are quite different. NanoDSF could also be extremely useful for those methyltransferases where we still lack robust MST methods. Especially if different approaches to optimize MST assays for those methyltransferases fail, nanoDSF could be very valuable. To further investigate the kinetics of the inhibitors, SPR could be used. This would be interesting for covalent inhibitors, which often display very slow dissociation rates.¹⁵⁰

In this project, we were able to present quite promising *in vitro* data. Nevertheless, the results from *in vivo* experiments have been less pleasant due to the lack of cell permeability of the compounds. Therefore, assays have to be implemented, which enable fast determination of the compounds' cell permeability. A parallel artificial membrane permeation assay (PAMPA-assay), in which the passive permeability of a compound can be tested, or a Caco-2 permeability assay, in which the passive and active permeation of a compound can be determined, would be very useful. Extensive permeability data might help to improve the design of new compounds. It could also help with the design of prodrugs, which is an often-used concept in medicinal chemistry to improve the bioavailability of inhibitors.

Another objective should be the metabolism of these inhibitors. During future *in vivo* testing, the inhibitors might be exposed to extensive metabolism within the cells, which could have a major impact on *in vivo* results. Therefore, it should be investigated which metabolites are generated, in which period of time these metabolites are generated, and which enzymes are involved in the metabolism of the inhibitors. To investigate these aspects, incubation of the compounds with CYP enzymes in combination with mass spectrometry could be very promising.

Outlook

The number of crystal structures available for enzymes of the NSUN family and DNMT2 is limited. Since crystal structures only represent snapshots of the protein in energy-minimized states, more crystal structures would be beneficial for scientists to develop inhibitors. Especially for DNMT2, where the enzymes' active site was not resolved in a sufficiently high resolution, other crystal structures that resolve this area in more detail are essential. The inhibitors designed within our second SAR study, capable of binding the active site cysteine of DNMT2 covalently, could rigidize this area, contributing to crystallize the active site of DNMT2 with an improved resolution. Currently, our collaborators from the [REDACTED] (University of Heidelberg) are striving to crystallize DNMT2 in complex with inhibitors of our second SAR study. Meanwhile, co-crystals have been obtained and currently undergo refinement cycles.

Furthermore, the design of cell-permeable tool compounds labeled with different fluorescent dyes would be desirable to visualize the methyltransferases *in cellulo*. These tool compounds could be designed to bind all or specific methyltransferases covalently. Moreover, it would be interesting to have tool compounds at hand, capable of crosslinking particular methyltransferases and their substrates. These approaches could facilitate investigations of the biochemistry and cellular functions of the respective methyltransferases of interest.

References

- (1) Helm, M.; Motorin, Y. Detecting RNA Modifications in the Epitranscriptome: Predict and Validate. *Nat Rev Genet* **2017**, *18* (5), 275–291. <https://doi.org/10.1038/nrg.2016.169>.
- (2) Sarkar, A.; Gasperi, W.; Begley, U.; Nevins, S.; Huber, S. M.; Dedon, P. C.; Begley, T. J. Detecting the Epitranscriptome. *WIREs RNA* **2021**, *12* (6). <https://doi.org/10.1002/wrna.1663>.
- (3) Jiang, X.; Liu, B.; Nie, Z.; Duan, L.; Xiong, Q.; Jin, Z.; Yang, C.; Chen, Y. The Role of m⁶A Modification in the Biological Functions and Diseases. *Signal Transduct Target Ther* **2021**, *6* (1), 74. <https://doi.org/10.1038/s41392-020-00450-x>.
- (4) Saletore, Y.; Meyer, K.; Korlach, J.; Vilfan, I. D.; Jaffrey, S.; Mason, C. E. The Birth of the Epitranscriptome: Deciphering the Function of RNA Modifications. *Genome Biol* **2012**, *13* (10), 175. <https://doi.org/10.1186/gb-2012-13-10-175>.
- (5) Meyer, K. D.; Saletore, Y.; Zumbo, P.; Elemento, O.; Mason, C. E.; Jaffrey, S. R. Comprehensive Analysis of mRNA Methylation Reveals Enrichment in 3' UTRs and near Stop Codons. *Cell* **2012**, *149* (7), 1635–1646. <https://doi.org/10.1016/j.cell.2012.05.003>.
- (6) Wiener, D.; Schwartz, S. The Epitranscriptome beyond M6A. *Nat Rev Genet* **2021**, *22* (2), 119–131. <https://doi.org/10.1038/s41576-020-00295-8>.
- (7) Fu, Y.; Dominissini, D.; Rechavi, G.; He, C. Gene Expression Regulation Mediated through Reversible m⁶A RNA Methylation. *Nat Rev Genet* **2014**, *15* (5), 293–306. <https://doi.org/10.1038/nrg3724>.
- (8) Barbieri, I.; Kouzarides, T. Role of RNA Modifications in Cancer. *Nat Rev Cancer* **2020**, *20* (6), 303–322. <https://doi.org/10.1038/s41568-020-0253-2>.
- (9) Ontiveros, R. J.; Stoute, J.; Liu, K. F. The Chemical Diversity of RNA Modifications. *Biochemical Journal* **2019**, *476* (8), 1227–1245. <https://doi.org/10.1042/BCJ20180445>.
- (10) Roundtree, I. A.; Evans, M. E.; Pan, T.; He, C. Dynamic RNA Modifications in Gene Expression Regulation. *Cell* **2017**, *169* (7), 1187–1200. <https://doi.org/10.1016/j.cell.2017.05.045>.
- (11) Delaunay, S.; Frye, M. RNA Modifications Regulating Cell Fate in Cancer. *Nat Cell Biol* **2019**, *21* (5), 552–559. <https://doi.org/10.1038/s41556-019-0319-0>.
- (12) Shi, H.; Chai, P.; Jia, R.; Fan, X. Novel Insight into the Regulatory Roles of Diverse RNA Modifications: Re-Defining the Bridge between Transcription and Translation. *Mol Cancer* **2020**, *19* (1), 78. <https://doi.org/10.1186/s12943-020-01194-6>.
- (13) Motorin, Y.; Helm, M. RNA Nucleotide Methylation: 2021 Update. *WIREs RNA* **2022**, *13* (1). <https://doi.org/10.1002/wrna.1691>.

References

- (14) Cully, M. Chemical Inhibitors Make Their RNA Epigenetic Mark. *Nat Rev Drug Discov* **2019**, *18* (12), 892–894. <https://doi.org/10.1038/d41573-019-00179-5>.
- (15) Boccaletto, P.; Stefaniak, F.; Ray, A.; Cappannini, A.; Mukherjee, S.; Purta, E.; Kurkowska, M.; Shirvanizadeh, N.; Destefanis, E.; Groza, P.; Avşar, G.; Romitelli, A.; Pir, P.; Dassi, E.; Conticello, S. G.; Aguilo, F.; Bujnicki, J. M. MODOMICS: A Database of RNA Modification Pathways. 2021 Update. *Nucleic Acids Res* **2022**, *50* (D1), D231–D235. <https://doi.org/10.1093/nar/gkab1083>.
- (16) Cantara, W. A.; Crain, P. F.; Rozenski, J.; McCloskey, J. A.; Harris, K. A.; Zhang, X.; Vendeix, F. A. P.; Fabris, D.; Agris, P. F. The RNA Modification Database, RNAMDB: 2011 Update. *Nucleic Acids Res* **2011**, *39* (Database), D195–D201. <https://doi.org/10.1093/nar/gkq1028>.
- (17) Paramasivam, A.; Vijayashree Priyadharsini, J.; Raghunandhakumar, S. N6-Adenosine Methylation (M6A): A Promising New Molecular Target in Hypertension and Cardiovascular Diseases. *Hypertension Research* **2020**, *43* (2), 153–154. <https://doi.org/10.1038/s41440-019-0338-z>.
- (18) Zhang, M.; Song, J.; Yuan, W.; Zhang, W.; Sun, Z. Roles of RNA Methylation on Tumor Immunity and Clinical Implications. *Front Immunol* **2021**, *12*, 641507. <https://doi.org/10.3389/fimmu.2021.641507>.
- (19) Xie, S.; Chen, W.; Chen, K.; Chang, Y.; Yang, F.; Lin, A.; Shu, Q.; Zhou, T.; Yan, X. Emerging Roles of RNA Methylation in Gastrointestinal Cancers. *Cancer Cell Int* **2020**, *20* (1), 585. <https://doi.org/10.1186/s12935-020-01679-w>.
- (20) Berulava, T.; Buchholz, E.; Elerdashvili, V.; Pena, T.; Islam, M. R.; Lbik, D.; Mohamed, B. A.; Renner, A.; von Lewinski, D.; Sacherer, M.; Bohnsack, K. E.; Bohnsack, M. T.; Jain, G.; Capece, V.; Cleve, N.; Burkhardt, S.; Hasenfuss, G.; Fischer, A.; Toischer, K. Changes in M6A RNA Methylation Contribute to Heart Failure Progression by Modulating Translation. *Eur J Heart Fail* **2020**, *22* (1), 54–66. <https://doi.org/10.1002/ehf.1672>.
- (21) Yan, L.; Wei, J.; Yang, F.; Wang, M.; Wang, S.; Cheng, T.; Liu, X.; Jia, Y.; So, K.; Zhang, L. Physical Exercise Prevented Stress-Induced Anxiety via Improving Brain RNA Methylation. *Advanced Science* **2022**, *9* (24), 2105731. <https://doi.org/10.1002/advs.202105731>.
- (22) Zaccara, S.; Jaffrey, S. R. A Unified Model for the Function of YTHDF Proteins in Regulating M6A-Modified mRNA. *Cell* **2020**, *181* (7), 1582–1595.e18. <https://doi.org/10.1016/j.cell.2020.05.012>.
- (23) Rottman, F. M.; Bokar, J. A.; Narayan, P.; Shambaugh, M. E.; Ludwiczak, R. N6-Adenosine Methylation in mRNA: Substrate Specificity and Enzyme Complexity. *Biochimie* **1994**, *76* (12), 1109–1114. [https://doi.org/10.1016/0300-9084\(94\)90038-8](https://doi.org/10.1016/0300-9084(94)90038-8).
- (24) Yang, C.; Hu, Y.; Zhou, B.; Bao, Y.; Li, Z.; Gong, C.; Yang, H.; Wang, S.; Xiao, Y. The Role of M6A Modification in Physiology and Disease. *Cell Death Dis* **2020**, *11* (11), 960. <https://doi.org/10.1038/s41419-020-03143-z>.
- (25) Tomikawa, C. 7-Methylguanosine Modifications in Transfer RNA (TRNA). *Int J Mol Sci* **2018**, *19* (12), 4080. <https://doi.org/10.3390/ijms19124080>.

References

- (26) Cui, L.; Ma, R.; Cai, J.; Guo, C.; Chen, Z.; Yao, L.; Wang, Y.; Fan, R.; Wang, X.; Shi, Y. RNA Modifications: Importance in Immune Cell Biology and Related Diseases. *Signal Transduct Target Ther* **2022**, *7* (1), 334. <https://doi.org/10.1038/s41392-022-01175-9>.
- (27) Xia, X.; Wang, Y.; Zheng, J. C. Internal M7G Methylation: A Novel Epitranscriptomic Contributor in Brain Development and Diseases. *Mol Ther Nucleic Acids* **2023**, *31*, 295–308. <https://doi.org/10.1016/j.omtn.2023.01.003>.
- (28) Shaheen, R.; Abdel-Salam, G. M. H.; Guy, M. P.; Alomar, R.; Abdel-Hamid, M. S.; Afifi, H. H.; Ismail, S. I.; Emam, B. A.; Phizicky, E. M.; Alkuraya, F. S. Mutation in WDR4 Impairs TRNA M7G46 Methylation and Causes a Distinct Form of Microcephalic Primordial Dwarfism. *Genome Biol* **2015**, *16* (1), 210. <https://doi.org/10.1186/s13059-015-0779-x>.
- (29) Bohnsack, K.; Höbartner, C.; Bohnsack, M. Eukaryotic 5-Methylcytosine (M5C) RNA Methyltransferases: Mechanisms, Cellular Functions, and Links to Disease. *Genes (Basel)* **2019**, *10* (2), 102. <https://doi.org/10.3390/genes10020102>.
- (30) Breiling, A.; Lyko, F. Epigenetic Regulatory Functions of DNA Modifications: 5-Methylcytosine and Beyond. *Epigenetics Chromatin* **2015**, *8* (1), 24. <https://doi.org/10.1186/s13072-015-0016-6>.
- (31) Trixl, L.; Lusser, A. The Dynamic RNA Modification 5-methylcytosine and Its Emerging Role as an Epitranscriptomic Mark. *WIREs RNA* **2019**, *10* (1). <https://doi.org/10.1002/wrna.1510>.
- (32) Balachander, K.; Priyadharsini, J. V.; Roy, A.; Paramasivam, A. Emerging Role of RNA M5C Modification in Cardiovascular Diseases. *J Cardiovasc Transl Res* **2022**. <https://doi.org/10.1007/s12265-022-10336-8>.
- (33) Martinez, F. J.; Lee, J. H.; Lee, J. E.; Blanco, S.; Nickerson, E.; Gabriel, S.; Frye, M.; Al-Gazali, L.; Gleeson, J. G. Whole Exome Sequencing Identifies a Splicing Mutation in *NSUN2* as a Cause of a Dubowitz-like Syndrome. *J Med Genet* **2012**, *49* (6), 380–385. <https://doi.org/10.1136/jmedgenet-2011-100686>.
- (34) Zhang, Q.; Liu, F.; Chen, W.; Miao, H.; Liang, H.; Liao, Z.; Zhang, Z.; Zhang, B. The Role of RNA m⁵C Modification in Cancer Metastasis. *Int J Biol Sci* **2021**, *17* (13), 3369–3380. <https://doi.org/10.7150/ijbs.61439>.
- (35) Song, H.; Zhang, J.; Liu, B.; Xu, J.; Cai, B.; Yang, H.; Straube, J.; Yu, X.; Ma, T. Biological Roles of RNA M5C Modification and Its Implications in Cancer Immunotherapy. *Biomark Res* **2022**, *10* (1), 15. <https://doi.org/10.1186/s40364-022-00362-8>.
- (36) Quiles-Jiménez, A.; Dahl, T. B.; Bjørås, M.; Alseth, I.; Halvorsen, B.; Gregersen, I. Epitranscriptome in Ischemic Cardiovascular Disease: Potential Target for Therapies. *Stroke* **2022**, *53* (6), 2114–2122. <https://doi.org/10.1161/STROKEAHA.121.037581>.
- (37) Bohnsack, M. T.; Sloan, K. E. The Mitochondrial Epitranscriptome: The Roles of RNA Modifications in Mitochondrial Translation and Human Disease. *Cellular and Molecular Life Sciences* **2018**, *75* (2), 241–260. <https://doi.org/10.1007/s00018-017-2598-6>.
- (38) Bove, G.; Amin, S.; Babaei, M.; Benedetti, R.; Nebbioso, A.; Altucci, L.; Del Gaudio, N. Interplay between m⁶A Epitranscriptome and Epigenome in Cancer: Current Knowledge and Therapeutic Perspectives. *Int J Cancer* **2022**. <https://doi.org/10.1002/ijc.34378>.

References

- (39) Ehrenhofer-Murray, A. Cross-Talk between Dnmt2-Dependent TRNA Methylation and Queuosine Modification. *Biomolecules* **2017**, *7* (4), 14. <https://doi.org/10.3390/biom7010014>.
- (40) Zhang, Y.; Zhang, X.; Shi, J.; Tuorto, F.; Li, X.; Liu, Y.; Liebers, R.; Zhang, L.; Qu, Y.; Qian, J.; Pahima, M.; Liu, Y.; Yan, M.; Cao, Z.; Lei, X.; Cao, Y.; Peng, H.; Liu, S.; Wang, Y.; Zheng, H.; Woolsey, R.; Quilici, D.; Zhai, Q.; Li, L.; Zhou, T.; Yan, W.; Lyko, F.; Zhang, Y.; Zhou, Q.; Duan, E.; Chen, Q. Dnmt2 Mediates Intergenerational Transmission of Paternally Acquired Metabolic Disorders through Sperm Small Non-Coding RNAs. *Nat Cell Biol* **2018**, *20* (5), 535–540. <https://doi.org/10.1038/s41556-018-0087-2>.
- (41) Fleissner, E.; Borek, E. A NEW ENZYME OF RNA SYNTHESIS: RNA METHYLASE. *Proceedings of the National Academy of Sciences* **1962**, *48* (7), 1199–1203. <https://doi.org/10.1073/pnas.48.7.1199>.
- (42) McDonald, A. G.; Boyce, S.; Tipton, K. F. ExplorEnz: The Primary Source of the IUBMB Enzyme List. *Nucleic Acids Res* **2009**, *37* (Database), D593–D597. <https://doi.org/10.1093/nar/gkn582>.
- (43) Wolf, S. S. The Protein Arginine Methyltransferase Family: An Update about Function, New Perspectives and the Physiological Role in Humans. *Cellular and Molecular Life Sciences* **2009**, *66* (13), 2109–2121. <https://doi.org/10.1007/s00018-009-0010-x>.
- (44) Husmann, D.; Gozani, O. Histone Lysine Methyltransferases in Biology and Disease. *Nat Struct Mol Biol* **2019**, *26* (10), 880–889. <https://doi.org/10.1038/s41594-019-0298-7>.
- (45) Kudithipudi, S.; Jeltsch, A. Role of Somatic Cancer Mutations in Human Protein Lysine Methyltransferases. *Biochimica et Biophysica Acta (BBA) - Reviews on Cancer* **2014**, *1846* (2), 366–379. <https://doi.org/10.1016/j.bbcan.2014.08.002>.
- (46) Morales, Y.; Cáceres, T.; May, K.; Hevel, J. M. Biochemistry and Regulation of the Protein Arginine Methyltransferases (PRMTs). *Arch Biochem Biophys* **2016**, *590*, 138–152. <https://doi.org/10.1016/j.abb.2015.11.030>.
- (47) Edwards, J. R.; Yarychkivska, O.; Boulard, M.; Bestor, T. H. DNA Methylation and DNA Methyltransferases. *Epigenetics Chromatin* **2017**, *10* (1), 23. <https://doi.org/10.1186/s13072-017-0130-8>.
- (48) Bestor, T. H.; Verdine, G. L. DNA Methyltransferases. *Curr Opin Cell Biol* **1994**, *6* (3), 380–389. [https://doi.org/10.1016/0955-0674\(94\)90030-2](https://doi.org/10.1016/0955-0674(94)90030-2).
- (49) Jurkowska, R. Z.; Jurkowski, T. P.; Jeltsch, A. Structure and Function of Mammalian DNA Methyltransferases. *ChemBioChem* **2011**, *12* (2), 206–222. <https://doi.org/10.1002/cbic.201000195>.
- (50) Blanco, S.; Frye, M. Role of RNA Methyltransferases in Tissue Renewal and Pathology. *Curr Opin Cell Biol* **2014**, *31*, 1–7. <https://doi.org/10.1016/j.ceb.2014.06.006>.
- (51) Bohnsack, K.; Höbartner, C.; Bohnsack, M. Eukaryotic 5-Methylcytosine (m⁵C) RNA Methyltransferases: Mechanisms, Cellular Functions, and Links to Disease. *Genes (Basel)* **2019**, *10* (2), 102. <https://doi.org/10.3390/genes10020102>.
- (52) Fischer, T. R.; Meidner, L.; Schwickert, M.; Weber, M.; Zimmermann, R. A.; Kersten, C.; Schirmeister, T.; Helm, M. Chemical Biology and Medicinal Chemistry of RNA

References

- Methyltransferases. *Nucleic Acids Res* **2022**, *50* (8), 4216–4245. <https://doi.org/10.1093/nar/gkac224>.
- (53) Lennard, L. Methyltransferases. In *Comprehensive Toxicology*; Elsevier, 2010; pp 435–457. <https://doi.org/10.1016/B978-0-08-046884-6.00421-8>.
- (54) Krishnamohan, A.; Jackman, J. E. A Family Divided: Distinct Structural and Mechanistic Features of the SpoU-TrmD (SPOUT) Methyltransferase Superfamily. *Biochemistry* **2019**, *58* (5), 336–345. <https://doi.org/10.1021/acs.biochem.8b01047>.
- (55) Cantoni, G. L. Biological Methylation: Selected Aspects. *Annu Rev Biochem* **1975**, *44* (1), 435–451. <https://doi.org/10.1146/annurev.bi.44.070175.002251>.
- (56) Schubert, H. L.; Blumenthal, R. M.; Cheng, X. Many Paths to Methyltransfer: A Chronicle of Convergence. *Trends Biochem Sci* **2003**, *28* (6), 329–335. [https://doi.org/10.1016/S0968-0004\(03\)00090-2](https://doi.org/10.1016/S0968-0004(03)00090-2).
- (57) Struck, A.-W.; Thompson, M. L.; Wong, L. S.; Micklefield, J. S-Adenosyl-Methionine-Dependent Methyltransferases: Highly Versatile Enzymes in Biocatalysis, Biosynthesis and Other Biotechnological Applications. *ChemBioChem* **2012**, *13* (18), 2642–2655. <https://doi.org/10.1002/cbic.201200556>.
- (58) Qian, C.; Zhou, M.-M. SET Domain Protein Lysine Methyltransferases: Structure, Specificity and Catalysis. *Cellular and Molecular Life Sciences* **2006**, *63* (23), 2755–2763. <https://doi.org/10.1007/s00018-006-6274-5>.
- (59) Abdelraheem, E.; Thair, B.; Varela, R. F.; Jockmann, E.; Popadić, D.; Hailes, H. C.; Ward, J. M.; Iribarren, A. M.; Lewkowicz, E. S.; Andexer, J. N.; Hagedoorn, P.; Hanefeld, U. Methyltransferases: Functions and Applications. *ChemBioChem* **2022**, *23* (18). <https://doi.org/10.1002/cbic.202200212>.
- (60) Kozbial, P. Z.; Mushegian, A. R. Natural History of S-Adenosylmethionine-Binding Proteins. *BMC Struct Biol* **2005**, *5* (1), 19. <https://doi.org/10.1186/1472-6807-5-19>.
- (61) Chouhan, B. P. S.; Maimaiti, S.; Gade, M.; Laurino, P. Rossmann-Fold Methyltransferases: Taking a “ β -Turn” around Their Cofactor, S-Adenosylmethionine. *Biochemistry* **2019**, *58* (3), 166–170. <https://doi.org/10.1021/acs.biochem.8b00994>.
- (62) Schapira, M. Structural Chemistry of Human RNA Methyltransferases. *ACS Chem Biol* **2016**, *11* (3), 575–582. <https://doi.org/10.1021/acschembio.5b00781>.
- (63) Anantharaman, V.; Koonin, E. V.; Aravind, L. SPOUT: A Class of Methyltransferases That Includes SpoU and TrmD RNA Methylase Superfamilies, and Novel Superfamilies of Predicted Prokaryotic RNA Methylases. *J Mol Microbiol Biotechnol* **2002**, *4* (1), 71–76.
- (64) Lv, F.; Zhang, T.; Zhou, Z.; Gao, S.; Wong, C. C.; Zhou, J.-Q.; Ding, J. Structural Basis for Sfm1 Functioning as a Protein Arginine Methyltransferase. *Cell Discov* **2015**, *1* (1), 15037. <https://doi.org/10.1038/celldisc.2015.37>.
- (65) Sofia, H. J. Radical SAM, a Novel Protein Superfamily Linking Unresolved Steps in Familiar Biosynthetic Pathways with Radical Mechanisms: Functional Characterization Using New Analysis and Information Visualization Methods. *Nucleic Acids Res* **2001**, *29* (5), 1097–1106. <https://doi.org/10.1093/nar/29.5.1097>.

References

- (66) Giessing, A. M. B.; Jensen, S. S.; Rasmussen, A.; Hansen, L. H.; Gondela, A.; Long, K.; Vester, B.; Kirpekar, F. Identification of 8-Methyladenosine as the Modification Catalyzed by the Radical SAM Methyltransferase Cfr That Confers Antibiotic Resistance in Bacteria. *RNA* **2009**, *15* (2), 327–336. <https://doi.org/10.1261/rna.1371409>.
- (67) Kaminska, K. H.; Purta, E.; Hansen, L. H.; Bujnicki, J. M.; Vester, B.; Long, K. S. Insights into the Structure, Function and Evolution of the Radical-SAM 23S RRNA Methyltransferase Cfr That Confers Antibiotic Resistance in Bacteria. *Nucleic Acids Res* **2010**, *38* (5), 1652–1663. <https://doi.org/10.1093/nar/gkp1142>.
- (68) Toh, S.-M.; Xiong, L.; Bae, T.; Mankin, A. S. The Methyltransferase YfgB/RlmN Is Responsible for Modification of Adenosine 2503 in 23S RRNA. *RNA* **2008**, *14* (1), 98–106. <https://doi.org/10.1261/rna.814408>.
- (69) Nicolet, Y. AdoMet Radical Proteins--from Structure to Evolution--Alignment of Divergent Protein Sequences Reveals Strong Secondary Structure Element Conservation. *Nucleic Acids Res* **2004**, *32* (13), 4015–4025. <https://doi.org/10.1093/nar/gkh728>.
- (70) Kimura, S.; Miyauchi, K.; Ikeuchi, Y.; Thiaville, P. C.; Crécy-Lagard, V. de; Suzuki, T. Discovery of the β -Barrel-Type RNA Methyltransferase Responsible for N^6 -Methylation of N^6 -Threonylcarbamoyladenine in tRNAs. *Nucleic Acids Res* **2014**, *42* (14), 9350–9365. <https://doi.org/10.1093/nar/gku618>.
- (71) Currie, M. A.; Brown, G.; Wong, A.; Ohira, T.; Sugiyama, K.; Suzuki, T.; Yakunin, A. F.; Jia, Z. Structural and Functional Characterization of the TYW3/Taw3 Class of SAM-Dependent Methyltransferases. *RNA* **2017**, *23* (3), 346–354. <https://doi.org/10.1261/rna.057943.116>.
- (72) Bestor, T. H. The DNA Methyltransferases of Mammals. *Hum Mol Genet* **2000**, *9* (16), 2395–2402. <https://doi.org/10.1093/hmg/9.16.2395>.
- (73) Schaefer, M.; Lyko, F. Solving the Dnmt2 Enigma. *Chromosoma* **2010**, *119* (1), 35–40. <https://doi.org/10.1007/s00412-009-0240-6>.
- (74) Jeltsch, A.; Nellen, W.; Lyko, F. Two Substrates Are Better than One: Dual Specificities for Dnmt2 Methyltransferases. *Trends Biochem Sci* **2006**, *31* (6), 306–308. <https://doi.org/10.1016/j.tibs.2006.04.005>.
- (75) Bateman, A.; Martin, M.-J.; Orchard, S.; Magrane, M.; Ahmad, S.; Alpi, E.; Bowler-Barnett, E. H.; Britto, R.; Bye-A-Jee, H.; Cukura, A.; Denny, P.; Dogan, T.; Ebenezer, T.; Fan, J.; Garmiri, P.; da Costa Gonzales, L. J.; Hatton-Ellis, E.; Hussein, A.; Ignatchenko, A.; Insana, G.; Ishtiaq, R.; Joshi, V.; Jyothi, D.; Kandasamy, S.; Lock, A.; Luciani, A.; Lugaric, M.; Luo, J.; Lussi, Y.; MacDougall, A.; Madeira, F.; Mahmoudy, M.; Mishra, A.; Moulang, K.; Nightingale, A.; Pundir, S.; Qi, G.; Raj, S.; Raposo, P.; Rice, D. L.; Saidi, R.; Santos, R.; Speretta, E.; Stephenson, J.; Tootoo, P.; Turner, E.; Tyagi, N.; Vasudev, P.; Warner, K.; Watkins, X.; Zaru, R.; Zellner, H.; Bridge, A. J.; Aimo, L.; Argoud-Puy, G.; Auchincloss, A. H.; Axelsen, K. B.; Bansal, P.; Baratin, D.; Batista Neto, T. M.; Blatter, M.-C.; Bolleman, J. T.; Boutet, E.; Breuza, L.; Gil, B. C.; Casals-Casas, C.; Echioukh, K. C.; Coudert, E.; Cuche, B.; de Castro, E.; Estreicher, A.; Famiglietti, M. L.; Feuermann, M.; Gasteiger, E.; Gaudet, P.; Gehant, S.; Gerritsen, V.; Gos, A.; Gruaz, N.; Hulo, C.; Hyka-Nouspikel, N.; Jungo, F.; Kerhornou, A.; Le Mercier, P.; Lieberherr, D.; Masson, P.; Morgat, A.; Muthukrishnan, V.; Paesano, S.; Pedruzzi, I.; Pilbout, S.; Pourcel, L.; Poux,

References

- S.; Pozzato, M.; Pruess, M.; Redaschi, N.; Rivoire, C.; Sigrist, C. J. A.; Sonesson, K.; Sundaram, S.; Wu, C. H.; Arighi, C. N.; Arminski, L.; Chen, C.; Chen, Y.; Huang, H.; Laiho, K.; McGarvey, P.; Natale, D. A.; Ross, K.; Vinayaka, C. R.; Wang, Q.; Wang, Y.; Zhang, J. UniProt: The Universal Protein Knowledgebase in 2023. *Nucleic Acids Res* **2023**, *51* (D1), D523–D531. <https://doi.org/10.1093/nar/gkac1052>.
- (76) Dong, A. Structure of Human DNMT2, an Enigmatic DNA Methyltransferase Homolog That Displays Denaturant-Resistant Binding to DNA. *Nucleic Acids Res* **2001**, *29* (2), 439–448. <https://doi.org/10.1093/nar/29.2.439>.
- (77) Van den Wyngaert, I.; Sprengel, J.; Kass, S. U.; Luyten, W. H. M. L. Cloning and Analysis of a Novel Human Putative DNA Methyltransferase. *FEBS Lett* **1998**, *426* (2), 283–289. [https://doi.org/10.1016/S0014-5793\(98\)00362-7](https://doi.org/10.1016/S0014-5793(98)00362-7).
- (78) Yoder, J. A Candidate Mammalian DNA Methyltransferase Related to Pmt1p of Fission Yeast. *Hum Mol Genet* **1998**, *7* (2), 279–284. <https://doi.org/10.1093/hmg/7.2.279>.
- (79) Hermann, A.; Schmitt, S.; Jeltsch, A. The Human Dnmt2 Has Residual DNA-(Cytosine-C5) Methyltransferase Activity. *Journal of Biological Chemistry* **2003**, *278* (34), 31717–31721. <https://doi.org/10.1074/jbc.M305448200>.
- (80) Goll, M. G.; Kirpekar, F.; Maggert, K. A.; Yoder, J. A.; Hsieh, C.-L.; Zhang, X.; Golic, K. G.; Jacobsen, S. E.; Bestor, T. H. Methylation of TRNA^{Asp} by the DNA Methyltransferase Homolog Dnmt2. *Science (1979)* **2006**, *311* (5759), 395–398. <https://doi.org/10.1126/science.1120976>.
- (81) Schaefer, M.; Pollex, T.; Hanna Katharina; Tuorto, F.; Meusburger, M.; Helm, M.; Lyko, F. RNA Methylation by Dnmt2 Protects Transfer RNAs against Stress-Induced Cleavage. *Genes Dev* **2010**, *24* (15), 1590–1595. <https://doi.org/10.1101/gad.586710>.
- (82) Jurkowski, T. P.; Meusburger, M.; Phalke, S.; Helm, M.; Nellen, W.; Reuter, G.; Jeltsch, A. Human DNMT2 Methylates TRNA^{Asp} Molecules Using a DNA Methyltransferase-like Catalytic Mechanism. *RNA* **2008**, *14* (8), 1663–1670. <https://doi.org/10.1261/rna.970408>.
- (83) Jurkowska, R. Z.; Jurkowski, T. P.; Jeltsch, A. Structure and Function of Mammalian DNA Methyltransferases. *ChemBioChem* **2011**, *12* (2), 206–222. <https://doi.org/10.1002/cbic.201000195>.
- (84) Jeltsch, A.; Ehrenhofer-Murray, A.; Jurkowski, T. P.; Lyko, F.; Reuter, G.; Ankri, S.; Nellen, W.; Schaefer, M.; Helm, M. Mechanism and Biological Role of Dnmt2 in Nucleic Acid Methylation. *RNA Biol* **2017**, *14* (9), 1108–1123. <https://doi.org/10.1080/15476286.2016.1191737>.
- (85) Jeltsch, A. Beyond Watson and Crick: DNA Methylation and Molecular Enzymology of DNA Methyltransferases. *ChemBioChem* **2002**, *3* (4), 274–293. [https://doi.org/10.1002/1439-7633\(20020402\)3:4<274::AID-CBIC274>3.0.CO;2-S](https://doi.org/10.1002/1439-7633(20020402)3:4<274::AID-CBIC274>3.0.CO;2-S).
- (86) Huang, Z.-X.; Li, J.; Xiong, Q.-P.; Li, H.; Wang, E.-D.; Liu, R.-J. Position 34 of TRNA Is a Discriminative Element for M5C38 Modification by Human DNMT2. *Nucleic Acids Res* **2021**, *49* (22), 13045–13061. <https://doi.org/10.1093/nar/gkab1148>.
- (87) Shanmugam, R.; Fierer, J.; Kaiser, S.; Helm, M.; Jurkowski, T. P.; Jeltsch, A. Cytosine Methylation of TRNA-Asp by DNMT2 Has a Role in Translation of Proteins Containing

References

- Poly-Asp Sequences. *Cell Discov* **2015**, *1* (1), 15010.
<https://doi.org/10.1038/celldisc.2015.10>.
- (88) Tuorto, F.; Liebers, R.; Musch, T.; Schaefer, M.; Hofmann, S.; Kellner, S.; Frye, M.; Helm, M.; Stoecklin, G.; Lyko, F. RNA Cytosine Methylation by Dnmt2 and NSun2 Promotes TRNA Stability and Protein Synthesis. *Nat Struct Mol Biol* **2012**, *19* (9), 900–905.
<https://doi.org/10.1038/nsmb.2357>.
- (89) Becker, M.; Müller, S.; Nellen, W.; Jurkowski, T. P.; Jeltsch, A.; Ehrenhofer-Murray, A. E. Pmt1, a Dnmt2 Homolog in *Schizosaccharomyces Pombe*, Mediates TRNA Methylation in Response to Nutrient Signaling. *Nucleic Acids Res* **2012**, *40* (22), 11648–11658.
<https://doi.org/10.1093/nar/gks956>.
- (90) Lin, M.-J.; Tang, L.-Y.; Reddy, M. N.; Shen, C.-K. J. DNA Methyltransferase Gene DDnmt2 and Longevity of *Drosophila*. *Journal of Biological Chemistry* **2005**, *280* (2), 861–864. <https://doi.org/10.1074/jbc.C400477200>.
- (91) Elhardt, W.; Shanmugam, R.; Jurkowski, T. P.; Jeltsch, A. Somatic Cancer Mutations in the DNMT2 TRNA Methyltransferase Alter Its Catalytic Properties. *Biochimie* **2015**, *112*, 66–72. <https://doi.org/10.1016/j.biochi.2015.02.022>.
- (92) King, M. Y.; Redman, K. L. RNA Methyltransferases Utilize Two Cysteine Residues in the Formation of 5-Methylcytosine. *Biochemistry* **2002**, *41* (37), 11218–11225.
<https://doi.org/10.1021/bi026055q>.
- (93) Liu, Y.; Santi, D. V. M⁵C RNA and m⁵C DNA Methyl Transferases Use Different Cysteine Residues as Catalysts. *Proceedings of the National Academy of Sciences* **2000**, *97* (15), 8263–8265. <https://doi.org/10.1073/pnas.97.15.8263>.
- (94) Hussain, S.; Sajini, A. A.; Blanco, S.; Dietmann, S.; Lombard, P.; Sugimoto, Y.; Paramor, M.; Gleeson, J. G.; Odom, D. T.; Ule, J.; Frye, M. NSun2-Mediated Cytosine-5 Methylation of Vault Noncoding RNA Determines Its Processing into Regulatory Small RNAs. *Cell Rep* **2013**, *4* (2), 255–261. <https://doi.org/10.1016/j.celrep.2013.06.029>.
- (95) Haag, S.; Warda, A. S.; Kretschmer, J.; Günnigmann, M. A.; Höbartner, C.; Bohnsack, M. T. NSUN6 Is a Human RNA Methyltransferase That Catalyzes Formation of m⁵C72 in Specific TRNAs. *RNA* **2015**, *21* (9), 1532–1543.
<https://doi.org/10.1261/rna.051524.115>.
- (96) Liu, R.-J.; Long, T.; Li, J.; Li, H.; Wang, E.-D. Structural Basis for Substrate Binding and Catalytic Mechanism of a Human RNA:M5C Methyltransferase NSun6. *Nucleic Acids Res* **2017**, *45* (11), 6684–6697. <https://doi.org/10.1093/nar/gkx473>.
- (97) Long, T.; Li, J.; Li, H.; Zhou, M.; Zhou, X.-L.; Liu, R.-J.; Wang, E.-D. Sequence-Specific and Shape-Selective RNA Recognition by the Human RNA 5-Methylcytosine Methyltransferase NSun6. *Journal of Biological Chemistry* **2016**, *291* (46), 24293–24303. <https://doi.org/10.1074/jbc.M116.742569>.
- (98) Yang, R.; Liang, X.; Wang, H.; Guo, M.; Shen, H.; Shi, Y.; Liu, Q.; Sun, Y.; Yang, L.; Zhan, M. The RNA Methyltransferase NSUN6 Suppresses Pancreatic Cancer Development by Regulating Cell Proliferation. *EBioMedicine* **2021**, *63*, 103195.
<https://doi.org/10.1016/j.ebiom.2020.103195>.

References

- (99) Wang, Z.-L.; Li, B.; Luo, Y.-X.; Lin, Q.; Liu, S.-R.; Zhang, X.-Q.; Zhou, H.; Yang, J.-H.; Qu, L.-H. Comprehensive Genomic Characterization of RNA-Binding Proteins across Human Cancers. *Cell Rep* **2018**, *22* (1), 286–298. <https://doi.org/10.1016/j.celrep.2017.12.035>.
- (100) Li, C.; Wang, S.; Xing, Z.; Lin, A.; Liang, K.; Song, J.; Hu, Q.; Yao, J.; Chen, Z.; Park, P. K.; Hawke, D. H.; Zhou, J.; Zhou, Y.; Zhang, S.; Liang, H.; Hung, M.-C.; Gallick, G. E.; Han, L.; Lin, C.; Yang, L. A ROR1–HER3–LncRNA Signalling Axis Modulates the Hippo–YAP Pathway to Regulate Bone Metastasis. *Nat Cell Biol* **2017**, *19* (2), 106–119. <https://doi.org/10.1038/ncb3464>.
- (101) PerezGrovas-Saltijeral, A.; Rajkumar, A. P.; Knight, H. M. Differential Expression of M5C RNA Methyltransferase Genes NSUN6 and NSUN7 in Alzheimer’s Disease and Traumatic Brain Injury. *Mol Neurobiol* **2023**, *60* (4), 2223–2235. <https://doi.org/10.1007/s12035-022-03195-6>.
- (102) Wang, W.; Huang, H.; Jiang, H.; Tian, C.; Tang, Y.; Gan, D.; Wen, X.; Song, Z.; He, Y.; Ou, X.; Fang, L. A Cross-Tissue Investigation of Molecular Targets and Physiological Functions of Nsun6 Using Knockout Mice. *Int J Mol Sci* **2022**, *23* (12), 6584. <https://doi.org/10.3390/ijms23126584>.
- (103) Schaefer, M.; Hagemann, S.; Hanna, K.; Lyko, F. Azacytidine Inhibits RNA Methylation at DNMT2 Target Sites in Human Cancer Cell Lines. *Cancer Res* **2009**, *69* (20), 8127–8132. <https://doi.org/10.1158/0008-5472.CAN-09-0458>.
- (104) Mehdipour, P.; Chen, R.; De Carvalho, D. D. The next Generation of DNMT Inhibitors. *Nat Cancer* **2021**, *2* (10), 1000–1001. <https://doi.org/10.1038/s43018-021-00271-z>.
- (105) Pappalardi, M. B.; Keenan, K.; Cockerill, M.; Kellner, W. A.; Stowell, A.; Sherk, C.; Wong, K.; Pathuri, S.; Briand, J.; Steidel, M.; Chapman, P.; Groy, A.; Wiseman, A. K.; McHugh, C. F.; Campobasso, N.; Graves, A. P.; Fairweather, E.; Werner, T.; Raoof, A.; Butlin, R. J.; Rueda, L.; Horton, J. R.; Fosbenner, D. T.; Zhang, C.; Handler, J. L.; Muliaditan, M.; Mebrahtu, M.; Jaworski, J.-P.; McNulty, D. E.; Burt, C.; Eberl, H. C.; Taylor, A. N.; Ho, T.; Merrihew, S.; Foley, S. W.; Rutkowska, A.; Li, M.; Romeril, S. P.; Goldberg, K.; Zhang, X.; Kershaw, C. S.; Bantscheff, M.; Jurewicz, A. J.; Minthorn, E.; Grandi, P.; Patel, M.; Benowitz, A. B.; Mohammad, H. P.; Gilmartin, A. G.; Prinjha, R. K.; Ogilvie, D.; Carpenter, C.; Heering, D.; Baylin, S. B.; Jones, P. A.; Cheng, X.; King, B. W.; Luengo, J. I.; Jordan, A. M.; Waddell, I.; Kruger, R. G.; McCabe, M. T. Discovery of a First-in-Class Reversible DNMT1-Selective Inhibitor with Improved Tolerability and Efficacy in Acute Myeloid Leukemia. *Nat Cancer* **2021**, *2* (10), 1002–1017. <https://doi.org/10.1038/s43018-021-00249-x>.
- (106) Yankova, E.; Blackaby, W.; Albertella, M.; Rak, J.; De Braekeleer, E.; Tzagkogeorga, G.; Pilka, E. S.; Aspris, D.; Leggate, D.; Hendrick, A. G.; Webster, N. A.; Andrews, B.; Fosbeary, R.; Guest, P.; Irigoyen, N.; Eleftheriou, M.; Gozdecka, M.; Dias, J. M. L.; Bannister, A. J.; Vick, B.; Jeremias, I.; Vassiliou, G. S.; Rausch, O.; Tzelepis, K.; Kouzarides, T. Small-Molecule Inhibition of METTL3 as a Strategy against Myeloid Leukaemia. *Nature* **2021**, *593* (7860), 597–601. <https://doi.org/10.1038/s41586-021-03536-w>.
- (107) Stacchiotti, S.; Schoffski, P.; Jones, R.; Agulnik, M.; Villalobos, V. M.; Jahan, T. M.; Chen, T. W.-W.; Italiano, A.; Demetri, G. D.; Cote, G. M.; Chugh, R.; Attia, S.; Gupta, A. A.; Loggers, E. T.; Van Tine, B.; Sierra, L.; Yang, J.; Rajarethinam, A.; Gounder, M. M. Safety

References

- and Efficacy of Tazemetostat, a First-in-Class EZH2 Inhibitor, in Patients (Pts) with Epithelioid Sarcoma (ES) (NCT02601950). *Journal of Clinical Oncology* **2019**, *37* (15_suppl), 11003–11003. https://doi.org/10.1200/JCO.2019.37.15_suppl.11003.
- (108) Hoy, S. M. Tazemetostat: First Approval. *Drugs* **2020**, *80* (5), 513–521. <https://doi.org/10.1007/s40265-020-01288-x>.
- (109) Knutson, S. K.; Warholic, N. M.; Wigle, T. J.; Klaus, C. R.; Allain, C. J.; Raimondi, A.; Porter Scott, M.; Chesworth, R.; Moyer, M. P.; Copeland, R. A.; Richon, V. M.; Pollock, R. M.; Kuntz, K. W.; Keilhack, H. Durable Tumor Regression in Genetically Altered Malignant Rhabdoid Tumors by Inhibition of Methyltransferase EZH2. *Proceedings of the National Academy of Sciences* **2013**, *110* (19), 7922–7927. <https://doi.org/10.1073/pnas.1303800110>.
- (110) Smyth, L. A.; Collins, I. Measuring and Interpreting the Selectivity of Protein Kinase Inhibitors. *J Chem Biol* **2009**, *2* (3), 131–151. <https://doi.org/10.1007/s12154-009-0023-9>.
- (111) Roskoski, R. Properties of FDA-Approved Small Molecule Protein Kinase Inhibitors: A 2023 Update. *Pharmacol Res* **2023**, *187*, 106552. <https://doi.org/10.1016/j.phrs.2022.106552>.
- (112) Petrossian, T. C.; Clarke, S. G. Uncovering the Human Methyltransferasome. *Molecular & Cellular Proteomics* **2011**, *10* (1), M110.000976. <https://doi.org/10.1074/mcp.M110.000976>.
- (113) Fontecave, M.; Atta, M.; Mulliez, E. S-Adenosylmethionine: Nothing Goes to Waste. *Trends Biochem Sci* **2004**, *29* (5), 243–249. <https://doi.org/10.1016/j.tibs.2004.03.007>.
- (114) Santi, D. V.; McHenry, C. S. 5-Fluoro-2'-Deoxyuridylate: Covalent Complex with Thymidylate Synthetase. *Proceedings of the National Academy of Sciences* **1972**, *69* (7), 1855–1857. <https://doi.org/10.1073/pnas.69.7.1855>.
- (115) Hartmann, K.-U.; Heidelberger, C. Studies on Fluorinated Pyrimidines. *Journal of Biological Chemistry* **1961**, *236* (11), 3006–3013. [https://doi.org/10.1016/S0021-9258\(19\)76419-9](https://doi.org/10.1016/S0021-9258(19)76419-9).
- (116) Langenbach, R. J.; Danenberg, P. V.; Heidelberger, C. Thymidylate Synthetase: Mechanism of Inhibition by 5-Fluoro-2'-Deoxyuridylate. *Biochem Biophys Res Commun* **1972**, *48* (6), 1565–1571. [https://doi.org/10.1016/0006-291X\(72\)90892-3](https://doi.org/10.1016/0006-291X(72)90892-3).
- (117) Danenberg, P. V.; Langenbach, R. J.; Heidelberger, C. Fluorinated Pyrimidines. Structures of Reversible and Irreversible Complexes of Thymidylate Synthetase and Fluorinated Pyrimidine Nucleotides. *Biochemistry* **1974**, *13* (5), 926–933. <https://doi.org/10.1021/bi00702a016>.
- (118) De Cesco, S.; Kurian, J.; Dufresne, C.; Mittermaier, A. K.; Moitessier, N. Covalent Inhibitors Design and Discovery. *Eur J Med Chem* **2017**, *138*, 96–114. <https://doi.org/10.1016/j.ejmech.2017.06.019>.
- (119) Sutanto, F.; Konstantinidou, M.; Dömling, A. Covalent Inhibitors: A Rational Approach to Drug Discovery. *RSC Med Chem* **2020**, *11* (8), 876–884. <https://doi.org/10.1039/D0MD00154F>.

References

- (120) Schmidt, T. C.; Welker, A.; Rieger, M.; Sahu, P. K.; Sotriffer, C. A.; Schirmeister, T.; Engels, B. Protocol for Rational Design of Covalently Interacting Inhibitors. *ChemPhysChem* **2014**, *15* (15), 3226–3235. <https://doi.org/10.1002/cphc.201402542>.
- (121) Baillie, T. A. Targeted Covalent Inhibitors for Drug Design. *Angewandte Chemie International Edition* **2016**, *55* (43), 13408–13421. <https://doi.org/10.1002/anie.201601091>.
- (122) Bauer, R. A. Covalent Inhibitors in Drug Discovery: From Accidental Discoveries to Avoided Liabilities and Designed Therapies. *Drug Discov Today* **2015**, *20* (9), 1061–1073. <https://doi.org/10.1016/j.drudis.2015.05.005>.
- (123) Mora-Ochomogo, M.; Lohans, C. T. β -Lactam Antibiotic Targets and Resistance Mechanisms: From Covalent Inhibitors to Substrates. *RSC Med Chem* **2021**, *12* (10), 1623–1639. <https://doi.org/10.1039/D1MD00200G>.
- (124) Waxman, D. J.; Strominger Jack L. Penicillin-Binding Proteins and the Mechanism of Action of Beta-Lactam Antibiotics. *Annu Rev Biochem* **1983**, *52* (1), 825–869.
- (125) Wallmark, B. Mechanism of Action of Omeprazole. *Scand J Gastroenterol* **1986**, *21* (sup118), 11–16. <https://doi.org/10.3109/00365528609090881>.
- (126) Keeling, D. J.; Fallowfield, C.; Milliner, K. J.; Tingley, S. K.; Ife, R. J.; Underwood, A. H. Studies on the Mechanism of Action of Omeprazole. *Biochem Pharmacol* **1985**, *34* (16), 2967–2973. [https://doi.org/10.1016/0006-2952\(85\)90023-1](https://doi.org/10.1016/0006-2952(85)90023-1).
- (127) Shin, J. M.; Cho, Y. M.; Sachs, G. Chemistry of Covalent Inhibition of the Gastric (H^+ , K^+)-ATPase by Proton Pump Inhibitors. *J Am Chem Soc* **2004**, *126* (25), 7800–7811. <https://doi.org/10.1021/ja049607w>.
- (128) Fischer, J.; Rotella, D. P. Serendipitous Target-Based Drug Discoveries. In *Successful Drug Discovery*; Wiley-VCH Verlag GmbH & Co. KGaA: Weinheim, Germany, 2015; pp 1–18. <https://doi.org/10.1002/9783527678433.ch1>.
- (129) Lei, J.; Zhou, Y.; Xie, D.; Zhang, Y. Mechanistic Insights into a Classic Wonder Drug—Aspirin. *J Am Chem Soc* **2015**, *137* (1), 70–73. <https://doi.org/10.1021/ja5112964>.
- (130) Renaud, J.-P.; Chung, C.; Danielson, U. H.; Egner, U.; Hennig, M.; Hubbard, R. E.; Nar, H. Biophysics in Drug Discovery: Impact, Challenges and Opportunities. *Nat Rev Drug Discov* **2016**, *15* (10), 679–698. <https://doi.org/10.1038/nrd.2016.123>.
- (131) Genick, C. C.; Wright, S. K. Biophysics: For HTS Hit Validation, Chemical Lead Optimization, and Beyond. *Expert Opin Drug Discov* **2017**, *12* (9), 897–907. <https://doi.org/10.1080/17460441.2017.1349096>.
- (132) Eggen, M.; Schindler, J. Impact and Evolution of Biophysics in Medicinal Chemistry. In *Biophysical Techniques in Drug Discovery*; The Royal Society of Chemistry, 2017; pp 1–22. <https://doi.org/10.1039/9781788010016-00001>.
- (133) Gao, K.; Oerlemans, R.; Groves, M. R. Theory and Applications of Differential Scanning Fluorimetry in Early-Stage Drug Discovery. *Biophys Rev* **2020**, *12* (1), 85–104. <https://doi.org/10.1007/s12551-020-00619-2>.

References

- (134) Niesen, F. H.; Berglund, H.; Vedadi, M. The Use of Differential Scanning Fluorimetry to Detect Ligand Interactions That Promote Protein Stability. *Nat Protoc* **2007**, *2* (9), 2212–2221. <https://doi.org/10.1038/nprot.2007.321>.
- (135) Pantoliano, M. W.; Petrella, E. C.; Kwasnoski, J. D.; Lobanov, V. S.; Myslik, J.; Graf, E.; Carver, T.; Asel, E.; Springer, B. A.; Lane, P.; Salemme, F. R. High-Density Miniaturized Thermal Shift Assays as a General Strategy for Drug Discovery. *SLAS Discovery* **2001**, *6* (6), 429–440. <https://doi.org/10.1177/108705710100600609>.
- (136) Lo, M.-C.; Aulabaugh, A.; Jin, G.; Cowling, R.; Bard, J.; Malamas, M.; Ellestad, G. Evaluation of Fluorescence-Based Thermal Shift Assays for Hit Identification in Drug Discovery. *Anal Biochem* **2004**, *332* (1), 153–159. <https://doi.org/10.1016/j.ab.2004.04.031>.
- (137) Strutz, W. Exploring Protein Stability by NanoDSF. *Biophys J* **2016**, *110* (3), 393a.
- (138) Baaske, P.; Wienken, C. J.; Reineck, P.; Duhr, S.; Braun, D. Optical Thermophoresis for Quantifying the Buffer Dependence of Aptamer Binding. *Angewandte Chemie International Edition* **2010**, *49* (12), 2238–2241. <https://doi.org/10.1002/anie.200903998>.
- (139) Wienken, C. J.; Baaske, P.; Rothbauer, U.; Braun, D.; Duhr, S. Protein-Binding Assays in Biological Liquids Using Microscale Thermophoresis. *Nat Commun* **2010**, *1* (1), 100. <https://doi.org/10.1038/ncomms1093>.
- (140) Jerabek-Willemsen, M.; André, T.; Wanner, R.; Roth, H. M.; Duhr, S.; Baaske, P.; Breitsprecher, D. MicroScale Thermophoresis: Interaction Analysis and Beyond. *J Mol Struct* **2014**, *1077*, 101–113. <https://doi.org/10.1016/j.molstruc.2014.03.009>.
- (141) Rainard, J. M.; Pandarakalam, G. C.; McElroy, S. P. Using Microscale Thermophoresis to Characterize Hits from High-Throughput Screening: A European Lead Factory Perspective. *SLAS Discovery* **2018**, *23* (3), 225–241. <https://doi.org/10.1177/2472555217744728>.
- (142) Zimmermann, R. A.; Schwickert, M.; Meidner, J. L.; Nidoieva, Z.; Helm, M.; Schirmeister, T. An Optimized Microscale Thermophoresis Method for High-Throughput Screening of DNA Methyltransferase 2 Ligands. *ACS Pharmacol Transl Sci* **2022**, *5* (11), 1079–1085. <https://doi.org/10.1021/acsptsci.2c00175>.
- (143) Freire, E.; Mayorga, O. L.; Straume, M. Isothermal Titration Calorimetry. *Anal Chem* **1990**, *62* (18), 950–959.
- (144) Velázquez-Campoy, A.; Ohtaka, H.; Nezami, A.; Muzammil, S.; Freire, E. Isothermal Titration Calorimetry. *Curr Protoc Cell Biol* **2004**, *23* (1). <https://doi.org/10.1002/0471143030.cb1708s23>.
- (145) Ghai, R.; Falconer, R. J.; Collins, B. M. Applications of Isothermal Titration Calorimetry in Pure and Applied Research—Survey of the Literature from 2010. *Journal of Molecular Recognition* **2012**, *25* (1), 32–52. <https://doi.org/10.1002/jmr.1167>.
- (146) Burnouf, D.; Ennifar, E.; Guedich, S.; Puffer, B.; Hoffmann, G.; Bec, G.; Disdier, F.; Baltzinger, M.; Dumas, P. KinITC: A New Method for Obtaining Joint Thermodynamic and Kinetic Data by Isothermal Titration Calorimetry. *J Am Chem Soc* **2012**, *134* (1), 559–565. <https://doi.org/10.1021/ja209057d>.

References

- (147) Johe, P.; Jung, S.; Endres, E.; Kersten, C.; Zimmer, C.; Ye, W.; Sönnichsen, C.; Hellmich, U. A.; Sotriffer, C.; Schirmeister, T.; Neuweiler, H. Warhead Reactivity Limits the Speed of Inhibition of the Cysteine Protease Rhodospain. *ACS Chem Biol* **2021**, *16* (4), 661–670. <https://doi.org/10.1021/acscchembio.0c00911>.
- (148) Falconer, R. J. Applications of Isothermal Titration Calorimetry - the Research and Technical Developments from 2011 to 2015. *Journal of Molecular Recognition* **2016**, *29* (10), 504–515. <https://doi.org/10.1002/jmr.2550>.
- (149) Luan, Y.; Blazer, L. L.; Hu, H.; Hajian, T.; Zhang, J.; Wu, H.; Houliston, S.; Arrowsmith, C. H.; Vedadi, M.; Zheng, Y. G. Design of a Fluorescent Ligand Targeting the S-Adenosylmethionine Binding Site of the Histone Methyltransferase MLL1. *Org Biomol Chem* **2016**, *14* (2), 631–638. <https://doi.org/10.1039/C5OB01794G>.
- (150) Strelow, J. M. A Perspective on the Kinetics of Covalent and Irreversible Inhibition. *SLAS Discovery* **2017**, *22* (1), 3–20. <https://doi.org/10.1177/1087057116671509>.
- (151) Śledź, P.; Jinek, M. Structural Insights into the Molecular Mechanism of the M6A Writer Complex. *Elife* **2016**, *5*. <https://doi.org/10.7554/eLife.18434>.